

5-2011

Co-development of biological soil crusts, soil-geomorphology, and landscape biogeochemistry in the Mojave Desert, Nevada, U.S.A. – Implications for ecological management

Amanda Jean Williams
University of Nevada, Las Vegas

Follow this and additional works at: <https://digitalscholarship.unlv.edu/thesesdissertations>



Part of the [Desert Ecology Commons](#), [Geomorphology Commons](#), [Soil Science Commons](#), and the [Terrestrial and Aquatic Ecology Commons](#)

Repository Citation

Williams, Amanda Jean, "Co-development of biological soil crusts, soil-geomorphology, and landscape biogeochemistry in the Mojave Desert, Nevada, U.S.A. – Implications for ecological management" (2011). *UNLV Theses, Dissertations, Professional Papers, and Capstones*. 1025.
<http://dx.doi.org/10.34917/2396460>

This Dissertation is protected by copyright and/or related rights. It has been brought to you by Digital Scholarship@UNLV with permission from the rights-holder(s). You are free to use this Dissertation in any way that is permitted by the copyright and related rights legislation that applies to your use. For other uses you need to obtain permission from the rights-holder(s) directly, unless additional rights are indicated by a Creative Commons license in the record and/or on the work itself.

This Dissertation has been accepted for inclusion in UNLV Theses, Dissertations, Professional Papers, and Capstones by an authorized administrator of Digital Scholarship@UNLV. For more information, please contact digitalscholarship@unlv.edu.

CO-DEVELOPMENT OF BIOLOGICAL SOIL CRUSTS, SOIL-GEOMORPHOLOGY,
AND LANDSCAPE BIOGEOCHEMISTRY IN THE MOJAVE DESERT,
NEVADA, U.S.A. – IMPLICATIONS FOR
ECOLOGICAL MANAGEMENT

by

Amanda Jean Williams

Bachelor of Science
University of Missouri – Columbia
2005

A dissertation submitted in partial fulfillment
of the requirements for the

Doctor of Philosophy in Geoscience
Department of Geoscience
College of Science

Graduate College
University of Nevada, Las Vegas
May 2011

Copyright by Amanda J. Williams 2011
All Rights Reserved



THE GRADUATE COLLEGE

We recommend the dissertation prepared under our supervision by

Amanda Jean Williams

entitled

**Co-Development of Biological Soil Crusts, Soil-Geomorphology, and
Landscape Biogeochemistry in the Mojave Desert, Nevada, U.S.A. –
Implications for Ecological Management**

be accepted in partial fulfillment of the requirements for the degree of

Doctor of Philosophy in Geoscience

Brenda Buck, Committee Chair

Margaret Rees, Committee Member

Stephen Rowland, Committee Member

Deborah Soukup, Committee Member

Lloyd Stark, Graduate Faculty Representative

Ronald Smith, Ph. D., Vice President for Research and Graduate Studies
and Dean of the Graduate College

May 2011

ABSTRACT

Co-Development of Biological Soil Crusts, Soil-Geomorphology, and Landscape Biogeochemistry in the Mojave Desert, Nevada, U.S.A. – Implications for Ecological Management

by

Amanda Jean Williams

Dr. Brenda J. Buck, Examination Committee Chair
Professor of Geology
University of Nevada, Las Vegas

Biological soil crusts (BSCs) are complex matrices of soil particles, mosses, lichens, and cyanobacteria that prevent erosion and influence water and energy balances, soil fertility, and vascular plant germination. The processes that form BSCs, the factors that control their distribution, and the ecosystem feedbacks that they sustain are poorly understood. This dissertation employed a novel interdisciplinary approach to address those research unknowns through investigations of the micromorphological structure, soil-geomorphic relationships, and biogeochemical feedbacks of BSCs in the Mojave Desert.

A micromorphological study of BSCs resulted in a succession model that illustrates how crust formative processes and structures change through time. Tall moss-lichen pinnacled crusts actively capture dust, precipitate authigenic minerals, experience alternating expansion-contraction from wet-dry cycles, and form a surface seal that together with dust capture produces Av horizons. The resulting unique bio-sedimentary structures control ecological function and further promote BSC growth. This is the first study to demonstrate a biological process leading to the formation of Av horizons and

suggests that BSCs are previously under-recognized critical agents of arid pedogenesis and landscape development.

From a soil-geomorphic study of BSCs a model was developed wherein the ratio of fine sand to rocks controls the relative distribution of three surface cover types – cyanobacteria crusts, moss-lichen crusts, and desert pavements with low to moderate moss-lichen cover. The biological and geological feedbacks that sustain these cover types vary predictably across intermontane basins, yielding new insights for land management. Moreover, the physical processes that control BSCs are common to most deserts, making these results applicable worldwide.

An ecological study of BSCs resulted in a conceptual model wherein the sand-to-rock-ratio, which constrains interspace cover by BSCs and desert pavements, ultimately determines the magnitude of the fertile island effect. Inferred biological-geological feedbacks produce three unique biogeochemical patterns that vary predictably across the landscape. These surface cover patterns are consistent within many deserts, potentially reflecting overarching controls of resource allocation that operate despite differences in total site productivity.

TABLE OF CONTENTS

ABSTRACT	iii
ACKNOWLEDGEMENTS	vii
LIST OF FIGURES	x
LIST OF TABLES	xiii
 CHAPTER 1 INTEGRATING STUDIES OF BIOLOGICAL SOIL CRUST MICROSTRUCTURE, SOIL-GEOMORPHIC RELATIONSHIPS, AND ECOLOGY	
Ecological Importance of Biological Soil crusts	1
Current Scientific Challenges and Study Objectives.....	1
Linking Microstructure, Soil-Geomorphic Relationships, and Ecology of Biological Soil Crusts.....	3
Literature Cited.....	7
 CHAPTER 2 MICROSTRUCTURE AND GENESIS OF BIOLOGICAL SOIL CRUSTS.....	
Abstract.....	10
Introduction and Background	11
Materials and Methods	14
Results	14
Interpretations	31
Discussion.....	42
Conclusions	58
Literature Cited	60
Figures	72
Tables.....	100
 CHAPTER 3 COEVOLUTION OF BIOLOGICAL SOIL CRUSTS AND SOIL-GEOMORPHOLOGY	
Abstract.....	104
Introduction	105
Background and Geologic Setting.....	108
Materials and Methods	110
Results	110
Interpretations	121
Discussion.....	124
Conclusions	140
Literature Cited.....	141
Figures	154
Tables.....	172

CHAPTER 4	BIOLOGICAL SOIL CRUSTS AND THE FERTILE ISLAND	
EFFECT		220
Abstract.....		220
Introduction		221
Background.....		224
Materials and Methods		227
Results		228
Interpretations		238
Discussion.....		248
Conclusions		260
Literature Cited.....		261
Figures		275
Tables.....		324
APPENDIX 1	METHODS	351
APPENDIX 2	ADDITIONAL MICROMORPHOLOGY OBSERVATIONS	377
APPENDIX 3	BIOLOGICAL SOIL CRUST MAP	381
APPENDIX 4	GEOMORPHIC MAP	383
VITA		385

ACKNOWLEDGEMENTS

First, I want to thank Brenda Buck, my AMAZING faculty advisor, whose scientific mind and dedication are inspirational. Brenda has given me endless support and freedom to pursue a project I am passionate about. She pushed me when I needed to be pushed and encouraged me when I was in need of kind words. Her input has made this dissertation a success, and I am very grateful for her willingness to be such an instrumental part of my academic life.

Thanks to my other committee members, Debbie Soukup, Peg Rees, Lloyd Stark, and Steve Rowland. I could not ask for a better group of people to guide my graduate program. Thank you for your support, advice, and input on my project.

I would like to express my sincere gratitude to the Bureau of Land Management for generously funding this project. Thanks to Sarah Peterson (BLM) and Bob Boyd (BLM) for initiating this study. I would especially like to thank Sarah for her continued support and logistical assistance with this project and for arranging my BSC training. Thanks to BLM and to USGS for providing access to Quickbird® data. Thanks, also, to Henry Sun (project PI, DRI) for making our funding subcontract possible.

I want to thank my other generous funding sources: UNLV Urban Sustainability Initiative for providing funding for my graduate fellowship and conference travel; thanks especially to Ron Smith and Tom Piechota; NSF-Nevada EPSCor, and the SEPHAS Fellowship Program (NSF-EPSCor RING-TRUE III, Grant No. 0447416) who provided graduate assistantship and research funding; thanks to the Farouk El-Baz Research Grant Program, the Geological Society of America Student Grant Program, ExxonMobil Scholarship Fund, UNLV Geoscience Scholarship program & Bernada French

Scholarship Fund, the Adams/GPSA Scholarship Fund, Summer Session Scholarship (GPSA) for funding. Thanks to NASA-EPSCoR (NSHE 08-55) for research funds.

I also want to thank several individuals who supported this project through thoughtful discussions, field assistance, and scientific counsel. Thanks to Doug Merkler (USDA-NRCS) for providing thoughtful field review of my geomorphology map and for sharing his vast knowledge of soil ecology, GIS, insolation modeling and remote sensing. Doug has been an incredible scientific mentor and friend, and I am grateful for his generosity. Thanks to Debbie Soukup for her wonderful help in the field and input on my project. Thanks to NRCS for providing access to NAIP imagery. Thanks to Brett McLaurin, Becki Huntoon, and Kyle House for providing advice and support in GIS and remote sensing applications. I sincerely thank Mengesha Beyene for his tireless efforts and assistance in the field, in the laboratory, and with remote sensing/GIS tasks. Thanks to John Brinda for sharing his bryophyte taxonomy expertise, resources, and many thoughtful conversations about BSC ecology. Thanks to Lloyd Stark and Crystal Erickson for providing laboratory equipment and project advice. Thanks so Andrew Hanson for use of his microscope. Thanks to John Egelin and Seth Page for their hard work in the lab. Thanks to Sean Mulcahy (UNLV EMIL) for sharing his expertise in SEM analyses. Thanks to Yuanxin Teng and the UNLV Environmental Soil Analysis Laboratory and Dirk Baron (CSUB) for providing reliable soil analyses and project input. Thanks to Scott Abella and Anton Westenveld for their fantastic statistical and project design advice. Thanks to Bruce Lund, David Charlet, and Lois Merkler for their help in the field and assistance with plant taxonomic identifications. Thanks to Dirk Goossens for providing advice on all “dusty” things. Thanks to Cathy Willey for her help with

permit acquisition. Thanks to Jayne Belnap for providing much needed project design advice. Thanks to Henry Sun and Clay Crow for laboratory and microscope assistance. Thanks to Craig Westenburg for his assistance with Quickbird® imagery acquisition. Thanks to Ben Williams for his gracious assistance with fieldwork and editing. Thanks to my wonderfully supportive department. I am fortunate to work with such fantastic students, faculty, and staff.

Finally, I want to thank my friends and family for all of their support. You graciously dealt with my craziness as I pursued this degree. I love you all. I owe an enormous THANK YOU to my husband, Ben. His love and encouragement kept me afloat through this entire process, and he deserves much credit for the success of this dissertation. Ben, you always dream big and set high standards and goals. Your passion and tenacity continue to be my inspiration!!!

Thank you all!

Mandy

LIST OF FIGURES

Figure 2.1	Morphology of Cyanobacteria Crusts	72
Figure 2.2	Morphology of Moss-Lichen Crusts	73
Figure 2.3	Location Map.....	74
Figure 2.4	Cross-section of a Cyanobacteria-dominated Crust	75
Figure 2.5	Cross-section of a Short Moss-Lichen Crust.....	76
Figure 2.6	Cross-section of a Tall Moss-Lichen Pinnacled Crust	77
Figure 2.7	Microscopic Images of Grains.....	78
Figure 2.8	Microscopic Images of Large Voids	79
Figure 2.9	Microscopic Images of Vesicular Pores	80
Figure 2.10	Microscopic Images of Upturned Sediments and Voids	81
Figure 2.11	Microscopic Images of Precipitates.....	82
Figure 2.12	Microscopic Images of Filaments	83
Figure 2.13	Microscopic Images of Squamulose Lichens	84
Figure 2.14	Microscopic Images of Gelatinous Lichens	85
Figure 2.15	Microscopic Images of Mosses	86
Figure 2.16	Microscopic Images of Filament Knobs.....	87
Figure 2.17	Microscopic Images of Filament Knobs and Tufts	88
Figure 2.18	Microscopic Images of Upturned and Curled Features	89
Figure 2.19	Microscopic Images of Pedestals and Towers.....	90
Figure 2.20	Microscopic Image of Sharp Protrusion.....	91
Figure 2.21	Microscopic Images of Bio-sediment Bridges	92
Figure 2.22	Microscopic Images of Curved Features	93
Figure 2.23	Model of BSC Evolution	94
Figure 2.24	Model of Pedestal Development	95
Figure 2.25	Model of Tower Development	96
Figure 2.26	Model of Toppling Events.....	97
Figure 2.27	Model of Mineral Av Horizon Formation	98
Figure 2.28	Revised BSC Succession Model	99
Figure 3.1	Morphology of Cyanobacteria Crusts	154
Figure 3.2	Morphology of Moss-Lichen Crusts	155
Figure 3.3	Location Map.....	156
Figure 3.4	Subregion Map	157
Figure 3.5	ANOVA Design for Geomorphic Surfaces.....	158
Figure 3.6	Cross-section of Hidden Valley Geomorphic Surfaces.....	159
Figure 3.7	BSC vs. Geomorphic Map Overlay.....	160
Figure 3.8	Geomorphic vs. BSC Map Overlay.....	161
Figure 3.9	ANOVA of Canopy Cover among Geomorphic Surfaces	162
Figure 3.10	ANOVA of Canopy Clay Content among Geomorphic Surfaces	163
Figure 3.11	ANOVA of Interspace Cover among Geomorphic Surfaces	164
Figure 3.12	ANOVA of Interspace Texture among Geomorphic Surfaces.....	165
Figure 3.13	Geomorphic Trajectory Model.....	166
Figure 3.14	Geomorphology Block Model.....	167
Figure 3.15	Summary of Geomorphic Surfaces and BSC Characteristics	168
Figure 3.16	Feedback Model of Geological and Biological Interactions	169

Figure 3.17	Disturbance and BSC Succession.....	170
Figure 3.18	Photos Illustrating the Influence of Sand on BSCs and Pedogenesis	171
Figure 4.1	Morphology of Cyanobacteria Crusts	275
Figure 4.2	Morphology of Moss-Lichen Crusts	276
Figure 4.3	Summary of Geomorphic Surface and BSC Characteristics	277
Figure 4.4	Location Map.....	278
Figure 4.5	Subregion Map	279
Figure 4.6	Cross-section of Geomorphic Surfaces within Hidden Valley.....	280
Figure 4.7	ANOVA Design for Geomorphic Surfaces	281
Figure 4.8	ANOVA Design for Interspace Surface Cover	282
Figure 4.9	t-test Design for Interspace Exotic Grass Cover	283
Figure 4.10	Paired t-test Design for All Canopies and Interspaces	284
Figure 4.11	Paired t-test Design for Canopies and Interspaces as a Function of Interspace Surface Cover	285
Figure 4.12	t-test of Cyanobacteria Ocular Estimates	286
Figure 4.13	NMS Ordination	287
Figure 4.14	Summary of Geomorphic Surface ANOVA.....	288
Figure 4.15	ANOVA of Canopy Cover among Geomorphic Surfaces	289
Figure 4.16	ANOVA of Canopy Clay and Cation Concentrations among Geomorphic Surfaces.....	290
Figure 4.17	ANOVA of Canopy C and N among Geomorphic Surfaces	291
Figure 4.18	ANOVA of Interspace Cover among Geomorphic Surfaces	292
Figure 4.19	ANOVA of Interspace Pinnacle Height and Texture among Geomorphic Surfaces.....	293
Figure 4.20	ANOVA of Interspace Cations Concentrations among Geomorphic Surfaces.....	294
Figure 4.21	ANOVA of Interspace EC and C:N Ratios among Geomorphic Surfaces.....	295
Figure 4.22	Summary of Interspace Surface Cover Class ANOVA.....	296
Figure 4.23	ANOVA of Soil Cover among Interspace Cover Classes	297
Figure 4.24	ANOVA of Pinnacle Ht. and Texture among Interspace Cover Classes.....	298
Figure 4.25	ANOVA of Cation Concentrations among Interspace Cover Classes.....	299
Figure 4.26	ANOVA of P, C, and N among Interspace Cover Classes.....	300
Figure 4.27	ANOVA of EC among Interspace Cover Classes	301
Figure 4.28	t-test of Soil Cover and Cation Concentrations for High vs. Low Exotic Grass Cover.....	302
Figure 4.29	t-test of Cl, S, and pH for High vs. Low Exotic Grass Cover	303
Figure 4.30	Paired t-test of Soil Cover for all Canopies and Interspaces	304
Figure 4.31	Paired t-test of Texture for all Canopies and Interspaces.....	305
Figure 4.32	Paired t-test of Cation Concentrations for all Canopies and Interspaces.....	306
Figure 4.33	Paired t-test of P and Anion Concentrations for all Canopies and Interspaces.....	307
Figure 4.34	Paired t-test of C, N, and EC for all Canopies and Interspaces.....	308

Figure 4.35	Paired t-test of Soil Cover for Canopies and Interspaces as a function of Interspace Cover (Parametric)	309
Figure 4.36	Paired t-test of Soil Cover for Canopies and Interspaces as a function of Interspace Cover (Non-Parametric)	310
Figure 4.37	Paired t-test of Soil Texture for Canopies and Interspaces as a function of Interspace Cover	311
Figure 4.38	Paired t-test of Soil Cation concentrations for Canopies and Interspaces as a function of Interspace Cover (Parametric).....	312
Figure 4.39	Paired t-test of Soil Cation Concentrations for Canopies and Interspaces as a function of Interspace Cover (Non-parametric).....	313
Figure 4.40	Paired t-test of Soil N, S, and P for Canopies and Interspaces as a function of Interspace Cover.....	314
Figure 4.41	Paired t-test of Soil C:N Ratios for Canopies and Interspaces as a function of Interspace Cover.....	315
Figure 4.42	Paired t-test of Soil Cover for Canopies and Interspaces as a function of Interspace Cover N and EC.....	316
Figure 4.43	Surface Trajectory and Soil Fertility	317
Figure 4.44	Cyanobacteria Fertility Model.....	318
Figure 4.45	Moss-Lichen Fertility Model.....	319
Figure 4.46	Rock (Desert Pavement) Fertility Model	320
Figure 4.47	Fertile Island Feedback Model	321
Figure 4.48	Landscape Block Model of Soil Fertility	322
Figure 4.49	Disturbance Response Model	323

LIST OF TABLES

Table 2.1	Bio-sedimentary Features	100
Table 2.2	Summary of Formative Processes.....	103
Table 3.1	Potential Factors Controlling BSC Distribution	172
Table 3.2	Surface Cover Composite Classes	174
Table 3.3	BSC Map Unit Summary	175
Table 3.4	BSC Map Unit Descriptions	176
Table 3.5	Geomorphic Map Unit and Soil Type Summary	187
Table 3.6	Geomorphic Map Unit Descriptions.....	188
Table 3.7	Soil Type Descriptions.....	201
Table 3.8	GIS Overlay Summary.....	209
Table 3.9	MRPP: Significance of Map Units	210
Table 3.10	Parametric Correlations of Canopy Cover.....	211
Table 3.11	Non-parametric Correlations of Canopy Cover.....	212
Table 3.12	Parametric Correlations of Interspace Cover.....	217
Table 3.13	Non-parametric Correlations of Interspace Cover.....	218
Table 4.1	GIS Overlay Summary.....	324
Table 4.2	Geomorphic Map Unit Summary	325
Table 4.3	Surface Cover Composite Classes	326
Table 4.4	Summary of Paired t-tests for Canopies and Interspaces of All Plots	327
Table 4.5	Summary of Paired t-tests for Canopies and Interspaces as a Function of Interspace Surface Cover	328
Table 4.6	Parametric Correlations of Canopy Cover.....	329
Table 4.7	Parametric Correlations of Interspace Cover.....	330
Table 4.8	Non-parametric Correlations of Canopy Cover.....	331
Table 4.9	Non-parametric Correlations of Interspace Cover.....	343
Table 4.10	Parametric Correlations within Rock-Covered Interspaces.....	349
Table 4.11	Non-parametric Correlations within Rock-Covered Interspaces.....	350

CHAPTER 1

INTEGRATING STUDIES OF BIOLOGICAL SOIL CRUST MICROSTRUCTURE, SOIL-GEOMORPHIC RELATIONSHIPS, AND ECOLOGY

Ecological Importance of Biological Soil Crusts

Biological soil crusts (BSCs) are complex matrices of soil particles, cyanobacteria, lichens, mosses, algae, microfungi, and bacteria (Friedmann and Galun 1974) that provide crucial soil cover in arid regions. Biological structures trap and bind sediments, fusing them into a desert skin that prevents erosion (Campbell et al. 1989, McKenna Neuman et al. 1996, Li et al. 2004, Bowker et al. 2008). BSC organisms are ecosystem engineers (Jones et al. 1997, Bowker 2007) that prevent desertification by impacting landscape stability (Booth 1941, McKenna Neuman et al. 1996, Canton et al. 2003, Li et al. 2004, Thomas and Dougill 2007, Chaudhary et al. 2009), managing soil moisture and temperature (Booth 1941, Belnap 1995, DeFalco et al. 2001, Belnap 2006), enhancing soil organic matter and nutrients (Kleiner and Harper 1977, Evans and Belnap 1999, Elbert et al. 2009), and influencing vascular plant germination (DeFalco et al. 2001, Li et al. 2005, Escudero et al. 2007). BSCs have far-reaching impacts, as crusts may comprise 70 percent of living soil cover in arid landscapes (Belnap 1994).

Current Scientific Challenges and Study Objectives

Processes that form BSCs, the factors that control their distribution in the landscape, and the ecosystem feedbacks they sustain are poorly understood. First, few studies have investigated bio-sedimentary features of BSCs (Campbell 1979, 1989, Danin and Ganor 1991, Belnap 2001, 2003) or their complex internal structures (Campbell

1979, Canton et al. 2003) that potentially influence ecosystem function. BSC micro-features warrant investigation because they contain insight into the genesis of crust morphology, soil development, and landscape evolution. Second, although BSCs play important biogeomorphic roles (Viles 2008, Viles et al. 2008), their landscape distribution patterns are challenging to predict. Soil-geomorphology controls many key factors that influence BSC growth (Peterson 1981, Bull 1991, Young et al. 2004, Bowker and Belnap 2008, Meadows et al. 2008, Robins et al. 2009). A few studies have used soil-geomorphic characteristics, such as parent material (Bowker and Belnap 2008), solar insolation (Kidron et al. 2010), and dust capture potential (Li et al. 2010) to estimate BSC biotic potential. No studies, however, have comprehensively analyzed how soil-geomorphic controls of surface characteristics and surface processes influence BSC distribution, or how those processes co-develop with BSCs. Finally, the feedbacks involving BSCs and soil resource allocation from the meter-scale to the landscape level have not been thoroughly investigated, and previous studies of fertile islands yielded inconsistent results. Some authors have suggested BSCs have little effect on the magnitude and distribution of fertile islands (Thompson et al. 2005), while other studies have shown that BSC types commonly influence canopy-interspace nutrient dynamics (Housman et al. 2007). Further study is needed to understand the true impact of BSC morphology and surface cover on fertile islands.

This dissertation addresses the current gaps in scientific knowledge of BSCs with the following objectives: (1) to understand the genesis of BSCs and crust microstructures that impact ecosystem function and water dynamics; (2) to investigate the relationships among geomorphology, soils, BSCs, and the feedback mechanisms that control their co-

development; and (3) to elucidate the soil-geomorphic and BSC controls of soil resource allocation and the fertile island effect. This unique interdisciplinary approach provides a more comprehensive perspective of BSC ecology that helps explain unravel relationships among biological and geological drivers.

Linking Microstructure, Soil-Geomorphic Relationships, and Ecology of Biological Soil Crusts

Chapter 2, *Micro-structure and Genesis of Biological Soil Crusts*, discusses a micromorphological investigation of BSC genesis and micro-structure in the Mojave Desert. In this study, I examined crust micro-features in thin section using petrographic microscopy, light microscopy, SEM, and EDS, and I linked those observations to crust macro-features and soil-geomorphology. The results indicate BSCs have complex internal and external morphologies that reflect a turbulent genetic history. The model that was developed from this study illustrates how crusts form through time under evolving species compositions and physical soil processes, and it demonstrates BSCs' important role in dust capture and pedogenesis. Here I also propose a new biological setting for Av horizon development.

BSC dust accretion and surface sealing form vesicular pores within the bio-rich zone and facilitate mineral Av horizon development below moss-lichen crusts. The BSC micro-features produced during crust succession potentially have large impacts on the distribution and movement of water. Because of their important role in dust capture, surface morphology, and water movement, I suggest BSCs be considered critical agents in arid pedogenesis and landscape evolution.

Chapter 3, *Co-development of BSCs and Soil-Geomorphology*, builds on the conclusions of Chapter 2, as I examine the soil-geomorphic feedbacks that control and co-develop with BSCs. In this study, extensive field mapping, descriptions of exposed soil profiles, and surface data collection characterize BSCs, geomorphic surfaces, and soil types. GIS overlays and statistical analyses of these data indicate that geomorphology controls the ratio of surficial sand to rocks; this ratio in turn constrains the formation of (1) cyanobacteria crusts, (2) extensive moss-lichen crusts, and (3) “desert pavements” with low to moderate moss-lichen crusts. The findings suggest that soil-geomorphic control of the sand-to-rock ratio determines the stability, disturbance regime, dust-capture potential, and textural framework, thus setting surface-cover trajectories. Geological and biological interactions sustain those unique surface conditions. Both cyanobacteria and moss-lichen crusts induce positive feedback mechanisms that allow them to “engineer” their own suitable habitats through sand stabilization and dust capture. Similarly, the physical processes controlling the development of desert pavements promote pavement integrity. The positive feedback mechanisms sustaining these surface characteristics support geomorphic continuity and ecological stability. Each feedback can be predicted across individual geomorphic surfaces within intermontane basins. Moreover, the physical processes controlling BSC distribution in this study area are ubiquitous to all arid regions, making these interpretations widely applicable. The new insights into BSCs and soil-geomorphic development could improve landscape models and help land managers and scientists address impacts of climate change and physical disturbances.

Chapter 4, *Biological Soil Crusts and the Fertile Island Effect*, investigates how the soil physical processes and landscape dynamics discussed in Chapters 2 and 3

influence ecological feedbacks, soil resource allocation, and fertile island dynamics. Extensive field data collection, soil surface sampling, and soil physicochemical analyses quantify biotic and abiotic characteristics. ANOVA, t-tests, and multivariate statistical analyses indicate interspace and canopy fertility is strongly tied to the age of landforms, input of fine sand, and interspace cover. Geomorphic processes control the sand-to-rock ratio, which in turn constrains interspace cover by cyanobacteria crusts, moss-lichen crusts, and desert pavements. Interspace cover ultimately determines the magnitude of the fertile island effect. Inferred feedback systems involving surface stability, dust inputs, water availability, biological activity, and canopy-interspace dynamics produce three unique biogeochemical patterns that support geomorphic and ecosystem stability. (1) Areas of “desert pavement” with low to moderate moss-lichen crust cover produce high canopy-interspace nutrient disparities through low interspace biological activity and high runoff. (2) High density moss-lichen crusts lead to the formation of low canopy-interspace nutrient disparities because enhanced biological activity and dust capture increases interspace nutrient availability. (3) Moderate canopy-interspace nutrient disparities and low overall fertility occur in areas with extensive cyanobacteria crusts, through low water availability and low dust capture potential. These patterns in biogeochemistry can be predicted as a function of soil-geomorphology, providing a hierarchical landscape perspective into soil resource allocation. This novel approach allows prediction of landform and ecosystem responses to climate change, exotic plant invasions, anthropogenic disturbances, and desertification dynamics. Overall, canopy-interspace nutrient disparities vary consistently among many deserts with similar soil

interspace cover, which suggests overarching patterns in resource allocation occur despite differences in total site productivity.

Literature Cited

- Belnap J. 2006. The potential roles of biological soil crusts in dryland hydrologic cycles. *Hydrological Processes* **20**:3159-3178.
- Belnap J. 2003. The world at your feet: Desert biological soil crusts. *Frontiers in Ecology and the Environment* **1**:181-189.
- Belnap J. 2001. Comparative structure of physical and biological soil crusts. Pages 177-191 *In* J. Belnap and O. L. Lange, editors. *Biological Soil Crusts: Structure, Function, and Management*, Springer-Verlag, Berlin.
- Belnap J. 1995. Surface disturbances: their role in accelerating desertification. *Environmental Monitoring and Assessment* **37**:39-57.
- S. B. Monsen, S. G. Kitchen. 1994. Potential role of cryptobiotic soil crust in semiarid rangelands. *Proceedings – Ecology and Management of Annual Rangelands*: 179-185.
- Booth W. E. 1941. Algae as pioneers in plant succession and their importance in erosion control. *Ecology* **22**:38-46.
- Bowker M. A. 2007. Biological soil crust rehabilitation in theory and practice: An underexploited opportunity. *Restoration Ecology* **15**:13-23.
- Bowker M. A., J. Belnap. 2008. A simple classification of soil types as habitats of biological soil crusts on the Colorado Plateau, USA. *Journal of Vegetation Science* **19**:831-840.
- Bowker M. A., J. Belnap, V. B. Chaudhary, and N. C. Johnson. 2008. Revisiting classic water erosion models in drylands: The strong impact of biological soil crusts. *Soil Biology & Biochemistry* **40**:2309-2316.
- Bull W. B. 1991. *Geomorphic Responses to Climatic Change*. Oxford University Press, New York.
- Campbell S. E. 1979. Soil stabilization by a prokaryotic desert crust: Implications for Precambrian land biota. *Origins of Life* **9**:335-348.
- Campbell S. E., J. Seeler, and S. Golubic. 1989. Desert crust formation and soil stabilization. *Arid Soil Research and Rehabilitation* **3**:217-228.
- Canton Y., A. Sole-Benet, and R. Lazaro. 2003. Soil–geomorphology relations in gypsiferous materials of the Tabernas Desert (Almeria, SE Spain). *Geoderma* **115**:193-222.

- Chaudhary V. B., M. A. Bowker, T. E. O'Dell, J. B. Grace, A. E. Redman, M. C. Rilling, and N. C. Johnson. 2009. Untangling the biological contributions to soil stability in semiarid shrublands. *Ecological Applications* **19**:110-122.
- Danin A., E. Ganor. 1991. Trapping of airborne dust by mosses in the Negev Desert, Israel. *Earth Surface Processes and Landforms* **16**:153-162.
- DeFalco L. A., J. K. Detling, C. R. Tracy, and S. D. Warren. 2001. Physiological variation among native and exotic winter annual plants associated with microbiotic crusts in the Mojave Desert. *Plant and Soil* **234**:1-14.
- Elbert W., B. Weber, B. Budel, M. O. Andreae, and U. Poschl. 2009. Microbiotic crusts on soil, rock and plants: neglected major players in the global cycles of carbon and nitrogen? *Biogeosciences Discuss.* **6**:6983-7015.
- Escudero A., I. Martinez, A. de la Cruz, M. A. G. Otalora, and F. T. Maestre. 2007. Soil lichens have species-specific effects on the seedling emergence of three gypsophile plant species. *Journal of Arid Environments* **70**:18-28.
- Evans R. D., J. Belnap. 1999. Long-Term consequences of disturbance on nitrogen dynamics in an arid ecosystem. *Ecology* **80**:150-160.
- Friedmann E. I., M. Galun. 1974. Desert algae, lichens and fungi. Pages 165-212. *In* G. W. Brown, editor. *Desert Biology*, Academic Press, New York.
- Housman D. C., C. M. Yeager, B. J. Darby, J. Sanford R.L., C. R. Kuske, D. A. Neher, and J. Belnap. 2007. Heterogeneity of soil nutrients and subsurface biota in a dryland ecosystem. *Soil Biology & Biochemistry* **39**:2138-2149.
- Jones C. G., J. H. Lawton, and M. Shachak. 1997. Positive and negative effects of organisms as physical ecosystem engineers. *Ecology* **78**:1946-1957.
- Kidron G. J., A. Vonshak, I. Dor, S. Barinova, and A. Abeliovich. 2010. Properties and spatial distribution of microbiotic crusts in the Negev Desert, Israel. *Catena* **82**:92-101.
- Kleiner E. F., K. T. Harper. 1977. Soil properties in relation to cryptogamic groundcover in Canyonlands National Park. *Journal of Range Management* **30**:202-205.
- Li X. R., X. H. Jia, L. Q. Long, and S. Zerbe. 2005. Effects of biological soil crusts on seed bank, germination and establishment of two annual plant species in the Tengger Desert (N China). *Plant and Soil* **277**:375-385.
- Li X. R., M. Z. He, S. Zerbe, X. J. Li, and L. C. Liu. 2010. Micro-geomorphology determines community structure of biological soil crusts at small scales. *Earth Surface Processes and Landforms* **35**:932-940.

- Li X. Y., L. Y. Liu, and J. H. Wang. 2004. Wind tunnel simulation of aeolian sandy soil erodibility under human disturbance. *Geomorphology* **59**:3-11.
- McKenna Neuman C., C. D. Maxwell, and J. W. Boulton. 1996. Wind transport of sand surfaces crusted with photoautotrophic microorganisms. *Catena* **27**:229-247.
- Meadows D. G., M. H. Young, and E. V. McDonald. 2008. Influence of relative surface age on hydraulic properties and infiltration on soils associated with desert pavements. *Catena* **72**:169-178.
- Peterson FF. 1981. Landforms of the Basin and Range, Defined for Soil Survey. Reno: UNR Max C. Fleishmann College of Agriculture, Nevada Agricultural Experiment Station. Technical Bulletin 28. 52 pp.
- Robins C. R., B. J. Buck, A. J. Williams, J. L. Morton, P. K. House, M. S. Howell, and M. L. Yonovitz. 2009. Comparison of flood hazard assessments on desert piedmonts and playas: A case study in Ivanpah Valley, Nevada. *Geomorphology* **103**:520-532.
- Thomas A. D., A. J. Dougill. 2007. Spatial and temporal distribution of cyanobacterial soil crusts in the Kalahari: Implications for soil surface properties. *Geomorphology* **85**:17-29.
- Thompson D. B., L. R. Walker, F. H. Landau, and L. R. Stark. 2005. The influence of elevation, shrub species, and biological soil crust on fertile islands in the Mojave Desert, USA. *Journal of Arid Environments* **61**:609-629.
- Viles H. A. 2008. Understanding dryland landscape dynamics: Do biological crusts hold the key? *Geography Compass* **2/3**:899-919.
- Viles H. A., L. A. Naylor, N. E. A. Carter, and D. Chaput. 2008. Biogeomorphological disturbance regimes: progress in linking ecological and geomorphological systems. *Earth Surface Processes and Landforms* **33**:1419-1435.
- Young M. H., E. V. McDonald, T. G. Caldwell, S. G. Benner, and D. G. Meadows. 2004. Hydraulic properties of a desert soil chronosequence in the Mojave Desert, USA. *Vadose Zone Journal* **3**:956-963.

CHAPTER 2

MICROSTRUCTURE AND GENESIS OF BIOLOGICAL SOIL CRUSTS

Abstract

Biological soil crusts (BSCs) are bio-sedimentary complexes that reduce erosion and influence hydrology, soil fertility, and plant germination. Despite their critical ecological roles, crust bio-sedimentary formation is poorly understood. A detailed micromorphological investigation of BSC development, moss-lichen pinnacle genesis, and crust microstructure was completed. BSC features were examined in thin section using petrographic microscopy, light microscopy, SEM, and EDS. These observations were linked to crust macro-features and soil-geomorphology. The complex bio-sedimentary structures of BSCs reflect a dynamic genetic history and diverse formative processes: (1) grain trapping and binding by biotic structures; (2) dust capture; (3) authigenic mineral precipitation; (4) surface sealing and erosion mitigation by biological, physical, and chemical cements; (5) expansion and contraction from wetting and drying cycles; (6) mass wasting processes, including toppling, creep, sloughing, and collapse; (7) bio-rich vesicular pore formation and heaving; and (8) dust accumulation and mineral Av horizon formation. These processes co-develop with BSC succession, controlling ecological function and biogeomorphic feedbacks. A new model of Av horizon development illustrates how BSC dust accretion and surface sealing form vesicular pores in the bio-rich zone and mineral Av horizons below moss-lichen pinnacles. BSC dust capture provides fine-grained material at the profile and landform levels, which increases soil water-holding capacity and alters surface topography. BSC dust accretion creates complex surficial and internal bio-sedimentary structures that capture surface water for

uptake by crust organisms. BSCs uniquely facilitate the accumulation, morphology, and ecosystem function of dust and should, therefore, be considered critical agents in arid pedogenesis and landscape evolution.

Introduction and Background

Biological soil crusts (BSCs) manage soil resources and provide critical ecosystem services throughout the world's deserts. These crusts are complex matrices of cyanobacteria, mosses, lichens, bacteria, and fungi that fuse around soil particles to create a living, protective membrane (Friedmann and Galun 1974, Eldridge and Greene 1994, Belnap et al. 2003). Similar to skin, crusts control the movement of water, gases, and, solutes across the soil surface (Belnap et al. 2003). BSCs prevent desertification through their impacts on soil erosion and deposition (e.g. Booth 1941, McKenna Neuman et al. 1996, Canton et al. 2003, Li et al. 2004, Thomas and Dougill 2007, Chaudhary et al. 2009), water and energy balances (e.g., Booth 1941, Belnap 1995, DeFalco et al. 2001, Belnap 2006) soil fertility (e.g., Kleiner and Harper 1977, Evans and Belnap 1999, Elbert et al. 2009), and plant community establishment (e.g., DeFalco et al. 2001, Li et al. 2005, Escudero et al. 2007). BSCs are extremely fragile and sensitive to physical impacts such as off-road vehicles, hiking, and grazing, making them excellent indicators of disturbance (Kleiner and Harper 1977, Campbell 1979, Campbell et al. 1989, Belnap and Gardner 1993, Belnap 1995, 1998, Ponzetti and McCune 2001, Berkeley et al. 2005).

BSC development follows a natural succession beginning with development of smooth cyanobacterial-algal crusts (Figure 2.1)(Belnap 2001). If conditions are favorable, moss-lichen crusts develop (see Chapter 3)(Ponzetti and McCune 2001, Bowker et al. 2006, 2008, Kidron et al. 2010, Li et al. 2010). Two types of moss-lichen

crusts have been described: (1) short moss-lichen crusts and (2) tall moss-lichen pinnacled crusts. Short moss-lichen crusts have less than 2 cm of vertical relief and gently rolling morphology. Tall moss-lichen crusts display a pinnacled or roughened topography with up to 5 cm of relief (Figure 2.2)(Belnap 2001). Several studies have approximated rates of crust recovery from disturbance, with estimates ranging from 10s to 1000s of years. These discrepancies in recovery responses are largely tied to differences in climate, soil texture, geomorphic stability, metabolic adaptations, and reproductive strategies of component organisms in these studies (Belnap and Warren 2002, Nagy et al. 2005, Zhang 2005, Thomas and Dougill 2007, Kidron et al. 2008, Williams et al. 2008, Langhans et al. 2010). These studies have identified recovery times of individual species and have not investigated recovery of structural and bio-sedimentary features with changing organisms.

Structural investigations of BSCs have primarily focused on species distributions (Belnap 2001, Garcia-Pichel and Belnap 2001, Davidson et al. 2002, Garcia-Pichel et al. 2003), with only a few studies investigating bio-sedimentary features (Campbell 1979, Campbell et al. 1989, Danin and Ganor 1991, Belnap 2001, 2003). Most sediment-related studies have focused on smooth cyanobacterial crusts (Booth 1941, Campbell 1979, Belnap and Gardner 1993, Issa et al. 1999, Garcia-Pichel and Pringault 2001, Issa et al. 2007, Thomas and Dougill 2007, Issa et al. 2009), while a few others have investigated moss growth in sandy environments (Danin and Ganor 1991, Belnap 2001,). Despite the conspicuous, complex surface morphology of moss-lichen pinnacles (Figure 2.2), few have critically analyzed their internal structure (Campbell 1979, Canton et al. 2003). Some researchers have speculated pinnacle morphology results from frost

heaving, which is an important mechanism in cold deserts (Belnap 2001, 2003).

However, no studies have formally investigated the genesis of this unique morphology, particularly in hotter or more arid deserts. In order to maximize ecological restoration and crust recovery, we need a better understanding of how crusts develop through time. Furthermore, if we are to ensure ecosystem function is returned to its natural state, we must understand the microstructural features that control distributions of soil water, nutrients, and energy.

Hidden Valley, Muddy Mountains Wilderness Area, in the Mojave Desert of southern Nevada (U.S.A.), is an ideal natural laboratory to investigate BSC microstructures of arid environments (Figure 2.3). This semi-enclosed basin contains a variety of alluvial and eolian geomorphic surfaces and soil types formed from limestone and sandstone parent materials. BSC types include cyanobacteria crusts, short moss-lichen crusts, and tall moss-lichen pinnacled crusts (Figures 2.1, 2.2). The two latter types of crusts may occur as colonies of mosses or lichens, or as a mixture of both taxa. The study area lies within the northern reaches of the Mojave Desert at approximately 1000 m elevation. The climate is characterized by hot, dry summers and cool, moist winters. The average annual temperature is 27 °C, and the average annual precipitation is 114 mm (Gorelow and Skrbac 2005). Most precipitation falls from January to March, when average highs range from 14-21 °C. Summers are primarily dry, but some precipitation may fall during the warmest months of July and August, when average highs range from 39-40 °C (Gorelow and Skrbac 2005). Given its proximity to the Las Vegas, NV metropolitan area and its designation as a Wilderness Area, the valley is a critical management concern for the Bureau of Land Management.

To better understand the structure, function, and genetic history of tall moss-lichen pinnacled crusts, I completed a micromorphological investigation of the biotic and mineral components of several BSC types. The objectives of my study included the following: (1) to investigate the surficial and internal structural components of BSCs in a variety of morphological stages and geomorphic settings; (2) to understand genesis of these crusts and the origin of BSCs' topographic relief; (3) to study BSCs' role in dust accretion and pedogenesis; and (4) to understand BSC microstructures that potentially influence soil resource allocation and water dynamics.

Materials and Methods

In June 2009, 70 BSC samples were collected within the Hidden Valley portion of the Muddy Mountains Wilderness Area, Nevada (Figure 2.3). Samples were photographed and described with respect to crust macro-features and soil-geomorphic characteristics. Samples were embedded in epoxy and prepared into thin sections. Bio-sedimentary features of thin sections were examined using petrographic microscopy, light microscopy, SEM, and EDS. Complete methods are described in Appendix 1.1.

Results

BSC Types, Landscape Setting, and Macro-features

BSC morphology and species composition vary as a function of soil-geomorphology (see Chapter 3). Three types of BSCs were identified, including cyanobacteria-dominated crusts, short moss-lichen crusts, and tall moss-lichen pinnacled crusts (Figures 2.1, 2.2, 2.4, 2.5, 2.6). Cyanobacteria-dominated crusts are primarily

composed of filamentous cyanobacteria and are identified by their light color and smooth surface topography. Cyanobacteria crusts commonly occur in conjunction with non-crustified bare soil. In this study, cyanobacteria crusts were not sampled discretely, but were sampled adjacent to or in association with short moss-lichen crusts. However, because of their unique surface morphology and characteristics, they are described separately. In this study, short moss-lichen crusts are composed of lichens, mosses, and cyanobacteria and have surface relief up to 2 cm. Tall moss-lichen pinnacled crusts are dominated by lichens and include some moss and cyanobacteria cover. These crusts have rough and complex surface morphologies with up to 5 cm of relief. The distribution of crust morphological types varies among geomorphic surfaces.

All BSC types contain two macro-scale zones: the upper, bio-rich zone that is highly cohesive and the lower, non-cohesive bio-poor zone (Figures 2.4, 2.5, 2.6). The bio-rich zone varies in thickness from 0.5 to 22 mm and is capped with cyanobacteria, lichen thalli, or mosses. In this zone, grains may be bound by bio-structures, coat bio-structures, embedded within biological exudates, cemented in authigenic minerals, or engulfed in some tissues. Often, grains appear oriented parallel to the surface of bio-structures. The bio-poor zone is primarily composed of loosely held sand that falls away when the bio-rich surface crust is detached from the underlying soil. In cross-section the bio-rich and bio-poor zones are commonly separated by a linear void.

Cyanobacteria-Dominated Crusts

Cyanobacteria-dominated crusts are relatively smooth and primarily composed of filamentous cyanobacteria (Figure 2.1). These crusts have flat surface topographies but also have few to many convex protrusions up to 3.8 mm tall and 2 mm wide (Figure

2.1A, B). The bio-rich zone is generally 1.5 mm thick and frequently is partially detached from the flat-lying bio-poor zone composed of sand (Figure 2.4).

Cyanobacteria crusts may cover square meters of soil or may occur as cm-scale patches adjacent to short moss-lichen crusts. Regardless of the biotic setting, their surface morphology remains relatively consistent.

Cyanobacteria-dominated crusts primarily form in sandy plant interspaces along recently abandoned inset fans approximately 0.5 m above active channels. These inset fans have sandy phases composed of sand with little gravel and gravelly phases composed of mixed sand and gravel. Cyanobacteria crusts are most prominent within sandy soil phases. Sandy areas may cover large expanses of alluvial surfaces, or may form in localized alluvial swales. These phases correspond to soils that are mixed thermic Typic Torripsamments. The gravelly phases correspond to sandy-skeletal mixed thermic Typic Torriorthents (Soil Survey Staff 2010b). Where surface clasts are present, their cover ranges from 31-70% within shrub interspaces. Gravels and cobbles are primarily composed of limestone. Soils within these recently abandoned inset fans show little pedogenic development and negligible dust input, with no Av horizon development.

Short Moss-Lichen Crusts

Short moss-lichen crusts are characterized by $\geq 50\%$ moss-lichen cover and topographic relief up to 2 cm (Figure 2.2B). These crusts are dominated by colonies of mosses as well as gelatinous and squamulose lichens but commonly include cyanobacteria. Moss and lichen colonies grow up to 6 cm in diameter. Short moss-lichen crusts have bio-rich zones up to 11 mm thick (Figure 2.5).

Similar to cyanobacteria crusts, short moss-lichen crusts commonly grow within plant interspaces of recently abandoned inset fans. Although they may occur in sandsheets, short moss-lichen crusts are most common within gravelly interspaces (Figure 2.2B). Other gravel-covered surfaces, such as those with desert pavements are not favorable for these types of crusts because they lack a source of sand, and rock fragment cover prevents moss and lichen colonization (see Chapter 3).

Tall Moss-Lichen Pinnacled Crusts

Tall moss-lichen pinnacled crusts form polygonal mounds 2-8 cm in diameter and up to 5 cm tall (Figure 2.2 A, C, E, D, F). Generally, pinnacles are composed of mixed colonies of mosses, gelatinous lichens, and squamulose lichens but may include discrete colonies of mosses (Figure 2.2D). Mosses and lichens cover at least 50% of most pinnacles, which may also include some interspersed cyanobacteria cover. The bio-rich zone is generally 22 mm thick and is commonly separated from the bio-poor zone by horizontal voids up to 5 mm wide (Figure 2.6). The size of the bio-poor zone varies as a function of the whole pinnacle's size. However, the zone may be as large as 20 mm tall and 55 mm wide.

Tall moss-lichen pinnacle mounds display complex surface morphologies that vary as a function of component organisms. Pinnacles are composed of mixed taxa, including mosses, lichens, and cyanobacteria, and have irregular surfaces marked by sharp peaks along the summits and up to 5 cm of relief (Fig 2.2E). Pinnacles with surfaces composed of 60% or greater squamulose lichens form compact pinnacle mounds up to 3 cm in diameter with 3 cm of vertical relief with distinct, rounded tops (Figure

2.2C). Crusts with 70% or greater moss cover grow as mosaics of interlocking moss pads that have smooth, rolling surfaces, with less than 1 cm of relief (Figure 2.2D).

Vertical surface cracks are common features of tall moss-lichen pinnacle mounds. In some areas, vertical cracks up to 0.5 cm wide form around individual pinnacle mounds that are 5-8 cm in diameter. These cracks penetrate the entire bio-rich zone (Figure 2.2E). This fracturing creates a network of polygonal cracks around pinnacles that resembles mud cracks. In addition, horizontal cracks up to 0.5 cm wide form below pinnacle mounds, separating the pinnacle from the mineral soil below (Figure 2.2E). In other cases, pinnacles that grow above underlying rock clasts have highly irregular connections to the rock surface. The pinnacle interior may be fully detached from the rock surface, while the pinnacle perimeter is connected via discontinuous silt or clay films. Cracking phenomena generally occur in association with crusts of 50% or greater lichen cover and are mostly absent when moss cover is greater than 70%.

Tall moss-lichen pinnacled crusts occur on a wide range of geomorphic surfaces that are mid- to late Holocene and older. The most widespread moss-lichen pinnacled crusts cover up to 88% of soil interspaces and occur along mid- to late Holocene alluvial surfaces and within shallow sand sheets over bedrock (Figure 2.2A)(see Chapter 3). These surfaces lie 1-1.5 m above active channels and have interspaces with 3-38% surface rock cover. Vesicular horizons may be up to 27 cm thick. Soils on mid- to late Holocene inset fans correspond to the Arizo soil series (Soil Survey Staff 2010a), which are sandy-skeletal mixed, thermic Typic Torriorthents (Soil Survey Staff 2010b).

Pleistocene surfaces contain scattered tall moss-lichen pinnacled crusts. These crusts cover up to 45% of interspace surfaces. These older alluvial surfaces include inset

fans, ballenas, and erosional fan remnants (Figure 2.2F)(Peterson 1981). In this study, crusts were sampled from two Pleistocene geomorphic surfaces. These surfaces lie 2 to 3 m above the active channel, generally have high surface rock cover composed of moderately to poorly interlocking desert pavements that cover 31-60% of interspace surfaces, and have low inputs of fine sand. Soil profiles have 10- to 16-cm- thick Av horizons and Stage III to IV petrocalcic horizons (Gile et al. 1966, Bachman and Machette 1977, Machette 1985). Soils that form in these Pleistocene surfaces are loamy, mixed, thermic shallow Typic Petrocalcids and correspond to the Irongold soil series (Soil Survey Staff 2010a, 2010b,).

Micromorphological Features

Crust Components

Grains

Grain size, orientation, and compaction vary with biological and sedimentary factors. Grain size commonly ranges from clay to medium sand with few coarse sand grains. Grains within the bio-rich zone and especially those grains attached to or embedded within biological structures are commonly finer than those in the bio-poor zone (Figures 2.4, 2.5, 2.6). For example, the bio-rich zone contains surface layers of compacted clays, silts, and very fine sands generally at least 0.3 mm thick (Figure 2.7A, B). Exposed surfaces are often highly compacted with clay or silt surface films. Strata of fine, densely packed grains also occur near concave edges. The thickest fine-grained layers, up to 2 mm, occur within tall moss-lichen pinnacle bio-rich zones. In contrast, coarse grains are mostly concentrated within the bio-poor zone, which is composed of poorly sorted, unconsolidated sands with some silt and clay. Aggregation and

compaction of grains are frequently associated with biological structures. However, some aggregates contain no visible biological tissues (Figure 2.7C).

Voids and cracks

Void morphology is highly variable within the bio-rich and bio-poor zones. Irregular, linear voids up to 5 mm wide with rough margins separate the bio-rich zone from the bio-poor zone (Figures 2.4, 2.5, 2.6). The bio-rich zone also contains large, irregular voids up to 24 mm by 36 mm with smooth margins of compacted clays, silts, and very fine sands (Figure 2.8A, B). Many voids contain photosynthetic tissue of lichens and mosses. In two-dimensional view, these photosynthetic tissues appear to be blocked from visible sunlight (Figure 2.8B). Both incipient and well-developed vesicular pores most commonly occur near the surface of the bio-rich zone (Figure 2.8A, 2.9). Vesicular pores are generally 0.1-0.5 mm in diameter but can be up to 0.8 mm wide. Well-developed vesicular pores are round with smooth margins and commonly occur in bio-rich zones capped by clay- to silt-rich surfaces. Biological filaments commonly grow among grains that surround vesicular pores. Vesicular pores are rare in crusts that contain more than 50% moss cover and primarily occur in association with surfaces dominated by filaments or lichens.

Soil cracks occur in conjunction with biological and sedimentary features (Figures 2.2E, 2.10). Horizontal to vertical linear voids commonly align parallel to all biological structures and are 0.5-1 mm wide (Figure 2.10A, C). Other vertical to sub-vertical surface cracks, up to 0.5 mm wide, penetrate the bio-rich zone (Figure 2.7C). These cracks are commonly associated with individual bio-structures but also occur in the absence of visible bio-structures. Loose sediment commonly infills cracks or depressions

that are open to the surface (Figure 2.2D, 2.10A). Bio-structures commonly appear to be torn, creating 5 to 100 μm diameter cracks or voids (Figure 2.10B) and also infill with grains (Figure 2.10B).

Authigenic minerals

Several authigenic minerals occur at or near the surface of all crust types, often in association with biological structures. Most commonly, mineral precipitates lie directly along or near biological structures or exudates (Figure 2.11). Calcium-rich carbonate is the most common precipitate, and may contain trace amounts of magnesium (Appendix 2A). Authigenic minerals occur as densely cemented zones or are finely disseminated within biological exudates. Carbonate commonly occurs as finely disseminated micrite or rhombohedral crystals up to 15 μm . Some EDS data indicate calcium chloride may be present, as round grains up to 4 μm in diameter, although this mineral was not verified (Appendix 2B). A single, angular, euhedral 4 μm barite crystal was also identified (Appendix 2C). Its crystal faces are slightly uneven and show minor pitting. Surface zones containing carbonate are up to 0.88-1 mm thick and commonly cap underlying zones of vesicular pores. Many mineral precipitates are visible to the naked eye as the conspicuous white coating seen along the protruding tops of moss-lichen pinnacles (Figure 2.2C). Authigenic minerals are primarily concentrated in the bio-rich zone, and were not concentrated within the bio-poor zone.

Petrographic microscopy revealed brown staining in association with many biological structures. These stains are likely organic compounds excreted from nearby tissues (Stoops 2003).

Cyanobacterial and fungal filaments

Cyanobacterial and fungal filaments are common features within the outer few millimeters of the bio-rich zone in all three crust types. Individual filaments occur as 3 μm wide strands or as sheathed bundles up to 200 μm wide and 800 μm long (Figures 2.12, 2.11C). Polysaccharide sheaths, or extracellular polymeric secretions (EPS), are often coated in clay- to sand-sized grains or mineral precipitates (Figure 2.12A, 2.11C). Grains as large as 65 μm may sit on top of taut filaments (Figure 2.12B). Because the samples were dry upon embedding, filaments commonly appear flattened under backscatter SEM. The epoxy embedding methods precluded differentiation of fungi, heterotrophic bacteria, and cyanobacteria. However, a majority of the filaments are covered in EPS and occur at or near the soil surface, suggesting many are cyanobacteria. Furthermore, a few images show green pigment in some surficial filaments, further supporting the presence of cyanobacteria (Figure 2.11C). A companion study identified high concentrations of *Microcoleus* from surface soils collected within the study area (see Chapter 4).

Biological filaments are ubiquitous in all crust types and primarily occur with compacted and aggregated grains. Filaments that encapsulate and weave around grains occur on most crust surfaces (Figure 2.7A, B). Filaments with associated EPS also cap many surfaces that show adjacent concave edges. Taut filaments span interior voids up to 2.8 mm in diameter and surface voids up to 1.4 mm wide (Figure 2.12). Irregular or incipient vesicular pores are associated with sediments in a dense mesh of filaments (Figure 2.9A). Most authigenic minerals at the soil surface occur in conjunction with filaments that are thought to be *Microcoleus* cyanobacteria (see Chapter 4). Authigenic

minerals are abundant within filament EPS, with the largest crystals, up to 15 μm , occurring toward exterior edges (Figure 2.11C).

Squamulose lichens

Squamulose lichens are common features in short moss-lichen crusts and tall moss-lichen pinnacles. These lichen thalli form irregular plates, or squamules, at the soil surface and are anchored by root-like structures called rhizines (Figure 2.13). The squamules vary from 0.18-0.25 mm thick and 0.23-2.5 mm in diameter. Rhizines have two basic morphologies: numerous, thin, hair-like rhizines; or single, thick, tap root-like rhizines. Thin hair-like, or rhizoidal, rhizines are most commonly 1-5 μm thick and 1.8 mm long (Figure 2.13A). Rhizoidal rhizines occur embedded in the soil matrix or are loosely held within void spaces below the squamule near the soil surface. This void space is up to 1.8 mm in diameter. Thick, single taproot-like rhizines occur as single shoots or are sparsely branched (Figure 2.13D). These rhizines are approximately 0.1 mm in diameter and as long as 5.25 mm. Thicker rhizines infrequently have enlarged areas, or bulbous features up to 1 mm in diameter (Figure 2.10C). Along a few pinnacles, rhizines are exposed along vertical edges. The dominant squamulose lichen genus found within these samples is *Placidium*. *Placidium lacinulatum* is characterized by a single, thick rhizine, while *Placidium squamulosum* produces many thin, rhizoidal rhizines.

As seen in SEM, fungal cortex tissue forms a honeycomb mesh, while algal layers are convoluted (Figure 2.10B, 2.11B). Rhizines interiors display linear, ribbon-like filaments of fungal tissue. Perithecia, lichen reproductive structures, show one or two layers of fungal tissue that commonly contain silicate grains or precipitates (Figure

2.13A, C). Other fissures or depressions within lichen squamule tissue also contain silicate grains (Figure 2.10B).

Layers of lichen exudates up to 200 μm thick are commonly detached from thalli and contain embedded grains or mineral precipitates (Figure 2.13D). Authigenic minerals commonly occur on the outer surface of the squamulose and gelatinous lichen thalli, within their associated exudates, and around their rhizines (Figure 2.13 A, D). Some of these crystals actually permeate the lichen tissue (Figure 2.11A, B). The largest crystals are most abundant towards the periphery of the tissues, with crystals up to 15 μm . Smaller crystals occur deeper in the tissues as finely disseminated clay-sized crystals or grains (Appendix 2C).

Vascular plant roots

Vascular plant roots are uncommon features that occur in large interior voids, usually near the base of pinnacle mounds. Roots are typically 0.6 mm in diameter. Roots often lie horizontal to the soil surface as seen in cross-section. Root hairs are rare and are 3-5 μm in diameter and commonly have attached clay and silt grains

Gelatinous lichens

Collema is the dominant gelatinous lichen present in short and tall moss-lichen crusts (Figure 2.14). When dry, *Collema* thalli commonly display an irregular, tree-like form in cross-section (Figure 2.14 A). A single “branch” or a mesh of filamentous rhizines connects these structures to the fine sediments below. Some thalli cap sharp protrusions at the soil surface (Figure 2.14B). Thalli are generally 65 μm thick and 600 μm long and are aligned perpendicular to the soil surface. *Collema* bio-structures commonly have thin layers of exudates (EPS) up to 50 μm thick that are covered in fine

sediments or coated in authigenic minerals. Authigenic minerals also occur along fissures in lichen thalli (Appendix 2A).

Mosses

Short and tall mosses occur throughout the study area. Short mosses are 1 mm long and extend 0.5 mm above the soil surface. Tall mosses grow up to as 6.8 mm tall and rise 3 mm above the soil surface. Both short and tall mosses grow among lichens or as discrete, single-species colonies within short moss-lichen crusts and tall moss-lichen pinnacled crusts (Figure 2.15). Shorter mosses, such as *Bryum* and *Pterygoneurum* inhabit tall lichen-dominated pinnacles, commonly as discrete individuals (Figure 2.15 B). *Syntrichia* is a common tall moss that grows as distinct pads in all moss-lichen crusts, but most commonly occurs within short moss-lichen crusts (Figure 2.15A). Under SEM, moss interiors appear convoluted with large spaces or holes that reflect internal structures. Bumps 5 μm in diameter, which are likely papillae, are seen on the adaxial surfaces of many moss leaves. Clay and silt grains commonly settle between these papillae-like features (Figure 2.15C). Most exposed moss leaves are coated with clay and silt grains (Figure 2.15C).

Mosses occur in a variety of soil textures and have unique relationships to adjacent grains. *Syntrichia* is strongly associated with loose, sandy substrates that are common to short moss-lichen crusts (Figures 2.2D, 2.15A). Shorter mosses, *Bryum* and *Pterygoneurum* are associated with the finer, more compacted substrates of tall moss-lichen crusts (Figure 2.15B). In many cases, sediments near mosses are finer and more compacted than surrounding substrates. Unlike cyanobacteria and lichen structures, authigenic minerals do not coat moss structures. Silt- and clay-sized particles may occur

around individual mosses or within moss leaves (Figure 2.15 A, B). Mosses often cap surfaces adjacent to concave vertical edges.

Bio-sedimentary Structures

Bio-sedimentary structures are unique features that include distinct soil aggregates that form in conjunction with specific biological components (Table 2.1A-C). Nine distinct morphological features were observed in this study: (1) filament sheets, (2) knobs, (3) upturned or curled features, (4) rafts, (5) pedestals, (6) towers, (7) hoo-dooes and sharp protrusions, (8) curved features, and (9) bio-sediment bridges. The unique characteristics of each feature are tied to associated biota, and their distribution varies as a function of crust type.

Filament sheets

Filament sheets are thin horizontal strata of filament-bound surface sediments (Figure 2.7A, B; Table 2.1A). Most filaments are thought to be cyanobacteria, such as *Microcoleus*. Fine-grained sediments with abundant filaments form sheets up to 250-300 µm thick and overlie coarser, looser sediments. These layers may be repeated with depth, resulting in distinct stratification. Fine-grained sediments are highly compacted and may be associated with authigenic minerals. Filament sheets cap zones of vesicular pores within tall moss-lichen crusts. These sheets are common features of the bio-rich zone in all crust types, but they are particularly pronounced in cyanobacteria-dominated crusts (Figure 2.4).

Knobs

Knobs are filament-rich, surface protrusions with convex summits that are found in all crust types (Figures 2.1B, 2.9A, 2.16, 2.17; Table 2.1A). Knobs commonly contain

authigenic minerals that cement grains or occur as finely disseminated crystals within filament EPS. The tallest knobs are linear features that are up to 3.8 mm tall, with loose grains infilling adjacent depressions (Figures 2.1B, 2.16A, B, 2.17A). Shorter knobs that protrude 1-2 mm form detached filament- and authigenic mineral-rich layers up to 1 mm thick (Figure 2.17B). This detachment results in linear voids, measuring 1.5 mm thick by 0.25 mm high, that align parallel to the convex summit of the knob (Figure 2.16B, 2.17B). Horizontal cracks up to 100 μ m wide occur along the base of some knobs. The tallest knobs may be oriented vertically or sub-vertically (Figures 2.9A, 2.16A). Individual filaments or bundles of filaments occur with attached silt and clay and extend vertically from a few knob summits (Figures 2.17 C, D). These grain and filament bundles form sharp protrusions that are 0.25 mm wide and 0.35 mm tall. Some knobs also contain well-developed or incipient vesicular pores and irregular pores (Figures 2.9A, 2.16B, 2.17A). Gelatinous and squamulose lichens commonly inhabit knob summits.

Upturned or curled biological features

Upturned or curled features are biological and bio-sedimentary structures that are partially detached or curl to protrude from the soil surface (Figures, 2.10A, 2.10C, 2.13B, 2.15B, 2.18A; Table 2.1A). These features occur in all crust types. The most common examples include squamulose thalli, gelatinous thalli, filaments, and filament sheets that curl and partially detach from the soil (Figure 2.10A, 2.13B). In most cases, biological structures also have sediments and precipitates attached to their tissues (Figure 2.13B). Commonly biotic structures curl, crack, break off, or stretch, as shown by thallus laterally thinning or detaching (Figure 2.10B). As some lichen thalli curl, they fuse to other lichen

thalli with the upper photosynthetic sides of the thalli touching. Edges of lichen thalli also curl downward into the soil, while the center of the thallus curls up. This curling forms small arch shapes or hummocky surfaces (Figure 2.18A). Fine, compacted grains surrounding some mosses form sheets that curl up and partially detach from the soil surface (Figure 2.15B).

Rafts

Bio-sediment rafts are lichen thalli with attached grains and authigenic minerals that are completely separated from the soil surface, forming a discrete aggregate (Figure 2.18B; Table 2.1B). These rafts are most commonly composed of single lichen squamules whose EPS material is embedded with silicate grains and authigenic minerals. Rafts are up to 1.1 mm thick and 2 mm long. Some rafts occur along short moss-lichen crusts but are most common along tall moss-lichen pinnacles, which show strong expression of upturned features.

Pedestals

Bio-sediment pedestals are comprised of lichen squamules that cap small protrusions of sediments, rising up to 0.75 mm above the adjacent soil surface (Figure 2.19A; Table 2.1B). Pedestals are common features found within tall moss-lichen pinnacled crusts. Pedestal sediments are most commonly composed of clays and silts and have finer textures than the underlying sediments. Pedestals are formed primarily in association with multiple hair-like rhizines, or rhizoidal rhizines, as those of *Placidium squamulosum*. Pedestals commonly display densely packed sediments and authigenic minerals below the perimeter of the lichen squamule (Figure 2.19A). Many pedestals have irregular interior void space up to 1.5 mm in diameter that contains loose rhizoidal

rhizines (Figure 2.13A). Loose rhizines are rarely longer than 1.5 mm and are commonly coated in authigenic minerals.

Towers

Bio-sediment towers are protruding features that are similar to pedestals but differ with respect to height and component rhizine morphology (Figures 2.13B, 2.13D, 2.19B, 2.19C; Table 2.1B). Towers are formed in association with single-rhizine squamulose lichens such as *Placidium lacinulatum*, whereas pedestals form in association with thin, rhizoidal rhizines. Towers are common to most tall moss-lichen pinnacles and are dominated by clay and silt-sized grains. Intact towers are up to 4.75 mm tall and are approximately 0.95 mm wide. These towers commonly lean up to 10 degrees from vertical, and many are cracked along the base. Authigenic minerals and grains below single-rhizine thalli are densely packed around the entire rhizine (Figure 2.13D). Some cracks up to 0.1 mm separate the rhizine from the adjacent soil (Figure 2.19C). Thick rhizines are up to 5.25 mm long and penetrate the entire length of tallest sediment towers (Figure 2.19C). A few single rhizines are also broken up, sheared or exposed along the sediment tower edges (Figure 2.19C).

Hoo-doo and sharp protrusions

Hoo-doo and sharp protrusions are bio-sedimentary projections that are capped by gelatinous lichens and filament meshes (Figures 2.14B, Figure 2.20; Table 2.1C). The term —hoo-doo” is used here because these protrusions closely resemble hoo-doo observed at the landscape-scale, although these are micro-scale features observed in thin section. Hoo-doo are vertical, linear features composed primarily of sand-sized grains with few silt or clay-sized grains (Figure 2.14B). Hoo-doo differ from knobs because

they have flat summits and show no obvious stratification. These structures are up to 1 mm wide and 6 mm tall.

Sharp protrusions are triangular features that are capped by filament-bound sediments (Figure 2.20). They are up to 1.5 mm long and are vertical to sub-vertical (Figure 2.12). Sharp protrusions differ from knobs because they have no obvious stratification and have pointed summits. Both features are somewhat rare but mostly occur within tall moss-lichen pinnacled crusts.

Bio-sediment bridges

Bio-sediment bridges are horizontal soil aggregates that overlie irregular voids (Figures 2.7C, 2.8B, 2.21; Table 2.1C). These bridges are only found in tall moss-lichen pinnacles. The features measure up to 12 mm thick by 25 mm long and commonly contain filaments or other biological structures. Associated voids are up to 24 mm by 36 mm. Lichen squamules commonly bridge small surface gaps as wide as 2 mm (Figure 2.8B). In two dimensions, these structures often appear to be free-hanging (Figures 2.8B, 2.21A). Commonly, free-hanging bridges partially close near-surface pores that contain mosses or lichens and appear to block interior photosynthetic material from light (Figures 2.8B, 2.21B). A few bridges contain no visible biological structures (Figure 2.7C).

These bridges are most common at the base of the bio-rich zone.

Curved features

Curved bio-sedimentary features are thumb-shaped aggregates of grains and biological structures that form —U or —L” shapes (Figure 2.22; Table 2.1C). These aggregates are up to 3.5 mm wide by 7 mm long and are composed of clay, silt, and sand. Curved features commonly occur in conjunction with bio-sediment bridges and interior

voids (Figure 2.21B, 2.22B). Some of the associated interior voids contain photosynthetic tissues that, in two-dimensions, appear to be blocked from visible light (Figure 2.21B). In other cases, lichens attached to these features are pointed downwards, away from direct light sources. Curved features commonly occur in conjunction with near surface voids that have smooth margins and show infilling of unconsolidated grains (Figure 2.21A). A few sharp protrusions of filament-bound sediments were found along the lower edge of these curved features (Figure 2.22B).

Interpretations

Model of BSC Formation

Given suitable environmental conditions, the development of BSCs will proceed from cyanobacteria to tall moss-lichen pinnacled crusts overlying an accompanying mineral Av horizon (Figure 2.23, Table 2.2). Advancing through this succession, surface topography builds, internal morphology becomes more complex, dust and organic substrates accumulate, and component crust taxa change. BSC succession includes the following steps: (1) cyanobacteria-dominated crusts, (2) short moss-lichen crusts, (3) tall moss-lichen pinnacled crusts, and (4) tall moss-lichen pinnacled crusts overlying mineral Av horizons.

Step 1: Cyanobacteria-Dominated Crusts

If a stable, fine-grained substrate is available, filamentous cyanobacteria will colonize the soil surface. Cyanobacteria are most extensive along sand sheets (see Chapter 3), as their unique life habits make them well-suited for high sand saltation. Cyanobacteria respond to shifting sands as they trap and bind materials and facilitate

precipitation of authigenic minerals. Cyanobacteria crusts create surface seals that stabilize soil and mitigate erosion. Trapping and binding, surface sealing, and mineral precipitation continue in all crust types but co-develop with changes in surface morphology and species composition.

Trapping & binding, sealing, mineral precipitation and erosion mitigation

Filamentous cyanobacteria trap and bind grains to form filament sheets and knobs (Figures 2.7A, 2.7B, 2.1B, 2.9A). Sticky EPS material of cyanobacterial sheaths traps clay and silt grains. Cyanobacterial filaments also grow around or bind to clay, silt, and sand-sized grains. In this study, cyanobacteria stabilize the primary soil materials, which are sand grains. To form sheets and knobs, filaments first move to the soil surface to stabilize the upper layer of sediment. Once at the surface, filaments trap atmospheric silt, clay, and very fine sand in their sheaths. Eventually, the fine sediment and filament mesh thickens to form a continuous surface seal that resists erosion. With time, another layer of fine sand is deposited at the surface, forcing cyanobacteria to move upward toward light. Cyanobacteria inhabit and stabilize new sands with another layer of filaments and fine grains. This process continues and, over time, produces interbedding strata of loose sands and compacted fine grains. Filament sheets develop where cyanobacteria form homogenous surface layers and grow uniformly. Knobs form in a similar fashion to sheets, but likely occur in areas where cyanobacteria are heterogeneously distributed. Trapping and binding promote the build-up of sediment in areas where cyanobacteria are present. If cyanobacteria are heterogeneously distributed, this accretion occurs along the tops of existing protrusions such as knob features (Figures 2.1B, 2.9A, 2.16, 2.17). Regardless of morphological setting, knobs appear to grow toward light, whether

vertically or diagonally. Authigenic minerals within cyanobacteria sheaths act as cementing agents that improve the integrity of these features. The stability from surface crusting and surface roughness associated with knob development enhance dust accumulation.

Step 2: Short Moss-Lichen Crusts

If sand sheet activity is low and geomorphic stability persists, mosses and lichens colonize cyanobacteria-stabilized surfaces to form short moss-lichen crusts. These crusts commonly form along sandy gravel bars of recently abandoned inset fans, where surface clasts reduce sand saltation and sand sheet movement (see Chapter 3). Short moss-lichen crusts augment stabilization processes displayed in cyanobacteria crusts. These crusts show strong expression of wetting and drying processes that promote expansion and contraction, changes in surface morphology, and dust capture.

Mosses and lichens increase sediment trapping and binding and further mitigate erosion. *Syntrichia* a tall, “sand-loving” moss, is the primary genus found in these short crusts and plays an important role in sediment binding and trapping. *Syntrichia* collects sand grains between leaves, while sand also piles up against moss individuals. In most cases, few silt, clay, or very fine sand grains have been captured around mosses as evidenced by the coarse nature of their substrates. Fine and medium sand grains commonly accumulate along the surface of the tall mosses to form cushion-like colonies. Mosses grow up through newly-deposited sand at a relatively uniform rate that keeps topographic relief to less than 1 cm. These mosses provide surface cover that protects newly captured sediments. Gelatinous lichens can also trap grains within their sticky thalli and exudates (Figure 2.14A). When wet, lichen thalli create a surface seal that

reduces erosion and influences the movement of moisture and gases. Authigenic minerals associated with lichen thalli could eventually be re-precipitated as cements for enhanced crust integrity (Appendix 2A).

Wetting/drying & expansion/contraction

Wetting and drying induce changes in lichen thallus shape, moss leaf orientation, and soil morphology. Expansion and contraction from wet-dry cycles lead to curling and cracking. Two major phenomena influence these dynamics – differential drying of biological structures and sediment and tissue expansion upon hydration. When biological tissues with attached soil particles are moistened, they expand and subsequently contract upon drying. Soil texture and biological tissue composition lead to disparate volumetric expansion and rates of desiccation. In addition, drying generally occurs sequentially from the soil surface downwards. This differential and sequential drying results in the curling, cracking, stretching, or breaking of lichen thalli that resembles aggregate curling in mud-crack morphology (Figures 2.10B, 2.13B). Fine grains and biological tissues are concentrated at the soil surface, thus magnifying differences in near-surface expansion and contraction.

Curling and cracking phenomena create distinct bio-sedimentary features. When lichen squamules curl, attached sediments, especially those embedded in exudates or in gelatinous thalli, peel upwards, leaving void space above the soil surface (Figure 2.13B). Some lichen curling causes thalli to break off along edges, or whole thalli to break away and form detached “rafts” (Figure 2.18B). Drying also causes lichen squamules to crack or stretch. Differential drying can be substantial within lichen towers, producing shear forces that break rhizines (Figure 2.19 C, 2.21B). In short moss-lichen crusts, curling

associated with drying may form “C” or “S” shapes that change the topography of nearby non-cohesive, sandy sediments (Figure 2.18A). As biological tissues dry, they also shrink, creating cracks between biological tissues and adjacent soil. Sediment may settle within these cracks and eventually be compacted by rehydrating and expanding tissues. For example, coarse grains are slightly compacted near most *Syntrichia* colonies. This relationship suggests that mosses contribute to sediment compaction in areas where sand grains would otherwise be relatively unconsolidated. A few squamulose rhizines have enlarged, bulbous features that expand and shrink substantially upon drying, creating void space or changing surface morphologies (Figure 2.10C, 2.19C).

Dust capture

Dust capture is enhanced within short and tall moss-lichen crusts. Wetting and drying processes increase surface topographic relief and dust capture potential. Within short moss-lichen crusts, thin layers of dust accumulate around or below many lichens (Figure 2.7A). Cracks in the lichen thallus also collect dust. As tissues reconnect upon wetting, grains become trapped within the lichen thallus. Similarly, as squamulose lichen perithecia open, grains settle into the voids, only to be embedded in the thallus when perithecia close (Figures 2.13A, C).

Step 3: Tall Moss-Lichen Pinnacled Crusts

If surfaces remain undisturbed, materials accumulate to form tall moss-lichen pinnacled crusts. Late Holocene and older surfaces have the prolonged stability sufficient for these crusts to develop (see Chapter 3). Pleistocene and older surfaces display scattered pinnacles between desert pavement clasts, while mid- to late Holocene inset fans have the most abundant tall moss-lichen pinnacles across their extensive fine-

grained surfaces. Formative processes from earlier successional steps such as stabilization, binding and trapping, and authigenic mineral precipitation continue. Dust capture is magnified and partially offset by concomitant mass wasting. The net effect is the accumulation of material and formation of new pores. Vesicular pores also develop within the bio-rich zone, which enhances heaving, surface roughness, and dust capture potential.

Magnified dust capture

As biota grow upward in response to light, dust accumulates along BSC surfaces. Finer particles are trapped at the surface, thickening the bio-rich zone. Surface sealing by silt and clay laminae, authigenic mineral precipitation, and expansion of hydrated biologic tissues protect dust from erosion. Dust capture increases topography and surface area. Expanded surface area and biotic cover enhance expansion-contraction processes, which further increase surface roughness and dust capture potential.

Dust accretion is particularly elevated where squamulose lichens form protruding accretionary features such as pedestals and towers (Figures 2.13A, 2.13B, 2.13D, 2.19, 2.21B, 2.22B). Rhizine morphology largely controls dust trapping dynamics and the formation of lichen pedestals versus towers (Figures 2.24, 2.25). Thin, hair-like rhizines cover the lower surface of the lichen thallus yielding a continuous set of anchors to the soil surface (Figure 2.24). As a result, lichen curling is low, and dust mostly accumulates around the circumference of the lichen squamule. Rhizines grow upward or outward to keep up with sediment accretion along the squamule's edge. No sediment, however, concurrently accumulates around interior rhizines. Over many wetting and drying cycles sediment builds around the squamule perimeter, leaving void space below the center of

squamule (Figure 2.24). In general, total dust accumulation is limited by rhizine morphology, so pedestals rarely exceed heights of 1 mm. In contrast, squamules with thick rhizines are only anchored by one or a few points. This reduction in surface anchoring allows greater squamule curling (Figure 2.25). Dust accretes around these thalli in a similar fashion to pedestals, over the course of many wet and dry cycles. Increased thallus curling, however, allows more complete infilling of dust around the entire rhizine, resulting in negligible void space below the lichen squamule (Figure 2.25). The net effect is enhanced dust capture with towers reaching heights of 4.75 mm. In addition, the towers may have mixed grain sizes, because the greater curling accommodates larger grains. Many towers contain long rhizines that grow through their entire length, which strengthens the structure (Figure 2.19 C, 2.21B).

Dust capture mechanisms influence pinnacle morphology. Pinnacled mounds with 60% or greater squamulose lichen cover have rounded tops and compact forms. This morphology is likely the result of successive dust accretion producing radial expansion over time (Figure 2.2C, 2.24, 2.25). When squamulose lichens are extensive, they form continuous surface cover, which further promotes smooth, rounded pinnacle morphology. In contrast, gelatinous lichens and filaments commonly cap pinnacles with sharper features (Figures 2.14B, 2.20). Given the angular nature of these structures, differential erosion may play a stronger role in their formation. Dry, gelatinous lichens leave more soil exposed, which could allow more eolian erosion than that in squamulose-dominated crusts. Cyanobacteria knob formation results in pointed features that further augment the sharp nature of these pinnacles. Heaving and collapsing processes may also contribute to the sharpness of pinnacle surfaces.

Bio-rich Av pore formation & heaving

Vesicular pores cause significant heaving that increases surface topography and dust capture potential. Vesicular pores are thought to form through surface sealing and thermal expansion of trapped air (Springer 1958, Miller 1971, Evenari et al. 1974, Figueira and Stoops 1983, Sullivan and Koppi 1991) in association with desert pavements (Springer 1958, McFadden et al. 1987, Wells et al. 1987, Anderson et al. 2002). In this model, surface sealing occurs because of biological crusting. As water infiltrates the soil, air becomes trapped within the bio-rich zone of tall moss-lichen pinnacles. Hydrated organic structures such as lichen thalli and filaments as well as surface crusts create a seal that prevents gases from escaping. Temperature changes drive water evapotranspiration and gas expansion. Expansion of trapped gases creates vesicular pores and interior voids with smooth margins. Vesicular pores are not formed in association with cushion-like colonies of $\geq 50\%$ moss cover, presumably because mosses do not facilitate crusting or sufficiently seal surfaces for vesicle formation. As vesicles develop, any available filaments or precipitation of authigenic minerals help to enhance the strength of the pores. In addition, when filament sheets dry and crack, they can curl up and then partially reattach upon wetting. This process forms small irregular pores that will later become vesicles. The expansion of trapped air associated with vesicular pore formation causes heaving and enhances surface roughness, which further facilitates dust trapping.

Cyanobacteria knobs of tall moss-lichen pinnacles show additional evidence of heaving. Many knobs display small, linear voids that parallel convex summits and contain vesicular pores throughout the structure (Figure 2.17A, B). Linear voids may

form as crystal growth causes heaving along the tops of knobs. Precipitation of authigenic minerals is greatest near summit of the knob, presumably because these areas contain the greatest concentration of active cyanobacteria and EPS material. The mineralization of EPS material releases Ca into solution and drives the precipitation of authigenic minerals, such as carbonate. Therefore, crystal growth and heaving are also highest in these areas. Cyanobacteria form new pores with small filament bundles (Figures 2.17C, D). As cyanobacteria grow upward they can form sharp bundles (Figures 2.17C, D). Growth and sediment capture eventually cause these bundles to become sufficiently heavy to tip over. Tipping bundles create new pores that may eventually become vesicles during subsequent wet-dry cycles (Figure 2.17A).

Wetting, drying, and dust capture associated with mosses and gelatinous lichens cause significant heaving to create sharp pinnacle features (Figures 2.10A, 2.15B). Within tall, pinnacled crusts single moss individuals such as *Bryum* or *Pterygoneurum* are scattered among squamulose and gelatinous lichen thalli. As moss and gelatinous lichen tissues shrink upon drying, cracks form between the biotic tissue and the soil. This creates space for dust to accumulate. Tissues expand upon rewetting and compact newly-captured grains. Over time, this sediment accumulation can no longer be accommodated. Heaving occurs and surface cracks develop, similar to features and processes found in Vertisols (Figures 2.10A, 2.15B). Differential pressures orient grains parallel to nearby biotic structures (Figures 2.10A, 2.15B). Various types of tissues may dry at different rates which would magnify differential drying and heaving. Heaving processes associated with short mosses and gelatinous lichens produce sharp pinnacle surface features.

Micro-scale mass wasting

Tall moss-lichen pinnacled crusts are characterized by net accumulation of material. Interior voids, curved features, and sediment bridges, however, reflect a complex history of mass-wasting within pinnacles (Figures 2.7C, 2.8B, 2.21, 2.22).

Sediment bridges overlying large interior voids record toppling events. Biologically mediated towers build up through sediment accretion and adjacent erosional down-cutting. Towers eventually tip over because of outside disturbances or because continual vertical growth produce instability (Figure 2.26). Tipped towers form sediment bridges that block much of the sunlight from the photosynthetic tissues in underlying voids (Figure 2.8B, 2.21B). Cracks below tilting towers and fragile, sharp aggregates also provide evidence of toppling events.

Thumb-like sedimentary structures reflect bending that occurs with creep processes along pinnacle mound surfaces. Thumbs bent into “ \perp ” or “ \cup ” shapes, may begin as knobs or towers (Figure 2.22). Over time, sediments deform as upward heaving is followed by downward gravitational settling. These “thumbs” can create smooth, interior pores that trap photosynthetic material (Figure 2.22A). These features suggest interior pore linings were once exposed at the pinnacle surface. In some cases, lichen thalli are oriented with their photosynthetic side downward, further indicating churning forces via creep, through heaving and collapsing. Many curved sedimentary features contain filaments, suggesting biological mediation enhances plastic deformation. Other curved features accompany bio-sediment bridges (Figures 2.21B, 2.22B).

Some free-hanging biological and sedimentary structures reflect sloughing or collapse. One common example is partial detachment of lichen thalli along vertical sides

of pinnacles. Sloughing and/or collapse augment creep processes to close near-surface pores. Lichen thalli may bridge surface voids to block other photosynthetic materials from light. In other cases, sediment bridges within the bio-poor zone may collapse and detach from the bio-rich zone (Figure 2.7C). Biological structures help sediments remain intact, while non-biologically mediated sediments slump or slough as semi-cohesive linear aggregates.

Step 4: Tall Moss-Lichen Pinnacled Crusts over Mineral Av Horizons

If surfaces remain undisturbed with sustained dust influx, mineral vesicular horizons will accumulate below tall moss-lichen pinnacles. Biologically-mediated mineral Av horizons are best expressed on mid-Holocene inset fans where tall moss-lichen pinnacles are most extensive, meter-scale surface roughness is high, and stability is prolonged (see Chapter 3). Earlier crust formative processes continue to operate at the surface. Dust accretion below moss-lichen pinnacles leads to significant dust accumulation and the formation of mineral Av horizons, a newly recognized biological process.

Mineral dust accumulation and Av formation

Wetting and drying cause expansion and contraction of pinnacle mounds, which facilitates mineral dust accretion, and vesicular horizon formation. Expansion and contraction form cracks along the basal edge of pinnacle mounds (Figure 2.27). During dry times, these voids that closely resemble mud cracks separate individual pinnacles from adjacent pinnacle mounds (Figure 2.2E). Horizontal cracks also develop along the base of the pinnacle mounds, separating them from the mineral soil below (Figure 2.2E). These cracks form when the bio-rich zone dries and contracts. This contraction is similar

to the curling associated with differential drying in mud cracks. Cracks forming between pinnacle mounds create an entry point for dust, while cracks below pinnacles create accommodation space for incoming sediment (Figure 2.27). Dry times are periods of high dust influx, when dust blows across the soil surface. Some of this dust is blown through the vertical cracks and into the horizontal voids below the pinnacle mounds. Dust trapped below pinnacle mounds is sheltered from erosion. As the bio-rich zone rehydrates during the next rainfall event, pinnacle mounds expand to seal the surface cracks, thus protecting and compacting newly accumulated dust. Over several wetting and drying cycles, a thick dust layer accumulates. BSCs seal surfaces to trap air and produce vesicular pores below pinnacle mounds. Dust accumulation and surface sealing produce Av horizons up to 27 cm thick. Rock cover in these areas can be as low as 22%, which is insufficient for such high dust capture. Therefore, BSC-related dust accumulation and surface sealing controls the formation of these thick mineral Av horizons.

Discussion

Models of BSC Development

Complex surface processes create pinnacle mound topography and form intricate external and internal morphologies. This study is the first comprehensive investigation of bio-sedimentary structures and origins of BSC topographic relief (Figure 2.2C). Other arid regions have documented that wetting and drying processes curl soil margins along surface cracks, creating micro-relief that is subsequently inhabited by lichens (Danin et al. 1998). Hoof traffic from native ungulates enhances micro-topography of BSCs in

some cold environments (Csotonyi and Addicott 2004), while others suggest frost heave and differential erosion produce most pinnacle topographic relief (Belnap 2001, 2003).

While frost heave may play a dominant role in cooler deserts, it has minimal influence on crust micro-topography in hot deserts like the Mojave Desert where soils rarely freeze.

My results show surface stabilization, accretionary processes, mass wasting, and heaving from wetting and drying collectively produce crust micro-features. Surface features and internal bio-sedimentary structures record a complex genetic history in which cyanobacteria crusts develop into tall moss-lichen pinnacled crusts over mineral Av horizons.

My succession model illustrates how BSC characteristics and crust-forming processes co-develop through time with changing organisms (Figure 2.28). If a fine-grained mineral substrate is available and restricted from outside disturbances, crust formation may begin (see Chapter 3). If environmental conditions permit, BSC development progresses from bare mineral soils to cyanobacteria-dominated crusts and eventually to extensive moss-lichen crusts (Figure 2.28)(Campbell 1979, Pluis and de Winder 1989, Eldridge and Greene 1994, Danin et al. 1998, Belnap 2001, Langhans et al. 2010). My study illustrates how physical processes change through this progression, starting with binding, trapping and stabilization and progress to include elevated dust accretion and low-magnitude mass wasting. These observations also provide two additional steps to earlier succession models. (1) Incremental dust accretion forms tall moss-lichen pinnacles (Figure 2.28, t_3); (2) dust accumulation leads to the formation of biologically-mediated mineral Av horizons below tall moss-lichen pinnacled crusts

(Figure 2.28, t₄). This progression in crust-forming processes likely influences rates of pedogenesis and landscape change.

Implications for Pedogenesis and Landscape Evolution

BSCs play an important role in early soil formation and landscape evolution. My results show micromorphological evidence that BSCs reduce erosion (Campbell et al. 1989, Belnap 1995, McKenna Neuman et al. 1996, Marticorena et al. 1997, Canton et al. 2003, Eldridge and Leys 2003, Li et al. 2004, Bowker et al. 2008, Lazaro et al. 2008), enhancing stability necessary to initiate pedogenesis. This study identifies new mechanisms through which BSCs influence the accretion and preservation of dust, which is a strong driver of arid soil development and landform surface change (see Chapter 3). Dust accretion associated with moss-lichen crusts controls ecological feedbacks through enhanced moisture availability and nutrient inputs (see Chapter 4). These phenomena increase microbial activity and fertility, partially offsetting nutrient disparities between shrub canopies and interspaces (see Chapter 4). Moss-lichen crusts support ecosystem stability by supplementing soil resource availability during times of drought or biotic stress. BSCs also influence landscape-scale biogeomorphic processes by impacting surface bio-sedimentary features, similar to marine microbially-induced sedimentary structures (e.g. Reid et al. 2000, Noffke et al. 2001a, Dupraz et al. 2009).

Stabilization

Life habits of terrestrial crust-forming cyanobacteria strongly parallel those of marine microbially induced sedimentary structures, biolaminates, and stromatolites. BSCs have been compared to terrestrial stromatolites (Campbell 1979, Issa et al. 1999). This study, however, illuminates new similarities between BSCs and marine structures.

Microcoleus is a dominant terrestrial cyanobacterium of BSCs (Booth 1941, Belnap and Gardner 1993, Issa et al. 1999, Garcia-Pichel and Pringault 2001, Issa et al. 2007, Thomas and Dougill 2007, Issa et al. 2009) that is also a common marine taxon responsible for sediment baffling, binding, and trapping as well as carbonate cementation in stromatolites and microbial mats (Black 1933, Grotzinger and Knoll 1999, Reid et al. 2000, Noffke et al. 2001a, Dupraz and Visscher 2005, Allwood et al. 2006, Dupraz et al. 2009). BSCs and marine microbial mats show similar sedimentary preferences. Microbial mat-forming cyanobacteria prefer moderately stable fine sands of 95% quartz (Noffke et al. 2002, Noffke 2009). In the Mojave Desert, *Microcoleus* cyanobacteria prefer moderately stable fine sands as initial substrates (see Chapter 3) but do not require high quartz contents, as light is not limiting along exposed soil surfaces. Fine sands also promote cyanobacteria growth in other arid regions (Bowker and Belnap 2008), which may occur because fine sands are the optimal size for filaments and less sticky than silts or clays (Noffke 2009). Terrestrial and marine cyanobacteria interact similarly with these incoming grains.

Terrestrial cyanobacteria actively stabilize sediments and impact grains analogous to cyanobacteria of marine stromatolites and microbial mats. My data suggest cyanobacteria play an active role in sediment aggregation and stabilization, as have other terrestrial studies (Booth 1941, Campbell 1979, Belnap and Gardner 1993, Issa et al. 1999, Garcia-Pichel and Pringault 2001, Issa et al. 2007, Thomas and Dougill 2007, Issa et al. 2009). Filament knobs and sheets (Figures 2.7B, 2.16) form similarly to marine bio-sedimentary structures (Campbell 1979, Grotzinger and Knoll 1999, Reid et al. 2000, Allwood et al. 2006). Incoming grains are either trapped in sticky EPS material, or

bound by cyanobacteria filaments (Campbell 1979, Tisdall and Oades 1982, Verrecchia et al. 1995, Zhang 2005, Issa et al. 2007, Thomas and Dougill 2007). EPS enhances cyanobacteria motility, allowing filaments to glide upward toward sunlight to regain soil surfaces after burial (Belnap and Gardner 1993, Garcia-Pichel and Pringault 2001). As in marine environments, many cycles of binding and trapping build up distinct strata (Campbell et al. 1989, Issa et al. 1999, Noffke et al. 2003a, Noffke 2008). Heterogeneously distributed cyanobacteria produce filament knobs (Figure 2.16), previously undescribed features that closely resemble rough stromatolites (Grotzinger and Knoll 1999). In contrast, homogeneously distributed cyanobacteria develop into filament sheets (Figure 2.7B)(Campbell et al. 1989, Issa et al. 1999) similar to smooth biolaminates (Noffke et al. 2001a, 2003b). Terrestrial cyanobacteria may form bundles (Figures 2.17C, 2.17D) resembling marine filament tufts (Noffke 2009). Bundles capture grains and eventually tip over to form new pores. As cyanobacteria form knobs and sheets they also influence authigenic mineral precipitates.

Similar to marine taxa, terrestrial filamentous cyanobacteria facilitate authigenic mineral precipitation. Precipitates found throughout the filament knobs and sheets are seemingly tied to metabolic processes. Carbonate minerals form within terrestrial cyanobacteria EPS (Figure 2.11C)(Campbell 1979), which could occur when sheath material is mineralized, as seen in marine stromatolites (Braissant et al. 2002, 2003). In aqueous environments, EPS sequesters cations such as calcium and magnesium (Dupraz and Visscher 2005, Dupraz et al. 2009). In terrestrial environments cyanobacteria sheaths commonly contain dust (Belnap and Gardner 1993) that is also rich in calcium (Reynolds et al. 2001, Reheis et al. 2009). As heterotrophic bacteria begin to mineralize

sheath material, they release calcium and magnesium and respire carbon dioxide (CO_2) (Dupraz and Visscher 2005, Dupraz et al. 2009). If CO_2 is transformed to bicarbonate (HCO_3^-), authigenic carbonate can precipitate (Dupraz and Visscher 2005, Dupraz et al. 2009). Some types of EPS may even serve as a precipitation template for carbonates (Dupraz and Visscher 2005, Dupraz et al. 2009). This process seemingly occurs in BSCs, as soil bacteria and fungi are widely known to biomineralize carbonates (Rivadeneyra et al. 1985, Ferrer et al. 1988, Monger et al. 1991, Rivadeneyra et al. 1991, 1996, 1998, Loisy et al. 1999, Gonzalez-Munoz et al. 2000, Braissant et al. 2002, Hammes and Verstraete 2002, Braissant et al. 2003, Lian et al. 2006). As authigenic crystals grow, lateral expansion is constrained along the soil surface, which can cause heaving that forms linear voids near knob summits (Figure 2.17B). Such features closely resemble gypsum heaving in cauliflower structures of marine environments (Gerdes et al. 2000). EDS data from this study indicate calcium chloride occurs in association with carbonate. However, this salt is rare in soils and is commonly found in brines or minerals of Antarctic dry valleys or hydrothermally modified marine waters (Garrett 2004, Warren 2010). The micro-conditions of EPS material could augment calcium chloride precipitation with readily available sources of calcium and a potential source of chloride from dust (Wells et al. 1987, Simonson 1995, Reynolds et al. 2001, McTainsh and Strong 2007). Because calcium chloride has not been reported in Mojave Desert soils, it likely is a transitory phase within these crusts. A barite crystal also was found in this study, but its origin has not been determined. The euhedral nature of the crystal suggests *in situ* precipitation. Slightly uneven crystal faces, however, may indicate pitting from eolian processes. Moreover, the 4 μm crystal was small enough for wind transport.

Lichen thalli facilitate authigenic mineral precipitation, which may also result from metabolic activity. Precipitation is greatest within exudates, fungal cortex tissue, and along rhizines (Figures 2.11, 2.13A, 2.13D). Heterotrophic bacterial mineralization of lichen exudates may catalyze precipitation, similar to EPS mineralization seen in cyanobacterial filaments. Precipitation on the outside of the thalli could result from fungal respiration (Dupraz et al. 2009). Lichen thalli are also hypothesized to excrete calcium to detoxify their carbonate-rich environment (Phillips et al. 1987, Monger et al. 1991). The largest crystals lie along thallus margins, suggesting those minerals experienced prolonged crystallization. Enlarged crystals may form through recrystallization of smaller grains (Folk 1974, Deutz et al. 2002), a process that would be favored near the lichen exterior where moisture wicks and evaporates. Alternatively, if organisms excrete calcium, large crystals may develop via overprinting, as precipitation occurs around existing crystals (Deutz et al. 2002). Precipitates form within perithecia and engulf some lichen thalli (Figures 2.11A, 2.11B). These authigenic minerals may be killing fungal tissue or the minerals could serve as a UV sunscreen. Minerals associated with lichen thalli could eventually be re-precipitated to enhance crust integrity.

Sediment stabilization and mineral precipitation by BSCs mitigates wind and water erosion. The role of BSCs in erosion prevention is well documented (Campbell et al. 1989, Belnap 1995, McKenna Neuman et al. 1996, Marticorena et al. 1997, Canton et al. 2003, Eldridge and Leys 2003, Li et al. 2004, Bowker et al. 2008, Lazaro et al. 2008, Chaudhary et al. 2009). My results provide microscopic evidence of erosion reduction, including biostructures that form resistant caps and biological binding of sediments (Booth 1941, Tisdall and Oades 1982, Danin and Ganor 1991, Belnap and Gardner

1993). Authigenic precipitates offer additional cementation to enhance structural stability of the crusts. Coarse sand grains embedded within crusts as well as compacted fine sediments serve as physical barriers. BSC stabilization and erosion mitigation preserve existing bio-sedimentary structures and protect newly deposited dust.

Dust Capture

Dust capture is the primary driver of pinnacle mound build-up, moss and lichen propagation, and arid pedogenesis. Dust provides nutrients and salts (Reheis 1990, Simonson 1995, Reynolds et al. 2001, Reheis et al. 2002, Reynolds et al. 2006, McTainsh and Strong 2007, Field et al. 2010) and changes the particle size distribution of soils (Reheis 1990, Reheis et al. 1995, Simonson 1995) for enhanced soil water-holding capacity (see Chapter 4). Dust build-up forms abiotic vesicular horizons as it forms desert pavements (McFadden et al. 1987, Anderson et al. 2002), facilitates changes in surface topography (Wells et al. 1987, Wood et al. 2005), and impacts runoff and infiltration dynamics (Wells and Dohrenwend 1985, Young et al. 2004, Wood et al. 2005, Meadows et al. 2008). My results show dust provides fine-grained substrates for BSCs and leads to the formation of biologically-mediated mineral Av horizons.

My data provide new evidence that all BSC organisms actively capture dust. Previous research showed some evidence of dust accretion along BSC surfaces (Campbell 1979, Campbell et al. 1989, Danin and Ganor 1991, Belnap and Gardner 1993, Verrecchia et al. 1995, Shachak and Lovett 1998, Reynolds et al. 2001, Belnap 2003). Most work investigated the role of cyanobacteria sheaths in dust trapping and aggregation (Booth 1941, Campbell 1979, Campbell et al. 1989, Belnap and Gardner 1993, Zhang 2005, Issa et al. 2007, Wu et al. 2010, Zaady and Offer 2010), while other studies

illustrated the role of mosses in dust capture and stabilization (Danin and Ganor 1991, Perez 1997). Some geochemical data indicate potential dust signatures in BSC sediments (Reynolds et al. 2001), while others suggested surface roughness associated with moss-lichen crusts contributes to dust capture potential (Belnap 2003, Li et al. 2010). In this study, elevated concentrations of fine grains within the bio-rich zone, as compared to the bio-poor zone, show direct evidence for dust input. This dust capture drives thickening of the bio-rich zone that commonly occurs during BSC succession (Budel et al. 2009). Previously undescribed bio-sedimentary features such as towers and pedestals (Figures 2.19, 2.24, 2.25) grow with dust capture and increase micro-topographic relief, thus in turn, increasing dust capture.

Surface dust capture is an important survival and propagation mechanism for BSC organisms. Crust organisms capture grains in sticky exudates, incorporate grains in bio-structures, and trap and bind sediments. By enhancing dust capture and fine particle concentrations, crust organisms also increase the local soil water holding capacity, fertility, and surface area availability. Dust accumulation within and around lichen thalli are well-known sources of nutrients to component organisms (Gadd 2007, Nash 2008), while fine-grains enhance soil moisture retention around bio-structures (Belnap and Gardner 1993). Dust capture increases surface roughness, providing new, exposed substrates for microbial colonization. Increased surface roughness further enhances dust capture and decreases rates of runoff for greater infiltration. Because crust organisms actively obtain optimal substrates for their growth, they act as local ecosystem engineers inducing a positive feedback for continued propagation (see Chapter 3).

Surface morphology and mechanisms of sediment accretion vary as a function of component taxa. In this study, moss genera actively capture their preferred grain size (Danin and Ganor 1991). *Syntrichia* mosses are best suited for sandy sediments because their large leaves fill void space between sand grains (Figure 2.15A), making them well equipped for rapid water uptake (John Brinda, *pers. comm.*) necessary in fast-draining, sandy soils. The large size and leaf morphology favor the trapping of sand grains, their preferred substrate. The cushion-like colonies of tall *Syntrichia* mosses accumulate sand uniformly, leading to low topographic relief and rolling morphologies (Figure 2.2D). Short mosses, *Bryum* and *Pterygoneurum*, are better suited for loamy material, as they have smaller leaves (Figure 2.15B) and prefer the higher water-holding capacity of silt- and clay-rich substrates of pinnacles (John Brinda, *pers. comm.*). These short mosses facilitate silt and clay capture along pinnacle surfaces, augmenting topographic relief (Figure 2.2E). Similarly, this study shows gelatinous lichens have different dust capture and build-up mechanisms than squamulose lichens. Squamulose lichens capture dust below thalli, while gelatinous lichens capture dust within cracks around or between thalli structures. Squamulose lichens form rounded, compact pinnacles through “radial” dust capture (Figure 2.2C), while heaving associated with gelatinous lichens create sharp surface features (Figure 2.2E). A companion study indicates squamulose lichens are favored in areas of high desert pavement cover (see Chapter 3). Squamulose lichens capture dust, building up protruding surface features (Figure 2.2F) that enhance substrate availability between rock fragments. These differences in dust accumulation mechanisms and surface topography support the hypothesis that BSC morphological types influence

ecosystem function (Eldridge and Rosentreter 1999). Dust capture by mosses and lichens is regulated by wetting and drying processes.

Wetting/Drying, Expansion/Contraction, and Heaving

Wetting and drying lead to expansion and contraction that change surface morphology, form surface cracks for dust capture, and produce new bio-sedimentary propagules. Wetting followed by sequential drying forms surface cracks and upturned or curled features (Figure 2.18A) similar to mud cracks documented in marine tidal and supratidal settings as well as terrestrial environments (Plummer and Gostin 1981, Danin et al. 1998, Noffke et al. 2001a). Cracks form within or around bio-structures (Figure 2.10), creating accommodation space for settling dust. *Collema* and other gelatinous lichens shrink substantially upon drying (Lange et al. 1998), which produces cracks. Dust settles into these voids. As lichens rewet, the increased volume from dust influx leads to heaving and oriented grains (Figure 2.10A), which resemble expansion-contraction features caused by wetting and drying in Vertisols (Yaalon and Kalmar 1972, Nordt et al. 2004). As lichen squamules curl, dust can fill in below thalli to form pedestals or towers. This curling may also cause lichen-sediment aggregates to detach, forming “rafts” (Figure 2.18B). Detached “rafts” have been identified in other regions and may act as propagules that are reattached nearby, or move large distances via wind currents (Wynn-Williams 1990). Wetting and drying are also responsible for heaving in vesicular horizons.

Vesicular Horizon Formation

This study provides new insight into the formation of vesicular and large irregular pores within the bio-rich zone of tall moss-lichen pinnacled crusts. Vesicular pores form

through sequential wetting and drying processes. Infiltrating water traps air bubbles within the soil. Surface crusts prevent gas exchange, and as soils reheat, expanding air forms vesicles (Springer 1958, Miller 1971, Evenari et al. 1974, Figueira and Stoops 1983, Sullivan and Koppi 1991). Vesicular pores are most often associated with Av horizons underlying desert pavements (Springer 1958, McFadden et al. 1987, Wells et al. 1987, Anderson et al. 2002). A few studies show vesicular pores occurring with BSCs (Danin et al. 1998, Issa et al. 1999, Canton et al. 2003, Marsh et al. 2006). My data provide further evidence that cyanobacteria and lichens seal surfaces to trap air and form vesicles within the bio-rich zone (Danin et al. 1998). Mosses generally do not produce surface crusts that block moisture flow (Eldridge and Rosentreter 2003). Presumably these crusts would permit air flow and thus could explain the lack of bio-rich vesicular pores associated with moss-dominated crusts. While these pores were only observed in tall moss-lichen pinnacled crusts, they could potentially form in earlier crust types given adequate conditions. My results also show BSCs actively form pores that eventually become vesicles. This air-trapping could form smooth margins of large irregular pores, similar to vesicle development. The air-trapping and expansion associated with these pores contributes to heaving and increased topographic relief along pinnacles.

Vesicular pores are ecologically important because these spherical voids are poorly connected, and thus, can impede water flow (Anderson et al. 2002, Meadows et al. 2008). Moreover, Av horizons, which contain high concentrations of these pores, are known to decrease infiltration rates in arid lands (Young et al. 2004, Wood et al. 2005, Meadows et al. 2008). Vesicular horizons impact where water infiltrates and runs off, and therefore, greatly influence vascular plant distributions (Hamerlynck et al. 2002,

Young et al. 2004, Wood et al. 2005, Meadows et al. 2008,). Micro-scale observations in this study show how vesicular pores may reduce water flow through the pinnacle mound. This water-trapping would provide a near-surface moisture reservoir that crust organisms could readily exploit. Overall, the dust trapping and surface sealing that forms vesicular pores enhances BSC growth by providing sources of both water and nutrients for these organisms.

Tall moss-lichen pinnacled crusts facilitate build-up of mineral Av horizons, a previously unrecognized biologically-mediated process. Dust accumulates below detached moss-lichen pinnacles during dry intervals, similar to dust accretion below desert pavement clasts (Figure 2.27)(McFadden et al. 1987, Wells et al. 1987). In this model, moss-lichen pinnacle mounds develop polygonal surface cracks (Figure 2.2C)(Danin et al. 1998) that are entry points for dust. These cracks are not seen in the cushion-like moss colonies that lie adjacent to pinnacles. My data could not sufficiently determine whether dust accumulation rates of these mosses increased or reduced mineral Av accumulation rates. Pinnacle mounds provide surface seals to protect dust and to facilitate vesicular pore formation (Springer 1958, Miller 1971, Evenari et al. 1974, Figueira and Stoops 1983, Sullivan and Koppi 1991). This dust accumulation produces mineral Av horizons up to 27 cm thick. This degree of accretion cannot be accounted for by traditional desert pavement dust capture models (McFadden et al. 1987, 1998, Anderson et al. 2002, Wood et al. 2005) because surface rock cover is generally 20% or less. Such low rock cover is insufficient for accumulation of thick, continuous dust layers (Goossens 1995). Therefore, I propose a new biological model of mineral Av

horizon formation, in which tall moss-lichen pinnacled crusts play a dominant role in dust accumulation (Figure 2.27).

Mineral Av accumulation below BSCs is a new step in the crust succession model that reflects prolonged surface stability (Figures 2.28). This time series is not based on chronosequence data. It assumes mineral Av thickness increases with time as dust incrementally accumulates (Figure 2.27)(McFadden et al. 1987, 1998, Anderson et al. 2002, Wood et al. 2005). A 27-cm-thick Av horizon reflects long periods of stability, as this dust accumulation may require hundreds to thousands of years (see Chapter 3). The dust accumulation by tall moss-lichen pinnacled crusts leads to the net accretion of material, despite the influence of micro-scale mass wasting processes.

Micro-scale Mass Wasting

Low magnitude mass wasting increases topographic complexity and forms intricate internal features in tall moss-lichen pinnacled crusts. Mass wasting is commonly associated with macro-scale geomorphic features. In tall moss-lichen pinnacle mounds, these same processes operate at the micro-scale. For example, toppling is a process commonly associated with the weathering of cliff faces (Figure 2.26)(Caine 1982) but also plays a role in the formation of bio-sediment bridges. Creep is widely recognized in hillslope evolution (Kirkby 1967) and produces some curved features observed in this study (Figure 2.22A). Sloughing or collapse form curved features and new voids (Figure 2.7C). Filaments typically aggregate suspended features (Belnap and Gardner 1993, Zhang 2005) involved in micro-scale mass wasting processes. Thus, biological filaments may augment the plasticity or integrity of these structures. Mass

wasting forms complex internal pores, cracks, and voids that can strongly influence water flow (Figure 2.8).

Implications for Hydrology

The influence of BSCs on surface hydrology has been highly debated. Some work indicates BSCs decrease infiltration and increase surface runoff (Yair 1990, Verrecchia et al. 1995, Mazor et al. 1996, Kidron et al. 1999, Eldridge et al. 2000, Marsh et al. 2006, Li et al. 2008), while others suggest crusts enhance infiltration (Perez 1997, Eldridge and Rosentreter 2003, Issa et al. 2009). Most studies agree organic structures of BSCs increase soil water-holding capacity (Booth 1941, Roberson and Firestone 1992, Verrecchia et al. 1995, Mazor et al. 1996, DeFalco et al. 2001, Issa et al. 2009, Rao et al. 2009). Discrepancies may be due to BSC organism structure or wettability, soil moisture content, measurement techniques, surface roughness, BSC successional age, degree of surface disturbance and soil morphology (Kidron et al. 1999, Belnap 2006, Kidron 2007, Eldridge et al. 2010, Fischer et al. 2010).

While I did not directly investigate soil water dynamics, my results show that surficial and internal structures vary as a function of BSC morphology, and that these features could strongly influence water distribution before, during, and after precipitation events. The micro-features identified in this study help explain previous conflicting results regarding the influence of BSCs on surface hydrology (Belnap 2006). (1) Some BSCs contain areas of dense vesicular pores (Figure 2.9). Vesicular pores in Av horizons have been shown to reduce infiltration rates (Young et al. 2004, Wood et al. 2005, Meadows et al. 2008). Therefore, well-developed Av horizons beneath some moss-lichen BSCs and vesicular pores within the bio-rich zone may explain previous studies that

reported increased runoff and decreased infiltration rates associated with some moss-lichen BSCs (Brotherson and Rushforth 1983, Eldridge et al. 2000, Li et al. 2008). Alternatively, those studies that found increased infiltration rates (Brotherson and Rushforth 1983, Eldridge and Rosentreter 2003) may have had BSCs that lacked vesicular pores or Av horizons. (2) BSCs contain irregular macropores (Figure 2.8). Depending on the size and connectivity of these pores, infiltration could be enhanced or decreased. (3) Irregular void space is also found between the bio-rich and bio-poor zones (Figures 2.4, 2.5, 2.6). This void space could potentially “perch” water within the upper bio-rich zone, increasing water availability for crust organisms. (4) Surface crusting and pore clogging would decrease infiltration but also could provide surface seals for decreased evapotranspiration. Soil water content, however, changes the degree of sealing and pore clogging (Yair 1990, Verrecchia et al. 1995, Mazor et al. 1996, Kidron et al. 1999, Fischer et al. 2010). (5) Surface cracking, along pinnacle surfaces or between pinnacle mounds would increase infiltration locally (Figures 2A, 7C)(Danin et al. 1998, Meadows et al. 2008). Surface cracking is ephemeral and would change with the water content of the soil (Danin et al. 1998) as induced by rainfall timing, amount, and intensity (Meadows et al. 2008). For example, cracking present at the beginning of a rainfall event would initially allow significant infiltration, but later expansion due to wetting would close cracks and reduce infiltration. (6) The rugose nature of BSC pinnacles potentially slows runoff (Figure 2.2C), while smooth cyanobacterial crusts and associated surface seals may increase runoff (Figure 2.1A)(Belnap 2006, Kidron 2007). (7) Laminae are common features within BSCs (Figures 2.7A, 2.7B). Any lamination, such as particle size, compaction, or cementation would slow infiltration and induce horizontal flow. The

distribution of these surface features could control BSC impacts on water dynamics, with effects being highly localized and variable. These observations show restoration of BSCs and ecological function requires more than reestablishment of crust organisms. The mineral dust and bio-sedimentary features of BSCs must be restored for natural hydrological dynamics to return. However, the rate at which those processes occur is still unknown.

Several gaps in our knowledge of BSC genesis remain. My study did not directly investigate the connection between the filament-rich zone and underlying soil substrates. Surface cracks across pinnacles, and polygonal cracks around pinnacle mounds suggest pinnacles could act like surface pavement clasts in dust accretion. Direct investigation of the pinnacle mound base is needed to better understand Av horizon formation at depths below those examined in study. While sedimentary features support morphotype-specific controls on BSC development, my results are purely observational. Experimental data would help solidify my proposed models. The observational nature of this study also prevents development time constraint. Long-term field-based experiments combined with micromorphological data collection would provide insight into the timing of stabilization, accretion, and mass-wasting processes.

Conclusions

Well-developed moss-lichen pinnacles are complex agglomerations of sedimentary and biotic structures that develop through dynamic surface processes: (1) grain trapping and binding by biotic structures; (2) dust capture; (3) authigenic mineral precipitation; (4) surface sealing and erosion mitigation by biological, physical, and

chemical cements; (5) expansion and contraction from wetting and drying cycles; (6) mass wasting processes, including toppling, creep, sloughing, and collapse; (7) bio-rich vesicular pore formation and heaving; and (8) dust accumulation and mineral Av horizon formation. The relative influence of these processes changes as a function of crust succession and component organisms.

The dynamic processes forming BSCs strongly influence pedogenesis, landscape evolution, and hydrologic function. A new model Av horizon development proposes that BSC dust accretion and surface sealing create vesicular pores in the bio-rich zone and form mineral Av horizons below moss-lichen pinnacles. Vesicular pores do not form readily below moss-dominated crusts that form poor surface seals. BSC dust capture supplies fine-grained materials to the soil surface, which modifies meter-scale surface topography, alters landform surface characteristics, and increases soil water-holding capacity. BSCs form unique internal and surficial bio-sedimentary structures that trap water for uptake by crust organisms. I propose BSCs be recognized as crucial agents in arid pedogenesis and landscape evolution because they play a unique role in the accumulation, morphology, ecological function of captured dust.

Literature Cited

- Allwood A. C., M. R. Walter, B. S. Kamber, C. P. Marshall, and I. W. Burch. 2006. Stromatolite reef from the Early Archaean era of Australia. *Nature* **441**:714-718.
- Anderson K., S. Wells, and R. Graham. 2002. Pedogenesis of vesicular horizons, Cima Volcanic Field, Mojave Desert, California. *Soil Science Society of America Journal* **66**:878-887.
- Bachman GO, Machette MN. 1977. Calcic soils and calcretes in the Southwestern United States. USGS Open-File Report 77-794. 163 pp.
- Belnap J. 2006. The potential roles of biological soil crusts in dryland hydrologic cycles. *Hydrological Processes* **20**:3159-3178.
- Belnap J. 2003. The world at your feet: Desert biological soil crusts. *Frontiers in Ecology and the Environment* **1**:181-189.
- Belnap J. 2001. Comparative structure of physical and biological soil crusts. Pages 177-191 *In* J. Belnap and O. L. Lange, editors. *Biological Soil Crusts: Structure, Function, and Management*, Springer-Verlag, Berlin.
- Belnap J. 1998. Environmental auditing choosing indicators of natural resource condition: A case study in Arches National Park, Utah, USA. *Environmental Management* **22**:635-642.
- Belnap J. 1995. Surface disturbances: their role in accelerating desertification. *Environmental Monitoring and Assessment* **37**:39-57.
- Belnap J., S. D. Warren. 2002. Patton's tracks in the Mojave Desert, USA: An ecological legacy. *Arid Land Research and Management* **16**:245-258.
- Belnap J., J. S. Gardner. 1993. Soil microstructure in soils of the Colorado Plateau: The role of the cyanobacterium *Microcoleus vaginatus*. *Great Basin Naturalist* **53**:40-47.
- Belnap J., C. V. Hawkes, and M. K. Firestone. 2003. Boundaries in miniature: Two examples from soil. *BioScience* **53**:739-749.
- Berkeley A., A. D. Thomas, and A. J. Dougill. 2005. Cyanobacterial soil crusts and woody shrub canopies in Kalahari rangelands. *African Journal of Ecology* **43**:137-145.
- Black M. 1933. The algal sediments of Andros Islands, Bahamas. *Royal Society of London Philosophical Transactions Series B*:165-192.

- Booth W. E. 1941. Algae as pioneers in plant succession and their importance in erosion control. *Ecology* **22**:38-46.
- Bowker M. A., J. Belnap. 2008. A simple classification of soil types as habitats of biological soil crusts on the Colorado Plateau, USA. *Journal of Vegetation Science* **19**:831-840.
- Bowker M. A., J. Belnap, V. B. Chaudhary, and N. C. Johnson. 2008. Revisiting classic water erosion models in drylands: The strong impact of biological soil crusts. *Soil Biology & Biochemistry* **40**:2309-2316.
- Bowker M. A., J. Belnap, D. W. Davidson, and H. Goldstein. 2006. Correlates of biological soil crust abundance across a continuum of spatial scales: support for a hierarchical conceptual model. *Journal of Applied Ecology* **43**:152-163.
- Braissant O., E. P. Verrecchia, and M. Aragno. 2002. Is the contribution of bacteria to terrestrial carbon budget greatly underestimated? *Naturwissenschaften* **89**:366-370.
- Braissant O., G. Cailleau, C. Dupraz, and E. P. Verrecchia. 2003. Bacterially induced mineralization of calcium carbonate in terrestrial environments: The roles of exopolysaccharides and amino acids. *Journal of Sedimentary Research* **73**:485-490.
- Brotherson J. D., S. R. Rushforth. 1983. Influence of cryptogamic crusts on moisture relationships of soils in Navajo National Monument, Arizona. *Great Basin Naturalist* **43**:73-78.
- Budel B., T. Darienko, K. Deutschewitz, S. Dojani, T. Friedl, K. I. Mohr, M. Salisch, W. Reisser, and B. Weber. 2009. Southern African biological soil crusts are ubiquitous and highly diverse in drylands, being restricted by rainfall frequency. *Microbial Ecology* **57**:229-247.
- Buick R., J. S. R. Dunlop, and D. I. Groves. 1981. Stromatolite recognition in ancient rocks: an appraisal of irregularly laminated structures in an Early Archaean chert-barite unit from North Pole, Western Australia. *Alcheringa* **5**:161-181.
- Caine N. 1982. Toppling failures from alpine cliffs on Ben Lomond, Tasmania. *Earth Surface Processes and Landforms* **7**:133-152.
- Campbell S. E. 1979. Soil stabilization by a prokaryotic desert crust: Implications for Precambrian land biota. *Origins of Life* **9**:335-348.
- Campbell S. E., J. Seeler, and S. Golubic. 1989. Desert crust formation and soil stabilization. *Arid Soil Research and Rehabilitation* **3**:217-228.

- Canton Y., A. Sole-Benet, and R. Lazaro. 2003. Soil–geomorphology relations in gypsiferous materials of the Tabernas Desert (Almeria, SE Spain). *Geoderma* **115**:193-222.
- Chaudhary V. B., M. A. Bowker, T. E. O'Dell, J. B. Grace, A. E. Redman, M. C. Rilling, and N. C. Johnson. 2009. Untangling the biological contributions to soil stability in semiarid shrublands. *Ecological Applications* **19**:110-122.
- Csotonyi J. T., J. F. Addicott. 2004. Influence of trampling-induced microtopography on growth of the soil crust bryophyte *Ceratodon purpureus* in Jasper National Park. *Canadian Journal of Botany* **82**:1382-1392.
- Danin A., E. Ganor. 1991. Trapping of airborne dust by mosses in the Negev Desert, Israel. *Earth Surface Processes and Landforms* **16**:153-162.
- Danin A., I. Dor, A. Sandler, and R. Amit. 1998. Desert crust morphology and its relations to microbiotic succession at Mt. Sedom, Israel. *Journal of Arid Environments* **38**:161-174.
- Davidson D. W., M. A. Bowker, D. George, S. L. Phillips, and J. Belnap. 2002. Treatment effects on performance of N-fixing lichens in disturbed soil crusts of the Colorado Plateau. *Ecological Applications* **12**:1391-1405.
- DeFalco L. A., J. K. Detling, C. R. Tracy, and S. D. Warren. 2001. Physiological variation among native and exotic winter annual plants associated with microbiotic crusts in the Mojave Desert. *Plant and Soil* **234**:1-14.
- Deutz P., I. P. Montanez, and H. C. Monger. 2002. Morphology and stable and radiogenic isotope composition of pedogenic carbonates in late Quaternary relict soils, New Mexico, U.S.A.: An integrated record of pedogenic overprinting. *Journal of Sedimentary Research* **72**:809-822.
- Dupraz C., P. T. Visscher. 2005. Microbial lithification in marine stromatolites and hypersaline mats. *TRENDS in Microbiology* **13**:429-438.
- Dupraz C., R. P. Reid, O. Braissant, A. W. Decho, R. S. Norman, and P. T. Visscher. 2009. Processes of carbonate precipitation in modern microbial mats. *Earth-Science Reviews* **96**:141-162.
- Elbert W., B. Weber, B. Budel, M. O. Andreae, and U. Pöschl. 2009. Microbiotic crusts on soil, rock and plants: neglected major players in the global cycles of carbon and nitrogen? *Biogeosciences Discuss.* **6**:6983-7015.
- Eldridge DJ, Rosentreter R. 2003. Shrub mounds enhance waterflow in a shrub-steppe community in southwestern Idaho, U.S.A. USDA Forest Service, Rocky Mountain Research Station Forest Service Proceedings RMRS-P-000. Ogden, UT, p. 1-8.

- Eldridge D. J., J. F. Leys. 2003. Exploring some relationships between biological soil crusts, soil aggregation and wind erosion. *Journal of Arid Environments* **53**:457-466.
- Eldridge D. J., R. Rosentreter. 1999. Morphological groups: a framework for monitoring microphytic crusts in arid landscapes. *Journal of Arid Environments* **41**:11-25.
- Eldridge D. J., R. S. B. Greene. 1994. Microbiotic soil crusts: A review of their roles in soil and ecological processes in the rangelands of Australia. *Australian Journal of Soil Research* **32**:389-415.
- Eldridge D. J., E. Zaady, and M. Shachak. 2000. Infiltration through three contrasting biological soil crusts in patterned landscapes in the Negev, Israel. *Catena* **40**:323-336.
- Eldridge D. J., M. A. Bowker, F. T. Maestre, P. Alonso, R. L. Mau, J. Papadopoulos, and A. Escudero. 2010. Interactive Effects of Three Ecosystem Engineers on Infiltration in a Semi-Arid Mediterranean Grassland. *Ecosystems* **13**:499-510.
- Escudero A., I. Martinez, A. de la Cruz, M. A. G. Otalora, and F. T. Maestre. 2007. Soil lichens have species-specific effects on the seedling emergence of three gypsophile plant species. *Journal of Arid Environments* **70**:18-28.
- Evans R. D., J. Belnap. 1999. Long-Term consequences of disturbance on nitrogen dynamics in an arid ecosystem. *Ecology* **80**:150-160.
- Evenari M., D. H. Yaalon, and Y. Gutterman. 1974. Note on soils with vesicular structure in deserts. *Zeitschrift fur Geomorphologie N.F.* **18**:162-172.
- Ferrer M. R., J. Quevedo-Sarmiento, M. A. Rivadeneyra, V. Bejar, R. Delgado, and A. Ramos-Cormenzana. 1988. Calcium carbonate precipitation by two groups of moderately halophilic microorganisms at different temperatures and salt concentrations. *Current Microbiology* **17**:221-227.
- Field J. P., J. Belnap, D. D. Breshears, J. C. Neff, G. S. Okin, J. J. Whicker, T. H. Painter, S. Ravi, M. C. Reheis, and R. L. Reynolds. 2010. The ecology of dust. *Frontiers in Ecology and the Environment* **8**:423-430.
- Figueira H., G. Stoops. 1983. Application of micromorphometric techniques to the experimental study of vesicular layer formation. *Pedologie* **33**:77-89.
- Fischer T., M. Veste, W. Wiehe, and P. Lange. 2010. Water repellency and pore clogging at early successional stages of microbiotic crusts on inland dunes, Brandenburg, NE Germany. *Catena* **80**:47-52.
- Folk R. L. 1974. The natural history of crystalline calcium carbonate: Effect of magnesium content and salinity. *Journal of Sedimentary Petrology* **44**:40-53.

- Friedmann E. I., M. Galun. 1974. Desert algae, lichens and fungi. Pages 165-212 *In* G. W. Brown, editor. Desert Biology, Academic Press, New York.
- Gadd G. M. 2007. Geomycology: biogeochemical transformations of rocks, minerals, metals and radionuclides by fungi, bioweathering and bioremediation. *Mycological Research* **111**:3-49.
- Garcia-Pichel F., O. Pringault. 2001. Cyanobacteria track water in desert soils. *Nature* **413**:380-381.
- Garcia-Pichel F., J. Belnap. 2001. Small-scale environments and distribution of biological soil crusts. Pages 193-201 *In* J. Belnap and O. L. Lange, editors. Biological Soil Crusts: Structure, Function, and Management. Springer, Berlin.
- Garcia-Pichel F., S. L. Johnson, D. Youngkin, and J. Belnap. 2003. Small-scale vertical distribution of bacterial biomass and diversity in biological soil crusts from arid lands in the Colorado Plateau. *Microbial Ecology* **46**:312-321.
- Garrett D. E. 2004. Part 2 - Calcium Chloride. Pages 237-457 *In* Anonymous Handbook of Lithium and Natural Calcium Chloride, Elsevier, Amsterdam.
- Gerdes G., T. Klenke, and N. Noffke. 2000. Microbial signatures in peritidal siliciclastic sediments: A catalogue. *Sedimentology* **47**:279-308.
- Gile L. H., F. F. Peterson, and R. B. Grossman. 1966. Morphological and genetic sequences of carbonate accumulation. *Soil Science* **101**:347-360.
- Gonzalez-Munoz M. T., K. B. Chekroun, A. B. Aboud, J. M. Arias, and M. Rodriguez-Gallego. 2000. Bacterially induced Mg-calcite formation: Role of Mg²⁺ in development of crystal morphology. *Journal of Sedimentary Research* **70**:559-564.
- Goossens D. 1995. Field experiments of aeolian dust accumulation on rock fragment substrata. *Sedimentology* **42**:391-402.
- Gorelow A. S., P. H. Skrbac. 2005. Climate of Las Vegas, NV. National Weather Service, Las Vegas, NV.
- Grotzinger J. P., A. H. Knoll. 1999. Stromatolites in Precambrian carbonates: Evolutionary mileposts or environmental dipsticks? *Annu. Rev. Earth Planet. Sci.* **27**:313-358.
- Hamerlynck E. P., J. R. McAuliffe, E. V. McDonald, and S. D. Smith. 2002. Ecological responses of two Mojave Desert shrubs to soil horizon development and soil water dynamics. *Ecology* **83**:768-779.

- Hammes F., W. Verstraete. 2002. Key roles of pH and calcium metabolism in microbial carbonate precipitation. *Reviews in Environmental Science & Biotechnology* **1**:3-7.
- Issa O. M., C. Defarge, J. Trichet, C. Valentin, and J. L. Rajot. 2009. Microbiotic soil crusts in the Sahel of Western Niger and their influence on soil porosity and water dynamics. *Catena* **77**:48-55.
- Issa O. M., J. Trichet, C. Defarge, A. Coute, and C. Valentin. 1999. Morphology and microstructure of microbiotic soil crusts on a tiger bush sequence (Niger, Sahel). *Catena* **37**:175-196.
- Issa O. M., C. Defarge, Y. L. Bissonais, B. Marin, O. Duval, A. Bruand, L. P. D'Acqui, S. Nordenberg, and M. Annerman. 2007. Effects of the inoculation of cyanobacteria on the microstructure and the structural stability of a tropical soil. *Plant Soil* **290**:209-219.
- Kidron G. J. 2007. Millimeter-scale microrelief affecting runoff yield over microbiotic crust in the Negev Desert. *Catena* **70**:266-273.
- Kidron G. J., A. Vonshak, and A. Abeliovich. 2008. Recovery rates of microbiotic crusts within a dune ecosystem in the Negev Desert. *Geomorphology* **100**:444-452.
- Kidron G. J., D. H. Yaalon, and A. Vonshak. 1999. Two causes for runoff initiation on microbiotic crusts: Hydrophobicity and pore clogging. *Soil Science* **164**:18-27.
- Kidron G. J., A. Vonshak, I. Dor, S. Barinova, and A. Abeliovich. 2010. Properties and spatial distribution of microbiotic crusts in the Negev Desert, Israel. *Catena* **82**:92-101.
- Kirkby M. J. 1967. Measurement and theory of soil creep. *Journal of Geology* **75**:359-378.
- Kleiner E. F., K. T. Harper. 1977. Soil properties in relation to cryptogamic groundcover in Canyonlands National Park. *Journal of Range Management* **30**:202-205.
- Lange O. L., J. Belnap, and H. Reichenberger. 1998. Photosynthesis of the cyanobacterial soil-crust lichen *Collema tenax* from arid lands in southern Utah, USA: Role of water content on light and temperature responses of CO₂ exchange. *Functional Ecology* **12**:195-202.
- Langhans T. M., C. Storm, and A. Schwabe. 2010. Regeneration processes of biological soil crusts, macro-cryptogams and vascular plant species after fine-scale disturbance in a temperate region: Recolonization or successional replacement? *Flora* **205**:46-60.
- Lazaro R., Y. Canton, A. Sole-Benet, J. Bevan, R. Alexander, L. G. Sancho, and J. Puigdefabregas. 2008. The influence of competition between lichen colonization and

- erosion on the evolution of soil surfaces in the Tabernas badlands (SE Spain) and its landscape effects. *Geomorphology* **102**:252-266.
- Li X. J., X. R. Li, W. M. Song, Y. P. Gao, J. G. Zheng, and R. L. Jia. 2008. Effects of crust and shrub patches on runoff, sedimentation, and related nutrient (C, N) redistribution in the desertified steppe zone of the Tengger Desert, Northern China. *Geomorphology* **96**:221-232.
- Li X. R., X. H. Jia, L. Q. Long, and S. Zerbe. 2005. Effects of biological soil crusts on seed bank, germination and establishment of two annual plant species in the Tengger Desert (N China). *Plant and Soil* **277**:375-385.
- Li X. R., M. Z. He, S. Zerbe, X. J. Li, and L. C. Liu. 2010. Micro-geomorphology determines community structure of biological soil crusts at small scales. *Earth Surface Processes and Landforms* **35**:932-940.
- Li X. Y., L. Y. Liu, and J. H. Wang. 2004. Wind tunnel simulation of aeolian sandy soil erodibility under human disturbance. *Geomorphology* **59**:3-11.
- Lian B., Q. Hu, J. Chen, J. Ji, and H. H. Teng. 2006. Carbonate biomineralization induced by soil bacterium *Bacillus megaterium*. *Geochimica et Cosmochimica Acta* **70**:5522-5535.
- Loisy C., E. P. Verrecchia, and P. Dufour. 1999. Microbial origin for pedogenic micrite associated with a carbonate paleosol (Champagne, France). *Sedimentary Geology* **126**:193-204.
- Machette M. N. 1985. Calcic soils of the southwestern United States. Pages 1-21 *In* D. L. Weide, editor. *Soils and Quaternary geomorphology of the southwestern United States*, Geological Society of America, Boulder, CO.
- Marsh J., S. Nouvet, P. Sanborn, and D. Coxson. 2006. Composition and function of biological soil crust communities along topographic gradients in grasslands of central British Columbia (Chilcotin) and southwestern Yukon (Kluane). *Canadian Journal of Botany* **84**:717-736.
- Marticorena B., G. Bergametti, D. Gillette, and J. Belnap. 1997. Factors controlling threshold friction velocity in semiarid and arid areas of the United States. *Journal of Geophysical Research* **102**:23277-23287.
- Mazor G., G. J. Kidron, A. Vonshak, and A. Abeliovich. 1996. The role of cyanobacterial exopolysaccharides in structuring desert microbial crusts. *FEMS Microbiology Ecology* **21**:121-130.

- McFadden L. D., S. G. Wells, and M. J. Jercinovich. 1987. Influences of eolian and pedogenic processes on the origin and evolution of desert pavements. *Geology* **15**:504-508.
- McFadden L. D., E. V. McDonald, S. G. Wells, K. Anderson, J. Quade, and S. L. Forman. 1998. The vesicular layer and carbonate collars of desert soils and pavements: formation, age and relation to climate change. *Geomorphology* **24**:101-145.
- McKenna Neuman C., C. D. Maxwell, and J. W. Boulton. 1996. Wind transport of sand surfaces crusted with photoautotrophic microorganisms. *Catena* **27**:229-247.
- McTainsh G., C. Strong. 2007. The role of aeolian dust in ecosystems. *Geomorphology* **89**:39-54.
- Meadows D. G., M. H. Young, and E. V. McDonald. 2008. Influence of relative surface age on hydraulic properties and infiltration on soils associated with desert pavements. *Catena* **72**:169-178.
- Miller D. E. 1971. Formation of vesicular structure in soil. *Soil Science Society of America Journal* **35**:635-637.
- Monger H. C., L. A. Daugherty, W. C. Lindemann, and C. M. Liddell. 1991. Microbial precipitation of pedogenic calcite. *Geology* **19**:997-1000.
- Nagy M. L., J. R. Johansen, L. L. St. Clair, and B. L. Webb. 2005. Recovery patterns of microbiotic soil crusts 70 years after arsenic contamination. *Journal of Arid Environments* **63**:304-323.
- Nash T. H. 2008. Nutrients, elemental accumulation, and mineral cycling. Pages 234-251 *In* T. H. Nash, editor. *Lichen Biology*, Cambridge University Press, Cambridge.
- Noffke N. 2009. The criteria for the biogenicity of microbially induced sedimentary structures (MISS) in Archean and younger, sandy deposits. *Earth-Science Reviews* **96**:173-180.
- Noffke N. 2008. Turbulent lifestyle: Microbial mats on Earth's sandy beaches—Today and 3 billion years ago. *GSA Today* **18**:4-9.
- Noffke N., R. Hazen, and N. Nhleko. 2003a. Earth's earliest microbial mats in a siliciclastic marine environment (2.9 Ga Mozaan Group, South Africa). *Geology* **31**:673-676.
- Noffke N., G. Gerdes, and T. Klenke. 2003b. Benthic cyanobacteria and their influence on the sedimentary dynamics of peritidal depositional systems (siliciclastic, evaporitic salty, and evaporitic carbonatic). *Earth-Science Reviews* **62**:163-176.

- Noffke N., A. H. Knoll, and J. P. Grotzinger. 2002. Sedimentary controls on the formation and preservation of microbial mats in siliciclastic deposits: A case study from the upper Neoproterozoic Nama Group, Namibia. *PALAIOS* **17**:533-544.
- Noffke N., G. Gerdes, T. Klenke, and W. E. Krumbein. 2001a. Microbially induced sedimentary structures – A new category within the classification of primary sedimentary structures. *Journal of Sedimentary Research*, **71**:649-646.
- Noffke N., G. Gerdes, T. Klenke, and W. E. Krumbein. 2001b. Microbially induced sedimentary structures indicating climatological, hydrological and depositional conditions within recent and Pleistocene coastal facies zones (southern Tunisia). *Facies* **44**:23-30.
- Nordt L. C., L. P. Wilding, W. C. Lynn, and C. C. Crawford. 2004. Vertisol genesis in a humid climate of the coastal plain of Texas, U.S.A. *Geoderma* **122**:83-102.
- Perez F. L. 1997. Microbiotic crusts in the high equatorial Andes, and their influence on paramo soils. *Catena* **173-198**..
- Peterson FF. Landforms of the Basin and Range, Defined for Soil Survey. Reno: UNR Max C.Fleishmann College of Agriculture, Nevada Agricultural Experiment Station; 1981. Report nr Technical Bulletin 28. 52 pp p.
- Phillips S. E., A. R. Milnes, and R. C. Foster. 1987. Calcified filaments - an example of biological influences in the formation of calcrete in South Australia. *Australian Journal of Soil Research* **25**:405-428.
- Pluis J. L. A., B. de Winder. 1989. Spatial patterns in algae colonization of dune blowouts. *Catena* **16**:499-506.
- Plummer P. S., V. A. Gostin. 1981. Shrinkage cracks: Desiccation or syneresis. *Journal of Sedimentary Petrology* **51**:1147-1156.
- Ponzetti J. M., B. P. McCune. 2001. Biotic soil crusts of Oregon's shrub steppe: Community composition in relation to soil chemistry, climate, and livestock activity. *The Bryologist* **104**:212-225.
- Rao B., Y. Liu, W. Wang, C. Hu, L. Dunhai, and S. Lan. 2009. Influence of dew on biomass and photosystem II activity of cyanobacterial crusts in the Hopq Desert, northwest China. *Soil Biology & Biochemistry* **41**:2387-2393.
- Reheis M., J. R. Budahn, P. J. Lamothe, and R. L. Reynolds. 2009. Compositions of modern dust and surface sediments in the Desert Southwest, United States. *Journal of Geophysical Research* **114**:F01028.

- Reheis M. C. 1990. Influence of climate and eolian dust on the major-element chemistry and clay mineralogy of soils in the northern Bighorn Basin, U.S.A. *Catena* **17**:219-248.
- Reheis M. C., J. R. Budahn, and P. J. Lamothe. 2002. Geochemical evidence for diversity of dust sources in the southwestern United States. *Geochimica et Cosmochimica Acta* **66**:1569-1587.
- Reheis M. C., J. C. Goodmacher, J. W. Harden, L. D. McFadden, T. K. Rockwell, R. R. Shroba, J. M. Sowers, and E. M. Taylor. 1995. Quaternary soils and dust deposition in southern Nevada and California. *GSA Bulletin* **107**:1003-1022.
- Reid R. P., P. T. Visscher, A. W. Decho, J. F. Stolz, B. M. Bebout, C. Dupraz, I. G. MacIntyre, H. W. Pearl, J. L. Pinckney, L. Prufert-Bebout, T. F. Steppe, and D. J. DesMarais. 2000. The role of microbes in accretion, lamination and early lithification of modern marine stromatolites. *Nature* **406**:989-991.
- Reynolds R., J. Neff, M. Reheis, and P. Lamothe. 2006. Atmospheric dust in modern soil on aeolian sandstone, Colorado Plateau (USA): Variation with landscape position and contribution to potential plant nutrients. *Geoderma* **130**:108-123.
- Reynolds R., J. Belnap, M. C. Reheis, P. J. Lamothe, and F. Luiszer. 2001. Aeolian dust in Colorado Plateau soils: Nutrient inputs and recent change in source. *PNAS* **98**:7123-7127.
- Rivadeneira M. A., G. Delgado, A. Ramos-Cormenzana, and R. Delgado. 1998. Biomineralization of carbonates by *Halomonas eurihalina* in solid and liquid media with different salinities: crystal formation sequence. *Res. Microbiol.* **149**:277-287.
- Rivadeneira M. A., A. Ramos-Cormenzana, G. Delgado, and R. Delgado. 1996. Process of carbonate precipitation by *Deleya halophila*. *Current Microbiology* **32**:308-313.
- Rivadeneira M. A., R. Delgado, E. Quesada, and A. Ramos-Cormenzana. 1991. Precipitation of calcium carbonate by *Deleya halophila* in media containing NaCl as sole salt. *Current Microbiology* **22**:185-190.
- Rivadeneira M. A., I. Perez-Garcia, V. Salmeron, and A. Ramos-Cormenzana. 1985. Bacterial precipitation of calcium carbonate in presence of phosphate. *Soil Biology & Biochemistry* **17**:171-172.
- Roberson E. B., M. K. Firestone. 1992. Relationship between desiccation and exopolysaccharide production in a soil *Pseudomonas* sp.. *Applied and Environmental Microbiology* **58**:1284-1291.
- Shachak M., G. M. Lovett. 1998. Atmospheric deposition to a desert ecosystem and its implications for management. *Ecological Applications* **8**:455-463.

- Simonson R. W. 1995. Airborne dust and its significance to soils. *Geoderma* **65**:1-43.
- Soil Survey Staff. 2010a. Official Soil Series Descriptions. USDA-NRCS, Washington, D.C.
- Soil Survey Staff. 2010b. Keys to Soil Taxonomy. USDA-NRCS, Washington, D.C.
- Springer M. E. 1958. Desert pavement and vesicular layer of some soils of the desert of the Lahontan Basin, Nevada. *Soil Science Society of America Journal* **22**:63-66.
- Stoops G. 2003. Guidelines for Analysis and Description of Soil and Regolith Thin Sections. Soil Science Society of America, Madison, Wisconsin, USA.
- Sullivan L. A., A. J. Koppi. 1991. Morphology and genesis of silt and clay coatings in the vesicular layer of a desert loam soil. *Australian Journal of Soil Research* **29**:579-586.
- Thomas A. D., A. J. Dougill. 2007. Spatial and temporal distribution of cyanobacterial soil crusts in the Kalahari: Implications for soil surface properties. *Geomorphology* **85**:17-29.
- Tisdall J. M., J. M. Oades. 1982. Organic matter and water-stable aggregates in soils. *Journal of Soil Science* **33**:141-163.
- Verrecchia E. P., A. Yair, G. J. Kidron, and K. Verrecchia. 1995. Physical properties of the psammophile cryptogamic crust and their consequences to the water regime of sandy soils, north-western Negev Desert, Israel. *Journal of Arid Environments* **29**:427-437.
- Warren J. K. 2010. Evaporites through time: Tectonic, climatic and eustatic controls in marine and nonmarine deposits. *Earth-Science Reviews* **98**:217-268.
- Wells S. G., J. C. Dohrenwend. 1985. Relict sheetflood bed forms on late Quaternary alluvial-fan surfaces in the southwestern United States. *Geology* **13**:512-516.
- Wells S. G., L. D. McFadden, and J. C. Dohrenwend. 1987. Influence of late Quaternary climatic changes on geomorphic and pedogenic processes on a desert piedmont, eastern Mojave Desert, California. *Quaternary Research* **27**:130-146.
- Williams W. J., D. J. Eldridge, and B. M. Alchin. 2008. Grazing and drought reduce cyanobacterial soil crusts in an Australian Acacia woodland. *Journal of Arid Environments* **72**:1064-1075.
- Wood Y. A., R. C. Graham, and S. G. Wells. 2005. Surface control of desert pavement pedologic process and landscape function, Cima Volcanic field, Mojave Desert, California. *Catena* **59**:205-230.

- Wu N., Y. M. Zhang, H. X. Pan, and J. Zhang. 2010. The role of nonphotosynthetic microbes in the recovery of biological soil crusts in the Gurbantunggut Desert, northwestern China. *Arid Land Research and Management* **24**:42-56.
- Wynn-Williams D. D. 1990. Microbial colonization processes in Antarctic fellfield soils - an experimental overview. *Proc. NIPR Symp. Polar Biol* **3**:164-178.
- Yaalon D. H., D. Kalmar. 1972. Vertical movement in an undisturbed soil: Continuous measurement of swelling and shrinkage with a sensitive apparatus. *Geoderma* **8**:231-240.
- Yair A. 1990. Runoff generation in a sandy area - the Nizzana Sands, Western Negev, Israel. *Earth Surface Processes and Landforms* **15**:597-609.
- Young M. H., E. V. McDonald, T. G. Caldwell, S. G. Benner, and D. G. Meadows. 2004. Hydraulic properties of a desert soil chronosequence in the Mojave Desert, USA. *Vadose Zone Journal* **3**:956-963.
- Zaady E., Z. Y. Offer. 2010. Biogenic soil crusts and soil depth: a long-term case study from the Central Negev desert highland. *Sedimentology* **57**:351-358.
- Zhang Y. 2005. The microstructure and formation of biological soil crusts in their early developmental stage. *Chinese Science Bulletin* **50**:117-121.

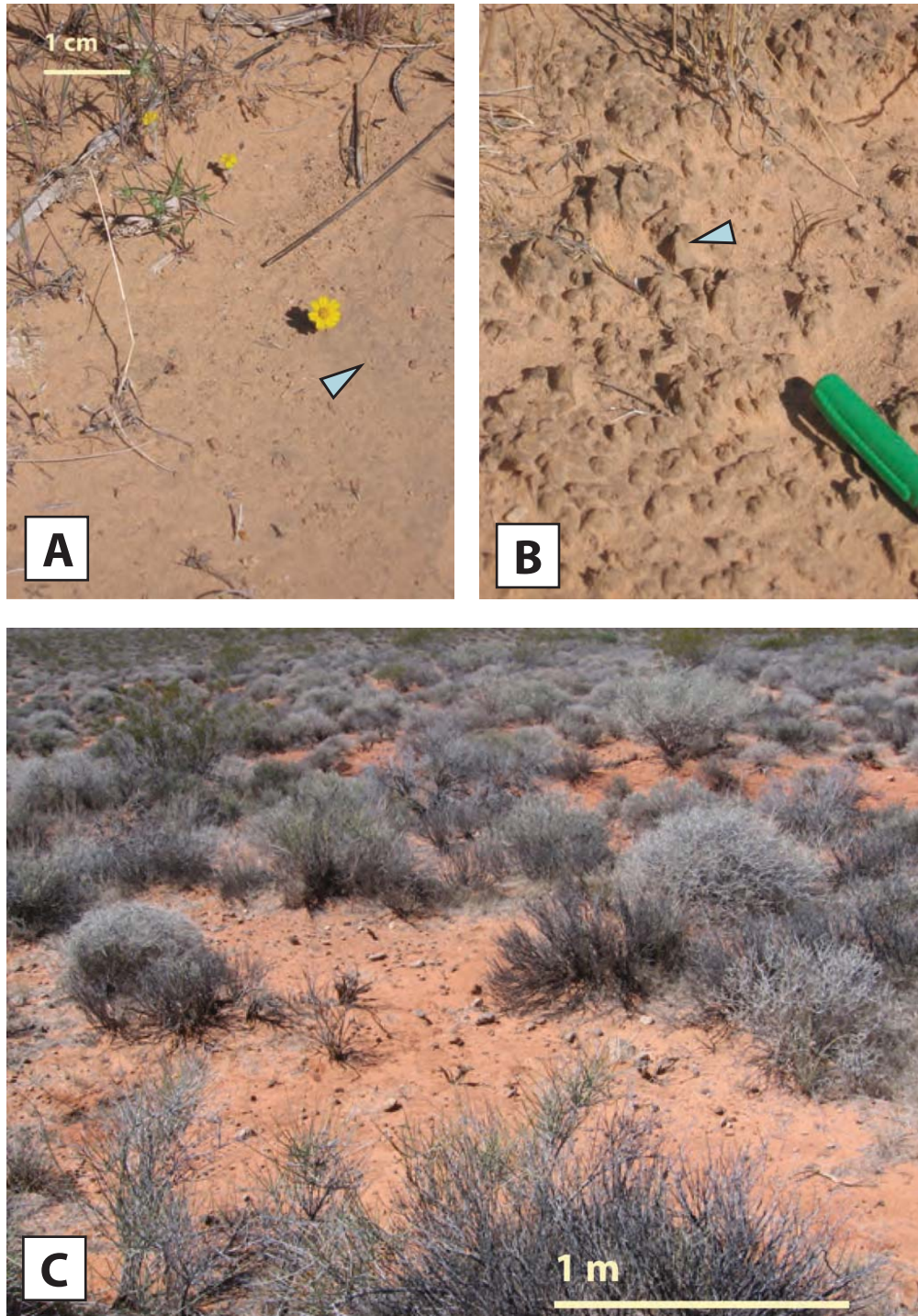


Figure 2.1: (A) Smooth cyanobacteria crusts have a slightly darkened surfaces with visible crusting. (B) Cyanobacteria-dominated crusts may have knob-like (arrow) surface protrusions that also display surface darkening (marker for scale). (C) Cyanobacterial crusts form smooth, light colored surfaces between shrubs.

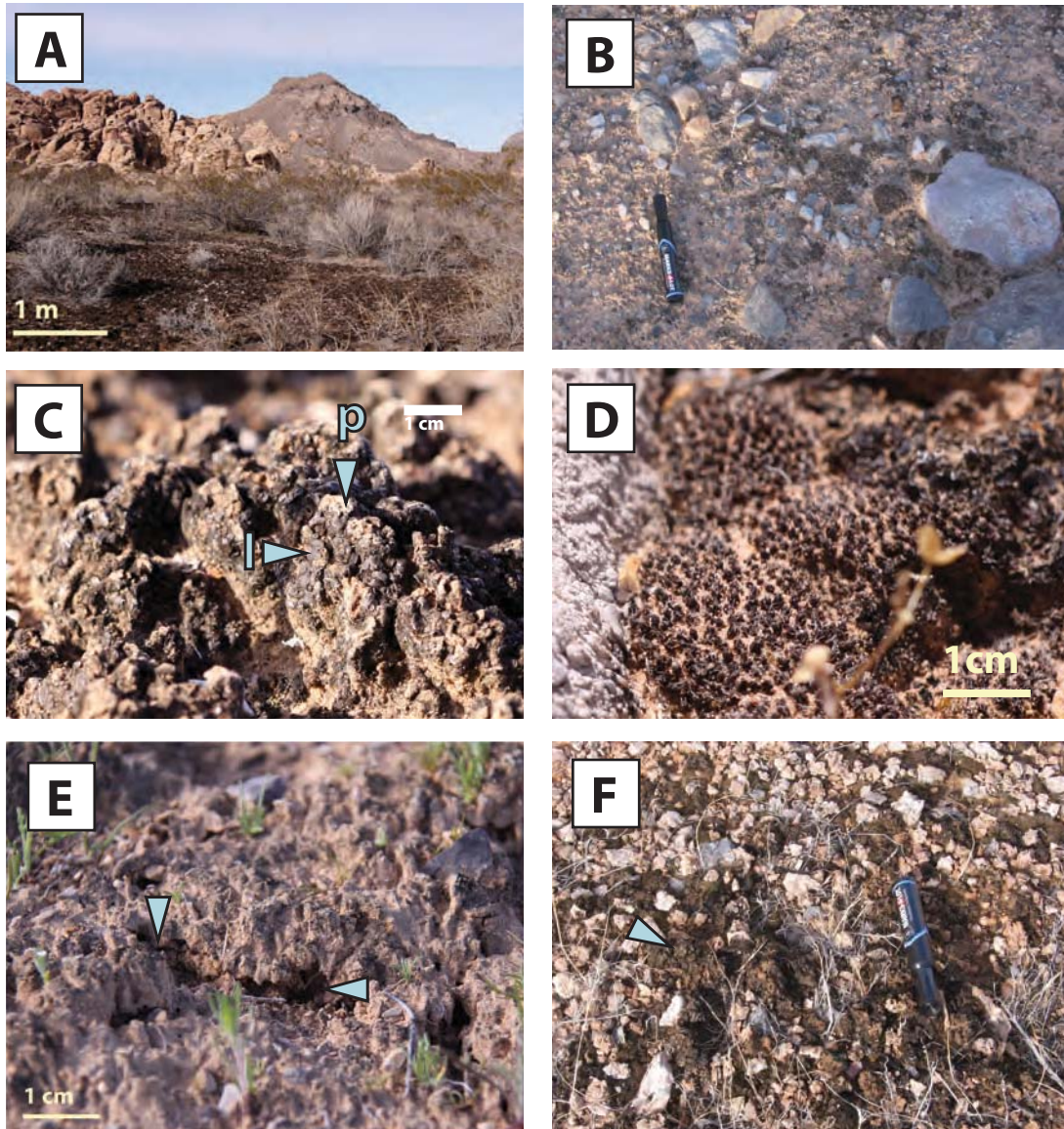


Figure 2.2: (A) Moss-lichen crusts have dark, rough surfaces that protect shrub interspaces from erosion (scale 1 m). (B) Short moss-lichen crusts are common in recent Holocene inset fans and have low surface relief, up to 2 cm (marker for scale). (C) Tall moss-lichen pinnaced crusts are composed of complex matrices of mosses, lichens, cyanobacteria, and sediments. Squamulose lichens (l) dominate this crust. Note the white-colored pinnacle summits that are cemented with calcium carbonate (p)(scale 1 cm). (D) Moss-dominated crusts have a rolling surface morphology and low topographic relief. Eolian sand grains accumulate along the moss surface (1 cm scale). (E) Dry moss-lichen pinnacles show vertical cracking (vertical arrow) between pinnacle mounds. Cracks may also occur below pinnacle mounds (horizontal arrow), separating the crust from the mineral soil below (scale 1 cm). (F) Tall moss-lichen pinnacles (arrow) occur between desert pavement clasts within Pleistocene and older alluvial surfaces (marker for scale).



Figure 2.3: The study area is located within the Muddy Mountains Wilderness Area, Nevada, U.S.A.

Cyanobacteria-dominated Crust

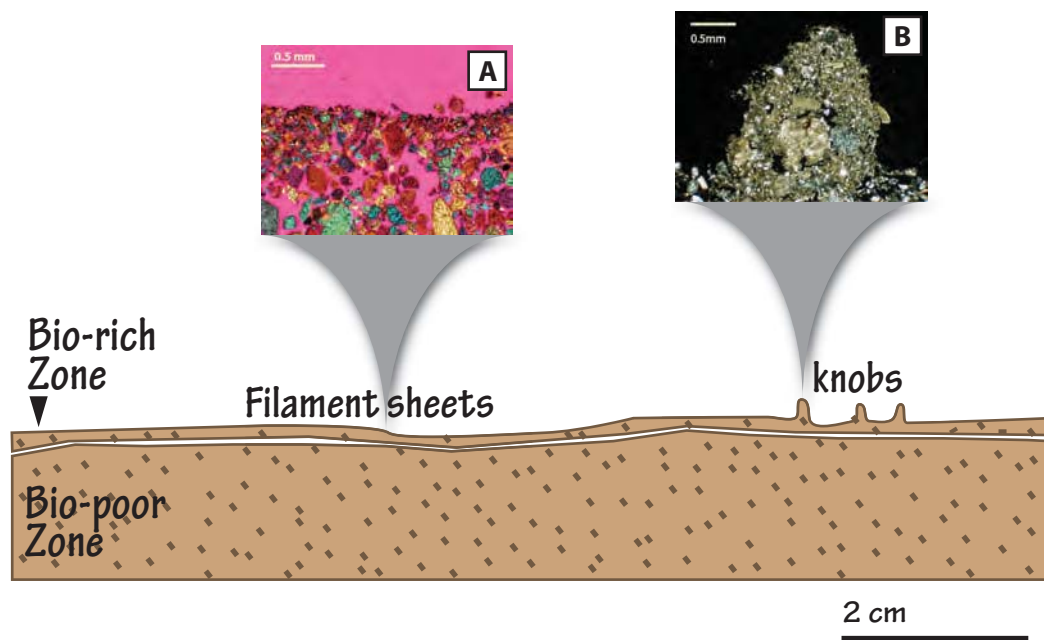


Figure 2.4: Cyanobacteria-dominated crusts have low surface relief and 1.5 mm thick bio-rich zones. (A) Filament sheets are common features. (See enlarged image in Fig. 7B.) (B) Filament knobs create minor topographic relief and are up to 3.8 mm tall and 2 mm wide. (See enlarged image in Fig. 16B).

Short Moss-Lichen Crust

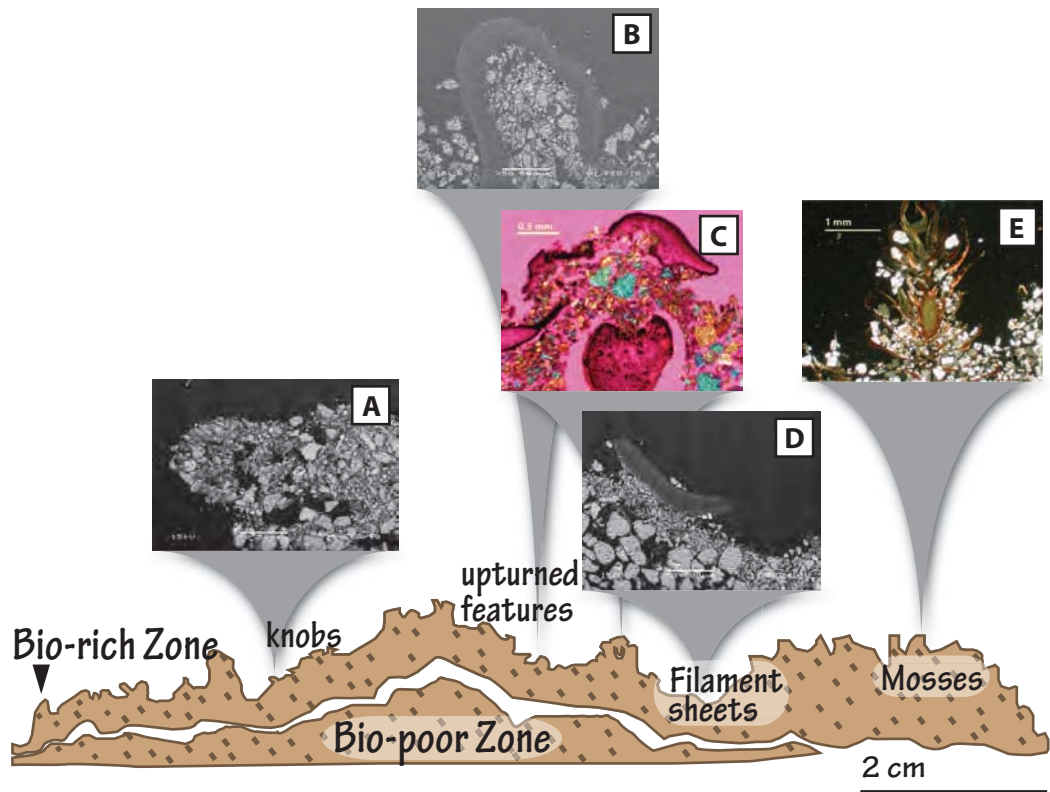


Figure 2.5: Short moss-lichen crusts have topographic relief up to 2 cm and are dominated by moss and lichen cover. The bio-rich layer is up to 11 mm thick. (A) Knobs are common features. (See enlarged image in Fig. 9A.) (B) Upturned lichen squamules increase topographic relief. (See enlarged image in Fig. 18A) (C) Enlarged rhizines are also associated with upturned sediment. (See enlarged image in Fig. 10C.) (D) Filament sheets may act as substrates for lichen thalli. (See enlarged image in Fig. 7A.) (E) Tall mosses such as *Syntherichia caninervis* commonly inhabit these crusts as discrete colonies (See enlarged image in Fig. 15A.)

Tall Moss-lichen Pinnacled Crust

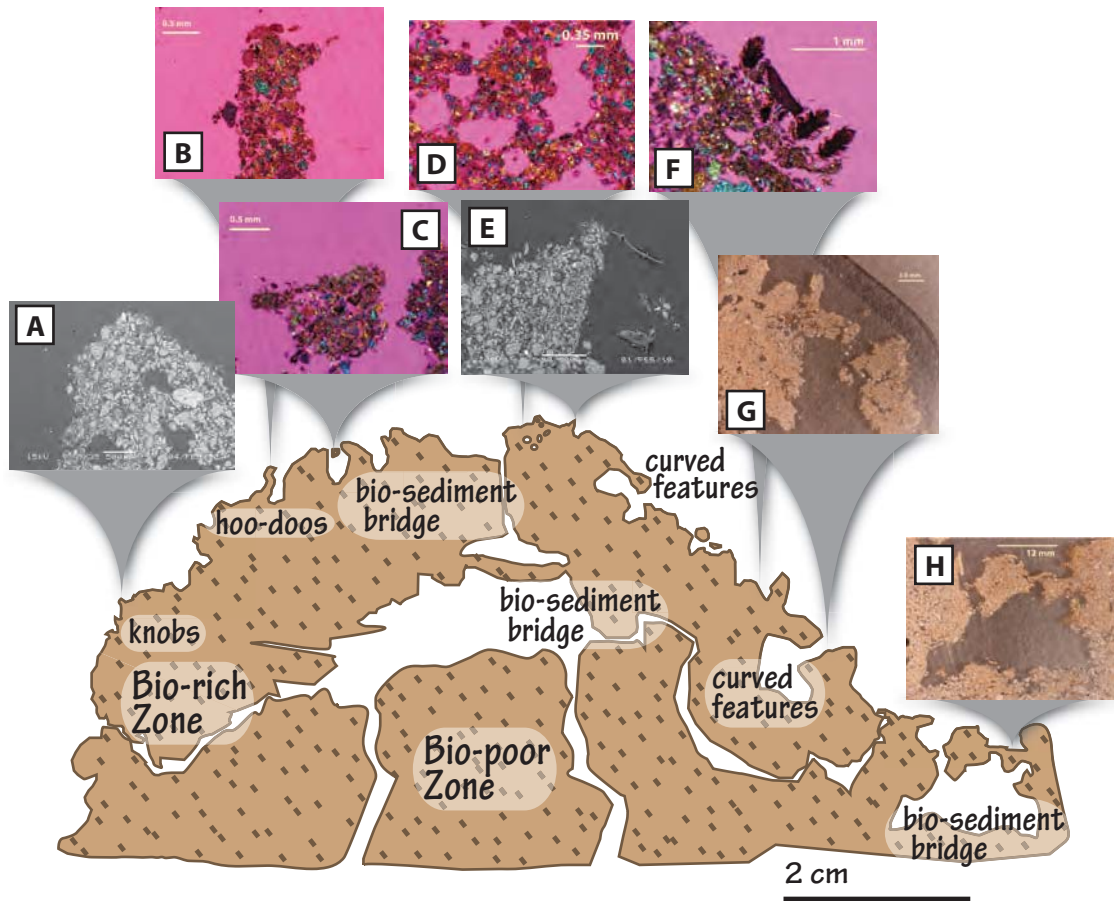


Figure 2.6: Tall moss-lichen pinnacled crusts have the greatest surface relief with bio-rich zones approximately 22 mm thick. Cover by mosses and lichens is extensive across pinnacle mounds. (A) Filament knobs are common and may contain well developed vesicular pores. (See enlarged image in Fig 17A.) (B) Hoo-doo structures are common protrusions that are often capped by gelatinous lichens. (See enlarged image in 14B.) (C) Small bio-sediment bridges often occur over surface depressions. (See enlarged image in Fig. 21A.) (D) Well-developed vesicular pores are common features within the bio-rich zone. (See enlarged image in Fig. 9C.) (E) Filament-bound sediments may cap sharp protrusions. (See enlarged image in Fig. 20). (F) Short mosses often grow within fine-grained sediments. (See enlarged image in Fig. 15B.) (G) Curved features and lichen-capped towers may form intact or suspended aggregates. (See enlarged image in Fig. 22B.) (H) Bio-sediment bridges may overlie large interior voids. (See enlarged image in Fig. 8B.)

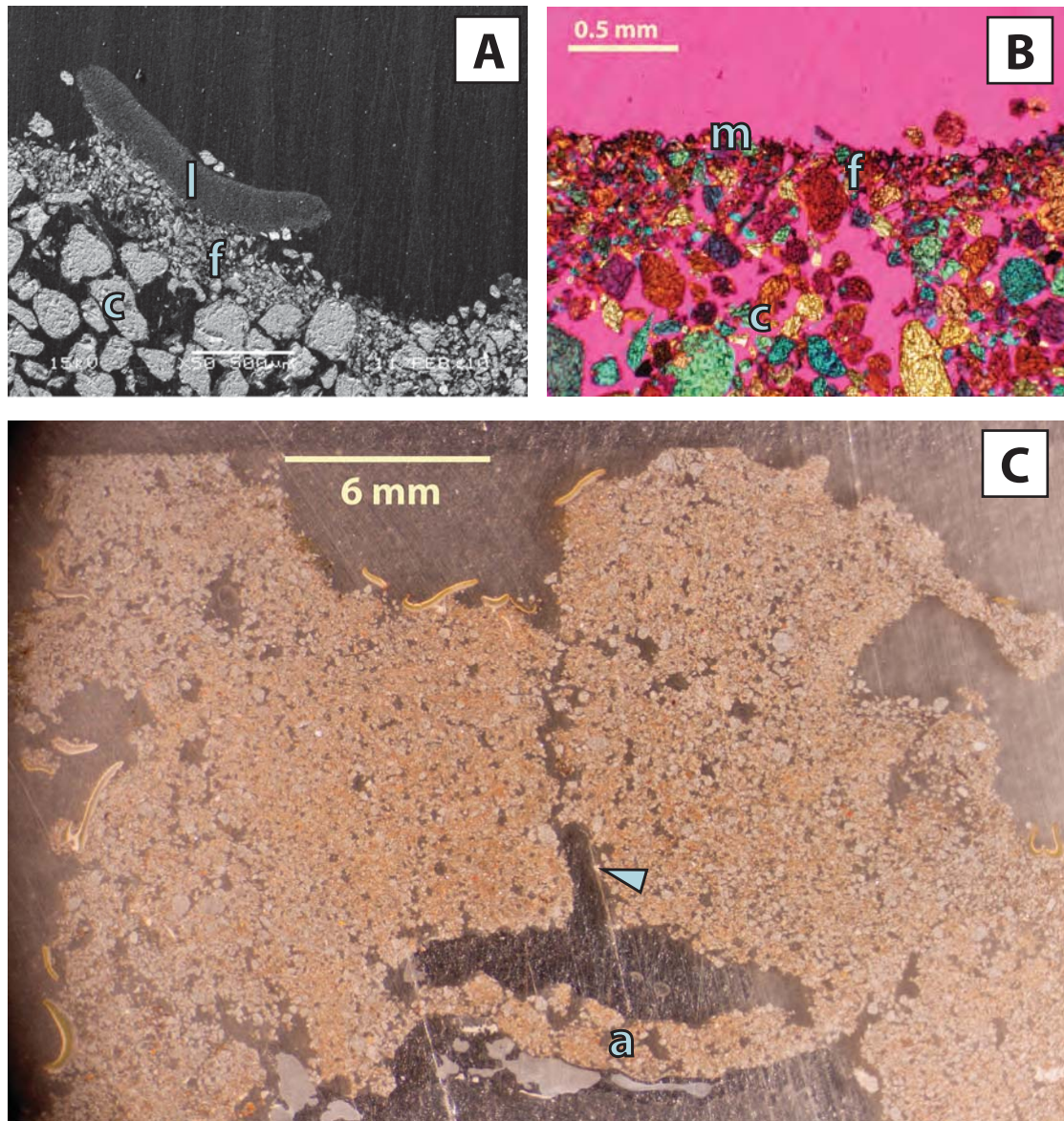


Figure 2.7: (A) A layer of fines (f), including clays, silts, and very fine sands, and a mesh of filaments overlie coarser, unconsolidated sands (c). A lichen squamule (l) inhabits the surface of this filament sheet (BES, scale 0.5 mm). (B) A thin filament sheet includes filaments that are likely *Microcoleus*. (m) forming a thin, layer of slightly compacted clays, silts, and very fine sands (f) above a layer of coarser, unconsolidated (c) sands (XPL image, scale 0.5 mm). (C) A vertical crack (arrow) penetrates surface pinnacle sediments. A non-biologically mediated aggregate (a) sloughs away from the upper bio-rich zone (light microscope image, scale 6 mm). (All images are oriented vertically with the top pointing upwards.)

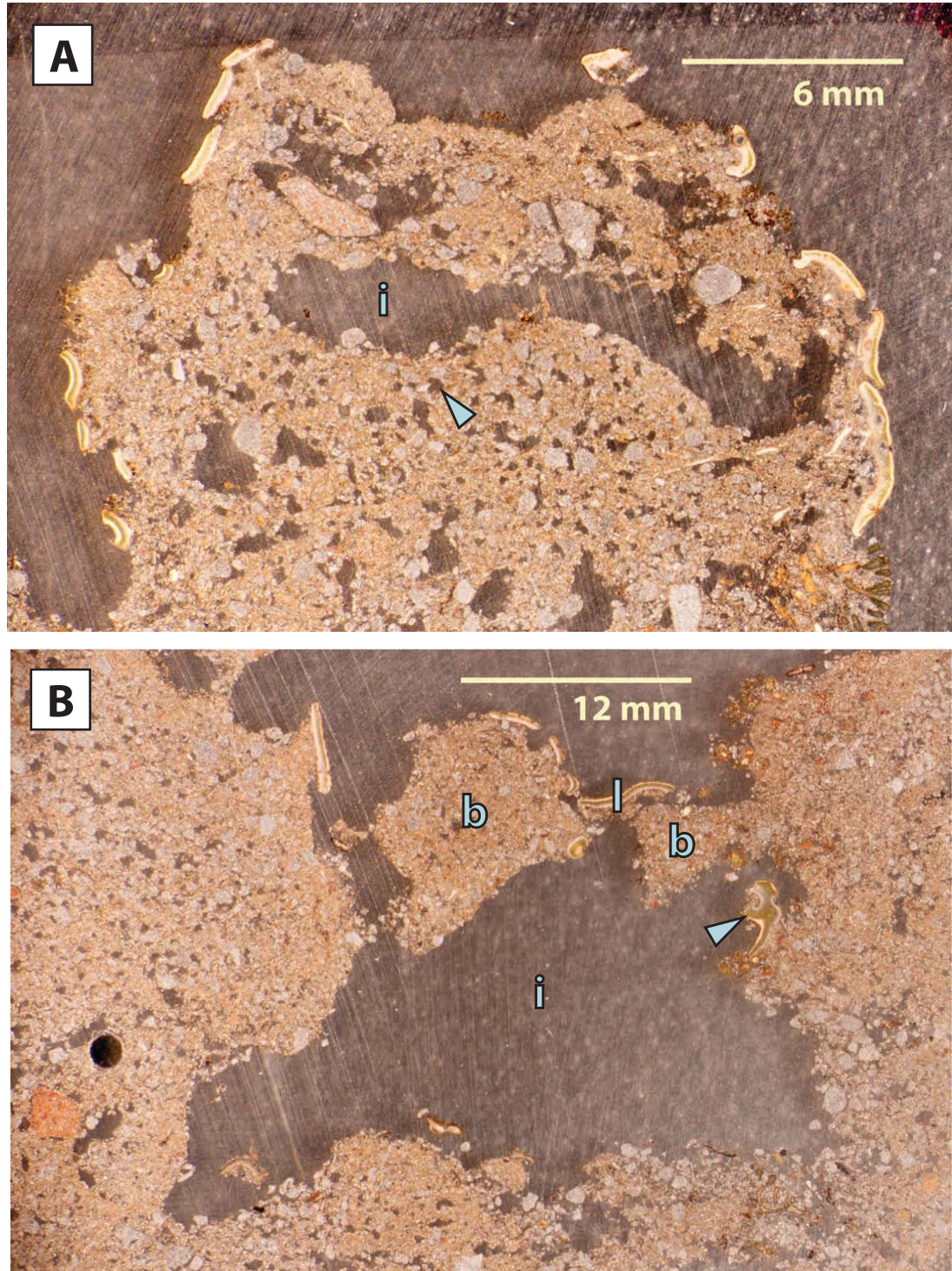


Figure 2.8: (A) Pinnacles display complex interior void space. Voids vary in size and may be irregularly shaped (i) or vesicular (arrow)(light microscope image, scale 6 mm). (B) Sediment bridges (b) overlie an irregular interior void (i). Note photosynthetic lichen squamules (arrow) appear to be blocked from sunlight. A squamulose lichen (l) at the soil surface also acts as a smaller sediment bridge (light microscope image, scale 12 mm). (All images are oriented vertically with the top pointing upwards.)

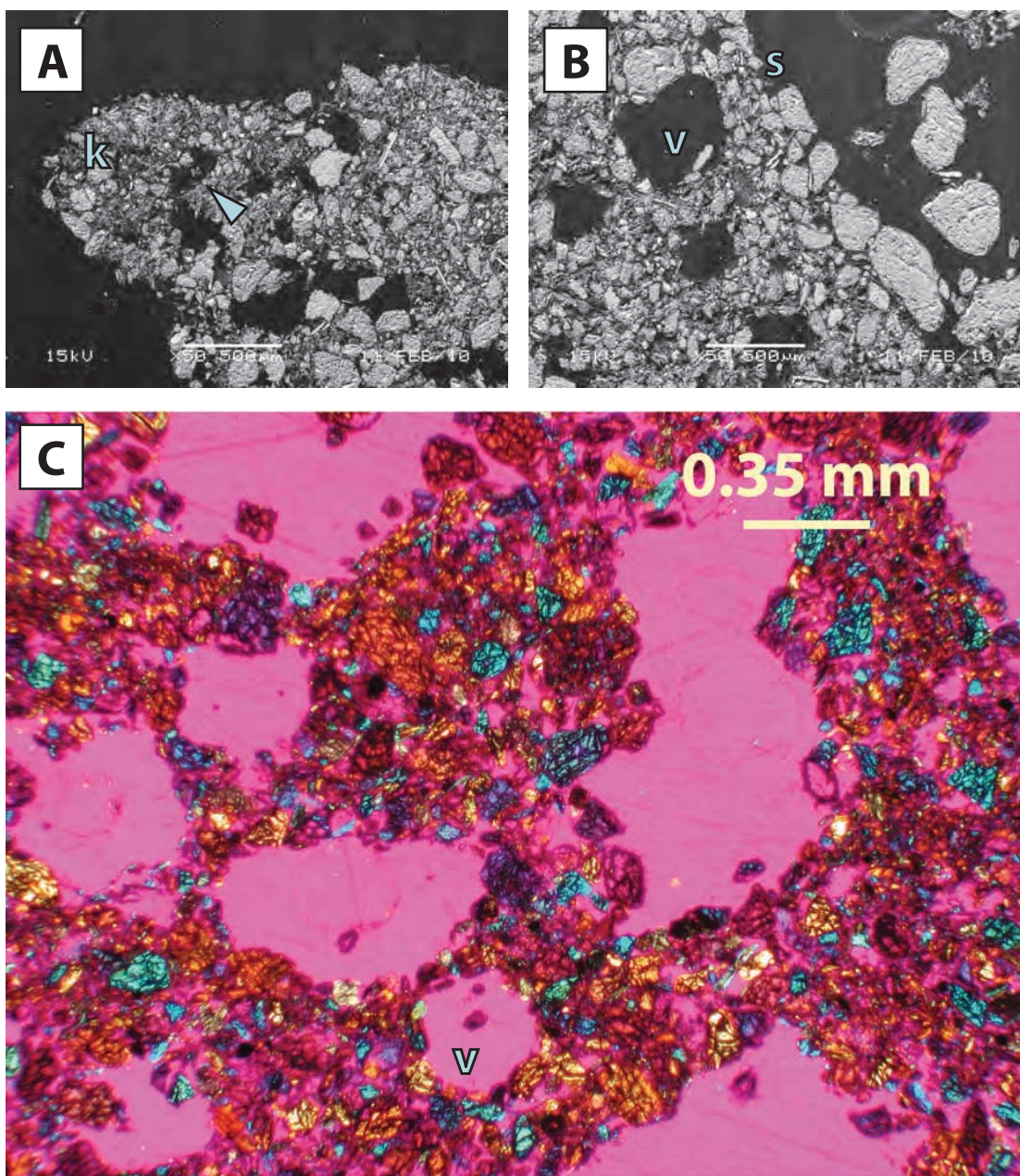


Figure 2.9: (A) A cyanobacterial knob (k) shows irregular pores (arrow). The surface is bound by cyanobacteria and cemented with carbonate (BES, scale 0.5 mm). (B) Vesicular pores (v) are found near the soil surface (s) within the bio-rich zone (petrographic image, scale 0.35 mm). (C) Vesicular pores (v) are common features of the upper bio-rich zone (BES, scale 0.5 mm). (All images are oriented vertically with the top pointing upwards.)

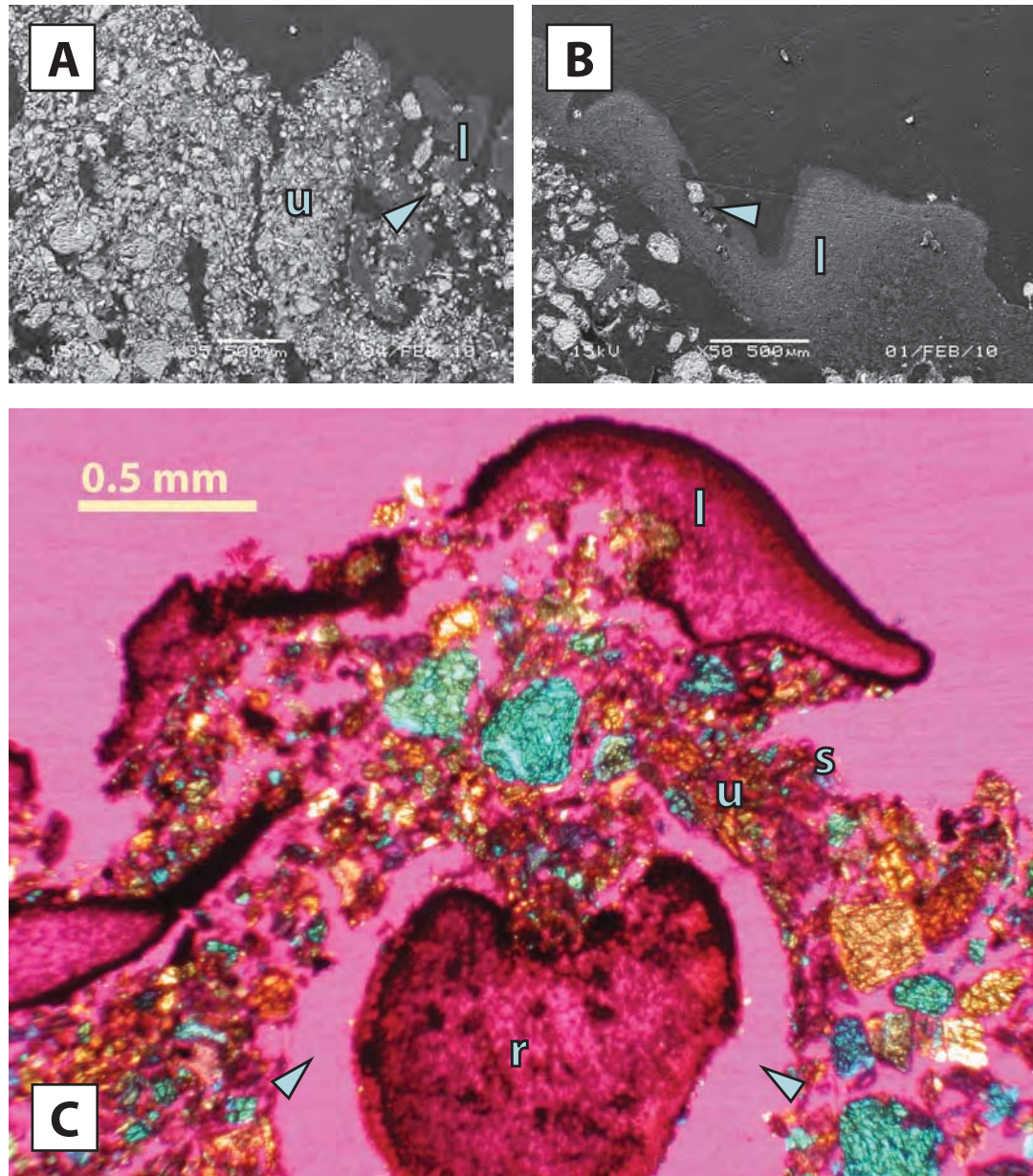


Figure 2.10: (A) Upturned sediment lies (u) adjacent to *Collema* lichen (l). Note linear vertical to subvertical cracks with infilling grains (arrow)(BES, scale 0.5 mm). (B) A crack or tear (arrow) in a lichen squamule (l) is infilled with grains (BES, scale 0.5 mm). (C) An enlarged rhizine (r) forms a bulb-like structure below the lichen squamule (l) at the soil surface (s). Note the linear cracks (arrows) between the rhizine and the adjacent soil. Sediment above enlarged rhizine appears to be upturned (u)(XPL, scale 0.5 mm). (All images are oriented vertically with the top pointing upwards.)

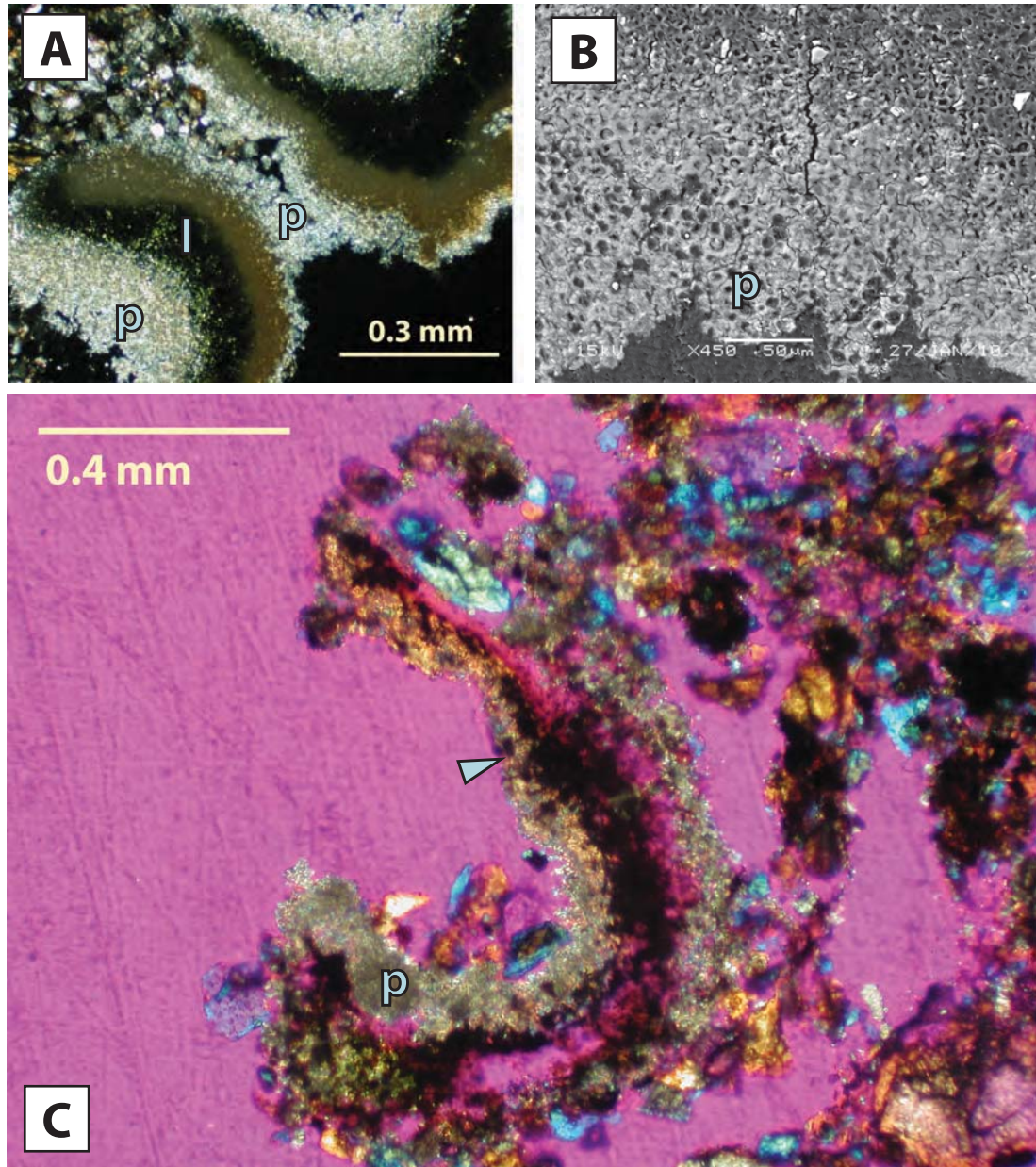


Figure 2.11: (A) Carbonate precipitates (p) cover lichen squamule (l) surfaces (petrographic image, scale 0.3 mm). (B) A close-up of the previous image shows calcium carbonate precipitates (p) permeating fungal cortex tissue along a lichen exterior (BES, scale 0.05 mm). (C) Calcium carbonate precipitates permeate cyanobacterial EPS material (arrow)(XPL image, scale 0.4 mm). (All images are oriented vertically with the top pointing upwards.)

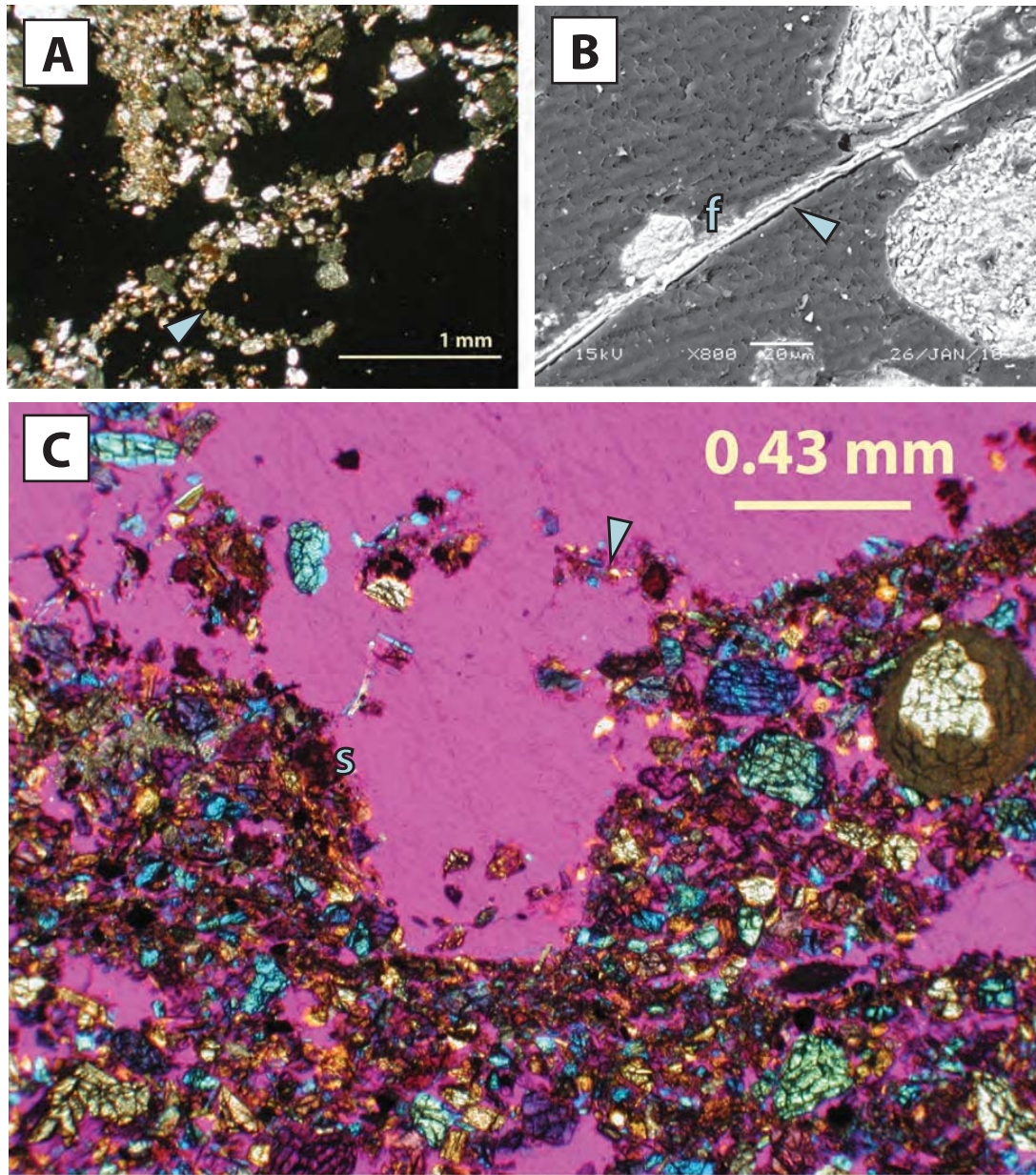


Figure 2.12: (A) Filaments (arrow) found within an interior pinnacle void are coated in grains (petrographic image, scale 1 mm). (B) Grains adhere to surface of a taut filament (arrow). Note clay-sized grains (f) are embedded within outer EPS material (BES, scale 0.2 mm). (C) Filaments (arrow) with attached grains bridge a small gap along the soil surface (s)(XPL image, scale 0.43 mm). (All images are oriented vertically with the top pointing upwards.)

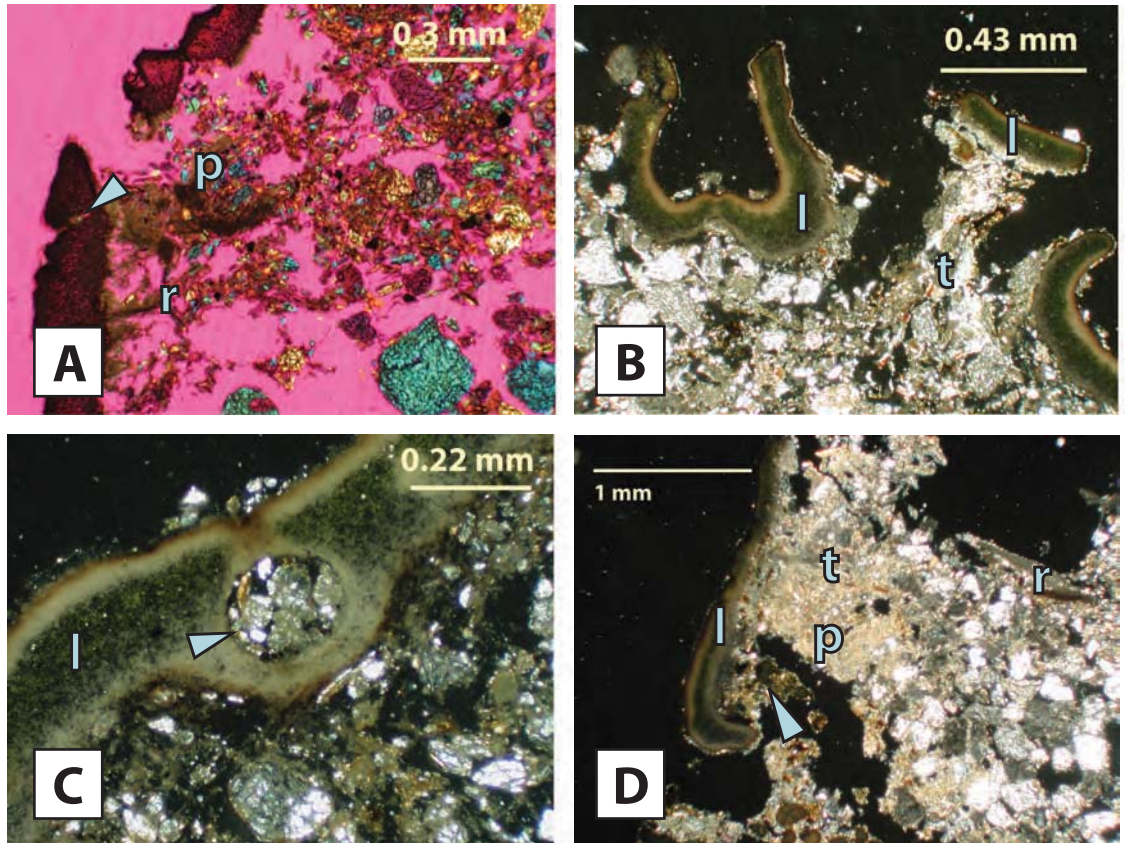


Figure 2.13: (A) Thin, filamentous rhizines (r) are partially surrounded by void space and are caked in carbonate precipitates (p, yellow minerals). Note an open perithecium (arrow) is filled with grains. Perithecia are lichen reproductive structures that release fungal spores (XPL image, scale 0.3 mm). (B) Dry lichen squamules (l) are curled and detached from the soil surface. One squamule tops a small bio-sediment tower (t) (petrographic image, scale 0.43 mm). (C) A closed perithecium (arrow) within a lichen squamule (l) is filled with grains (petrographic image, scale 0.22 mm). (D) A lichen squamule (l) tops a small sediment tower (t). The tower is cemented in carbonate precipitates (p) and contains a long, thick rhizine (r). Exudates (arrow) filled with precipitates and grains detach from the lower lichen squamule edge (petrographic image, scale 1 mm). (All images are oriented vertically with the top pointing upwards.)

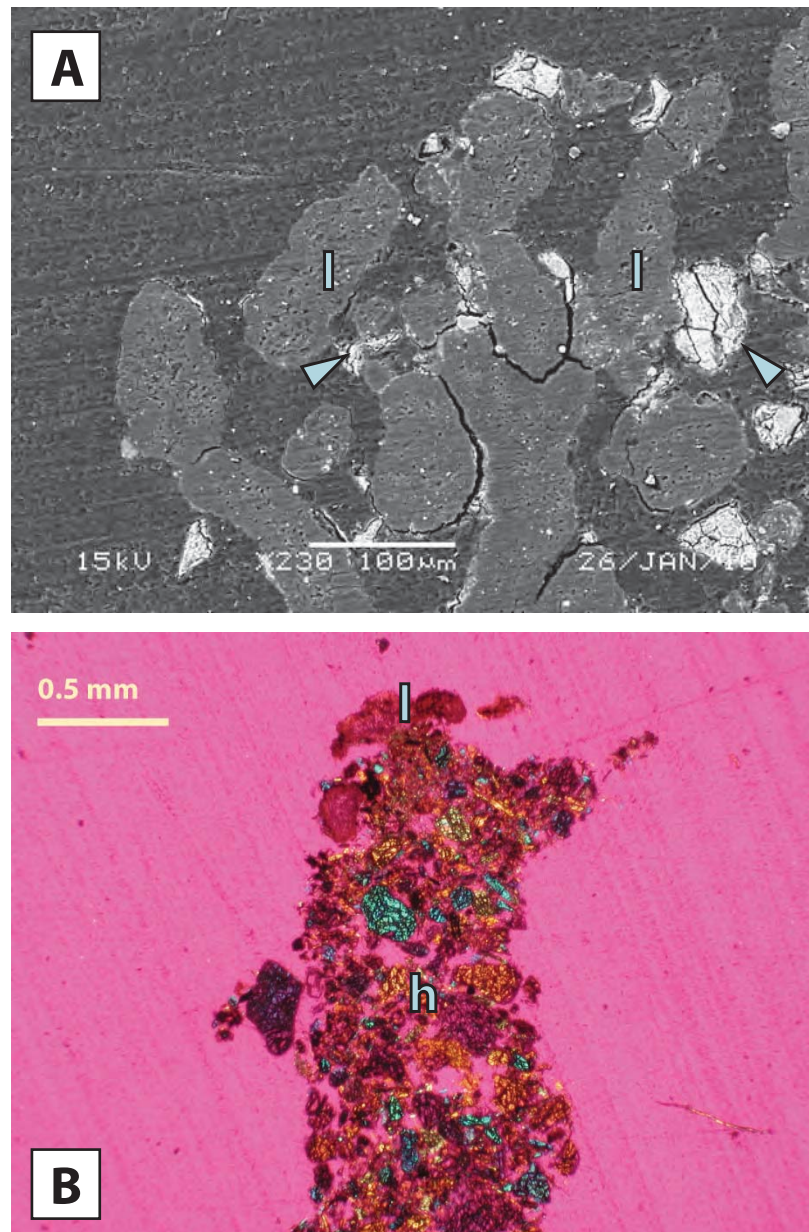


Figure 2.14: (A) A gelatinous lichen thallus (l), likely *Collema*, has a branching, tree-like morphology. Note grains trapped among thallus (arrows)(BES, scale 0.1 mm). (B) A gelatinous lichen thallus (l), tops a hoo-doo bio-sedimentary structure (h)(XPL image, scale 0.5 mm). (All images are oriented vertically with the top pointing upwards.)

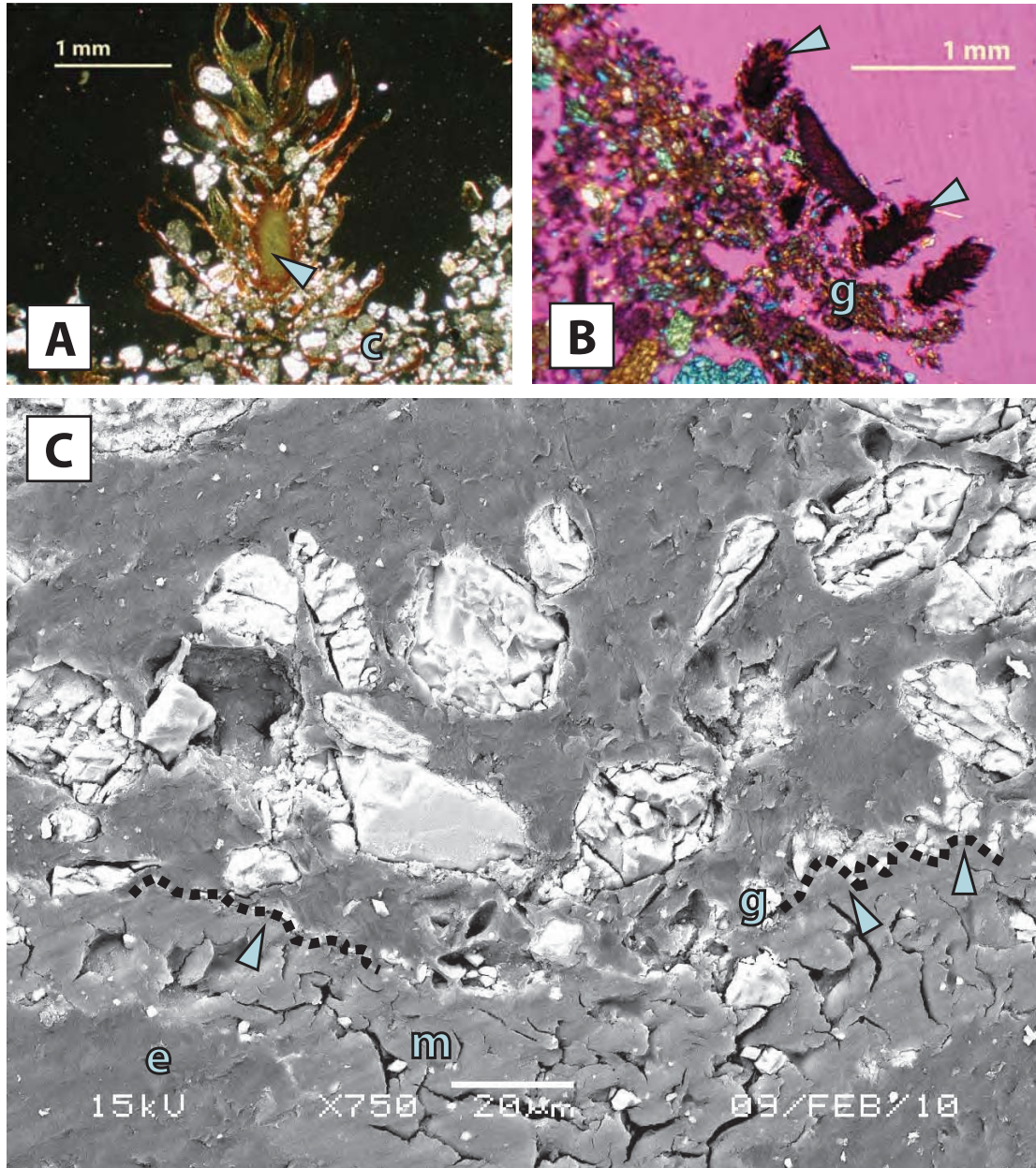


Figure 2.15: (A) A “tall” moss (arrow), likely *Syntrichia caninervis*, grows within loose, coarser grains (c). Note sediments occur among leaves (petrographic image, scale 1mm). (B) “Short” mosses (arrows) grow on a layer of fine, compacted grains (g) that is partially detached and upturned from the soil surface. These mosses are likely *Bryum* or *Pterygoneurum* (XPL image, scale 1 mm). (C) Fine grains (g) have settled among moss papillae (arrows and dotted outline), which are small bumps found on moss leaves. Epoxy (e) appears as a slightly darker tone than the moss tissue (m)(BES image, scale 0.02 mm). (All images are oriented vertically with the top pointing upwards.)

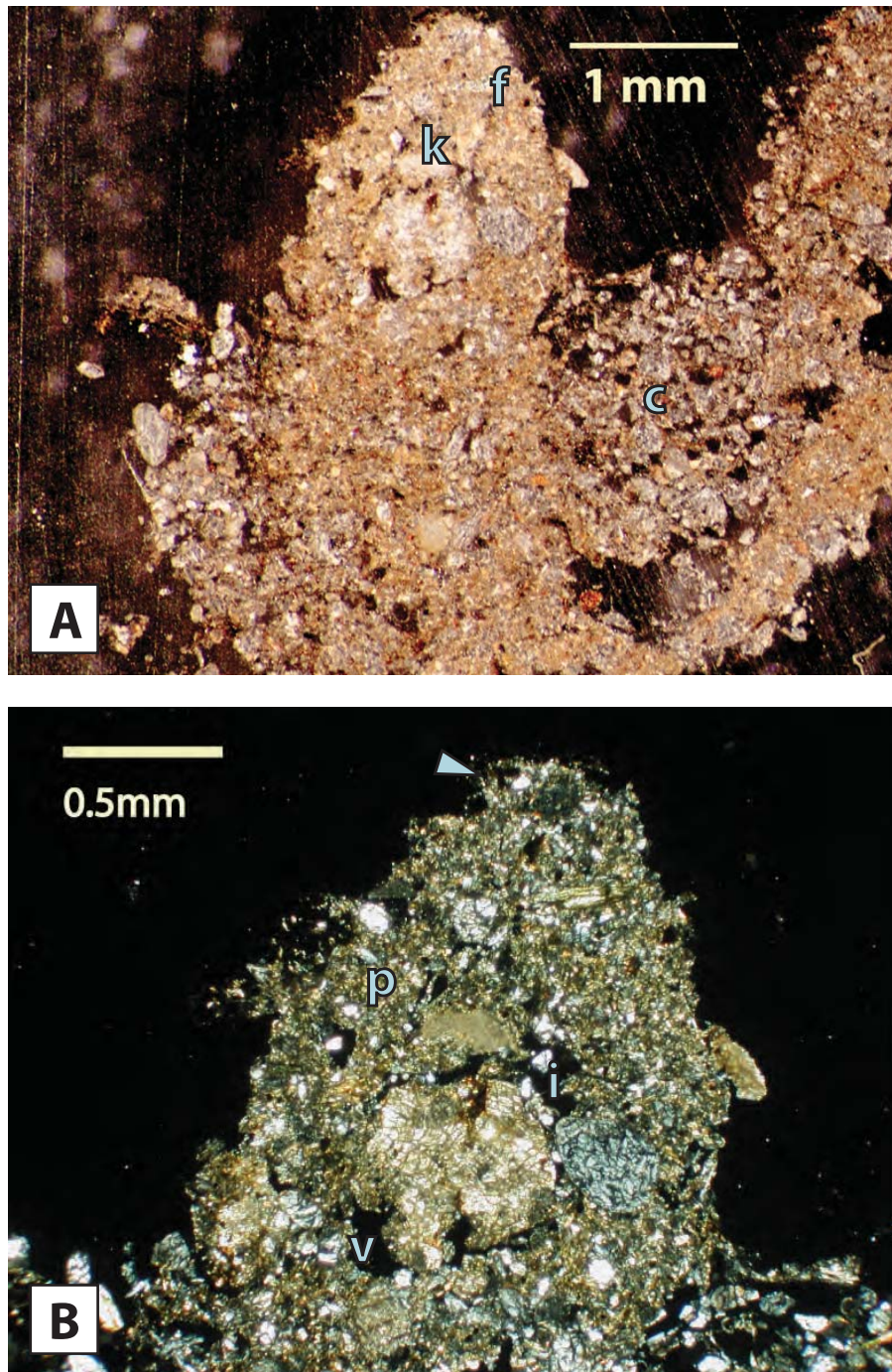


Figure 2.16: (A) Knobs (k) are bio-sedimentary structures composed primarily of fine grains (f) and extensive networks of filaments. Coarser, unconsolidated grains (c) infill adjacent depressions (light microscope image, scale 1 mm). (B) A close-up of the previous image shows the knob is cemented with carbonate precipitates (p). The knob contains poorly-developed vesicular pores (v) and irregular pores (i). Exposed filaments (arrow) are seen near the soil surface. (petrographic image, scale 0.5 mm). (All images are oriented vertically with the top pointing upwards.)

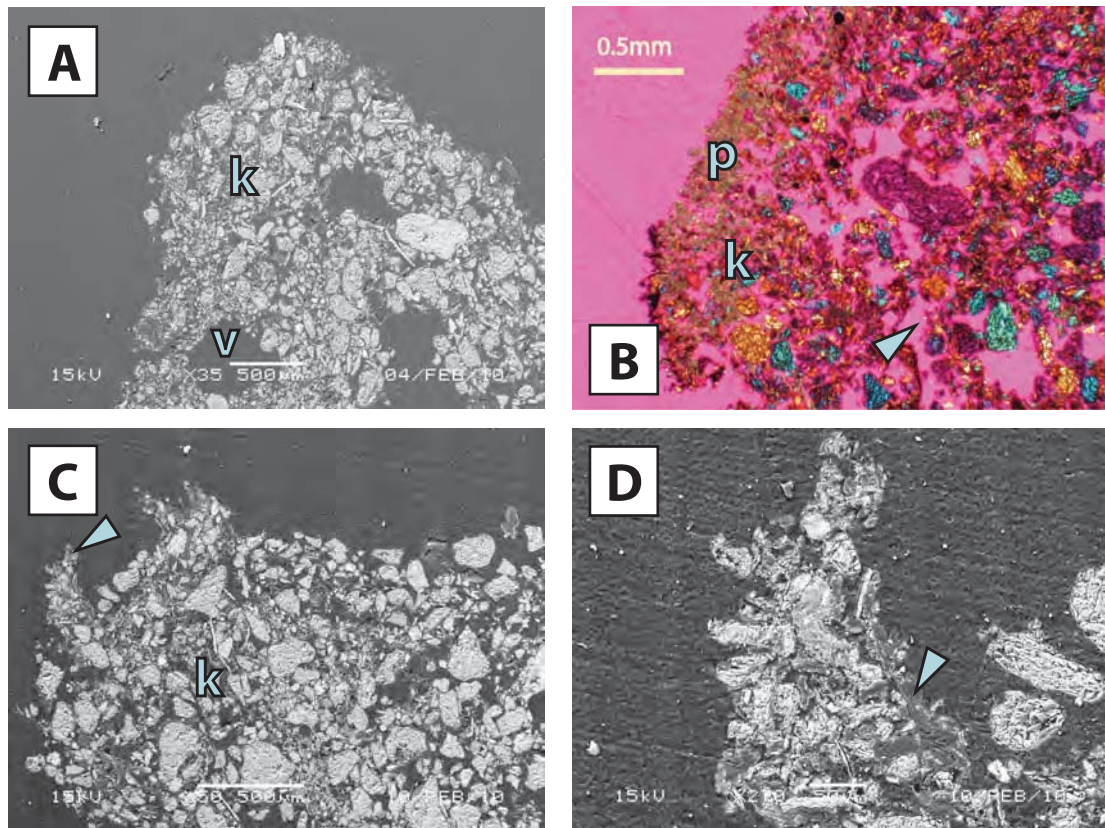


Figure 2.17: (A) A tall knob (k) protrudes 2 mm above the adjacent soil surface and contains well-developed vesicular pores (v) and networks of filaments (BES, scale 0.5 mm). (B) A short knob (k) protrudes <1 mm beyond the adjacent soil surface. Filaments are covered in carbonate precipitates (p, yellow). A linear void (arrow) 1 mm from the soil surface parallels the knob perimeter (XPL image, scale 0.5 mm). (C) A knob (k) surface displays sharp protrusions (arrow), or tufts, composed of filaments, precipitates, and grains (BES, scale 0.5 mm). (D) Close-up of sharp protrusion from previous image shows network of filaments (arrow), grains, and precipitates (BES, scale 0.05 mm). (All images are oriented vertically with the top pointing upwards.)

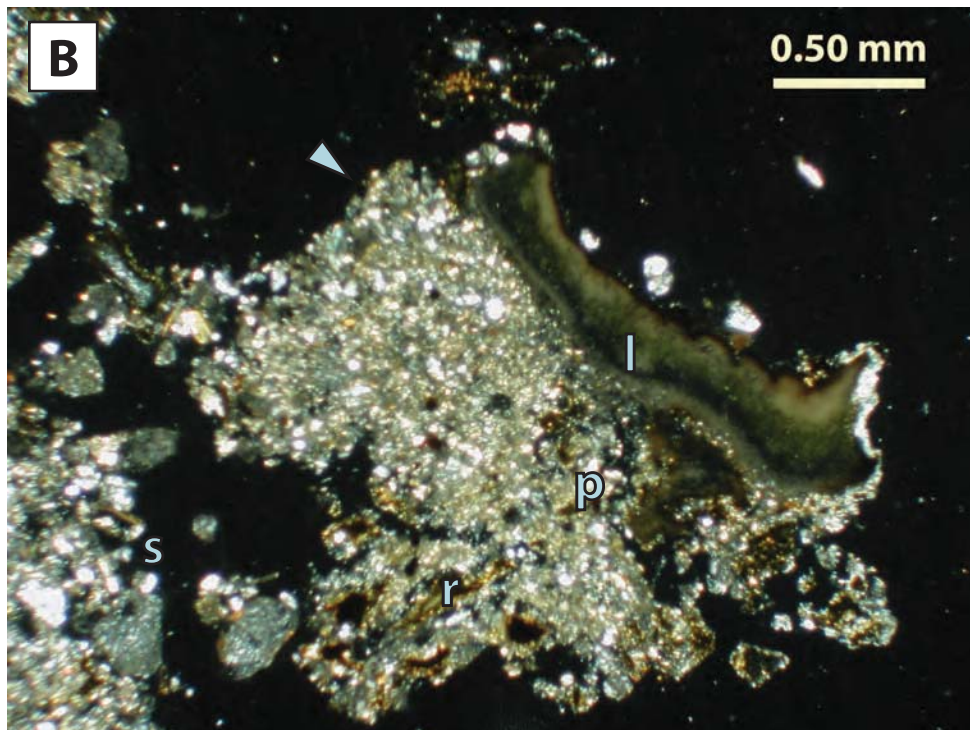
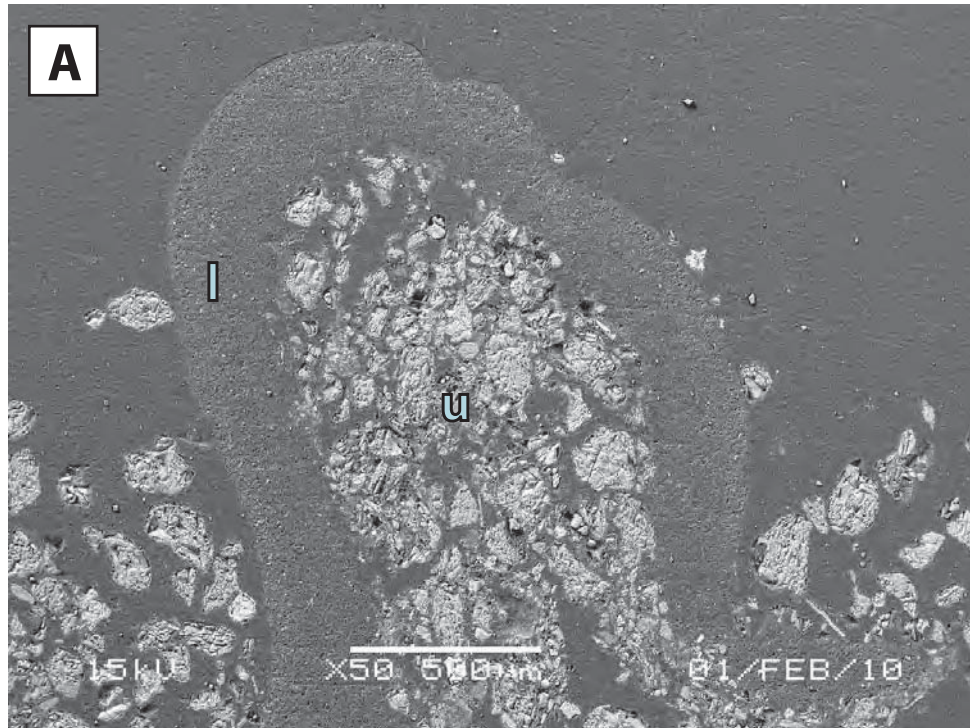


Figure 2.18: (A) A lichen squamule (l) curls to form a “c”. Note upturned soil (u) fills the interior space of the “c” (BES, scale 0.5 mm). (B) A raft (arrow), which is formed by a lichen squamule (l), rhizines (r), grains, and mineral precipitates (p), is completely detached from the soil surface (s)(petrographic image, scale 0.5 mm). (All images are oriented vertically with the top pointing upwards.)

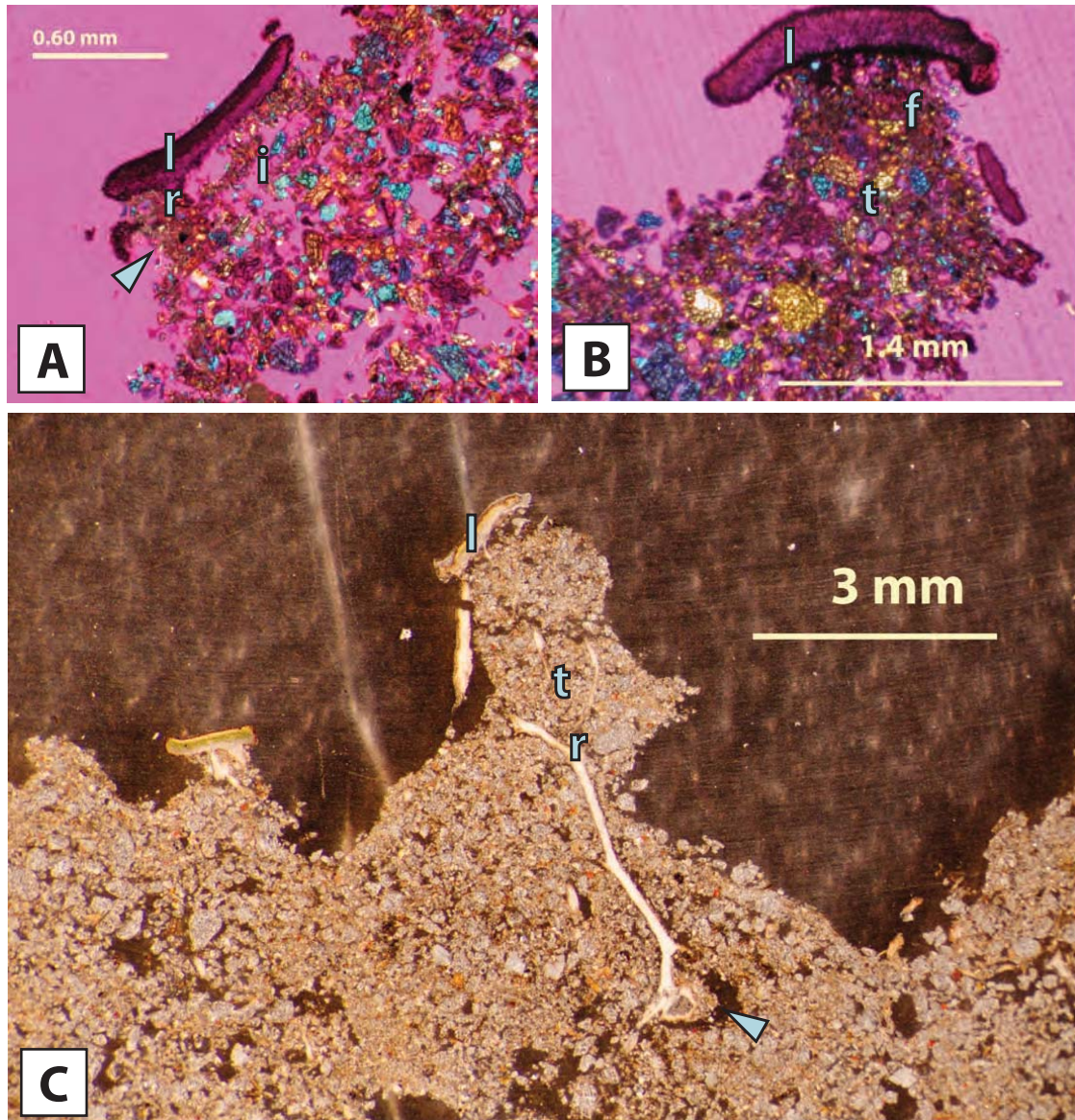


Figure 2.19: (A) A lichen squamule (l) with multiple hair-like, or rhizoidal, rhizines (r) tops a bio-sediment pedestal (arrow). The outer edge of the pedestal is formed in compacted, clays and silts, while the interior contains irregular interior void space (i)(XPL image, scale 0.6 mm). (B) A lichen squamule (l) tops a bio-sediment tower (t). The tower contains a thick, rhizine surrounded by fine grains (f). The tower sediments are finer grained than the sediments below (XPL image, 1.4 mm). (C) The tower (t) is topped by a lichen squamule (l) and contains a thick rhizine (r) that is branched. Note some of the rhizine tissue appears to be broken, while an exposed rhizine covers one vertical side of the tower. Note the void (arrow) space between the enlarged rhizine and the adjacent soil (light microscope image, scale 3 mm). (All images are oriented vertically with the top pointing upwards.)

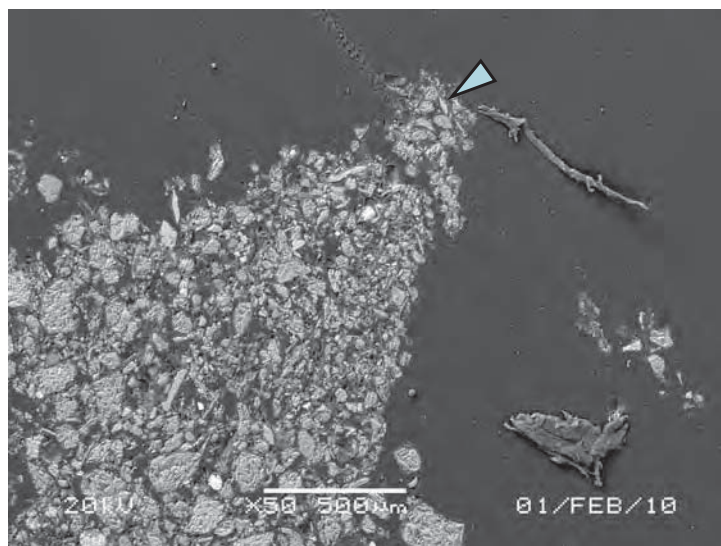


Figure 2.20: A mesh of filaments and grains (arrow) cap a sharp protrusion. Note the subvertical right-hand edge. The morphology of this structure partially resembles knob features with its fine-grained particles, but it also resembles hoo-doo features with an incut edge (right side)(BES, scale 0.5 mm). (All images are oriented vertically with the top pointing upwards.)

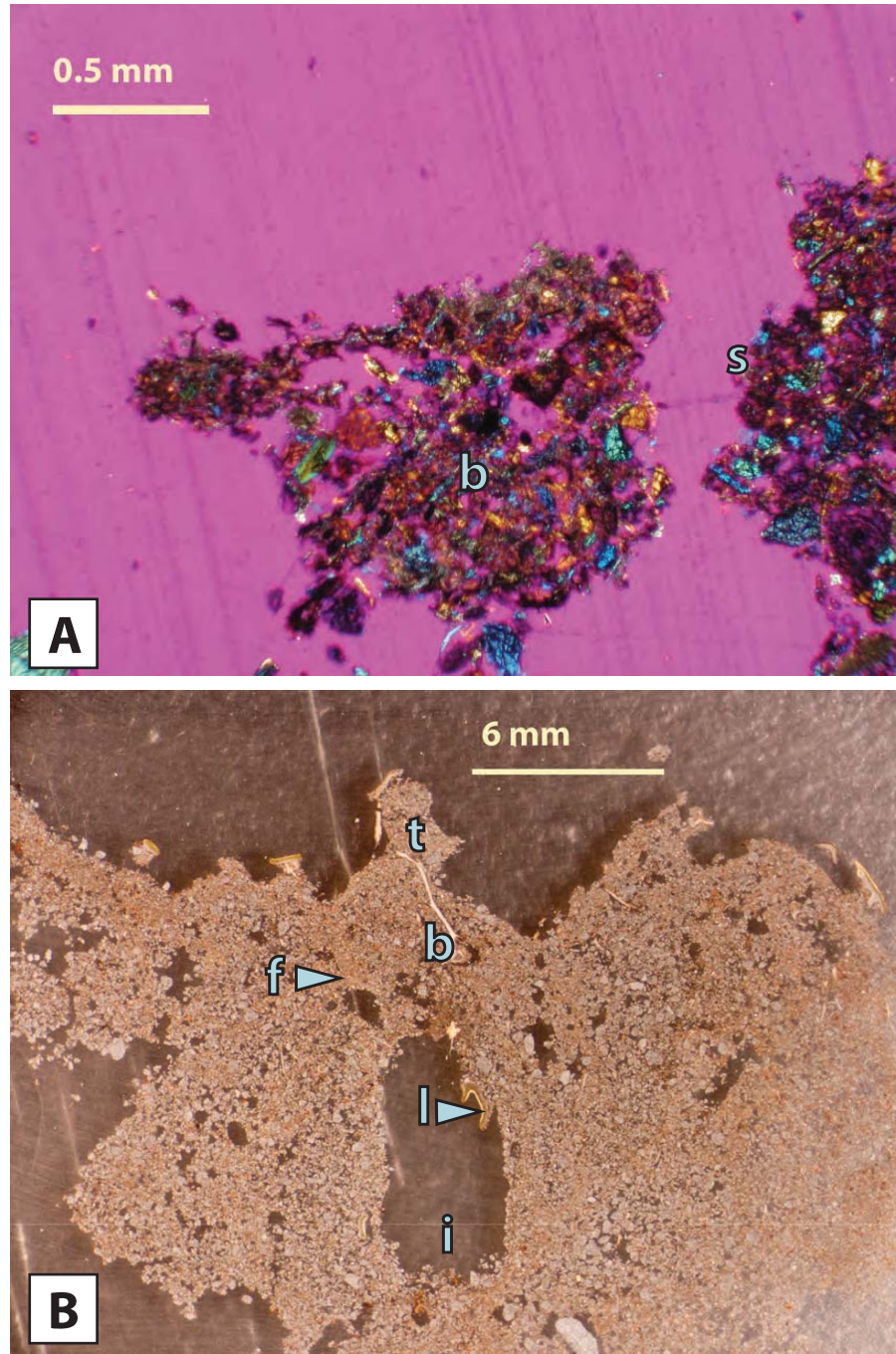


Figure 2.21: (A) A bio-sediment bridge (b) appears suspended above a depression along the soil surface (s). The bridge is an aggregate of grains and filaments (XPL image, scale 0.5 mm). (B) A bio-sediment bridge (b) overlies a large irregular interior void (i). A lichen squamule (l) is found within the void and appears to be blocked from sunlight. The perimeter of the void is mostly smooth and is composed of silt and clay grains. Another fine-grained lamina is found along left side of the sediment bridge (f). A tower (t) topped by a lichen squamule overlies the sediment bridge. The composite aggregate of the bridge and the lichen tower make a curved feature (light microscope image, scale 6 mm). (All images are oriented vertically with the top pointing upwards.)

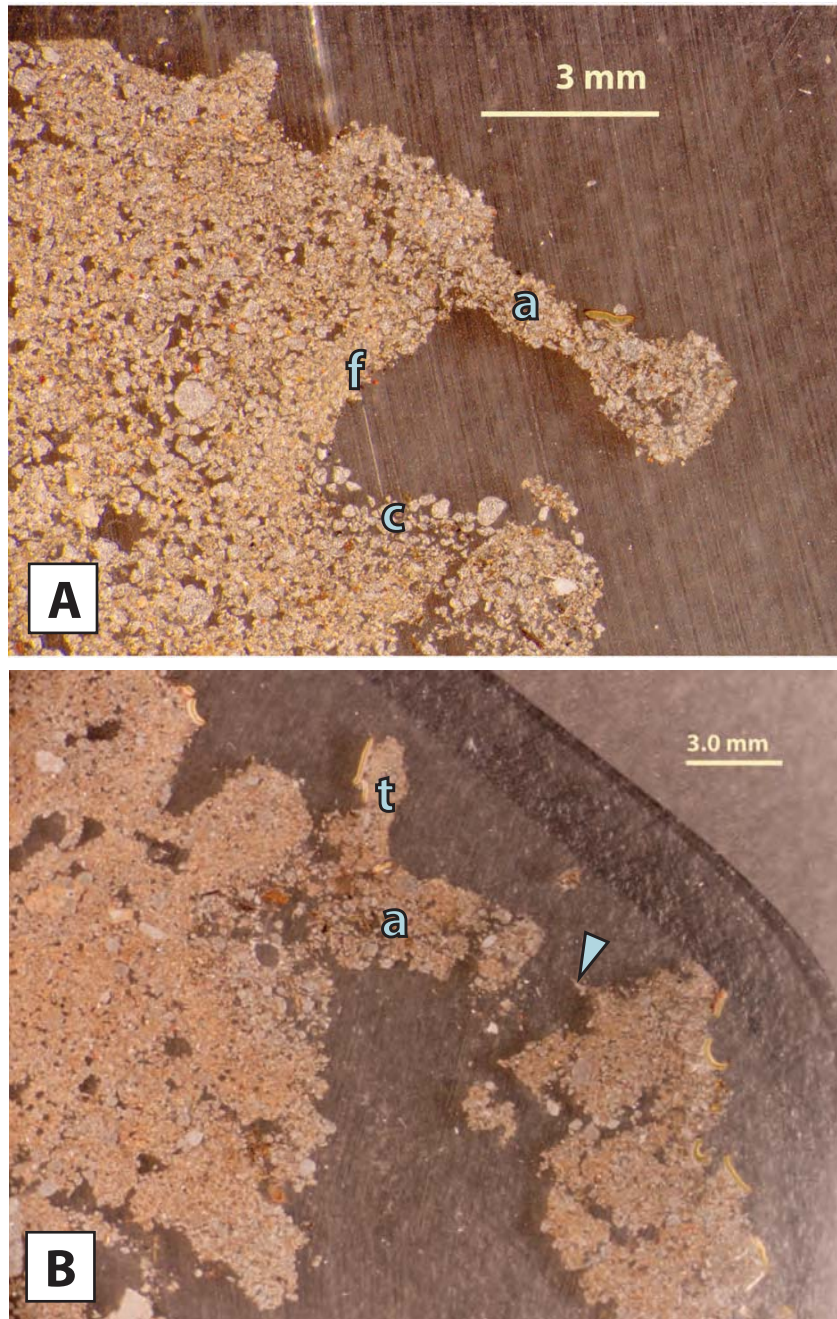


Figure 2.22: (A) A curved sedimentary structure forms a “U-shaped” aggregate (a) that encloses an exposed void. The perimeter of the void has a smooth margin formed in fine, compacted grains (f)(light microscope image, scale 3 mm). Coarser, unconsolidated grains infill the base of the void (c). (B) A curved aggregate (a) is partially suspended from the adjacent soil aggregate to the right. A small, sharp point (arrow) tops the rightmost aggregate. A squamulose lichen tower (t) tops the curved aggregate (a)(light microscope image, scale 3 mm). (All images are oriented vertically with the top pointing upwards.)

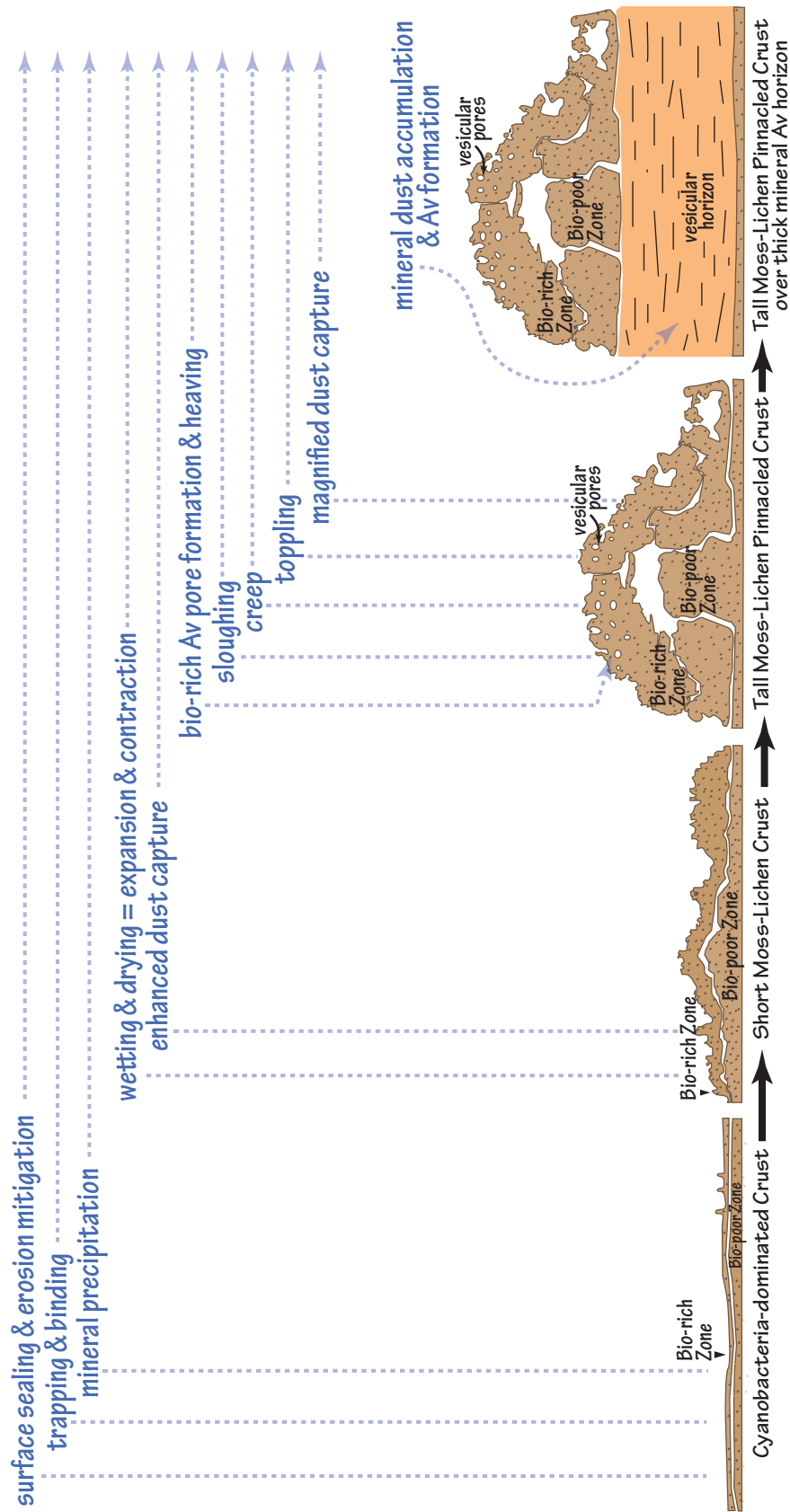
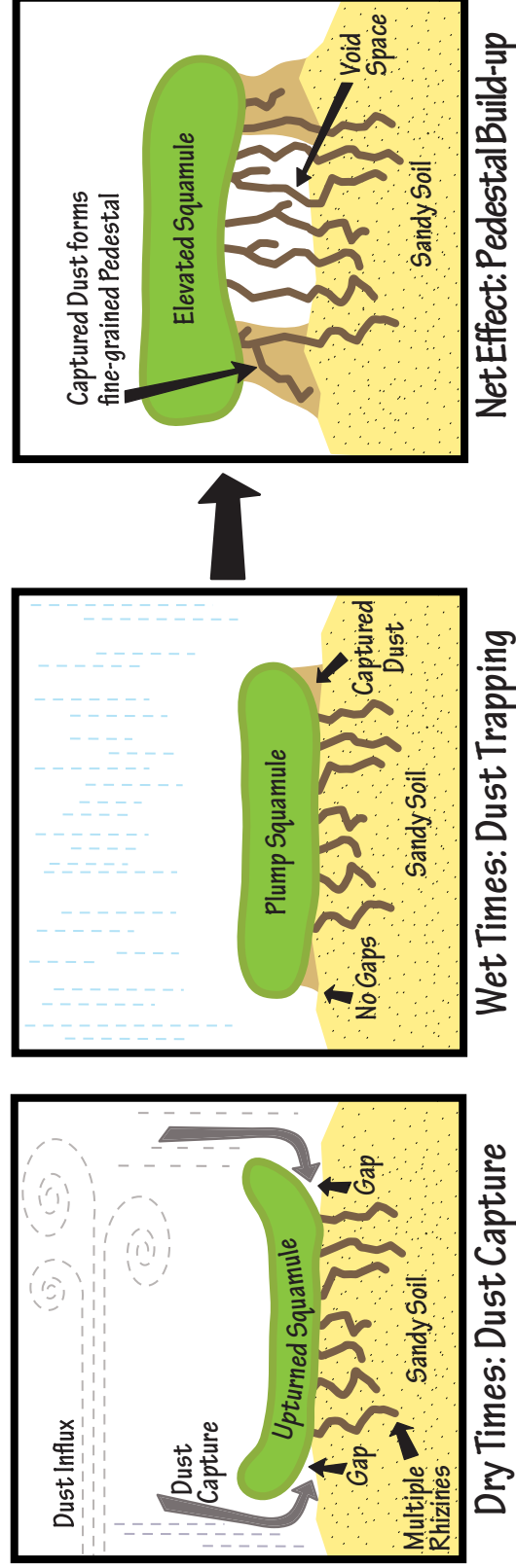


Figure 2.23: An idealized model illustrates biological soil crust development through time. Cyanobacteria colonize geomorphically stable fine-grained sediments. These crusts seal surfaces, mitigate erosion, trap and bind materials, and facilitate mineral precipitation processes. If conditions are favorable, mosses and lichens colonize the site to form short moss-lichen crusts. Wetting/drying, expansion/contraction and dust capture lead to the accretion of material and increased surface topography. Dust accretion magnifies as tall moss-lichen pinnacled crusts form. Vesicular pores develop within the bio-rich zone. Heaving, sloughing, creep, and topping processes increase surface topography and internal morphological complexity. These tall moss-lichen pinnacles may crack and detach from the soil surface. Dust accumulates below the pinnacle mounds to form a thick, mineral Av horizon.

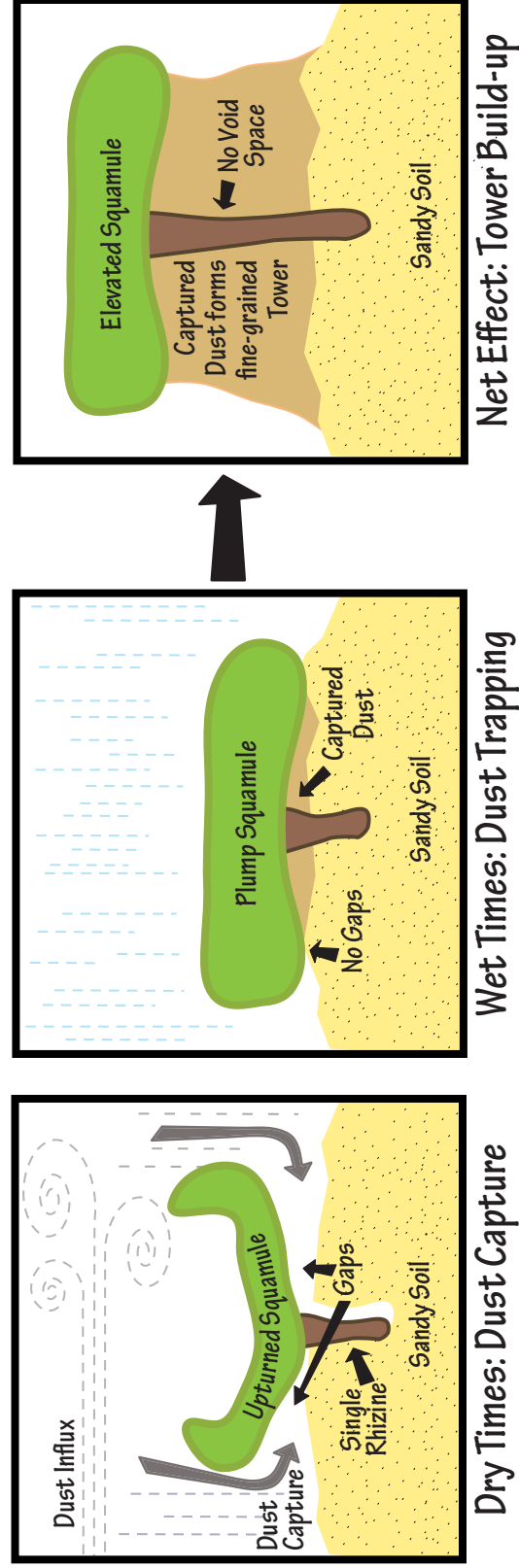
Pedestal Development below Squamulose Lichen with Multiple, Thin Rhizines



Alternating Wet & Dry Times build up Pedestal below Lichen Squamule

Figure 2.24: Proposed 2-D model of pedestal development below squamulose lichen with multiple, thin rhizines. During dry times, disk-shaped lichen thalli with multiple, thin rhizines shrink and curl along their edges. This upturning creates small gaps along the entire thalli perimeter for dust capture. During wet times, the squamule rehydrates and expands to trap dust. Several alternating wet and dry cycles lead to the capture of dust around the squamule edge. This process elevates the squamule to form a pedestal. Because the multiple rhizines act like anchors, dust accumulation occurs only along the perimeter of the thallus. This creates interior void space below the center of squamule.

Tower Development below Squamulose Lichen with Single, Thick Rhizines



Alternating Wet & Dry Times build up Tower below Lichen Squamule

Figure 2.25: Proposed 2-D model of tower development below squamulose lichens with single, thick rhizines. During dry times, a disk-shaped lichen squamule with a single thick rhizine shrinks and curls around all edges. This upturning produces gaps below the entire squamule that may capture dust. During wet times, the squamule rehydrates and expands to trap this sediment. Several alternating wet and dry cycles lead to the capture of dust below the squamule. This process elevates the squamule to form a tower. Because the single rhizine allows complete curling of the squamule, dust accumulation is relatively uniform around the tower. This results in little void space around the rhizine or below the tower.

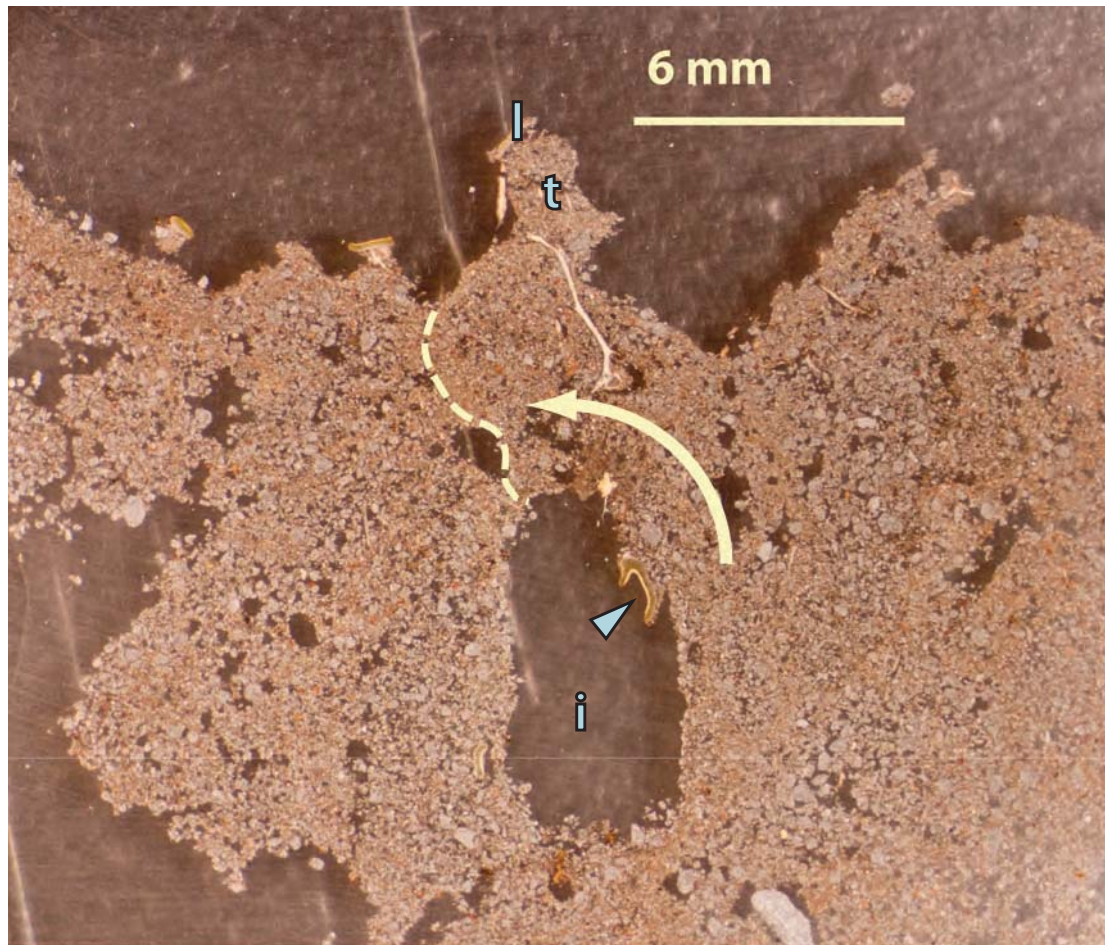


Figure 2.26: An arrow indicates a proposed “toppling” event. A lichen tower (t) likely built up by accretion below the lichen squamule (l). Eventually this tower became unstable and toppled over. This event trapped a lichen squamule (arrow) within the irregular interior void (i). The dashed line marks the contact between the two previously exposed surfaces. This contact is reflected by a vertical lamina of fine grains that suggests surface sealing and crusting associated with its previous exposure.

Mineral Dust Accumulation & Av Formation below Tall Moss-Lichen Pinnacles

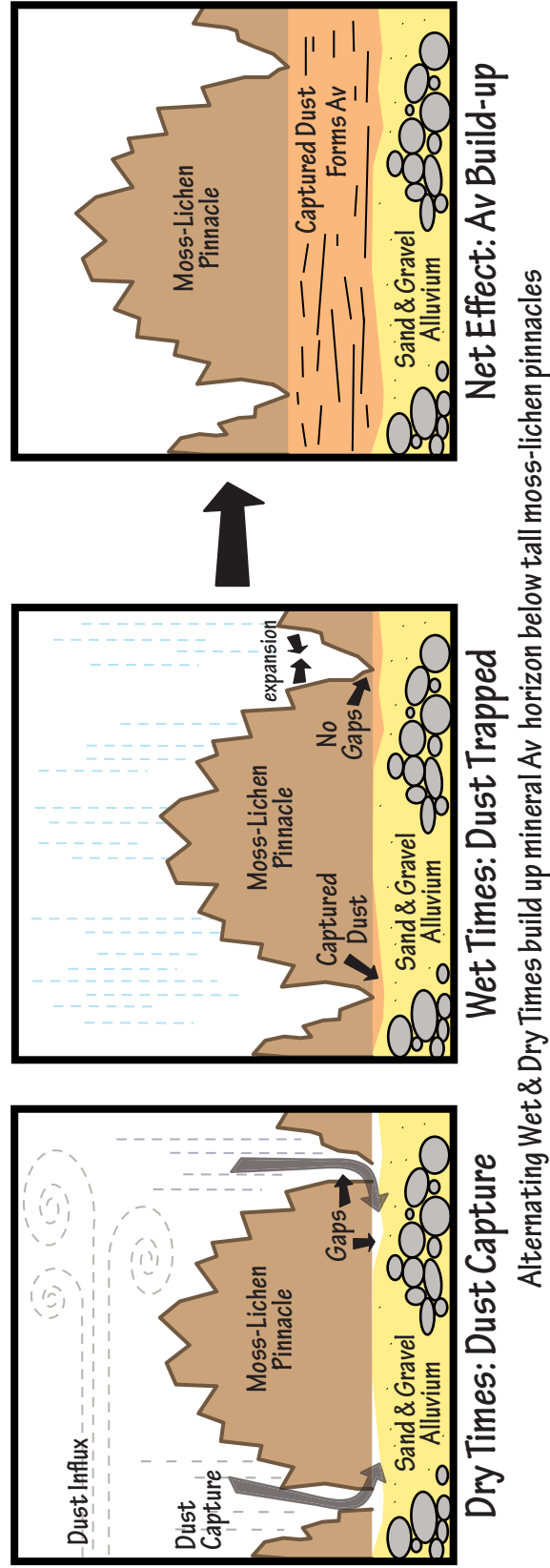


Figure 2.27: Proposed model of Av accumulation below tall moss-lichen pinnacle mounds. During dry times, pinnacle mounds shrink. Cracks form below and between pinnacle mounds, similar to mud cracks. Cracking and slight upturning create gaps between and below pinnacle mounds where dust may enter and be trapped. During wet times, pinnacle mounds rehydrate and expand, to seal gaps and to trap this sediment. Several alternating wet and dry cycles lead to the capture of dust below the pinnacle mounds. This process elevates the pinnacle mounds to form a dust-rich layer. The moss-lichen crust surface forms a seal that traps air to form vesicular pores over subsequent wet and dry cycles. Vesicular pores form within the pinnacle mound and below the pinnacle mound in the dust-rich layer. The net effect is the formation of an Av horizon below and within tall moss-lichen pinnacles.

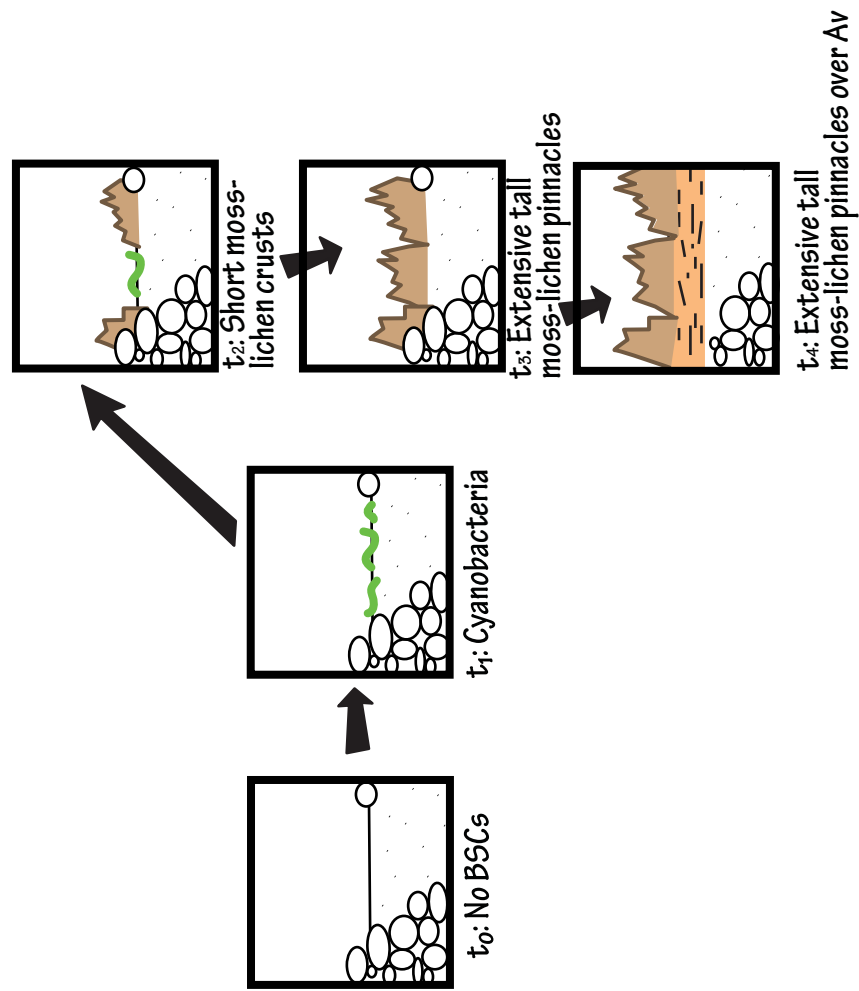


Figure 2.28: Crust development proceeds from bare mineral soil to cyanobacteria crusts to short moss-lichen crusts to tall moss-lichen pinnacled crusts with or without underlying mineral Av horizons.

Bio-sedimentary Features

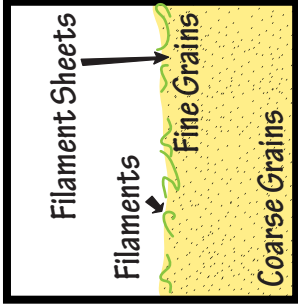
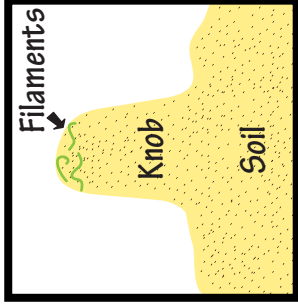
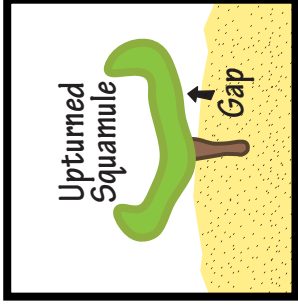
Feature	Characteristics	Occurrence	General Morphology	Examples
Filament sheets	Horizontal strata of compacted clays, silts, and very fine sands among mesh of filaments that are probable cyanobacteria; strata may be up to 250-300 µm thick and often overlie layers of loose, unconsolidated fine to coarse sands; may contain authigenic minerals.	All crust types, most pervasive in cyanobacteria-dominated crusts		Figures 1A, 4, 7A, 7B
Knobs	Protrusions of clay, silt, and sand; 2 mm wide and up to 3.8 mm tall; summits are convex; short knobs contain linear voids 1.5 by 0.25 mm linear voids that align parallel with the knob summit, 1 mm from the surface; taller knobs may also contain poorly-developed vesicular pores; and sharp protrusions of filaments, silt and	All crust types, most pervasive in cyanobacteria-dominated crusts		Figures 1B, 4, 5, 6, 9A, 16, 17
Upturned features	Biological or bio-sedimentary structures partially detached from the soil surface; examples include lichen thalli, filaments, and filament sheets; biological structures may curl upwards and downwards in conjunction with attached grains.	All crust types		Figures 5, 6, 10A, 10C, 13B, 15B, 17C, 17D, 18A

Table 2.1(A): Summary of bio-sedimentary features

Bio-sedimentary Features

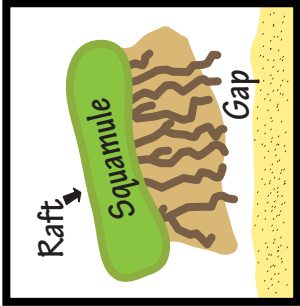
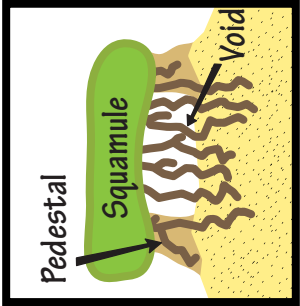
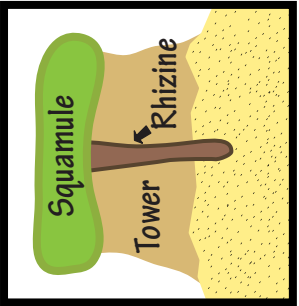
Feature	Characteristics	Occurrence	General Morphology	Examples
Rafts	Lichen thalli completely separated from the soil surface; grains or precipitates may be attached to or embedded within rhizines or exudates; rafts may form bio-sedimentary aggregates up to 1.1 mm thick and 2 mm long.	Short moss-lichen crusts, Tall moss-lichen pinnacled crusts		Figure 18B
Pedestals	Lichen squamules cap small sediment protrusions up to 0.75 mm tall; occur in conjunction with multiple-rhizine squamulose lichens such as <i>Placidium squamulosum</i> ; pedestals contain clays and silts; particles are often finer than underlying grains; interior of pedestal may contain a 1.5 mm diameter void with precipitate coated rhizines up to 1.5 mm long.	Tall moss-lichen pinnacled crusts		Figure 19A
Towers	Lichen squamules cap large, linear sediment protrusions up to 4.75 mm tall and 0.95 mm wide; <i>Placidium lacinulatum</i> lichen thalli have single, thick rhizines; towers contain sands but are dominated by silts and clays; rhizines may penetrate entire length of tower running parallel with 0.1 mm wide linear voids	Tall moss-lichen pinnacled crusts		Figures 6, 13B, 13D, 19B, 19C, 21B, 22B

Table 2.1(B): Summary of bio-sedimentary features - continued

Bio-sedimentary Features

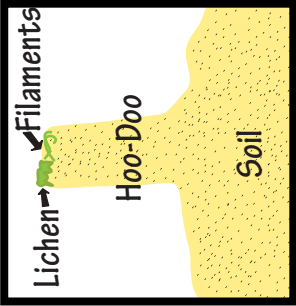
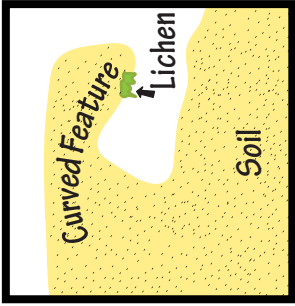
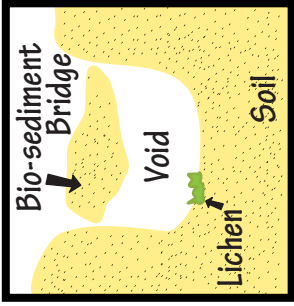
Feature	Characteristics	Occurrence	General Morphology	Examples
Hoo-doo & Sharp protrusions	Gelatinous lichens and filaments top "hoo-doo-like" protrusions and sharp bio-sediment aggregates; grain sizes include mostly sand with some clay and silt; protrusions show no obvious stratification and are up to 1 mm wide and 6 mm tall.	Tall moss-lichen pinnacled crusts		Figures 6, 14B, 20
Curved features	Thumb-like aggregates of grains and bio-structures that form "U" or "L" shapes; features may be up to 3.5 mm wide and 7 mm long; contain clay, silt, and sand; commonly occur in conjunction with sediment bridges and interior voids containing photosynthetic biostructures.	Tall moss-lichen pinnacled crusts		Figures 6, 22
Bio-sediment bridges	Horizontal, linear soil aggregates that may or may not contain biotic structures; aggregates are up to 12 mm wide and 24 mm long; often overlie interior voids as large as 24 mm by 36 mm; interior voids may contain photosynthetic biostructures; aggregates are comprised of sand, silt, and clay.	Tall moss-lichen pinnacled crusts		Figures 6, 7C, 8B, 21

Table 2.1(C): Summary of bio-sedimentary features - continued

Summary of Formative Processes

Category	Process	Description	Features
Stabilization	Binding	Biostructures enmesh and stabilize grains	Filament sheets, knobs, rafts, pedestals, towers
	Trapping	Biostructures capture grains and prevent immediate removal	Filament sheets, knobs, rafts, pedestals, towers
	Differential Erosion	Areas stabilized by physical, chemical, and biological cements mitigate effects of erosion compared to non-cemented areas	Filament sheets, knobs, pedestals, towers, hoo-doo
Accretion	Authigenic Mineral Precipitation	Minerals precipitate in situ, often in conjunction with metabolic processes of component biota	Filament sheets, knobs, pedestal, towers, pores
	Dust Capture	Atmospheric dust is captured and bound by biotic structures	Filament sheets, knobs, pedestals, towers
Wetting & Drying	Surface Sealing	Surface is sealed by biological structures, authigenic minerals, or physical crusts; augments air trapping in the formation of vesicular pores	Filament sheets, knobs, pedestals, towers
	Differential Drying	Biological structures dry from the exterior towards the interior; differences in drying rates of biological structures and soil textures causes curling	Upturned features, rafts, pedestals, towers
	Heaving	Expansion processes associated with wetting and drying; trapped air located below surface seals will expand and heave upon drying	Vesicular and irregular pores
Mass-Wasting	Toppling	Mass movement of aggregate with rotation along basal axis	Bio-sediment bridges
	Creep	Downslope movement of bio-sedimentary structures associated with wetting and drying cycles	Curved features
	Sloughing (Collapse)	Destabilization and downward movement of bio-sedimentary structures or soil aggregates	Bio-sediment bridges

Table 2.2: Summary of processes forming biological soil crusts and bio-sediment features

CHAPTER 3
CO-DEVELOPMENT OF BIOLOGICAL SOIL CRUSTS AND
SOIL-GEOMORPHOLOGY

Abstract

Biological soil crusts (BSCs) are bio-sedimentary features that are critical to geomorphic and ecological processes because they mitigate erosion, manage water and energy balances, fix C and N, and influence plant communities. This study investigated the relationship of BSCs to soil-geomorphology and the feedback mechanisms that control their co-development. Extensive mapping, surface characterization, GIS overlays and statistical analyses investigated relationships among BSCs, geomorphic surfaces, and soil types. Results indicate that geomorphic processes control the surface sand-to-rock ratio, which constrains the development of three surface cover types across intermontane basins. (1) Cyanobacteria crusts grow where abundant sand and negligible rocks form highly unstable, saltating sand sheets. Cyanobacteria allow moderate sand saltation that reduces growth potential of mosses and lichens. (2) Extensive tall moss-lichen pinnacled crusts are favored on mid- to late Holocene surfaces composed of mixed rock and sand. Moss-lichen crusts along these surfaces induce a positive feedback mechanism of dust capture that forms biologically-mediated Av horizons and promotes further crust propagation. (3) Low to moderate moss-lichen crusts with some form of “desert pavement” grow along early Holocene and older geomorphic surfaces with high rock cover and little surficial sand. Rock cover reduces BSC growth potential and supports “desert pavement” processes. Overall, geomorphic relationships predict abundance of BSCs and biogeomorphic feedbacks across intermontane basins. These findings also

provide important insight into soil physical processes that control crusts worldwide. The co-development of BSCs and soil-geomorphic processes should be incorporated into landscape models, as scientists and land managers address issues of climate change and anthropogenic disturbance.

Introduction

Biological soil crusts (BSCs) provide crucial soil cover in arid landscapes. These crusts are complex matrices of soil particles, cyanobacteria, lichens, mosses, algae, microfungi, and bacteria (see Chapter 2)(Friedmann and Galun 1974). Biotic structures grow around surface sediments, fusing into a desert skin that mitigates erosion (Campbell et al. 1989, Belnap and Gardner 1993, McKenna Neuman et al. 1996, Eldridge and Leys 2003, Bowker et al. 2008). BSC organisms are ecosystem engineers (Bowker 2007) that prevent desertification through soil organic matter and nutrients inputs (e.g., Kleiner and Harper 1977, Evans and Belnap 1999, Elbert et al. 2009), management of soil moisture and temperature (e.g., Chapter 2, Booth 1941, Belnap 1995, DeFalco et al. 2001, Belnap 2006), enhancement of landscape stability (e.g. Booth 1941, McKenna Neuman et al. 1996, Canton et al. 2003, Li et al. 2004, Thomas and Dougill 2007, Chaudhary et al. 2009), and interactions with vascular plant communities (e.g., DeFalco et al. 2001, Li et al. 2005, Escudero et al. 2007). The ecological impacts of BSCs are potentially enormous, as crusts can comprise 70 percent of the living soil cover in arid landscapes (Belnap 1994).

BSCs vary widely in their species compositions and surface morphologies. Early succession crusts, or smooth crusts, are primarily composed of filamentous cyanobacteria

that stabilize soil for less-motile organisms (Figure 3.1)(see Chapter 2)(Belnap 2001). Filamentous cyanobacteria influence texture by capturing small volumes of dust within their sticky, polysaccharide sheaths (see Chapter 2)(Belnap and Gardner 1993). Once soils are stable, mosses and lichens colonize the surface along with cyanobacteria to form short moss-lichen crusts (Figure 3.2)(see Chapter 2)(Belnap 2001). Over time, moss-lichen BSCs collect significant amounts of dust, which leads to formation of tall moss-lichen pinnacled crusts (Figure 3.2) (see Chapter 2). Dust capture (Belnap and Gardner 1993) and surface sealing form vesicular pores within or below moss-lichen crusts (see Chapter 2) (Danin et al. 1998, Issa et al. 1999, Canton et al. 2003, Marsh et al. 2006), while mineral Av horizons build-up below the pinnacle mounds (see Chapter 2). The exact age of these crusts is unknown; although, some estimate crust succession takes 10s to 1000s of years (Belnap and Warren 2002, Nagy et al. 2005, Zhang 2005, Thomas and Dougill 2007, Kidron et al. 2008, Williams et al. 2008, Langhans et al. 2010).

A number of predictive models for BSC distribution have been developed for deserts of the southwestern U.S. and other parts of the world (Eldridge and Greene 1994, Kidron et al. 2000, Ponzetti and McCune 2001, Belnap et al. 2006, Bowker et al. 2006, Thomas and Dougill 2006, Bowker 2007, Bowker and Belnap 2008, Rivera-Aguilar et al. 2009). Such studies have identified factors that may influence BSC distribution and species composition (Table 1). Currently, no predictive models exist for Mojave Desert crusts. Many of the studies that explain BSC distribution have come from cooler, or wetter deserts with different soil types (Ponzetti and McCune 2001, Bowker et al. 2006a, 2006b, Bowker and Belnap 2008). Furthermore, only a few studies have considered the interaction of BSCs with physical soil-forming processes or geomorphic processes

(Brostoff 2002, Bowker et al. 2005, Thomas and Dougill 2006, 2007, Wang et al. 2007, Bowker and Belnap 2008, Lazaro et al. 2008). Many BSC-geomorphic studies have focused on erosional relationships or substrate availability (Booth 1941, Campbell et al. 1989, Pluis and de Winder 1989, Belnap 1995, McKenna Neuman et al. 1996, Marticorena et al. 1997, Eldridge 1999, Canton et al. 2003, Eldridge and Leys 2003, Li et al. 2004, Bowker et al. 2008, Guo et al. 2008, Lazaro et al. 2008). Other biogeomorphic studies have focused on parent material influences (Bowker and Belnap 2008) or solar insolation and dust capture controls of BSC distribution (Kidron et al. 2010, Li et al. 2010). Given the dust-capturing abilities of BSCs (see Chapter 2), crusts could play a synergistic role in soil-geomorphic evolution.

Surface stability (Kidron et al. 2000, Bowker et al. 2005, Thompson et al. 2006, Bowker and Belnap 2008, Rivera-Aguilar et al. 2009), topography (Bowker et al. 2005, 2006b, Lazaro et al. 2008, Li et al. 2010), rock cover (Kaltenecker et al. 1999, Quade 2001), soil texture or mineralogy (Belnap 2002, Canton et al. 2003, Bowker et al. 2005, Thompson et al. 2005, Bowker et al. 2006, Bowker and Belnap 2008, Budel et al. 2009, Rivera-Aguilar et al. 2009), and hydrological dynamics (Lazaro et al. 2008, Rivera-Aguilar et al. 2009, Bowker et al. 2010b) are key factors influencing BSC distribution and species composition that commonly vary as a function of soil-geomorphology (Peterson 1981, Bull 1991, Young et al. 2004, Bowker and Belnap 2008, Meadows et al. 2008, Robins et al. 2009). For example in the Chihuahuan Desert, the soil-geomorphic template forms a framework upon which vegetation communities are built (Monger and Bestelmeyer 2006). Moreover, the soil-geomorphic template also has been hypothesized to influence ecological responses to climate and land use change (Peters et al. 2006).

Like the Chihuahuan Desert, the Mojave Desert lies within the Basin and Range physiographic province. Both deserts display similar expression of intermontane-basin landforms that correspond to predictable soil properties (Peterson 1981). I hypothesize that the geomorphic controls on soil properties also control BSC distribution within the Mojave Desert.

The objectives of this study are (1) to investigate the relationships among geomorphology, soils, and BSC distribution in the Mojave Desert; (2) to understand the landscape feedback mechanisms that control geomorphic stability, pedogenesis, and BSC development within the region; (3) to develop a physical process model that explains the co-development of BSCs, soils, and geomorphology; and (4) to use soil-geomorphic relationships to predict BSC distribution for land management applications.

Background and Geologic Setting

The study site lies within the Hidden Valley Area of Critical Environmental Concern (ACEC), inside the Muddy Mountains Wilderness Area (MMWA), Clark County, NV (Figure 3.3). The site lies at 36°20'N and 114°42'W. The area is ideal for studying BSC-soil-geomorphic interactions as the valley contains well-developed BSCs, variable crust distribution, and numerous geomorphic surfaces. The site also displays soils and vegetation communities that are common to the Mojave Desert.

The study area lies within the Mojave Desert climate zone, characterized by hot, dry summers and cool, moist winters. The site has thermic temperature and aridic moisture regimes, with average annual temperatures of 27°C and mean annual precipitation of 114 mm (Gorelow and Skrbac 2005, Soil Survey Staff 2010b). Most

precipitation falls from January to March, when average highs range from 14-21°C.

Summers are primarily dry with some precipitation during the warmest months of July and August, when average highs range from 39-40°C (Gorelow and Skrbac 2005).

Hidden Valley is a semi-enclosed basin that drains to the north by a single wash (Figure 3.4). Mountains formed in carbonate and sandstone bedrock rise up to an elevation of 1642 m and surround the basin floor that lies at 1000 m. These mountains formed during Sevier-age thrusting when Paleozoic carbonates were thrust eastward over younger Jurassic Aztec Sandstone along the Muddy Mountain Thrust Fault (Beard et al. 2007). Erosion of the upper plate of the thrust created a structural window that exposes the underlying Aztec Sandstone, forming the basin known as Hidden Valley (Figure 3.4). The valley contains distinct alluvial geomorphic surfaces, with interspersed sand sheets, and colluvium. These geomorphic surfaces display varied soil characteristics and surface morphology. A 2.8 km² subregion of Hidden Valley that contains variable geomorphic and BSC characteristics was chosen for this investigation (Figure 3.4).

The study area is a significant management concern to BLM, as Hidden Valley contains some of the most well developed BSCs within the Mojave Desert. Off-highway vehicles (OHVs) have been prohibited since the area was designated a Federal Wilderness in 2002, but OHV tracks continue to scar the landscape. Hidden Valley was previously grazed, but the trampling effects of livestock on the area's BSCs are unknown. Despite apparent disturbance to the area, Hidden Valley's crusts have remained relatively pristine compared to other Mojave Desert locations. As Hidden Valley becomes increasingly popular to hikers and sightseers, off-trail foot traffic and illegal OHV use are becoming significant management concerns.

Materials and Methods

Detailed field mapping and characterization of BSCs and soil-geomorphology were completed with the 2.8 km² subregion of Hidden Valley, in the Muddy Mts. Wilderness, NV, U.S.A. (Complete methods are described in Appendices 1.2, 1.3, and 1.4). Detailed field mapping delineates BSC and geomorphic features (Appendix 1.2). Extensive data collection included BSC features, vascular vegetation, surface characteristics, soil development, and geomorphic characteristics. Geomorphic units are correlated to soil types (Appendix 1.2) and surface soil samples were collected and analyzed for physical properties (Appendix 1.2). Data were compiled and processed for analyses (Table 3.2, Appendix 1.2). GIS overlays quantified spatial relationships among BSC types and geomorphic surfaces (Appendix 1.3). Statistical analyses (Appendix 1.4) including ANOVAs (Figure 3.5) and correlation coefficients quantify relationships among BSC and soil-geomorphic characteristics.

Results

Mapping and Characterization

BSC species composition varies throughout the site and includes three morphotypes: (1) cyanobacteria, (2) short moss-lichen, and (3) tall moss-lichen pinnacled crusts (Figures 3.1, 3.2). Cyanobacterial crusts are smooth and dominated by filamentous cyanobacteria such as *Microcoleus*. These crusts may also have associated physical or chemical crusting (see Chapter 2) and occur in conjunction with bare soil. Short moss-lichen crusts are characterized rolling surface morphologies and less than 2 cm of vertical relief. In these crusts, moss and lichen colonies are generally scattered among

cyanobacteria crusts dominated by taxa such as *Microcoleus*. Mosses include *Syntrichia caninervis*, *Bryum*, and *Pterygoneurum*. Gelatinous lichens are primarily *Collema*. Squamulose lichens include *Placidium*, *Psora decipiens*, and *Peltula*. Tall moss-lichen pinnacled crusts are also composed the same moss, lichen, and cyanobacteria taxa but have rougher, “pinnacle” morphology with up to 5 cm of vertical microrelief. The density of the three crust types varies throughout the site.

Vascular vegetation within the basin of Hidden Valley is dominated by *Larrea tridentata*, *Ambrosia dumosa*, *Menodora spinescens*, *Krameria erecta*, *Coleogyne ramosissima*, *Psoralea fremontii*, *Hymenoclea salsola*, *Pleuraphis rigida*, and *Ephedra nevadensis*. Other common species include *Opuntia basilaris*, *Cylindropuntia echinocarpa*, *Encelia farinosa*, *Prunus fasciculata*, *Krascheninnikovia lanata*, *Salvia dorrii*, *Sphaeralcea ambigua*, *Eriogonum fasciculatum*, *Eriogonum inflatum*, *Lycium copperi*, *Tiquilia canescens*, *Chilopsis linearis*, and *Lycium andersonii* (Baldwin et al. 2002). *Bromus rubens* is a common invasive species that can be found throughout the valley, within plant interspaces, below shrubs, or invading BSC patches.

BSC Mapping and Characterization

In this study, 10 map units delineate the range of interspace BSC types and morphologies (Tables 3.3, 3.4). (See map in Appendix 3.) Units are divided according to their relative aerial cover by cyanobacteria-bare crusts, short moss-lichen crusts and tall moss-lichen pinnacled crusts. Short moss-lichen crusts generally occur in conjunction with cyanobacteria crusts and are included within the cyanobacteria-bare map units. Tall moss-lichen (ML) map units have high density tall moss-lichen pinnacled crusts, or \geq 40% mean interspace cover. ML.1 and ML.3 have $>50\%$ mean tall moss-lichen

interspace cover, while ML.1 has approximately 42% cover (Tables 3.4D, 3.4E, 3.4F). ML.1 also has greater mean cyanobacteria-bare cover (26%) than ML.2 and ML.3, which have 11% and 15%, respectively. Tall moss-lichen units also vary with respect to rock cover and soil surface characteristics. ML.1 has 10% mean interspace rock cover, while ML.2 and ML.3 have 26% and 27%, respectively. Map unit ML.3 is also unique in that it commonly occurs in shallow soils with bedrock at depths of 9 cm or less (Table 3.4D, 3.4E, 3.4F). Scattered tall moss-lichen units (S) have low to moderate density tall moss-lichen crusts, or 5-20% mean interspace cover. S.1 and S.2 both have moderate density tall moss-lichen crusts, with approximately 16% mean interspace cover (Table 3.4G, 3.4H). S.2 has much greater cyanobacteria-bare cover (29%) than S.1 (17%). S.3 has low to moderate moss-lichen cover (13%) and cyanobacteria-bare cover (11%), while S.4 has low moss-lichen densities (8%) and low cyanobacteria-bare cover (6%)(Table 3.4I, 3.3J). Units S.1, S.2, S.3, and S.4 have moderate to high mean interspace rock density, from 36-83%, with clasts lying among scattered BSCs. Map unit S.2 contains moderate density embedded surface gravel with mean interspace cover at 36% (Table 3.4H), while S.1 has high density (57%) non-embedded surface gravel (Table 3.4G). Map unit S.3 has high density (72%) partially embedded surface gravel composed of >50% petrocalcic clasts. These areas commonly occur on flat, elevated soil surfaces (Table 3.4I). Map unit S.4 has the highest mean interspace rock cover (83%) and commonly occurs along slopes of 15% or greater (Table 3.4J). The cyanobacteria-bare units (CB) have high composite cover by cyanobacteria and bare soil, with interspace mean cover of $\geq 45\%$. These units vary according to their relative density of short moss-lichen crusts. Map unit CB.1 has the greatest interspace cyanobacteria-bare cover (68%) and the lowest interspace short

moss-lichen cover (2%)(Table 3.4A). In contrast, CB.2 has 64% bare soil and cyanobacteria interspace cover and 10% short moss and lichen interspace cover (Table 3.4B). Map unit CB.3 includes variable short moss-lichen crusts and variable cyanobacteria-bare cover. This unit commonly lies adjacent to the active washes (Table 3.4C). Four additional surface features were delineated including limestone bedrock, sandstone bedrock, active washes, and off-road vehicle tracks (Table 3.4K). None of these features were formally described because they lacked BSC development.

Geomorphic Mapping and Characterization

The geomorphic map contains 12 units defined as alluvial, colluvial or eolian (Figure 3.6; Tables 3.5, 3.6). (See map in Appendix 4.) Based on surface and soil characteristics, the alluvial units are estimated to range in age from recent, active channels to earliest Pleistocene or late Miocene relict fans (Sowers et al. 1989, Bull 1991, Harden et al. 1991, Reheis et al. 1992, Peterson et al. 1995, Bell et al. 1998, 1999, Brock and Buck 2005, Page et al. 2005, Brock and Buck 2009, House et al. 2010). The alluvium in this basin is primarily composed of locally-derived limestone clasts, and to a lesser extent, sandstone clasts. Much of the eolian sand is seemingly derived from the nearby outcrops of Aztec Sandstone and commonly incorporated with alluvium. Recent active channels (Table 3.6A), Qay₄, have negligible soil development. They display fresh bar-and-channel morphology and lie adjacent to recently abandoned, latest Holocene inset fans, Qay₃, which display similar characteristics (Table 3.6B). Mean interspace rock cover for these units is 46%. Mid- to late Holocene inset fans, Qay₂ and Qay₁, are characterized by intermediate interspace rock cover that range from 18-25% and muted to faint, bar-and-swale morphology (Tables 3.6C, 3.6D). These surfaces have Av horizons

ranging from 15-27 cm in thickness and display Stage I-II carbonate morphology (Gile et al. 1966, Bachman and Machette 1977, Machette 1985). The mid- to late Holocene Qay₂ surfaces have much more interspace sand than the recently abandoned Qay₃ inset fans and start a notable trend in which interspace rock cover increases with increasing age. This trend continues up through the oldest QTa surfaces. The early to late Pleistocene Qai inset fan surfaces have high interspace rock or desert pavement cover, ranging from 36-49% (Tables 3.6E, 3.6F, 3.6G). Surfaces are planar, and desert pavements may be poorly to moderately interlocking. These surfaces have Av horizons ranging from 10-13 cm thick and show strong Stage III-V carbonate morphology. Early Pleistocene ballenas, Qao₂, have poorly interlocking desert pavements composed of limestone and petrocalcic fragments and 18-cm-thick Av horizons (Table 3.6 H)(Peterson 1981). Soil profiles exposed on sideslope shoulders show Stage II Bk horizons that overlie Stage III-IV Bkkm, or petrocalcic horizons. Mean rock fragment cover is 63% within interspaces. Map units Qao₁ and QTa are late Miocene to earliest Pleistocene erosional fan remnants (Tables 3.6I, 3.6J) that lie several meters above the early Pleistocene ballenas, or Qao₂. They have poorly to moderately interlocking desert pavements composed of petrocalcic clasts and 8-9-cm-thick Av horizons and shallow Stage V-VI Bkkm horizons. Mean interspace rock fragment cover is 63-80%. These late Miocene to earliest Pleistocene erosional fan remnants have likely been protected from backslope erosion by underlying bedrock that outcrops locally. Colluvium, Qc, is highly variable within the field area and could range from latest Pleistocene to Holocene in age (Table 3.6K)(House et al. 2010). Colluvial deposits commonly occur below steep cliffs with particle sizes ranging from fine sand up to boulder-sized talus. Mean interspace rock cover is 83%. Eolian units,

Qea, are Holocene sand sheets with an eolian/fluvial gravel lag (Table 3.6L). The single layer of rocks on the soil surface covers approximately 30% of interspaces. These sand sheets may have Stage I fine carbonate filaments. Map units composed of sandstone and limestone bedrock, and off-highway vehicle (OHV) tracks are also delineated (Table 3.6M).

Characterization of these geomorphic surfaces is primarily based upon data collected from surface characterization plots and soil profiles. A few units were less rigorously characterized. Qay₄ surface characteristics were estimated visually, but not characterized with plot data. No soil profile exposures were available, as the active channels are topographically the lowest unit in the landscape. Late Miocene to earliest Pleistocene QTa erosional fan remnants did not receive plot data characterization, but surface characteristics were estimated based on ocular estimates adjacent to the exposed profile. Ocular estimates from Late Miocene to earliest Pleistocene QTa had comparable surface characteristics to those found in the earliest Pleistocene Qao₁ erosional fan remnants. No colluvial, or Qc, soil profiles were described, as there were no available exposures. However, these surfaces were characterized with plot data.

Soil Characterization

Eight soil types correspond to the 12 geomorphic surfaces in the area (Tables 3.5, 3.7). Geomorphic units correlate with four USDA Official Soil Series. Four units do not successfully correlate but are named according to their soil taxonomy or depositional setting. Because wilderness restrictions prevent soil pits, soils data are limited to surface exposures from 14 locations. Therefore, soil characteristics are not comprehensively described nor mapped but roughly estimated. Soil types were assumed to correlate across

a single geomorphic surface and characteristics were generally extrapolated from one arroyo profile description. Profiles of active channels, Qay₄, were not described, so these units were classified as Unspecified Entisols (Table 3.7A). Recently abandoned or latest Holocene Qay₃ inset fans included two phases, gravel bars and sandy swales, that both displayed negligible soil development. These inset fans were classified as 2-Phase Entisols (Table 3.7B) and named according to their respective taxonomic classifications: (1) sandy-skeletal, mixed, thermic Typic Torriorthents and (2) mixed, thermic Typic Torripsamments. Mid- to late Holocene Qay₂ and Qay₁ inset fans have Stage I-II carbonate morphology and 15-27-cm-thick Av horizons (Table 3.7C). Their pedons are classified as sandy-skeletal, mixed, thermic Typic Torriorthents, which correlate to the Arizo series. The Pleistocene Qai inset fans have Stage III-IV Bkkm horizons within 45 cm of the soil surface and 9-16-cm-thick Av horizons (Table 3.7D). Pedons on Pleistocene Qai inset fans are classified as loamy, mixed, thermic shallow Typic Petrocalcids, which correlate with the Irongold Series. The early Pleistocene Qao₂ ballenas have shallow Bkkm horizons within 28 cm of the soil surface, which are overlain, by diagnostic calcic horizons (Table 3.7E). The soils were classified as loamy-skeletal, mixed, thermic, shallow Calcic Petrocalcids, which correspond to the Ferrogold Series. The late Miocene to earliest Pleistocene Qao₁ and QTa erosional fan remnants have shallow Stage V-VI petrocalcic horizons at a depth of 8-9 cm (Table 3.7F). These pedons were classified as loamy-skeletal, mixed thermic, shallow, Typic Petrocalcids, which did not directly correlate with any existing soil series. They are referred to as shallow Typic Petrocalcids. Latest Pleistocene to Holocene colluvial, or Qc, units are highly variable, and their profiles are not exposed, so these units were classified as

Unspecified Colluvium (Table 3.7G). Holocene Qea surfaces are deep sand sheets with negligible soil development that may show Stage I carbonate filaments (Table 3.7H). Their pedons classify as mixed, thermic Typic Torripsamments, which correlate to the Bluepoint Series.

GIS Analyses

GIS overlays reveal relationships between BSCs map units and geomorphic map units. Overall, there are three dominant BSC surface cover types: (1) cyanobacteria-bare crusts, (2) high density tall moss-lichen pinnacled crusts, and (3) scattered low to moderate density tall moss-lichen crusts that commonly display some type of “desert pavement” or pavement-like rock cover. These surface cover types correspond to specific geomorphic surfaces and correlated soil types (Table 3.8). Sixty-six percent of the extensive cyanobacteria-bare crusts, which occur in CB.1, lie within deep Holocene sand sheets, or Qea. High density tall moss-lichen pinnacled crust units ML.1 and ML.2 have 57-59% of their surfaces that lie within mid- to late Holocene Qay₁ and Qay₂ inset fans. Sixty-three to eighty-seven percent of units with scattered low to moderate density tall moss-lichen crusts (S.1, S.2, and S.3), which commonly display moderate to high density rock cover, lie within Pleistocene and older surfaces, or Qai, Qao, and QTa. Those geomorphic surfaces include inset fans, ballenas, and erosional fan remnants older than mid-Holocene.

Despite these overarching patterns, BSC map units show complicated overlapping relationships with geomorphic surfaces (Figures 3.7, 3.8). The cyanobacteria-bare CB.1 and CB.2 map units predominantly occur along active sand sheets, Qea. However, mid- to late Holocene Qay₂ and several other alluvial surfaces also share some overlap with

CB.1 (Figure 3.7). High density, tall moss-lichen BSC map units ML.1 and ML.2 overlap significantly with Qea sand sheets. High density tall moss-lichen unit ML.3, which commonly occurs in thin soils adjacent to exposed Aztec Sandstone bedrock, overlaps with Qea sand sheets and several alluvial surfaces. While units of scattered tall moss-lichen crusts commonly occur along alluvial surfaces older than mid-Holocene, they also overlap with Qea sand sheets and young Qay surfaces. Similar complexities arise when comparing soil geomorphic overlap with various crust units (Figure 3.8). Sand sheets, or Qea, have the greatest cover by cyanobacteria-bare BSC map units CB.1 and CB.2. However, the younger alluvial Qay₃, Qay₂ and Qay₁ surfaces also have significant cover by BSC map units CB.1 and CB.2. Pleistocene Qai alluvial surfaces also have small overlaps with the cyanobacteria-bare units. Mid- to late Holocene Qay₂ and Qay₁ inset fans show the greatest cover by high density tall moss-lichen BSC map units ML.1 and ML.2. However, these BSC map units comprise only a fraction of the total surface area of these geomorphic surfaces. Areas of scattered tall moss-lichen crusts are most strongly expressed on Pleistocene and older Qai, Qao, and QTa surfaces. The young Qay alluvial surfaces and active sand sheets, Qea, also show some cover by scattered tall-moss lichen units.

Statistics

Multi-Response Permutation Procedure (MRPP)

The Multi-Response Permutation Procedure (MRPP) indicates all BSC, geomorphic, and interpreted soil map units effectively differentiate between different types of soil interspace cover (Table 3.9). This analysis does not indicate which types of surface cover correspond to various map units but merely indicates whether different map

units, or groups, display differences in surface cover. MRPP results are reported as association values (A) and p -values of significance. When $A=1$, group members are identical; and when $A=0$, group members are not similar. McCune and Grace (2002) state that $A>0.3$ are high values for ecological data sets. MRPP analyses show BSC map units had the greatest association values with $A=0.52$ at $p=0.00000000$. Geomorphic map units have the next highest association values with $A=0.35$ at $p=0.00000657$. Correlated soil types have high association values of $A=0.29$ at $p=0.00000875$.

ANOVA

Parametric and non-parametric ANOVA also found significant relationships in the plant canopy and interspace characteristics among four geomorphic surface groups (Figures 3.9, 3.10, 3.11, 3.12). Groups tested include mid- to late Holocene inset fans Qay_2 - Qay_1 , sand sheets Qea , Pleistocene Qai inset fans, and the late Miocene to earliest Pleistocene QTa - Qao_1 erosional fan remnants (Figure 3.5). Mid- to late Holocene Qay_1 - Qay_2 surfaces have elevated canopy cover by *Bromus* exotic grass, *Collema* lichen, *Placidium* lichen, and moss-lichen cover (Figure 3.9). Pleistocene Qai surfaces have elevated canopy cover by *Coleogyne ramosissima*, *Collema* lichen, and *Placidium* lichen (Figure 3.9). Late Miocene to earliest Pleistocene QTa - Qao_1 erosional fan remnants have elevated canopy cover by *Coleogyne ramosissima*, *Collema* lichen, *Placidium* lichen, limestone clasts, and total rock cover (Figure 3.9). Pleistocene Qai inset fans also have elevated canopy clay contents (Figure 3.10). Mid- to late Holocene Qay_1 - Qay_2 surfaces have elevated interspace cover by mosses, *Collema* lichen, *Placidium* lichen, and moss-lichen (Figure 3.11). Sand sheet, or Qea , surfaces have elevated interspace non-grass plant litter (Figure 3.11). Pleistocene Qai surfaces have elevated interspace total rock

cover (Figure 3.11). Late-Miocene to earliest Pleistocene QTa-Qao₁ surfaces have elevated interspace petrocalcic clast cover and total rock cover (Figure 3.11). Total interspace sand is elevated in mid- to late Holocene Qay₁-Qay₂ inset fans and Qea sand sheets, while interspace clay and silt are elevated in the Pleistocene Qai surfaces (Figure 3.12).

Correlation Coefficients

Parametric and non-parametric correlation coefficients (Tables 3.10, 3.11) reveal important relationships among soil canopy characteristics. Canopy cyanobacteria, total BSCs, rock cover, *Hymenoclea*, and litter are negatively correlated with Canopy *Bromus* cover. Bare soil is positively related to *Hymenoclea*, *Menodora*, fine sand, and total sand but negatively related to *Ambrosia* canopies, silt and very fine sand. *Placidium* is negatively correlated to *Pleuraphis* canopies and fine sand, and *Psora* is positively correlated to *Tiquilia* and *Krascheninnikovia* canopies. In addition, *Larrea* is negatively correlated with limestone cover, total rock cover and *Coleogyne*. *Hymenoclea* is negatively related to *Ambrosia* and *Bromus*. Rock categories are positively correlated to silt contents but negatively correlated to fine sand and total sand. *Pleuraphis* is negatively correlated to silt content and positively correlated to fine sand and total sand.

Parametric and non-parametric correlation coefficients (Tables 3.12, 3.13) indicate significant relationships among soil interspace characteristics. Mosses and all lichens show positive correlations. Limestone and total rock cover are negatively correlated to cyanobacteria cover, total BSC cover, and fine sand. *Placidium* lichen is negatively correlated to bare soil and fine sand and positively correlated to silt and very fine sand. Moss cover is negatively related to clay content. Maximum pinnacle height is

positively correlated to cover by mosses, *Collema* lichen, *Placidium* lichen, total moss-lichen, and total BSCs. Total rock cover is positively correlated to silt but negatively correlated to fine sand and total sand. Bare soil cover is negatively correlated to petrocalcic cover, silt, and very fine sand and positively correlated to fine sand and total sand.

Interpretations

Geomorphic Trajectory and Landscape Models

The ratio of fine sand to rocks constrains the development of three alternative surface-cover trajectories: (1) cyanobacteria crusts, (2) tall moss-lichen pinnacled crusts, and (3) “desert pavement” with low to moderate BSCs (Figure 3.13). The relative concentration of surficial fine sand and rocks controls BSC type and distribution by impacting stability, surface roughness, and morphology of the fine-grained matrix. Geomorphic processes determine relative elevation and proximity to sand sources, allowing prediction of the sand-to-rock ratio and surface cover within intermontane basins (Figure 3.14).

Cyanobacteria Crust Trajectories

Cyanobacteria dominate sand sheets and geomorphic surfaces composed primarily of sand and few rocks that display high sand saltation (Figure 3.13, 3.14). These crusts commonly occur in conjunction with bare soil. With negligible gravel present in these sand sheets, sand grains are free to move as allowed by local vegetation and wind patterns (Figure 3.15). While gravel lags may be common along these surfaces, they often do not significantly reduce sand saltation. These characteristics are best

expressed along deep active sand sheets, but they also occur in sandy swales of recently abandoned inset fans or as thin sand sheets overlying mid- to late Holocene inset fans (Figures 3.6, 3.14, 3.15). Surfaces composed of fine sands provide the optimal fine-grained substrate for extensive cyanobacteria propagation. Filamentous cyanobacteria are better adapted to sand sheet activity than other BSC organisms because they can move to reclaim soil surfaces after burial.

Moss-lichen Crust Trajectories

Moss-lichen crusts, which eventually form biologically-mediated Av horizons, are best expressed on geomorphically stable inset fans composed of mixed sand and gravel (Figures 3.13, 3.14). These crusts also contain some cyanobacteria cover. Rocks that are embedded near the soil surface impart additional stability and reduce sand saltation (Figure 3.15). These surfaces still have large expanses of surficial sand for BSC development, but decreased sand saltation increases stability and allows non-motile microorganisms such as mosses and lichens to colonize. Recently abandoned Qay₃ inset fans, formed in mixed sand and gravel, experience occasional alluvial activity, which supports growth of patchy, short moss-lichen crusts interspersed with cyanobacteria crusts (Figures 3.14, 3.15). Because of intermittent destruction by channel avulsion, there may not be sufficient time to form tall moss-lichen pinnacled crusts or Av horizons on these very young surfaces. In contrast, mid- to late Holocene inset fans do not experience alluvial activity yet have mixed sand and gravel that provide extensive and stable fine-grained substrates (Figures 3.14, 3.15). The increased surface stability facilitates development of extensive tall moss-lichen pinnacles (Figure 3.15), which incrementally capture dust to form biologically-mediated Av horizons (see Chapter 2).

Dust accumulation on pinnacle surfaces increases microtopography and surface roughness that augments surficial dust accretion and creates new surfaces for moss and lichen colonization. Mid- to late Holocene surfaces have high surface roughness that enhances landform-scale dust capture and often are located near dust sources such as modern channels and playas. Dust accretion leads to the accumulation of clay, silt, and very fine sand at the surface, which together with vesicular pore development (see Chapter 2), increases water-holding capacity and soil fertility for crust organisms. Moss and lichen dust capture has different biological consequences than that of “desert pavements.”

“Desert Pavement” Trajectories

Surfaces with high rock cover density and low fine-grained substrate availability provide unsuitable habitats for extensive BSC growth (Figures 3.13, 3.14). In my model, I term these surfaces “desert pavements,” but this includes a wide range of surfaces from well-developed, tightly interlocking desert pavements to highly degraded desert pavements and eroded surfaces that have moderate to high density rock cover. Rock covered surfaces follow a trajectory that forms well-developed, tightly interlocking desert pavements and minimizes potential growth by BSCs.

In the Mojave Desert, “desert pavements” with the least BSC cover occur along early-Holocene to latest Pleistocene surfaces. These surfaces are elevated from sand influx. With little sand to dilute gravelly alluvium, rock cover is high (Figure 3.15). Over time, dust accumulates below surface rocks to form abiotically-mediated Av horizons and tightly interlocking “desert pavements.” Such high rock cover provides negligible fine-grained substrates for BSC colonization (Figure 3.15). In addition, the

smooth morphology of well-developed “desert pavement” surfaces supports less dust capture than rougher surfaces (Figure 3.15) and tends to increase runoff and decrease infiltration. These conditions provide only marginal BSC habitat and support very few crusts. Low biological colonization and activity associated with “desert pavements” minimizes biotic disturbance and promotes pavement integrity.

Late Pleistocene and older inset fans and ballenas have poorly to moderately interlocking “desert pavements,” with some exposed clay- and silt-rich surfaces (Figures 3.14, 3.15). Backslope erosion has disrupted “desert pavements” and created spaces where scattered tall moss-lichen pinnacled crusts commonly develop. However, these smooth “desert pavement” surfaces still have low dust capture potential, high runoff, and decreased infiltration, which further restricts BSC growth potential. While lower rock cover facilitates greater crust development than areas with interlocking “desert pavements,” total BSC cover is lower than along mid-Holocene and younger inset fans and sand sheets.

Discussion

Feedback Model

Geological processes provide a framework for three types of soil interspace cover in the Mojave Desert. The relative input of fine sand combined with surface stability controls the initial development of cyanobacteria crusts, moss-lichen crusts or “desert pavement” with low to moderate BSCs. While the original trajectory is set by sand influx, surface cover types are sustained by self-enhancing biological and geological feedback mechanisms (Figure 3.16).

Cyanobacteria Feedbacks

Extensive fine sand provides the optimal substrate for terrestrial cyanobacteria growth and propagation (Figures 3.13, 3.16)(see Chapter 2)(Bowker and Belnap 2008). Studies from marine siliciclastic systems show fine sand composed of $\geq 95\%$ quartz favors filamentous cyanobacteria growth and microbial mat formation (Noffke et al. 2002, Noffke 2009). Quartz-dominated fine sands are the optimal grain size for filamentous cyanobacteria, less sticky than silts and clays, and sufficiently translucent for photosynthesis (Noffke et al. 2002, Noffke 2009). While the sands in this study contain lower quartz concentrations, light is not a limiting factor along these exposed soil surfaces (see Chapter 2). Because these substrates are optimal for filamentous cyanobacteria, understanding the distribution of fine sand is critical to predicting their growth across the landscape.

Geological and geomorphic processes control where fine sands occur, and thus, where cyanobacteria are most extensive. The Mojave Desert is a weathering-limited environment in which fine sands are fairly uncommon and occur only under special conditions (Bull 1991). Limestone and dolomite are dominant bedrock types that typically weather into gravel or boulders. The primary sources of sand are sand sheets derived from sandstone bedrock, arroyos, or playa margins (Figure 3.14)(Peterson 1981, Soil Survey Staff 2007, House et al. 2010). In this study, cyanobacteria are most extensive on active sand sheets, with 66% of the cyanobacteria-bare unit (CB.1) occurring along Holocene sand sheets (Qea)(Figure 3.14, Table 3.8). Sand sheets are generally found near sandstone bedrock outcrops or may overlie mid-Holocene or younger surfaces (Figures 3.6, 3.14). These surfaces lie at topographic lows and are more

likely to receive sand inputs than older, elevated surfaces. Other studies show that surfaces dominated by fine sand, such as sand sheets or dunes, favor cyanobacteria development (McKenna Neuman et al. 1996, Kidron et al. 2000, Belnap 2001, Wang et al. 2007, Bowker and Belnap 2008). The deficiency in fine sand of the Mojave Desert contrasts with deserts like the Colorado Plateau that contain extensive fine sands that weather from abundant sandstone bedrock. The prevalence of fine sands may explain the ubiquity of BSCs in the Colorado Plateau. Geomorphic stability of sandy surfaces varies from desert to desert. Sand sheets of cooler or wetter deserts, such as the Colorado Plateau, may have low sand saltation because higher water availability reduces sand sheet activity and supports greater vascular plant cover. Under the drier conditions of the Mojave Desert, sand-dominated geomorphic surfaces are characterized by high sand sheet activity.

Filamentous cyanobacteria life habits are well suited to sand saltation and sand sheet activity. These cyanobacteria are highly motile. Cyanobacteria filaments may be buried by sand grains, but after a rewetting event, they can move up toward sunlight to reclaim the soil surface (Campbell 1979, Belnap and Gardner 1993, Garcia-Pichel and Pringault 2001). However, if sand sheet activity is too high and propagules are too deeply buried, cyanobacteria will not reach the soil surface. Therefore, as in marine siliciclastic environments, moderately stable fine sands seem to be optimal for filamentous cyanobacteria such as *Microcoleus* (Noffke et al. 2002, Noffke 2009). Growth in the face of moderate instability is unique to filamentous cyanobacteria.

A positive feedback exists between cyanobacteria and active or saltating sand (Figure 3.16). Cyanobacteria bind sand grains, capture minute volumes of dust, and

partially stabilize fine sands (see Chapter 2)(Booth 1941, Campbell 1979, Belnap and Gardner 1993, Issa et al. 1999, Zaady and Offer 2010). Cyanobacteria further increase surface stability by forming surface crusts through fine-grained dust accretion and facilitation of calcium carbonate precipitation (see Chapter 2)(Campbell 1979, Campbell et al. 1989, Belnap and Gardner 1993, Verrecchia et al. 1995, Danin et al. 1998, McKenna Neuman and Maxwell 2002, Wang et al. 2007). Cyanobacteria stabilize sand sheets sufficiently for their own growth but still permit sand saltation. Such conditions are generally too unstable for moss-lichen crusts or “desert pavement” development. Therefore, these processes create a self-enhancing feedback that favors cyanobacteria propagation over other crust organisms and facilitates persistence of sand sheet activity in the absence of climate change or other extrinsic perturbations to the system.

Moss-Lichen Feedbacks

Moss-lichen crusts require stable, fine-grained substrates for initial colonization and high surface roughness for dust accretion and extensive propagation (Figures 3.13, 3.16). Mosses and lichens are relatively non-motile and require stability, in this case low sand saltation, for establishment and propagation (McKenna Neuman et al. 1996, Kidron et al. 2000, Belnap 2001, Wang et al. 2007, Guo et al. 2008). Cyanobacteria crusts augment stability of fine-grained surfaces. BSC development generally progresses from bare, fine-grained mineral soil to cyanobacteria-dominated crusts and eventually to moss-lichen crusts (Figure 3.17) (see Chapter 2)(Campbell 1979, Eldridge and Greene 1994, Danin et al. 1998, Belnap 2001, Langhans et al. 2010). However, in many cases, a climate or textural change is needed to adequately stabilize sand-dominated surfaces and to enhance dust capture for extensive moss and lichen growth.

Under current climatic conditions in the Mojave Desert, mixed sand and rock surfaces provide the optimal balance of stability, fine-grained surface availability, and surface roughness for moss and lichen propagation (Figure 3.15). These characteristics are best expressed on mid- to late Holocene inset fans, whose surfaces and profiles are composed of mixed sand and gravel. At the time of mapping, 57-59% of the extensive tall moss-lichen units ML.1 and ML.2 occurred along mid- to late Holocene inset fans (Qay₁-Qay₂)(Figure 3.14, Table 3.8). Along these surfaces, cyanobacteria-stabilized sands infill gravel to provide initial fine-grained substrates for moss and lichen colonization (Figure 3.18A, B)(Campbell 1979 Eldridge and Greene 1994, Belnap 2001, Eldridge et al. 2006, Langhans et al. 2010). In contrast, gravel bars that lack sandy matrices (Figure 3.18C, D) do not display BSCs. Surface rocks embedded within sands stabilize the sandy matrix and limit sand sheet activity (Figure 3.15). Rocks must be embedded for effective stabilization because non-embedded gravel lags can shift with sand saltation, permitting continued sand sheet activity (Buck et al. 2002). Observations of surface rock fragments alone do not sufficiently reflect subsurface characteristics such as stone embedding or stability (Buck et al. 2002). My observations suggest that profiles with sandy-skeletal particle size control sections, or $\geq 35\%$ rock fragments by volume within the upper decimeters of soil, provide the optimal mix of embedded rocks and fine sand (Table 3.6)(Soil Survey Staff 2010b). Embedded rocks from old gravel bars, as found along younger surfaces that retain their bar and swale morphology, increase surface roughness. High surface roughness enhances dust accretion (McFadden et al. 1986, Wells et al. 1987), providing new fine-grained substrates for mosses and lichens (see Chapter 2).

The presence of mid- to late Holocene surfaces, does not ensure extensive moss-lichen pinnacle cover. On a landscape scale, mid- to late Holocene surfaces composed of mixed rock and sand represent the most likely areas where extensive, tall moss-lichen pinnacled crusts can be found (Figure 3.14). Because these surfaces lie low in the landscape, often near to sand sources, they are commonly overlain by thin sand sheets with sufficient sand saltation to preclude extensive moss and lichen growth. In fact, while the most extensive moss-lichen crusts (ML.1 and ML.2) do occur along mid- to late Holocene surfaces in the study area, they cover only 10-19% of the total surface area of these landforms (Figure 3.8). If an area lacks sandstone bedrock, arroyos will contain far less sand, confining most surface sand to active channels, recently abandoned inset fans, or playa margins. In these conditions, sand-depleted Holocene surfaces would support few BSCs and display early pavement development (House et al. 2010). As in sandy areas, cyanobacteria and short moss-lichen crusts would colonize recently abandoned inset fans (House et al. 2010). Their distribution, however, would likely be less continuous. Because of the low geomorphic stability of recently abandoned inset fans, they are less likely to support development of tall moss-lichen pinnacles.

After colonizing a surface, mosses and lichens capture dust, creating a positive feedback mechanism that enhances growth and propagation of tall moss-lichen pinnacled crusts, vesicular pores in the bio-rich zone, and mineral Av horizons (see Chapter 2). Mosses and lichens incrementally accrete dust at the soil surface to form pinnacle topography, transforming short moss-lichen crusts into tall moss-lichen pinnacled crusts (Figure 3.17)(see Chapter 2). BSC bio-structures and surface dust accumulation lead to surface sealing that prevents erosion (Campbell et al. 1989, Belnap 1995, McKenna

Neuman et al. 1996, Marticorena et al. 1997, Danin et al. 1998, Canton et al. 2003, Eldridge and Leys 2003, Li et al. 2004, Bowker et al. 2008, Lazaro et al. 2008, Chaudhary et al. 2009) and over many wetting and drying cycles supports vesicular pore formation within the bio-rich zone (see Chapter 2)(Springer 1958, Miller 1971, Evenari et al. 1974, Figueira and Stoops 1983, Sullivan and Koppi 1991, Danin et al. 1998).

Wetting and drying creates surface polygonal cracks around moss-lichen pinnacle mounds that facilitate dust accumulation below pinnacles and the development of dust-rich mineral Av horizons (see Chapter 2). Dust accretion serves several purposes. Incremental dust accumulation provides new fine-grained substrates (Reheis 1990, Reheis et al. 1995, Simonson 1995) for BSC colonization (see Chapter 2) and a potential source of nutrients (see Chapter 4)(Reheis 1990, Simonson 1995, Reynolds et al. 2001, Reheis et al. 2002, Reynolds et al. 2006, McTainsh and Strong 2007, Field et al. 2010).

Dust also enhances water availability in several ways. Fine-grained dust increases water-holding capacity of the surface soil (Campbell 1979, Reheis 1990, Danin and Ganor 1991, Belnap and Gardner 1993, Reheis et al. 1995, Simonson 1995, Li et al. 2010).

Dust-related microstructures, such as vesicular pores of the bio-rich zone, capillary discontinuities, and mineral Av horizons, help maintain water near the soil surface for uptake by mosses, lichens, and cyanobacteria (see Chapter 2). Surface sealing within crusts reduces evaporation potential (Verrecchia et al. 1995, Mazor et al. 1996). Surface roughness associated with moss-lichen pinnacles may decrease runoff (see Chapter 2)(Wells et al. 1987, Wood et al. 2005), provide new substrates for BSC colonization (see Chapter 2) and further increase dust capture potential (see Chapter 2)(McFadden et al. 1986, Wells et al. 1987, Li et al. 2010). Overall, the compounding impacts of moss-

lichen dust capture greatly increases soil water, nutrient, and surface area availability, which further promote BSC growth and enhance dust accretion. It is important to note that initial sand input hastens BSC colonization, which eventually augments dust accretion and Av development (Figure 3.18). Therefore, this initial source of sand provides a catalyst that increases early rates of BSC-facilitated dust capture (Chapter 2) and associated pedogenic development (Chapter 4).

The thickness of biologically-mediated mineral Av horizons below extensive moss-lichen crusts reflects prolonged stability and dust capture. A study from the Negev estimated dust accumulation rates of live cyanobacteria crusts to be $277 \text{ g/m}^2/\text{year}$, or roughly 0.31 mm/year (Zaady and Offer 2010). If the same dust accretion rate was applied to this study, the 27-cm-thick Av horizon found below moss-lichen pinnacled crusts along mid-Holocene surfaces (Table 3.6D) would require 871 years to accumulate. Another study from the Negev estimated that moss-lichen interspaces accreted dust at a rate of $0.13 \text{ g/m}^2/\text{year}$ (Shachak and Lovett 1998). If calculated according to the methods of Zaady et al. (2010), dust accretes at approximately 0.00015 mm/year . At this rate, the 27cm Av would take 1.8 million years accumulate, far exceeding the mid-Holocene surface age. If modern average dust influx rates from the Mojave Desert are used (Reheis 2006), at $14 \text{ g/m}^2/\text{year}$, it would take 16,900 years to accumulate a dust-rich horizon of 27 cm. These Mojave Desert influx rates are based on several locations that differ with respect to proximity to dust sources, landform surface morphology, topography, and elevation. These data may underestimate moss-lichen dust accretion along mid-Holocene surfaces, as several outside factors are not considered. (1) Sand availability is high at this study site and may comprise a significant volume of the Av horizon, leading to much

higher dust accretion rates. For example, the fine, medium and coarse sand fractions collectively comprise 39% of the upper 3cm of soil from this horizon. (2) Macro-porosity associated with vesicular pore formation and bioturbation are not considered and could decrease horizon density. (3) The high surface roughness of mid-Holocene surfaces and tall moss-lichen pinnacled crusts may enhance local dust accretion rates over areas with lower surface roughness (McFadden et al. 1986). (4) The Mojave Desert dust accretion rates are based on modern measurements from 1984 to 1999 (Reheis 2006), which include time periods of increased anthropogenic activities and may not reflect the historical dust influx rates associated with climates from the past 100s to 1000s of years. Nevertheless, a 27-cm-thick biologically-mediated Av horizon suggests that moss-lichen crusts are long-lived surface features, which required sustained long-term stability for copious dust accretion. Dust accretion feedbacks associated with moss-lichen crusts lead to biological and geological characteristics dissimilar to those of “desert pavements.”

“Desert Pavement” Feedbacks

Older, topographically elevated surfaces commonly lack fine-grained substrates for widespread BSC establishment, and instead favor “desert pavement” development or with increased time, may lead to degradation of existing pavements (Figures 3.13, 3.16). Early Holocene and older geomorphic surfaces are topographically removed from significant sources of eolian sand influx, which results in a low sand-to-rock ratio. High rock cover favors the accumulation of dust below rock fragments (McFadden et al. 1986, 1987, Wells et al. 1987, Goossens 1995, Anderson et al. 2002, Wood et al. 2005). This process forms desert pavements and abiotically-mediated Av horizons. As desert pavement processes proceed, clast shattering leads to more extensive rock cover

(McFadden et al. 2005), and pavements become smooth and tightly interlocking (Anderson et al. 2002, Wood et al. 2005). Although these surfaces are highly stable, high rock cover density provides few exposed areas of fine-grained substrates for BSC colonization.

Areas with the highest rock cover and the most tightly interlocking “desert pavements,” such as the latest Pleistocene to early Holocene surfaces support the lowest BSC and plant canopy cover (Figure 3.14). Latest Pleistocene to early Holocene surfaces from nearby basins such as the Ivanpah Valley (House et al. 2010) or other parts of the Mojave Desert (Bell et al. 1998, 1999) are described as having smooth, tightly interlocking desert pavements that support negligible BSCs and sparse vascular plant cover (Hamerlynck et al. 2002). These observations along with my data support the theory that areas with high surface rock densities, that lack a high eolian sediment input, provide unsuitable habitats for BSC colonization (Tables 3.12, 3.13)(Kaltenecker et al. 1999, Quade 2001).

Tightly interlocking desert pavements with associated Av horizons prevent biotic colonization through decreased water availability (Hamerlynck et al. 2002, Wood et al. 2005, Meadows et al. 2008) and negligible exposure of fine-grained surfaces. The development of “desert pavements” is a self-enhancing feedback mechanism that further supports pavement integrity and prevents establishment of biological communities (Figure 3.16, Table 3.8)(Wells et al. 1987, Meadows et al. 1990, Valentin 1994, McFadden et al. 1998, Hamerlynck et al. 2002, Young et al. 2004, Wood et al. 2005, Schafer et al. 2007). Well-developed “desert pavements” will persist until extrinsic factors such as climate change or off-road-driving (Quade 2001, Goossens and Buck

2009) disrupt surface rock cover, or change hydrologic conditions, allowing for biologic colonization. In the absence of such extrinsic factors, well-developed “desert pavements” will eventually be degraded when surfaces become increasingly isolated and topographically elevated as new channels incise older alluvial fans. The high run-off associated with “desert pavement” surfaces, in time, facilitates incision and disruption of surface clasts (Wells and Dohrenwend 1985, Wells et al. 1987).

Disturbance to interlocking “desert pavements” exposes fine-grain substrates, allowing scattered moss and lichen colonization. Pleistocene and older surfaces have undergone backslope erosion and incision that disrupted surface rock fragments to form less dense, poorly interlocking “desert pavements” (Figures 3.14, 3.15)(Wells et al. 1987, Bull 1991, Wood et al. 2005). Gaps between clasts provide loamy surface substrates for initial BSC development (see Chapter 2)(Kaltenecker et al. 1999, Quade 2001). Once established at the surface, mosses and lichens accrete dust incrementally, forming scattered colonies of tall moss-lichen pinnacled crusts (Figure 3.17). At the time of mapping, 63-87% of areas with scattered tall moss-lichen pinnacles, which generally occurred with some form of “desert pavement” or high rock cover, overlapped with Pleistocene and older alluvial surfaces. The surface mosaics of “desert pavement” and scattered tall moss-lichen pinnacles are expected to persist under current environmental conditions. Together, these poorly-interlocking “desert pavements” and scattered moss-lichen crusts will decrease erosion and enhance dust trapping (see Chapter 2)(McFadden et al. 1986, 1987, Quade 2001, Soil Survey Staff 2010a, 2010b), thus facilitating vesicular horizon formation (see Chapter 2)(McFadden et al. 1987, Anderson et al. 2002).

Biogeomorphic and Ecological Stability

The self-enhancing feedback mechanisms associated with the three surface cover types promote ecological stability and geomorphic continuity (Figure 3.16).

Cyanobacteria crusts, moss-lichen crusts, and “desert pavements” are sustained by biological and geological drivers, which will help maintain the current geomorphic trajectory, imparting geomorphic continuity. The BSC organisms and the plant communities that they support are uniquely adapted to current hydrological patterns, stability conditions, and soil resource allocation (see Chapter 4). Therefore, the continuity in geomorphic and biological communities supports ecological stability (see Chapter 4). These feedback processes have important implications for land management.

Land Management Implications

The biogeomorphic insights from this study can enhance management of arid ecological communities. The process-based models predict surface characteristics as well as specific geomorphic surfaces that support various BSC types. This approach contrasts with previous models based on isolated correlations of BSC distribution. Moreover, these broader, landscape process models may explain and integrate many of the environmental controls of crust development described by previous authors.

My conceptual models emphasize surficial controls of BSC distribution and biogeomorphic interactions across the landscape. Previous research identified several factors that can control BSC distribution and species composition (Table 1). Previous work has linked BSCs to soil-geomorphic characteristics (Pluis and de Winder 1989, Eldridge 1999, Brostoff 2002, Dougill and Thomas 2004, Bowker et al. 2005, Thomas and Dougill 2006, 2007, Wang et al. 2007, Bowker and Belnap 2008, Guo et al. 2008,

Lazaro et al. 2008, Li et al. 2010). Most geomorphic studies focus on substrate stability and erosional controls of BSC distribution (Booth 1941, Campbell et al. 1989, Pluis and de Winder 1989, Belnap 1995, McKenna Neuman et al. 1996, Marticorena et al. 1997, Eldridge 1999, Canton et al. 2003, Eldridge and Leys 2003, Li et al. 2004, Bowker et al. 2008, Guo et al. 2008, Lazaro et al. 2008). Others have used soil parent material distributions to predict BSC development (Bowker and Belnap 2008) and identified solar insolation and dust capture controls of crust growth (Kidron et al. 2010, Li et al. 2010). The data from this study indicate the most important controls of local BSC distribution – fine-grained substrate availability, stability, and inferred water availability - vary as a function of geomorphic and soil physical processes.

My results suggest geomorphic surfaces can be used to predict BSC distribution for more effective and efficient land management in other parts of the Mojave Desert or areas that display intermontane-basin geomorphology (Figure 3.14)(Peterson 1981). Therefore, geomorphic and soil maps could better inform land management plans for crust conservation or to help set goals for ecological restoration when suitable reference conditions are unavailable. For example, conservation and restoration of moss-lichen crusts should be focused on mid- to late Holocene inset fans formed in mixed rock and sand, or within the corresponding Arizo soil series (Soil Survey Staff 2010a), as these areas have greatest potential for extensive moss-lichen growth. Similarly, sand sheets that correlate to the Bluepoint soil series (Soil Survey Staff 2010a) have the greatest cyanobacteria crust development and would be best-suited to cyanobacteria inoculation. Pleistocene and older inset fans with moderately to poorly interlocking “desert pavements,” as well as corresponding the Irongold soil series, Ferrogold series soil, and

shallow Typic Petrocalcids (Soil Survey Staff 2010a), have some potential for scattered moss-lichen growth after inoculation. In other regions, one could apply geomorphic principles to predict the sand-to-rock ratio (Figure 3.13), or relative surface area availability, stability, and water availability along various landforms to estimate BSC growth potential. However, effectively applying these factors to land management requires clear understanding of how soil physical processes interact with locally-significant biotic processes (Monger and Bestelmeyer 2006, Stallins 2006, Viles 2008, Viles et al. 2008, Kidron et al. 2010).

By integrating this wider landscape perspective into biotic-abiotic interactions, my models not only identify the local environmental controls of BSC distribution but may also explain the nutrient limitations and soil chemical controls identified in other studies. Several authors have suggested that nutrient availability limits the biotic potential of later succession or moss-lichen BSCs (Eldridge and Greene 1994, Kidron et al. 2000, Ponzetti and McCune 2001, Belnap et al. 2006, Bowker et al. 2006, Thomas and Dougill 2006, Bowker 2007, Rivera-Aguilar et al. 2009). These studies were conducted in cooler or wetter environments (Eldridge and Greene 1994, Kidron et al. 2000, Ponzetti and McCune 2001, Belnap et al. 2006, Bowker et al. 2006, Thomas and Dougill 2006, Bowker 2007, Rivera-Aguilar et al. 2009), where water may be less limiting than in the Mojave Desert (Noy-Meir 1973). My data, along with work from companion studies (see Chapters 2, 4), however, suggest that dust accretion by BSCs provides a source of nutrients, increases water availability, and provides new fine-grained substrates for propagation, allowing these organisms to engineer their own favorable habitat. Active dust capture by BSCs could explain the apparent high fertility associated with moss-

lichen crusts (Eldridge and Greene 1994, Kidron et al. 2000, Ponzetti and McCune 2001, Belnap et al. 2006, Bowker et al. 2006, Thomas and Dougill 2006, Bowker 2007, Rivera-Aguilar et al. 2009). Therefore, fertilizer applications or micronutrient additions to BSCs may not be a sufficient trigger for moss-lichen crust development, as previously suggested (Bowker et al. 2005, 2006). Instead, land managers should recognize the importance of fine-grained dust in the establishment, health, and continued propagation of moss-lichen crusts.

This study highlights the important role of dust accumulation in BSC development, restoration potential, and dust emissions. My models suggest that dust accumulation rates may be just as critical to restoration as biotic propagation time. If BSC growth and ecological function are to be restored, one must wait for moss-lichen colonization, biologically-mediated dust capture and Av formation, and development of BSC microfeatures that impact ecosystem function (Figure 3.17)(see Chapter 2). In addition, disturbed BSC surfaces should be considered potential dust sources. While moss-lichen crusts are excellent dust collectors (see Chapter 2)(Belnap and Gardner 1993, Shachak and Lovett 1998, Reynolds et al. 2001), BSC disturbance can lead to wind erosion that causes dust emissions and air pollution (see Chapters 2, 4)(Campbell et al. 1989, Belnap 1995, McKenna Neuman et al. 1996, Eldridge and Leys 2003, Li et al. 2004, Goossens and Buck 2009), as well as loss of nutrient-rich surface soils (see Chapter 4)(Reheis 1990, Reheis et al. 1995, Simonson 1995, Reynolds et al. 2001, Reheis et al. 2002). Therefore, land managers should strive to maintain BSC-protected dust and seek ways to restore dust-related surface features (see Chapter 2) following disturbance.

Study Limitations

The aforementioned interpretations and hypotheses of BSC development, biogeomorphic interactions, and surface morphological change are based on observational data without time constraint. Currently, we have no age control on previous disturbance (Figure 3.17). The study area was grazed prior to its wilderness area designation in 2002, approximately six years before this study began. However, the severity and extent of anthropogenic disturbances to BSCs by grazing (Kleiner and Harper 1977, Kaltenecker et al. 1999, Ponzetti and McCune 2001, Thomas and Dougill 2007), foot traffic (Brostoff 2002), and OHVs (Belnap 1995, Belnap and Warren 2002) are difficult to quantify. We also lack constraint on the fire (Johansen et al. 1984, Eldridge and Bradstock 1994, Brooks 1999, Bowker et al. 2004, Hilty et al. 2004, Ford and Johnson 2006, Ravi et al. 2007), climatic (Bull 1991, Belnap et al. 2004), and geomorphic disturbances (Wells et al. 1987, Bull 1991, Kidron et al. 2000, Monger and Bestelmeyer 2006, Stallins 2006) that may have left signatures on the current BSC distribution (see Chapter 4). Therefore, we do not know how long BSCs have been developing on these surfaces (Figure 3.17), whether they have been intact during the past 100s to even 1000s of years. We do not know what role BSCs have played in surface dust capture and morphological change within geological time frames. Nor do we understand the complex interplay between crusts and desert pavement formation. Without constraint on the timing of disturbance, we are forced to examine this landscape as a snapshot in time. Therefore, my conceptual models use soil physical processes to explain the distribution of BSCs across the landscape, relying on ideas and assumptions that should be tested in the future.

Conclusions

Self-enhancing geological and biological feedbacks constrain the stability, disturbance regime, dust-capture, and textural framework that ultimately control BSC distribution within the Mojave Desert. Geomorphic processes regulate the sand-to-rock ratio, which controls the development of three surface cover types across intermontane basin landforms. (1) Cyanobacteria crusts grow where high sand and negligible rocks form highly unstable, saltating sand sheets. Filamentous cyanobacteria support moderate sand saltation that minimizes moss and lichen colonization. (2) Tall moss-lichen pinnacled crusts are most extensive on stable surfaces composed of mixed rocks and sand, such as mid- to late Holocene inset fans. These biogeomorphic conditions support a dust capture feedback that forms biologically-mediated Av horizons and promotes BSC propagation. (3) Scattered, low to moderate density moss-lichen crusts are favored on stable surfaces with high rock cover and little surficial sand, as is expressed along early Holocene and older alluvial surfaces. Rock cover minimizes BSC colonization and supports “desert pavement” processes. By predicting BSC growth potential across various geomorphic surfaces, land managers can set realistic crust restoration goals and identify sensitive areas to protect. In the future, these biological and geological feedbacks should be incorporated into arid landscape models, as scientists address impacts of climate change and anthropogenic disturbances.

Literature Cited

- Anderson K., S. Wells, and R. Graham. 2002. Pedogenesis of vesicular horizons, Cima Volcanic Field, Mojave Desert, California. *Soil Science Society of America Journal* **66**:878-887.
- Bachman GO, Machette MN. 1977. Calcic soils and calcretes in the Southwestern United States. USGS Open-File Report 77-794. 163 pp.
- Baldwin B. G., S. Boyd, B. J. Ertter, R. W. Patterson, T. J. Rosatti, D. H. Wilken, and M. Wetherwax. 2002. The Jepson Desert Manual: Vascular Plants of Southeastern California. 626 pp.
- Barker D. H., L. R. Stark, J. F. Zimpfer, N. D. McLetchie, and S. D. Smith. 2005. Evidence of drought-induced stress on biotic crust moss in the Mojave Desert. *Plant, Cell and Environment* **28**:939-947.
- Beard L. S., R. E. Anderson, D. L. Block, R. G. Bohannon, R. J. Brady, S. B. Castor, E. M. Duebendorfer, J. E. Faulds, T. J. Felger, K. A. Howard, M. A. Kuntz, and V. S. Williams. 2007. Preliminary Geologic Map of the Lake Mead 30' x 60' Quadrangle, Clark County, Nevada, and Mohave County, Arizona.
- Bell J. W., A. R. Ramelli, and S. J. Caskey. 1998. Geologic map of the Tule Springs Park quadrangle, Nevada. **1:24,000**.
- Bell J. W., A. R. Ramelli, C. M. dePolo, F. Maldonado, and D. L. Schmidt. 1999. Geologic map of the Corn Creek Springs quadrangle, Nevada. **1:24,000**.
- Belnap J. 2006. The potential roles of biological soil crusts in dryland hydrologic cycles. *Hydrological Processes* **20**:3159-3178.
- Belnap J. 2002. Impacts of off-road vehicles on nitrogen cycles in biological soil crusts: resistance in different U.S. deserts. *Journal of Arid Environments* **52**:155-165.
- Belnap J. 2001. Comparative structure of physical and biological soil crusts. Pages 177-191 *In* J. Belnap and O. L. Lange, editors. *Biological Soil Crusts: Structure, Function, and Management*, Springer-Verlag, Berlin.
- Belnap J. 1995. Surface disturbances: their role in accelerating desertification. *Environmental Monitoring and Assessment* **37**:39-57.
- S. B. Monsen, S. G. Kitchen. 1994. Potential role of cryptobiotic soil crust in semiarid rangelands. *Proceedings – Ecology and Management of Annual Rangelands*. p.179-185.

- Belnap J., S. D. Warren. 2002. Patton's tracks in the Mojave Desert, USA: An ecological legacy. *Arid Land Research and Management* **16**:245-258.
- Belnap J., J. S. Gardner. 1993. Soil microstructure in soils of the Colorado Plateau: The role of the cyanobacterium *Microcoleus vaginatus*. *Great Basin Naturalist* **53**:40-47.
- Belnap J., S. L. Phillips, and T. Troxler. 2006. Soil lichen and moss cover and species richness can be highly dynamic: The effects of invasion by the annual exotic grass *Bromus tectorum*, precipitation, and temperature on biological soil crusts in SE Utah. *Applied Soil Ecology* **32**:63-76.
- Belnap J., S. L. Phillips, and M. E. Miller. 2004. Response of desert biological soil crusts to alterations in precipitation frequency. *Oecologia* **141**:306-316.
- Berkeley A., A. D. Thomas, and A. J. Dougill. 2005. Cyanobacterial soil crusts and woody shrub canopies in Kalahari rangelands. *African Journal of Ecology* **43**:137-145.
- Booth W. E. 1941. Algae as pioneers in plant succession and their importance in erosion control. *Ecology* **22**:38-46.
- Bowker M. A. 2007. Biological soil crust rehabilitation in theory and practice: An underexploited opportunity. *Restoration Ecology* **15**:13-23.
- Bowker M. A., J. Belnap. 2008. A simple classification of soil types as habitats of biological soil crusts on the Colorado Plateau, USA. *Journal of Vegetation Science* **19**:831-840.
- Bowker M. A., S. Soliveres, and F. T. Maestre. 2010a. Competition increases with abiotic stress and regulates the diversity of biological soil crusts. *Journal of Ecology* **98**:551-560.
- Bowker M. A., J. Belnap, and D. W. Davidson. 2010b. Microclimate and Propagule Availability are Equally Important for Rehabilitation of Dryland N-Fixing Lichens. *Restoration Ecology* **18**:30-33.
- Bowker M. A., J. Belnap, and M. E. Miller. 2006a. Spatial modeling of biological soil crusts to support rangeland assessment and monitoring. *Rangeland Ecol. Manage.* **59**:519-529.
- Bowker M. A., J. Belnap, V. B. Chaudhary, and N. C. Johnson. 2008. Revisiting classic water erosion models in drylands: The strong impact of biological soil crusts. *Soil Biology & Biochemistry* **40**:2309-2316.

- Bowker M. A., J. Belnap, D. W. Davidson, and H. Goldstein. 2006b. Correlates of biological soil crust abundance across a continuum of spatial scales: support for a hierarchical conceptual model. *Journal of Applied Ecology* **43**:152-163.
- Bowker M. A., J. Belnap, D. W. Davidson, and S. L. Phillips. 2005. Evidence for micronutrient limitations of biological soil crusts: importance to arid-lands restoration. *Ecological Applications* **15**:1941-1951.
- Bowker M. A., J. Belnap, R. Rosentreter, and B. Graham. 2004. Wildfire-resistant biological soil crusts and fire-induced loss of soil stability in Palouse prairies, USA. *Applied Soil Ecology* **26**:41-52.
- Brock A. L., B. J. Buck. 2009. Polygenetic development of the Mormon Mesa, NV petrocalcic horizons: Geomorphic and paleoenvironmental interpretations. *Catena* **77**:65-75.
- Brock A. L., B. J. Buck. 2005. A new formation process for calcic pendants from the Pahrnagat Valley, Nevada, USA, and implication for dating Quaternary landforms. *Quaternary Research* **63**:359-367.
- Brooks M. L. 1999. Alien annual grasses and fire in the Mojave Desert. *Madrono* **46**:13-19.
- Brostoff W. N. 2002. Cryptobiotic crusts of a seasonally inundated Dune–Pan system at Edwards Air Force Base, Western Mojave Desert, California. *Journal of Arid Environments* **51**:339-361.
- Buck B. J., J. Kipp J., and H. C. Monger. 2002. Inverted Clast Stratigraphy in an Eolian Archaeological Environment. *Geoarchaeology* **17**:665-687.
- Budel B., T. Darienko, K. Deutschewitz, S. Dojani, T. Friedl, K. I. Mohr, M. Salisch, W. Reisser, and B. Weber. 2009. Southern African biological soil crusts are ubiquitous and highly diverse in drylands, being restricted by rainfall frequency. *Microbial Ecology* **57**:229-247.
- Bull W. B. 1991. *Geomorphic Responses to Climatic Change*. Oxford University Press, New York.
- Campbell S. E. 1979. Soil stabilization by a prokaryotic desert crust: Implications for Precambrian land biota. *Origins of Life* **9**:335-348.
- Campbell S. E., J. Seeler, and S. Golubic. 1989. Desert crust formation and soil stabilization. *Arid Soil Research and Rehabilitation* **3**:217-228.

- Canton Y., A. Sole-Benet, and R. Lazaro. 2003. Soil–geomorphology relations in gypsiferous materials of the Tabernas Desert (Almeria, SE Spain). *Geoderma* **115**:193-222.
- Chaudhary V. B., M. A. Bowker, T. E. O'Dell, J. B. Grace, A. E. Redman, M. C. Rilling, and N. C. Johnson. 2009. Untangling the biological contributions to soil stability in semiarid shrublands. *Ecological Applications* **19**:110-122.
- Cole C., L. R. Stark, M. L. Bonine, and D. N. McLetchie. 2010. Transplant survivorship of bryophyte soil crusts in the Mojave Desert. *Restoration Ecology* **18**:198-205.
- Danin A., E. Ganor. 1991. Trapping of airborne dust by mosses in the Negev Desert, Israel. *Earth Surface Processes and Landforms* **16**:153-162.
- Danin A., I. Dor, A. Sandler, and R. Amit. 1998. Desert crust morphology and its relations to microbiotic succession at Mt. Sedom, Israel. *Journal of Arid Environments* **38**:161-174.
- DeFalco L. A., J. K. Detling, C. R. Tracy, and S. D. Warren. 2001. Physiological variation among native and exotic winter annual plants associated with microbiotic crusts in the Mojave Desert. *Plant and Soil* **234**:1-14.
- Dougill A. J., A. D. Thomas. 2004. Kalahari sand soils: Spatial heterogeneity, biological soil crusts and land degradation. *Land Degradation & Development* **15**:233-242.
- Elbert W., B. Weber, B. Budel, M. O. Andreae, and U. Poschl. 2009. Microbiotic crusts on soil, rock and plants: neglected major players in the global cycles of carbon and nitrogen? *Biogeosciences Discuss.* **6**:6983-7015.
- Eldridge D. J. 1999. Distribution and floristics of moss- and lichen-dominated soil crusts in a patterned *Callitris glaucophylla* woodland in eastern Australia. *Acta Oecologica* **20**:159-170.
- Eldridge D. J., J. F. Leys. 2003. Exploring some relationships between biological soil crusts, soil aggregation and wind erosion. *Journal of Arid Environments* **53**:457-466.
- Eldridge D. J., R. S. B. Greene. 1994. Microbiotic soil crusts: A review of their roles in soil and ecological processes in the rangelands of Australia. *Australian Journal of Soil Research* **32**:389-415.
- Eldridge D. J., R. A. Bradstock. 1994. The effect of time since fire on the cover and composition of cryptogamic soil crusts on a eucalypt shrubland soil. *Cunninghamia* **3**:521-527.

- Eldridge D. J., D. Freudenberger, and T. B. Koen. 2006. Diversity and abundance of biological soil crust taxa in relation to fine and coarse-scale disturbances in a grassy eucalypt woodland in eastern Australia. *Plant and Soil* **281**:255-268.
- Eldridge D. J., M. A. Bowker, F. T. Maestre, P. Alonso, R. L. Mau, J. Papadopoulos, and A. Escudero. 2010. Interactive Effects of Three Ecosystem Engineers on Infiltration in a Semi-Arid Mediterranean Grassland. *Ecosystems* **13**:499-510.
- Escudero A., I. Martinez, A. de la Cruz, M. A. G. Otalora, and F. T. Maestre. 2007. Soil lichens have species-specific effects on the seedling emergence of three gypsophile plant species. *Journal of Arid Environments* **70**:18-28.
- Evans R. D., J. Belnap. 1999. Long-Term consequences of disturbance on nitrogen dynamics in an arid ecosystem. *Ecology* **80**:150-160.
- Evenari M., D. H. Yaalon, and Y. Gutterman. 1974. Note on soils with vesicular structure in deserts. *Zeitschrift fur Geomorphologie N.F.* **18**:162-172.
- Field J. P., J. Belnap, D. D. Breshears, J. C. Neff, G. S. Okin, J. J. Whicker, T. H. Painter, S. Ravi, M. C. Reheis, and R. L. Reynolds. 2010. The ecology of dust. *Frontiers in Ecology and the Environment* **8**:423-430.
- Figueira H., G. Stoops. 1983. Application of micromorphometric techniques to the experimental study of vesicular layer formation. *Pedologie* **33**:77-89.
- Ford P. L., G. V. Johnson. 2006. Effects of dormant- vs. growing-season fire in shortgrass steppe: Biological soil crust and perennial grass responses. *Journal of Arid Environments* **67**:1-14.
- Friedmann E. I., M. Galun. 1974. Desert algae, lichens and fungi. Pages 165-212 *In* G. W. Brown, editor. *Desert Biology*, Academic Press, New York.
- Garcia-Pichel F., O. Pringault. 2001. Cyanobacteria track water in desert soils. *Nature* **413**:380-381.
- Gile L. H., F. F. Peterson, and R. B. Grossman. 1966. Morphological and genetic sequences of carbonate accumulation. *Soil Science* **101**:347-360.
- Goossens D. 1995. Field experiments of aeolian dust accumulation on rock fragment substrata. *Sedimentology* **42**:391-402.
- Goossens D., B. Buck. 2009. Dust emission by off-road driving: Experiments on 17 arid soil types, Nevada, USA. *Geomorphology* **107**:118-138.
- Gorelow A. S., P. H. Skrbac. 2005. *Climate of Las Vegas, NV*. National Weather Service, Las Vegas, NV.

- Guo Y., H. Zhao, X. Zuo, S. Drake, and X. Zhao. 2008. Biological soil crust development and its topsoil properties in the process of dune stabilization, Inner Mongolia, China. *Environ Geol* **54**:653-662.
- Hamerlynck E. P., J. R. McAuliffe, E. V. McDonald, and S. D. Smith. 2002. Ecological responses of two Mojave Desert shrubs to soil horizon development and soil water dynamics. *Ecology* **83**:768-779.
- Harden J. W., E. M. Taylor, C. Hill, R. K. Mark, L. D. McFadden, M. C. Reheis, J. M. Sowers, and S. G. Wells. 1991. Rates of Soil Development from Four Soil Chronosequences in the Southern Great Basin. *Quaternary Research* **35**:383-399.
- Hilty J. H., D. J. Eldridge, R. Rosentreter, M. C. Wicklow-Howard, and M. Pellant. 2004. Recovery of biological soil crusts following wildfire in Idaho. *Journal of Range Management* **57**:89-96.
- House PK, Buck BJ, Ramelli AR. 1994. Geologic Assessment of Piedmont and Playa Flood Hazards in the Ivanpah Valley Area, Clark County, Nevada (online only). NV Bureau of Mines and Geology Report 53. Reno, NV.
- Issa O. M., J. Trichet, C. Defarge, A. Coute, and C. Valentin. 1999. Morphology and microstructure of microbiotic soil crusts on a tiger bush sequence (Niger, Sahel). *Catena* **37**:175-196.
- Johansen J. R., L. L. St. Clair, B. L. Webb, and G. T. Nebeker. 1984. Recovery patterns of cryptogamic soil crusts in desert rangelands following fire disturbance. *The Bryologist* **87**:238-243.
- Kaltenecker JH, Wicklow-Howard MC, Rosentreter R. 1999. Biological Soil Crusts in Three Sagebrush Communities Recovering from a Century of Livestock Trampling. USDA Forest Service Proceedings RMRS-P-11. Ogden, UT.
- Kidron G. J., A. Vonshak, and A. Abieliovich. 2008. Recovery rates of microbiotic crusts within a dune ecosystem in the Negev Desert. *Geomorphology* **100**:444-452.
- Kidron G. J., I. Herrnsstadt, and E. Barzilay. 2002. The role of dew as a moisture source for sand microbiotic crusts in the Negev Desert, Israel. *Journal of Arid Environments* **52**:517-533.
- Kidron G. J., E. Barzilay, and E. Sachs. 2000. Microclimate control upon sand microbiotic crusts, western Negev Desert, Israel. *Geomorphology* **36**:1-18.
- Kidron G. J., A. Vonshak, I. Dor, S. Barinova, and A. Abieliovich. 2010. Properties and spatial distribution of microbiotic crusts in the Negev Desert, Israel. *Catena* **82**:92-101.

- Kleiner E. F., K. T. Harper. 1977. Soil properties in relation to cryptogamic groundcover in Canyonlands National Park. *Journal of Range Management* **30**:202-205.
- Lange O. L., J. Belnap, and H. Reichenberger. 1998. Photosynthesis of the cyanobacterial soil-crust lichen *Collema tenax* from arid lands in southern Utah, USA: Role of water content on light and temperature responses of CO₂ exchange. *Functional Ecology* **12**:195-202.
- Lange O. L., B. Budel, A. Meyer, and E. Kilian. 1993. Further evidence that activation of net photosynthesis by dry cyanobacterial lichens requires liquid water. *The Lichenologist* **25**:175-189.
- Langhans T. M., C. Storm, and A. Schwabe. 2010. Regeneration processes of biological soil crusts, macro-cryptogams and vascular plant species after fine-scale disturbance in a temperate region: Recolonization or successional replacement? *Flora* **205**:46-60.
- Lazaro R., Y. Canton, A. Sole-Benet, J. Bevan, R. Alexander, L. G. Sancho, and J. Puigdefabregas. 2008. The influence of competition between lichen colonization and erosion on the evolution of soil surfaces in the Tabernas badlands (SE Spain) and its landscape effects. *Geomorphology* **102**:252-266.
- Li X. R., X. H. Jia, L. Q. Long, and S. Zerbe. 2005. Effects of biological soil crusts on seed bank, germination and establishment of two annual plant species in the Tengger Desert (N China). *Plant and Soil* **277**:375-385.
- Li X. R., M. Z. He, S. Zerbe, X. J. Li, and L. C. Liu. 2010. Micro-geomorphology determines community structure of biological soil crusts at small scales. *Earth Surface Processes and Landforms* **35**:932-940.
- Li X. Y., L. Y. Liu, and J. H. Wang. 2004. Wind tunnel simulation of aeolian sandy soil erodibility under human disturbance. *Geomorphology* **59**:3-11.
- Machette M. N. 1985. Calcic soils of the southwestern United States. Pages 1-21 *In* D. L. Weide, editor. *Soils and Quaternary geomorphology of the southwestern United States*, Geological Society of America, Boulder, CO.
- Maestre F. T. 2003. Small-scale spatial patterns of two soil lichens in semi-arid Mediterranean steppe. *Lichenologist* **35**:71-81.
- Maestre F. T., C. Escolar, I. Martinez, and A. Escudero. 2008. Are soil lichen communities structured by biotic interactions? A null model analysis. *Journal of Vegetation Science* **19**:261-266.
- Marsh J., S. Nouvet, P. Sanborn, and D. Coxson. 2006. Composition and function of biological soil crust communities along topographic gradients in grasslands of

- central British Columbia (Chilcotin) and southwestern Yukon (Kluane). *Canadian Journal of Botany* **84**:717-736.
- Marticorena B., G. Bergametti, D. Gillette, and J. Belnap. 1997. Factors controlling threshold friction velocity in semiarid and arid areas of the United States. *Journal of Geophysical Research* **102**:23277-23287.
- Mazor G., G. J. Kidron, A. Vonshak, and A. Abieliovich. 1996. The role of cyanobacterial exopolysaccharides in structuring desert microbial crusts. *FEMS Microbiology Ecology* **21**:121-130.
- McCune B., B. A. Caldwell. 2009. A single phosphorus treatment doubles growth of cyanobacterial lichen transplants. *Ecology* **90**:567-570.
- McFadden L. D., S. G. Wells, and M. J. Jercinovich. 1987. Influences of eolian and pedogenic processes on the origin and evolution of desert pavements. *Geology* **15**:504-508.
- McFadden L. D., S. G. Wells, and J. C. Dohrenwend. 1986. Influences of Quaternary climatic changes on processes of soil development on desert loess deposits of the Cima Volcanic Field, California. *Catena* **13**:361-389.
- McFadden L. D., M. C. Eppes, A. R. Gillespie, and B. Hallet. 2005. Physical weathering in arid landscapes due to diurnal variation in the direction of solar heating. *GSA Bulletin* **117**:161-173.
- McFadden L. D., E. V. McDonald, S. G. Wells, K. Anderson, J. Quade, and S. L. Forman. 1998. The vesicular layer and carbonate collars of desert soils and pavements: formation, age and relation to climate change. *Geomorphology* **24**:101-145.
- McKenna Neuman C., C. Maxwell. 2002. Temporal aspects of the abrasion of microphytic crusts under grain impact. *Earth Surface Processes and Landforms* **27**:891-908.
- McKenna Neuman C., C. D. Maxwell, and J. W. Boulton. 1996. Wind transport of sand surfaces crusted with photoautotrophic microorganisms. *Catena* **27**:229-247.
- McTainsh G., C. Strong. 2007. The role of aeolian dust in ecosystems. *Geomorphology* **89**:39-54.
- Meadows D. G., M. H. Young, and E. V. McDonald. 2008. Influence of relative surface age on hydraulic properties and infiltration on soils associated with desert pavements. *Catena* **72**:169-178.

- Meadows P. S., J. Tait, and S. A. Hussain. 1990. Effects of estuarine infauna on sediment stability and particle sedimentation. *Hydrobiologia* **190**:263-266.
- Miller D. E. 1971. Formation of vesicular structure in soil. *Soil Science Society of America Journal* **35**:635-637.
- Monger H. C., B. T. Bestelmeyer. 2006. The soil-geomorphic template and biotic change in arid and semi-arid ecosystems. *Journal of Arid Environments* **65**:207-218.
- Nagy M. L., J. R. Johansen, L. L. St. Clair, and B. L. Webb. 2005. Recovery patterns of microbiotic soil crusts 70 years after arsenic contamination. *Journal of Arid Environments* **63**:304-323.
- Noffke N. 2009. The criteria for the biogenicity of microbially induced sedimentary structures (MISS) in Archean and younger, sandy deposits. *Earth-Science Reviews* **96**:173-180.
- Noffke N., A. H. Knoll, and J. P. Grotzinger. 2002. Sedimentary controls on the formation and preservation of microbial mats in siliciclastic deposits: A case study from the upper Neoproterozoic Nama Group, Namibia. *PALAIOS* **17**:533-544.
- Noy-Meir I. 1973. Desert ecosystems: Environment and producers. *Annual Review of Ecology and Systematics* **4**:25-51.
- Page W. R., S. C. Lundstrom, A. G. Harris, V. E. Langenheim, J. B. Workman, S. A. Mahan, J. B. Paces, G. L. Dixon, P. D. Rowley, B. C. Burchfiel, J. W. Bell, and E. I. Smith. 2005. Geologic and Geophysical Maps of the Las Vegas 30' x 60' Quadrangle, Clark and Nye Counties, Nevada, and Inyo County, California: **1:100,000**.
- Peters D. P. C., B. T. Bestelmeyer, J. E. Herrick, E. L. Fredrickson, H. C. Monger, and K. M. Havstad. 2006. Disentangling complex landscapes: New insights into arid and semiarid system dynamics. *BioScience* **56**:491-501.
- Peterson FF. 1981. Landforms of the Basin and Range, Defined for Soil Survey. UNR Max C. Fleishmann College of Agriculture, Nevada Agricultural Experiment Station; Technical Bulletin 28. 52 pp. Reno, NV.
- Peterson F. F., J. W. Bell, R. I. Dorn, A. R. Ramelli, and T. L. Ku. 1995. Late Quaternary geomorphology and soils in Crater Flat, Yucca Mountain area, southern Nevada. *GSA Bulletin* **107**:379-395.
- Pluis J. L. A., B. de Winder. 1989. Spatial patterns in algae colonization of dune blowouts. *Catena* **16**:499-506.

- Ponzetti J. M., B. P. McCune. 2001. Biotic soil crusts of Oregon's shrub steppe: Community composition in relation to soil chemistry, climate, and livestock activity. *The Bryologist* **104**:212-225.
- Quade J. 2001. Desert pavements and associated rock varnish in the Mojave Desert: How old can they be? *Geology* **29**:855-858.
- Rao B., Y. Liu, W. Wang, C. Hu, L. Dunhai, and S. Lan. 2009. Influence of dew on biomass and photosystem II activity of cyanobacterial crusts in the Hopq Desert, northwest China. *Soil Biology & Biochemistry* **41**:2387-2393.
- Ravi S., P. D'Odorico, T. M. Zobeck, T. M. Over, and S. L. Collins. 2007. Feedbacks between fires and wind erosion in heterogeneous arid lands. *Journal of Geophysical Research* **112**:G04007.
- Reheis M. 2006. A 16-year record of eolian dust in Southern Nevada and California, USA: Controls on dust generation and accumulation. *Journal of Arid Environments* **67**:487-520.
- Reheis M. C. 1990. Influence of climate and eolian dust on the major-element chemistry and clay mineralogy of soils in the northern Bighorn Basin, U.S.A. *Catena* **17**:219-248.
- Reheis M. C., J. R. Budahn, and P. J. Lamothe. 2002. Geochemical evidence for diversity of dust sources in the southwestern United States. *Geochimica et Cosmochimica Acta* **66**:1569-1587.
- Reheis M. C., J. M. Sowers, E. M. Taylor, L. D. McFadden, and J. W. Harden. 1992. Morphology and genesis of carbonate soils on the Kyle Canyon fan, Nevada, U.S.A. *Geoderma* **52**:303-342.
- Reheis M. C., J. C. Goodmacher, J. W. Harden, L. D. McFadden, T. K. Rockwell, R. R. Shroba, J. M. Sowers, and E. M. Taylor. 1995. Quaternary soils and dust deposition in southern Nevada and California. *GSA Bulletin* **107**:1003-1022.
- Reynolds R., J. Neff, M. Reheis, and P. Lamothe. 2006. Atmospheric dust in modern soil on aeolian sandstone, Colorado Plateau (USA): Variation with landscape position and contribution to potential plant nutrients. *Geoderma* **130**:108-123.
- Reynolds R., J. Belnap, M. C. Reheis, P. J. Lamothe, and F. Luiszer. 2001. Aeolian dust in Colorado Plateau soils: Nutrient inputs and recent change in source. *PNAS* **98**:7123-7127.
- Rivera-Aguilar V., H. Godinez-Alvarez, R. Moreno-Torres, and S. Rodriguez- Zaragoza. 2009. Soil physico-chemical properties affecting the distribution of biological soil

- crusts along an environmental transect at Zapotitlan drylands, Mexico. *Journal of Arid Environments* **73**:1023-1028.
- Rivera-Aguilar V., G. Montejano, S. Rodriguez-Zaragoza, and A. Duran-Diaz. 2006. Distribution and composition of cyanobacteria, mosses and lichens of the biological soil crusts of the Tehuacan Valley, Puebla, Mexico. *Journal of Arid Environments* **67**:208-225.
- Robins C. R., B. J. Buck, A. J. Williams, J. L. Morton, P. K. House, M. S. Howell, and M. L. Yonovitz. 2009. Comparison of flood hazard assessments on desert piedmonts and playas: A case study in Ivanpah Valley, Nevada. *Geomorphology* **103**:520-532.
- Schafer D. S., M. H. Young, S. F. Zitzer, T. G. Caldwell, and E. V. McDonald. 2007. Impacts of interrelated biotic and abiotic processes during the past 125,000 years of landscape evolution in the Northern Mojave Desert, Nevada, USA. *Journal of Arid Environments* **69**:633-657.
- Schoeneberger P. J., D. A. Wysocki, E. C. Benham, and W. D. Broderson. 2002. Field book for describing and sampling soils, Version 2.0. Natural Resources Conservation Service, National Soil Survey Center, Lincoln, NE.
- Shachak M., G. M. Lovett. 1998. Atmospheric deposition to a desert ecosystem and its implications for management. *Ecological Applications* **8**:455-463.
- Simonson R. W. 1995. Airborne dust and its significance to soils. *Geoderma* **65**:1-43.
- Soil Survey Staff. 2010a. Official Soil Series Descriptions. USDA-NRCS, Washington, D.C.
- Soil Survey Staff. 2010b. Keys to Soil Taxonomy. USDA-NRCS, Washington, D.C.
- Soil Survey Staff. 2007. Soil survey of the Clark County area, NV. USDA-NRCS, Washington, D.C.
- Sowers J. M., R. G. Amundson, O. A. Chadwick, J. W. Hardin, A. J. T. Jull, T. L. Ku, L. D. McFadden, M. C. Reheis, E. M. Taylor, and B. J. Szabo. 1989. Geomorphology and pedology on the Kyle Canyon Alluvial Fan, southern Nevada. Pages 93-112 *In* T. J. Rice, editor. Soils, geomorphology, and pedology in the Mojave Desert, California, Nevada: Field Tour Guidebook for the Soil Science Society of America Annual Meeting Pre-Meeting Tour, October 12-14.
- Springer M. E. 1958. Desert pavement and vesicular layer of some soils of the desert of the Lahontan Basin, Nevada. *Soil Science Society of America Journal* **22**:63-66.
- Stallins J. A. 2006. Geomorphology and ecology: Unifying themes for complex systems in biogeomorphology. *Geomorphology* **77**:207-216.

- Sullivan L. A., A. J. Koppi. 1991. Morphology and genesis of silt and clay coatings in the vesicular layer of a desert loam soil. *Australian Journal of Soil Research* **29**:579-586.
- Thomas A. D., A. J. Dougill. 2006. Distribution and characteristics of cyanobacterial soil crusts in the Molopo Basin, South Africa. *Journal of Arid Environments* **64**:270-283.
- Thomas A. D., A. J. Dougill. 2007. Spatial and temporal distribution of cyanobacterial soil crusts in the Kalahari: Implications for soil surface properties. *Geomorphology* **85**:17-29.
- Thompson D. B., L. R. Walker, F. H. Landau, and L. R. Stark. 2005. The influence of elevation, shrub species, and biological soil crust on fertile islands in the Mojave Desert, USA. *Journal of Arid Environments* **61**:609-629.
- Thompson W. A., D. J. Eldridge, and S. P. Bonser. 2006. Structure of biological soil crust communities in *Callitris glaucophylla* woodlands of New South Wales, Australia. *Journal of Vegetation Science* **17**:271-280.
- Valentin C. 1994. Surface sealing as affected by various rock fragment covers in West Africa. *Catena* **23**:87-97.
- Verrecchia E. P., A. Yair, G. J. Kidron, and K. Verrecchia. 1995. Physical properties of the psammophile cryptogamic crust and their consequences to the water regime of sandy soils, north-western Negev Desert, Israel. *Journal of Arid Environments* **29**:427-437.
- Viles H. A. 2008. Understanding dryland landscape dynamics: Do biological crusts hold the key? *Geography Compass* **2/3**:899-919.
- Viles H. A., L. A. Naylor, N. E. A. Carter, and D. Chaput. 2008. Biogeomorphological disturbance regimes: progress in linking ecological and geomorphological systems. *Earth Surface Processes and Landforms* **33**:1419-1435.
- Wang W. B., C. Y. Yang, D. S. Tang, D. H. Li, Y. D. Liu, and C. X. Hu. 2007. Effects of sand burial on biomass, chlorophyll fluorescence and extracellular polysaccharides of man-made cyanobacterial crusts under experimental conditions. *Science in China Series C: Life Sciences* **50**:530-534.
- Wells S. G., J. C. Dohrenwend. 1985. Relict sheetflood bed forms on late Quaternary alluvial-fan surfaces in the southwestern United States. *Geology* **13**:512-516.
- Wells S. G., L. D. McFadden, and J. C. Dohrenwend. 1987. Influence of late Quaternary climatic changes on geomorphic and pedogenic processes on a desert piedmont, eastern Mojave Desert, California. *Quaternary Research* **27**:130-146.

- Williams W. J., D. J. Eldridge, and B. M. Alchin. 2008. Grazing and drought reduce cyanobacterial soil crusts in an Australian Acacia woodland. *Journal of Arid Environments* **72**:1064-1075.
- Wood Y. A., R. C. Graham, and S. G. Wells. 2005. Surface control of desert pavement pedologic process and landscape function, Cima Volcanic field, Mojave Desert, California. *Catena* **59**:205-230.
- Young M. H., E. V. McDonald, T. G. Caldwell, S. G. Benner, and D. G. Meadows. 2004. Hydraulic properties of a desert soil chronosequence in the Mojave Desert, USA. *Vadose Zone Journal* **3**:956-963.
- Zaady E., Z. Y. Offer. 2010. Biogenic soil crusts and soil depth: a long-term case study from the Central Negev desert highland. *Sedimentology* **57**:351-358.
- Zhang Y. 2005. The microstructure and formation of biological soil crusts in their early developmental stage. *Chinese Science Bulletin* **50**:117-121.



Figure 3.1: (A) Smooth cyanobacteria crusts have slightly darkened surfaces where the sticky sheaths of filamentous cyanobacteria have captured and cemented dust (arrow, scale 1 cm). (B) Cyanobacterial crusts form smooth, light colored surfaces between shrubs (scale 1 m).

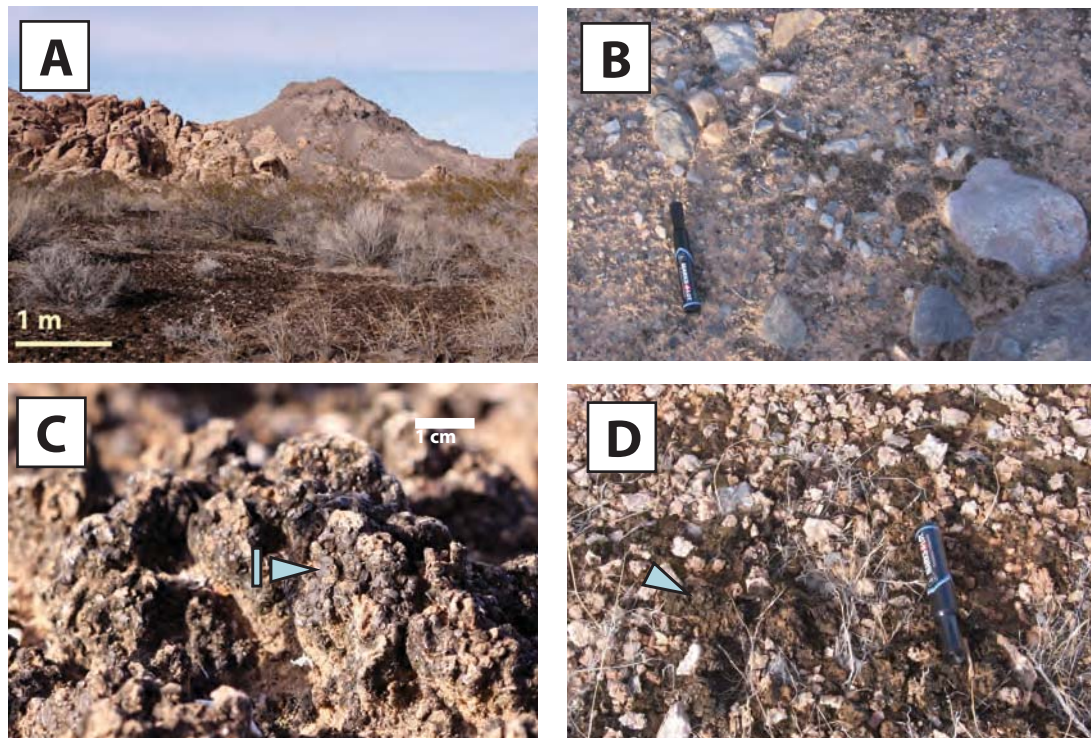


Figure 3.2: (A) Moss-lichen crusts have dark, rough surfaces that protect shrub interspaces from erosion (scale 1 m). (B) Short moss-lichen crusts have low surface relief, up to 2 cm (marker for scale). (C) Tall moss-lichen pinnacled crusts are composed of complex matrices of mosses, lichens, cyanobacteria, and sediments. Squamulose lichens (l) dominate this crust (scale 1 cm). (D) Scattered, tall moss-lichen pinnacles (arrow) grow between surface rock fragments (marker for scale).

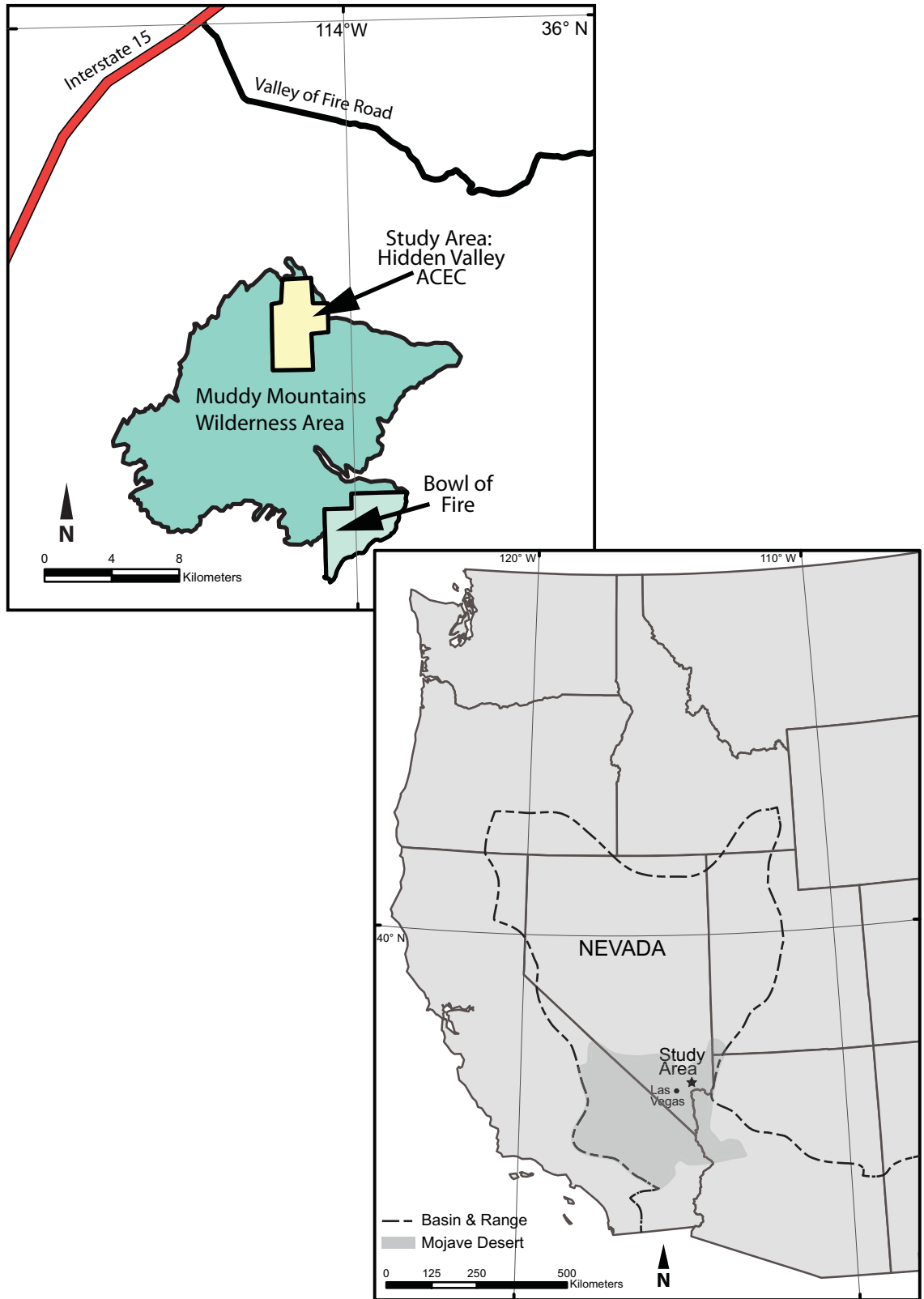


Figure 3.3: The study area is located within the Hidden Valley Area of Critical Environmental Concern of the Muddy Mountains Wilderness Area, Nevada, U.S.A.

Hidden Valley, Muddy Mountains Wilderness Area, NV (NAIP Imagery)

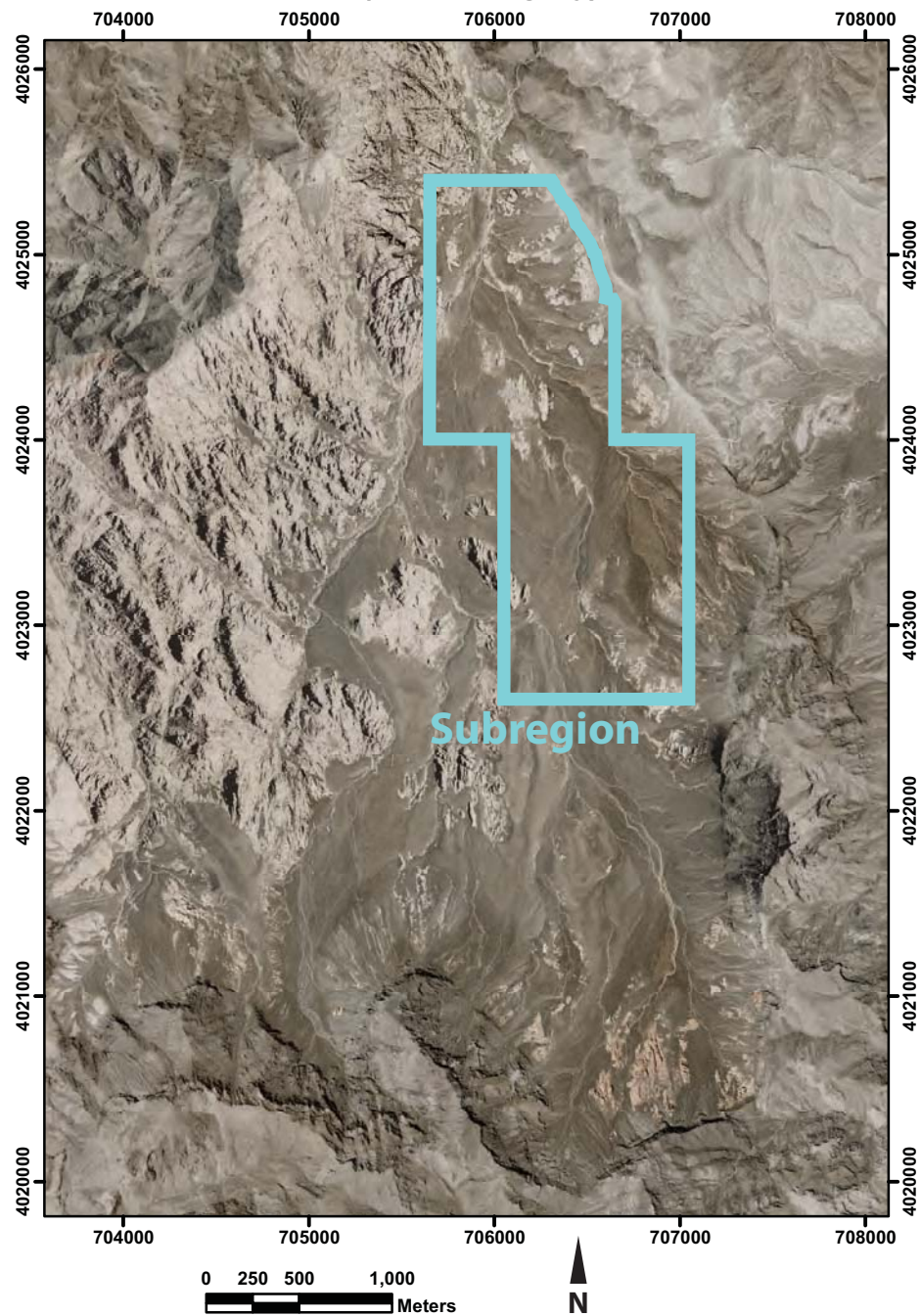


Figure 3.4: Hidden Valley is a semi-enclosed basin in the Muddy Mountains Wilderness Area, Nevada (USA). BSC mapping was completed throughout the entire valley. Geomorphic mapping was completed within the subregion outlined in turquoise. (See location in Figure 3.3.)

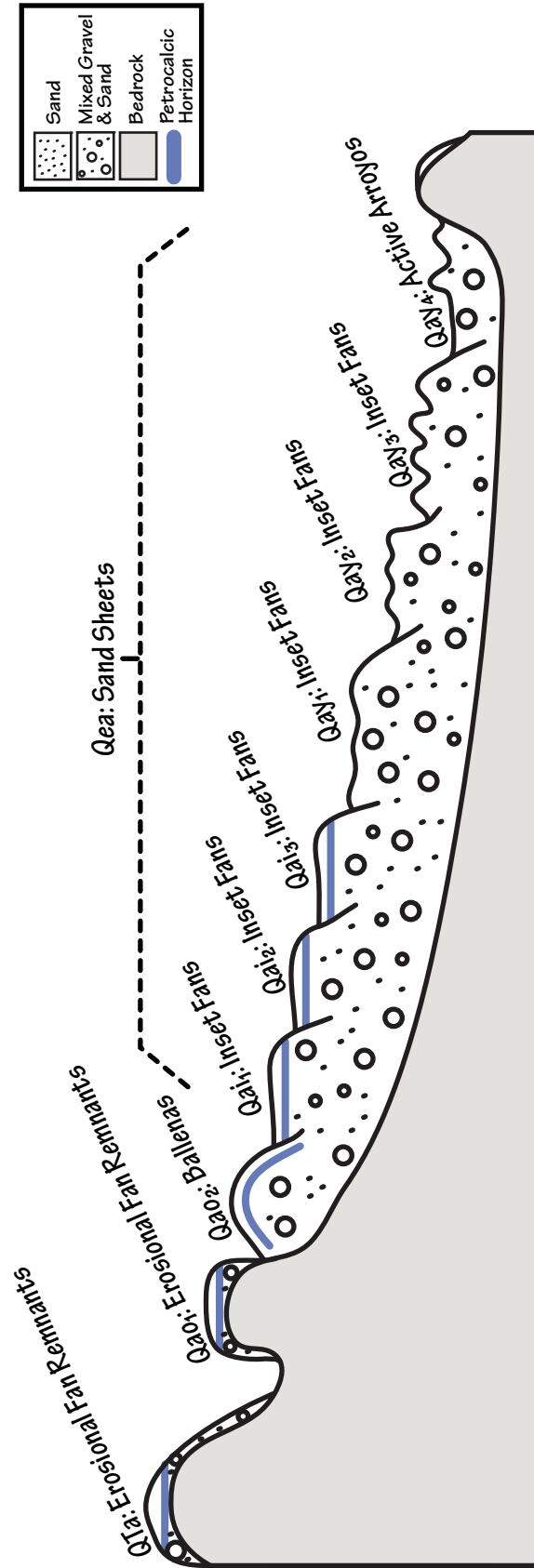


Figure 3.6: A schematic cross-section summarizes geomorphic surfaces found within the mapping subregion of Hidden Valley. Bedrock underlies all surfaces and outcrops as inselbergs throughout the valley. Surfaces range in age from Late Miocene or earliest Pleistocene to recent Holocene. Ages were estimated using topographic relief, cross-cutting relationships, soil surface morphology, desert pavement development, and stage of pedogenic carbonate accumulation and correlated to other soil-geomorphic investigations (see text for details). Most surfaces are formed in alluvium. Qea sand sheets, however, may overlie Qai or Qay surfaces. Colluvium is not shown in this cross-section, but may occur below the cliff faces surrounding the valley.

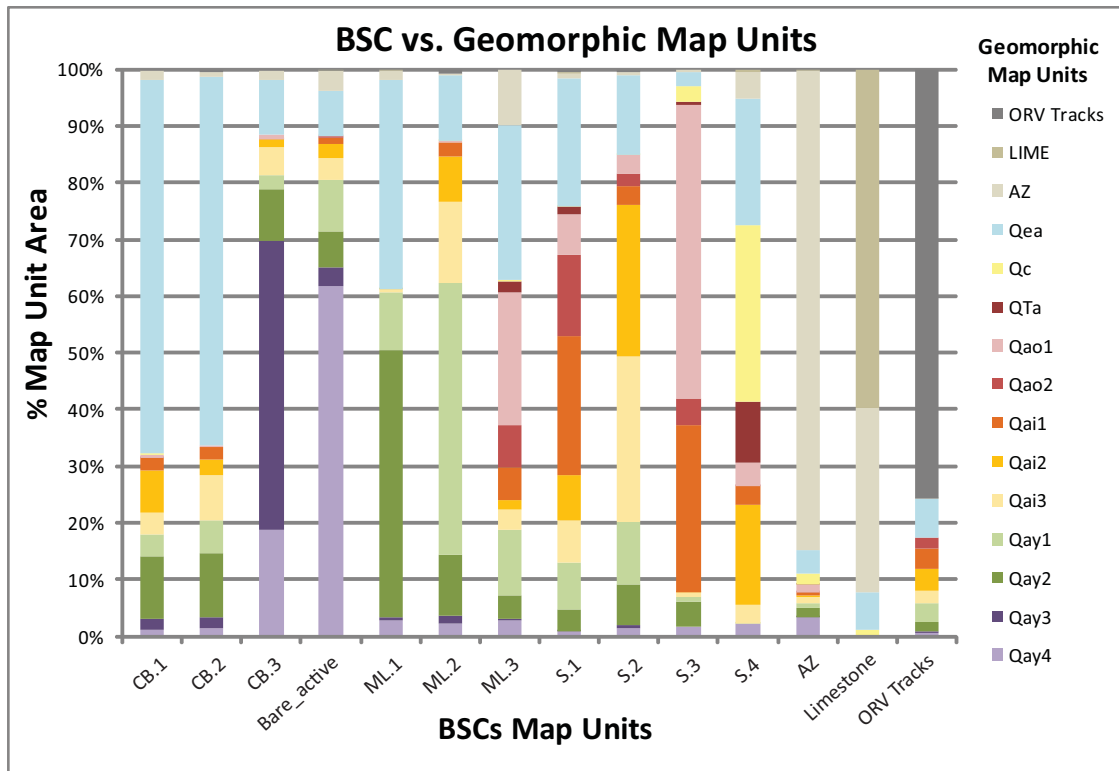


Figure 3.7: Results from GIS overlays of BSC units as a function of geomorphic units. Results show percent cover of BSC units that lie within with various geomorphic units. Bare_active refers to active channels with no BSCs. AZ refers to Aztec Sandstone, while LIME stands for limestone.

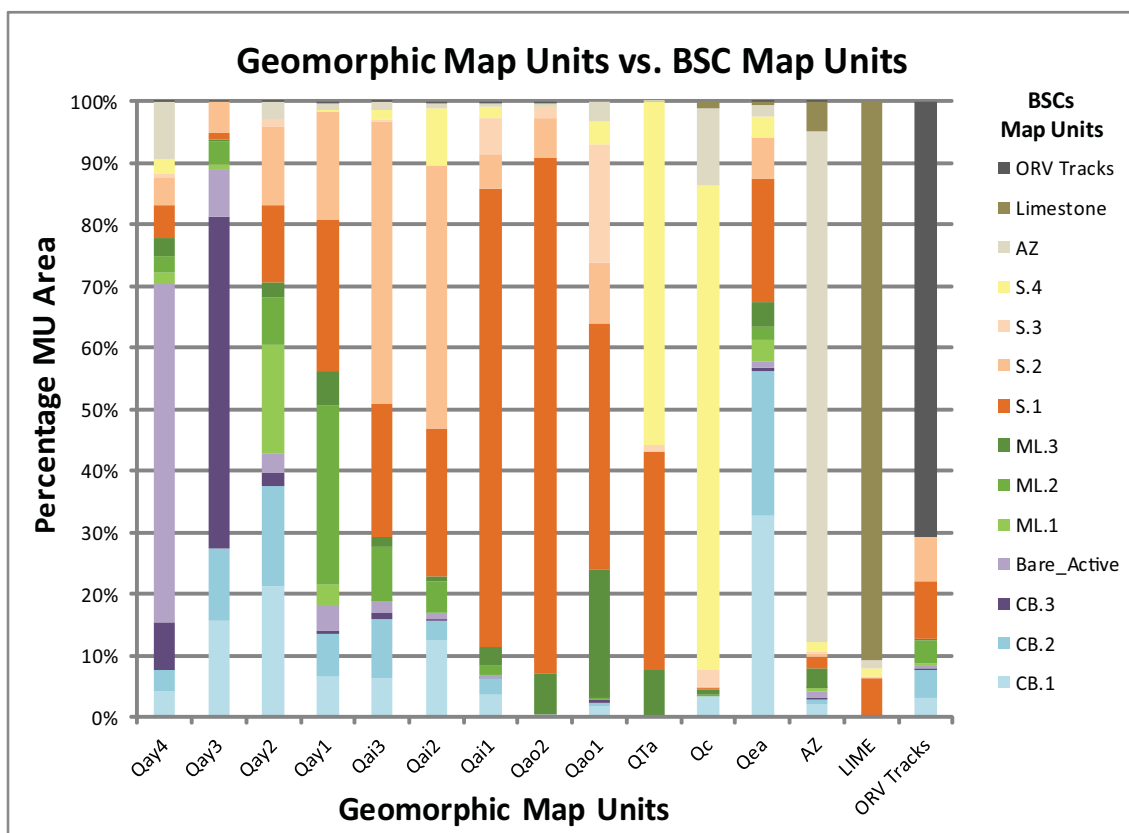


Figure 3.8: Results from GIS overlays of geomorphic units as a function of BSC units. Results show percentage of each geomorphic surface covered by various BSC units. Bare_Active refers to active channels with no BSCs. AZ refers to Aztec Sandstone, while LIME stands for limestone.

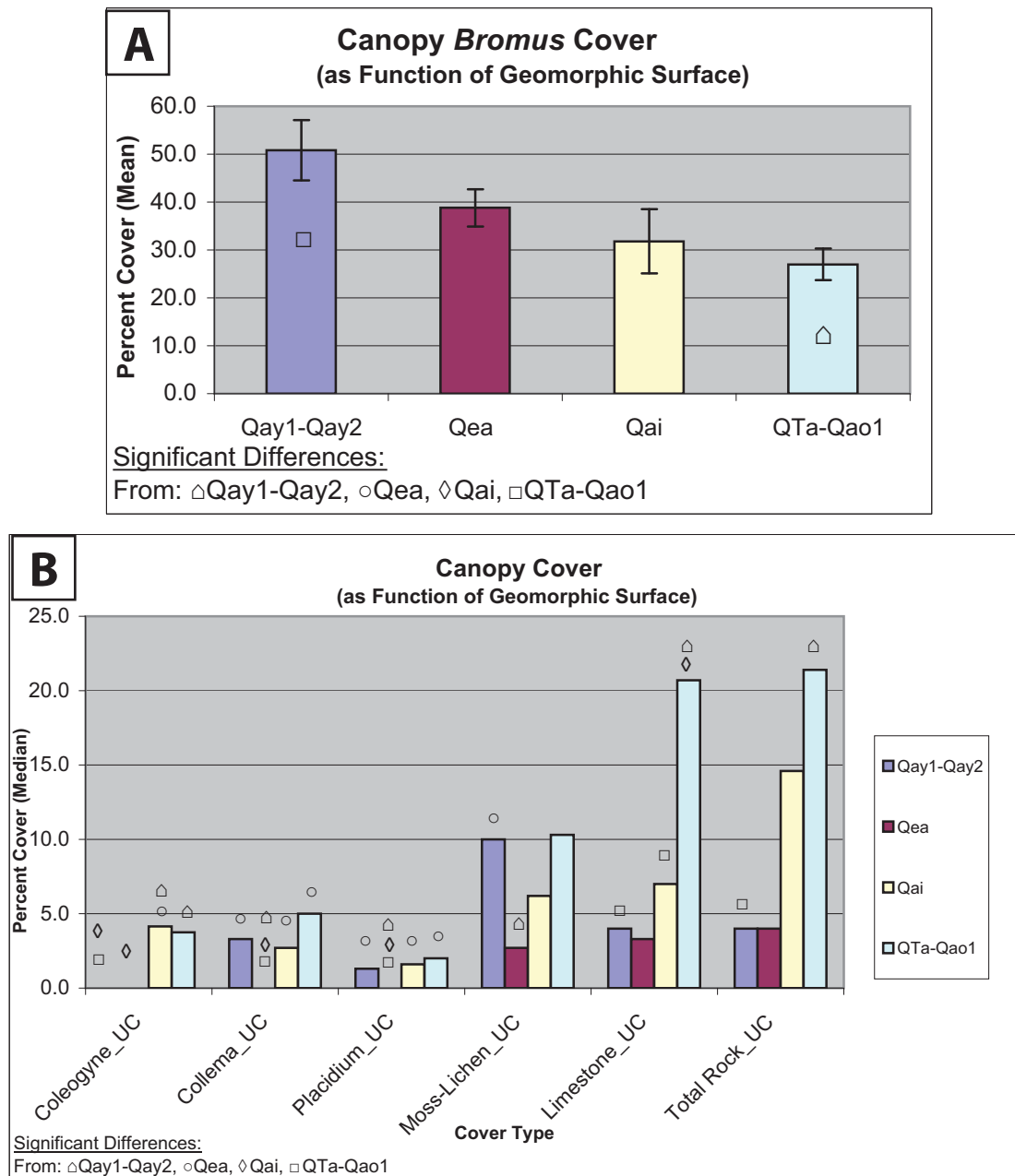


Figure 3.9: ANOVAs compare differences in canopy surface cover among various geomorphic surfaces. Significant differences are denoted by the following symbols: △ denotes significant differences from Qay1-Qay2; ○ denotes significant differences from Qea; ◇ denotes significant differences from Qai; □ denotes significant differences from QTa-Qao1. (A) Parametric ANOVA shows significant differences in mean canopy *Bromus* cover among geomorphic surfaces. Bars represent mean standard error. (B) Non-parametric ANOVAs show significant differences in median canopy *Coleogyne*, *Collema*, *Placidium*, moss-lichen, limestone, and total rock cover.

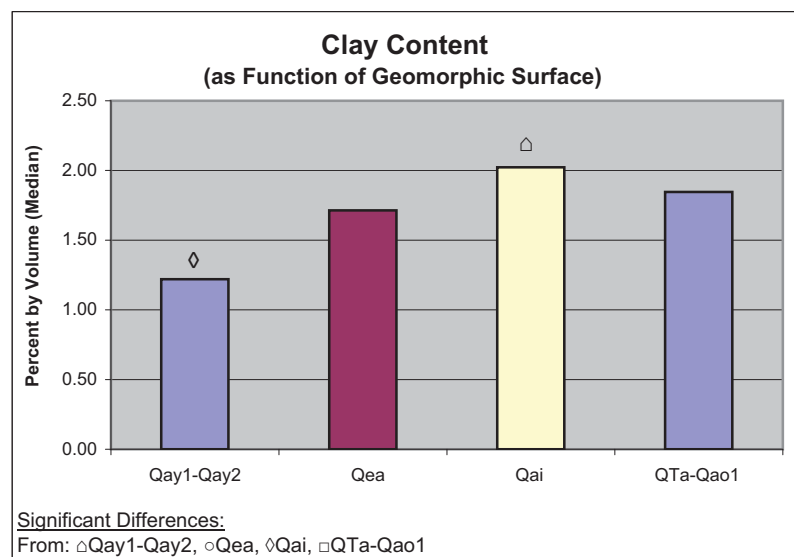


Figure 3.10: Non-parametric ANOVA compares differences in median canopy surface clay content among various geomorphic surfaces. Significant differences are denoted by the following symbols: △ denotes significant differences from Qay1-Qay2; ○ denotes significant differences from Qea; ◇ denotes significant differences from Qai; □ denotes significant differences from QTa-Qao1.

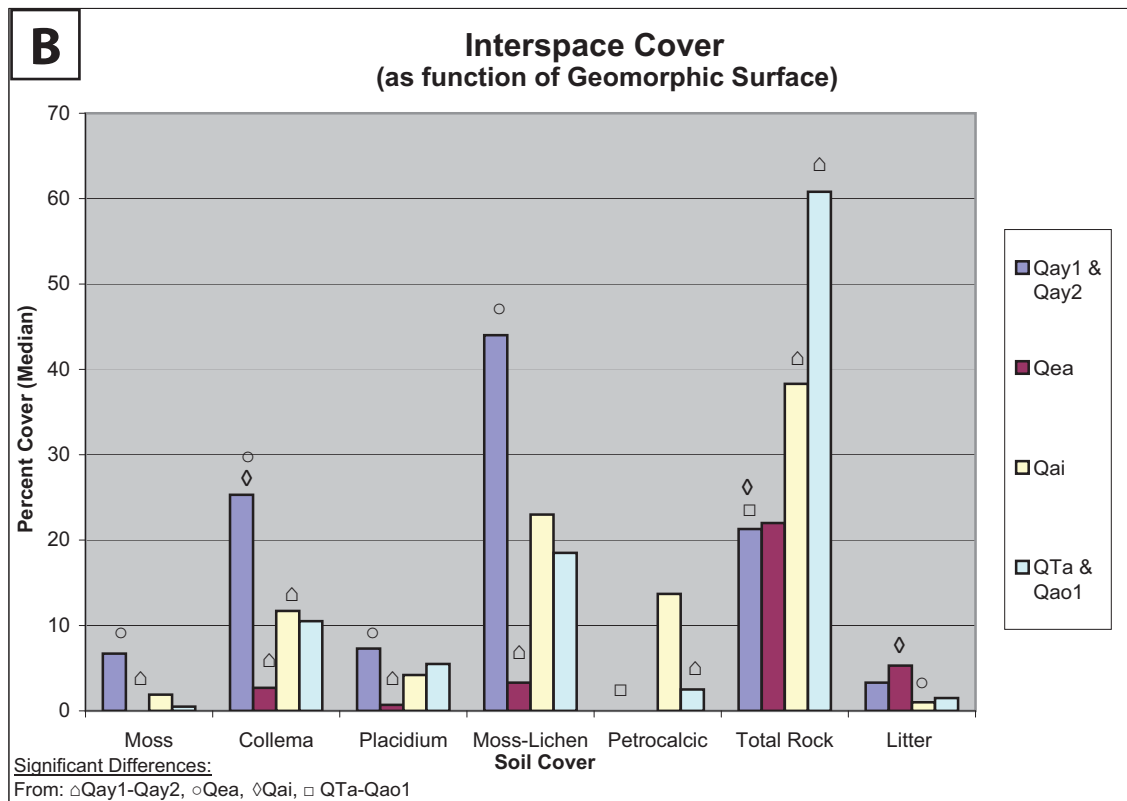
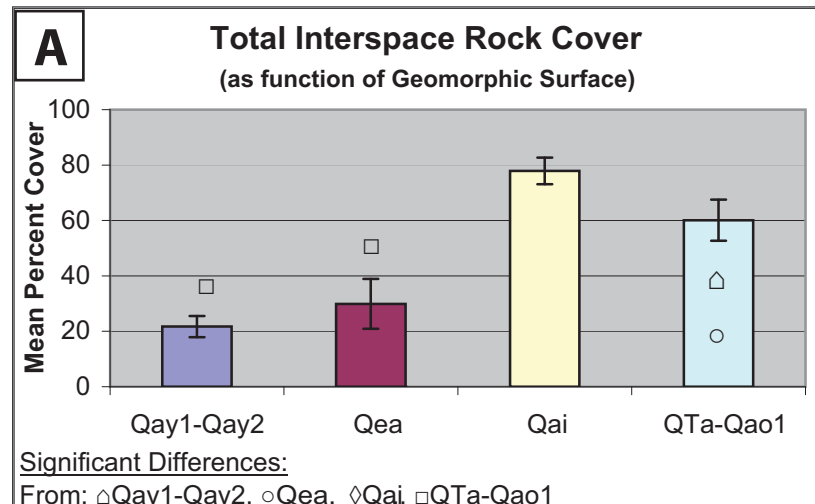


Figure 3.11: ANOVAs compare differences in interspace surface cover among various geomorphic surfaces. Significant differences are denoted by the following symbols: \triangle denotes significant differences from Qay1-Qay2; \circ denotes significant differences from Qea; \diamond denotes significant differences from Qai; \square denotes significant differences from QTa-Qao1. (A) Parametric ANOVA shows significant differences in mean interspace total rock cover among geomorphic surfaces. Bars reflect mean standard error. (B) Non-parametric ANOVAs show significant differences in median interspace moss, *Collema*, *Placidium*, moss-lichen, petrocalcic clast, total rock, and litter cover.

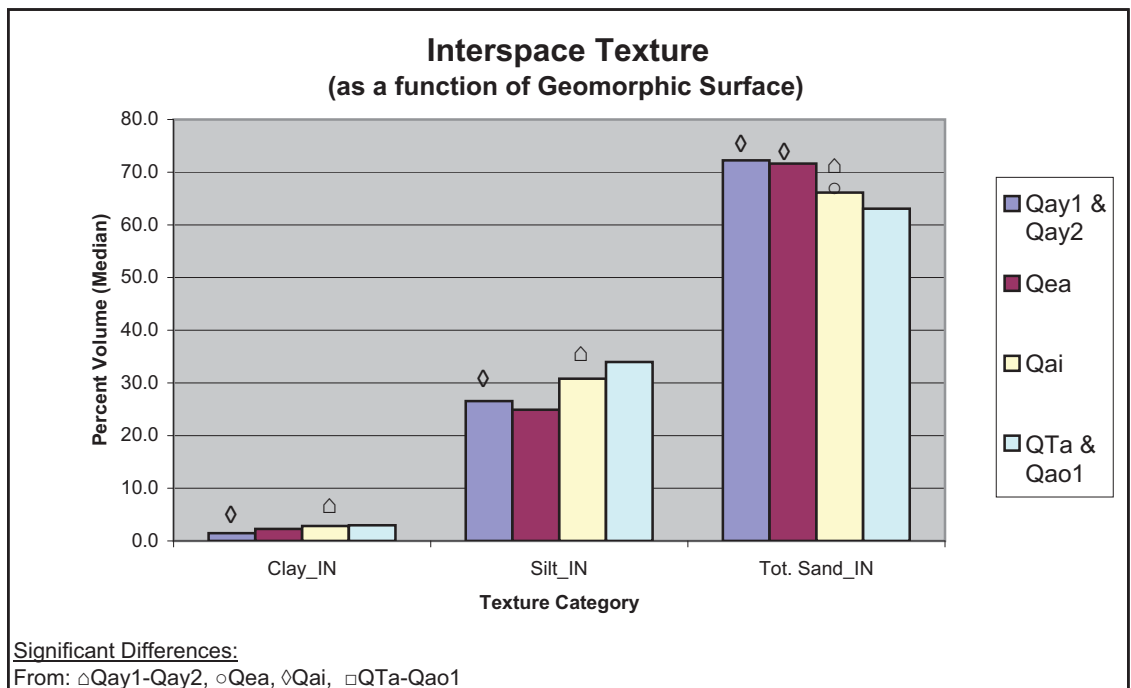


Figure 3.12: Non-parametric ANOVAs compare differences in median interspace surface clay, silt, and total sand content among various geomorphic surfaces. Significant differences are denoted by the following symbols: \triangle denotes significant differences from Qay1-Qay2; \circ denotes significant differences from Qea; \diamond denotes significant differences from Qai; \square denotes significant differences from QTa-Qao1.

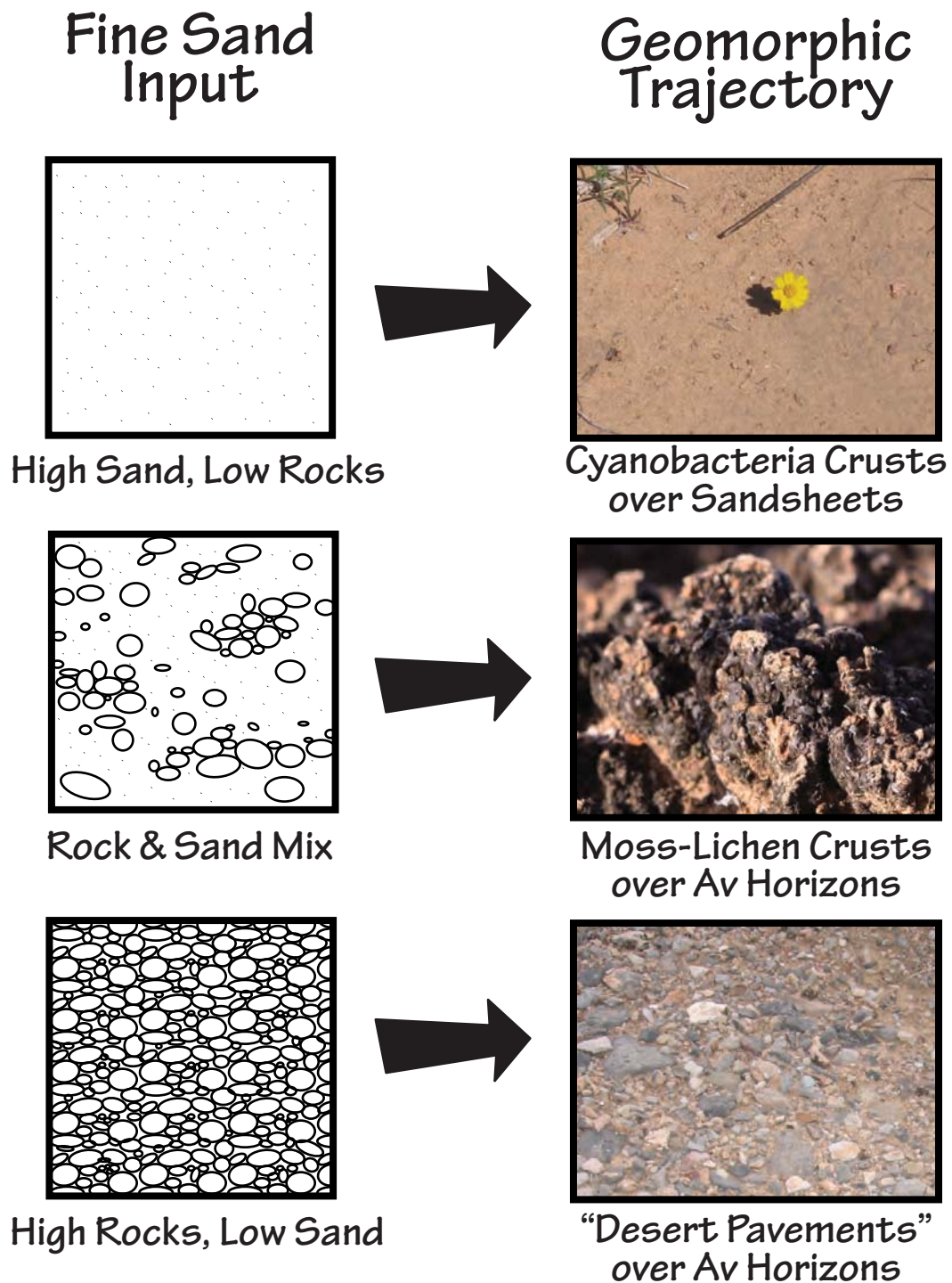


Figure 3.13: Soil profile particle size influences surface cover trajectories. Profiles composed of sand, or sandy particle size control sections lead to cyanobacteria crust development. Profiles composed of sand and $\geq 35\%$ rock fragments, or sandy-skeletal particle size control sections, lead to moss-lichen crust development over biologically-mediated Av horizons. Gravel-dominated deposits lead to "desert pavements" over Av horizons, which correspond to loamy or loamy-skeletal particle size control sections.

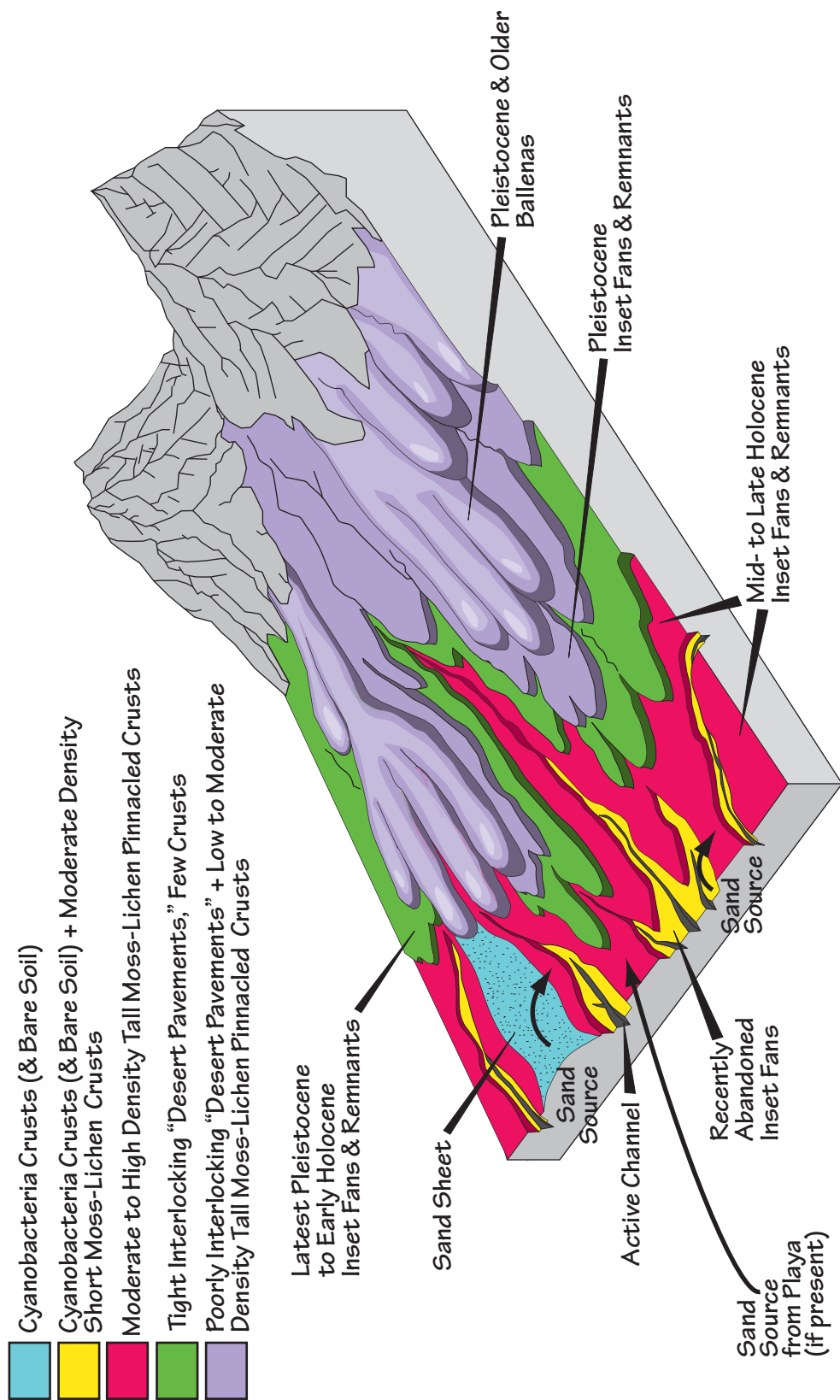


Figure 3.14: Geomorphic surfaces predict interspace cover by BSCs and "desert pavements". Sand sources include sand sheets, active channels, and alluvial flats or playas (not shown). Block model adapted after Peterson (1981).

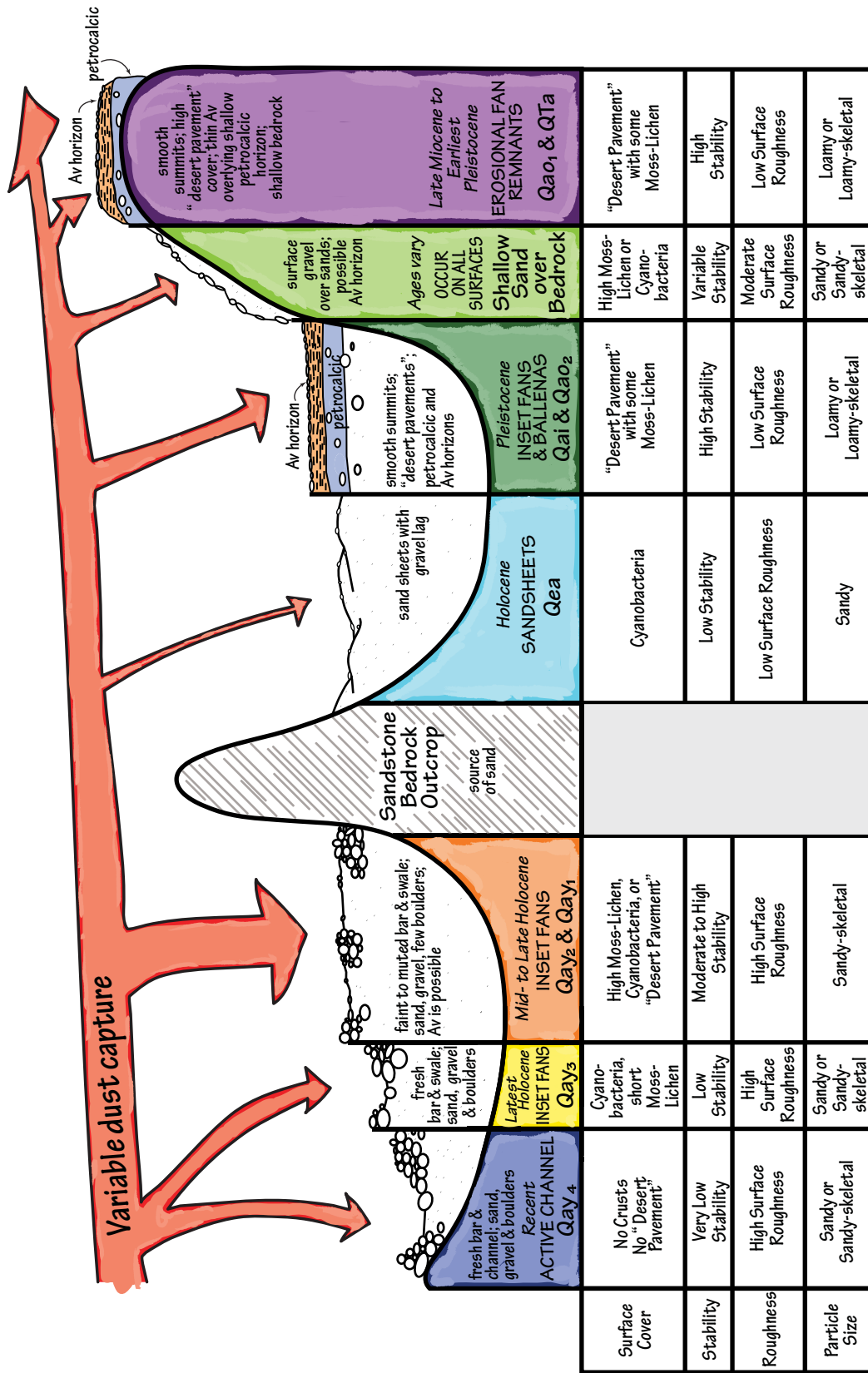


Figure 3.15: BSC and desert pavement cover (row 1) as a function of geomorphic stability (row 2), surface roughness (row 3), inferred dust capture (arrows) and soil particle size control (row 4). Sandstone bedrock outcrops throughout the study area.

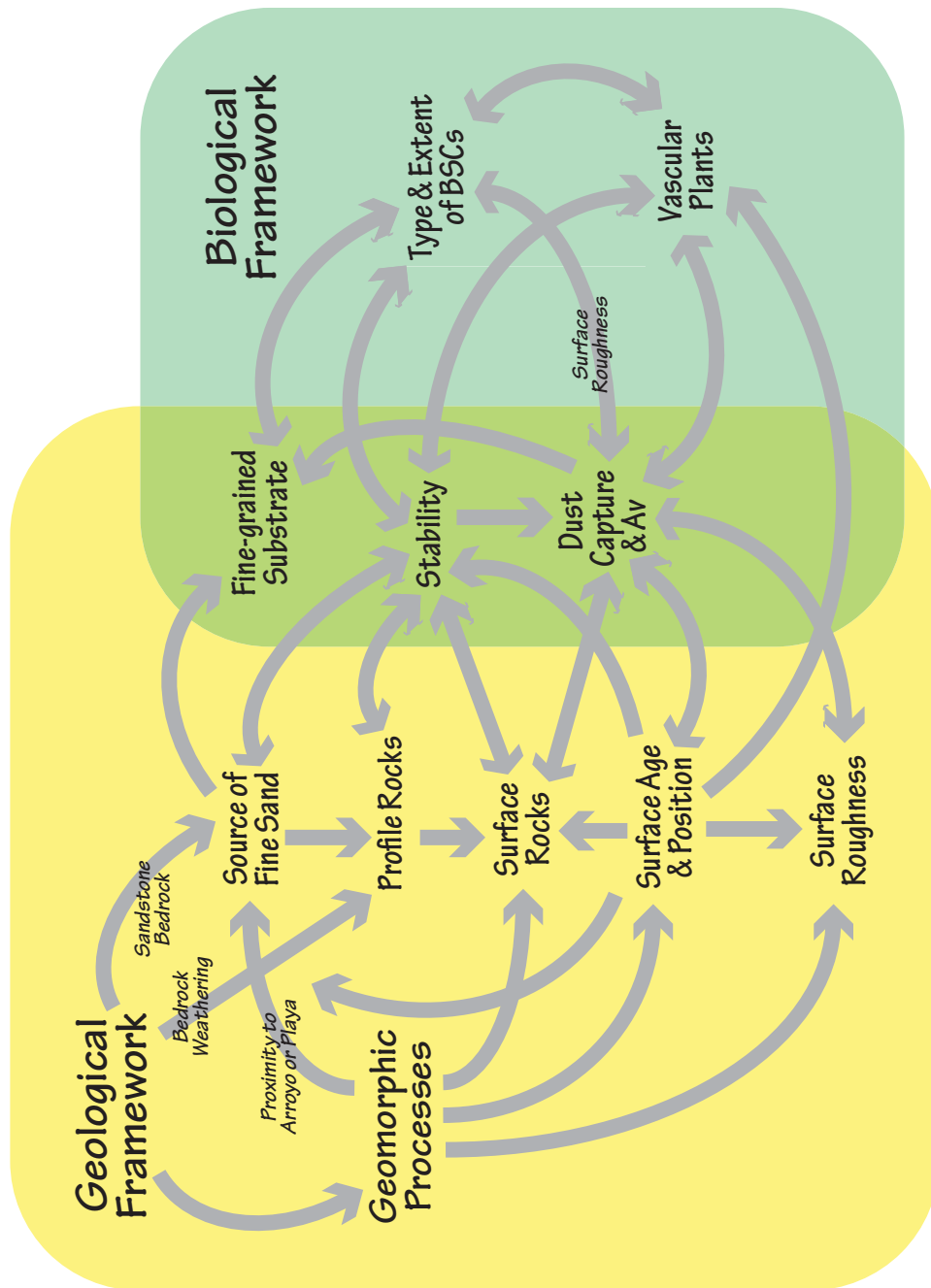


Figure 3.16: Within stable climatic intervals, interactions between geological and biological processes lead to three self-enhancing surface cover trajectories - cyanobacteria crusts, moss-lichen crusts, and "desert pavement." Geological processes influence sand inputs and surface characteristics, which largely determine the initial cover type. If sand input is kept constant, the original surface cover trajectory continues. The biotic framework further enhances feedbacks that support persistence of that surface trajectory.

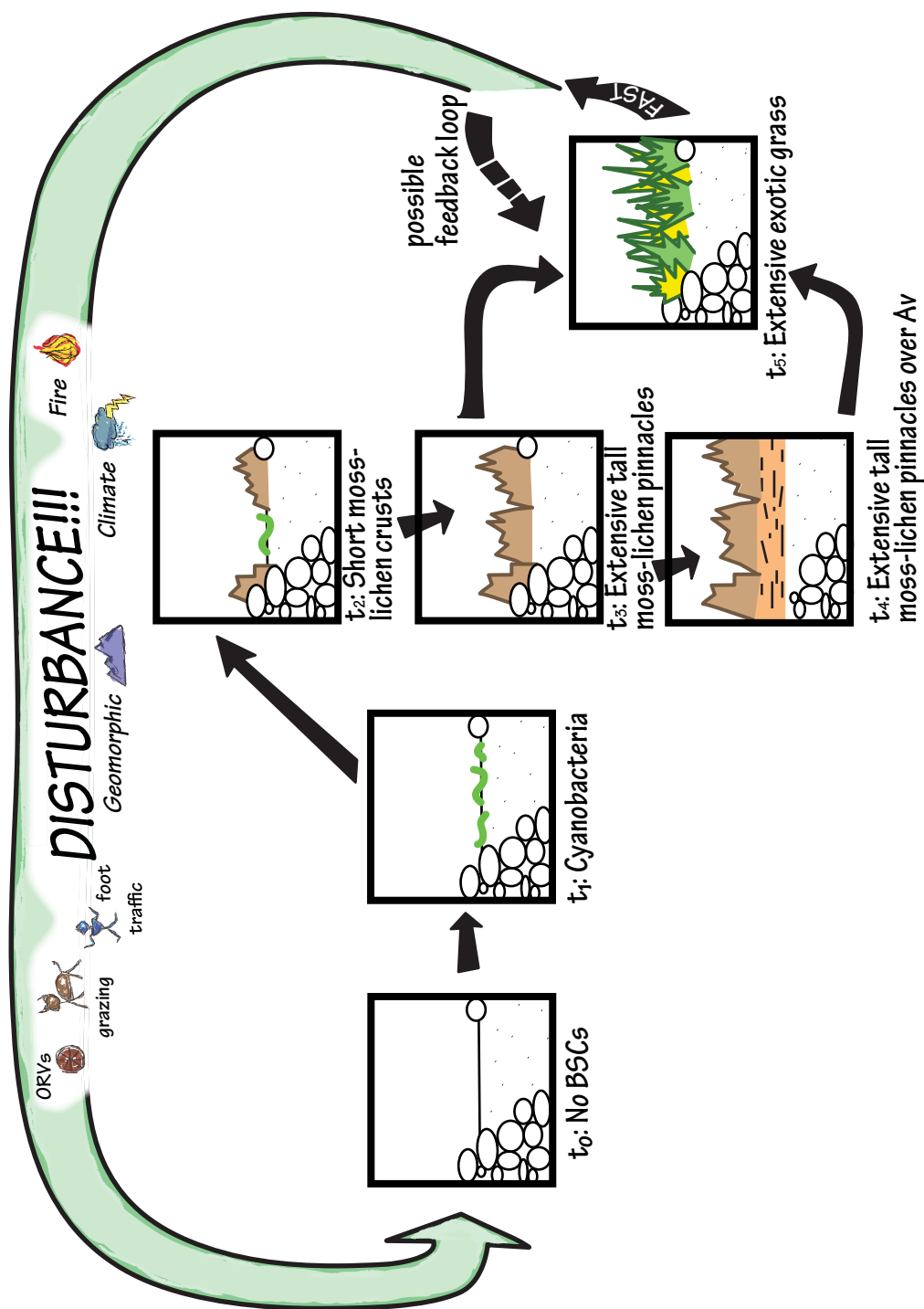


Figure 3.17: Crust development proceeds from bare mineral soil to cyanobacteria crusts to short moss-lichen crusts to tall moss-lichen pinnacled crusts with or without underlying mineral Av horizons. Moss-lichen crusts favor exotic grass invasions and wildfires (see Chapter 4). Natural and anthropogenic disturbances can reset crust succession back to an earlier stage of development.

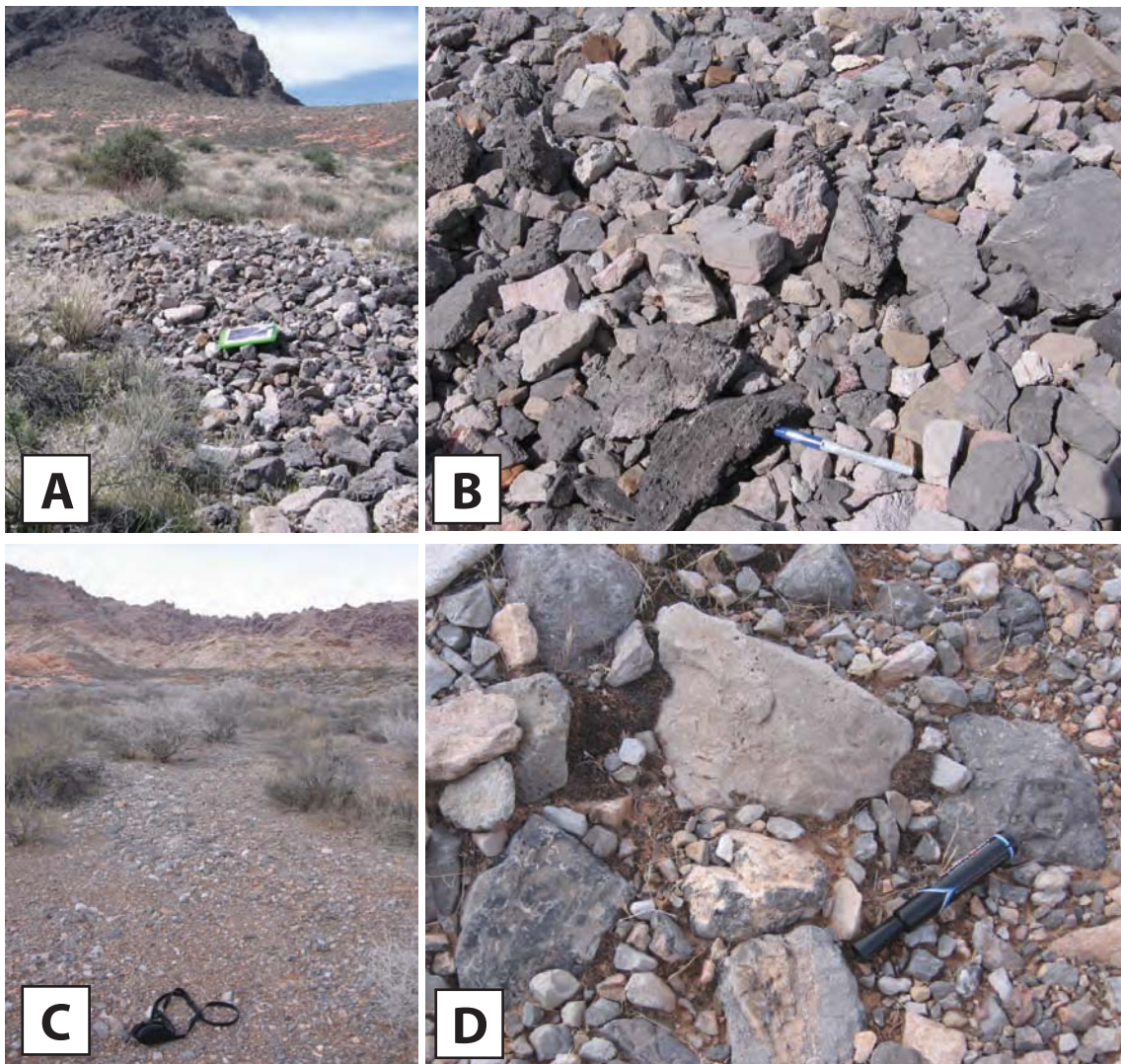


Figure 3.18: (A) A late Holocene to recent alluvial deposit shows no sand infilling (clipboard for scale). (B) A close-up of the previous images illustrates how lack of sand prevents development of BSCs (marker for scale). (C) A late Holocene to recent alluvial deposit displays infilling by sand (camera case for scale). (D) Sand infilling provides a fine-grained substrate for BSC growth. BSCs may capture dust and hasten the rates of pedogenesis (marker for scale).

Potential Factors Controlling BSC Distribution

Factors	Select References
soil stability	(Kidron et al. 2000, Bowker et al. 2005, Thompson et al. 2006, Bowker and Belnap 2008, Rivera-Aguilar et al. 2009)
soil type	(Brostoff 2002, Bowker et al. 2006a Bowker and Belnap 2008)
soil parent material	(Brostoff 2002, Bowker et al. 2005)
dust accretion	(Li et al. 2010)
surface rock cover	(Kaltenecker et al. 1999, Quade 2001)
sedimentation and erosion	(Kidron et al. 2000, McKenna Neuman and Maxwell 2002, Thomas and Dougill 2006, Wang et al. 2007, Lazaro et al. 2008)
disturbance	(Kleiner and Harper 1977, Ponzetti and McCune 2001, Belnap 2002, McKenna Neuman and Maxwell 2002, Bowker et al. 2004, Berkeley et al. 2005, Thomas and Dougill 2007, Eldridge et al. 2006, Thompson et al. 2006)
elevation	(Bowker et al. 2006a)
timing, amount, type of precipitation	(Ponzetti and McCune 2001, Belnap et al. 2004, Barker et al. 2005, Belnap et al. 2006, Bowker et al. 2006a, Budel et al. 2009)
humidity, dew, fog	(Lange et al. 1993, 1998, Kidron et al. 2002, Rao et al. 2009, Rivera-Aguilar et al. 2009)
topography	(Bowker et al. 2005, Lazaro et al. 2008, 2006b, Li et al. 2010)
local hydrology	(Lazaro et al. 2008, Rivera-Aguilar et al. 2009, Bowker et al. 2010b)
faunal activity	(Kleiner and Harper 1977, Kaltenecker et al. 1999, Ponzetti and McCune 2001, Brostoff 2002, Belnap et al. 2006, Thomas and Dougill 2007, Eldridge et al. 2010)
solar insolation and temperature	(Kidron et al. 2000, Belnap et al. 2006, Bowker et al. 2006b, Rivera-Aguilar et al. 2006, Cole et al. 2010, Li et al. 2010)
soil depth	(Canton et al. 2003)

Table 3.1(A): Previous research identified several potential factors that control BSC distribution.

Potential Factors Controlling BSC Distribution

Factors	Select References
soil texture and mineralogy	(Belnap 2002, Canton et al. 2003, Bowker et al. 2005, Thompson et al. 2005, Bowker et al. 2006b, Bowker and Belnap 2008, Budel et al. 2009, Rivera-Aguilar et al. 2009)
soil chemistry and fertility	(Ponzetti and McCune 2001, Canton et al. 2003, Bowker et al. 2005, 2006b, Rivera-Aguilar et al. 2009, McCune and Caldwell 2009)
vascular plant litter, protection, shading, competition	(Kaltenecker et al. 1999, Maestre 2003, Berkeley et al. 2005, Belnap et al. 2006, Eldridge et al. 2006, Rivera-Aguilar et al. 2006, Thomas and Dougill 2006, Eldridge et al. 2010)
BSC community interactions	(Maestre et al. 2008, Bowker et al. 2010a)
BSC development time or succession	(Belnap and Warren 2002, Thompson et al. 2006, Bowker 2007, Budel et al. 2009)

Table 3.1(B): Previous research identified several potential factors that control BSC distribution.

Surface Cover Composite Classes

Composite Class	Component Categories
Total Canopy Cover	Sum of all plant canopies from line intercept data
Moss-lichen	Sum of moss and all lichen cover from point count data
Total BSCs	Sum of cyanobacteria, moss, and all lichen from point count data
Cyanobacteria-Bare	Sum of cyanobacteria and bare soil cover from point count data
Total Rock	Sum of surface rock cover from limestone, sandstone, and petrocalcic clasts from point count data

Table 3.2: Summary of surface cover composite classes used in data compilation

BSC Map Unit Summary

BSC Map Units	Mean Interspace Cover		
	Moss-lichen	Cyanobacteria-bare	Rock
CB.1: High Density Cyanobacteria-Bare Crusts	2%	68%	18%
CB.2: High Density Cyanobacteria-Bare Crusts, Low to Moderate Density Short Moss-Lichen Crusts	10%	64%	20%
CB.3: Variable Density Cyanobacteria-Bare Crusts, Variable Density Short Moss-Lichen Crusts	9%	45%	46%
ML.1: High Density Tall Moss-Lichen Pinnacled Crusts, Moderate Density Cyanobacteria-Bare Crusts	52%	26%	10%
ML.2: Moderately-High Density Tall Moss-Lichen Pinnacled Crusts, Low to Moderate Density Cyanobacteria-Bare Crusts	42%	11%	26%
ML.3: High Density Tall Moss-Lichen Pinnacled Crusts, Low to Moderate Density Cyanobacteria-Bare Crusts	51%	15%	27%
S.1: Scattered, Moderate Density Tall Moss-Lichen Pinnacled Crusts, Low to Moderate Density Cyanobacteria-Bare Crusts	16%	17%	57%
S.2: Scattered, Moderate Density Tall Moss-Lichen Pinnacled Crusts, Moderate Density Cyanobacteria-Bare Crusts	16%	29%	36%
S.3: Scattered, Low to Moderate Density Tall Moss-Lichen Pinnacled Crusts, Low to Moderate Density Cyanobacteria-Bare Crusts	13%	11%	72%
S.4: Scattered, Low Density Tall Moss-Lichen Pinnacled Crusts, Low Density Cyanobacteria-Bare Crusts	8%	6%	83%

Table 3.3: Summary of BSC map units and respective surface cover

BSC Map Unit Descriptions

CB.1: High Density Cyanobacteria-Bare Crusts



Crusts: Nearly continuous cover by cyanobacteria and bare soil; few/no moss or lichen

Soil: Sandy surface soils; variable, non-embedded surface gravel

Dominant Vegetation: *Pleuraphis rigida*, *Larrea tridentata*, *Ambrosia dumosa*, *Menodora spinescens*, *Psoralea argemone*, *Hymenoclea salsola*, *Coleogyne ramosissima*, *Ephedra nevadensis*; also: *Lycium andersonii*, *Krameria erecta*, *Bromus rubens*, *Opuntia basilaris*

	Range (%)	Mean (%)		Range (%)	Mean (%)
Total Canopy Cover	32-36	34	Total Interspace Cover	64-68	66
Total BSCs	32-39	35	Total BSCs	28-54	45
Moss-Lichen	2-7	4	Moss-Lichen	0-3	2
Cyanobacteria-Bare	30-43	38	Cyanobacteria-Bare	48-81	68
Rock Fragments	0-4	2	Rock Fragments	1-38	18
Grass Litter	23-49	36	Grass Litter	3-12	7

Notes: Lowest moss-lichen crust cover of all CB, ML, and S units

Table 3.4(A): Description of BSC Map Unit CB.1

BSC Map Unit Descriptions

CB.2: High Density Cyanobacteria-Bare Crusts, Low to Moderate Density Short Moss-Lichen Crusts



Crusts: Extensive high density cyanobacteria-bare crusts with scattered low to moderate density short moss-lichen crusts

Soil: Sandy surface soils; variable, non-embedded surface gravel

Dominant Vegetation: *Larrea tridentata*, *Ephedra nevadensis*, *Menodora spinescens*, *Ambrosia dumosa*, *Pleuraphis rigida*, *Lycium andersonii*; also: *Bromus rubens*, *Cylindropuntia echinocarpa*, *Psoralea fremontii*, *Lycium cooperi*

	Range (%)	Mean (%)		Range (%)	Mean (%)
Total Canopy Cover	27-33	29	Total Interspace Cover	68-73	71
Total BSCs	25-42	35	Total BSCs	53-61	57
Moss-Lichen	5-9	7	Moss-Lichen	2-14	10
Cyanobacteria-Bare	23-33	29	Cyanobacteria-Bare	53-87	64
Rock Fragments	0-6	3	Rock Fragments	7-29	20
Grass Litter	35-55	44	Grass Litter	1-4	2

Notes: Highest cyanobacteria crust cover and lowest grass litter cover (i.e., Red Brome) among CB, ML, and S units.

Table 3.4(B): Description of BSC Map Unit CB.2

BSC Map Unit Descriptions

CB.3: Variable Density Cyanobacteria-Bare Crusts, Variable Density Short Moss-Lichen Crusts



Crusts: Scattered, variable density short moss-lichen crusts with scattered, variable density cyanobacteria-bare crusts

Soil: Variable; surface sands and gravels display fresh bar and swale morphology; surfaces commonly occur 10s of centimeters above active channel.

Dominant Vegetation: *Psoralea fremontii*, *Hymenoclea salsola*, *Menodora spinescens*, *Coleogyne ramosissima*, *Prunus fasciculata*, *Ephedra nevadensis*, *Krameria erecta*, *Encelia farinosa*; also: *Pleuraphis rigida*, *Larrea tridentata*, *Bromus rubens*, *Eriogonum fasciculatum*, *Chilopsis linearis*

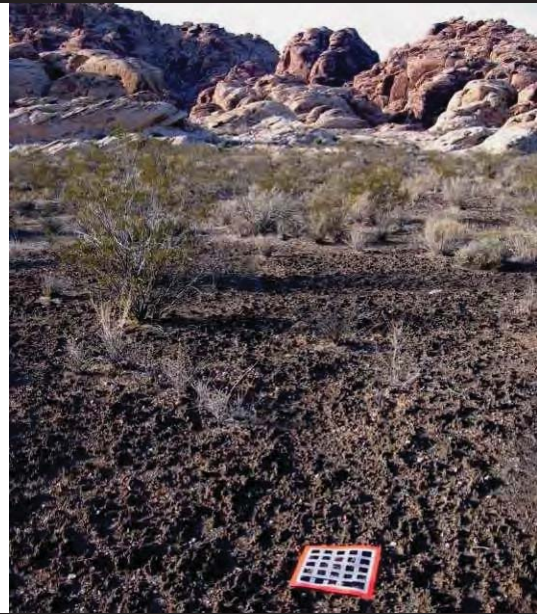
	Range (%)	Mean (%)		Range (%)	Mean (%)
Total Canopy Cover	19-34	29	Total Interspace Cover	66-81	71
Total BSCs	6-33	23	Total BSCs	16-29	22
Moss-Lichen	1-13	6	Moss-Lichen	2-13	9
Cyanobacteria-Bare	6-49	32	Cyanobacteria-Bare	8-75	45
Rock Fragments	4-37	18	Rock Fragments	31-70	46
Grass Litter	7-29	18	Grass Litter	1-4	3

Notes: Lowest total litter cover (by grasses and others) and highest bare soil cover among all units CB, ML, and S units. May occur in small patches with areas mapped as Bare/Active.

Table 3.4(C): Description of BSC Map Unit CB.3

BSC Map Unit Descriptions

ML.1: High Density Tall Moss-Lichen Pinnacled Crusts, Moderate Density Cyanobacteria-Bare Crusts



Crusts: High density, continuous tall moss-lichen pinnacled crusts; moderate density cyanobacteria-bare crusts

Soil: Sandy surface soils; few surface rock fragments

Dominant Vegetation: *Larrea tridentata*, *Ambrosia dumosa*, *Ephedra nevadensis*, *Lycium andersonii*, *Menodora spinescens*; also: *Pleuraphis rigida*, *Hymenoclea salsola*, *Bromus rubens*, *Krameria erecta*

	Range (%)	Mean (%)		Range (%)	Mean (%)
Total Canopy Cover	22-41	29	Total Interspace Cover	59-78	71
Total BSCs	21-66	39	Total BSCs	67-88	77
Moss-Lichen	5-25	14	Moss-Lichen	44-59	52
Cyanobacteria-Bare	11-42	26	Cyanobacteria-Bare	23-29	26
Rock Fragments	3-5	4	Rock Fragments	3-16	10
Grass Litter	6-57	37	Grass Litter	5-12	9

Notes: Lowest interspace rock fragment cover, highest moss-lichen interspace cover, and highest total BSC interspace cover among all CB, ML, and S units.

Table 3.4(D): Description of BSC Map Unit ML.1

BSC Map Unit Descriptions

ML.2: Moderately-High Density Tall Moss-Lichen Pinnacled Crusts, Low to Moderate Density Cyanobacteria-Crusts



Crusts: Moderately-high density, continuous tall moss-lichen pinnacled crusts; low to moderate density cyanobacteria-bare crusts

Soil: Moderate gravel cover, some 0.5 m cobbles; muted to faint bar and swale surface morphology

Dominant Vegetation: *Larrea tridentata*, *Menodora spinescens*, *Ephedra nevadensis*, *Ambrosia dumosa*, *Krameria erecta*; also: *Pleuraphis rigida*, *Prunus fasciculata*, *Bromus rubens*, *Coleogyne ramosissima*, *Hymenoclea salsola*, *Eriogonum fasciculatum*

	Range (%)	Mean (%)		Range (%)	Mean (%)
Total Canopy Cover	11-41	26	Total Interspace Cover	59-89	74
Total BSCs	8-33	19	Total BSCs	34-62	48
Moss-Lichen	6-10	8	Moss-Lichen	32-50	42
Cyanobacteria-Bare	1-23	11	Cyanobacteria-Bare	6-15	11
Rock Fragments	3-12	6	Rock Fragments	21-33	26
Grass Litter	49-72	60	Grass Litter	5-24	17

Notes: Highest exotic grass interspace cover and total litter interspace cover among all CB, ML, and S units.

Table 3.4(E): Description of BSC Map Unit ML.2

BSC Map Unit Descriptions

ML.3: High Density Tall Moss-Lichen Pinnacled Crusts, Low to Moderate Density Cyanobacteria-Bare Crusts



Crusts: High density, continuous tall moss-lichen pinnacled crusts; low to moderate density cyanobacteria-bare crusts

Soil: Sandy surface soils with moderate limestone and sandstone rock fragments; soils are commonly shallow, $\leq 8\text{cm}$ thick, overlying Aztec sandstone bedrock

Dominant Vegetation: *Coleogyne ramosissima*, *Hymenoclea salsola*, *Ambrosia dumosa*, *Ephedra nevadensis*, *Pleuraphis rigida*, *Menodora spinescens*, *Larrea tridentata*; also: *Encelia farinosa*, *Eriogonum fasciculatum*, *Bromus rubens*, *Krameria erecta*

	Range (%)	Mean (%)		Range (%)	Mean (%)
Total Canopy Cover	11-17	13	Total Interspace Cover	83-89	87
Total BSCs	23-35	28	Total BSCs	62-67	64
Moss-Lichen	3-27	11	Moss-Lichen	47-54	51
Cyanobacteria-Bare	15-23	20	Cyanobacteria-Bare	13-17	15
Rock Fragments	6-21	15	Rock Fragments	11-35	27
Grass Litter	15-50	36	Grass Litter	2-19	8

Table 3.4(F): Description of BSC Map Unit ML.3

BSC Map Unit Descriptions

S.1: Scattered, Moderate Density Tall Moss-Lichen Pinnaced Crusts, Low to Moderate Density Cyanobacteria-Bare Crusts



Crusts: Moderate density tall moss-lichen pinnaced crusts with low to moderate density cyanobacteria-bare crusts; BSCs are scattered among rock fragments; crust distribution may vary with topography, where summits *may* have fewer crusts than north-to-east-facing sideslopes.

Soil: High density, upturned surface gravel with fine-textured surface soils
Dominant Vegetation: *Ambrosia dumosa*, *Ephedra nevadensis*, *Coleogyne ramosissima*, *Larrea tridentata*, *Encelia farinosa*, *Hymenoclea salsola*, *Lycium andersonii*, *Psoralea fremontii*, *Krameria erecta*; also: *Menodora spinescens*, *Tiquilia canescens*, *Bromus rubens*

	Range (%)	Mean (%)		Range (%)	Mean (%)
Total Canopy Cover	10-32	23	Total Interspace Cover	68-90	77
Total BSCs	10-34	18	Total BSCs	12-43	28
Moss-Lichen	0-13	6	Moss-Lichen	3-24	16
Cyanobacteria-Bare	5-29	13	Cyanobacteria-Bare	7-31	17
Rock Fragments	15-24	19	Rock Fragments	38-67	57
Grass Litter	24-48	38	Grass Litter	0-16	7

Table 3.4(G): Description of BSC Map Unit S.1

BSC Map Unit Descriptions

S.2: Scattered, Moderate Density Tall Moss-Lichen Pinnaced Crusts, Moderate Density Cyanobacteria-Bare Crusts



Crusts: Moderate density tall moss-lichen pinnaced crusts with moderate density cyanobacteria-bare crusts; BSCs are scattered among surface rock fragments

Soil: Moderate to high density, embedded limestone surface gravel fragments with fine-textured surface soils; few 0.25 to 0.5 m cobbles

Dominant Vegetation: *Ambrosia dumosa*, *Coleogyne ramosissima*, *Menodora spinescens*, *Ephedra nevadensis*, *Larrea tridentata*, *Lycium andersonii*, *Prunus fasciculata*, *Psoralea fremontii*; also: *Krameria erecta*, *Bromus rubens*

	Range (%)	Mean (%)		Range (%)	Mean (%)
Total Canopy Cover	32-47	41	Total Interspace Cover	53-68	59
Total BSCs	42-52	47	Total BSCs	41-45	43
Moss-Lichen	7-13	9	Moss-Lichen	9-25	16
Cyanobacteria-Bare	35-45	41	Cyanobacteria-Bare	26-34	29
Rock Fragments	10-17	14	Rock Fragments	31-41	36
Grass Litter	15-22	17	Grass Litter	16-21	18

Notes: Highest canopy cover among CB, ML, and S units.

Table 3.4(H): Description of BSC Map Unit S.2

BSC Map Unit Descriptions

S.3: Scattered, Low to Moderate Density Tall Moss-Lichen Pinnaced Crusts, Low to Moderate Density Cyanobacteria-Bare Crusts



Crusts: Low to moderate density tall moss-lichen pinnaced crusts with low to moderate density cyanobacteria-bare crusts; scattered BSCs are scattered among rock fragments

Soil: High density petrocalcic and limestone gravel, fine textured surface soils; gravel is partially embedded; surfaces commonly lie along elevated landforms

Dominant Vegetation: *Coleogyne ramosissima*, *Hymenoclea salsola*, *Menodora spinescens*, *Ephedra nevadensis*, *Encelia farinosa*, *Ambrosia dumosa*; also: *Bromus rubens*, *Lycium andersonii*, *Psoralea fremontii*, *Sphaeralcea ambigua*

	Range (%)	Mean (%)		Range (%)	Mean (%)
Total Canopy Cover	11-30	21	Total Interspace Cover	70-89	79
Total BSCs	23-27	25	Total BSCs	16-35	23
Moss-Lichen	4-10	7	Moss-Lichen	7-21	13
Cyanobacteria-Bare	17-22	19	Cyanobacteria-Bare	5-16	11
Rock Fragments	15-38	25	Rock Fragments	61-81	72
Grass Litter	15-34	26	Grass Litter	2-7	5

Table 3.4(I): Description of BSC Map Unit S.3

BSC Map Unit Descriptions

S.4: Scattered, Low Density Tall Moss-Lichen Pinnacled Crusts, Low Density Cyanobacteria-Bare Crusts



Crusts: Low density tall moss-lichen pinnacled crusts and low density cyanobacteria-bare crusts; BSCs are scattered among surface rock fragments

Soil: High density gravel and large boulders with sandy to loamy surface soils; commonly occur on steep slopes ($\geq 15\%$) and in association with limestone or sandstone bedrock

Dominant Vegetation: *Ambrosia dumosa*, *Coleogyne ramosissima*, *Larrea tridentata*, *Ephedra nevadensis*, *Krascheninnikovia lanata*; also: *Hymenoclea salsola*, *Eriogonum inflatum*, *Bromus rubens*, *Pleuraphis rigida*, *Cylindropuntia echinocarpa*, *Sphaeralcea ambigua*, *Menodora spinescens*, *Krameria erecta*, *Opuntia basilaris*, *Encelia farinosa*, *Tiquilia canescens*

	Range (%)	Mean (%)		Range (%)	Mean (%)
Total Canopy Cover	8-32	21	Total Interspace Cover	68-93	79
Total BSCs	9-16	12	Total BSCs	11-15	14
Moss-Lichen	0-9	5	Moss-Lichen	4-11	8
Cyanobacteria-Bare	1-16	7	Cyanobacteria-Bare	4-8	6
Rock Fragments	14-37	27	Rock Fragments	80-86	83
Grass Litter	20-56	40	Grass Litter	3-9	6

Table 3.4(J): Description of BSC Map Unit S.4

BSC Map Unit Descriptions





Additional Units	
<p>Bare-Active: No BSC development; commonly occurs in active alluvial channel; often adjacent to Unit CB.3</p>	
<p>AZ: Aztec Sandstone bedrock; outcrops as inselbergs; no BSC development but commonly occurs adjacent to Unit ML.3</p>	
<p>Limestone: Limestone bedrock outcrop</p>	
<p>OHV Tracks: Off-highway vehicle disturbance or decommissioned roads</p>	

Table 3.4(K): Description of additional map units

Geomorphic Map Unit Summary

Geomorphic Unit	Characteristics	Mean Interspace Rock Cover	Correlated Soil Types
Qay₄	Youngest alluvium; recent active channels; fresh bar and channel morphology; negligible soil development	not collected	Unspecified Entisols
Qay₃	Recently abandoned alluvium; latest Holocene inset fans; fresh bar and swale morphology; negligible soil development	46%	2-Phase Entisols sandy-skeletal, mixed, thermic Typic Torriorthents; mixed thermic Typic Torripsamments
Qay₂	Youngest inactive alluvium; mid- to late Holocene inset fans; muted bar and swale; 15cm Av horizon; Stage I carbonate	18%	Arizo Series sandy-skeletal, mixed, thermic Typic Torriorthents
Qay₁	Young inactive alluvium; mid-Holocene inset fans; faint bar and swale; 27cm Av horizon; Stage II carbonate	25%	
Qai₃	Intermediate alluvium; late Pleistocene inset fans; moderately interlocking pavements; 10cm Av; Stage III Bkkm; Stage I Bk	36%	Irongold Series loamy, mixed, thermic shallow Typic Petrocalcids
Qai₂	Intermediate alluvium; mid- to late Pleistocene inset fans; moderately interlocking pavements; 13cm Av; Stage IV Bkkm; Stage I Bk	36%	
Qai₁	Intermediate alluvium; early to mid-Pleistocene inset fans; variable pavements morphology; 16cm Av; Stage V Bkkm	49%	
Qao₂	Old alluvium; early Pleistocene ballenas; poorly interlocking pavements; 18 cm Av; Stage III-V Bkkm; Stage II Bk with 5% secondary carbonate	63%	Ferrogold Series loamy-skeletal, mixed, thermic, shallow Calcic Petrocalcids
Qao₁	Old alluvium; earliest Pleistocene erosional fan remnants; variable pavement morphology; 9 cm Av; Stage V Bkkm	63%	Shallow Typic Petrocalcids loamy-skeletal, mixed, thermic, shallow Typic Petrocalcids
QTa	Oldest alluvium; late Miocene to earliest Pleistocene erosional fan remnants; variable pavements; 8 cm Av; Stage VI Bkkm;	80%	
Qc	Latest Pleistocene to Holocene colluvium; variable soils	83%	Unspecified Colluvium
Qea	Holocene sand sheets with eolian/fluvial gravel lag; sand sheets >1m thick; up to Stage I carbonate morphology	30%	Bluepoint Series Mixed, thermic Typic Torripsamments

Table 3.5: Summary of geomorphic units, their respective soil taxonomic classification, and correlated soil types

Geomorphic Map Unit Descriptions


Qay₄
Youngest Alluvium; recent active channels

<p>Characteristics: Qay₄ are active washes composed of poorly to moderately sorted limestone boulders, gravels, and sand. Fresh bar and channel morphology and patchy vegetation characterize these surfaces. Deposits range from broad sheet-like sandy and gravelly areas with few channels to incised washes with single channels that truncate low terraces. Channels may be braided with interspersed gravel bars and sandy fluvial/eolian deposits. Sands are likely fluvial deposits but may be reworked by eolian processes. Soils show negligible pedogenesis with no secondary carbonate accumulation or Av development. Sandstone bedrock outcrops within the unit.</p> <p>Canopy surface rock fragments: Transect data were not collected within active channels, as these sites showed no BSC development.</p> <p>Interspace surface rock fragments: not collected</p> <p>Profile rock fragments: not collected</p> <p>Canopy surface textures: not collected</p> <p>Interspace surface textures: not collected</p>
Vegetation: variable; see vegetation commonly associated adjacent Qay ₃
Classification of pedon: Unspecified Entisols
<p>Notes: Qay₄ units commonly truncate or lie adjacent to Qay₃ terraces, making them difficult to map in detail. Polygon boundaries are best approximations based on aerial imagery and field reconnaissance. Given the active nature of these washes, their boundaries and morphology are anticipated to change from year to year.</p>

Table 3.6(A): Description of geomorphic map unit Qay₄

Geomorphic Map Unit Descriptions



Qay₃	
Recently abandoned alluvium; latest Holocene	
	
<p>Characteristics: Qay₃ are recently abandoned inset fans composed of poorly to moderately sorted limestone boulders, gravels, and sand. Surfaces flank active channels and lie approximately 0.5 m higher. Fresh bar and swale morphology and moderate shrub cover characterize these surfaces. Deposits may be broad sheet-like sandy and gravelly areas, or they may be highly incised terraces truncated by nearby active channels. Deposits are commonly composed of gravel bars with interspersed sandy fluvial/eolian deposits. Though sands may be fluvial, they have likely been reworked by eolian processes. Soils are marked by negligible soil formation, with no secondary carbonate accumulation or Av horizon development. Soils include two phases, sandy-skeletal phases associated with gravel bars and sandy phases associated with the interspersed sand. A patchy, single grain mantle of gravel lag may overlie sandy phases.</p> <p>Canopy surface rock fragments: mostly limestone; range 4-37%; mean 18%</p> <p>Interspace surface rock fragments: mostly limestone; range 31-70%; mean 46%</p> <p>Profile rock fragments: primarily limestone; range 5-55% by volume</p> <p>Canopy surface textures: fine sand, loamy fine sand</p> <p>Interspace surface textures: sand, fine sand, loamy fine sandy</p>	
<p>Vegetation: <i>Encelia farinosa</i>, <i>Menodora spinescens</i>, <i>Larrea tridentata</i>, <i>Hymenoclea salsola</i>, <i>Psoralea argemone</i>, <i>Eriogonum fasciculatum</i>, <i>Krameria erecta</i>, <i>Ephedra nevadensis</i>, <i>Coleogyne ramosissima</i>, <i>Bromus rubens</i>, <i>Prunus fasciculata</i>, <i>Pleuraphis rigida</i>, <i>Chilopsis linearis</i></p>	
<p>Classification of pedon: Includes two taxonomic phases of soils (based on % rock fragments): (1) Sandy-skeletal, mixed thermic Typic Torriorthents; and (2) Sandy, mixed thermic Typic Torripsamments</p>	
<p>Notes: Qay₃ surfaces are commonly truncated by or lie adjacent to Qay₄ washes, making them difficult to map in detail. Polygon boundaries are best approximations based on aerial imagery and field reconnaissance. Qay₃ are mapped sparingly, and their distribution is expected to accompany Qay₄.</p>	

Table 3.6(B): Description of geomorphic map unit Qay₃

Geomorphic Map Unit Descriptions



Qay₂	
Youngest inactive alluvium; mid- to late Holocene	
	
<p>Characteristics: Qay₂ surfaces are inset fans composed of poorly to moderately sorted boulders, gravels, and sands. Surfaces often flank Qay₄ and Qay₃ and generally lie approximately 1 m above the active channel. These surfaces are slightly modified from their original depositional topography and generally display muted bar and swale morphology. In some areas, subdued gravel bars are still present. Soil profiles are composed of mixed sands and gravels and may be overlain by sand sheets up to 20 cm thick. A patchy, single grain mantle of gravel lag may overlie the surface. Av horizons may be up to 15 cm thick with common fine vesicular pores that are often associated with tall, moss-lichen pinnacled crusts. Soils are characterized by a Bk horizon with <0.5 mm carbonate pendants on clast sides/bottoms, which corresponds to Stage I carbonate morphology. Secondary carbonate is < 5% by volume.</p> <p>Canopy surface rock fragments: mostly limestone; range 3-12%; mean 7%</p> <p>Interspace surface rock fragments: mostly limestone; range 3-31%; mean 18%</p> <p>Profile rock fragments: primarily limestone; generally >35% by volume, with individual horizon fragments ranging from 20-50% by volume</p> <p>Canopy surface textures: fine sandy loam, loamy sand, loamy fine sand</p> <p>Interspace surface textures: fine sandy loam, loamy sand, loamy fine sand</p>	
<p>Vegetation: <i>Larrea tridentata</i>, <i>Hymenoclea salsola</i>, <i>Psoralea fremontii</i>, <i>Menodora spinescens</i>, <i>Krascheninnikovia lanata</i>, <i>Krameria erecta</i>, <i>Ephedra nevadensis</i>, <i>Coleogyne ramosissima</i> (uncommon), <i>Ambrosia dumosa</i>, <i>Eriogonum fasciculatum</i>, <i>Bromus rubens</i>, <i>Pleuraphis rigida</i>, <i>Prunus fasciculata</i>, <i>Lycium andersonii</i></p>	
<p>Classification of pedon: Sandy-skeletal mixed, thermic Typic Torriorthents</p>	
<p>Notes: Qay₂ commonly shares gradational boundaries with Qea. Without extensive subsurface data, differentiating between sand sheets <20 cm and sand sheets >1m is impractical. Boundaries between these units are best approximations based on field reconnaissance of surface features and aerial imagery.</p>	

Table 3.6(C): Description of geomorphic map unit Qay₂

Geomorphic Map Unit Descriptions



Qay₁	
Young inactive alluvium; mid-Holocene	
	
<p>Characteristics: Qay₁ are inset fans composed of poorly to moderately sorted gravels and sands with rare boulders. Surfaces often flank Qay₄ and Qay₃ and lie approximately 1.5 m above the active channel. These surfaces are significantly modified from their original depositional topography but still display faint bar and swale morphology. Original gravel bars are detectable in some areas. Soil profiles are composed of mixed sands and gravels and may be overlain by sand sheets up to 20 cm thick. A patchy, single grain mantle of gravel lag may overlie the surface. Av horizons are up to 27 cm thick with common fine vesicular pores that are often associated with tall, moss-lichen pinnacled crusts. Vesicular pores are found both within and below moss-lichen crusts. Soils display Bk horizons with thin continuous carbonate coats on clasts, which corresponds to Stage II carbonate morphology. Secondary carbonate is < 5% by volume. Soils commonly overlie fanglomerate deposits of weakly cemented gravels. Fanglomerate cementation more closely resembles groundwater rather than pedogenic processes.</p> <p>Canopy surface rock fragments: mostly limestone; range 3-15%; mean 6%</p> <p>Interspace surface rock fragments: mostly limestone; range 9-38%; mean 25%</p> <p>Profile rock fragments: primarily limestone; generally >35% by volume, with individual horizon fragments varying from 15-60% by volume</p> <p>Canopy surface textures: loamy sand, loamy fine sand, fine sandy loam</p> <p>Interspace surface textures: loamy sand, loamy fine sand, fine sandy loam</p> <p>Vegetation: <i>Larrea tridentata</i>, <i>Ambrosia dumosa</i>, <i>Hymenoclea salsola</i>, <i>Lycium andersonii</i>, <i>Menodora spinescens</i>, <i>Ephedra nevadensis</i>, <i>Bromus rubens</i>, <i>Pleuraphis rigida</i>, <i>Krameria erecta</i>, <i>Encelia farinosa</i>, <i>Coleogyne ramosissima</i> (uncommon)</p> <p>Classification of pedon: Sandy-skeletal mixed, thermic Typic Torriorthents</p> <p>Notes: Qay₁ may share gradational boundaries with Qea. Without extensive subsurface data, differentiating between sand sheets <20 cm and sand sheets >1m is impractical. Boundaries between units are approximations based on field reconnaissance of surface features and aerial imagery.</p>	

Table 3.6(D): Description of geomorphic map unit Qay₁

Geomorphic Map Unit Descriptions


Qai₃	
Intermediate Alluvium, late Pleistocene	
	
<p>Characteristics: Qai₃ are inset fans with planar surfaces and extensive gravel pavement cover. Surfaces lie approximately 0.5-1 meter above Qay₁. Pavements are primarily composed of poorly interlocking limestone gravels, though moderately interlocking pavements are possible. Pavements commonly overlie Av horizons up to 10 cm thick. Av horizons contain common fine vesicular pores. Soils are shallow and characterized by a Bkkm, or petrocalcic, horizon that is completely engulfed by secondary carbonate and found within 45 cm of the surface. This horizon corresponds to Stage III carbonate morphology. A Bk horizon overlies the Bkkm and has fine carbonate pendants on the bottoms of clasts, though secondary carbonate remains <5% by volume. Sand sheet mantles up to 20 cm thick are possible.</p> <p>Canopy surface rock fragments: mostly limestone; mean 6%</p> <p>Interspace surface rock fragments: mostly limestone; mean 36%</p> <p>Profile rock fragments: primarily limestone; are generally <35% by volume, with individual horizon fragments varying from 25-30% by volume</p> <p>Canopy surface textures: loamy sand</p> <p>Interspace surface textures: fine sandy loam</p>	
<p>Vegetation: <i>Menodora spinescens</i>, <i>Ambrosia dumosa</i>, <i>Lycium andersonii</i>, <i>Larrea tridentata</i>, <i>Ephedra nevadensis</i>, <i>Coleogyne ramosissima</i>, <i>Psoralea fremontii</i>, <i>Krameria erecta</i>, <i>Bromus rubens</i></p>	
<p>Classification of pedon: Loamy, mixed, thermic, shallow Typic Petrocalcids</p>	
<p>Notes: Qai₃ may share gradational boundaries with Qea. Without extensive subsurface data, differentiating between sandy sheets <20 cm and sand sheets >1m is impractical. Therefore, boundaries between these units are best approximations based on field reconnaissance of surface features and aerial imagery.</p>	

Table 3.6(E): Description of geomorphic map unit Qai₃

Geomorphic Map Unit Descriptions

Qai₂

Intermediate Alluvium, mid- to late Pleistocene



Characteristics: Qai₂ are inset fans with planar surfaces and extensive gravel pavement cover. Surfaces lie approximately 0.5 meter above Qai₃. Pavements are primarily composed of non-interlocking limestone gravels, though interlocking pavements are possible. Pavements overlie Av horizons up to 13 cm thick that contain common fine vesicular pores. Soils are shallow and characterized by a Bkkm, or petrocalcic, horizon within 42 cm of the surface. The Bkkm is completely indurated with secondary carbonate and has a laminar cap < 1 mm thick, which corresponds to incipient Stage IV carbonate morphology. A Bk horizon overlies the Bkkm and contains a few Stage I carbonate nodules and thin carbonate coats on the bottoms of clasts. Secondary carbonate within the Bk is <5% by volume. Sand sheet mantles up to 20 cm thick are possible.

Canopy surface rock fragments: mostly limestone; range 14-17%; mean 15%

Interspace surface rock fragments: mostly limestone; range 31-41%; mean 36%

Profile rock fragments: primarily limestone; generally <30% by volume, with individual horizon fragments varying from 20-40% by volume

Canopy surface textures: loamy sand

Interspace surface textures: fine sandy loam

Vegetation: *Coleogyne ramosissima*, *Larrea tridentata*, *Ephedra nevadensis*, *Ambrosia dumosa*, *Hymenoclea salsola*, *Lycium andersonii*, *Prunus fasciculata*, *Menodora spinescens*, *Psoralea fremontii*, *Bromus rubens*, *Krameria erecta*

Classification of pedon: Loamy, mixed, thermic, shallow Typic Petrocalcids

Notes: Qai₂ may share gradational boundaries with Qea. Without extensive subsurface data, differentiating between sandy sheets <20 cm and sand sheets >1m is impractical. Therefore, boundaries between these units are best approximations based on field reconnaissance of surface features and aerial imagery.

Table 3.6(F): Description of geomorphic map unit Qai₂

Geomorphic Map Unit Descriptions

Qai₁

Intermediate Alluvium; early to mid-Pleistocene



Characteristics: Qai₁ are inset fans with planar surfaces and extensive gravel pavement cover. Surfaces lie approximately 0.5-1 m above Qai₂. Pavements are primarily composed of poorly interlocking, upturned limestone and petrocalcic gravels. Pavements overlie Av horizons up to 16 cm thick that contain common fine vesicular pores. Soils are shallow and with a Bkkm, or petrocalcic, horizon within 16 cm of the surface. The Bkkm is completely indurated with secondary carbonate and has a 10 cm thick laminar cap, which corresponds to Stage V carbonate morphology. Sand sheet mantles up to 20 cm thick are possible. Soils commonly overlie fanglomerate deposits of weakly consolidated cemented gravels. Fanglomerate cementation is thought to be groundwater-derived and not pedogenic.

Canopy surface rock fragments: limestone & petrocalcic; range 6-17%; mean 13%

Interspace surface rock fragments: limestone & petrocalcic; range 33-60%; mean 49%

Profile rock fragments: limestone & petrocalcic; upper horizons have approximately 20% gravel by volume; cemented horizons have up to 60% gravel by volume.

Canopy surface textures: fine sandy loam, loamy fine sand

Interspace surface textures: fine sandy loam, very fine sandy loam

Vegetation: *Psoralea fremontii*, *Lycium andersonii*, *Hymenoclea salsola*, *Coleogyne ramosissima*, *Larrea tridentata*, *Ephedra nevadensis*, *Ambrosia dumosa*, *Bromus rubens*, *Krameria erecta*

Classification of pedon: Loamy, mixed, thermic shallow Typic Petrocalcids

Notes: Qai₁ may share gradational boundaries with Qea. Without extensive subsurface data, differentiating between sand sheets <20 cm and sand sheets >1m is impractical. Boundaries between units are approximations based on field reconnaissance of surface features and aerial imagery.

Table 3.6(G): Description of geomorphic map unit Qai₁

Geomorphic Map Unit Descriptions



Qao₂	
Old alluvium, early Pleistocene	
	
<p>Characteristics: Qao₂ are ballenas with deeply dissected ridge-and-ravine topography and concordant ridge crests. Surfaces lie approximately 1 m above Qai₁ surfaces. Poorly interlocking pavements of upturned limestone and petrocalcic clasts overlie Av horizons up to 18 cm thick that contain common fine vesicular pores. Soils are shallow with a Bkkm, or petrocalcic, at a depth of 28 cm. The Bkkm may be locally exposed along eroding side slopes. The Bkkm ranges from stage III-V carbonate morphology. A Bk horizon overlies the Bkkm. The Bk contains Stage II carbonate pendants on the bottoms of petrocalcic gravels. Overall the Bk has approximately 5 percent secondary carbonate by volume, which corresponds to a diagnostic calcic horizon. Sand sheet mantles up to 20 cm thick occur in some areas.</p> <p>Canopy surface rock fragments: limestone & petrocalcic; mean 23%</p> <p>Interspace surface rock fragments: limestone & petrocalcic; mean 63%</p> <p>Profile rock fragments: limestone & petrocalcic; upper horizons have >35% gravel by volume; individual horizon fragments vary between 20-85%</p> <p>Canopy surface textures: fine sandy loam</p> <p>Interspace surface textures: fine sandy loam</p>	
<p>Vegetation: <i>Larrea tridentata</i>, <i>Coleogyne ramosissima</i>, <i>Lycium andersonii</i>, <i>Ephedra Menodora spinescens</i>, <i>Ambrosia dumosa</i>, <i>Bromus rubens</i>, <i>Hymenoclea salsola</i></p>	
<p>Classification of pedon: Loamy-skeletal, mixed, thermic, shallow Calcic Petrocalcids</p>	
<p>Notes: Qao₂ may share gradational boundaries with Qea. Without extensive subsurface data, differentiating between sandy sheets <20 cm and sand sheets >1m is impractical. Boundaries between units are best approximations based on field reconnaissance of surface features and aerial imagery.</p>	

Table 3.6(H): Description of geomorphic map unit Qao₂

Geomorphic Map Unit Descriptions

Qao₁

Old Alluvium; earliest Pleistocene



Characteristics: Qao₁ are erosional fan remnants formed in old alluvium with deeply dissected ridge-and-ravine topography and laterally concordant ridge crests. Ridges are commonly rounded but may be planar where bedrock and/or a petrocalcic horizons are locally exposed by erosion. Surfaces lie several meters above Qao₂ surfaces. Bedrock exposures suggest these fan remnants have largely been protected from backslope erosion by underlying bedrock that outcrops locally. Poorly to moderately interlocking pavements of limestone and petrocalcic clasts overlie Av horizons up to 9 cm thick that contain common fine vesicular pores. Soils are shallow with a Bkkm, or petrocalcic, at a depth of 9 cm. The Bkkm displays strong stage V morphology with a 1 cm thick laminar cap sandwiched between two carbonate-indurated horizons. No brecciation was observed in the Bkkm.

Canopy surface rock fragments: limestone & petrocalcic; range 15-38%; mean 24%

Interspace surface rock fragments: limestone & petrocalcic; range 35-81%; mean 63%

Profile rock fragments: limestone & petrocalcic; upper horizons have approximately 50% rock fragments by volume

Canopy surface textures: loamy fine sand, fine sandy loam

Interspace surface textures: loamy fine sand, very fine sandy loam, fine sandy loam, sandy loam

Vegetation: *Sphaeralcea ambigua*, *Ambrosia dumosa*, *Krameria erecta*, *Menodora spinescens*, *Psoralea fremontii*, *Ephedra nevadensis*, *Hymenoclea salsola*, *Larrea tridentata*, *Coleogyne ramosissima*, *Encelia farinosa*, *Tiquilia canescens*, *Bromus rubens*

Classification of pedon: Loamy-skeletal, mixed, thermic, shallow Typic Petrocalcids

Table 3.6(I): Description of geomorphic map unit Qao₁

Geomorphic Map Unit Descriptions



QTa	
Oldest Alluvium; late Miocene to earliest Pleistocene	
	
<p>Characteristics: QTa are erosional fan remnants that form the oldest alluvial surfaces in the basin. These surfaces display deeply dissected ridge-and-ravine topography and discordant ridge crests. Ridge crests are generally planar, especially where bedrock and/or petrocalcic horizons are locally exposed by erosion. Surfaces lie several meters above Qao₁ summits. Bedrock exposures suggest these fan remnants have largely been protected from backslope erosion by underlying bedrock that outcrops locally. Poorly to moderately interlocking pavements are composed of limestone and petrocalcic gravels, cobbles, and stones. These pavements overlie Av horizons up to 8 cm thick that contain common fine vesicular pores. Soils are shallow to a Bkkm, or petrocalcic, at a depth of 8 cm. The Bkkm extends to a depth of 110 cm where it contacts Aztec sandstone bedrock cemented with secondary carbonate. The Bkkm displays strong stage VI morphology with a sequence of laminar caps 14 cm thick overlying a brecciated, carbonate-cemented horizon.</p> <p>Canopy surface rock fragments: limestone & petrocalcic; approximate mean 30%</p> <p>Interspace surface rock fragments: limestone & petrocalcic; approximate mean 80%</p> <p>Profile rock fragments: limestone & petrocalcic; upper horizon has approximately 60% rock fragments by volume</p> <p>Canopy surface textures: loamy fine sand, fine sandy loam</p> <p>Interspace surface textures: loamy fine sand, very fine sandy loam, fine sandy loam, sandy loam</p>	
<p>Vegetation: <i>Coleogyne ramosissima</i>, <i>Ambrosia dumosa</i>, <i>Larrea tridentata</i>, <i>Ephedra nevadensis</i>, <i>Bromus rubens</i></p>	
<p>Classification of pedon: Loamy-skeletal, mixed, thermic, shallow Typic Petrocalcids</p>	

Table 3.6(J): Description of geomorphic map unit QTa

Geomorphic Map Unit Descriptions



Qc	
Colluvium; latest Pleistocene to Holocene	
	
<p>Characteristics: Qc are hillslope, or colluvial, deposits of coarse, poorly sorted angular boulders, cobbles, stones, gravels, and sands. These deposits commonly cover slopes below the steep cliff faces that surround the valley. Colluvium composition is highly variable depending on local slope characteristics, but it ranges from angular boulder- to gravel-sized talus to fine grained mantles dominated by sand. Because exposures for this unit were not found, profiles were not described.</p> <p>Canopy surface rock fragments: limestone &/or sandstone; range 14-37%; mean 29%</p> <p>Interspace surface rock fragments: limestone &/or sandstone; range 80-86%; mean 83%</p> <p>Profile rock fragments: primarily limestone, some sandstone</p> <p>Canopy surface textures: fine sandy loam</p> <p>Interspace surface textures: fine sandy loam</p>	
<p>Vegetation: <i>Ephedra nevadensis</i>, <i>Ambrosia dumosa</i>, <i>Coleogyne ramosissima</i>, <i>Hymenoclea salsola</i>, <i>Encelia farinosa</i>, <i>Bromus rubens</i>, <i>Sphaeralcea ambigua</i>, <i>Krameria erecta</i>, <i>Tiquilia canescens</i>, <i>Menodora spinescens</i>, <i>Eriogonum inflatum</i>, <i>Krascheninnikovia lanata</i></p>	
<p>Classification of pedon: not determined</p>	
<p>Notes: Qc form gradational boundaries with alluvial and eolian units throughout the basin, where colluvium forms thin to thick mantles over other surfaces. These gradients were impractical to map in detail. Qc polygon boundaries in this area are best approximations based on aerial imagery and surface reconnaissance.</p>	

Table 3.6(K): Description of geomorphic map unit Qc

Geomorphic Map Unit Descriptions


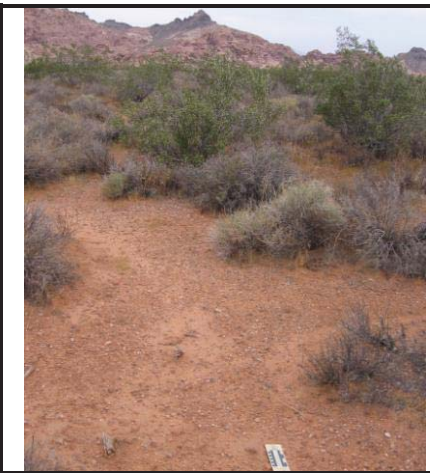
Qea	
Holocene sand sheets with gravel lag	
	
<p>Characteristics: Qea are deep sand sheets or mantles of unconsolidated, fine eolian sand overlain by a thin veneer of fluvial gravel. Eolian mantles vary in thickness but are generally at least 1 m thick and overlie alluvium or bedrock. Sand sheet surfaces are generally flat with broad undulations and small coppices forming around shrubs. Surface rock fragments form a single layer of gravel lag that may be an inflationary veneer and/or a thin alluvial veneer. Sand sources are presumed to have weathered out of local Aztec sandstone bedrock but may include small amounts of eolian silt and clay. Soils may show incipient accumulation of secondary carbonate in the form of fine, carbonate filaments, or Stage I carbonate morphology.</p> <p>Canopy surface rock fragments: primarily limestone; 0-31%; mean 9%</p> <p>Interspace surface rock fragments: primarily limestone; range 1-82%; mean 30%</p> <p>Profile rock fragments: primarily limestone; range 0-2% by volume</p> <p>Canopy surface textures: fine sand, fine sandy loam, loamy fine sand</p> <p>Interspace surface textures: fine sandy loam, loamy fine sand, loamy sand</p>	
<p>Vegetation: <i>Ambrosia dumosa</i>, <i>Menodora spinescens</i>, <i>Ephedra nevadensis</i>, <i>Eriogonum fasciculatum</i>, <i>Coleogyne ramosissima</i>, <i>Hymenoclea salsola</i>, <i>Encelia farinosa</i>, <i>Psoralea argemone</i>, <i>Larrea tridentata</i>, <i>Bromus rubens</i>, <i>Pleuraphis rigida</i>, <i>Lycium andersonii</i>, <i>Cylindropuntia echinocarpa</i>, <i>Sphaeralcea ambigua</i>, <i>Krameria erecta</i>, <i>Opuntia basilaris</i>, <i>Eriogonum inflatum</i>, <i>Krascheninnikovia lanata</i>, <i>Lycium cooperi</i></p>	
<p>Classification of pedon: Mixed, thermic Typic Torripsamments</p>	
<p>Notes: Qea form gradational boundaries with alluvial units throughout the basin, where the thick eolian mantle thins to sand sheets less than 20 cm thick. These gradients were impractical to map in detail. Therefore, Qea polygon boundaries in this area are best approximations based on aerial imagery and surface reconnaissance.</p>	

Table 3.6(L): Description of geomorphic map unit Qea

Geomorphic Map Unit Descriptions




Additional Units	
AZ: Aztec Sandstone bedrock; outcrops as inselbergs	
Limestone: Limestone bedrock outcrop	
OHV Tracks: Off-highway vehicle disturbance or decommissioned roads	

Table 3.6(M): Description of additional map units

Soil Unit Descriptions


Unspecified Entisols
Taxonomy: unspecified Entisols
Geomorphic Surfaces: Qay ₄ ; Recent active washes

<p>Characteristics: Unspecified Entisols soils form in active washes. Soils are characterized by negligible pedogenesis with no secondary carbonate accumulation or Av development. Alluvium is composed of poorly to moderately sorted limestone boulders, gravels, and sand. Fresh bar and channel morphology and patchy vegetation characterize these surfaces. Deposits range from broad sheet-like sandy and gravelly areas with few channels to incised washes with single channels that truncate low terraces. Channels are braided with interspersed gravel bars and sandy fluvial/eolian deposits. Sands are commonly fluvial deposits but are also reworked by eolian processes. Sandstone bedrock commonly outcrops within the unit.</p> <p>Canopy surface rock fragments: Transect data were not collected within active channels, as these sites showed no BSC development.</p> <p>Interspace surface rock fragments: not collected</p> <p>Profile rock fragments: not collected</p> <p>Canopy surface textures: not collected</p> <p>Interspace surface textures: not collected</p>
Vegetation: variable; see vegetation commonly associated 2-phase Entisols
<p>Notes: Unspecified Entisols commonly truncate or lie adjacent to 2-phase Entisols, making detailed mapping difficult. Polygon boundaries are best approximations based on aerial imagery and field reconnaissance. Given the active nature of these washes, their boundaries and morphology are anticipated to change from year to year.</p>

Table 3.7(A): Description of soil types: Unspecified Entisols

Soil Unit Descriptions


Entisols (2 Phases)	
Taxonomy: (1) Sandy-skeletal, mixed thermic Typic Torriorthents; and (2) Sandy, mixed thermic Typic Torripsammments	
Geomorphic Surfaces: Qay ₃ ; latest Holocene inset fans	
	
<p>Characteristics: Two-phase Entisols are formed in recently abandoned inset fans. Soils are characterized by negligible soil formation with no secondary carbonate accumulation or Av horizon development. Alluvium is composed of poorly to moderately sorted limestone boulders, gravels, and sand. The inset fans flank active channels and lie approximately 0.5 m higher. Fresh bar and swale morphology and moderate shrub cover characterize these surfaces. Alluvial deposits may occur as broad sheet-like sandy and gravelly areas, or they may be highly incised terraces truncated by nearby active channels. Deposits are commonly composed of interspersed gravel bars and sandy fluvial/eolian deposits. Though sands may be fluvial, they are likely reworked by eolian processes. Soils are split into two phases, sandy-skeletal phases associated with gravel bars and sandy phases associated with sandy swales. A patchy, single grain mantle of gravel lag may overlie sandy phases.</p> <p>Canopy surface rock fragments: mostly limestone; range 4-37%; mean 18%</p> <p>Interspace surface rock fragments: mostly limestone; range 31-70%; mean 46%</p> <p>Profile rock fragments: primarily limestone; range 5-55% by volume</p> <p>Canopy surface textures: fine sand, loamy fine sand</p> <p>Interspace surface textures: sand, fine sand, loamy fine sandy</p>	
<p>Vegetation: <i>Encelia farinosa</i>, <i>Menodora spinescens</i>, <i>Larrea tridentata</i>, <i>Hymenoclea salsola</i>, <i>Psorothamnus fremontii</i>, <i>Eriogonum fasciculatum</i>, <i>Krameria erecta</i>, <i>Ephedra nevadensis</i>, <i>Coleogyne ramosissima</i>, <i>Bromus rubens</i>, <i>Prunus fasciculata</i>, <i>Pleuraphis rigida</i>, <i>Chilopsis linearis</i></p>	
<p>Notes: Two-phase Entisols are commonly truncated by or lie adjacent to active washes, making them difficult to map in detail. Polygon boundaries are best approximations based on aerial imagery and field reconnaissance. Two-phase Entisols are mapped sparingly, and their distribution is expected to accompany most active channels.</p>	

Table 3.7(B): Description of soil types: 2-Phase Entisols

Soil Unit Descriptions

Arizo	
Taxonomy: Sandy-skeletal mixed, thermic Typic Torriorthents	
Geomorphic Surfaces: Qay ₁ , Qay ₂ ; mid- to late Holocene inset fans	
	
<p>Characteristics: Arizo soils form in inset fans composed of poorly to moderately sorted boulders, gravels, and sands. Soil profiles are generally composed of mixed sands and gravels and may be overlain by sand sheets up to 20 cm thick with patchy, single grain mantle of gravel lag. Av horizons up to 15-27 cm thick with common fine vesicular pores are possible. Vesicular pores are found within and below tall moss-lichen pinnaced crusts. Soils display a Bk horizon with thin, discontinuous to continuous <1 mm carbonate coats on clasts, corresponding to Stage I-II carbonate morphology. Secondary carbonate is < 5% by volume. Surfaces often flank the Unspecified and 2-phase Entisols and lie 1-1.5 m above the active channel. Soil surfaces are modified from their original depositional topography and display faint to muted bar and swale morphology. In some areas, subdued gravel bars may still be visible. Soils commonly overlie fanglomerate deposits of weakly consolidated cemented gravels. Fanglomerate cementation is thought to be groundwater-derived and not pedogenic.</p> <p>Canopy surface rock fragments: mostly limestone; range 3-15%; mean 6%</p> <p>Interspace surface rock fragments: mostly limestone; range 3-38%; mean 22%</p> <p>Profile rock fragments: primarily limestone; generally >35% by volume, with individual horizon fragments ranging from 15-60% by volume</p> <p>Canopy surface textures: fine sandy loam, loamy sand, loamy fine sand</p> <p>Interspace surface textures: fine sandy loam, loamy sand, loamy fine sand</p> <p>Vegetation: <i>Larrea tridentata</i>, <i>Hymenoclea salsola</i>, <i>Psoralea argemonea</i>, <i>Menodora spinescens</i>, <i>Krascheninnikovia lanata</i>, <i>Krameria erecta</i>, <i>Ephedra nevadensis</i>, <i>Coleogyne ramosissima</i> (uncommon), <i>Ambrosia dumosa</i>, <i>Eriogonum fasciculatum</i>, <i>Bromus rubens</i>, <i>Pleuraphis rigida</i>, <i>Prunus fasciculata</i>, <i>Lycium andersonii</i>, <i>Encelia farinosa</i></p> <p>Notes: Arizo soils may share gradational boundaries with the Bluepoint series that form in deep sand sheets. Without extensive subsurface data, differentiating between sand sheets <20 cm and sand sheets >1m is impractical. Boundaries between these units are best approximations based on field reconnaissance of surface features and aerial imagery.</p>	

Table 3.7(C): Description of soil types: Arizo Series

Soil Unit Descriptions

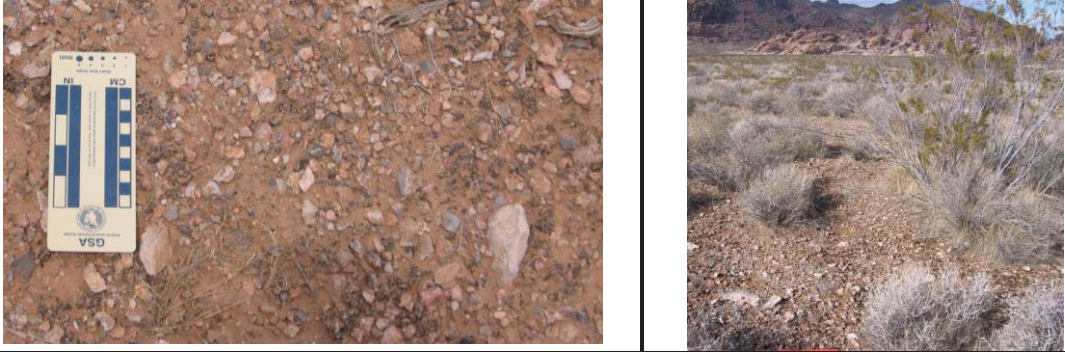
Irongold	
Taxonomy: Loamy, mixed, thermic, shallow Typic Petrocalcids	
Geomorphic Surfaces: Qai₁ , Qai₂ , and Qai₃ ; early to late Pleistocene inset fans	
	
<p>Characteristics: Irongold soils form in inset fans with planar surfaces and extensive gravel pavement cover. Pavements are primarily composed of poorly interlocking, upturned limestone and petrocalcic gravels, though some moderately interlocking pavements are possible. Pavements generally overlie Av horizons up to 10-16 cm thick. Av horizons contain common fine vesicular pores. Soils are shallow with a Bkkm, or petrocalcic, within 16-45 cm of the surface. Secondary carbonate morphology of this horizon ranges from Stage III-V. The Bkkm is generally completely indurated by carbonate. Laminar caps may be absent, <1 mm thick, or as thick as 10 cm. A Bk horizon may overlie the Bkkm with Stage I filaments and/or Stage I carbonate nodules. Secondary carbonate within the Bk is <5% by volume. Sand sheet mantles up to 20 cm thick are possible. The inset fans in which these soils form, lie approximately 0.5-3 m above the inset fans of the Arizo soil series.</p> <p>Canopy surface rock fragments: mostly limestone; range 6-17%; mean 13%</p> <p>Interspace surface rock fragments: mostly limestone; range 31-60%; mean 42%</p> <p>Profile rock fragments: limestone & petrocalcic; generally <35% by volume, with individual horizon fragments varying from 20-40% by volume</p> <p>Canopy surface textures: loamy sand, fine sandy loam, loamy fine sand</p> <p>Interspace surface textures: fine sandy loam, very fine sandy loam</p>	
<p>Vegetation: <i>Menodora spinescens</i>, <i>Ambrosia dumosa</i>, <i>Lycium andersonii</i>, <i>Larrea tridentata</i>, <i>Ephedra nevadensis</i>, <i>Coleogyne ramosissima</i>, <i>Psoralea fremontii</i>, <i>Krameria erecta</i>, <i>Bromus rubens</i>, <i>Hymenoclea salsola</i>, <i>Prunus fasciculata</i>,</p>	
<p>Notes: Irongold soils may share gradational boundaries with the Bluepoint series that form in deep sand sheets. Without extensive subsurface data, differentiating between sand sheets <20 cm and sand sheets >1m is impractical. Boundaries between these units are best approximations based on field reconnaissance of surface features and aerial imagery.</p>	

Table 3.7(D): Description of soil types: Irongold Series

Soil Unit Descriptions


Ferrogold	
Taxonomy: Loamy-skeletal, mixed, thermic, shallow Calcic Petrocalcids	
Geomorphic Surfaces: Qao ₂ ; early Pleistocene ballenas (ca. 1-0.5 Ma)	
	
<p>Characteristics: Ferrol soils form in ballenas with deeply dissected ridge-and-ravine topography and concordant ridge crests. Poorly interlocking pavements of upturned limestone and petrocalcic clasts overlie Av horizons up to 18 cm thick that contain common fine vesicular pores. Soils are shallow with a Bkkm, or petrocalcic, at a depth of 28 cm. The Bkkm may be locally exposed along eroding side slopes. The Bkkm ranges from stage III-V carbonate morphology. A Bk horizon overlies the Bkkm and contains Stage II carbonate pendants on the bottoms of petrocalcic gravels. Overall the Bk has approximately 5 percent secondary carbonate by volume, which corresponds to a diagnostic calcic horizon. Sand sheet mantles up to 20 cm thick are possible. The ballena summits of the Irongold series lie approximately 1-4 m above the inset fan surfaces of the Irongold soils.</p> <p>Canopy surface rock fragments: limestone & petrocalcic; mean 23%</p> <p>Interspace surface rock fragments: limestone & petrocalcic; mean 63%</p> <p>Profile rock fragments: limestone & petrocalcic; upper horizons have >35% gravel by volume; individual horizon fragments vary between 20-85%</p> <p>Canopy surface textures: fine sandy loam</p> <p>Interspace surface textures: fine sandy loam</p>	
<p>Vegetation: <i>Larrea tridentata</i>, <i>Coleogyne ramosissima</i>, <i>Lycium andersonii</i>, <i>Ephedra Menodora spinescens</i>, <i>Ambrosia dumosa</i>, <i>Bromus rubens</i>, <i>Hymenoclea salsola</i></p>	
<p>Notes: Ferrogold soils may share gradational boundaries with the Bluepoint series that form in deep sand sheets. Without extensive subsurface data, differentiating between sand sheets <20 cm and sand sheets >1m is impractical. Boundaries between these units are best approximations based on field reconnaissance of surface features and aerial imagery.</p>	

Table 3.7(E): Description of soil types: Ferrogold Series

Soil Unit Descriptions

shallow Typic Petrocalcids

Taxonomy: Loamy-skeletal, mixed, thermic, shallow Typic Petrocalcids

Geomorphic Surfaces: QTa and Qao₁; late Miocene to earliest Pleistocene erosional fan remnants



Characteristics: Shallow Typic Petrocalcids develop in erosional fan remnants that display deeply dissected ridge-and-ravine topography and laterally concordant or discordant ridge crests. Ridge summits may be rounded or planar. Bedrock exposures suggest these fan remnants have largely been protected from backslope erosion by underlying bedrock that outcrops locally. Poorly to moderately interlocking pavements of limestone and petrocalcic clasts overlie Av horizons to 8-9 cm thick that contain common fine vesicular pores. Soils are shallow with a Bkkm, or petrocalcic, horizon at a depth of 8-9 cm. The Bkkm is commonly exposed along eroding side slopes and displays strong stage V-VI morphology. Laminar carbonate horizons range from with a 1-14 cm. The indurated carbonate horizon may show brecciation and can be as thick as 102 cm. Often this indurated horizon directly overlies Aztec Sandstone bedrock that is cemented with secondary carbonate. These remnant surfaces in which these soils form lie several meters above the ballenas of the Ferrogold series.

Canopy surface rock fragments: limestone & petrocalcic; range 15-24%; mean 20%

Interspace surface rock fragments: limestone & petrocalcic; range 35-81%; mean 60%

Profile rock fragments: limestone & petrocalcic; upper horizons have approximately 55% rock fragments by volume

Canopy surface textures: loamy fine sand, fine sandy loam

Interspace surface textures: loamy fine sand, very fine sandy loam, fine sandy loam, sandy loam

Vegetation: *Sphaeralcea ambigua*, *Ambrosia dumosa*, *Krameria erecta*, *Menodora spinescens*, *Psoralea fremontii*, *Ephedra nevadensis*, *Hymenoclea salsola*, *Larrea tridentata*, *Coleogyne ramosissima*, *Encelia farinosa*, *Tiquilia canescens*, *Bromus rubens*

Table 3.7(F): Description of soil types: shallow Typic Petrocalcids

Soil Unit Descriptions

Unspecified Colluvium	
Taxonomy: not determined	
Geomorphic Surfaces: Qc; latest Pleistocene to Holocene colluvium	
	
<p>Characteristics: Unspecified colluvial soils are formed in hillslope, or colluvial, deposits of coarse, poorly sorted angular boulders, cobbles, stones, gravels, and sands. These deposits commonly cover slopes below the steep cliff faces that surround the valley. Colluvium composition is highly variable depending on local slope characteristics, but it ranges from angular boulder- to gravel-sized talus to fine-grained mantles dominated by sand. Because cross-sectional exposures for this unit were not found, profiles were not described.</p> <p>Canopy surface rock fragments: limestone &/or sandstone; range 14-37%; mean 26%</p> <p>Interspace surface rock fragments: limestone &/or sandstone; range 80-86%; mean 83%</p> <p>Profile rock fragments: primarily limestone, some sandstone</p> <p>Canopy surface textures: fine sandy loam</p> <p>Interspace surface textures: fine sandy loam</p>	
<p>Vegetation: <i>Ephedra nevadensis</i>, <i>Ambrosia dumosa</i>, <i>Coleogyne ramosissima</i>, <i>Hymenoclea salsola</i>, <i>Encelia farinosa</i>, <i>Bromus rubens</i>, <i>Sphaeralcea ambigua</i>, <i>Krameria erecta</i>, <i>Tiquilia canescens</i>, <i>Menodora spinescens</i>, <i>Eriogonum inflatum</i>, <i>Krascheninnikovia lanata</i></p>	
<p>Notes: Unspecified colluvial soils form gradational boundaries with alluvial and eolian soils throughout the basin, where colluvium may form thin to thick mantles over other geomorphic surfaces. These gradients were impractical to map in detail. Unspecified colluvium polygon boundaries in this area are best approximations based on aerial imagery and surface reconnaissance.</p>	

Table 3.7(G): Description of soil types: Unspecified Colluvium

Soil Unit Descriptions

Bluepoint	
Taxonomy: Mixed, thermic Typic Torripsamments	
Geomorphic Surfaces: Qea; Holocene sand sheets with variable gravel lag	
	
	<p>Characteristics: Bluepoint soils form in deep sand sheets or of mantles of unconsolidated, fine eolian sand overlain by a thin veneer of fluvial gravel. Soils may show incipient accumulation of secondary carbonate in the form of fine, carbonate filaments, or Stage I carbonate morphology. Eolian mantles vary in thickness but are commonly at least 1 m thick and overlie alluvium or bedrock. Sand sheet surfaces are generally flat with broad undulations and small coppices forming around shrubs. Surface rock fragments are primarily a single layer of patchy gravel lag that may be an inflationary veneer and/or a thin alluvial veneer. Sand is presumed to have weathered from local Aztec Sandstone bedrock and includes small volumes of eolian silt and clay.</p> <p>Canopy surface rock fragments: mostly limestone; range 0-31%; mean 9%</p> <p>Interspace surface rock fragments: mostly limestone; range 1-82%; mean 30%</p> <p>Profile rock fragments: primarily limestone; range 0-2% by volume</p> <p>Canopy surface textures: fine sand, fine sandy loam, loamy fine sand</p> <p>Interspace surface textures: fine sandy loam, loamy fine sand, loamy sand</p> <p>Vegetation: <i>Ambrosia dumosa</i>, <i>Menodora spinescens</i>, <i>Ephedra nevadensis</i>, <i>Eriogonum fasciculatum</i>, <i>Coleogyne ramosissima</i>, <i>Hymenoclea salsola</i>, <i>Encelia farinosa</i>, <i>Psoralea fremontii</i>, <i>Larrea tridentata</i>, <i>Bromus rubens</i>, <i>Pleuraphis rigida</i>, <i>Lycium andersonii</i>, <i>Cylindropuntia echinocarpa</i>, <i>Sphaeralcea ambigua</i>, <i>Krameria erecta</i>, <i>Opuntia basilaris</i>, <i>Eriogonum inflatum</i>, <i>Krascheninnikovia lanata</i>, <i>Lycium cooperi</i></p> <p>Notes: Bluepoint soils form gradational boundaries with alluvial soils throughout the basin, where the thick eolian mantle thins to sand sheets less than 20 cm thick. These gradients were impractical to map in detail. Bluepoint polygon boundaries in this area are best approximations based on aerial imagery and surface reconnaissance</p>

Table 3.7(H): Description of soil types: Bluepoint Series

GIS Overlay Summary

Crust Cover	Dominant Geomorphic Surface (% Overlap)
Cyanobacteria-Bare Crusts BSC Map Unit CB.1	Qea (66%) <i>Deep Holocene Sand Sheets</i>
High Density Tall Moss-Lichen Crusts BSC Map Units ML.1 & ML.2	Qay ₁ & Qay ₂ (57-59%) <i>Alluvium (Mid- to Late Holocene)</i>
Scattered Low to Moderate Density Tall Moss-Lichen Crusts ("Desert Pavement") BSC Map Units S.1, S.2, & S.3	Qai ₃ & Older (63-87%) <i>Alluvium (Pleistocene or older)</i>

Table 3.8: Summary of three dominant crust types and their overlap with geomorphic units. Unit CB.1 has high density cyanobacteria-bare cover and has the greatest overlap with active sand sheets, Qea. Units ML.1 and ML.2 have high density tall moss-lichen pinnacled crusts and have the greatest overlap with mid- to late Holocene inset fans Qay₁ and Qay₂. Units S.1, S.2, and S.3 have low to moderate density tall moss-lichen crusts with and often include "desert pavement" or pavement-like rock cover and have the greatest overlap Pleistocene and older alluvial surfaces.

MRPP: Significance of Map Units

Categories	MRPP Association Values	MRPP Significance
BSC Map Units	A=0.52	p=0.00000000
Geomorphic Map Units	A=0.35	p=0.00000657
Correlated Soil Types	A=0.29	p=0.00000875

Table 3.9: Multi-response Permutation Procedures (MRPP) tested the effectiveness of BSC map units, geomorphic map units and correlated soil types in grouping interspace cover. MRPP results are reported as association values (A). When A=1, group members are identical; and when A=0, group members are not similar (McCune and Grace, 2002). McCune and Grace (2002) state $A > 0.3$ are high values for ecological data sets. Results indicate all three categories differentiate different types of interspace cover, including rocks, bare soil, BSCs, and plant litter.

Parametric Product Moment Correlation Coefficients

	Canopy Cyanobacteria	Canopy Total BSC	Canopy Plant Litter	Canopy <i>Bromus</i>
Canopy Cyanobacteria	1.000	.906**	-.186	-.480**
Canopy Total BSC%_UC	.906**	1.000	-.178	-.558**
Canopy Plant Litter	-.186	-.178	1.000	-.467**
Canopy <i>Bromus</i>	-.480**	-.558**	-.467**	1.000
Canopy Silt	-.316	-.297	.143	.045
Canopy Very Fine Sand	-.298	-.209	.019	.165
Canopy Fine Sand	.260	.251	-.060	-.106
Canopy Sand	.206	.152	-.149	.032
Canopy Total Sand	.264	.264	-.146	-.017

	Pearson's R < -0.449999, Sig. at 0.05
	Pearson's R > 0.4499999, Sig. at 0.05

Table 3.10: Parametric correlation coefficients of canopy cover characteristics are calculated as Pearson's R-values. Cells in blue show significant negative relationships at the 0.05 level, with R-values of -0.45 or less. Cells in orange show significant positive relationships at the 0.05 level, with R-values of 0.45 or greater.

Non-parametric Correlation Coefficients

	Canopy Cyanobacteria	Canopy Moss	Canopy Collema	Canopy Placidium	Canopy Psora	Canopy Peltula
Canopy Cyanobacteria	1.000	.095	-.056	-.093	-.284	-.187
Canopy Moss	.095	1.000	-.019	.001	-.028	-.106
Canopy <i>Collema</i>	-.056	-.019	1.000	.401*	.102	-.057
Canopy <i>Placidium</i>	-.093	.001	.401*	1.000	.173	.227
Canopy <i>Psora</i>	-.284	-.028	.102	.173	1.000	-.041
Canopy <i>Peltula</i>	-.187	-.106	-.057	.227	-.041	1.000
Canopy Moss-Lichen	-.058	.665**	.558**	.404*	.147	-.057
Canopy Total BSC	.903**	.355*	.155	.032	-.260	-.203
Canopy Limestone	-.342*	-.262	.222	.205	.165	-.106
Canopy Sandstone	.205	.025	-.055	-.294	-.086	-.060
Canopy Petrocalcic	-.133	-.217	.039	.352*	.088	.340*
Canopy Total Rock	-.335*	-.415*	.195	.281	.171	.073
Canopy Bare	.211	.215	.086	-.242	-.058	-.157
Canopy Plant Litter	-.187	-.010	-.143	-.109	.158	.138
Canopy <i>Bromus</i>	-.447**	-.049	-.123	-.111	.076	.122
<i>Coleogyne</i>	.087	.121	.022	.283	.139	.218
<i>Pleurophus</i>	.195	-.151	-.044	-.476**	-.118	-.082
<i>Hymenoclea</i>	-.101	.199	.078	-.055	-.157	-.110
<i>Larrea</i>	.219	.213	-.333*	-.268	-.196	.100
<i>Lycium andersonii</i>	.350*	-.148	-.060	-.061	-.073	-.051
<i>Dead Shrub</i>	.161	.223	-.339*	-.001	-.156	.090
<i>Psorothamnus</i>	.154	.237	-.034	-.055	-.108	-.075
<i>Menodora</i>	.168	.312	-.153	-.261	-.215	-.150
<i>Krameria</i>	-.175	-.035	.119	.074	-.108	-.075
<i>Encelia</i>	-.106	-.329	.295	.037	.144	-.082
<i>Tiquilia</i>	-.106	-.204	.172	.177	.676**	-.029
<i>Krascheninnikovia</i>	-.285	.155	-.025	.067	.717**	-.029
<i>Eriogonum fasciculatum</i>	.016	-.253	.074	-.185	-.041	-.029
<i>Ambrosia</i>	.113	-.278	.047	.011	-.244	.051
Canopy Clay	.095	-.316	-.063	.191	.124	.171
Canopy Silt	-.293	-.291	.190	.440**	.252	.122
Canopy Very Fine Sand	-.264	-.228	.334*	.292	.056	.268
Canopy Fine Sand	.259	.215	-.232	-.517**	-.217	-.138
Canopy Sand	.164	.329	-.139	-.053	-.032	-.236
Canopy Total Sand	.254	.288	-.162	-.430**	-.229	-.122



 rho < -0.449999, Sig. at 0.05
 rho > 0.449999, Sig. at 0.05

Table 3.11(A): Non-parametric correlation coefficients of canopy characteristics are calculated as rho-values. Cells in blue show significant negative relationships at the 0.05 level, with rho-values of -0.45 or less. Cells in orange show significant positive relationships at the 0.05 level, with rho-values of 0.45 or greater.

Non-parametric Correlation Coefficients

	Canopy Moss-Lichen	Canopy Total BSC	Canopy Limestone	Canopy Sandstone	Canopy Petrocalcic	Canopy Total Rock
Canopy Cyanobacteria	-.058	.903**	-.342*	.205	-.133	-.335*
Canopy Moss	.665**	.355*	-.262	.025	-.217	-.415*
Canopy <i>Collema</i>	.558**	.155	.222	-.055	.039	.195
Canopy <i>Placidium</i>	.404*	.032	.205	-.294	.352*	.281
Canopy <i>Psora</i>	.147	-.260	.165	-.086	.088	.171
Canopy <i>Peltula</i>	-.057	-.203	-.106	-.060	.340*	.073
Canopy Moss-Lichen	1.000	.301	.039	-.041	-.132	-.091
Canopy Total BSC	.301	1.000	-.283	.163	-.157	-.312
Canopy Limestone	.039	-.283	1.000	.021	.103	.925**
Canopy Sandstone	-.041	.163	.021	1.000	-.033	.030
Canopy Petrocalcic	-.132	-.157	.103	-.033	1.000	.397*
Canopy Total Rock	-.091	-.312	.925**	.030	.397*	1.000
Canopy Bare	.096	.303	-.073	.163	-.370*	-.194
Canopy Plant Litter	-.024	-.182	.411*	-.168	-.081	.338*
Canopy <i>Bromus</i>	-.139	-.528**	-.513**	-.091	.021	-.457**
<i>Coleogyne</i>	.118	.186	.175	.102	.403*	.259
<i>Pleuraphis</i>	-.235	.108	-.399*	.068	-.124	-.383*
<i>Hymenoclea</i>	.184	.051	.400*	.151	-.057	.308
<i>Larrea</i>	-.177	.119	-.485**	-.128	-.262	-.514**
<i>Lycium andersonii</i>	-.184	.312	-.252	-.106	.309	-.045
<i>Dead Shrub</i>	-.082	.123	-.407*	-.380*	-.313	-.449**
<i>Psorothamnus</i>	.268	.219	.196	.290	-.141	.103
<i>Menodora</i>	.171	.208	-.232	.185	-.251	-.328
<i>Krameria</i>	.119	-.131	.106	-.157	-.141	.036
<i>Encelia</i>	-.055	-.127	.358*	.028	-.059	.313
<i>Tiquilia</i>	.090	-.106	.220	-.060	-.103	.220
<i>Krascheninnikovia</i>	.114	-.252	.016	-.060	.216	.024
<i>Eriogonum fasciculatum</i>	-.187	-.057	.114	.522**	-.103	.138
<i>Ambrosia</i>	-.103	.033	-.094	.062	.158	-.020
Canopy Clay	-.199	.002	.262	-.140	.367*	.397*
Canopy Silt	.026	-.327	.464**	-.170	.407*	.572**
Canopy Very Fine Sand	.052	-.258	.324	-.018	.429**	.436**
Canopy Fine Sand	-.107	.276	-.444**	.254	-.383*	-.523**
Canopy Sand	.141	.145	-.260	-.101	-.353*	-.443**
Canopy Total Sand	-.014	.289	-.463**	.187	-.397*	-.569**



 rho<-0.449999, Sig. at 0.05
 rho>0.449999, Sig. at 0.05

Table 3.11(B): Non-parametric correlation coefficients of canopy characteristics are calculated as rho-values. Cells in blue show significant negative relationships at the 0.05 level, with rho-values of -0.45 or less. Cells in orange show significant positive relationships at the 0.05 level, with rho-values of 0.45 or greater.

Non-parametric Correlation Coefficients

	Canopy Bare	Canopy Plant Litter	Canopy Bromus	<i>Coleogyne</i>	<i>Pleuraphis</i>	<i>Hymenoclea</i>
Canopy Cyanobacteria	.211	-.187	-.447**	.087	.195	-.101
Canopy Moss	.215	-.010	-.049	.121	-.151	.199
Canopy <i>Collema</i>	.086	-.143	-.123	.022	-.044	.078
Canopy <i>Placidium</i>	-.242	-.109	-.111	.283	-.476**	-.055
Canopy <i>Psora</i>	-.058	.158	.076	.139	-.118	-.157
Canopy <i>Peltula</i>	-.157	.138	.122	.218	-.082	-.110
Canopy Moss-Lichen	.096	-.024	-.139	.118	-.235	.184
Canopy Total BSC	.303	-.182	-.528**	.186	.108	.051
Canopy Limestone	-.073	.411*	-.513**	.175	-.399*	.400*
Canopy Sandstone	.163	-.168	-.091	.102	.068	.151
Canopy Petrocalcic	-.370*	-.081	.021	.403*	-.124	-.057
Canopy Total Rock	-.194	.338*	-.457**	.259	-.383*	.308
Canopy Bare	1.000	.010	-.315	.172	.096	.482**
Canopy Plant Litter	.010	1.000	-.474**	.294	-.250	.261
Canopy <i>Bromus</i>	-.315	-.474**	1.000	-.422*	.212	-.508**
<i>Coleogyne</i>	.172	.294	-.422*	1.000	-.272	.232
<i>Pleuraphis</i>	.096	-.250	.212	-.272	1.000	-.071
<i>Hymenoclea</i>	.482**	.261	-.508**	.232	-.071	1.000
<i>Larrea</i>	-.031	-.222	.295	-.488**	.178	-.407*
<i>Lycium andersonii</i>	.024	-.252	-.013	-.049	.131	-.195
<i>Dead Shrub</i>	.120	-.090	.186	-.031	-.082	-.105
<i>Psoralea</i>	.273	.253	-.402*	.126	-.217	.270
<i>Menodora</i>	.501**	-.111	-.026	.051	.208	.210
<i>Krameria</i>	.193	-.038	.103	-.235	-.217	.209
<i>Encelia</i>	.020	.260	-.210	-.029	.053	.230
<i>Tiquilia</i>	-.157	.244	-.106	-.136	-.082	-.110
<i>Krascheninnikovia</i>	.070	-.016	.203	.318	-.082	-.110
<i>Eriogonum fasciculatum</i>	.165	-.187	.049	-.136	.341*	.170
<i>Ambrosia</i>	-.476**	-.120	.154	-.109	-.048	-.613**
Canopy Clay	-.446**	.185	-.148	.237	-.255	-.321
Canopy Silt	-.639**	.188	.009	.061	-.530**	-.222
Canopy Very Fine Sand	-.523**	.122	.062	-.109	-.257	-.113
Canopy Fine Sand	.613**	-.164	.010	-.101	.524**	.214
Canopy Sand	.350*	-.169	.062	.073	.080	.039
Canopy Total Sand	.601**	-.206	.032	-.106	.530**	.201



 rho < -0.4499999, Sig. at 0.05
 rho > 0.4499999, Sig. at 0.05

Table 3.11(C): Non-parametric correlation coefficients of canopy characteristics are calculated as rho-values. Cells in blue show significant negative relationships at the 0.05 level, with rho-values of -0.45 or less. Cells in orange show significant positive relationships at the 0.05 level, with rho-values of 0.45 or greater.

Non-parametric Correlation Coefficients

	<i>Larrea</i>	<i>Lycium andersonii</i>	<i>Dead Shrub</i>	<i>Psoralea</i>	<i>Menodora</i>
Canopy Cyanobacteria	.219	.350 ⁺	.161	.154	.168
Canopy Moss	.213	-.148	.223	.237	.312
Canopy <i>Collema</i>	-.333 ⁺	-.060	-.339 ⁺	-.034	-.153
Canopy <i>Placidium</i>	-.268	-.061	-.001	-.055	-.261
Canopy <i>Psora</i>	-.196	-.073	-.156	-.108	-.215
Canopy <i>Peltula</i>	.100	-.051	.090	-.075	-.150
Canopy Moss-Lichen	-.177	-.184	-.082	.268	.171
Canopy Total BSC	.119	.312	.123	.219	.208
Canopy Limestone	-.485 ^{**}	-.252	-.407 ⁺	.196	-.232
Canopy Sandstone	-.128	-.106	-.380 ⁺	.290	.185
Canopy Petrocalcic	-.262	.309	-.313	-.141	-.251
Canopy Total Rock	-.514 ^{**}	-.045	-.449 ^{**}	.103	-.328
Canopy Bare	-.031	.024	.120	.273	.501 ^{**}
Canopy Plant Litter	-.222	-.252	-.090	.253	-.111
Canopy <i>Bromus</i>	.295	-.013	.186	-.402 ⁺	-.026
<i>Coleogyne</i>	-.488 ^{**}	-.049	-.031	.126	.051
<i>Pleuraphis</i>	.178	.131	-.082	-.217	.208
<i>Hymenoclea</i>	-.407 ⁺	-.195	-.105	.270	.210
<i>Larrea</i>	1.000	.231	.353 ⁺	-.235	.151
<i>Lycium andersonii</i>	.231	1.000	.011	-.134	-.049
<i>Dead Shrub</i>	.353 ⁺	.011	1.000	-.127	.150
<i>Psoralea</i>	-.235	-.134	-.127	1.000	.282
<i>Menodora</i>	.151	-.049	.150	.282	1.000
<i>Krameria</i>	-.186	-.134	.128	.376 ⁺	.037
<i>Encelia</i>	-.393 ⁺	-.147	-.268	-.036	-.149
<i>Tiquilia</i>	-.136	-.051	-.155	-.075	-.150
<i>Krascheninnikovia</i>	-.136	-.051	-.065	-.075	-.150
<i>Eriogonum fasciculatum</i>	-.136	-.051	-.130	-.075	.141
<i>Ambrosia</i>	.109	.171	-.164	.021	-.173
Canopy Clay	-.026	.322	.030	-.045	-.246
Canopy Silt	-.140	.069	-.209	-.169	-.413 ⁺
Canopy Very Fine Sand	-.076	-.045	-.419 ⁺	-.291	-.450 ^{**}
Canopy Fine Sand	.179	.018	.175	.045	.306
Canopy Sand	.012	-.246	.386 ⁺	.325	.431 ^{**}
Canopy Total Sand	.167	-.079	.169	.109	.382 ⁺



 rho < -0.449999, Sig. at 0.05
 rho > 0.449999, Sig. at 0.05

Table 3.11(D): Non-parametric correlation coefficients of canopy characteristics are calculated as rho-values. Cells in blue show significant negative relationships at the 0.05 level, with rho-values of -0.45 or less. Cells in orange show significant positive relationships at the 0.05 level, with rho-values of 0.45 or greater.

Non-parametric Correlation Coefficients

	<i>Krameria</i>	<i>Encelia</i>	<i>Tiquilia</i>	<i>Krascheninnikovia</i>	<i>Eriogonum fasciculatum</i>	<i>Ambrosia</i>
Canopy Cyanobacteria	-.175	-.106	-.106	-.285	.016	.113
Canopy Moss	-.035	-.329	-.204	.155	-.253	-.278
Canopy <i>Collema</i>	.119	.295	.172	-.025	.074	.047
Canopy <i>Placidium</i>	.074	.037	.177	.067	-.185	.011
Canopy <i>Psora</i>	-.108	.144	.676**	.717**	-.041	-.244
Canopy <i>Peltula</i>	-.075	-.082	-.029	-.029	-.029	.051
Canopy Moss-Lichen	.119	-.055	.090	.114	-.187	-.103
Canopy Total BSC	-.131	-.127	-.106	-.252	-.057	.033
Canopy Limestone	.106	.358*	.220	.016	.114	-.094
Canopy Sandstone	-.157	.028	-.060	-.060	.522**	.062
Canopy Petrocalcic	-.141	-.059	-.103	.216	-.103	.158
Canopy Total Rock	.036	.313	.220	.024	.138	-.020
Canopy Bare	.193	.020	-.157	.070	.165	-.476**
Canopy Plant Litter	-.038	.260	.244	-.016	-.187	-.120
Canopy <i>Bromus</i>	.103	-.210	-.106	.203	.049	.154
<i>Coleogyne</i>	-.235	-.029	-.136	.318	-.136	-.109
<i>Pleuraphis</i>	-.217	.053	-.082	-.082	.341*	-.048
<i>Hymenoclea</i>	.209	.230	-.110	-.110	.170	-.613**
<i>Larrea</i>	-.186	-.393*	-.136	-.136	-.136	.109
<i>Lycium andersonii</i>	-.134	-.147	-.051	-.051	-.051	.171
Dead Shrub	.128	-.268	-.155	-.065	-.130	-.164
<i>Psoralea</i>	.376*	-.036	-.075	-.075	-.075	.021
<i>Menodora</i>	.037	-.149	-.150	-.150	.141	-.173
<i>Krameria</i>	1.000	.164	-.075	-.075	-.075	-.041
<i>Encelia</i>	.164	1.000	.294	-.082	.271	-.202
<i>Tiquilia</i>	-.075	.294	1.000	-.029	-.029	-.170
<i>Krascheninnikovia</i>	-.075	-.082	-.029	1.000	-.029	-.170
<i>Eriogonum fasciculatum</i>	-.075	.271	-.029	-.029	1.000	-.170
<i>Ambrosia</i>	-.041	-.202	-.170	-.170	-.170	1.000
Canopy Clay	-.145	-.016	.203	-.024	-.057	.350*
Canopy Silt	.007	.193	.285	.073	-.089	.266
Canopy Very Fine Sand	-.001	.246	.106	-.024	.057	.232
Canopy Fine Sand	-.059	-.203	-.285	-.024	.171	-.217
Canopy Sand	.142	-.096	-.106	.057	-.252	-.220
Canopy Total Sand	-.041	-.178	-.268	-.057	.089	-.258



 rho<-0.449999, Sig. at 0.05
 rho>0.449999, Sig. at 0.05

Table 3.11(E): Non-parametric correlation coefficients of canopy characteristics are calculated as rho-values. Cells in blue show significant negative relationships at the 0.05 level, with rho-values of -0.45 or less. Cells in orange show significant positive relationships at the 0.05 level, with rho-values of 0.45 or greater.

Parametric Product Moment Correlation Coefficients

	Interspace Total BSC	Interspace Limestone
Interspace Total BSC	1.000	-.799**
Interspace Limestone	-.799**	1.000
Interspace Silt	-.229	.439**
Interspace Fine Sand	.265	-.486**
Interspace Sand	-.175	.047
Interspace Total Sand	.226	-.431**

	Pearson's R < -0.449999, Sig. at 0.05
	Pearson's R > 0.449999, Sig. at 0.05

Table 3.12: Parametric correlation coefficients of interspace cover characteristics are calculated as Pearson's R-values. Cells in blue show significant negative relationships at the 0.05 level, with R-values of -0.45 or less. Cells in orange show significant positive relationships at the 0.05 level, with R-values of 0.45 or greater.

Non-Parametric Correlation Coefficients

	Interspace Cyanobacteria	Interspace Moss	Interspace Collema	Interspace Placidium	Interspace Psora	Interspace Peltula
Interspace Cyanobacteria	1.000	-.331*	-.234	-.086	-.370*	-.019
Interspace Moss	-.331*	1.000	.724**	.349*	.017	.041
Interspace Collema	-.234	.724**	1.000	.586**	.013	.111
Interspace Placidium	-.086	.349*	.586**	1.000	.119	.428**
Interspace Psora	-.370*	.017	.013	.119	1.000	-.081
Interspace Peltula	-.019	.041	.111	.428**	-.081	1.000
Interspace Moss-Lichen	-.242	.799**	.967**	.666**	.006	.166
Total BSC	.516**	.400*	.608**	.387*	-.248	.104
Interspace Limestone	-.501*	-.296	-.336*	-.154	.293	-.109
Interspace Sandstone	-.019	.284	.072	-.347*	-.050	-.349*
Interspace Petrocalcic	-.207	.021	-.080	.266	.244	.023
Interspace Total Rock	-.559**	-.203	-.328	-.060	.273	-.017
Interspace Bare	.169	-.187	-.264	-.465**	-.087	-.142
Interspace Plant Litter	.099	-.075	-.220	-.112	.002	-.062
Interspace <i>Bromus</i>	-.206	.081	.356*	.051	.149	.045
Interspace Max. Pinnacle Ht.	-.168	.525**	.710**	.657**	.108	.328
Interspace Clay	.268	-.525**	-.279	.110	.187	-.047
Interspace Silt	-.262	-.152	.017	.463**	.278	.080
Interspace Very Fine Sand	-.215	.188	.312	.559**	.109	.169
Interspace Fine Sand	.293	.123	-.051	-.550**	-.268	-.098
Interspace Sand	-.081	.101	-.062	-.184	-.205	-.069
Interspace Total Sand	.145	.237	.053	-.388*	-.252	-.055



rho < -0.449999, Sig. at 0.05

rho > 0.449999, Sig. at 0.05

Table 3.13(A): Non-parametric correlation coefficients of interspace characteristics are calculated as rho-values. Cells in blue show significant negative relationships at the 0.05 level, with rho-values of -0.45 or less. Cells in orange show significant positive relationships at the 0.05 level, with rho-values of 0.45 or greater.

Non-Parametric Correlation Coefficients

	Interspace Moss-Lichen	Interspace Total BSC	Interspace Total Rock	Interspace Bare	Interspace Plant Litter	Interspace <i>Bromus</i>
Interspace Cyanobacteria	-.242	.516**	-.559**	.169	.099	-.206
Interspace Moss	.799**	.400*	-.203	-.187	-.075	.081
Interspace <i>Collema</i>	.967**	.608**	-.328	-.264	-.220	.356*
Interspace <i>Placidium</i>	.666**	.387*	-.060	-.465**	-.112	.051
Interspace <i>Psora</i>	.006	-.248	.273	-.087	.002	.149
Interspace <i>Peltula</i>	.166	.104	-.017	-.142	-.062	.045
Interspace Moss-Lichen	1.000	.613**	-.306	-.276	-.227	.224
Total BSC	.613**	1.000	-.837**	.029	-.061	.074
Interspace Limestone	-.362*	-.801**	.867**	-.245	.087	-.021
Interspace Sandstone	.099	.198	-.303	.423*	-.073	-.179
Interspace Petrocalcic	-.006	-.219	.468**	-.450**	-.217	-.284
Interspace Total Rock	-.306	-.837**	1.000	-.360*	-.042	-.207
Interspace Bare	-.276	.029	-.360*	1.000	.046	-.219
Interspace Plant Litter	-.227	-.061	-.042	.046	1.000	-.030
Interspace <i>Bromus</i>	.224	.074	-.207	-.219	-.030	1.000
Interspace Max. Pinnacle Ht.	.705**	.498**	-.327	-.306	-.066	.278
Interspace Clay	-.311	-.156	.352*	-.243	-.097	-.178
Interspace Silt	.016	-.322	.582**	-.615**	-.140	.051
Interspace Very Fine Sand	.326	.130	.033	-.464**	.141	.192
Interspace Fine Sand	-.060	.320	-.575**	.597**	.154	-.074
Interspace Sand	-.056	-.167	-.036	.251	-.089	.043
Interspace Total Sand	.061	.301	-.561**	.569**	.149	.002



rho < -0.449999, Sig. at 0.05
rho > 0.449999, Sig. at 0.05

Table 3.13(B): Non-parametric correlation coefficients of interspace characteristics are calculated as rho-values. Cells in blue show significant negative relationships at the 0.05 level, with rho-values of -0.45 or less. Cells in orange show significant positive relationships at the 0.05 level, with rho-values of 0.45 or greater.

CHAPTER 4

BIOLOGICAL SOIL CRUSTS AND THE FERTILE ISLAND EFFECT

Abstract

Biological soil crusts (BSCs) composed of cyanobacteria, mosses, and lichens manage soil resources and provide critical soil cover in arid regions. This study evaluated the influences of soil-geomorphology, distribution of BSCs, and desert pavements on the development of fertile islands within the Mojave Desert, Nevada, U.S.A. Statistical analyses of field and laboratory data indicated that fertility patterns are strongly tied to the age of landforms, input of fine sand, and interspace cover. Geomorphic processes control the sand-to-rock ratio and the formation of three surface cover types, which ultimately determine fertile island magnitude. (1) High canopy-interspace nutrient disparities develop on rock-covered surfaces that display “desert pavement” cover, with low to moderate density moss-lichen crusts. (2) Moderate canopy-interspace nutrient disparities and low overall fertility are supported by cyanobacteria crusts that develop on sand-dominated surfaces. (3) Low canopy-interspace nutrient disparities develop where high density moss-lichen crusts form along stable, rock-covered surfaces. These well-developed BSCs elevate interspace fertility, which increases a site’s susceptibility to exotic grass invasions. The sand-to-rock ratio, surface cover, and fertile island patterns vary predictably across intermontane basins, explaining landscape-scale biogeochemical patterns. Soil cover control of fertile island magnitude is strikingly similar across many deserts. This similarity could reflect universal biogeochemical patterns that develop regardless of total ecosystem productivity. These new perspectives should be considered as scientists, policy makers,

and land managers address climate change, exotic plant invasions, anthropogenic disturbances, and desertification dynamics.

Introduction

Biological soil crusts (BSCs) play principal roles in arid ecosystem dynamics. These crusts are complex matrices of cyanobacteria, algae, lichens, mosses, microfungi, and bacteria (Friedmann and Galun 1974) that fuse around soil to create a protective, desert skin (see Chapters 2, 3) (Campbell et al. 1989, Belnap and Gardner 1993, McKenna Neuman et al. 1996, Eldridge and Leys 2003, Bowker et al. 2008). BSC organisms are ecosystem engineers that (Bowker 2007) manage soil moisture and temperature (Booth 1941, Belnap 1995, DeFalco et al. 2001, Belnap 2006), promote landscape stability (see Chapter 3)(Booth 1941, McKenna Neuman et al. 1996, Canton et al. 2003, Li et al. 2004, Thomas and Dougill 2007, Chaudhary et al. 2009), and influence vascular plant growth (e.g., (DeFalco et al. 2001, Li et al. 2005, Escudero et al. 2007)). The ecological impact of BSCs is tied to their morphology and species composition. Early succession, smooth cyanobacteria crusts (Figure 4.1) have different impacts on soil water (Eldridge and Greene 1994, Eldridge and Rosentreter 1999, Evans and Johansen 1999, Kidron et al. 2002, Belnap 2006), temperature (Belnap 1995, Belnap et al. 2003, Belnap 2006), and dust capture (Chapters 2, 3) than short moss-lichen crusts and later succession, tall moss-lichen pinnacled crusts (Figure 4.2)(see Chapters 2, 3). The ecological impacts of BSCs are potentially enormous, as these crusts can comprise up to 70 percent of living cover across arid soils (Belnap 1994).

BSCs strongly influence soil fertility in arid regions. Crusts fix carbon (C), nitrogen (N), and contribute organic matter (Kleiner and Harper 1977, Belnap 2002, Barger et al. 2006, Bowker 2007, Elbert et al. 2009). BSCs prevent erosional losses of soil nutrients (Belnap 1995, Barger et al. 2006, Bowker 2007) and capture large volumes of nutrient-rich dust (see Chapters 2, 3)(Danin and Ganor 1991, Belnap and Gardner 1993, Shachak and Lovett 1998). BSCs' variable influence on water infiltration and runoff (see Chapters 2)(Booth 1941, Yair 1990, Eldridge and Rosentreter 2003, Belnap 2006, Issa et al. 2009) potentially cause feedback mechanisms that alter nutrient allocation within the soil (DeFalco et al. 2001, Eldridge and Rosentreter 2003, Li et al. 2008).

Crust influence on soil nutrient and moisture availability has also been shown to impact the fertile island effect Bromley et al. 1997, Shachak and Lovett 1998, Harper and Belnap 2001, Neff et al. 2005, Thompson et al. 2005, Housman et al. 2006, Okin et al. 2006, Li et al. 2008). The fertile island effect is a widely recognized phenomenon wherein soil resources are concentrated below shrub canopies (Charley and West 1977, Schlesinger et al. 1990, 1996, Kieft et al. 1998, Schlesinger and Pilmanis 1998, Aguiar and Sala 1999, Bolling and Walker 2002, Titus et al. 2002, Ewing et al. 2007, Li et al. 2007). Heterogeneity, or "patchiness," in soil resources is associated with increased desertification and catastrophic ecosystem shifts (Aguiar and Sala 1999, Rietkerk et al. 2004, Ridolfi et al. 2008). This process is most strongly expressed in arid shrublands with extensive plant interspaces (Charley and West 1977, Schlesinger et al. 1990, 1996, Kieft et al. 1998, Schlesinger and Pilmanis 1998, Bolling and Walker 2002, Titus et al. 2002, Ewing et al. 2007, Li et al. 2007). Wind and water erosion (Gibbens et al. 1983,

Schlesinger et al. 1990, Abrahams et al. 1994, Kieft et al. 1998, Aguiar and Sala 1999, Okin et al. 2001, Golodets and Boeken 2006, Okin et al. 2006), differences in water runoff, infiltration, and evapotranspiration (Schlesinger et al. 1990, Abrahams et al. 1994, Martinez-Meza and Whitford 1996, Bromley et al. 1997, Whitford et al. 1997, Dunkerley 2000, Walker et al. 2001, Howes and Abrahams 2003, Caldwell et al. 2008, Li et al. 2008), biological activity (Lajtha and Schlesinger 1986, Schlesinger et al. 1996, Schlesinger and Pilmanis 1998, Aguilera et al. 1999, Zaady et al. 2001, Titus et al. 2002, Ewing et al. 2007), plant canopy capture of dust and water-entrained sediment (Gibbens et al. 1983, Whitford et al. 1997, Shachak and Lovett 1998, Li et al. 2007, Li et al. 2008), plant uptake (Schlesinger et al. 1996, Schlesinger and Pilmanis 1998), and plant litter and organic residue accumulation (Charley and West 1977, Schlesinger et al. 1996, Zaady et al. 1996, Schlesinger and Pilmanis 1998, Zaady et al. 2001, Titus et al. 2002) concentrate water and nutrients around shrub canopies (Schlesinger et al. 1990, 1996, Schlesinger and Pilmanis 1998, Bolling and Walker 2002, Howes and Abrahams 2003). Changes in nutrient allocation and hydrological dynamics favor the establishment of shrubs over grasses, leading to increased desertification (Gibbens et al. 1983, Schlesinger and Jones 1984, Schlesinger et al. 1990, Bromley et al. 1997, Kieft et al. 1998, Schlesinger and Pilmanis 1998, Aguiar and Sala 1999, Ridolfi et al. 2008). Desert pavements may also affect the location of fertile islands. Interlocking desert pavements prevent plant germination, and associated Av horizons decrease infiltration, further limiting plant growth (Wells et al. 1987, Hamerlynck et al. 2002, Wood et al. 2005, Meadows et al. 2008). A previous study within the Mojave Desert concluded that fertile island magnitude was consistent across a wide elevation gradient and that BSCs had little

detectible influence on soil fertility (Thompson et al. 2005). However, a study performed in the Colorado Plateau concluded that BSCs directly influence interspace-canopy nutrient dynamics and the fertile island effect (Housman et al. 2007).

Given the potential significance of BSCs in soil resource allocation, predicting their distribution is critical to understanding fertile island dynamics. A companion study found that soil-geomorphic processes control the relative distribution of three interspace cover types (see Chapter 3). (1) Cyanobacteria crusts form along sand sheets composed primarily of fine sand (Table 4.1, Figure 4.3). (2) High density moss-lichen crusts occur along stable surfaces composed of mixed sand and gravel such as mid- to late Holocene inset fans (Table 4.1, Figure 4.3). (3) Poorly-interlocking “desert pavements” with low to moderate density moss-lichen crusts develop along rock-covered surfaces, such as Pleistocene and older alluvial surfaces (Table 4.1, Figure 4.3).

This study was undertaken to investigate the relationships between soil-geomorphology, soil surface cover, and shrub canopies and their effect on biogeochemical trajectories within a portion of the Mojave Desert. Landscape controls on BSC development and soil resources were also studied to develop a comprehensive conceptual framework explaining the distribution and extent of Mojave Desert islands of fertility.

Background

The 2.8 km² study area lies within a portion of the Hidden Valley Area of Critical Environmental Concern (ACEC), in the Muddy Mountains Wilderness Area, Nevada, U.S.A. (Figures 4.4, 4.5) at 36°20'N and 114°42'W. The area is ideal for studying BSCs

and soil ecological relationships, as the valley contains well-developed BSCs, variable crust distribution, common vascular plant communities, and diverse soil-geomorphology. The study area is located within the Mojave Desert climate zone and is characterized by hot, dry summers and cool, moist winters. The average annual temperature is 27 °C, and the mean annual precipitation is 114 mm. Most precipitation falls from January to March, when average high temperatures range from 14-21 °C. Summers are dry with some precipitation during the warmest months of July and August, when average high temperatures range from 39-40 °C (Gorelow and Skrbac 2005).

Hidden Valley is a semi-enclosed basin that drains by a single wash (Figure 4.5). A ring of carbonate and sandstone mountains rise up to an elevation of 1642 m, providing a source of fine sand and limestone gravel soil parent materials to the basin floor, which lies at 1000 m. The valley contains a suite of alluvial geomorphic surfaces, with interspersed sand sheets and colluvium, ranging in age from late Miocene or earliest Pleistocene to active drainages (Figure 4.6). The youngest alluvial surfaces occur at topographic lows and are inset against older, topographically higher surfaces. Each geomorphic surface displays unique soil characteristics and surface morphology that are a reflection of geomorphic processes and degree of pedogenesis (Table 4.2). The oldest alluvial surfaces, Late Miocene to earliest Pleistocene QTa and Qao₁ erosional fan remnants have smooth, poorly to moderately interlocking desert pavements, Av horizons and shallow Stage V-VI petrocalcic horizons that serve as a root-limiting layer (see Chapter 3)(Peterson 1981, McFadden et al. 1987, Soil Survey Staff 2010). Early Pleistocene Qao₂ ballenas (Peterson 1981) and Qai inset fans, also display smooth, poorly to moderately interlocking desert pavements with Av horizons that overlie Stage III-V

petrocalcic horizons. The surfaces of the mid- to late Holocene inset fans, Qay₁ and Qay₂, are composed of mixed sand and gravel with faint to muted bar and swale morphology. Soil profiles display stage I Bk horizons with thin coats of secondary carbonate on clasts, and 15-27 cm thick Av horizons forming below tall moss-lichen pinnacled crusts (see Chapters 2, 3). Recently abandoned Qay₃ inset fans have negligible soil development and distinct bar and swale surface morphology, creating high surface roughness. Active channels, or Qay₄, have distinct bar and channel surface morphology that creates high surface roughness. These channels experience ephemeral alluvial activity. Colluvium, or Qc, occurs throughout the field area along steep slopes below cliff faces and is composed of mixed sand, gravel, and boulders. Holocene active sand sheets, Qea, form sandy mantles over alluvium or over bedrock. These surfaces have high sand saltation activity, negligible soil development, and the thickness of the eolian sand ranges from a few cm to over 2 m thick (see Chapter 3).

Vascular plant communities are composed of common Mojave Desert taxa. Dominant species include *Larrea tridentata*, *Ambrosia dumosa*, *Menodora spinescens*, *Krameria erecta*, *Coleogyne ramosissima*, *Psorothamnus fremontii*, *Hymenoclea salsola*, *Pleuraphis rigida*, and *Ephedra nevadensis*. Other common species include *Opuntia basilaris*, *Cylindropuntia echinocarpa*, *Encelia farinosa*, *Prunus fasciculata*, *Krascheninnikovia lanata*, *Salvia dorrii*, *Sphaeralcea ambigua*, *Eriogonum fasciculatum*, *Eriogonum inflatum*, *Lycium copperi*, *Tiquilia canescens*, *Chilopsis linearis* and *Lycium andersonii* (see Chapter 3)(Baldwin et al. 2002). *Bromus rubens* is a common invasive grass that can be found throughout the valley, below shrubs or within plant interspaces (see Chapter 3).

Three primary types of BSCs dominate the study area and develop through a natural succession. (1) Smooth crusts form first and are dominated by filamentous cyanobacteria such as *Microcoleus*. These crusts are commonly associated with bare soil and also include physical and/or chemical crusting that augments soil stability (Figure 4.1)(see Chapter 2). Next, (2) Short moss-lichen crusts develop. These crusts have rolling surface morphology and less than 2 cm of relief (see Chapter 2). Short moss-lichen crusts contain cyanobacteria such as *Microcoleus* but are dominated by mosses and lichens. Mosses include *Syntrichia caninervis*, *Bryum*, and *Pterygoneurum*. Gelatinous lichens are predominantly *Collema*. Squamulose lichens include *Placidium*, *Psora decipiens*, and *Peltula*. Eventually, (3) tall moss-lichen pinnacled crusts (see Chapter 2) develop as mosses, lichens, and cyanobacteria collect dust, creating the rougher “pinnacled” morphology. Tall moss-lichen pinnacled crusts have complex surface microtopography with up to 5 cm of vertical relief. The density of these three BSC types, as well as desert pavements, varies throughout the site (Figures 4.1, 4.2, 4.3).

Materials and Methods

Overview of Methods

This study’s methods were selected to investigate the relationships between BSCs and surficial biogeochemical properties and how those relationships differ across the landscape. (Detailed methods are described in Appendices 1.2 and 1.4). Within the 2.8 km² study area (see Chapter 3) characterizations of geomorphology, soils and BSCs were completed (Appendix 1.2). Detailed descriptions of BSCs, geomorphology, and soils can be found in Chapter 3. Bulk soil samples were analyzed to quantify physical and

chemical properties (Appendix 1.2.2.3). Geographic Information System (GIS) analyses were used to characterize the geomorphic and topographic relationships of BSCs throughout the site (Appendices 1.2.5). Field, laboratory, and GIS output were compiled (Table 4.3, Appendix 1.2.6). Finally, statistical analyses quantified the relationships of surface cover types to soil physicochemical and soil-geomorphic characteristics (Appendix 1.4). A hierarchical approach was taken for these analyses, which began by exploring multivariate relationships (Appendix 1.4.2) and successively working down to meter-scale relationships. Landscape (Figure 4.7, Appendix 1.4.3.1) and soil surface cover (Figure 4.8, 4.9, Appendices 1.4.3.2, 1.4.4.1) relationships were analyzed through ANOVAs and t-tests. Relationships between canopies and interspaces were quantified using a series of paired t-tests (Figures 4.10, 4.11, Appendix 1.4.4.2). Finally a series of correlation coefficients explored relationships between variables (Appendix 1.4.5).

Results

Cyanobacteria Study

Ocular estimates of surface crusting are an effective proxy of cyanobacteria presence or absence (Figure 4.12). Samples predicted to have high cyanobacteria cover, as indicated by $\geq 35\%$ surface crusting, had significantly greater filamentous cyanobacterial concentrations, or 36% presence, than those predicted to have low cover based on $\leq 10\%$ surface crusting which had 0.8% presence.

Plot Data, Lab Analyses, & Solar Insolation

Shrub canopy cover, interspace/canopy soil cover, soil physicochemical properties, solar insolation, and other site characteristics were highly variable among the

36 plots. Data summaries by plot and by individual characteristics are summarized in the digital data set (see attached DVD in this dissertation). Relationships between geomorphic surfaces and between interspace and canopy types that are statistically significant at the 0.05 level are described below.

Statistics

NMS

A three dimensional NMS ordination illustrates select correlations between biological and environmental variables (Figure 4.13). The ordination groups individual plots according to differences in biological interspace surface cover, as recorded in point counts. The values of surface cover are weighted by percent total interspace cover. The species similarities are simplified into three dimensions, but only two dimensions are shown in the Figure 4.13. This ordination displays strong relationships, with relatively low stress of 9.4 and significance at the $p=0.0196$ level. The ordination indicates mosses, *Collema* lichen, *Psora* lichen, *Placidium* lichen, *Peltula* lichen, and *Bromus* exotic grass are all positively associated to each other. These cover types, however, are negatively associated with non-grass plant litter and cyanobacteria. Environmental overlays are shown as vectors that point toward species with which they are most strongly associated. The magnitude of these relationships is indicated by the length of the vectors, with the longest lines corresponding to the strongest relationships of the vectors to the ordination axes. The data in this NMS plot (Figure 4.13) indicate that mosses, all lichens, and *Bromus* exotic grass are positively related to maximum pinnacle height, potassium (K), boron (B), calcium (Ca), electrical conductivity (EC_e), and iron (Fe), while non-grass plant litter and cyanobacteria are positively related to bare soil. Carbon to nitrogen (C:N)

ratios and nitrate (NO₃) are negatively related to all surface cover types. Copper (Cu) has a moderate positive relationship to cyanobacteria cover and litter.

ANOVAs for Geomorphic Surface Groups

Parametric and non-parametric ANOVAs indicate important differences in soil surface cover, canopy cover, and soil physicochemical relationships between four groups of geomorphic surfaces (Fig. 4.14). Results from individual ANOVAs can be found in Figures 4.15-4.21.

Mid- to late Holocene Qay₁-Qay₂ inset fans, which are composed of mixed surficial gravel and sand, are characterized by high density moss-lichen cover and elevated soil fertility. Relative to other surface types, mid- to late Holocene surfaces have elevated canopy cover by *Bromus* exotic grass, *Collema* lichen, *Placidium* lichen, and elevated interspace cover by mosses, *Collema*, *Placidium*, and moss-lichen. Mid- to late Holocene surfaces also contain the tallest interspace moss-lichen pinnacles of all geomorphic surfaces. Canopies have elevated zinc (Zn), molybdenum (Mo), and total N. Interspaces have elevated total sand, magnesium (Mg), Fe, K, Ca, Fe, nickel (Ni), cobalt (Co), EC_e, and B, but have the lowest Cu concentrations. C:N ratios are also significantly lower than other surfaces.

Surficial sand sheets, or Qea, are characterized by high cyanobacteria cover and low fertility. Canopies have low moss-lichen crust cover, and interspaces have low cover by mosses, lichens, and rocks. Sand sheets also have the shortest interspace moss-lichen crusts. Canopies have the lowest concentrations of Zn, Mo, N, total C, organic C, and total N. Interspaces have elevated total sand and non-grass plant litter but have low Mg,

Fe, K, Mg, Ca, Fe, Ni, Co, B, EC values, and C:N ratios. Cu is slightly elevated, although this relationship is not significant.

Pleistocene inset fans, or Qai, are characterized by high rock cover, moderate lichen cover, low interspace fertility, and moderate canopy fertility. Pleistocene inset fans have elevated cover by *Coleogyne ramosissima* and elevated canopy soil cover by limestone clasts, *Collema* lichen, and *Placidium* lichen. Interspaces have elevated total rock cover. Canopies have elevated clay contents, while interspaces have elevated clay and silt contents. Canopies have elevated Mo concentrations. Interspaces have low Mg and K concentrations but slightly elevated Ni concentrations.

Late Miocene to earliest Pleistocene erosional fan remnants, or QTa-Qao₁, are characterized by high rock cover, low interspace fertility, and high canopy fertility. Canopies along these erosional fan remnants have low *Bromus* exotic grass cover, and elevated cover by *Coleogyne ramosissima*, *Collema* lichen, *Placidium* lichen, limestone clasts, and total rocks. Canopies also have elevated total N, total C, and organic C. Interspaces have low Mg and K and elevated Cu and C:N ratios.

ANOVAs for Interspace Surface Cover Groups

Parametric and non-parametric ANOVAs indicate important differences in soil surface characteristics, adjacent canopy cover, and soil physicochemical relationships between the three types of soil interspace cover (Figure 4.22). These three major interspace cover groups tested are areas with $\geq 31\%$ cyanobacteria-bare soil cover, $\geq 32\%$ moss-lichen cover, and $\geq 53\%$ interspace rock cover (“desert pavements”). Results from individual ANOVAs can be found in Figures 4.23-4.27.

Compared to other cover types, cyanobacteria-bare interspaces are characterized by low fertility. These interspaces, which commonly occur in conjunction with bare soil, are associated with *Pleuraphis rigida* and *Menodora spinescens* canopies. Cover by total BSCs, cyanobacteria, bare soil, and cyanobacteria-bare are all elevated, but cover by surface rocks and moss-lichen crusts are low. Pinnacle relief is the lowest of all groups. Interspace fine sand and total sand are elevated. K, Ca, Fe, Mg, Ni, B, extractable phosphorus (P), C:N ratios, EC_e total C, inorganic C, organic C, and total N are low. Cu is significantly elevated when compared to other surface cover groups.

Compared to other cover types, high density moss-lichen interspaces, which also include some cyanobacteria cover, are associated with high fertility. These interspaces have elevated cover by total BSCs, mosses, *Placidium* lichen, moss-lichen, *Collema* lichen, and *Bromus* exotic grasses. These surfaces also have the greatest pinnacle relief. Moss-lichen interspaces have elevated fine sand, total sand, and very fine sand. Interspaces have elevated K, Ca, Fe, Ni, Mg, Fe, B, total C, organic C, and total N. However, interspace Cu, inorganic C, C:N ratios are low.

Compared to other cover types, rock covered interspaces (“desert pavement”) are associated with low to moderate overall fertility but high inorganic and organic carbon. Interspace cover by total rocks, limestone clasts, petrocalcic clasts, and sandstone clasts are elevated. Rock interspaces also have elevated silt, clay, and very fine sand. Concentrations of interspace K, Ca, Ni, Mg, and B, and EC_e values are low compared to moss-lichen interspaces. Extractable P, C:N ratios, total C, inorganic C, organic C, and total N are elevated.

Independent Samples t-Tests for *Bromus* Cover Groups

Parametric and non-parametric ANOVAs indicate important differences in soil surface characteristics and soil physicochemical relationships between areas of high and low *Bromus* exotic grass cover (Figure 4.22). Results from individual ANOVAs can be found in Figures 4.28-4.29. Areas of high *Bromus* exotic grass occur in conjunction with *Ephedra nevadensis* canopies as well as *Collema* lichen interspace cover. High *Bromus* cover is also associated with elevated Ca, Mg, Ni, and total sulfur (S). However, areas with low *Bromus* cover are associated with higher chloride (Cl⁻) and pH relative to areas of low exotic grass cover.

Canopy versus Interspace Paired T-tests for All Plots

Parametric and non-parametric ANOVAs indicate important differences in soil surface characteristics and soil physicochemical relationships between all shrub canopies and associated interspaces (Table 4.4). Results from individual ANOVAs can be found in Figures 4.30-4.34.

When all types of interspaces are combined, they commonly have higher cover by total BSCs, *Collema* lichen, *Placidium* lichen, moss-lichen, limestone clasts, and total rock cover, while interspaces have elevated non-grass plant litter and *Bromus* exotic grass litter. Canopies have elevated fine sand and total sand. Interspaces have elevated silt and clay. Canopies tend to have elevated fertility with greater concentrations of K, Mg, Ca, manganese (Mn), Fe, B, Ni, Cu, Co, extractable P, Cl, sulfate (SO₄), NO₃, organic C, total N, and higher EC_e levels. However, Na, inorganic C, and C:N ratios are generally greater in interspaces.

Canopy versus Interspace Paired t-Tests for Plots of Different Interspace Cover

Parametric and non-parametric ANOVAs indicate important differences between shrub canopy and interspace characteristics among interspaces dominated by cyanobacteria-bare soil crusts, high density moss-lichen crusts, and high rock cover (“desert pavements”) with low density moss-lichen crusts (Table 4.5). Results from individual ANOVAs can be found in Figures 4.35-4.42. Overall, canopies have higher fertility, but the disparity between canopy and interspace fertility varies as a function of interspace cover.

Areas of high cyanobacteria-bare interspaces are characterized by a moderate disparity in fertility between canopies and interspaces, with low canopy fertility and even lower interspace fertility. These interspaces have elevated cover by *Collema* lichen, cyanobacteria-bare, limestone clasts, total rocks, and bare soil as compared to their associated canopies. These canopies have greater cover by *Bromus* exotic grass, mosses, and non-grass plant litter. Interspaces have higher concentrations of fine sand. Associated canopies have low fertility as compared to other canopies, but these canopies have elevated nutrients compared to cyanobacteria-bare interspaces. For example, K, Mg, Ca, Co, Ni, B, extractable P, and EC_e are elevated in these canopies. In contrast to other interspace types, cyanobacteria-bare interspaces have greater Cu concentrations than their associated canopies, although this relationship was not statistically significant.

Areas with high density moss-lichen interspace cover are characterized by a low disparity between canopies and interspaces, with moderate fertility overall. Compared to their associated canopies, these interspaces have elevated cover by mosses, *Placidium* lichen, moss-lichen, total BSCs, *Collema*, total rock, and limestone clasts. These

canopies have elevated cover by *Bromus* exotic grass and non-grass plant litter. There were no statistically significant differences in soil texture between these canopies and interspaces. Only a few nutrients were significantly elevated within canopies, with nutrient disparities often being quite low. K, Mg, Cu, and B were elevated in interspaces. While differences in most cations were low, the disparity in Cu was the greatest among all surface cover types. Na, C:N ratios, and EC_e were elevated in moss-lichen interspaces, although EC_e was not statistically significant. SO₄, NO₃, and total N were greater in canopies.

Areas of dense rock cover (“desert pavements”) within interspaces are characterized by the highest nutrient disparities between canopies and interspaces among all surface cover types, as these canopies have the highest fertility of all areas. Nutrients including K, Mg, Ca, Fe, Ni, Co, B, Mn, extractable P, Cl, SO₄, NO₃, EC_e and total N are all elevated within canopies. C:N ratios are elevated in rock-dominated interspaces. Rock-dominated interspaces have elevated cover by *Placidium* lichen, *Collema* lichen, moss-lichen, total rock, limestone clasts, petrocalcic clasts, and bare soil. Associated canopies have elevated cover by *Bromus* exotic grass and non-grass plant litter. Fine sand and very fine sand are elevated in canopies.

Correlation Coefficients

Parametric and non-parametric correlation coefficients show important relationships among canopy and interspace cover, soil surface characteristics, and soil physicochemical properties (Tables 4.6-4.9). Cover by rocks, mosses and/or lichens, and cyanobacteria appear to have disparate relationships to the various characteristics.

Soil canopy cover and vascular plant species show some significant correlations to canopy soil chemistry and surface characteristics (Tables 4.6, 4.8). *Pleuraphis* canopies are negatively correlated to *Placidium* lichen cover, silt content, and total C concentrations but positively associated with fine sand and total sand contents. *Tiquilia* and *Krascheninnikovia* canopies are positively correlated to *Psora* lichen. *Larrea* canopies and *Bromus* exotic grass cover are negatively associated with rock cover. *Bromus* is also negatively associated with BSC cover and non-grass plant litter. *Larrea* and *Coleogyne* canopies are negatively associated. *Hymenoclea* canopies are positively associated with bare soil and negatively associated with *Bromus* cover and *Ambrosia* canopies. *Ambrosia* is also negatively associated with bare soil. *Menodora* canopies are positively correlated with bare soil, but negatively associated with very fine sand, soil K, and soil Ca. Dead shrubs are negatively associated with soil K and B. *Psorothamnus* canopies are negatively associated with Na and Ni. *Krameria* is negatively associated with Na. *Encelia* is positively associated with soil B. *Eriogonum* is positively associated with sandstone clasts. Soil C:N ratios are positively correlated to non-grass plant litter but negatively associated with moss cover. Canopy cyanobacteria-bare cover is negatively associated with silt, very fine sand, K, Mg, organic C, and EC but positively associated with fine sand total sand and extractable P. Canopy *Placidium* is positively correlated with Mo and total N but negatively correlated with fine sand. Canopy rock cover is positively associated with silt, K, Mg, Ca, Fe, Ni, B, SO₄, NO₃, total C, organic C, C:N ratios, inorganic C, EC, but negatively associated with fine sand and total sand. Total canopy BSC cover is negatively associated with total C.

Soil interspace cover also shows important and significant correlations to interspace soil chemistry and surface characteristics (Tables 4.7, 4.9). BSC organisms generally are positively correlated with each other and maximum pinnacle height, but they are negatively correlated with rock cover. Cyanobacteria cover is negatively correlated to total C and inorganic C. Mosses are negatively related to clay and Cu but positively related to Ca, B, and EC_e. Most lichens are positively correlated to cations such as K, Mg, Ca, Ni, and B. *Collema* and total moss-lichen cover, however, are negatively correlated to Cu. Lichens are generally positively correlated to EC_e, but negatively correlated to pH. *Placidium* is positively correlated to silt, very fine sand, and total N and negatively correlated to bare soil and fine sand. *Peltula* is positively correlated to Cl. Total BSC cover is negatively associated with total C, inorganic C, and C:N ratios. *Psora* lichens are negatively correlated to equinox and winter insolation. Rock cover is positively correlated to silt, total C, inorganic C, and C:N ratios but negatively correlated to fine sand, and total sand. Bare soil is negatively correlated to petrocalcic cover, silt, very fine sand, and total C, but positively correlated to fine sand and total sand. *Bromus* exotic grass cover is positively associated with Mg concentrations.

Parametric and non-parametric correlations also reveal important relationships among slope, surface cover, and soil chemistry in areas that display $\geq 53\%$ interspace rock cover (Tables 4.10, 4.11). Interspace rock cover is negatively correlated with total interspace BSC cover and interspace organic C but positively correlated with interspace Cu. Total interspace BSC cover is negatively correlated with interspace pH. Percent

slope is positively correlated with interspace pH, Mn, and Zn and negatively correlated to total BSC cover.

Interpretations

Fertile Island Feedback Models

The ratio of fine sand to rocks controls interspace cover by cyanobacteria crusts, high density moss-lichen crusts, and “desert pavements” with low to moderate density moss-lichen crusts (see Chapter 3) that ultimately determines the magnitude of the fertile island effect (Figure 4.43) and landscape biogeochemistry. Inferred dust capture, erosion, water availability, and biological activity produce three unique biogeochemical signatures: (1) low, (2) moderate, and (3) high magnitude fertile islands, or canopy-interspace nutrient disparities (Figures 4.44, 4.45, 4.46). While, geological processes regulate the biological framework (Figure 4.47), biotic-abiotic interactions sustain resource allocation patterns. These self-enhancing processes support geomorphic continuity and ecological stability, allowing persistence of biological communities adapted to current conditions (Fig. 4.47). These feedback mechanisms vary as a function of geomorphic surfaces within intermontane basins. Therefore, geomorphology provides a tool for extrapolating meter-scale relationships to the landscape level and helps explain biogeochemical signatures of individual landforms (Figure 4.48).

Canopy-Interspace Interactions and Fertile Island Development

Vascular plants influence local hydrology, producing biogeochemical conditions unlike those of interspaces (Figures 4.44, 4.45, 4.46). Shrubs increase water availability by shading the soil surface, providing an organic-rich mulch that reduces evaporation,

capturing run-on water, and trapping dust for enhanced soil water-holding capacity (Schlesinger and Jones 1984, Schlesinger et al. 1990, Bromley et al. 1997, De Soyza et al. 1997, Shachak and Lovett 1998, Zaady et al. 2001, Howes and Abrahams 2003, Li et al. 2008, Li et al. 2008). However, in some cases, plant canopy unsaturated hydraulic conductivity may be lower than that of interspaces (Caldwell et al. 2008). Vascular plants decrease leaching via root uptake or by capturing precipitation within branches (Martinez-Meza and Whitford 1996, Whitford et al. 1997). Shrubs influence infiltration and leaching through stem flow and pore formation (Martinez-Meza and Whitford 1996, Whitford et al. 1997, Dunkerley 2000, Li et al. 2008). Water dynamics were not measured in this study. However, salts provided a proxy for water availability because other studies have shown that soluble salt concentrations reflect the degree of leaching within soil profiles (Young et al. 2004, Wood et al. 2005, Buck et al. 2006). Shrub canopies contain elevated anion concentrations (Figure 4.33B), indicating the presence of soluble salts and low leaching conditions.

Fertile island feedbacks lead to the concentration of nutrients within shrub canopies. Shrub canopies augment the capture of dust and other nutrient-rich substrates (Schlesinger et al. 1990, Shachak and Lovett 1998, Zaady et al. 2001). Litter production around shrubs creates a barrier to SO_x and NO_x volatility losses (Schlesinger et al. 1990, Martinez-Meza and Whitford 1996, Schlesinger et al. 1996, Bolling and Walker 2002, Thompson et al. 2006, Ewing et al. 2007). Enhanced organic production and moisture retention increase microbial populations and activity that promote soil nutrient availability (Charley and West 1977, Schlesinger and Pilmanis 1998, Robinson et al. 2002, Thompson et al. 2006, Ewing et al. 2007). Plant nutrient uptake, litter production,

and bioturbation bio-accumulate resources within canopy surface soils (Charley and West 1977, Schlesinger et al. 1990, 1996, Zaady et al. 1996, Schlesinger and Pilmanis 1998, Bolling and Walker 2002, Titus et al. 2002). In some cases, the presence of surface BSCs has been shown to enhance plant uptake of nutrients (Harper and Belnap 2001). Shrubs shelter soil resources from nutrient losses due to erosion or physical disturbances (De Soyza et al. 1997, Parsons et al. 2003, Li et al. 2004, Puigdefábregas 2005, Golodets and Boeken 2006, Okin et al. 2006, Li et al. 2008). Over time, resource sinks around shrub canopies act as ecological memory, wherein resources from previous rainfall events will be stored for invigorated biological activity in future precipitation events (Schwinning et al. 2004). While shrub canopies have elevated fertility, the relative magnitude of the canopy-interspace nutrient disparity varies as a function of soil interspace cover.

Cyanobacteria Feedbacks: Moderate Fertile Island Magnitude

Surfaces composed of sand with negligible rocks favor cyanobacteria crusts, which display moderate canopy-interspace nutrient disparities and low overall fertility (Figure 4.43). Cyanobacteria-dominated interspaces act as “Hyper-Deserts of Fertility” among canopy “Desolate Islands of Fertility” (Figure 4.44). Within intermontane basins, the moderate sand saltation that occurs along sand sheets promotes the growth and propagation of filamentous cyanobacteria (see Chapter 3). Both sand sheet activity and cyanobacteria growth promote low fertility (Figure 4.48) through low water availability, low dust influx, and high eolian erosion (Figure 4.44, 4.47). As cyanobacteria trap and bind sand grains, they also capture small volumes of dust within their sticky sheaths (see Chapter 2) (see Chapter 2)(Booth 1941, Campbell 1979, Belnap and Gardner 1993, Issa et al. 1999, Zaady and Offer 2010). Dust provides a primary source of soil nutrients in

many deserts (Reheis 1990, Simonson 1995, Reynolds et al. 2001, Reheis et al. 2002, Reynolds et al. 2006, McTainsh and Strong 2007, Field et al. 2010). Because dust accretion is negligible within cyanobacteria crusts, total dust-related nutrient influx is low. In addition, high eolian erosion along sand sheets limits resource retention and accumulation within these interspace soils (Gibbens et al. 1983, Okin et al. 2001, Zaady et al. 2001, Okin et al. 2006).

Areas dominated by cyanobacteria crusts have low water availability and low organic matter production that further limit fertility. Sandy soils inhabited by cyanobacteria facilitate leaching and low surface water availability (Noy-Meir 1973, Austin et al. 2004). Moreover, cyanobacteria crusts produce very limited organic matter as compared to moss-lichen crusts (Chapter 2), which further restricts water-holding capacity, while their facilitation of surface crusting favors runoff (Yair 1990, Verrecchia et al. 1995, Eldridge et al. 2000, Canton et al. 2010). Cyanobacteria facilitate carbonate precipitation (see Chapter 2), but inorganic C still remains low compared to other soil interspace cover types (Figure 4.22).

Fertile island processes elevate nutrients within shrub canopies to produce moderate canopy-interspace nutrient disparities. Despite the nutrient build-up within canopies, low fertility of interspace cyanobacteria crusts leads to low overall nutrient accumulation. In addition, canopies within these sand sheets show high burrowing activity, which may further reduce stability and retention of nutrients. In contrast, feedbacks supporting moss-lichen crusts lead to much higher interspace fertility.

Moss-Lichen Feedbacks: Low Fertile Island Magnitude

Geologic processes that create stable surfaces composed of mixed rock and sand support the development of high fertility moss-lichen crusts and low canopy-interspace nutrient disparities (Figure 4.43). In these areas, moss-lichen interspaces act as “Oases of Fertility” among shrub “Islands of Fertility” (Figure 4.45). Mid- to late Holocene surfaces support the most extensive moss-lichen crusts (Figure 4.48) and have high surface roughness that promotes dust capture (see Chapter 3). Moss and lichen micro-structures accrete large volumes of dust (see Chapters 2, 3) and their biological structures prevent erosion (see Chapter 2)(Barger et al. 2006). Dust accumulation forms moss-lichen pinnacle micro-relief that provides new fine-grained surfaces for BSC colonization (see Chapters 2, 3) and increases surface roughness for even greater dust capture potential (see Chapters 2, 3)(McFadden et al. 1986, Wells et al. 1987). This high dust influx enhances fertility and influences local surface hydrology (Figure 4.45)(see Chapter 2).

Tall moss-lichen crusts and associated dust capture have complex influences on the distribution and availability of water. Fine-grained dust increases soil water-holding capacity and forms surface micro-features and Av horizons that trap water within moss-lichen bio-rich zones (see Chapter 2). Moss-lichen crusts have high organic matter concentrations, accumulate large volumes of dust, and display high surface roughness, which collectively enhance moisture retention and decrease runoff (see Chapter 2). Moss-lichen crusts also create surface seals that may delay evaporation (see Chapter 2). High Na concentrations (Figure 4.39), as reported in other studies (Drahorad and Felix-Henningsen 2009), and elevated EC reflect the presence of soluble salts, which suggest leaching is relatively low within tall moss-lichen crusts.

Solar insolation can also influence BSC distribution to accentuate hydrological phenomena and biogeochemical dynamics. Solar insolation influences potential evapotranspiration and can be used as a proxy for moisture availability (Merkler et al. 2005). Slope and aspect relationships influence the distribution of moss-lichen crusts versus cyanobacteria crusts in some areas (Veste et al. 2001, Kidron et al. 2010). Solar insolation was tested at the landscape scale but did not appear to broadly influence distribution of BSC types. The shortage of significant relationships could be due to the imagery resolution, as the 10 m DEM used for insolation calculations may be too coarse to capture meter-scale BSC patterns. Nevertheless, correlation coefficients indicate *Psora decipiens*, a squamulose lichen, is negatively associated with winter and equinox insolation (Table 4.9D). This indicates that during wetter periods such as fall, winter, and spring, *Psora* growth is favored on mesic sites that are partially shaded.

Elevated water availability within moss-lichen interspaces leads to high solubilization of nutrients, biological nutrient fixation, and elevated interspace fertility. While dust capture by mosses and lichens provides an initial nutrient source, the nutrients from these incoming organic and mineral substrates may not be immediately available. High moisture retention leads to high biological activity. Metabolic activity associated with moss-lichen crusts releases organic acids that break down mineral substrates (Arocena et al. 2003, Souza-Egipsy et al. 2004), while organic substrates are likely decomposed by heterotrophic crust organisms (Garcia-Pichel et al. 2003, Darby et al. 2010). Mosses and lichens produce chelating agents that can solubilize some cations (Elix and Stocker-Worgotter 2008). Moreover, cyanobacteria and cyanolichens fix nitrogen (Evans and Belnap 1999, Belnap 2002, Davidson et al. 2002, Johnson et al.

2005, Housman et al. 2006, Marsh et al. 2006), which may reduce nitrogen limitations to biological activity and organic decomposition (Garcia-Pichel et al. 2003). This biological activity results in high solubility and availability of anions and cations, within interspace soils dominated by moss-lichen crusts. This further explains the elevated micronutrient concentrations commonly observed near moss-lichen crusts (Bowker et al. 2006, Housman et al. 2007, Guo et al. 2008, Drahorad and Felix-Henningsen 2009). High nutrient availability within moss-lichen interspaces may also lead to greater canopy fertility than that of cyanobacteria crusts.

While not all nutrients are elevated within moss-lichen interspaces, most anomalies can be explained through inferred chemical species behavior. For example, NO_3 and Cu are negatively associated with mosses and lichens (Figure 4.13, Table 4.9), (Figure 4.26). The negative relationship between Cu and moss-lichen crusts (Figure 4.13, Tables 4.8B, 4.8D) may be due to organic chelation and cation leaching. Moss cell walls have relatively high cation exchange capacity (CEC) that allows them to uptake heavy metals (Bates 2008). Higher valence cations and heavy metals preferentially bind to organic acids and compounds of cell walls, including polymeric uronic acids, phenolic compounds, amino acids, silicates, and sulfate esters. Copper has one of the highest binding preferences to cell walls among all cations (Bates 2008), which could reduce Cu availability in soil solution. Alternatively, as mosses die and decompose Cu-chelating acids such as phenolic compounds could bind or mobilize copper, allowing it to leach from the upper centimeters of soil. Lichens also produce phenolics that may interact with copper (Elix and Stocker-Worgotter 2008). High moisture retention of moss-lichen crusts could delay evapotranspiration and lead to volatilization of interspace NO_3

(Schlesinger et al. 1990, Johnson et al. 2005) or could enhance leaching. While N is commonly oxidized within BSCs (Johnson et al. 2005), some suggest denitrification rates within crusts are negligible because of a lack of denitrifying microorganisms (Johnson et al. 2007). In such cases, leaching may be the primary cause for N losses from surface soils (Johnson et al. 2007). The inferred high water availability in the upper bio-rich zone facilitates carbonate precipitation by BSC organisms (see Chapter 2). This could lead to the precipitation of calcium phosphate, which reduces P availability (Lajtha and Schlesinger 1988). Precipitation of calcium-phosphates may also explain why other studies reported P availability to be negatively associated with moss-lichen crusts (Bowker et al. 2006) and why P is only moderately elevated within moss-lichen crusts in this study (Figure 4.22). While these inferred relationships help explain potential chemical species behavior, these proposed mechanisms need to be tested. Moreover, the chemistry data in this study represent one point in time and do not account for the ephemeral nature of these chemical relationships as they relate to seasonality and precipitation pulses (Austin et al. 2004, Belnap et al. 2005).

Patterns in moss-lichen biogeochemistry suggest that these crusts may offset the resource heterogeneity associated with desertification, shedding new light into fertile island dynamics. In other regions, desertification associated with shrub invasions of grasslands increases soil resource heterogeneity (e.g., Schlesinger et al. 1990, Kieft et al. 1998, Aguiar and Sala 1999, Ridolfi et al. 2008). My results, however, indicate moss-lichen crusts reduce the canopy-interspace nutrient disparities and offset the resource partitioning associated with desertification (Aguiar and Sala 1999, Rietkerk et al. 2004, Ridolfi et al. 2008).

Desert Pavement Feedbacks: High Fertile Island Magnitude

Geological drivers that generate stable surfaces with high rock cover and low sand influx produce interspaces with “desert pavements” and low to moderate density moss-lichen crusts, which display high canopy-interspace nutrient disparities (Figure 4.43). “Desert pavement” interspaces act as “Moderate Deserts of Fertility” among canopies that are “Rich Islands of Fertility” (Figure 4.46). These characteristics are most commonly expressed along Pleistocene and older geomorphic surfaces in this study area (Figure 4.48). However, the data analyzed in this “desert pavement” group included a few additional rock-covered areas, including Holocene alluvial surfaces, sand sheets with high rock cover, and rocky, colluvial slopes. Along stable, rock-covered surfaces, dust accretes incrementally below surface clasts (Goossens 1995), eventually leading to smooth, desert pavement surfaces (McFadden et al. 1986, Wells et al. 1987, Goossens 1995, Anderson et al. 2002, Wood et al. 2005). Rock-covered surfaces provide few fine-grained substrates for BSCs and prevent plant colonization (see Chapter 3)(Wells et al. 1987, Quade 2001, Wood et al. 2005, Meadows et al. 2008), limiting bioturbation and biological activity. Desert pavement hydrological phenomena further reduce biological activity and restrict interspace fertility.

Water dynamics of desert pavements vary as a function of surface age and morphology. Av horizons associated with desert pavements decrease moisture availability to a greater or lesser extent, depending on the degree of development. In general, older desert pavements with well-developed Av horizons have lower infiltration and greater runoff potential than younger, or rougher surfaces (Wells et al. 1987, Young et al. 2004, Wood et al. 2005, Meadows et al. 2008). This lack of water availability

strongly contrasts with the high water availability inferred to occur in association with dense moss-lichen crusts (see Chapter 2). In this study, “desert pavements” and Av horizons are most common along Pleistocene and older alluvial surfaces, where water availability and moisture exchange are low (see Chapter 3).

Low water availability and high runoff along desert pavement interspaces leads to moderate interspace fertility and concomitant concentration of soil resources around shrub canopies. While incoming dust provides a source of nutrients to interspaces, low moisture availability, negligible plant germination, and low BSC establishment inhibit microbial activity. This lack of biological activity prevents overturn and release of nutrients into soil solution. Low water availability may limit precipitation of calcium phosphates, a common process that makes P unavailable in arid soils (Lajtha and Schlesinger 1988). Without water available to facilitate precipitation, P will not become fixed in calcium phosphate minerals, which would explain why extractable P is higher within “desert pavement” interspaces than BSC-dominated surfaces (Figure 4.22). Runoff may wash water, organic residues, and soil resources away from interspaces only to concentrate them within shrub canopies (Schlesinger et al. 1996, Schlesinger and Pilmanis 1998, Stavi et al. 2009). In fact, these runoff dynamics seem to play a dominant role in surface chemistry as fertility in these rock-covered surfaces is strongly related to slope angle. For example, interspace pH, Mn, and Zn are positively correlated with percent slope (Table 4.11), while total BSC cover is negatively correlated to slope. Mn and Zn do not readily solubilize at high pH levels under oxidizing conditions. However, Mn has a tendency to mobilize and reprecipitate quickly with changing pH and water content (McBride 1994), conditions that could fluctuate rapidly on steep, rocky slopes.

Because metal ions such as Zn commonly adsorb to Mn-oxides (McBride 1994), this mobilization-precipitation could also influence Zn mobility. Overall, low water availability and hydrological dynamics support the strong nutrient disparities between “desert pavement” interspaces and associated shrub canopies.

Discussion

Applicability of Model to Other Arid Regions

The fertile island model presented in this study can be used to explain the results and discrepancies reported in previous fertile island studies. While climate controls total ecosystem productivity and fertility, interactions between BSCs and soil-geomorphology drive resource allocation across arid soil surfaces. Therefore, careful analysis of geology, geomorphology, soils, and BSCs provides a more comprehensive understanding of fertile island dynamics.

Mojave Desert

The “desert pavement” trajectory of my fertile island model explains the lack of BSC-driven fertile island patterns previously reported for the Mojave Desert. Thompson et al. (2005) found that the relative disparity between canopy and interspace nutrients remained relatively constant among their sites, despite differences in elevation, shrub species, and BSC cover. The geomorphic characteristics and BSC cover of their study sites fit within my model’s “desert pavement” trajectory. Site descriptions suggest that those study plots lie along Pleistocene alluvial surfaces (Figure 4.48) that display poorly interlocking “desert pavements” with fine-grained Av horizons and shallow petrocalcic horizons. Their limestone-derived soils had only 25% moss-lichen cover, which fits the

“desert pavement” trajectory. My data and model suggest differences in fertility within that trajectory are primarily controlled by factors such as slope dynamics and rock cover but are less influenced by BSC cover.

While I measured a different suite of soil chemical constituents, fertility data from my “desert pavement” units reveal similar disparities in canopy-interspace nutrients as the equivalent age sites of Thompson et al. (2005). Mean soil organic matter was 40-50% higher within canopies than interspaces within their sites. While not statistically significant, my “desert pavement” canopies have 20% higher organic C concentrations than associated interspaces. My data also show similar patterns in total N. Thompson et al. (2005) report that mean canopy total N was elevated by 100%, while my median total N was 80% higher within canopies than interspaces. Overall, these observations suggest high rock cover produces consistent biogeochemical patterns with high canopy-interspace nutrient disparities. The relative cover by rocks and sand also plays an important role in the longevity of these distinct fertility patterns.

The development time of fertile islands is a critical factor controlling the magnitude of resource disparities between canopies and interspaces. Schlesinger et al. (1996) investigated the impact of time in fertile island development, by comparing young shrublands formed in historic grassland areas of the Chihuahuan Desert to older, longer-lived, shrublands of the Mojave Desert. It is difficult to assess the applicability of our model to their Mojave Desert sites because characteristics such as rock fragment size and cover and geomorphic setting are not described. The granite and granodiorite soil parent materials in their study could lead to different surface cover types. Weathering could lead to either the formation of sand sheets (Figure 4.48) that support cyanobacteria crusts

or coarse, rocky surfaces that form desert pavements and Av horizons on older geomorphic surfaces (Figure 4.48). The data from Schlesinger et al. (1996) resemble patterns from our “desert pavement” trajectory. While slight inconsistencies are seen in PO_4 , K, C, and Mg, my canopy-interspace nutrient disparities and total nutrient concentrations are similar to their results. Any apparent anomalies between the studies could be due to differences in incoming dust composition or differences in leaching dynamics and geochemistry between their granitic soils and our limestone- and sandstone-derived soils. While canopy-interspace nutrient disparities and total nutrient concentrations are quite similar between our “desert pavement” sites and their Mojave Desert sites, their fertility data are also comparable to our cyanobacteria crust units.

Both “desert pavement” and cyanobacteria trajectories could support moderate to high canopy-interspace nutrient disparities and long-lived fertile islands in the Mojave Desert. Schlesinger et al. (1996) noted that autocorrelation of soil resources is much higher in the Mojave Desert than other arid regions. The authors propose that the fertile islands of the Mojave Desert are strongly developed because these areas have remained shrublands for thousands of years, whereas many Chihuahuan Desert sites have only been shrublands since the 1800s. They suggest resources are highly concentrated within canopies because generations of shrubs occupy the same fertility island loci over time. Desert pavements and associated Av horizons limit plant germination (Musick 1975, Wood et al. 2005), forcing shrubs to grow in existing coppices, thus maintaining the location of existing fertile islands. Alternatively, sand saltation of the sand sheets that support cyanobacteria crusts (see Chapter 3) would also constrain plant germination to more stabilized areas, such as canopies of live or dead shrubs (Holmgren et al. 1997). In

addition, cyanobacteria crusts can, in some cases, inhibit vascular plant germination (Li et al. 2005). On the other hand, if the authors compared cyanobacteria from the Chihuahuan Desert, which are predicted to have moderate nutrient disparities, to the “desert pavement” surfaces of the Mojave Desert, which are predicted to have high nutrient disparities, this could explain some of the differences in nutrient auto correlation (Schlesinger et al. 1996).

Chihuahuan Desert

The moderate canopy-interspace nutrient disparities associated with relatively young, or recently invaded, shrublands (Schlesinger et al. 1996) of the Chihuahuan Desert can be explained by the fertile island patterns of the cyanobacteria crust trajectory. The extensive shrub invasions of previous grasslands began in the 1800s (Buffington and Herbel 1965). Without complete descriptions of soil-geomorphic and BSC characteristics, the direct application of my model to the Chihuahuan Desert study of Schlesinger et al. (1996) is difficult. However, many of these young shrublands occupy sandy soils that form sand sheets (Figure 4.48) with shrubs such as *Larrea tridentata* (De Soyza et al. 1997) or mesquite coppice dunes (Gibbens et al. 1983, Gibbens et al. 2005), which commonly support cyanobacteria crusts (Ritchie et al. 2003). Thus, many of the Chihuahuan Desert sites (Schlesinger et al. 1996) potentially fit the cyanobacteria crust trajectory.

As predicted by my model, Chihuahuan Desert data closely resemble those of my cyanobacteria units, where high eolian erosion strips interspace resources. Canopy-interspace nutrient disparities as well as total nutrient concentrations of the Chihuahuan Desert sites are comparable to our Mojave Desert cyanobacteria data. However, there are

some apparent differences. Their Chihuahuan sites have higher canopy-interspace nutrient disparities in N and PO₄ but lower disparities in K than our cyanobacteria sites. Their Chihuahuan sites also have lower SO₄ and Na concentrations and higher K, Ca, Mg concentrations than our cyanobacteria sites. These apparent anomalies could be due to differences in the composition or amount of dust, parent material, or leaching dynamics. These differences may be due to the age of shrub invasions from the Mojave and Chihuahuan Deserts, as the most limiting nutrients such as N are concentrated in canopies before less-limiting nutrients (Schlesinger et al. 1996). Similar resource patterns occur in the sandy soils of the Colorado Plateau.

Colorado Plateau

Fertile islands of the Colorado Plateau align with the patterns predicted by the cyanobacteria and moss-lichen trajectories. Of all the studies examined, the Colorado Plateau displays some of the most complex fertile island patterns. A study by Housman et al. (2007) suggests that differences in canopy and interspace fertility do not vary consistently as a function of plant or BSC types. While soil-geomorphic characteristics are difficult to decipher from their site descriptions, the sandy loam soils in this study support two major types of BSCs - moss-lichen crusts and cyanobacteria crusts.

Close examination of the Housman et al. (2007) data set (see Houseman et al. 2007 Supplementary Data) revealed strong similarities in canopy-interspace nutrient disparities in soils of the Mojave Desert and the Colorado Plateau. For these analyses, I compiled their canopy and interspace geochemical data by crust cover type and compared it to my geochemical data. Overall, the canopy-interspace disparities of most nutrients are quite similar for the Mojave Desert and Colorado Plateau moss-lichen sites. Nutrient

disparities within cyanobacteria crusts of the Mojave Desert and Colorado Plateau are also comparable. While these relationships do not necessarily reflect statistical significance, the similarity in canopy-interspace resource allocation within the respective cover types is quite striking.

The primary difference between BSC geochemistry from the Mojave Desert samples and those of the Colorado Plateau are seen in total nutrient concentrations. The Colorado Plateau moss-lichen crusts had interspaces nutrient concentrations that were commonly 2 times higher than those of the Mojave Desert moss-lichen interspaces. Cyanobacteria interspaces in Colorado Plateau had concentrations that were at least 3-15 times higher for many nutrients than the Mojave Desert cyanobacteria interspaces. The higher fertility in the Colorado Plateau, particularly those differences seen in cyanobacteria crusts, may be due to this deserts' greater availability of water. (1) The cooler and wetter conditions of the Colorado Plateau allow for more biological activity and organic production that would favor higher fertility. (2) Higher water availability would allow cyanobacteria to remain hydrated and sticky for longer periods, thus facilitating greater capture of nutrient-rich dust. (3) Despite low rock cover in the Colorado Plateau, sandy surfaces remain relatively stable because moist soils are less prone to sand saltation (Chapter 3). This enhanced stability prevents erosional losses of interspace soil resources that could occur in the drier soils of the Mojave Desert. (4) While moss-lichen crusts in the Colorado Plateau collect dust, they may not have sufficient dust influx to form the thick Av horizons seen in the Mojave Desert (see Chapter 3). Therefore, these sites could display different leaching dynamics than those of the Mojave Desert. (5) The spacing of plants in the Colorado Plateau sites (Housman et

al. 2007), is closer than that of the Mojave Desert sites, which could mask some fertile island patterns.

The consistency in canopy-interspace nutrient disparities that exist in disparate climatic conditions with large differences in total fertility supports the resource allocation hypothesis of Thompson et al. (2005). They suggested fertile island patterns remain relatively constant with increasing effective precipitation and concomitant increases in soil resource availability. Combining the model of Thompson et al. (2005) with my fertile island model provides a more comprehensive perspective into arid resource allocation that is applicable to many soil types, biogeomorphic settings, and climatic conditions. Therefore, I propose that the BSC and “desert pavement” cover control the ratio of canopy to interspace nutrients, and this resource disparity remains consistent as moisture or resources are added to the system.

Limitations to the Model

The applicability of this fertile island model should be tested in other arid regions, particularly where biogeochemical and biogeomorphic processes are vastly different. This model warrants additional testing in several conditions: (1) areas where coarse-grained parent materials do not facilitate the formation of cyanobacteria crusts or moss-lichen crusts; (2) along clay- and silt-rich playa deposits that may support cyanobacteria crust or scattered moss-lichen crusts, but have unique geomorphic and hydrologic dynamics that could strongly influence biogeochemical cycling; (3) within salty environments, such as gypsum parent materials, where soil chemistry is strongly affected by high salt concentrations. In addition my model is based on areas dominated by wind erosion, which form circular islands of fertility (Aguilar and Sala 1999). This fertile

island model may have limited applicability in areas of banded vegetation, where resource heterogeneity develops through water-dominated erosion (Aguilar and Sala 1999).

The landscape biogeochemical model (Figure 4.48) has applications to intermontane basins as well as other geomorphic settings. This model may be directly applicable to the Basin and Range Province (U.S.A.) such as the Mojave, Chihuahuan, Great Basin, and Sonoran Deserts, in which equivalent-aged landforms express similar soil characteristics (Peterson 1981). Within intermontane basins, the soil-geomorphic template (Monger and Bestelmeyer 2006) provides a useful tool for predicting the sand-to-rock ratio along surfaces of varying age and depositional setting (see Chapter 3). While the landform model (Figure 4.48) may not be directly applicable to other geomorphic settings, it clearly illustrates how geomorphic controls on the sand-to-rock ratio and surface cover (Figure 4.47)(see Chapter 3) can be used to predict landscape-scale biogeochemical patterns.

Environmental Perturbations and Fertile Island Dynamics

The three fertile island patterns will respond differently to environmental perturbations. Geologic processes influence susceptibility to physical impacts, while biological and geomorphic responses determine the longevity of disturbance effects (Stavi et al. 2009). Several perturbations could derail natural self-enhancing feedbacks, leading to ecological and biogeomorphic instability (Figure 4.49) and long-term changes to fertile island patterns.

Climate change effects to the timing, intensity and amount of precipitation could have dramatic impacts on surface cover and biogeochemical feedbacks. Long-term

“mega-droughts” are predicted for the arid regions of the southwestern U.S. (Fawcett et al. 2011). More extreme and variable rainfall events, such as those predicted for this region (IPCC 2007) are expected to have significant impacts to terrestrial ecosystem dynamics (Knapp et al. 2008). For example, shorter and more frequent rainfall events can cause physiological stress and in some cases senescence of cyanobacteria, mosses, and lichens (Bowker et al. 2002, Belnap et al. 2004, Barker et al. 2005). Increased UV radiation due to stratospheric ozone depletion (Boucher 2010) may reduce BSC protective pigment production, further decreasing physiological efficiency (Belnap et al. 2008). The biotic stress induced by climate and atmospheric changes could increase competitive interactions among BSC organisms, resulting in decreased crust cover and species richness (Bowker et al. 2010, Maestre et al. 2010). Mortality of moss-lichen crusts that protect and enhance interspace fertility would lead to increased resource heterogeneity and greater canopy-interspace nutrient disparities. If sand sheet-stabilizing cyanobacteria die back, the vascular plant, microbial, and faunal communities that they support (Robinson et al. 2002, Zaady and Bouskila 2002, Thomas and Dougill 2006, Darby et al. 2007, Thomas and Dougill 2007, Darby et al. 2010) would be negatively impacted by elevated eolian activity, such as sand abrasion and erosional losses of interspace nutrients (McKenna Neuman et al. 1996, Okin et al. 2001, McKenna Neuman and Maxwell 2002, Field et al. 2010). The droughts predicted for the southwest U.S. would also promote resource heterogeneity within “desert pavement” sites, as decreased water availability would support fewer vascular plants and fewer fertile islands (Wells et al. 1987).

Fertile island patterns and water allocation will become increasingly important as climate changes. Overall, water is the most-limiting factor to biological productivity in desert regions (Noy-Meir 1973). My model suggests that high fertility commonly reflects water-driven productivity and biogeochemical phenomena, such as fixation of C and N, biologically-induced dust capture, and solubilization of nutrients from biological activity. Nevertheless, nutrient limitations to productivity could become important in two scenarios. (1) If ecosystems become extremely degraded by erosion, the loss of biological structures, organic matter, and fine-grained material could lead to nutrient limitations. In such cases, micronutrients that become less available in high pH soils, such as Fe, Cu, Mn, and Zn, could become limiting for the few organisms that could survive in these highly-eroded soils. (2) If climates become wetter and less water-limited, areas of high fertility, that are also areas of high water availability, will be most susceptible to exotic plant invasions (Bromley et al. 1997, Kieft et al. 1998, Aguiar and Sala 1999, Walker et al. 2001, DeFalco et al. 2003, Ridolfi et al. 2008).

Exotic grass invasions threaten ecosystems with extensive moss-lichen cover (Figure 4.49). Moss-lichen crusts appear to be highly susceptible to exotic grass establishment (Figure 4.49, Figure 4.13). Other studies from the Mojave Desert have shown similar relationships, where exotic grass germination is elevated in moss-lichen crusts (DeFalco et al. 2001), within deep, fertile soils, or in soils with high water-availability (Gelbard and Belnap 2003, Su et al. 2007, Rao and Allen 2010). These findings agree with this study, which found exotic grass cover is elevated within fertile moss-lichen interspaces (Figure 4.22), where water availability is inferred to be high (Chapter 2). These grasses are also strongly associated with *Collema*, a nitrogen-fixing

cyanolichen (Figure 4.22). These invasions occur, in part, because non-native annuals such as *Bromus* can scavenge N and other soil resources more efficiently than many non-native annuals (DeFalco et al. 2003). However, research from other regions suggests exotic grass invasions are negatively associated with BSCs (Stohlgren et al. 2001), and certain BSC mosses (Serpe et al. 2006) and lichens (Deines et al. 2007) can prevent exotic grass germination.

Grass invasions support feedback loops between exotics such as *Bromus* and fire disturbance (Knapp 1998, Brooks 1999). If exotic non-bunch grasses like *Bromus* overtake BSC interspaces, fire frequency and intensity is expected to increase (Knapp 1998, Brooks 1999, DeFalco et al. 2001, Belnap et al. 2006). Grass invasions and wildfires will significantly decrease biodiversity because frequent and intense fires reduce BSC and perennial shrub cover, favoring monocultures of exotic grasses (Evans et al. 2001, DeFalco et al. 2003, Hilty et al. 2004, Belnap et al. 2006, Abella et al. 2009). Ecosystem hydrologic dynamics will also change as shrub cover diminishes (Dunkerley 2000) and if important BSC microstructures (see Chapter 2) are destroyed. Finally, fire-induced losses of crust and shrub cover will increase interspace and canopy susceptibility to wind erosion and loss of soil resources that eventually could mask previous fertile island patterns (Ravi et al. 2007, 2009, 2010).

Off-highway vehicle disturbances (OHV) and associated ecological impacts are intensifying in arid regions. For instance, the number of off-highway drivers in southern Nevada recently increased four-fold during a 10-year period (Spivey 2008). Physical impacts by OHVs upset desert pavement and moss-lichen crust integrity, exposing fine-grained Av horizons to erosion, causing dust emissions and significant negative impacts

to human health (Belnap et al. 2009, Goossens and Buck 2009)(Figure 4.49). These surface disturbances alter local hydrology, which would impair ecological communities adapted to desert pavement water dynamics (Schlesinger and Jones 1984, Wells et al. 1987, Young et al. 2004, Wood et al. 2005, Meadows et al. 2008). OHV disturbance and erosion transform biogeochemical sinks within shrub canopies or moss-lichen crusts from “conserving” systems to “leaky” systems (Belnap et al. 2005). Erosional loss of soil resources can have long-lasting effects. One study from the Mojave Desert showed OHV activity significantly reduced fertility associated with shrub canopies (Bolling and Walker 2002). Even 88 years after disturbance, canopy nutrient concentrations were significantly lower than those in non-disturbed sites.

Interactions among climate, exotic invasions, and OHV disturbances will only amplify the effects of global desertification (Schlesinger et al. 1990, Field et al. 2010). Climate change will intensify exotic grass invasions and wildfires, as increased atmospheric CO₂ concentrations favor exotic grass growth and reproduction over native annuals (Smith et al. 2000). Fire (Bowker et al. 2004, Hilty et al. 2004) or OHV (Belnap and Gillette 1998) disturbances to BSCS combined with climate-induced mortality of vascular plants will exponentially increase eolian erosion and loss of soil resources (Munson et al. 2011). In addition, OHV activity will directly amplify existing dust emissions, further degrading air quality (Goossens and Buck 2009). Erosional feedbacks and reduced landscape stability could eventually lead to degradation of entire ecosystems, widespread irreversible soil loss, and dust bowl conditions.

Conclusions

Geological and biological interactions determine surface cover characteristics and the magnitude of the fertile island effect. Soil-geomorphic factors control the ratio of rocks to sand and the development of three surface cover types and three unique biogeochemical patterns. (1) Cyanobacteria crust interspaces occur along sandy surfaces and lead to the formation of moderate canopy-interspace nutrient disparities and low overall fertility. (2) High density moss-lichen crusts grow along stable surfaces composed of mixed rock and sand and support high overall fertility with low canopy-interspace nutrient disparities. While elevated interspace fertility offsets resource heterogeneity associated with desertification, it increases the susceptibility of moss-lichen crusts to exotic grass invasion. (3) High rock cover favors the formation of “desert pavements” with low to moderate density moss-lichen cover, which produce high canopy-interspace nutrient disparities. Inferred biological and geological interactions involving stability, dust inputs, water availability, and biological activity sustain these unique geochemical patterns across the landscape. Surface control on fertile island patterns are consistent throughout many deserts and could reflect overarching ecological controls on canopy-interspace nutrient disparities that are universal to arid regions, regardless of climate or total productivity. The proposed models of fertile island magnitude and biogeochemical-biogeomorphic interactions help predict landscape response to climate change, exotic grass invasions, anthropogenic disturbance, and desertification.

Literature Cited

- Abella S. R., E. C. Engel, C. L. Lund, and J. E. Spencer. 2009. Early post-fire plant establishment on a Mojave Desert burn. *Madrono* **56**:137-148.
- Abrahams A. D., A. J. Parsons, and J. Wainwright. 1994. Resistance to overland flow on semiarid grassland and shrubland hillslopes, Walnut Gulch, southern Arizona. *Journal of Hydrology* **156**:431-446.
- Aguilar M. R., O. E. Sala. 1999. Patch structure, dynamics and implications for the functioning of arid ecosystems. *TREE* **14**:273-277.
- Aguilera L. E., J. R. Gutierrez, and P. L. Meserve. 1999. Variation in soil micro-organisms and nutrients underneath and outside the canopy of *Adesmia bedwellii* (Papilionaceae) shrubs in arid coastal Chile following drought and above average rainfall. *Journal of Arid Environments* **42**:61-70.
- Anderson K., S. Wells, and R. Graham. 2002. Pedogenesis of vesicular horizons, Cima Volcanic Field, Mojave Desert, California. *Soil Science Society of America Journal* **66**:878-887.
- Arocena J. M., L. P. Zhu, and K. Hall. 2003. Mineral accumulations induced by biological activity on granitic rocks in Qinghai Plateau, China. *Earth Surface Processes and Landforms* **28**:1429-1437.
- Austin A. T., L. Yahdjian, J. M. Stark, J. Belnap, A. Porporato, U. Norton, D. A. Ravetta, and S. M. Schaeffer. 2004. Water pulses and biogeochemical cycles in arid and semiarid ecosystems. *Oecologia* **141**:221-235.
- Baldwin B. G., S. Boyd, B. J. Ertter, R. W. Patterson, T. J. Rosatti, D. H. Wilken, and M. Wetherwax. 2002. *The Jepson Desert Manual: Vascular Plants of Southeastern California*. 626 pp.
- Barger N. N., J. E. Herrick, J. Van Zee, and J. Belnap. 2006. Impacts of biological soil crust disturbance and composition on C and N loss from water erosion. *Biogeochemistry* **77**:247-263.
- Barker D. H., L. R. Stark, J. F. Zimpfer, N. D. McLetchie, and S. D. Smith. 2005. Evidence of drought-induced stress on biotic crust moss in the Mojave Desert. *Plant, Cell and Environment* **28**:939-947.
- Bates J. W. 2008. Mineral nutrition and substratum ecology. Pages p. 299-356 *In* B. Goffinet and A. J. Shaw, editors. *Bryophyte Biology*, Cambridge University Press, Cambridge.

- Belnap J. 2006. The potential roles of biological soil crusts in dryland hydrologic cycles. *Hydrological Processes* **20**:3159-3178.
- Belnap J. 2002. Nitrogen fixation in biological soil crusts from southeast Utah, USA. *Biol. Fertil. Soils* **35**:128-135.
- Belnap J. 1995. Surface disturbances: their role in accelerating desertification. *Environmental Monitoring and Assessment* **37**:39-57.
- S. B. Monsen, S. G. Kitchen, editors. 1994. Potential role of cryptobiotic soil crust in semiarid rangelands. *Proceedings – Ecology and Management of Annual Rangelands* p. 179-185.
- Belnap J., D. A. Gillette. 1998. Vulnerability of desert biological soil crusts to wind erosion: the influences of crust development, soil texture, and disturbance. *Journal of Arid Environments* **39**:133-142.
- Belnap J., J. S. Gardner. 1993. Soil microstructure in soils of the Colorado Plateau: The role of the cyanobacterium *Microcoleus vaginatus*. *Great Basin Naturalist* **53**:40-47.
- Belnap J., S. L. Phillips, and T. Troxler. 2006. Soil lichen and moss cover and species richness can be highly dynamic: The effects of invasion by the annual exotic grass *Bromus tectorum*, precipitation, and temperature on biological soil crusts in SE Utah. *Applied Soil Ecology* **32**:63-76.
- Belnap J., S. L. Phillips, and M. E. Miller. 2004. Response of desert biological soil crusts to alterations in precipitation frequency. *Oecologia* **141**:306-316.
- Belnap J., R. Prasse, and K. T. Harper. 2003. Influence of biological soil crusts on soil environments and vascular plants. *In* J. Belnap and O. L. Lange, editors. *Biological Soil Crusts: Structure, Function, and Management*, Springer-Verlag, Berlin.
- Belnap J., S. L. Phillips, S. Flint, J. Money, and M. Caldwell. 2008. Global change and biological soil crusts: effects of ultraviolet augmentation under altered precipitation regimes and nitrogen additions. *Global Change Biology* **14**:670-686.
- Belnap J., J. R. Welter, N. B. Grimm, N. Barger, and J. A. Ludwig. 2005. Linkages between microbial and hydrological processes in arid and semiarid watersheds. *Ecology* **86**:298-307.
- Belnap J., R. L. Reynolds, M. C. Reheis, S. E. Phillips, F. E. Urban, and H. L. Goldstein. 2009. Sediment losses and gains across a gradient of livestock grazing and plant invasion in a cool, semi-arid grassland, Colorado Plateau, USA *Aeolian Research* **1**:27-43.

- Bolling J. D., L. R. Walker. 2002. Fertile island development around perennial shrubs across a Mojave Desert chronosequence. *Western North American Naturalist* **62**:88-100.
- Booth W. E. 1941. Algae as pioneers in plant succession and their importance in erosion control. *Ecology* **22**:38-46.
- Boucher O. 2010. Stratospheric ozone, ultraviolet radiation and climate change. *Weather* **65**:105-110.
- Bowker M. A. 2007. Biological soil crust rehabilitation in theory and practice: An underexploited opportunity. *Restoration Ecology* **15**:13-23.
- Bowker M. A., S. Soliveres, and F. T. Maestre. 2010. Competition increases with abiotic stress and regulates the diversity of biological soil crusts. *Journal of Ecology* **98**:551-560.
- Bowker M. A., J. Belnap, V. B. Chaudhary, and N. C. Johnson. 2008. Revisiting classic water erosion models in drylands: The strong impact of biological soil crusts. *Soil Biology & Biochemistry* **40**:2309-2316.
- Bowker M. A., J. Belnap, D. W. Davidson, and H. Goldstein. 2006. Correlates of biological soil crust abundance across a continuum of spatial scales: support for a hierarchical conceptual model. *Journal of Applied Ecology* **43**:152-163.
- Bowker M. A., J. Belnap, R. Rosentreter, and B. Graham. 2004. Wildfire-resistant biological soil crusts and fire-induced loss of soil stability in Palouse prairies, USA. *Applied Soil Ecology* **26**:41-52.
- Bowker M. A., S. C. Reed, J. Belnap, and S. L. Phillips. 2002. Temporal variation in community composition, pigmentation, and Fv /Fm of desert cyanobacterial soil crusts. *Microbial Ecology* **43**:13-25.
- Bromley J., J. Brouwer, A. P. Barker, and C. Valentin. 1997. The role of surface water redistribution in an area of patterned vegetation in a semi-arid environment, south-west Niger. *Journal of Hydrology* **198**:1-29.
- Brooks M. L. 1999. Alien annual grasses and fire in the Mojave Desert. *Madrono* **46**:13-19.
- Buck B. J., K. Wolff, D. J. Merkler, and N. J. McMillan. 2006. Salt mineralogy of Las Vegas Wash, Nevada: Morphology and subsurface evaporation. *Soil Science Society of America Journal* **70**:1639-1651.
- Buffington L. C., C. H. Herbel. 1965. Vegetational Changes on a Semidesert Grassland Range from 1858 to 1963. *Ecological Monographs* **35**:139-164.

- Caldwell T. G., M. H. Young, J. Zhu, and E. V. McDonald. 2008. Spatial structure of hydraulic properties from canopy to interspace in the Mojave Desert. *Geophys. Res. Lett.* **35**:L19406.
- Campbell S. E. 1979. Soil stabilization by a prokaryotic desert crust: Implications for Precambrian land biota. *Origins of Life* **9**:335-348.
- Campbell S. E., J. Seeler, and S. Golubic. 1989. Desert crust formation and soil stabilization. *Arid Soil Research and Rehabilitation* **3**:217-228.
- Canton Y., A. Sole-Benet, and R. Lazaro. 2003. Soil–geomorphology relations in gypsiferous materials of the Tabernas Desert (Almeria, SE Spain). *Geoderma* **115**:193-222.
- Charley J. L., N. E. West. 1977. Micro-patterns of nitrogen mineralization activity in soils of some shrub-dominated semi-desert ecosystems of Utah. *Soil Biol. Biochem.* **9**:357-365.
- Chaudhary V. B., M. A. Bowker, T. E. O'Dell, J. B. Grace, A. E. Redman, M. C. Rilling, and N. C. Johnson. 2009. Untangling the biological contributions to soil stability in semiarid shrublands. *Ecological Applications* **19**:110-122.
- Danin A., E. Ganor. 1991. Trapping of airborne dust by mosses in the Negev Desert, Israel. *Earth Surface Processes and Landforms* **16**:153-162.
- Darby B. J., D. A. Neher, and J. Belnap. 2010. Impact of biological soil crusts and desert plants on soil microfaunal community composition. *Plant and Soil* **328**:421-431.
- Darby B. J., D. A. Neher, and J. Belnap. 2007. Soil nematode communities are ecologically more mature beneath late- than early-successional stage biological soil crusts. *Applied Soil Ecology* **35**:203-212.
- Davidson D. W., M. A. Bowker, D. George, S. L. Phillips, and J. Belnap. 2002. Treatment effects on performance of N-fixing lichens in disturbed soil crusts of the Colorado Plateau. *Ecological Applications* **12**:1391-1405.
- De Soyza A. G., W. G. Whitford, E. Martinez-Meza, and J. Van Zee. 1997. Variation in creosotebush (*Larrea tridentata*) canopy morphology in relation to habitat, soil fertility and associated annual plant communities. *American Midland Naturalist* **137**:13-26.
- DeFalco L. A., D. R. Bryla, V. Smith-Longozo, and R. S. Nowak. 2003. Are Mojave Desert annual species equal? Resource acquisition and allocation for the invasive grass *Bromus madritensis* subsp. *rubens* (Poaceae) and two native species. *American Journal of Botany* **90**:1045-1053.

- DeFalco L. A., J. K. Detling, C. R. Tracy, and S. D. Warren. 2001. Physiological variation among native and exotic winter annual plants associated with microbiotic crusts in the Mojave Desert. *Plant and Soil* **234**:1-14.
- Deines L., R. Rosentreter, D. J. Eldridge, and M. D. Serpe. 2007. Germination and seedling establishment of two annual grasses on lichen-dominated biological soil crusts. *Plant and Soil* **295**:23-35.
- Dunkerley D. 2000. Hydrologic effects of dryland shrubs: defining the spatial extent of modified soil water uptake rates at an Australian desert site. *Journal of Arid Environments* **45**:159-172.
- Elbert W., B. Weber, B. Budel, M. O. Andreae, and U. Poschl. 2009. Microbiotic crusts on soil, rock and plants: neglected major players in the global cycles of carbon and nitrogen? *Biogeosciences Discuss.* **6**:6983-7015.
- Eldridge DJ, Rosentreter R. 2003. Shrub mounds enhance waterflow in a shrub-steppe community in southwestern Idaho, U.S.A. USDA Forest Service, Rocky Mountain Research Station Proceedings RMRS-P-000. p.1-8. Ogden, UT.
- Eldridge D. J., J. F. Leys. 2003. Exploring some relationships between biological soil crusts, soil aggregation and wind erosion. *Journal of Arid Environments* **53**:457-466.
- Eldridge D. J., R. Rosentreter. 1999. Morphological groups: a framework for monitoring microphytic crusts in arid landscapes. *Journal of Arid Environments* **41**:11-25.
- Eldridge D. J., R. S. B. Greene. 1994. Microbiotic soil crusts: A review of their roles in soil and ecological processes in the rangelands of Australia. *Australian Journal of Soil Research* **32**:389-415.
- Eldridge D. J., E. Zaady, and M. Shachak. 2000. Infiltration through three contrasting biological soil crusts in patterned landscapes in the Negev, Israel. *Catena* **40**:323-336.
- Elix J. A., E. Stocker-Worgotter. 2008. Biochemistry and secondary metabolites. Pages p. 104-133 *In* T. H. Nash, editor. *Lichen Biology*, Cambridge University Press, Cambridge.
- Escudero A., I. Martinez, A. de la Cruz, M. A. G. Otalora, and F. T. Maestre. 2007. Soil lichens have species-specific effects on the seedling emergence of three gypsophile plant species. *Journal of Arid Environments* **70**:18-28.
- Evans R. D., J. Belnap. 1999. Long-Term consequences of disturbance on nitrogen dynamics in an arid ecosystem. *Ecology* **80**:150-160.

- Evans R. D., J. R. Johansen. 1999. Microbiotic crusts and ecosystem processes. *Critical Reviews in Plant Sciences* **18**:183-225.
- Evans R. D., R. Rimer, L. Sperry, and J. Belnap. 2001. Exotic plant invasion alters nitrogen dynamics in an arid grassland. *Ecological Applications* **11**:1301-1310.
- Ewing S. A., R. J. Southard, J. L. Macalady, A. S. Hartshorn, and M. J. Johnson. 2007. Soil microbial fingerprints, carbon, and nitrogen in a Mojave Desert creosote-bush ecosystem. *Soil Science Society of America Journal* **71**:469-475.
- Fawcett P. J., J. P. Werne, R. S. Anderson, J. M. Heikoop, E. T. Brown, M. A. Berke, S. J. Smith, F. Goff, L. Donohoo-Hurley, L. M. Cisneros-Dozal, S. Schouten, J. S. Sinninghe Damste, Y. Huang, J. Toney, J. Fessenden, G. WoldeGabriel, V. Atudorei, J. W. Geissman, and C. D. Allen. 2011. Extended megadroughts in the southwestern United States during Pleistocene interglacials. *Nature* **470**:518-521.
- Field J. P., J. Belnap, D. D. Breshears, J. C. Neff, G. S. Okin, J. J. Whicker, T. H. Painter, S. Ravi, M. C. Reheis, and R. L. Reynolds. 2010. The ecology of dust. *Frontiers in Ecology and the Environment* **8**:423-430.
- Friedmann E. I., M. Galun. 1974. Desert algae, lichens and fungi. Pages 165-212 *In* G. W. Brown, editor. *Desert Biology*, Academic Press, New York.
- Garcia-Pichel F., S. L. Johnson, D. Youngkin, and J. Belnap. 2003. Small-scale vertical distribution of bacterial biomass and diversity in biological soil crusts from arid lands in the Colorado Plateau. *Microbial Ecology* **46**:312-321.
- Gelbard J. L., J. Belnap. 2003. Roads as conduits for exotic plant invasions in a semiarid landscape. *Conservation Biology* **17**:420-432.
- Gibbens R. P., J. M. Tromble, J. T. Hennessy, and M. Cardenas. 1983. Soil movement in mesquite dunelands and former grasslands of southern New Mexico from 1933 to 1980. *Journal of Range Management* **36**:145-148.
- Gibbens R. P., R. P. McNeely, K. M. Havstad, R. F. Beck, and B. Nolen. 2005. Vegetation changes in the Jornada Basin from 1858 to 1998. *Journal of Arid Environments* **61**:651-668.
- Golodets C., B. Boeken. 2006. Moderate sheep grazing in semiarid shrubland alters small-scale soil surface structure and patch properties. *Catena* **65**:285-291.
- Goossens D. 1995. Field experiments of aeolian dust accumulation on rock fragment substrata. *Sedimentology* **42**:391-402.
- Goossens D., B. Buck. 2009. Dust emission by off-road driving: Experiments on 17 arid soil types, Nevada, USA. *Geomorphology* **107**:118-138.

- Gorelow A. S., P. H. Skrbac. 2005. Climate of Las Vegas, NV. National Weather Service, Las Vegas, NV.
- Guo Y., H. Zhao, X. Zuo, S. Drake, and X. Zhao. 2008. Biological soil crust development and its topsoil properties in the process of dune stabilization, Inner Mongolia, China. *Environ Geol* **54**:653-662.
- Hamerlynck E. P., J. R. McAuliffe, E. V. McDonald, and S. D. Smith. 2002. Ecological responses of two Mojave Desert shrubs to soil horizon development and soil water dynamics. *Ecology* **83**:768-779.
- Harper K. T., J. Belnap. 2001. The influence of biological soil crusts on mineral uptake by associated vascular plants. *Journal of Arid Environments* **47**:347-357.
- Hilty J. H., D. J. Eldridge, R. Rosentreter, M. C. Wicklow-Howard, and M. Pellant. 2004. Recovery of biological soil crusts following wildfire in Idaho. *Journal of Range Management* **57**:89-96.
- Holmgren M., M. Scheffer, and M. A. Huston. 1997. The interplay of facilitation and competition in plant communities. *Ecology* **78**:1966-1975.
- Housman D. C., H. H. Powers, A. D. Collins, and J. Belnap. 2006. Carbon and nitrogen fixation differ between successional stages of biological soil crusts in the Colorado Plateau and Chihuahuan Desert. *Journal of Arid Environments* **66**:620-634.
- Housman D. C., C. M. Yeager, B. J. Darby, J. Sanford R.L., C. R. Kuske, D. A. Neher, and J. Belnap. 2007. Heterogeneity of soil nutrients and subsurface biota in a dryland ecosystem. *Soil Biology & Biochemistry* **39**:2138-2149.
- Howes D. A., A. D. Abrahams. 2003. Modeling runoff and runoff in a desert shrubland ecosystem, Jornada Basin, New Mexico. *Geomorphology* **53**:45-73.
- IPCC. 2007. IPCC Fourth Assessment Report: Climate Change. Accessed online at www.ipcc.ch.
- Issa O. M., C. Defarge, J. Trichet, C. Valentin, and J. L. Rajot. 2009. Microbiotic soil crusts in the Sahel of Western Niger and their influence on soil porosity and water dynamics. *Catena* **77**:48-55.
- Issa O. M., J. Trichet, C. Defarge, A. Coute, and C. Valentin. 1999. Morphology and microstructure of microbiotic soil crusts on a tiger bush sequence (Niger, Sahel). *Catena* **37**:175-196.
- Johnson S. L., S. Neuer, and F. Garcia-Pichel. 2007. Export of nitrogenous compounds due to incomplete cycling within biological soil crusts of arid lands. *Environmental Microbiology* **9**:680-689.

- Johnson S. L., C. R. Budinoff, J. Belnap, and F. Garcia-Pichel. 2005. Relevance of ammonium oxidation within biological soil crust communities. *Environmental Microbiology* **7**:1-12.
- Kidron G. J., I. Herrnsstadt, and E. Barzilay. 2002. The role of dew as a moisture source for sand microbiotic crusts in the Negev Desert, Israel. *Journal of Arid Environments* **52**:517-533.
- Kidron G. J., A. Vonshak, I. Dor, S. Barinova, and A. Abeliovich. 2010. Properties and spatial distribution of microbiotic crusts in the Negev Desert, Israel. *Catena* **82**:92-101.
- Kieft T. L., C. S. White, S. R. Loftin, R. Aguilar, J. A. Craig, and D. A. Skaar. 1998. Temporal dynamics in soil carbon and nitrogen resources at a grassland-shrubland ecotone. *Ecology* **79**:671-683.
- Kleiner E. F., K. T. Harper. 1977. Soil properties in relation to cryptogamic groundcover in Canyonlands National Park. *Journal of Range Management* **30**:202-205.
- Knapp A. K., C. Beier, D. D. Briske, A. T. Classen, Y. Luo, M. Reichstein, M. D. Smith, S. D. Smith, J. E. Bell, P. A. Fay, J. L. Heisler, S. W. Leavitt, R. Sherry, B. Smith, and E. Weng. 2008. Consequences of more extreme precipitation regimes for terrestrial ecosystems. *BioScience* **58**:1-11.
- Knapp P. A. 1998. Spatio-temporal patterns of large grassland fires in the intermountain west, U.S.A. *Global Ecology and Biogeography Letters* **7**:259-272.
- Lajtha K., W. H. Schlesinger. 1988. The biogeochemistry of phosphorus cycling and phosphorus availability along a desert soil chronosequence. *Ecology* **69**:24-39.
- Lajtha K., W. H. Schlesinger. 1986. Plant response to variations in nitrogen availability in a desert shrubland community. *Biogeochemistry* **2**:29-37.
- Li J., G. S. Okin, L. Alvarez, and H. Epstein. 2008. Effects of wind erosion on the spatial heterogeneity of soil nutrients in two desert grassland communities. *Biogeochemistry* **88**:73-88.
- Li J., C. Zhao, H. Zhu, Y. Li, and F. Wang. 2007. Effect of plant species on shrub fertile island at an oasis-desert ecotone in the South Junggar Basin, China. *Journal of Arid Environments* **71**:350-361.
- Li X. J., X. R. Li, W. M. Song, Y. P. Gao, J. G. Zheng, and R. L. Jia. 2008. Effects of crust and shrub patches on runoff, sedimentation, and related nutrient (C, N) redistribution in the desertified steppe zone of the Tengger Desert, Northern China. *Geomorphology* **96**:221-232.

- Li X. R., X. H. Jia, L. Q. Long, and S. Zerbe. 2005. Effects of biological soil crusts on seed bank, germination and establishment of two annual plant species in the Tengger Desert (N China). *Plant and Soil* **277**:375-385.
- Li X. Y., L. Y. Liu, and J. H. Wang. 2004. Wind tunnel simulation of aeolian sandy soil erodibility under human disturbance. *Geomorphology* **59**:3-11.
- Maestre F. T., M. A. Bowker, C. Escolar, M. D. Puche, S. Solivares, S. Maltez-Mouro, P. Garcia-Palacios, A. P. Castillo-Monroy, I. Martinez, and A. Escudero. 2010. Do biotic interactions modulate ecosystem functioning along stress gradients? Insights from semi-arid plant and biological soil crust communities. *Phil. Tran. R. Soc. B.* **365**:2057-2070.
- Marsh J., S. Nouvet, P. Sanborn, and D. Coxson. 2006. Composition and function of biological soil crust communities along topographic gradients in grasslands of central British Columbia (Chilcotin) and southwestern Yukon (Kluane). *Canadian Journal of Botany* **84**:717-736.
- Martinez-Meza E., W. G. Whitford. 1996. Stemflow, throughfall and channelization of stemflow by roots in three Chihuahuan desert shrubs. *Journal of Arid Environments* **32**:271-287.
- McBride M. B. 1994. *Environmental Chemistry of Soils*. Oxford University Press, New York, New York.
- McFadden L. D., S. G. Wells, and M. J. Jercinovich. 1987. Influences of eolian and pedogenic processes on the origin and evolution of desert pavements. *Geology* **15**:504-508.
- McFadden L. D., S. G. Wells, and J. C. Dohrenwend. 1986. Influences of Quaternary climatic changes on processes of soil development on desert loess deposits of the Cima Volcanic Field, California. *Catena* **13**:361-389.
- McKenna Neuman C., C. Maxwell. 2002. Temporal aspects of the abrasion of microphytic crusts under grain impact. *Earth Surface Processes and Landforms* **27**:891-908.
- McKenna Neuman C., C. D. Maxwell, and J. W. Boulton. 1996. Wind transport of sand surfaces crusted with photoautotrophic microorganisms. *Catena* **27**:229-247.
- McTainsh G., C. Strong. 2007. The role of aeolian dust in ecosystems. *Geomorphology* **89**:39-54.
- Meadows D. G., M. H. Young, and E. V. McDonald. 2008. Influence of relative surface age on hydraulic properties and infiltration on soils associated with desert pavements. *Catena* **72**:169-178.

- Merkler D., Drohan P.J. and M. Sappington. 2005 Spatial and temporal variation of solar insolation over landscapes as a tool for mapping soils in the field. SSSA, International Meeting.
- Monger H. C., B. T. Bestelmeyer. 2006. The soil-geomorphic template and biotic change in arid and semi-arid ecosystems. *Journal of Arid Environments* **65**:207-218.
- Munson S. M., J. Belnap, G. S. Okin, and G. S. Okin. 2011. Responses of wind erosion to climate-induced vegetation changes on the Colorado Plateau. *Proceedings of the National Academy of Sciences* (available online).
- Musick H. B. 1975. Barrenness of desert pavement in Yuma County, Arizona. *Journal of the Arizona Academy of Science* **10**:24-28.
- Neff J. C., R. L. Reynolds, J. Belnap, and P. Lamothe. 2005. Multi-decadal impacts of grazing on soil physical and biogeochemical properties in southeastern Utah. *Ecological Applications* **15**:87-95.
- Noy-Meir I. 1973. Desert ecosystems: Environment and producers. *Annual Review of Ecology and Systematics* **4**:25-51.
- Okin G. S., D. A. Gillette, and J. E. Herrick. 2006. Multi-scale controls on and consequences of aeolian processes in landscape change in arid and semi-arid environments. *Journal of Arid Environments* **65**:253-275.
- Okin G. S., B. Murray, and W. H. Schlesinger. 2001. Degradation of sandy arid shrubland environments: observations, process modelling, and management implications. *Journal of Arid Environments* **47**:123-144.
- Parsons A. J., J. Wainwright, W. H. Schlesinger, and A. D. Abrahams. 2003. The role of overland flow in sediment and nitrogen budgets of mesquite dunefields, southern New Mexico. *Journal of Arid Environments* **53**:61-71.
- Peterson FF. 1981. Landforms of the Basin and Range, Defined for Soil Survey. UNR Max C.Fleishmann College of Agriculture, Nevada Agricultural Experiment Station; Technical Bulletin 28. 52 pp. Reno, NV.
- Puigdefábregas J. 2005. The role of vegetation patterns in structuring runoff and sediment fluxes in drylands. *Earth Surface Processes and Landforms* **30**:133-147.
- Quade J. 2001. Desert pavements and associated rock varnish in the Mojave Desert: How old can they be? *Geology* **29**:855-858.
- Rao L. E., E. B. Allen. 2010. Combined effects of precipitation and nitrogen deposition on native and invasive winter annual production in California deserts. *Oecologia* **162**:1035-1046.

- Ravi S., P. D'Odorico, T. E. Huxman, and S. L. Collins. 2010. Interactions Between Soil Erosion Processes and Fires: Implications for the Dynamics of Fertility Islands. *Rangeland Ecol. Manage.* **63**:267-274.
- Ravi S., P. D'Odorico, T. M. Zobeck, T. M. Over, and S. L. Collins. 2007. Feedbacks between fires and wind erosion in heterogeneous arid lands. *Journal of Geophysical Research* **112**:G04007.
- Ravi S., P. D'Odorico, L. Wang, C. S. White, G. S. Okin, S. A. Macko, and S. L. Collins. 2009. Post-Fire Resource Redistribution in Desert Grasslands: A Possible Negative Feedback on Land Degradation. *Ecosystems* **12**:434-444.
- Reheis M. C. 1990. Influence of climate and eolian dust on the major-element chemistry and clay mineralogy of soils in the northern Bighorn Basin, U.S.A. *Catena* **17**:219-248.
- Reheis M. C., J. R. Budahn, and P. J. Lamothe. 2002. Geochemical evidence for diversity of dust sources in the southwestern United States. *Geochimica et Cosmochimica Acta* **66**:1569-1587.
- Reynolds R., J. Neff, M. Reheis, and P. Lamothe. 2006. Atmospheric dust in modern soil on aeolian sandstone, Colorado Plateau (USA): Variation with landscape position and contribution to potential plant nutrients. *Geoderma* **130**:108-123.
- Reynolds R., J. Belnap, M. C. Reheis, P. J. Lamothe, and F. Luiszer. 2001. Aeolian dust in Colorado Plateau soils: Nutrient inputs and recent change in source. *PNAS* **98**:7123-7127.
- Ridolfi L., F. Laio, and P. D'Odorico. 2008. Fertility island formation and evolution in dryland ecosystems. *Ecology and Society* **13**:1-13.
- Rietkerk M., S. C. Dekker, P. C. de Ruiter, and J. van de Koppel. 2004. Self-organized patchiness and catastrophic shifts in ecosystems. *Science* **305**:1926-1929.
- Ritchie J. C., J. E. Herrick, and C. A. Ritchie. 2003. Variability in soil redistribution in the northern Chihuahuan Desert based on ¹³⁷Cesium measurements. *Journal of Arid Environments* **55**:737-746.
- Robinson B. S., S. S. Bamforth, and P. J. Dobson. 2002. Density and diversity of protozoa in some arid Australian soils. *J. Eukaryot. Microbiol.* **49**:449-453.
- Schlesinger W. H., A. M. Pilmanis. 1998. Plant-soil interactions in deserts. *Biogeochemistry* **42**:169-187.

- Schlesinger W. H., C. S. Jones. 1984. The comparative importance of overland runoff and mean annual rainfall to shrub communities of the Mojave Desert. *Bot. Gaz.* **145**:116-124.
- Schlesinger W. H., J. A. Raikes, A. E. Hartley, and A. F. Cross. 1996. On the spatial pattern of soil nutrients in desert ecosystems. *Ecology* **77**:364-374.
- Schlesinger W. H., J. F. Reynolds, G. L. Cunningham, L. F. Huenneke, W. M. Jarrell, R. A. Virginia, and W. G. Whitford. 1990. Biological feedbacks in global desertification. *Science* **247**:1043-1048.
- Schoeneberger P. J., D. A. Wysocki, E. C. Benham, and W. D. Broderson. 2002. Field book for describing and sampling soils, Version 2.0. Natural Resources Conservation Service, National Soil Survey Center, Lincoln, NE.
- Schwinning S., O. E. Sala, M. E. Loik, and J. R. Ehleringer. 2004. Thresholds, memory, and seasonality: understanding pulse dynamics in arid/semi-arid ecosystems. *Oecologia* **141**:191-193.
- Serpe M. D., J. M. Orm, T. Barkes, and R. Rosentreter. 2006. Germination and seed water status of four grasses on moss-dominated biological soil crusts from arid lands. *Plant Ecology* **185**:163-178.
- Shachak M., G. M. Lovett. 1998. Atmospheric deposition to a desert ecosystem and its implications for management. *Ecological Applications* **8**:455-463.
- Simonson R. W. 1995. Airborne dust and its significance to soils. *Geoderma* **65**:1-43.
- Smith S. D., T. E. Huxman, S. F. Zitzer, T. N. Charlet, D. C. Housman, J. S. Coleman, L. K. Fenstermaker, J. R. Seemann, and R. S. Nowak. 2000. Elevated CO₂ increases productivity and invasive species success in an arid ecosystem. *Nature* **408**:79-82.
- Soil Survey Staff. 2010. Keys to Soil Taxonomy. USDA-NRCS, Washington, D.C.
- Souza-Egipsy V., J. Wierzchos, C. Sancho, A. Belmonte, and C. Ascaso. 2004. Role of biological soil crust cover in bioweathering and protection of sandstones in a semi-arid landscape (Torrollones de Gabarda, Huesca, Spain). *Earth Surface Processes and Landforms* **29**:1651-1661.
- Spivey S. 2008. Off-road fans, critics face off. *Las Vegas Review-Journal*. March 18, 2008, Section 10B.
- Stavi I., H. Lavee, E. D. Ungar, and P. Sarah. 2009. Ecogeomorphic feedbacks in semiarid rangelands: A review. *Pedosphere* **19**:217-229.

- Stohlgren T. J., Y. Otsuki, C. A. Villa, M. Lee, and J. Belnap. 2001. Patterns of plant invasions: a case example in native species hotspots and rare habitats. *Biological Invasions* **3**:37-50.
- Su Y. G., X. R. Li, Y. W. Cheng, H. J. Tan, and R. L. Jia. 2007. Effects of biological soil crusts on emergence of desert vascular plants in North China. *Plant Ecology* **191**:11-19.
- Thomas A. D., A. J. Dougill. 2007. Spatial and temporal distribution of cyanobacterial soil crusts in the Kalahari: Implications for soil surface properties. *Geomorphology* **85**:17-29.
- Thomas A. D., A. J. Dougill. 2006. Distribution and characteristics of cyanobacterial soil crusts in the Molopo Basin, South Africa. *Journal of Arid Environments* **64**:270-283.
- Thompson D. B., L. R. Walker, F. H. Landau, and L. R. Stark. 2005. The influence of elevation, shrub species, and biological soil crust on fertile islands in the Mojave Desert, USA. *Journal of Arid Environments* **61**:609-629.
- Thompson T. L., E. Zaady, P. Huancheng, T. B. Wilson, and D. A. Martens. 2006. Soil C and N pools in patchy shrublands of the Negev and Chihuahuan Deserts. *Soil Biology & Biochemistry* **38**:1943-1955.
- Titus J. H., R. S. Nowak, and S. D. Smith. 2002. Soil resource heterogeneity in the Mojave Desert. *Journal of Arid Environments* **52**:269-292.
- Verrecchia E. P., A. Yair, G. J. Kidron, and K. Verrecchia. 1995. Physical properties of the psammophile cryptogamic crust and their consequences to the water regime of sandy soils, north-western Negev Desert, Israel. *Journal of Arid Environments* **29**:427-437.
- Veste M., T. Littmann, S. W. Breckle, and A. Yair. 2001. The role of biological soil crusts on desert sand dunes in the northwestern Negev, Israel. Pages 357-367 *In* S. W. Breckle, M. Veste, and W. Wucherer, editors. *Sustainable Land-Use in Deserts*, Springer, Berlin.
- Walker L. R., D. B. Thompson, and F. H. Landau. 2001. Experimental manipulations of fertile islands and nurse plant effects in the Mojave Desert, USA. *Western North American Naturalist* **61**:25-35.
- Wells S. G., L. D. McFadden, and J. C. Dohrenwend. 1987. Influence of late Quaternary climatic changes on geomorphic and pedogenic processes on a desert piedmont, eastern Mojave Desert, California. *Quaternary Research* **27**:130-146.

- Whitford W. G., J. Anderson, and P. M. Rice. 1997. Stemflow contribution to the „fertile island’ effect in creosotebush, *Larrea tridentata*. *Journal of Arid Environments* **35**:451-457.
- Wood Y. A., R. C. Graham, and S. G. Wells. 2005. Surface control of desert pavement pedologic process and landscape function, Cima Volcanic field, Mojave Desert, California. *Catena* **59**:205-230.
- Yair A. 1990. Runoff generation in a sandy area - the Nizzana Sands, Western Negev, Israel. *Earth Surface Processes and Landforms* **15**:597-609.
- Young M. H., E. V. McDonald, T. G. Caldwell, S. G. Benner, and D. G. Meadows. 2004. Hydraulic properties of a desert soil chronosequence in the Mojave Desert, USA. *Vadose Zone Journal* **3**:956-963.
- Zaady E., Z. Y. Offer. 2010. Biogenic soil crusts and soil depth: a long-term case study from the Central Negev desert highland. *Sedimentology* **57**:351-358.
- Zaady E., A. Bouskila. 2002. Lizard burrows association with successional stages of biological soil crusts in an arid sandy region. *Journal of Arid Environments* **50**:235-246.
- Zaady E., Z. Y. Offer, and M. Shachak. 2001. The content and contributions of deposited aeolian organic matter in a dry land ecosystem of the Negev Desert, Israel. *Atmospheric Environment* **35**:769-776.
- Zaady E., P. M. Groffman, and M. Shachak. 1996. Litter as a regulator of N and C dynamics in macrophytic patches in Negev Desert soils. *Soil Biol. Biochem.* **28**:39-46.



Figure 4.1: (A) Smooth cyanobacteria crusts have slightly darkened surfaces where the sticky sheaths of filamentous cyanobacteria have captured and cemented dust (arrow, scale 1 cm). This crusting is usually visible to the naked eye. (B) Cyanobacterial crusts form smooth, light colored surfaces between shrubs (scale 1 m).

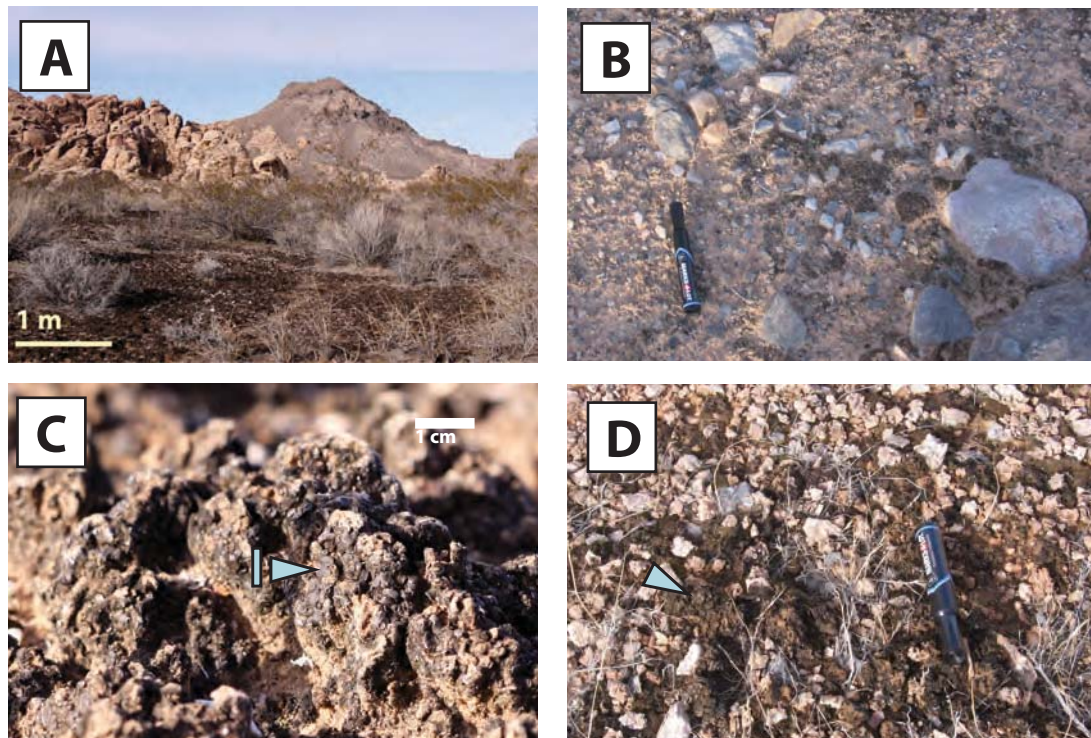


Figure 4.2: (A) Moss-lichen crusts have dark, rough surfaces that protect shrub interspaces from erosion (scale 1 m). (B) Short moss-lichen crusts are common in recent Holocene inset fans and have low surface relief, up to 2 cm (marker for scale). (C) Tall moss-lichen pinnaced crusts are composed of complex matrices of mosses, lichens, cyanobacteria, and sediments. Squamulose lichens (l) dominate this crust (scale 1 cm). (D) Tall moss-lichen pinnacles (arrow) grow between desert pavement clasts along this alluvial surface (marker for scale).

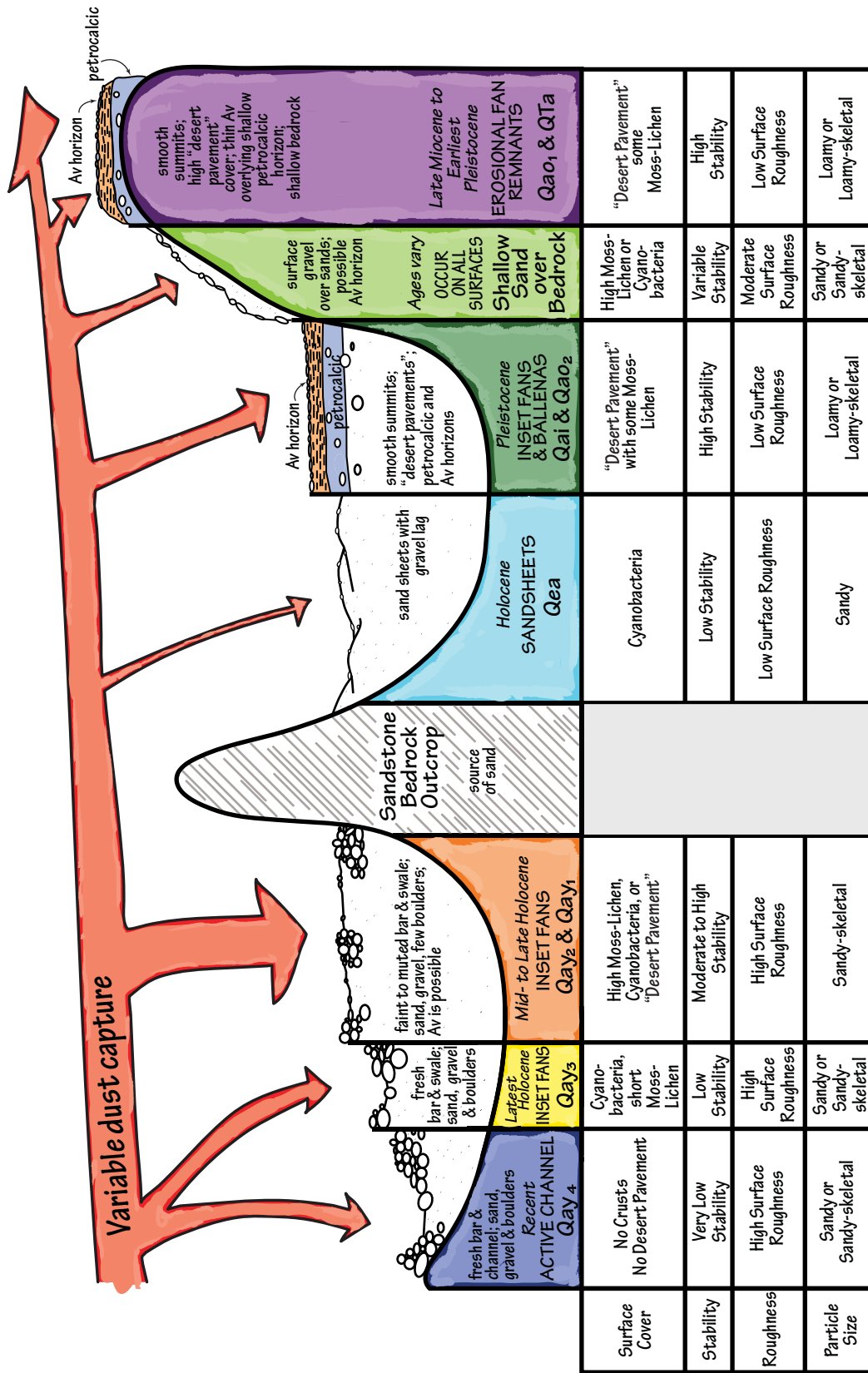


Figure 4.3: BSC and desert pavement cover (row 1) as a function of geomorphic stability (row 2), surface roughness (row 3), inferred dust capture (arrows) and soil particle size control (row 4)(see Chapter 3). Sandstone bedrock outcrops throughout the study area.

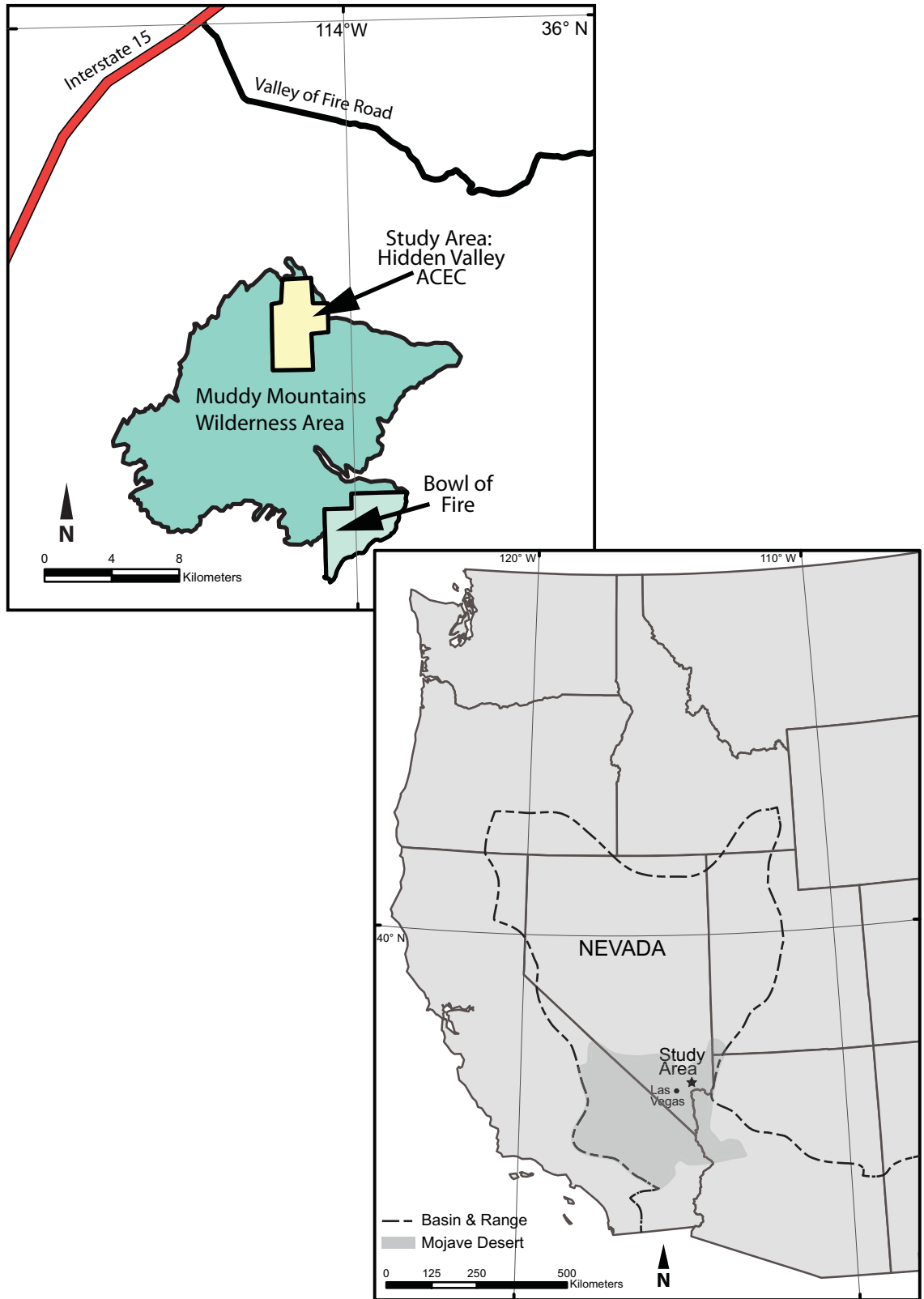


Figure 4.4: The study area is located within the Hidden Valley Area of Critical Environmental Concern of the Muddy Mountains Wilderness Area, Nevada, U.S.A.

Hidden Valley, Muddy Mountains Wilderness Area, NV (NAIP Imagery)

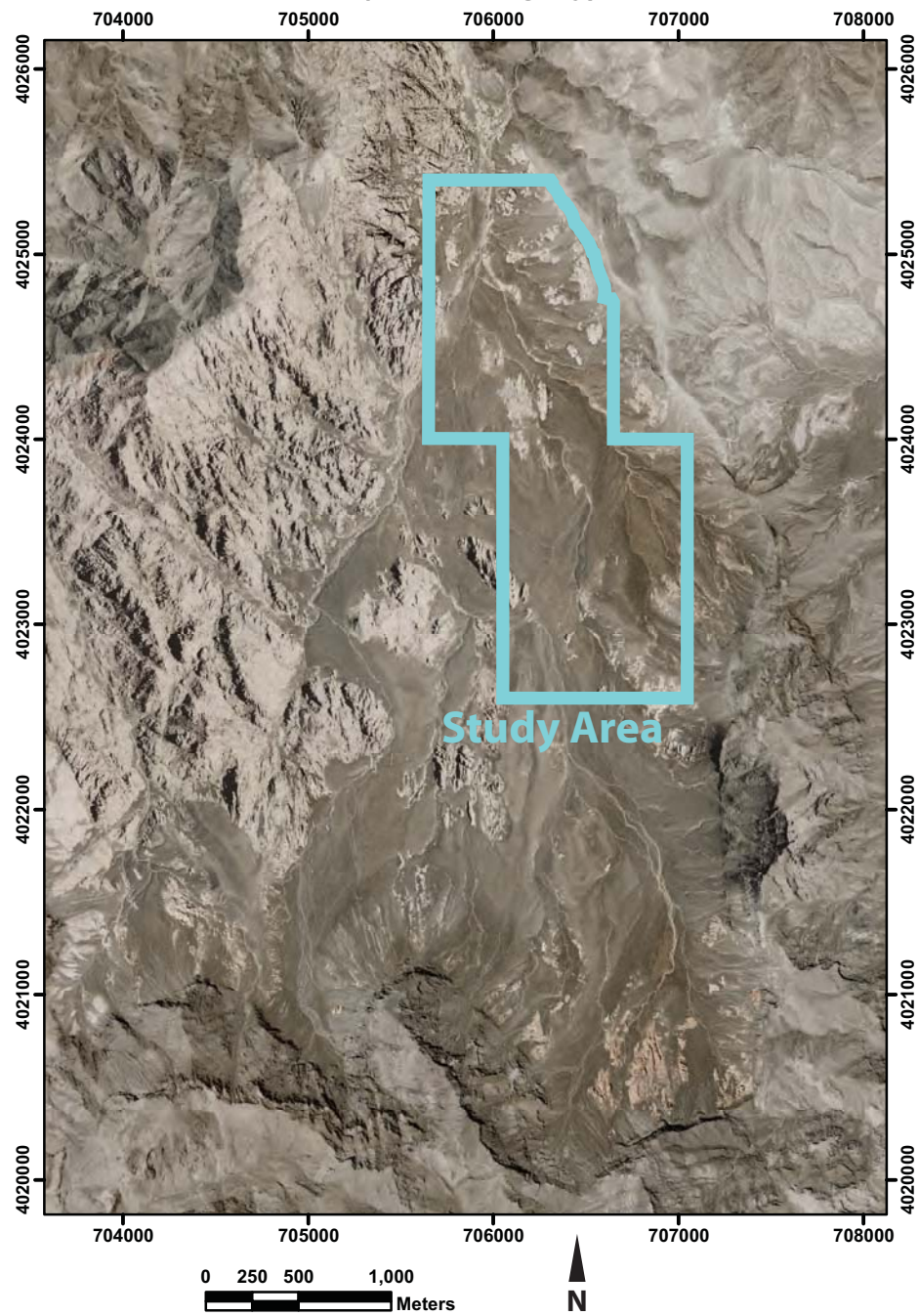


Figure 4.5: Hidden Valley is a semi-enclosed basin in the Muddy Mountains Wilderness Area, NV (USA). Data were collected within study area outlined in turquoise.

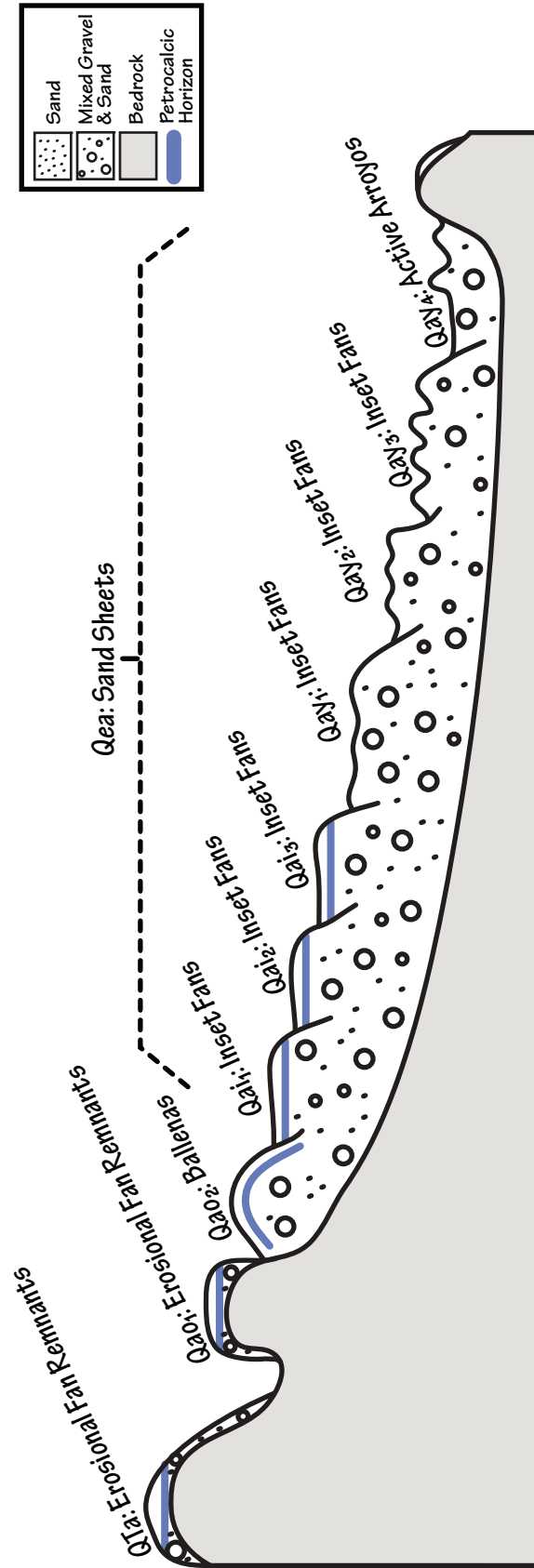
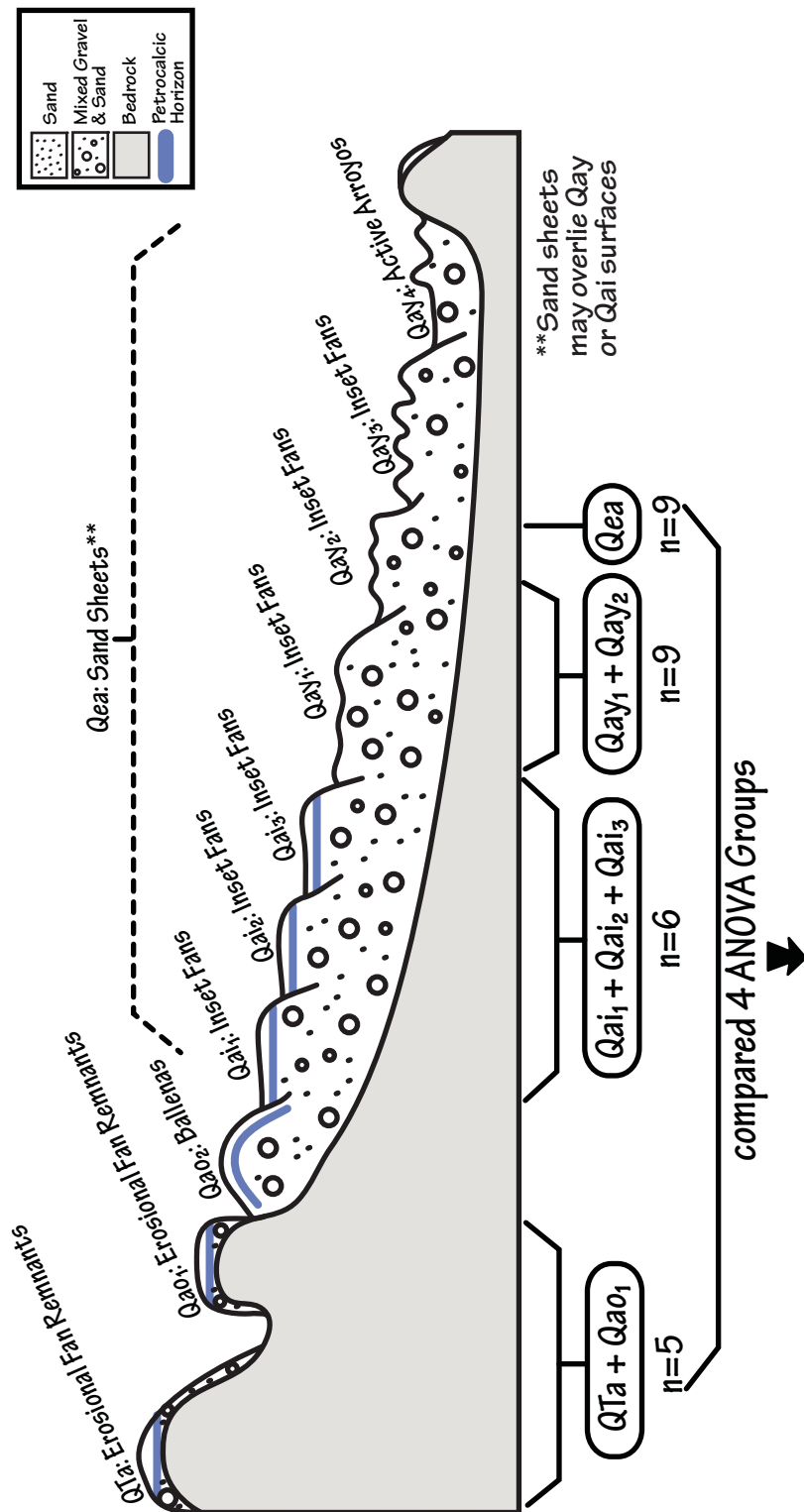


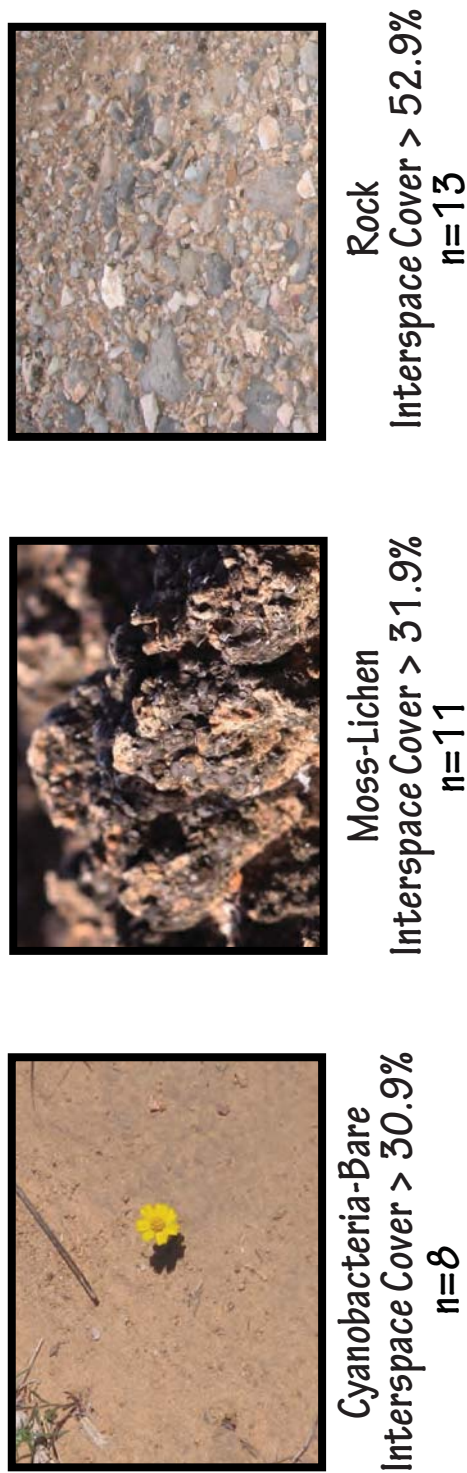
Figure 4.6: A cross-section summarizes geomorphic surfaces found within the mapping subregion of Hidden Valley. Bedrock underlies all surfaces outcrops as inselbergs throughout the valley. Surfaces range in age from Late Miocene or earliest Pleistocene to recent. Most surfaces are formed in alluvium; however, Qea sand sheets may overlie Qai or Qay surfaces. Colluvium is not shown in this cross-section, but may occur below the cliff faces surrounding the valley.



Comparisons of Surface Characteristics from Canopies and Interspaces:

vascular plant canopy cover; cyanobacteria crust, moss, *Collema* lichen, *Placidium* lichen, *Peltula* lichen, bare soil, limestone clasts, sandstone clasts, petrocalcic clasts, *Bromus* exotic grass litter, non-grass plant litter, moss-lichen crusts, total BSCs, bare-cyanobacteria, total rocks, clay, silt, very fine sand, fine sand, sand, total sand, K, Ca, Fe, Mg, B, Mn, Cu, Zn, Mo, Ni, NO₃, SO₄, Cl, extractable P, total S, total N, total C, inorganic C, organic C, carbonate, pH, EC, seasonal solar insolation, maximum pinnacle height

Figure 4.7: Parametric and non-parametric ANOVAs compared differences in soil characteristics from point counts, line intercept data, metadata, and solar insolation analyses. Differences were calculated from among four groups of geomorphic surfaces, including QTa + Qao1, all Qai surfaces, Qay1 + Qay2, and Qea. Plots from other geomorphic surfaces were not included in these analyses.

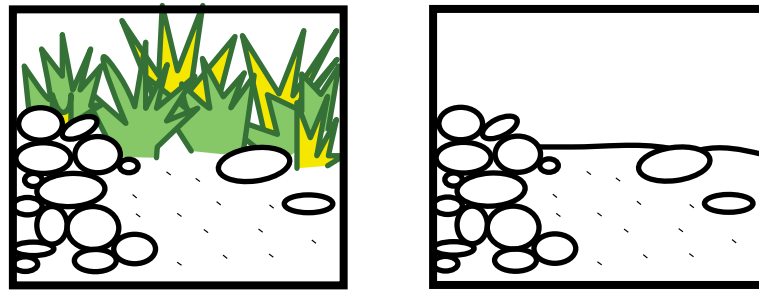


3 ANOVA Groups compare mean and median values

Comparisons of Surface Characteristics from Interspaces:
 adjacent vascular plant canopy cover; cyanobacteria crust, moss, *Collema* lichen, *Placidium* lichen, *Peltula* lichen, bare soil, limestone clasts, sandstone clasts, petrocalcic clasts, *Bromus* exotic grass litter, non-grass plant litter, moss-lichen crusts, total BSCs, bare-cyanobacteria, total rocks, clay, silt, very fine sand, fine sand, total sand, K, Ca, Na, Fe, Mg, B, Mn, Cu, Zn, Mo, Ni, NO₃, SO₄, Cl, extractable P, total S, total N, total C, inorganic C, organic C, carbonate, pH, EC, seasonal solar insolation, maximum pinnacle height

Figure 4.8: Parametric and non-parametric ANOVAs compared differences in mean/median values of interspace soil characteristics from point counts, line intercept data, metadata, and solar insolation analyses for three interspace cover classes. For these analyses, plots were classified as having >30.9% cyanobacteria-bare interspace cover (cover by cyanobacteria crusts and bare soil), > 31.9% moss-lichen interspace cover, and >52.9% rock interspace cover. Plots could come from any geomorphic surface. Those plots that did not fall into one of these categories were removed from the analyses.

Exotic *Bromus* Grass Cover Classes



High *Bromus*
Interspace Cover > 14%
n=8

Low *Bromus*
Interspace Cover < 5%
n=11

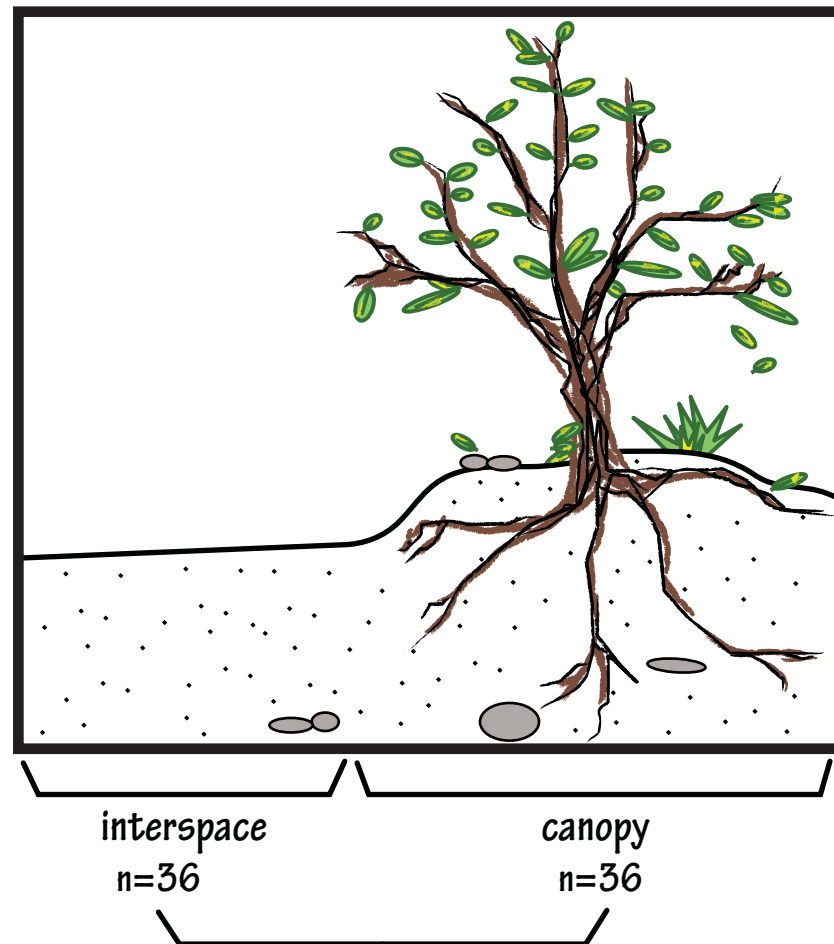
t-tests compared mean and median values of
interspace characteristics for 2 groups



Comparisons of Surface Characteristics from Interspaces:

adjacent vascular plant canopy cover; cyanobacteria crust, moss, *Collema* lichen, *Placidium* lichen, *Peltula* lichen, bare soil, limestone clasts, sandstone clasts, petrocalcic clasts, *Bromus* exotic grass litter, non-grass plant litter, moss-lichen crusts, total BSCs, bare-cyanobacteria, total rocks, clay, silt, very fine sand, fine sand, sand, total sand, K, Na, Ca, Fe, Mg, B, Mn, Cu, Zn, Mo, Ni, NO₃, SO₄, Cl, extractable P, total S, total N, total C, inorganic C, organic C, carbonate, pH, EC, seasonal solar insolation, maximum pinnacle height

Figure 4.9: Parametric and non-parametric *t*-tests compared differences in mean and median values for interspace soil characteristics from point counts, line intercept data, metadata, and solar insolation analyses for two interspace cover classes. For these analyses, plots were classified as having >14% exotic *Bromus* grass interspace cover or <5% exotic *Bromus* grass interspace cover. Plots could come from any geomorphic surface and may occur with other surface cover types. Plots that did not fall into one of these two categories were removed from the analyses.



paired t -tests compared mean and median values of interspace vs. canopy characteristics for all plots



Comparisons of Surface Characteristics:

cyanobacteria crust, moss, *Collema* lichen, *Placidium* lichen, *Peltula* lichen, bare soil, limestone clasts, sandstone clasts, petrocalcic clasts, *Bromus* exotic grass litter, non-grass plant litter, moss-lichen crusts, total BSCs, bare-cyanobacteria, total rocks, clay, silt, very fine sand, fine sand, sand, total sand, K, Ca, Fe, Mg, B, Mn, Cu, Zn, Mo, Ni, NO_3 , SO_4 , Cl, extractable P, total S, total N, total C, inorganic C, organic C, carbonate, pH, EC

Figure 4.10: Parametric and non-parametric paired t -tests compared differences in mean and median values from point counts and physicochemical data from all shrub canopies and interspaces combined.

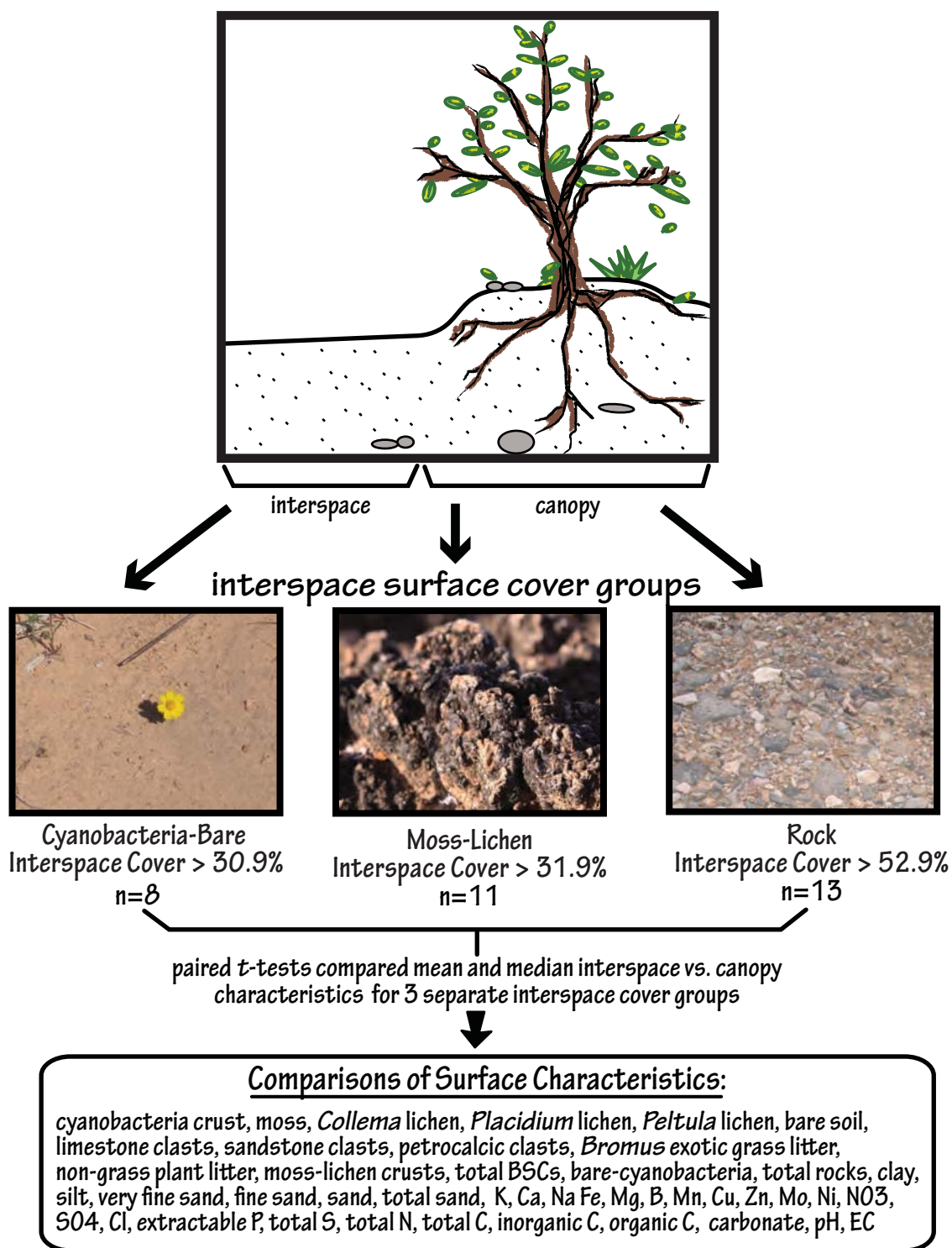


Figure 4.11: Parametric and non-parametric *t*-tests compared differences between interspace and canopy soil characteristics from point count and physicochemistry data separately for three groups. For these analyses, plots were classified as having >30.9% cyanobacteria-bare interspace cover, > 31.9% moss-lichen interspace cover, and >52.9% rock interspace cover. Plots could come from any geomorphic surface. Plots that did not fall into one of these categories were removed from the analyses.

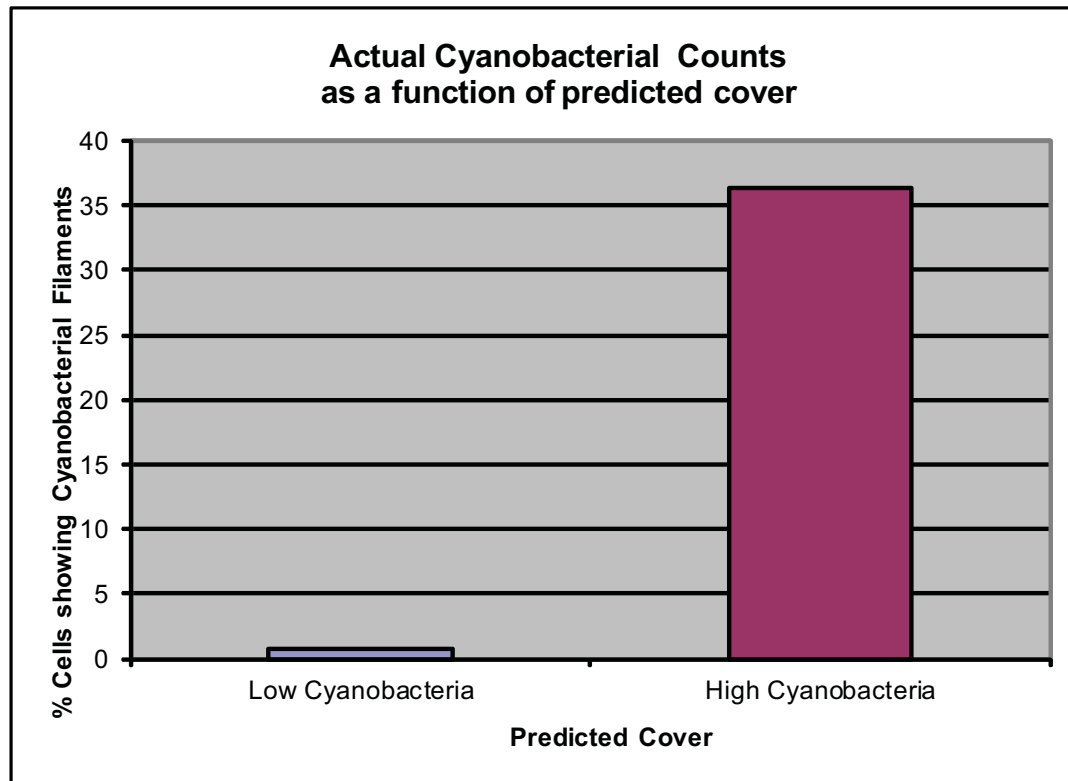


Figure 4.12: A parametric t -test indicates a significant difference in actual cyanobacteria counts between groups predicted to have low cyanobacteria and high cyanobacteria according to ocular estimates. This analysis indicates that ocular estimates of cyanobacteria presence/absence are effective.

NMS Ordination Interspace Cover and Environmental Characteristics

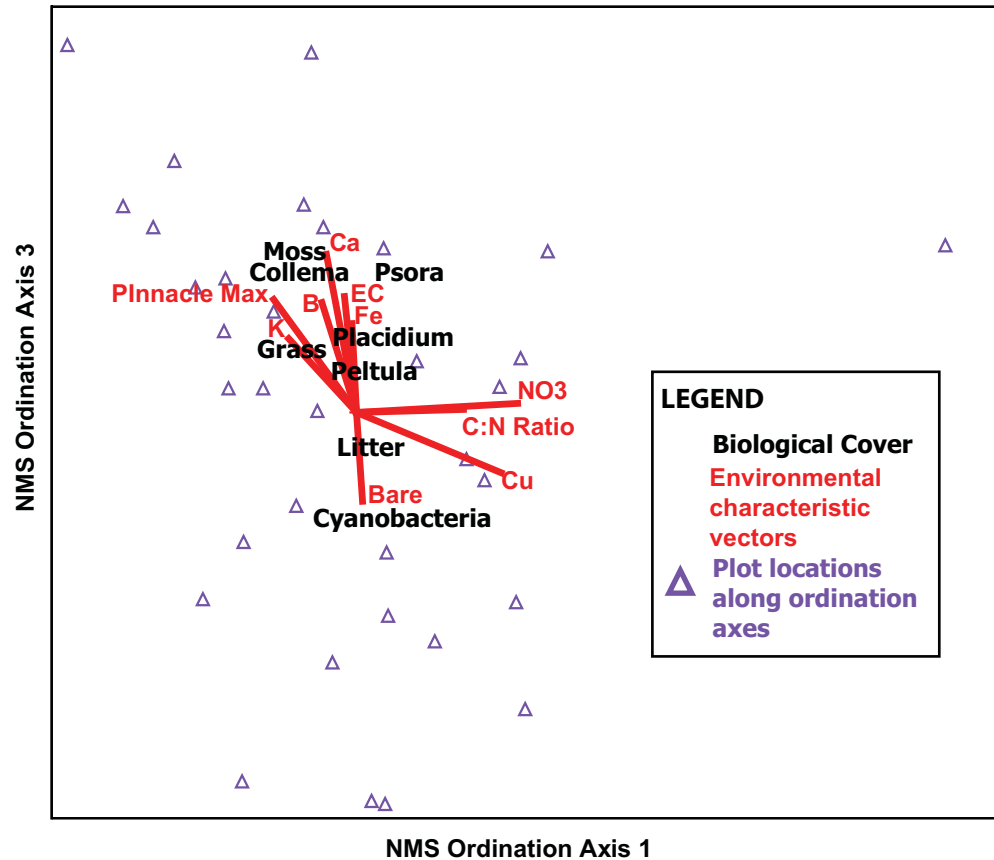


Figure 4.13: A non-metric multidimensional scaling groups plots (purple triangles) in a 3-D ordination. Two axes are shown. Plots are grouped according to similarities in interspace biological soil surface cover (black text). Biological cover types that are most commonly associated lie close together along the plot. The ordination indicates that mosses, *Collema* lichen, *Psora* lichen, *Placidium* lichen, *Peltula* lichen, and *Bromus* exotic grass are all positively associated with each other but negatively associated with non-grass plant litter and cyanobacteria. Environmental overlays are shown as vectors (red). Vectors point in the direction of those surface cover types with which they are most commonly associated. The magnitude of these relationships is indicated by the length of the vectors, with the longest lines corresponding to the strongest relationships. These vectors indicate that mosses, all lichens, and exotic *Bromus* are positively related to maximum pinnacle height, K, B, Ca, EC_e, and Fe, while non-grass plant litter and cyanobacteria are positively related to bare soil. C:N ratios and NO₃ are negatively related to all surface cover types. A positive relationship may also exist between Cu and cyanobacteria.

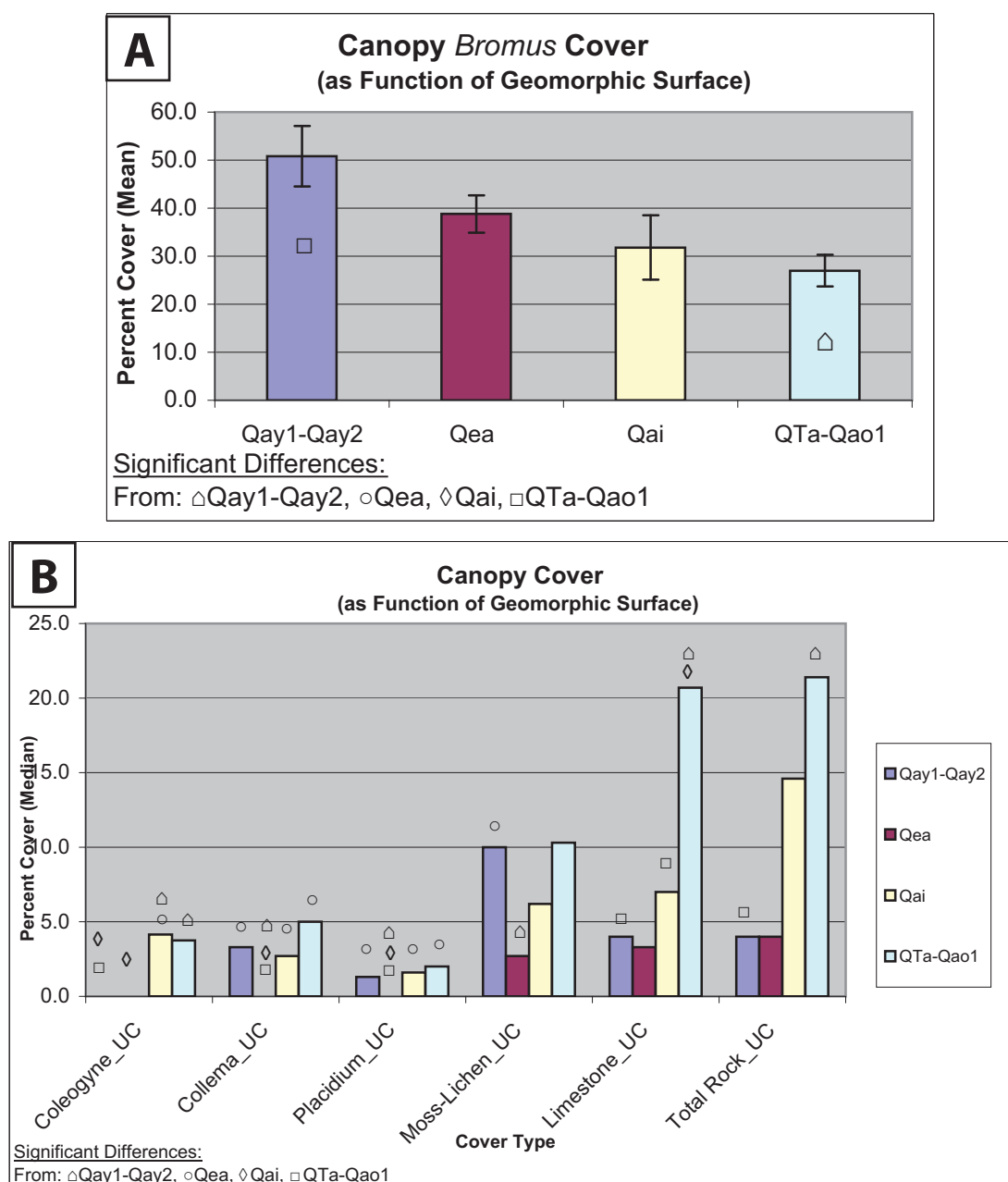


Figure 4.15: ANOVAs compare differences in canopy surface cover among various geomorphic surfaces. Significant differences are denoted by the following symbols: △ denotes significant differences from Qay1-Qay2; ○ denotes significant differences from Qea; ◇ denotes significant differences from Qai; □ denotes significant differences from QTa-Qao1. (A) Parametric ANOVA shows significant differences in mean canopy *Bromus* cover among geomorphic surfaces. Bars represent mean standard error. (B) Non-parametric ANOVAs show significant differences in median canopy *Coleogyne*, *Collema*, *Placidium*, moss-lichen, limestone, and total rock cover. (See Figure 7 for methods.)

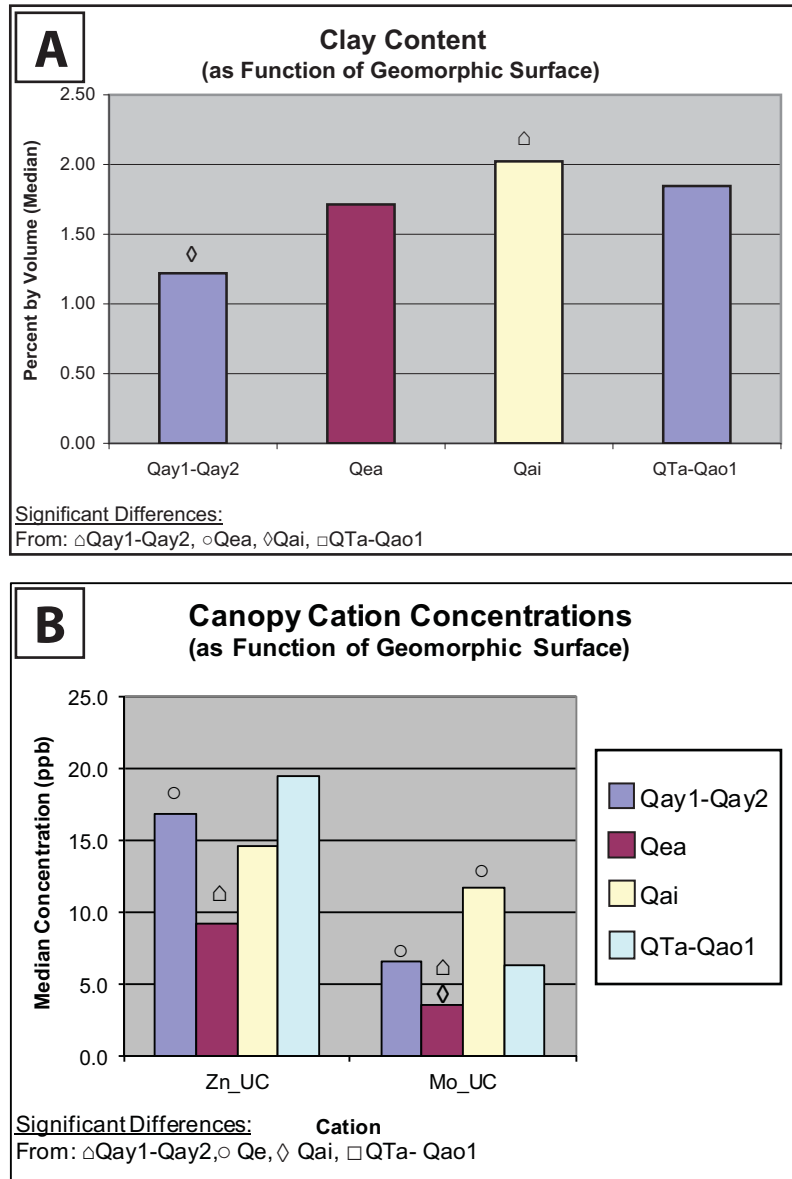


Figure 4.16: Non-parametric ANOVAs compare differences in median canopy surface texture and cations among various geomorphic surfaces. Significant differences are denoted by the following symbols: △ denotes significant differences from Qay1-Qay2; ○ denotes significant differences from Qea; ◇ denotes significant differences from Qai; □ denotes significant differences from QTa-Qao1. Non-parametric ANOVAs indicate differences in (A) canopy clay content and (B) canopy Zn and Mo concentrations. (See Figure 7 for methods.)

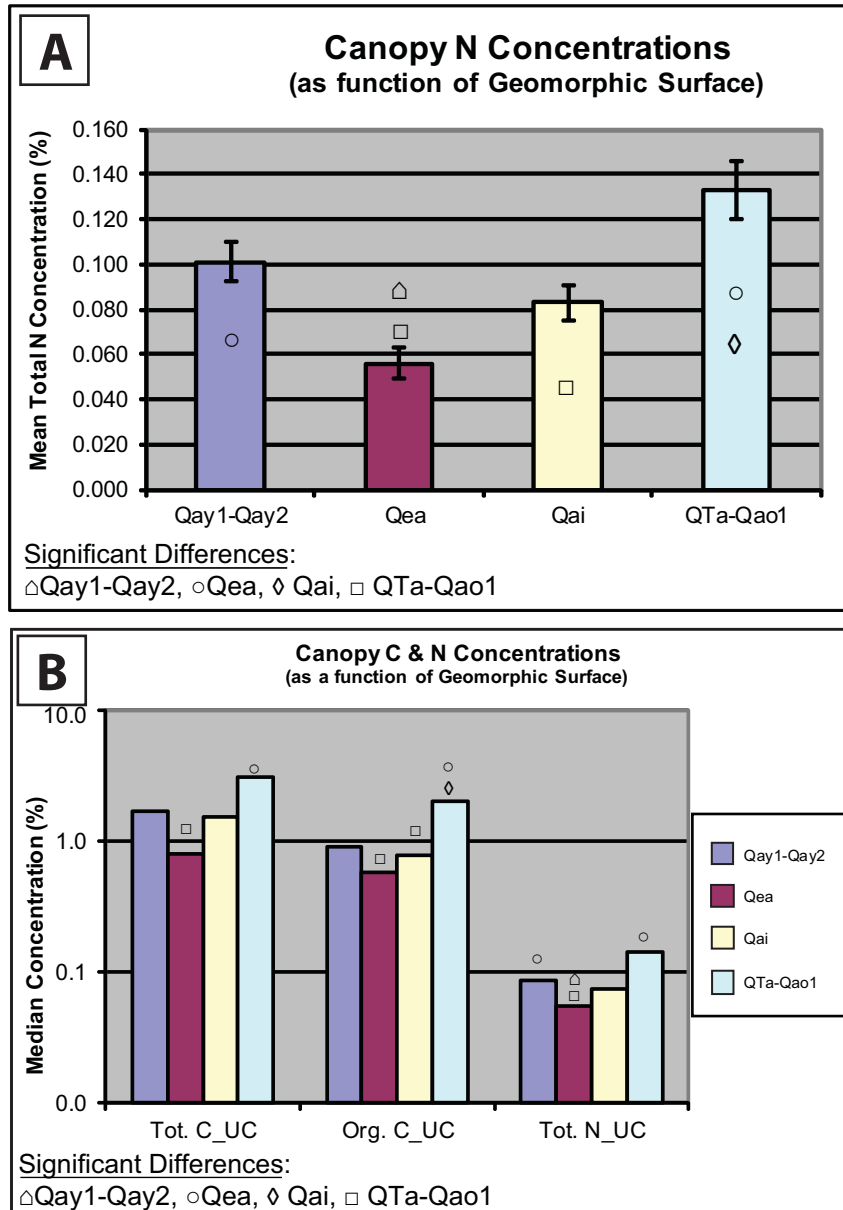


Figure 4.17: ANOVAs compare differences in canopy surface chemistry among various geomorphic surfaces. Significant differences are denoted by the following symbols: \triangle denotes significant differences from Qay1-Qay2; \circ denotes significant differences from Qea; \diamond denotes significant differences from Qai; \square denotes significant differences from QTa-Qao1. (A) Parametric ANOVA shows significant differences in mean canopy N concentrations among geomorphic surfaces. Bars represent mean standard error. (B) Non-parametric ANOVAs show significant differences in median canopy total C, organic C, and total N. (See Figure 7 for methods.)

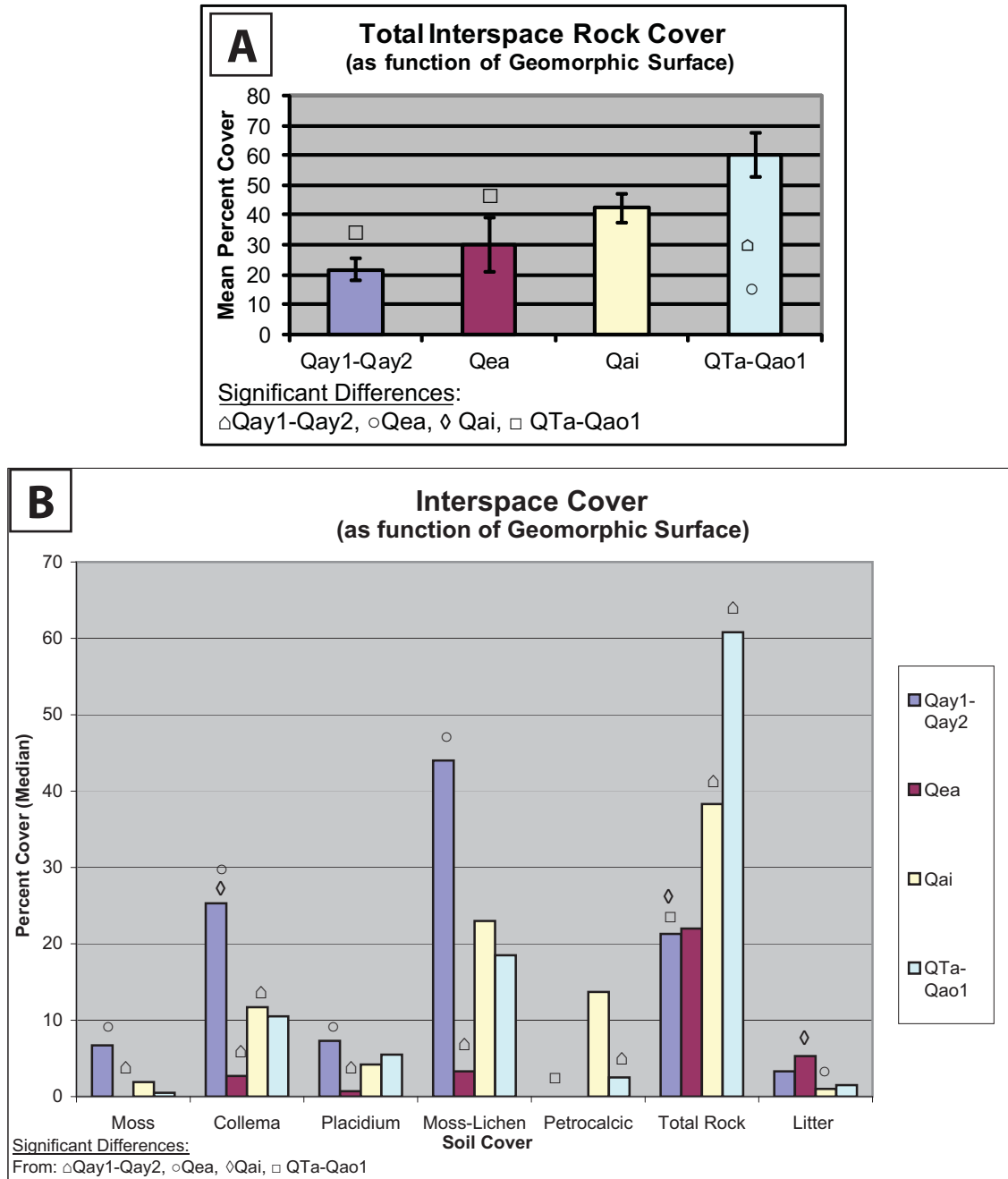


Figure 4.18: ANOVAs compare differences in interspace surface cover among various geomorphic surfaces. Significant differences are denoted by the following symbols: △ denotes significant differences from Qay1-Qay2; ○ denotes significant differences from Qea; ◇ denotes significant differences from Qai; □ denotes significant differences from QTa-Qao1. (A) Parametric ANOVA shows significant differences in mean interspace total rock cover among geomorphic surfaces. Bars reflect mean standard error. (B) Non-parametric ANOVAs show significant differences in median interspace moss, *Collema*, *Placidium*, moss-lichen, petrocalcic clast, total rock, and litter cover. (See Figure 7 for methods.)

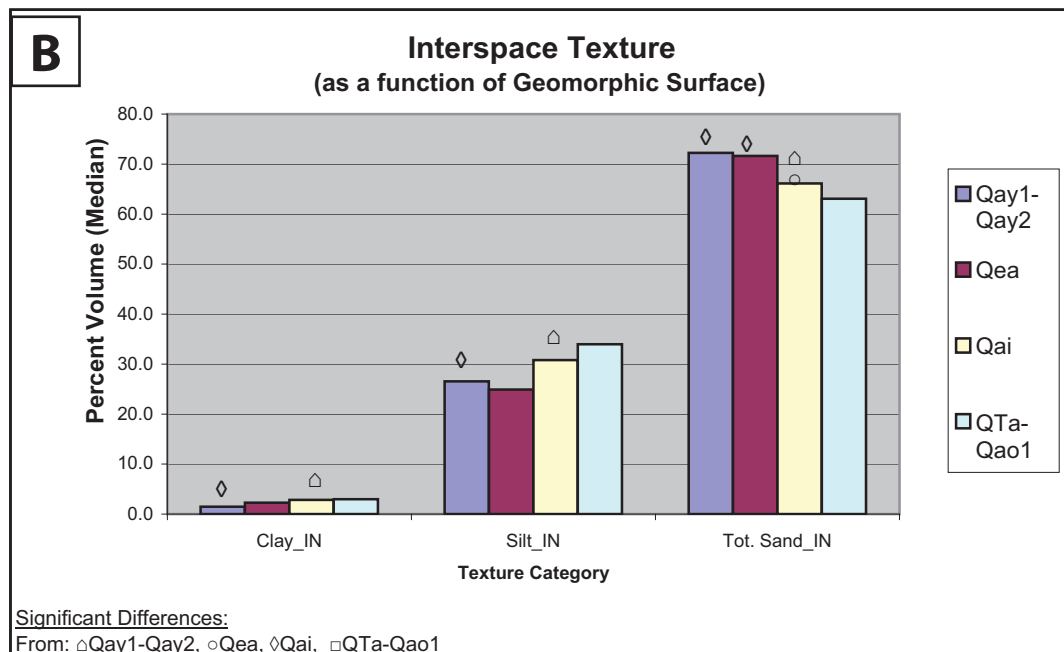
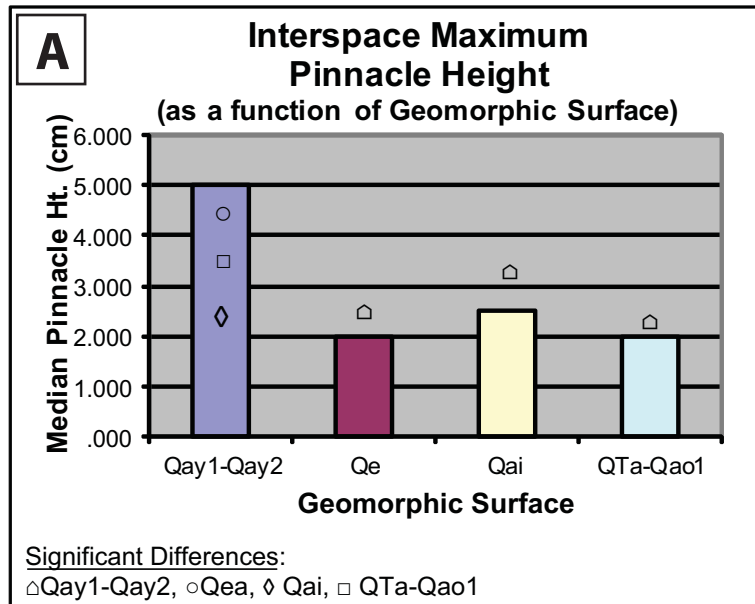


Figure 4.19: ANOVAs compare differences in interspace maximum pinnacle height and interspace texture among various geomorphic surfaces. Significant differences are denoted by the following symbols: △ denotes significant differences from Qay1-Qay2; ○ denotes significant differences from Qe; ◇ denotes significant differences from Qai; □ denotes significant differences from QTa-Qao1. (A) Non-parametric ANOVA shows significant differences in median maximum pinnacle height. Maximum pinnacle height refers to the greatest topographic microrelief found in moss-lichen pinnacles within shrub interspaces. (B) Non-parametric ANOVAs compare differences in median interspace surface clay, silt, and total sand content. (See Figure 7 for methods.)

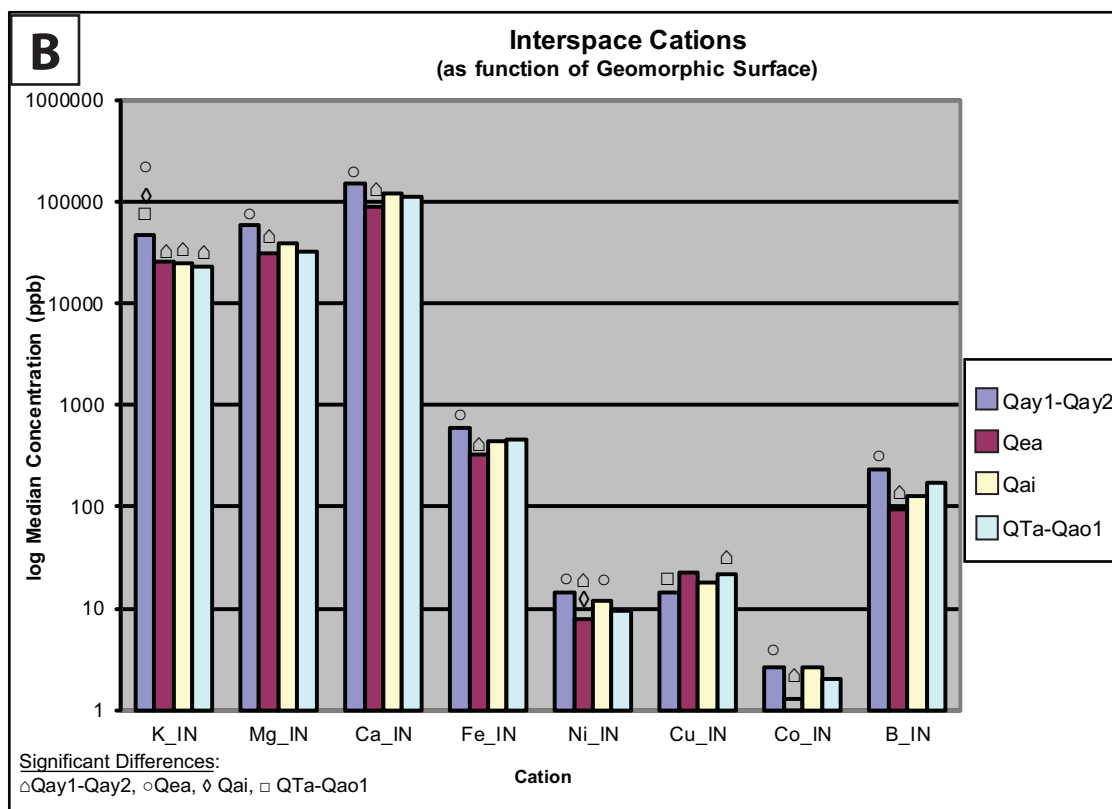
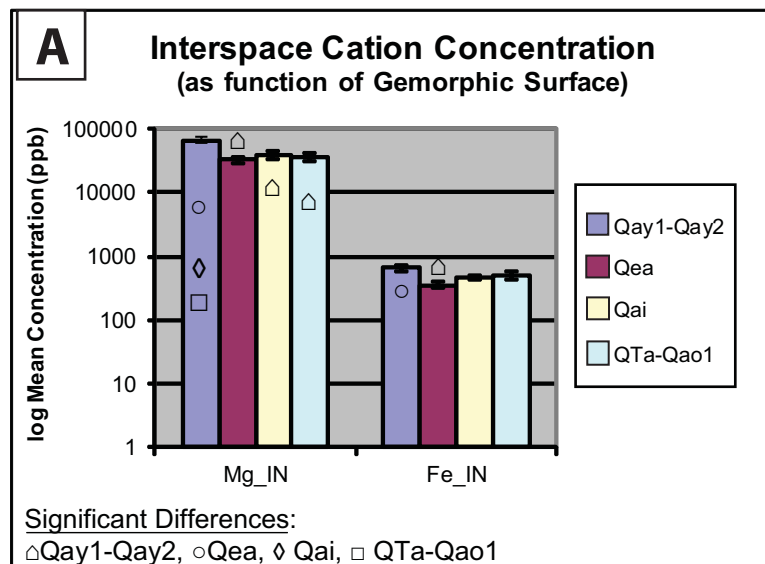


Figure 4.20: ANOVAs compare differences in interspace surface cations among various geomorphic surfaces. Significant differences are denoted by the following symbols: △ denotes significant differences from Qay1-Qay2; ○ denotes significant differences from Qea; ◇ denotes significant differences from Qai; □ denotes significant differences from QTa-Qao1. (A) Parametric ANOVAs show significant differences in mean interspace Mg and Fe among geomorphic surfaces. Bars reflect mean standard error. (B) Non-parametric ANOVAs show significant differences in median interspace K, Mg, Ca, Fe, Ni, Cu, Co, and B. (See Figure 7 for methods.)

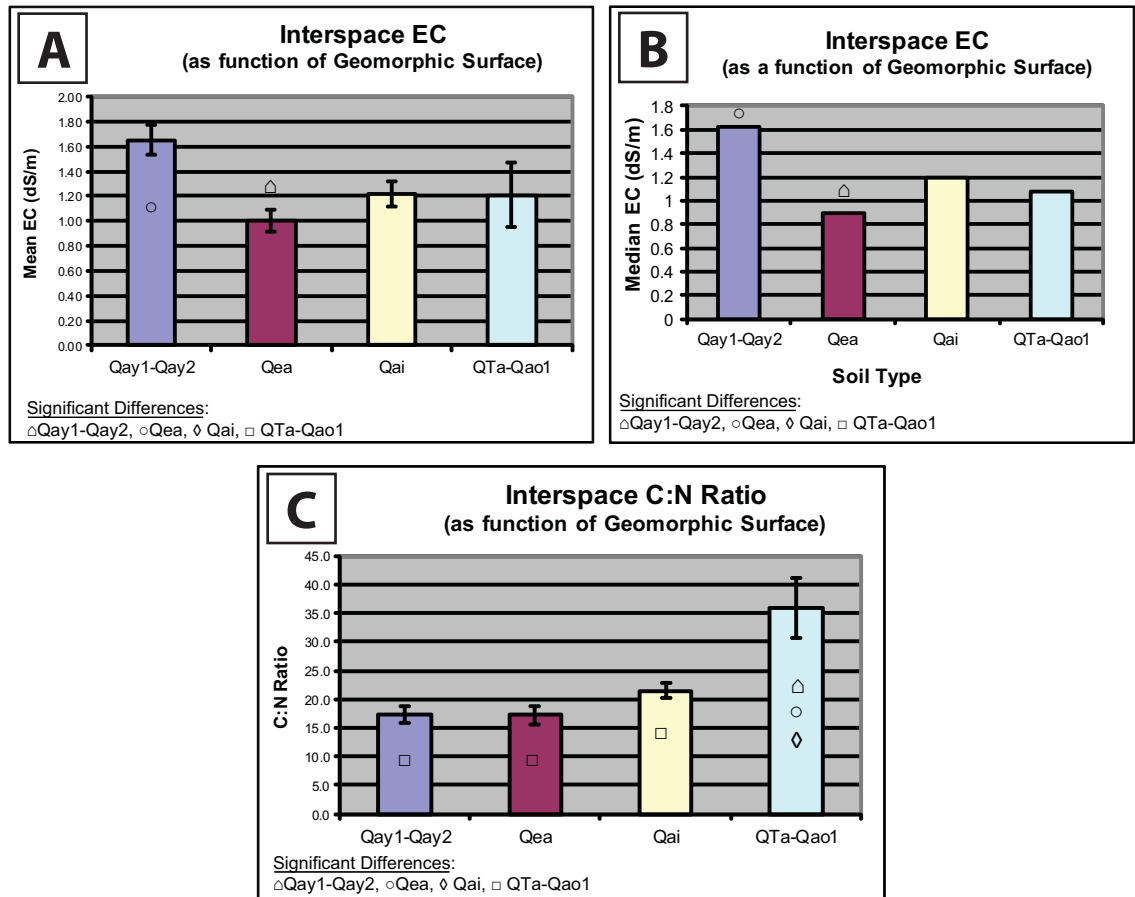


Figure 4.21: ANOVAs compare differences in interspace surface chemistry among various geomorphic surfaces. Significant differences are denoted by the following symbols: △ denotes significant differences from Qay1-Qay2; ○ denotes significant differences from Qea; ◇ denotes significant differences from Qai; □ denotes significant differences from QTa-Qao1. Bars represent mean standard error for parametric analyses (A) Parametric ANOVA shows significant differences in mean interspace EC among geomorphic surfaces. (B) Non-parametric ANOVA shows significant differences in median interspace EC. (C) Parametric ANOVA shows significant differences in mean interspace C:N ratios. (See Figure 7 for methods.)

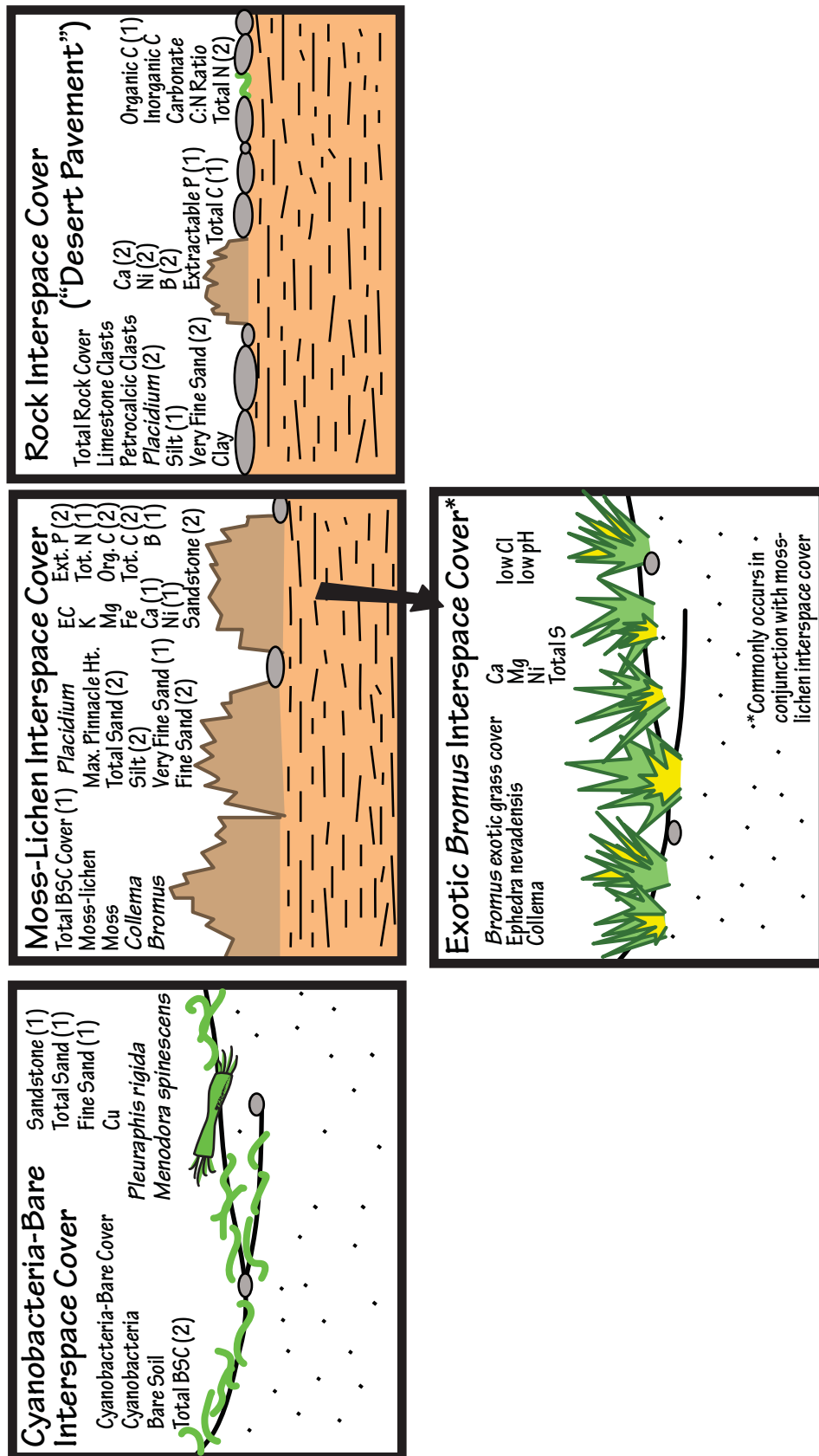


Figure 4.22: Interspace characteristics vary as a function of surface cover. ANOVA results show interspace mean/median characteristics vary with cover by cyanobacteria-bare soil (predominantly cyanobacteria cover with some bare soil), moss-lichen (includes some cyanobacteria), and rocks ("desert pavement"). T-test results show characteristics vary with exotic grass cover. Exotic grasses are not mutually exclusive from other cover types. These grasses are most extensive in areas of high moss-lichen crust density. Elevated characteristics are listed for each respective cover type. Characteristics elevated in more than one ANOVA group are labeled 1 or 2 for the first and second highest mean/median values. (See Figures 8 and 9 for methods.)

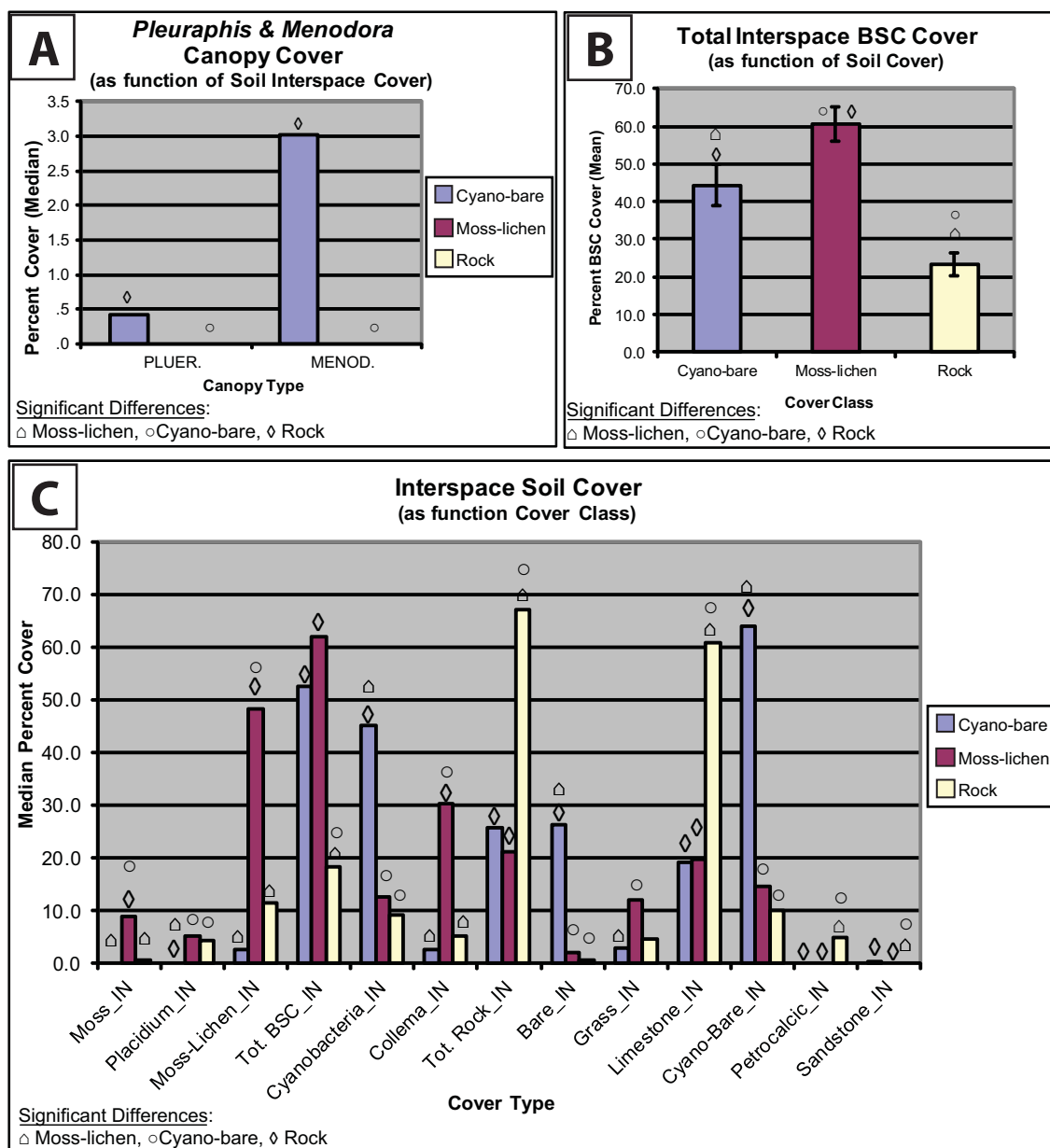


Figure 4.23: ANOVAs compare differences in surface cover among three interspace surface cover categories. Significant differences are denoted by the following symbols: \triangle denotes significant differences from the moss-lichen category; \circ denotes significant differences from the cyanobacteria-bare category; \diamond denotes significant differences from the rock category (“desert pavement”). (A) Non-parametric ANOVAs show significant differences in median vascular plant cover adjacent to interspaces. Differences are reported for *Pleuraphis* and *Menodora*. (B) Parametric ANOVA shows significant differences in mean interspace BSC cover. Bars represent mean standard error. (C) Non-parametric ANOVAs show significant differences in median interspace cover by moss, *Placidium* lichen, moss-lichen, total BSC, cyanobacteria, *Collema* lichen, total rock, bare soil, grass litter, limestone clasts, cyanobacteria-bare, petrocalcic clasts, and sandstone clasts. (See Figure 8 for methods.)

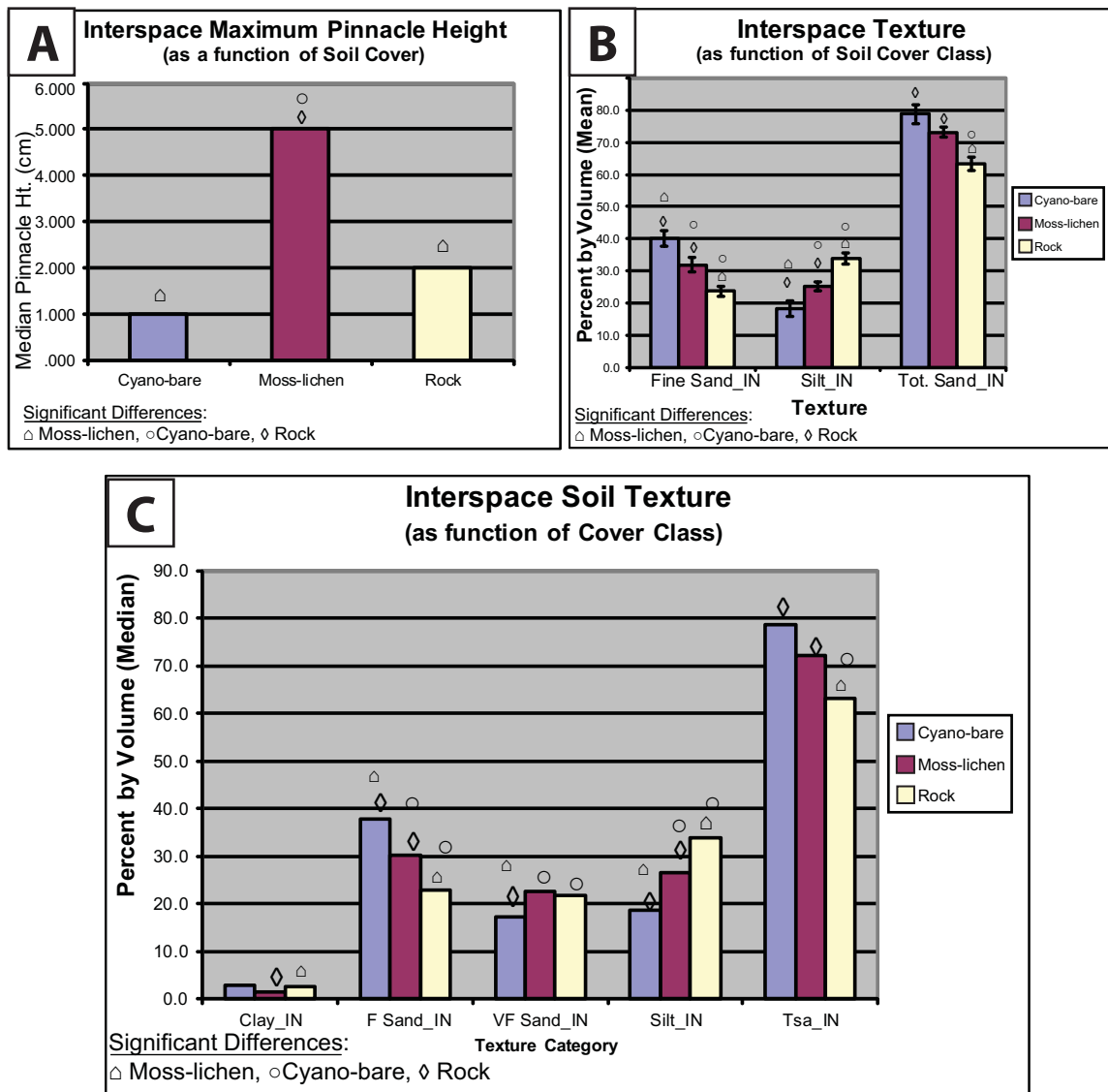


Figure 4.24: ANOVAs compare differences in soil characteristics among three inter-space surface cover classes. Significant differences are denoted by the following symbols: \triangle denotes significant differences from the moss-lichen class; \circ denotes significant differences from the cyanobacteria-bare class; \diamond denotes significant differences from the rock class (“desert pavement”). (A) Non-parametric ANOVA shows significant differences in median maximum pinnacle height. Maximum pinnacle height refers to the greatest topographic microrelief found in moss-lichen pinnacles within shrub interspaces. (B) Parametric ANOVAs show significant differences in mean interspace fine sand, silt, and total sand. Bars represent mean standard error. (C) Non-parametric ANOVAs show significant differences in median interspace clay, fine sand, very fine sand, silt, and total sand. (See Figure 8 for methods.)

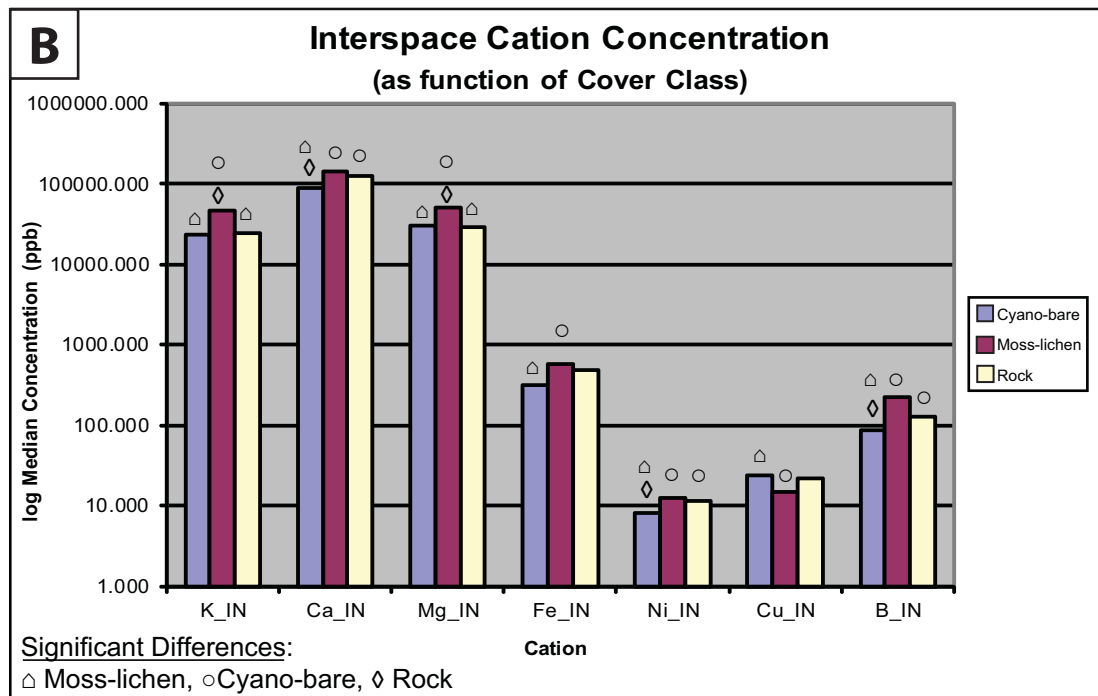
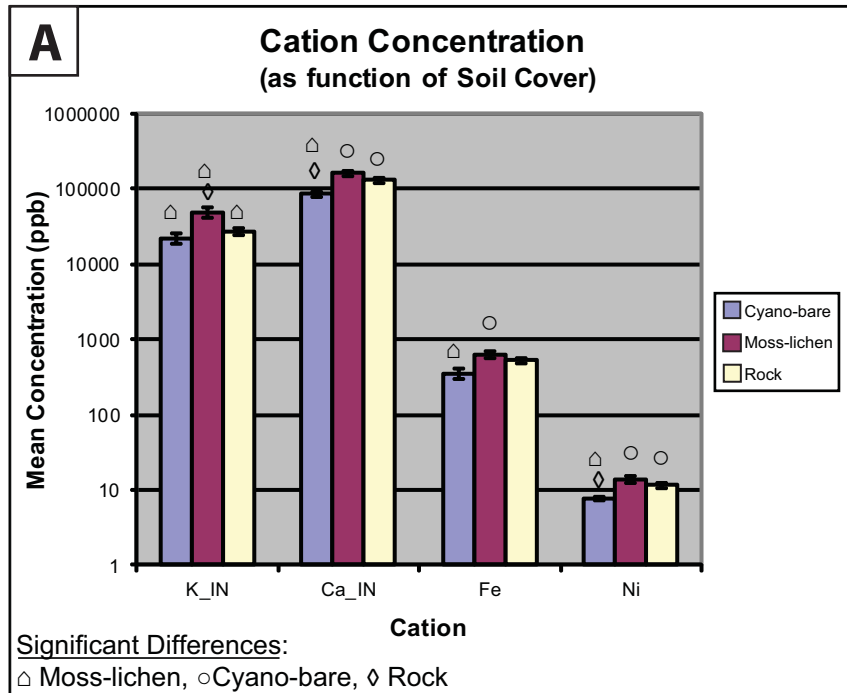


Figure 4.25: ANOVAs compare differences in soil chemistry among three interspace surface cover classes. Significant differences are denoted by the following symbols: \triangle denotes significant differences from the moss-lichen class; \circ denotes significant differences from the cyanobacteria-bare class; \diamond denotes significant differences from the rock class (“desert pavement”). (A) Parametric ANOVAs show significant differences in mean interspace K, Ca, Fe, and Ni. Bars represent mean standard error. (B) Non-parametric ANOVAs show significant differences in median interspace K, Ca, Mg, Fe, Ni, Cu, and B. (See Figure 8 for methods.)

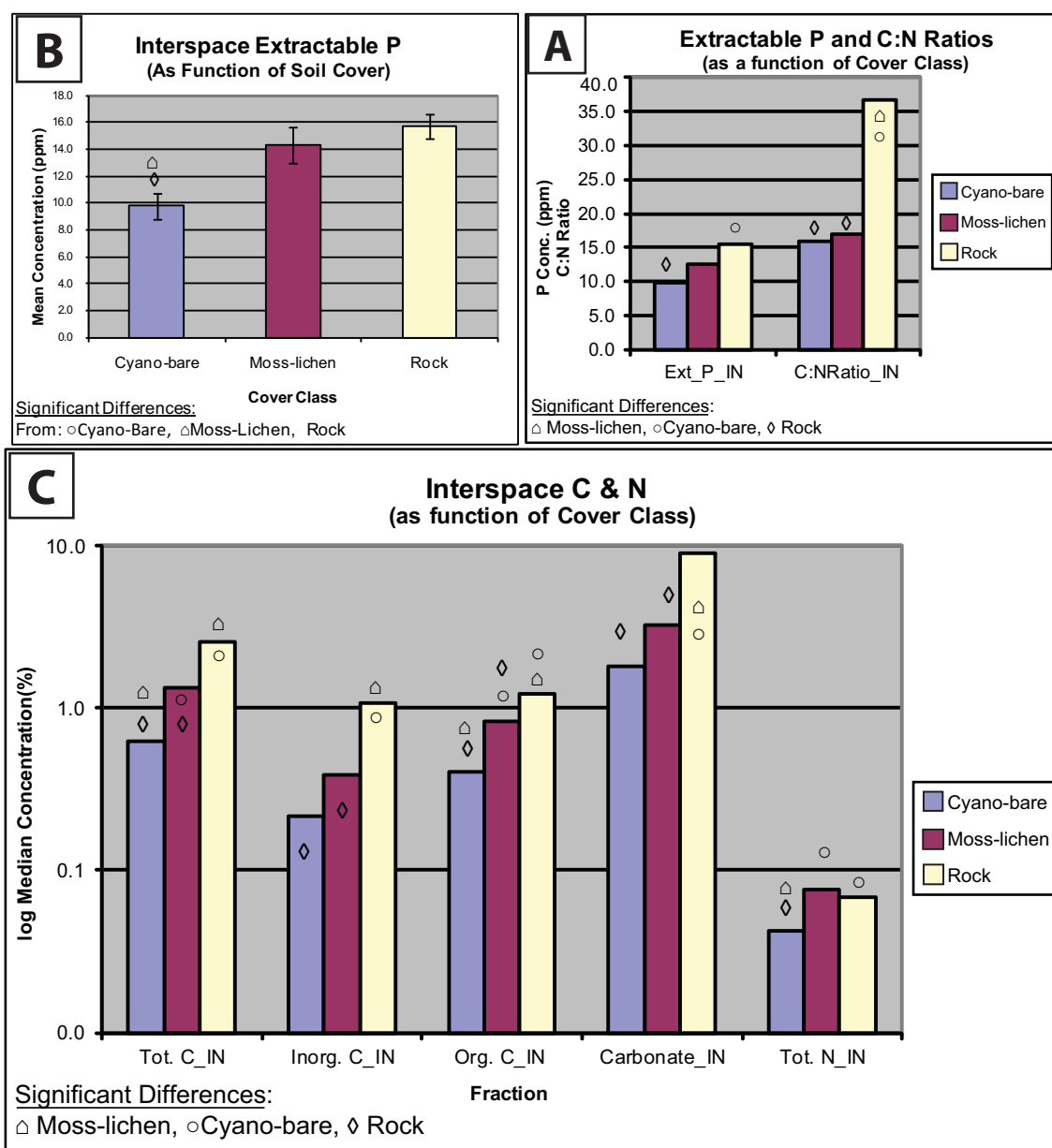


Figure 4.26: ANOVAs compare differences in soil chemistry among three interspace surface cover classes. Significant differences are denoted by the following symbols: △ denotes significant differences from the moss-lichen class; ○ denotes significant differences from the cyanobacteria-bare class; ◇ denotes significant differences from the rock class (“desert pavement”). (A) Parametric ANOVA shows significant differences in mean interspace extractable P. Bars represent mean standard error. (B) Non-parametric ANOVAs show significant differences in mean interspace extractable P and C:N ratios. (C) Non-parametric ANOVAs show significant differences in median interspace total C, inorganic C, organic C, carbonate, and total N. Parametric ANOVA (not shown) reported similar results. (See Figure 8 for methods.)

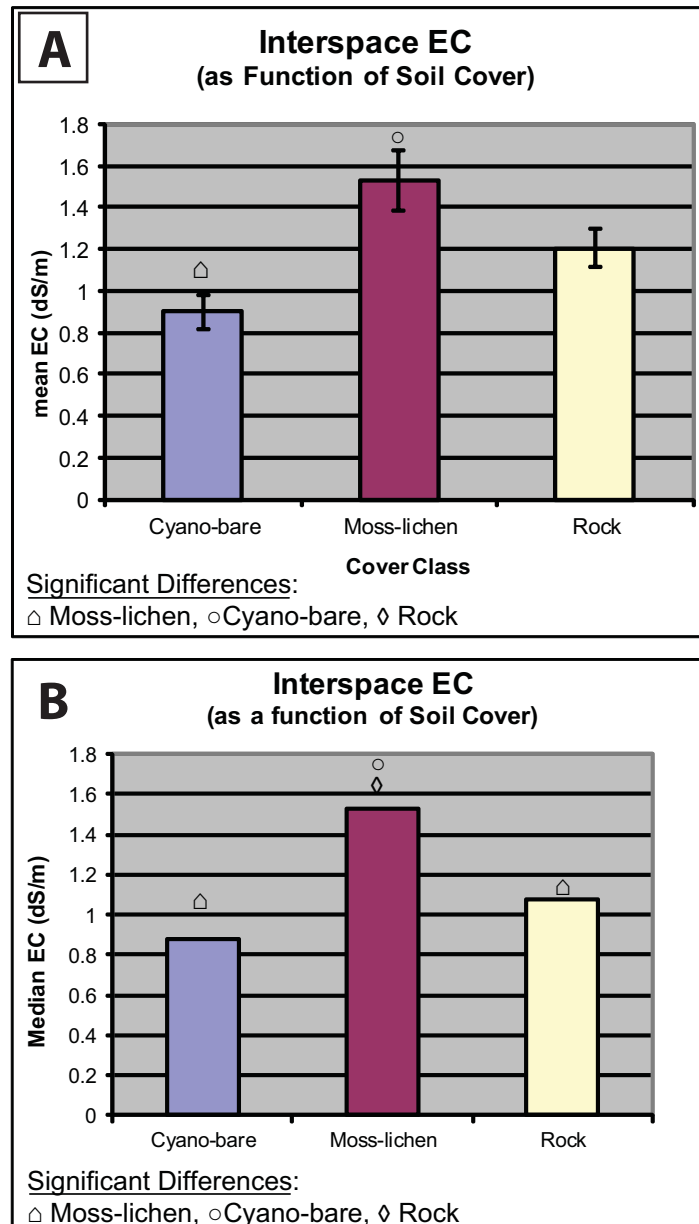


Figure 4.27: ANOVAs compare differences in soil EC among three interspace surface cover classes. Significant differences are denoted by the following symbols: \triangle denotes significant differences from the moss-lichen class; \circ denotes significant differences from the cyanobacteria-bare class; \diamond denotes significant differences from the rock class (“desert pavement”). (A) Parametric ANOVA shows significant differences in mean interspace EC. Bars represent mean standard error. (B) Non-parametric ANOVA shows significant differences in median interspace EC. (See Figure 8 for methods.)

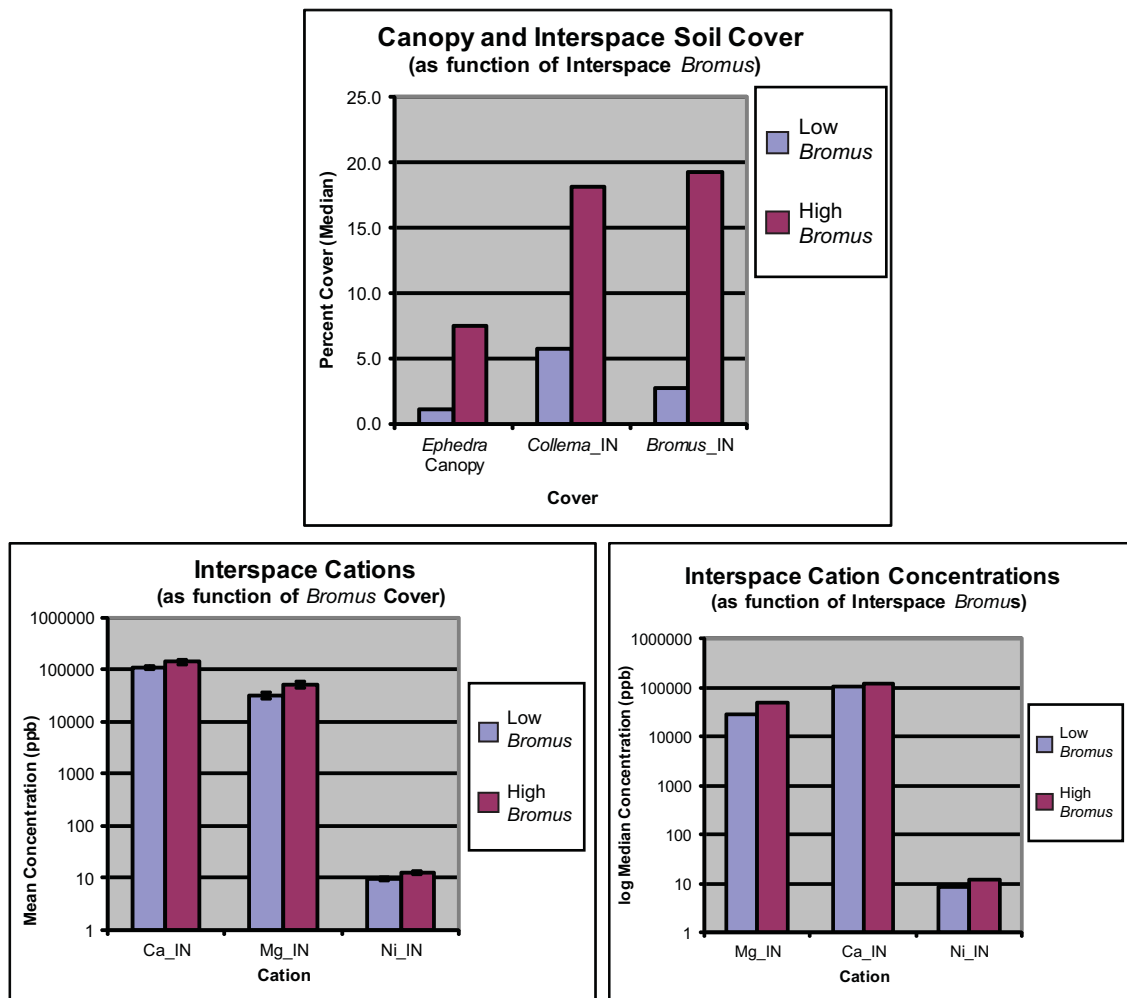


Figure 4.28: *T*-tests compare differences in soil cover, adjacent canopy cover, and soil chemistry associated areas of low and high exotic *Bromus* grass cover. (A) Non-parametric *t*-tests show significant differences in median *Ephedra* canopy cover, interspace *Collema* lichen cover, and interspace *Bromus* cover. (B) Parametric *t*-tests show significant differences in mean interspace Ca, Mg, and Ni. Bars represent mean standard error. (C) Non-parametric *t*-tests show significant differences in Mg, Ca, and Ni. (See Figure 9 for methods.)

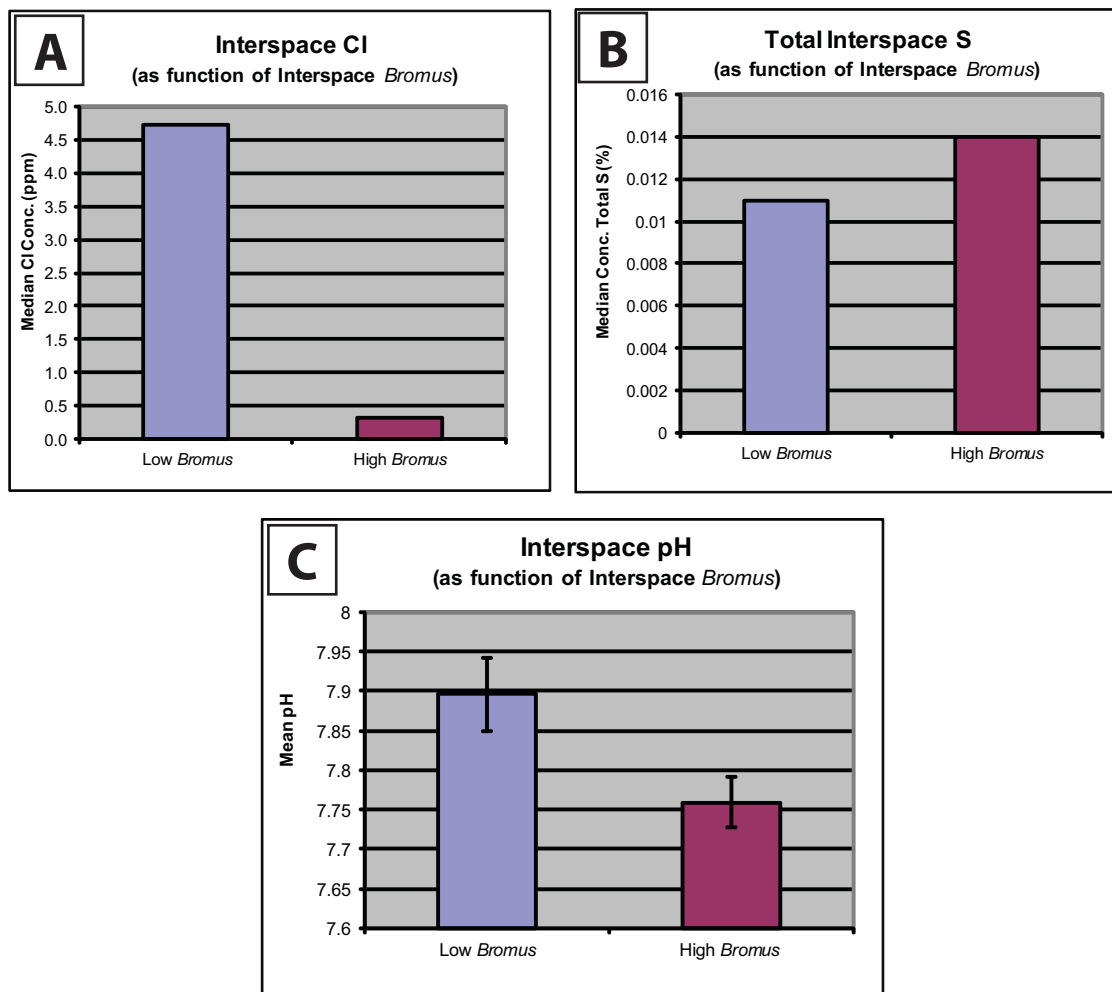


Figure 4.29: T-tests compare differences in soil chemistry associated areas of low and high exotic *Bromus* grass cover. (A) Non-parametric t-tests show significant differences in median interspace Cl. (B) Non-parametric t-tests show significant differences in median interspace total S. (C) Parametric t-tests show significant differences in mean interspace pH. Bars represent mean standard error. (See Figure 9 for methods.)

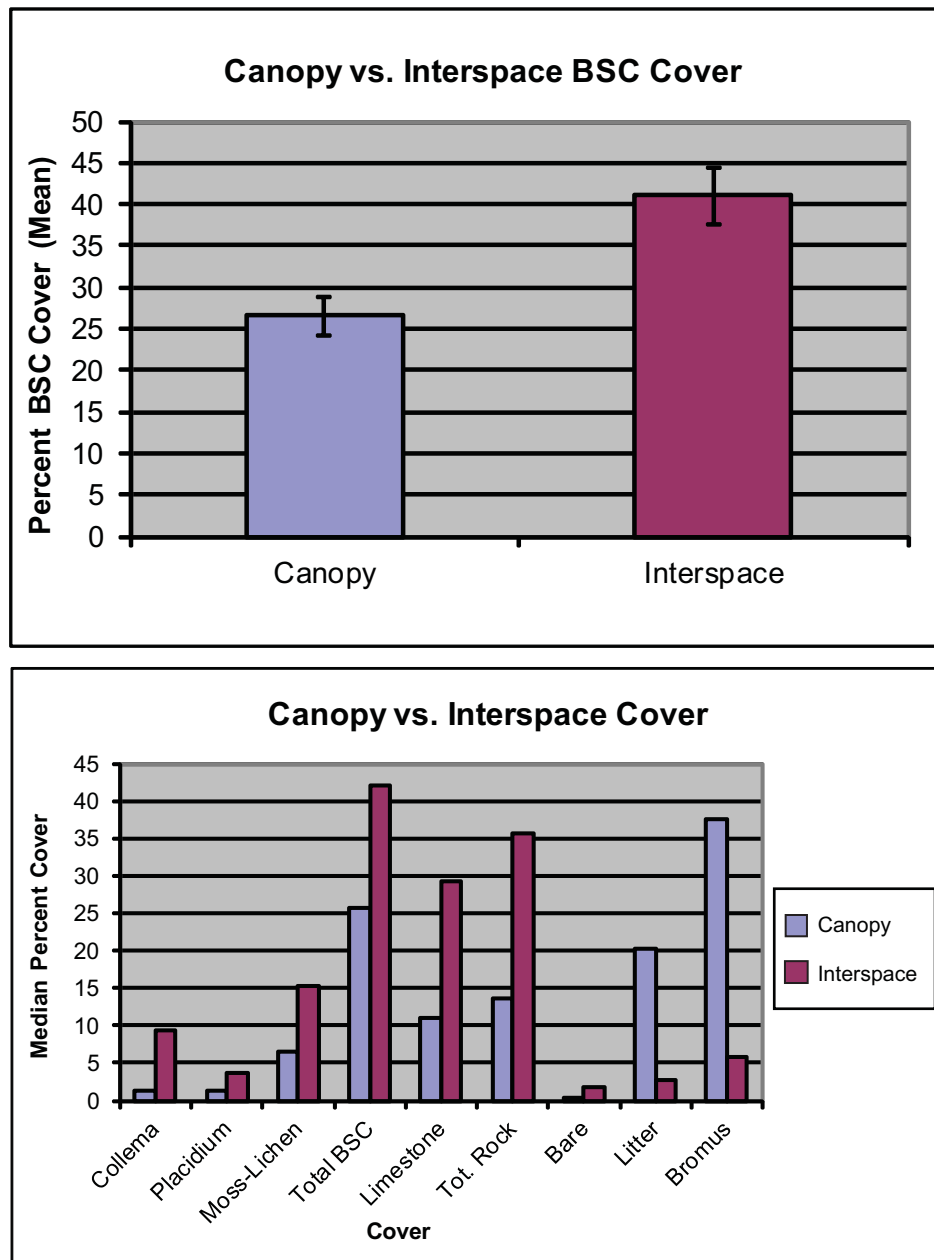


Figure 4.30: T-tests compare differences in soil cover between all shrub canopies and interspaces. (A) Parametric t-tests show significant differences in mean BSC cover. Bars represent mean standard error. (B) Non-parametric t-tests show significant differences in median soil cover by *Collema* lichen, *Placidium* lichen, moss-lichen, total BSCs, limestone clasts, total rock, bare soil, plant litter, and *Bromus* exotic grass litter. (See Figure 10 for methods.)

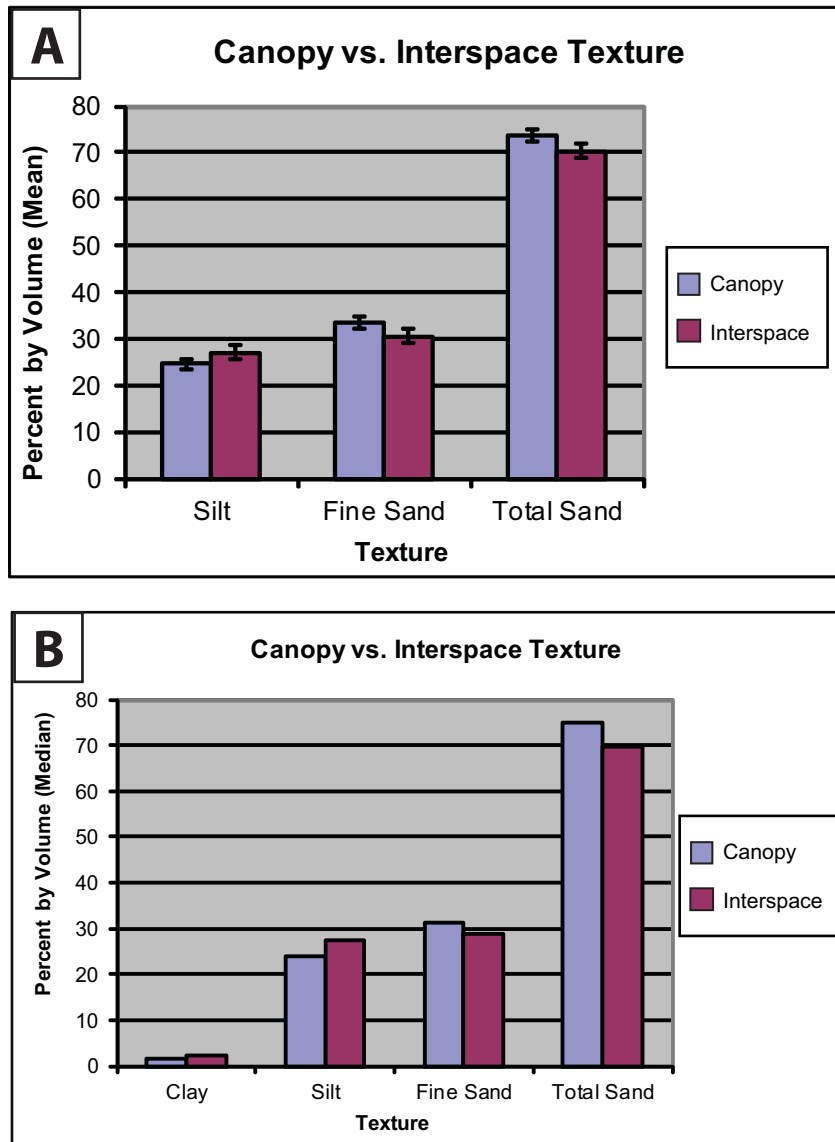


Figure 4.31: *T*-tests compare differences in soil texture between all shrub canopies and interspaces. (A) Parametric *t*-tests show significant differences in mean silt, fine sand and total sand volumes. Bars represent mean standard error. (B) Non-parametric *t*-tests show significant differences in median clay, silt, fine sand, and total sand volumes. (See Figure 10 for methods.)

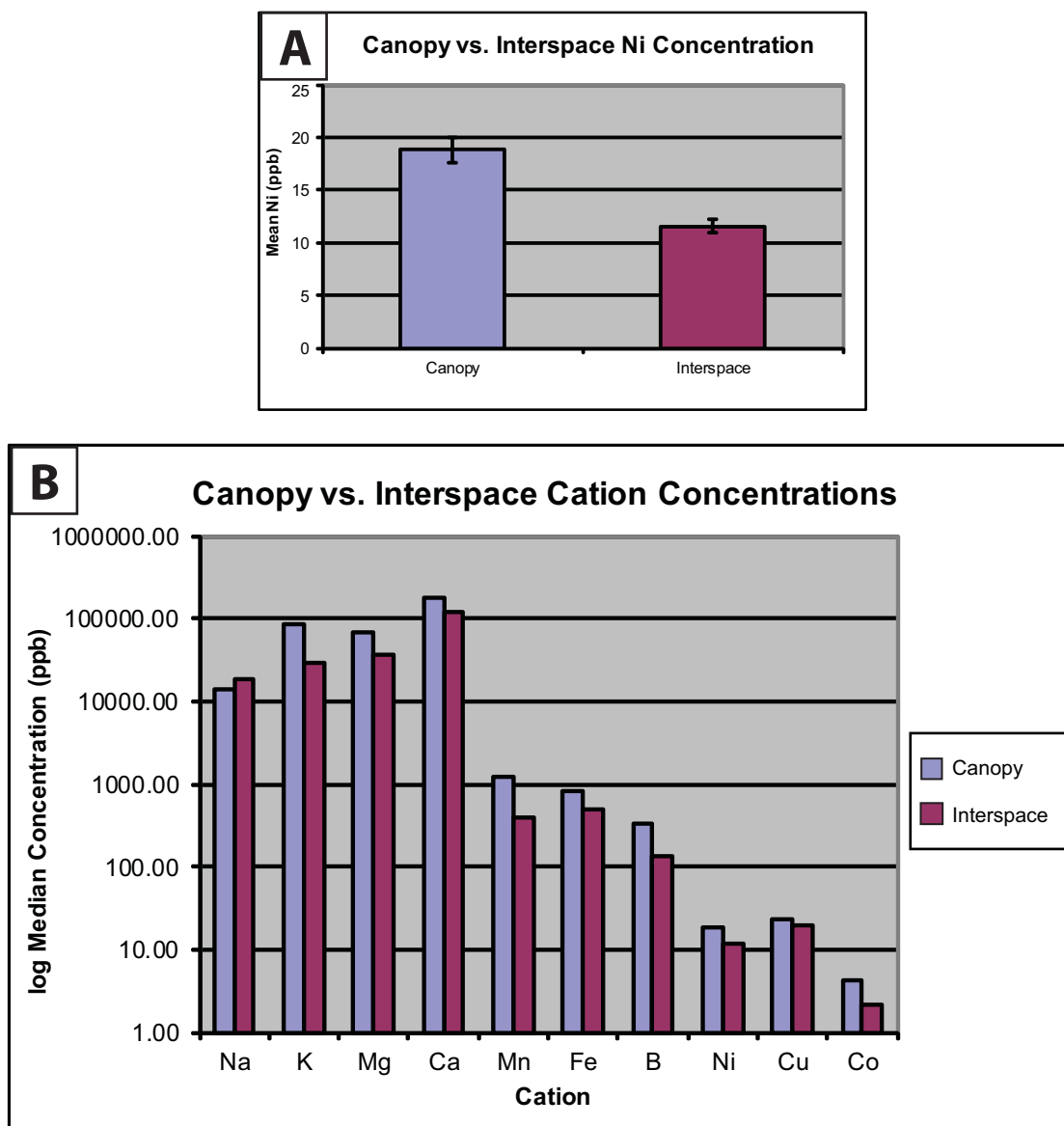


Figure 4.32: *T*-tests compare differences in soil chemistry between all shrub canopies and interspaces. (A) Parametric *t*-tests show significant differences in mean Ni concentrations. Bars represent mean standard error. (B) Non-parametric *t*-tests show significant differences in median Na, K, Mg, Ca, Mn, Fe, B, Ni, Cu, and Co concentrations. (See Figure 10 for methods.)

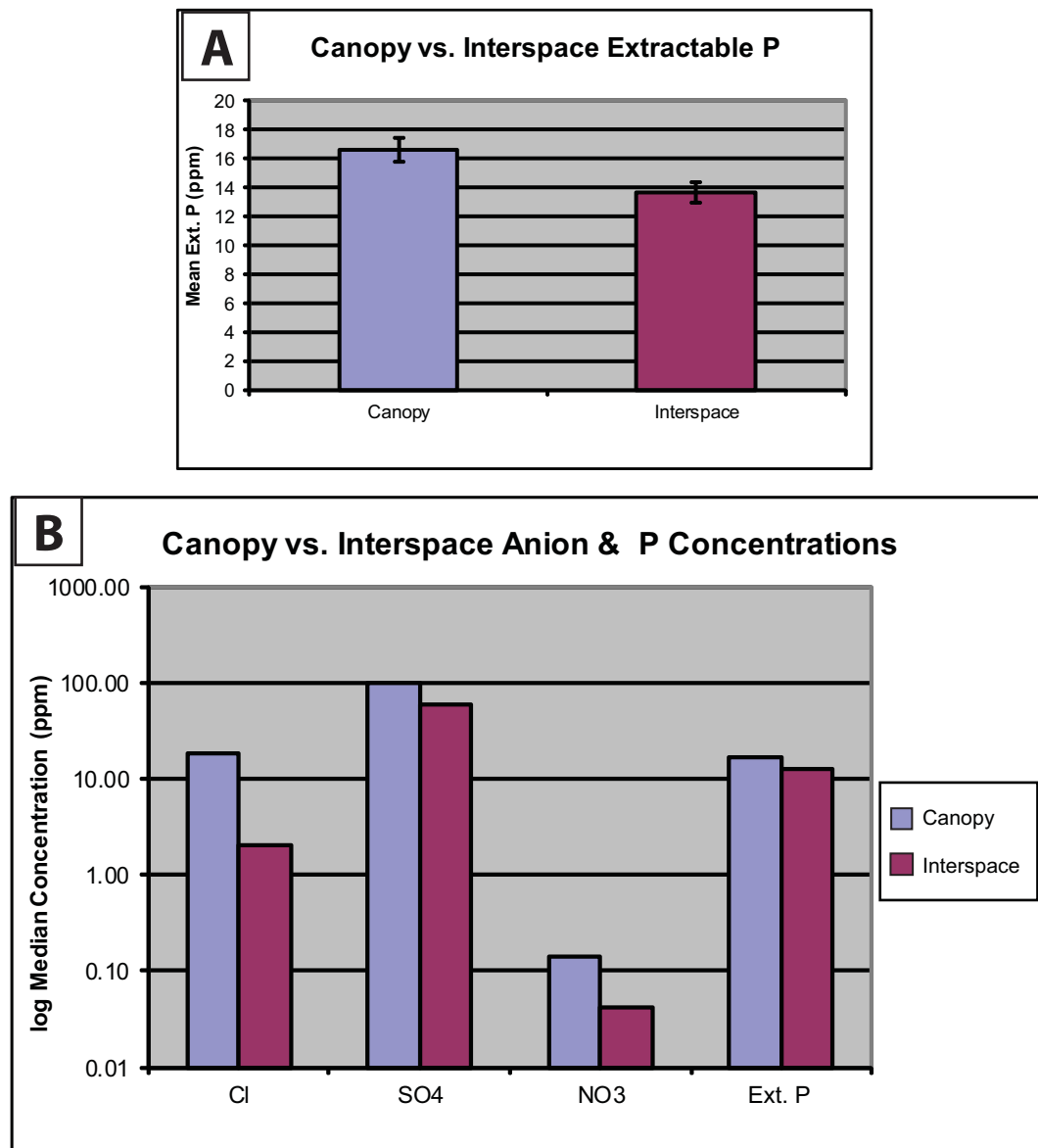


Figure 4.33: *T*-tests compare differences in soil chemistry between all shrub canopies and interspaces. (A) Parametric *t*-tests show a significant difference in mean extractable P concentrations. Bars represent mean standard error. (B) Non-parametric *t*-tests show significant differences in median Cl, SO₄, NO₃, and extractable P concentrations. (See Figure 10 for methods.)

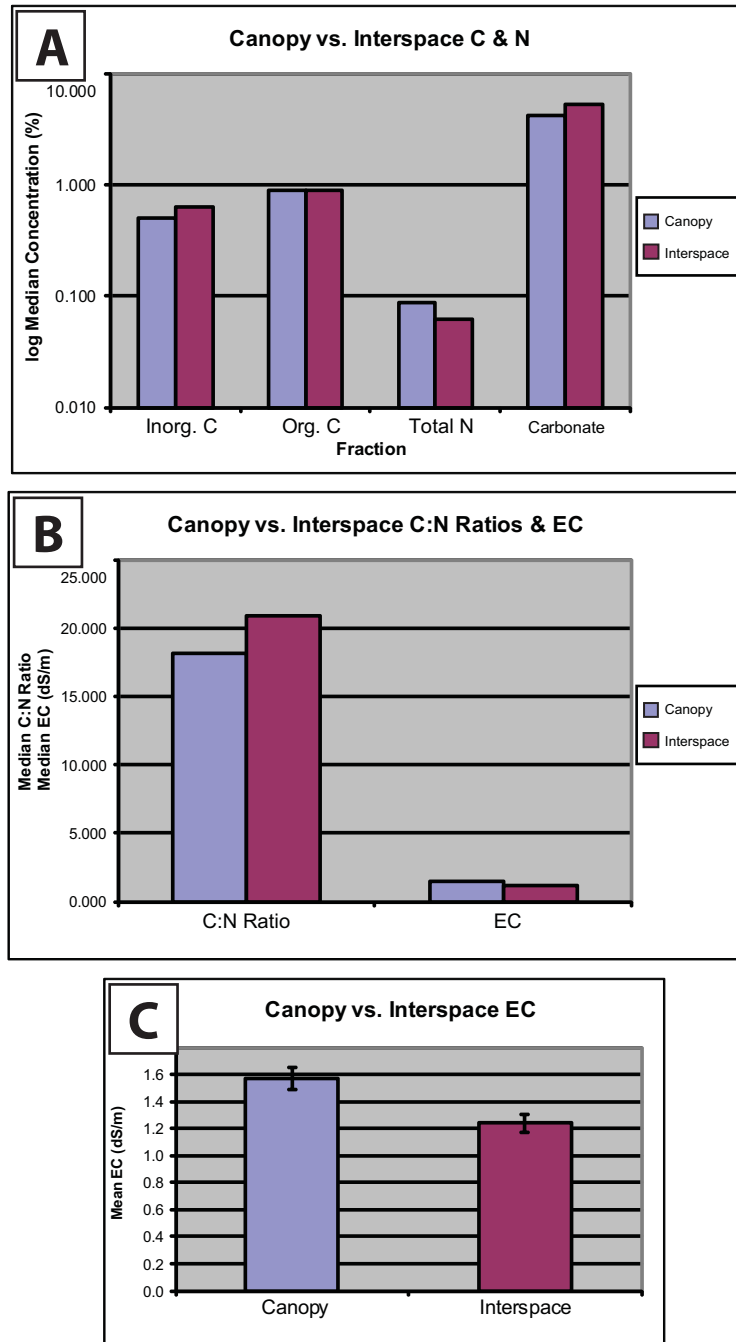


Figure 4.34: T-tests compare differences in soil chemistry between all shrub canopies and interspaces. (A) Non-parametric t-tests show a significant difference in median inorganic C, organic, C, total N, and carbonate concentrations. (B) Non-parametric t-tests show significant differences in median C:N ratios and EC. (C) Parametric t-tests show a significant difference in mean EC. Bars represent mean standard error. (See Figure 10 for methods.)

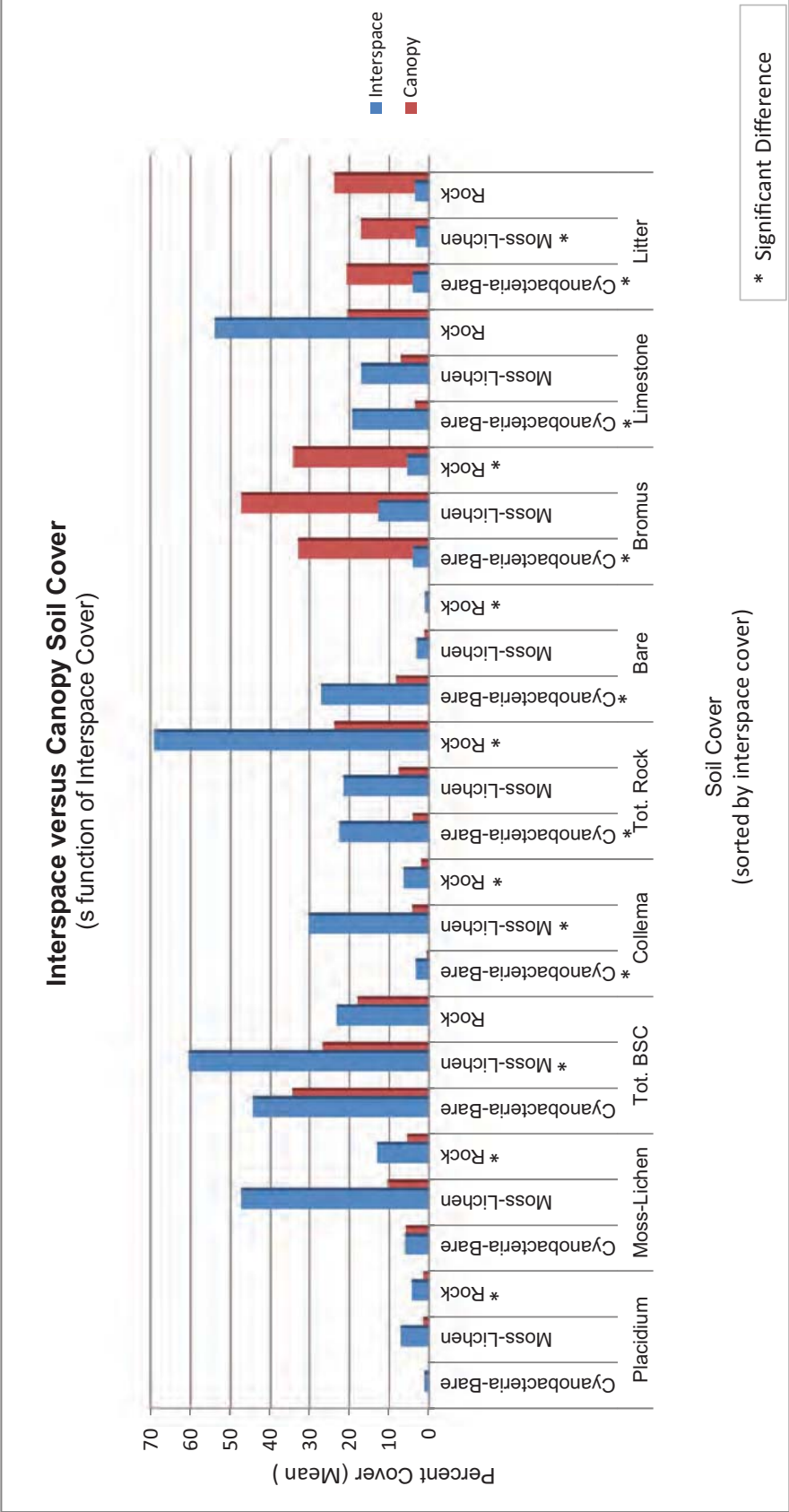


Figure 4.35: Parametric t -tests show significant differences between canopy and interspace soil cover for three interspace cover classes, which include cyanobacteria-bare, moss-lichen, and rock (“desert pavement”). Significant differences are denoted by *. Significant differences in surface cover are reported for *Placidium* lichen, moss-lichen, total BSCs, *Collema* lichen, total rock, bare soil, *Bromus* exotic grass litter, limestone clasts, and non-grass plant litter. (See Figure 11 for methods.)

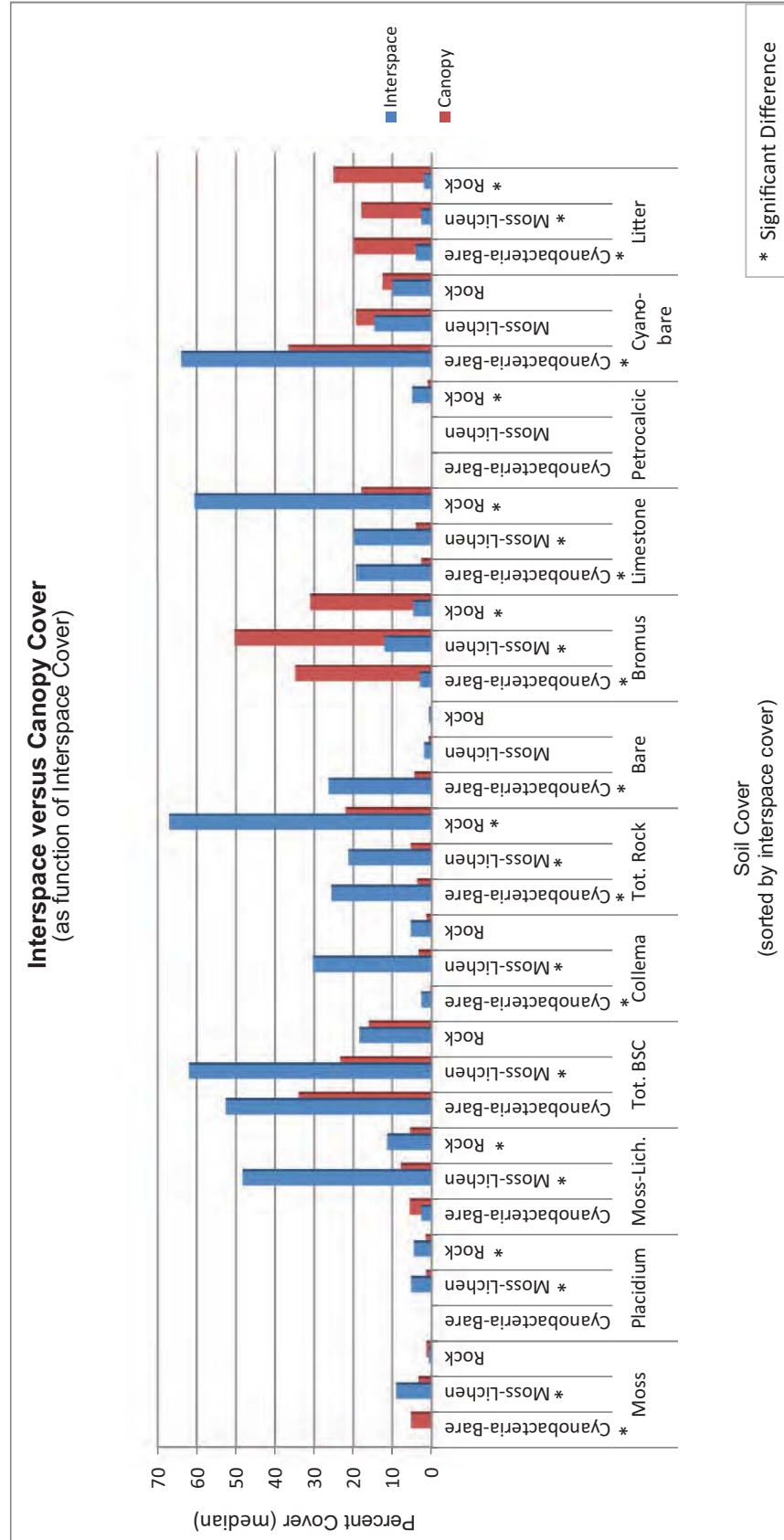


Figure 4.36: Non-parametric t -tests show significant differences between canopy and interspace soil cover for three interspace cover classes, which include cyanobacteria-bare, moss-lichen, and rock (“desert pavement”). Significant differences are denoted by *. Significant differences in surface cover are reported for moss, *Placidium* lichen, moss-lichen, total BSCs, *Collema* lichen, total rock, bare soil, *Bromus* exotic grass litter, limestone clasts, petrocalcic clasts, cyanobacteria-bare, and non-grass plant litter. (See Figure 11 for methods.)

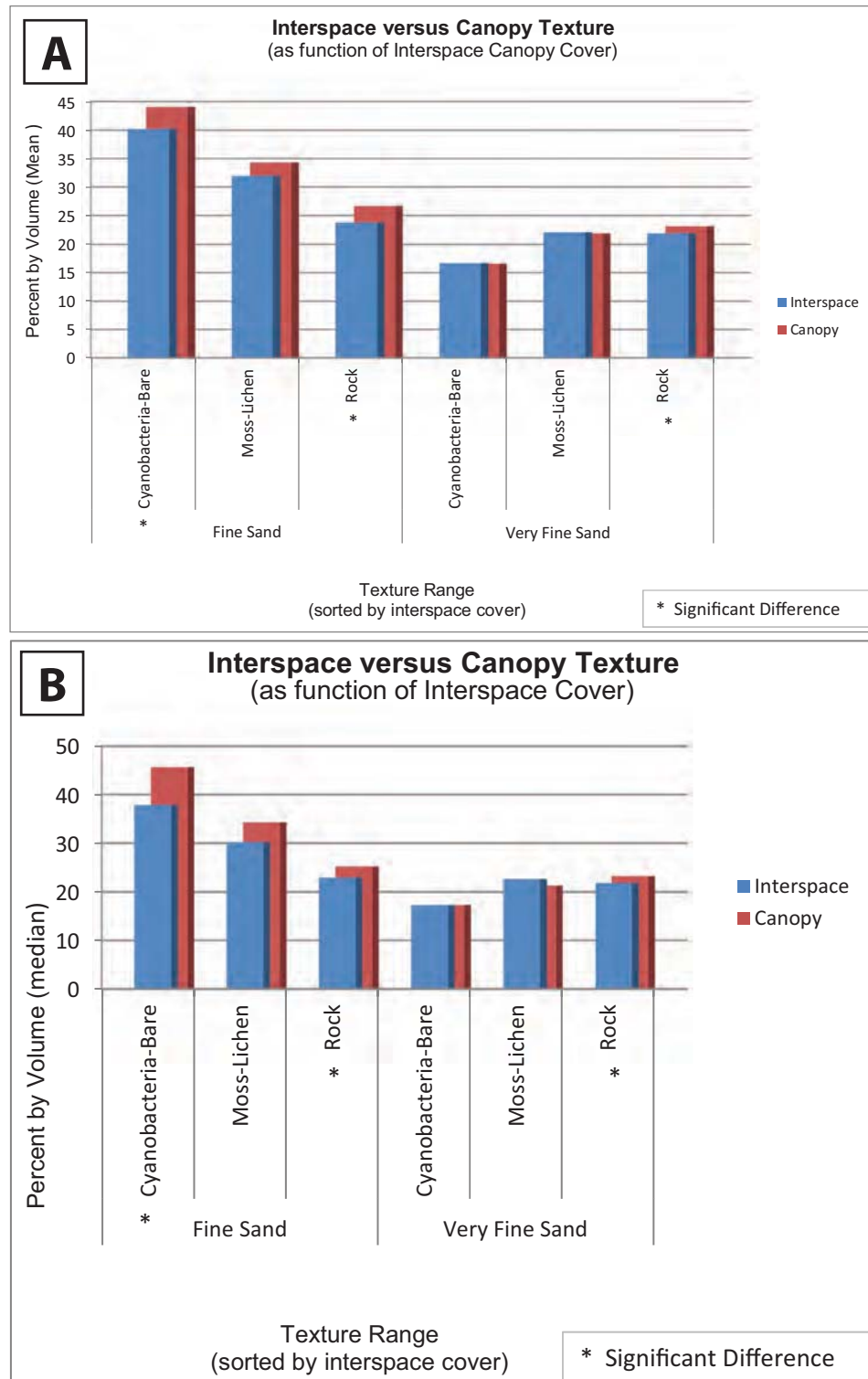


Figure 4.37: T-tests show significant differences between canopy and interspace soil texture for three interspace cover classes, which include cyanobacteria-bare, moss-lichen, and rock (“desert pavement”). Significant differences are denoted by *. (A) Parametric t-tests and (B) non-parametric t-test show significant differences fine sand and very fine sand. (See Figure 11 for methods.)

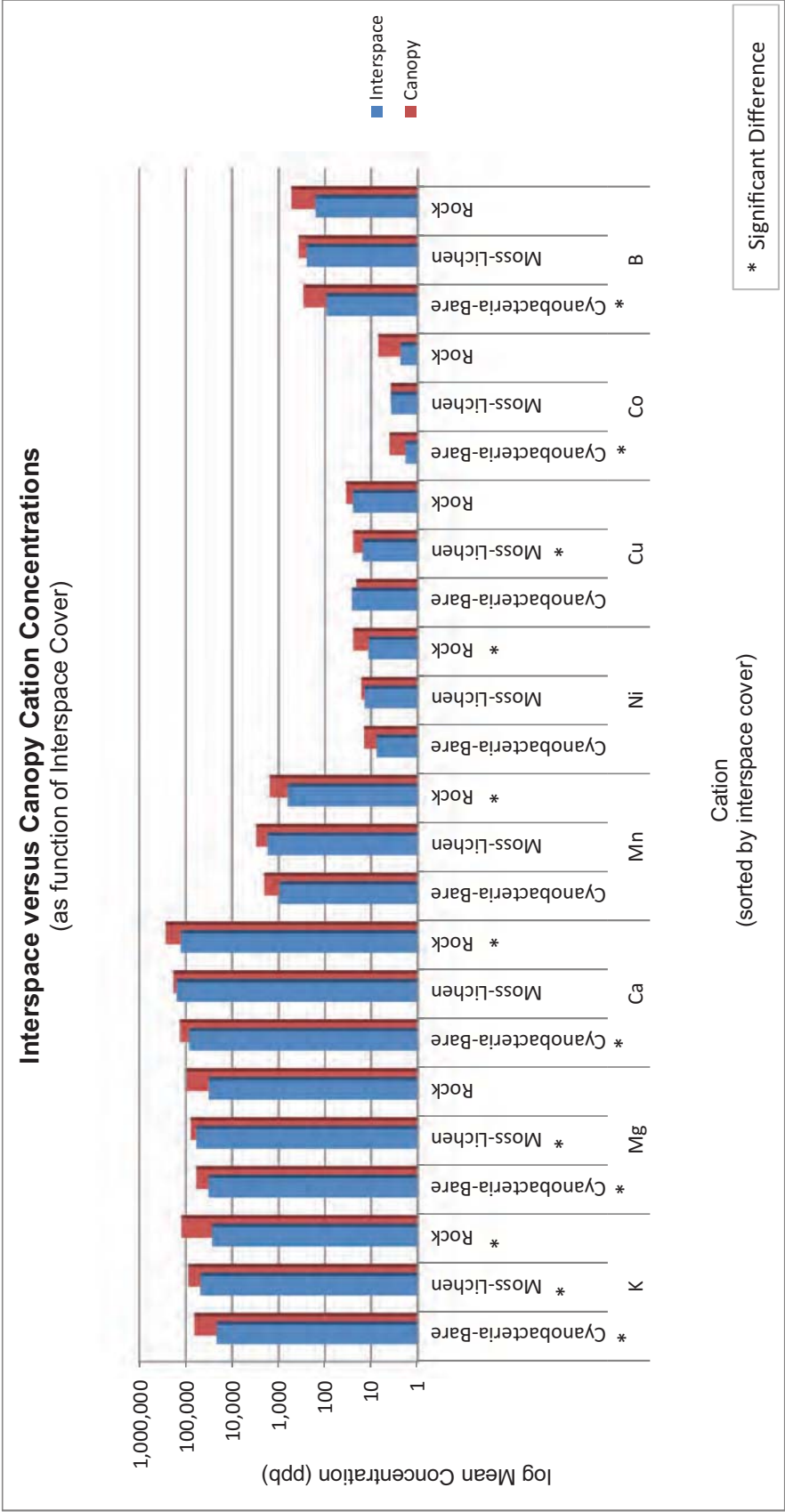


Figure 4.38: Parametric t-tests show significant differences between canopy and interspace soil chemistry for three interspace cover classes, which include cyanobacteria-bare, moss-lichen, and rock (“desert pavement”). Significant differences are denoted by *. Significant differences are reported for K, Mg, Ca, Mn, Ni, Cu, Co, and B concentrations. (See Figure 11 for methods.)

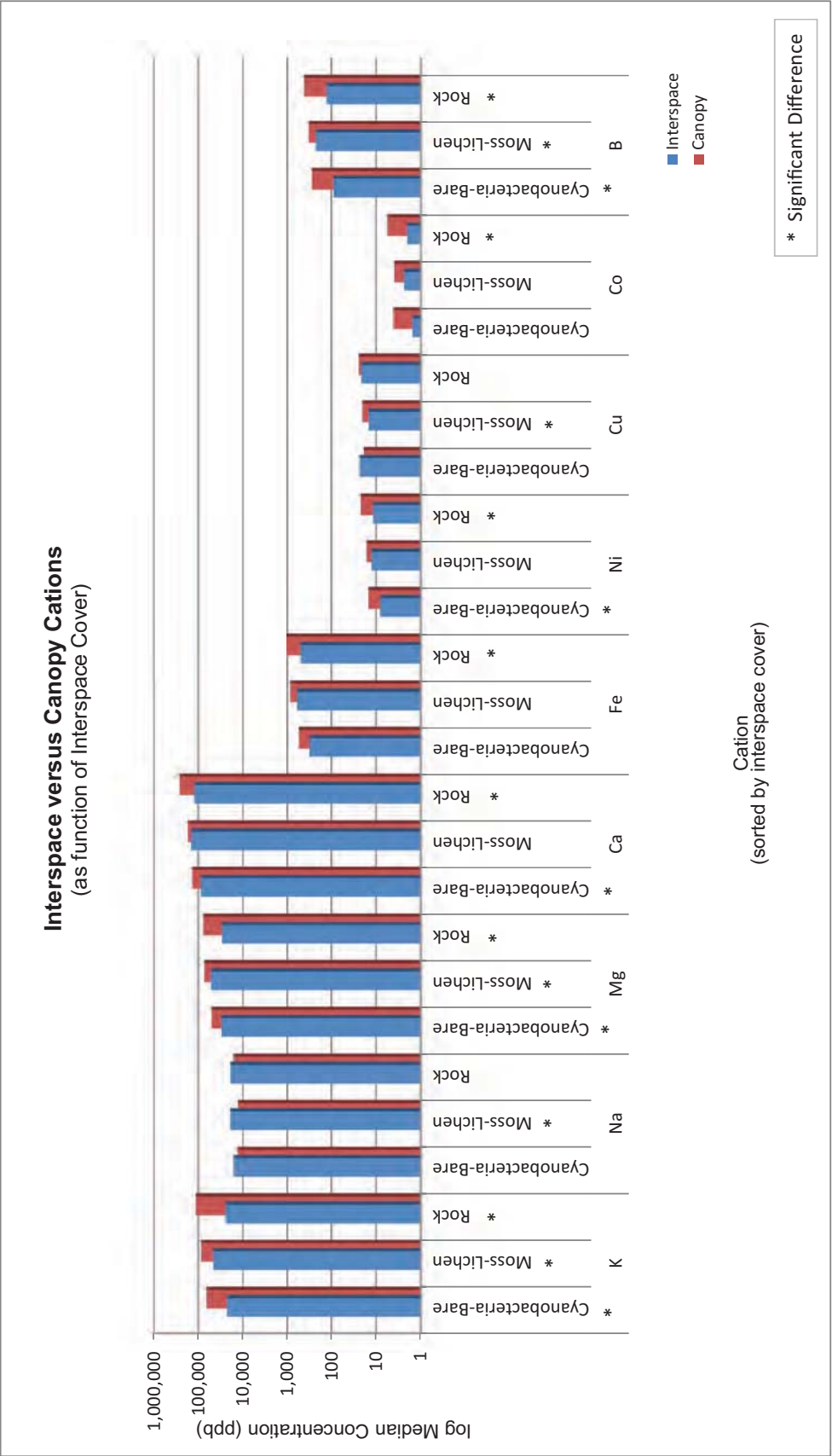


Figure 4.39: Non-parametric t-tests show significant differences between canopy and interspace soil chemistry for three interspace cover classes, which include cyanobacteria-bare, moss-lichen, and rock (“desert pavement”). Significant differences are denoted by *. Significant differences are reported for K, Na, Mg, Ca, Fe, Ni, Cu, Co, and B concentrations. (See Figure 11 for methods.)

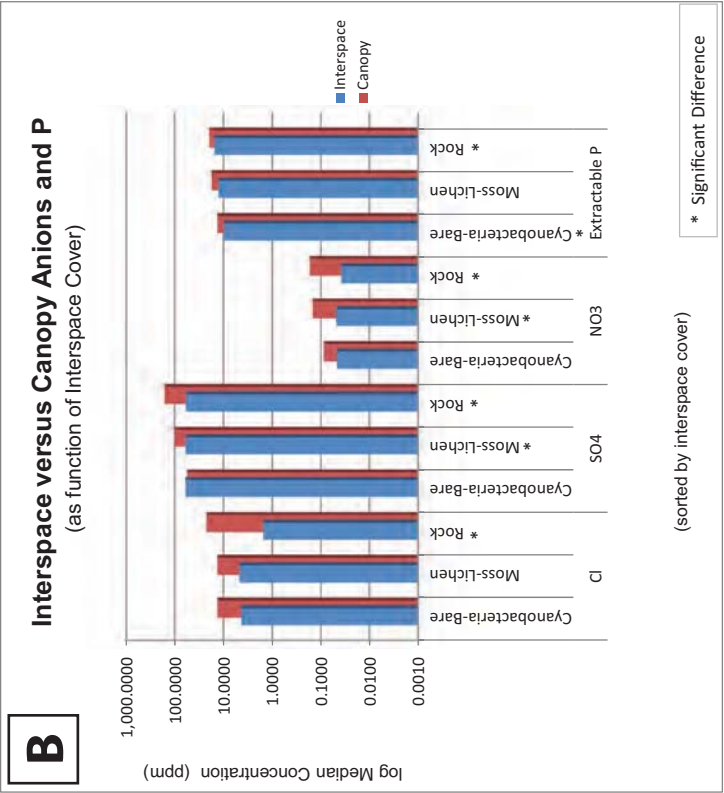
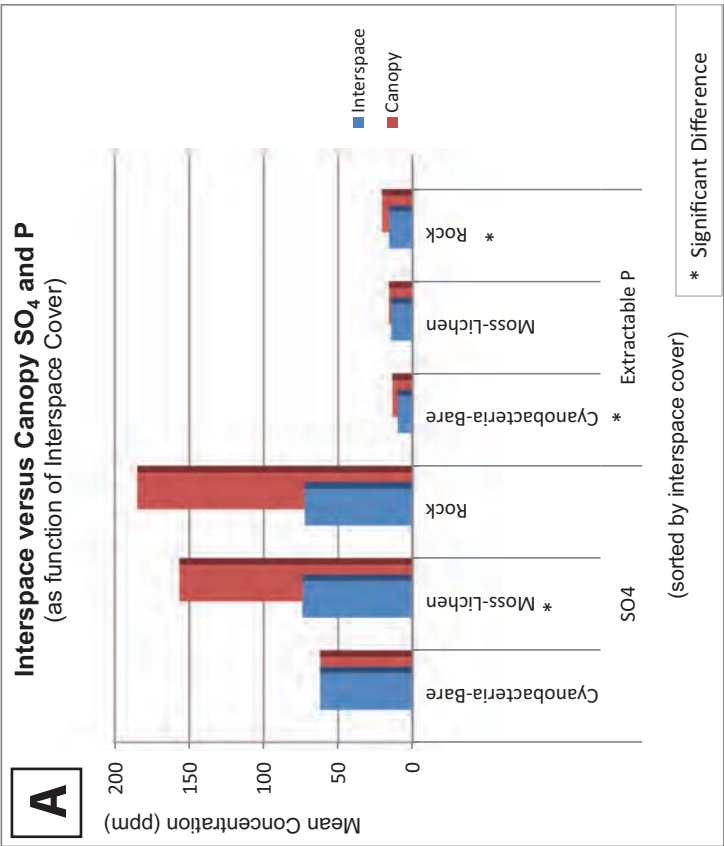


Figure 4.40: T-tests show significant differences between canopy and interspace soil chemistry for three interspace cover classes, which include cyanobacteria-bare, moss-lichen, and rock (“desert pavement”). Significant differences are denoted by *. (A) Parametric t-tests show significant differences in SO₄ and extractable P concentrations. (B) Non-parametric t-test show significant differences in Cl, SO₄, NO₃, and extractable P concentrations. (See Figure 11 for methods.)

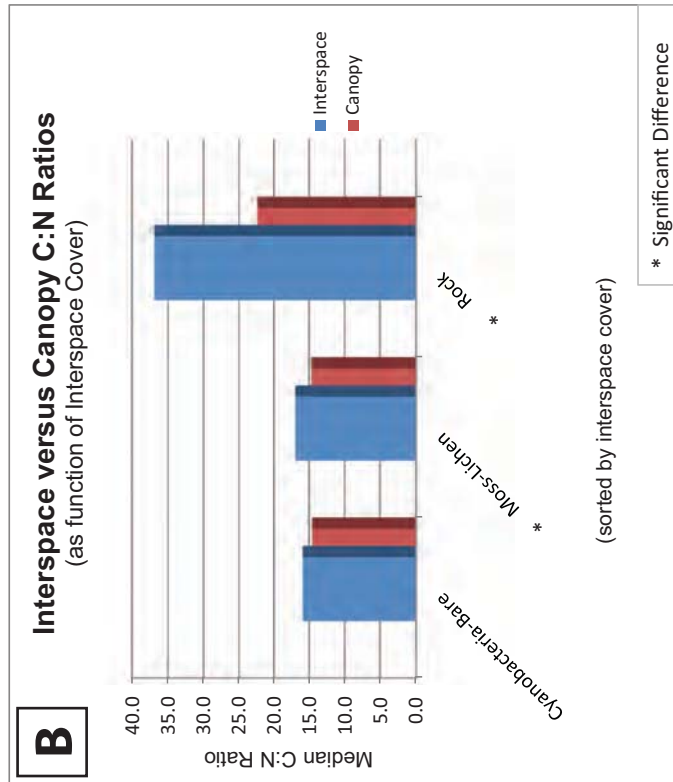
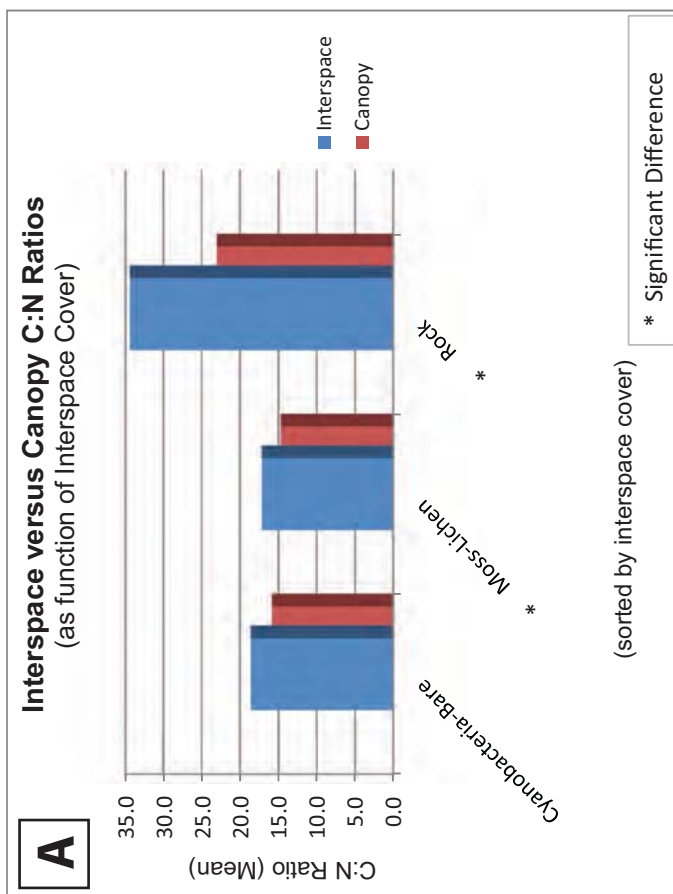


Figure 4.41: *T*-tests show significant differences between canopy and interspace soil chemistry for three interspace cover classes, which include cyanobacteria-bare, moss-lichen, and rock (“desert pavement”). Significant differences are denoted by *. (A) Parametric *t*-tests and (B) non-parametric *t*-tests show significant differences in C:N ratios. (See Figure 11 for methods.)

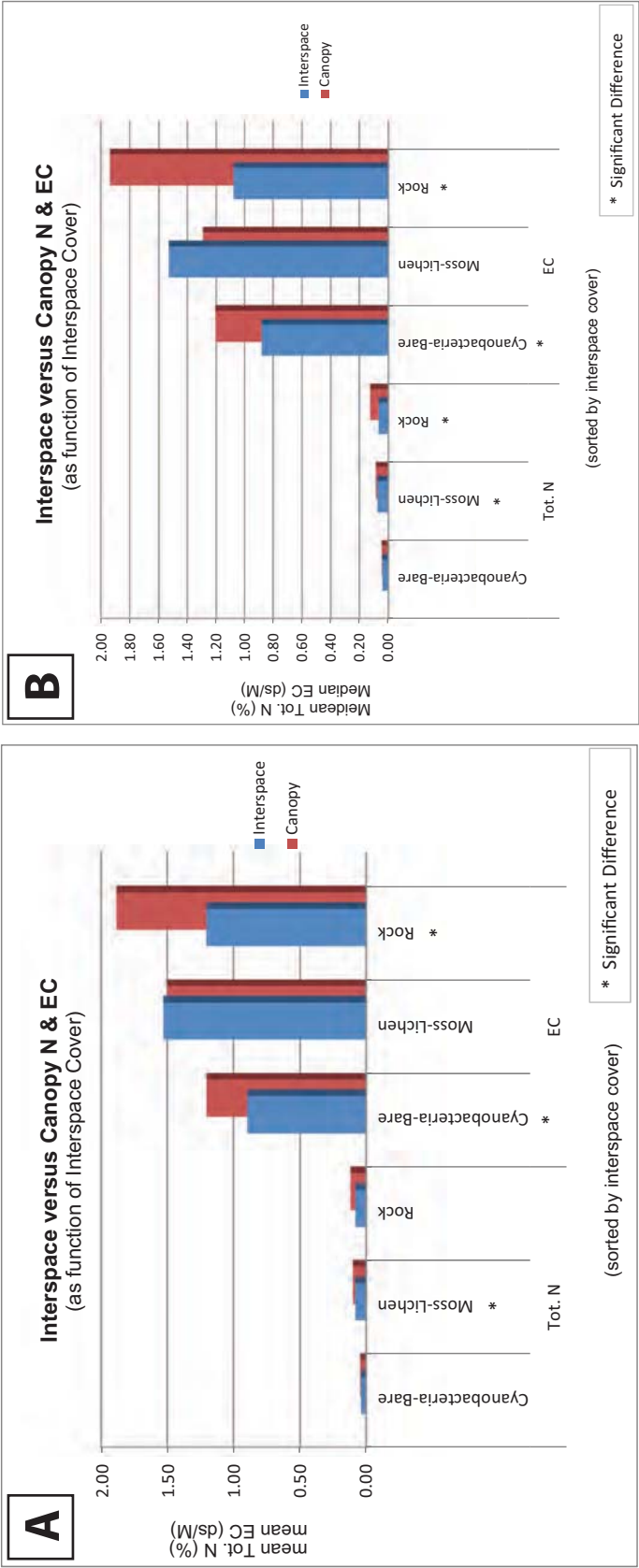


Figure 4.42: *T*-tests show significant differences between canopy and interspace soil chemistry for three interspace cover classes, which include cyanobacteria-bare, moss-lichen, and rock (“desert pavement”). Significant differences are denoted by *. (A) Parametric *t*-tests and (B) non-parametric *t*-tests show significant differences in total N and EC. (See Figure 11 for methods.)

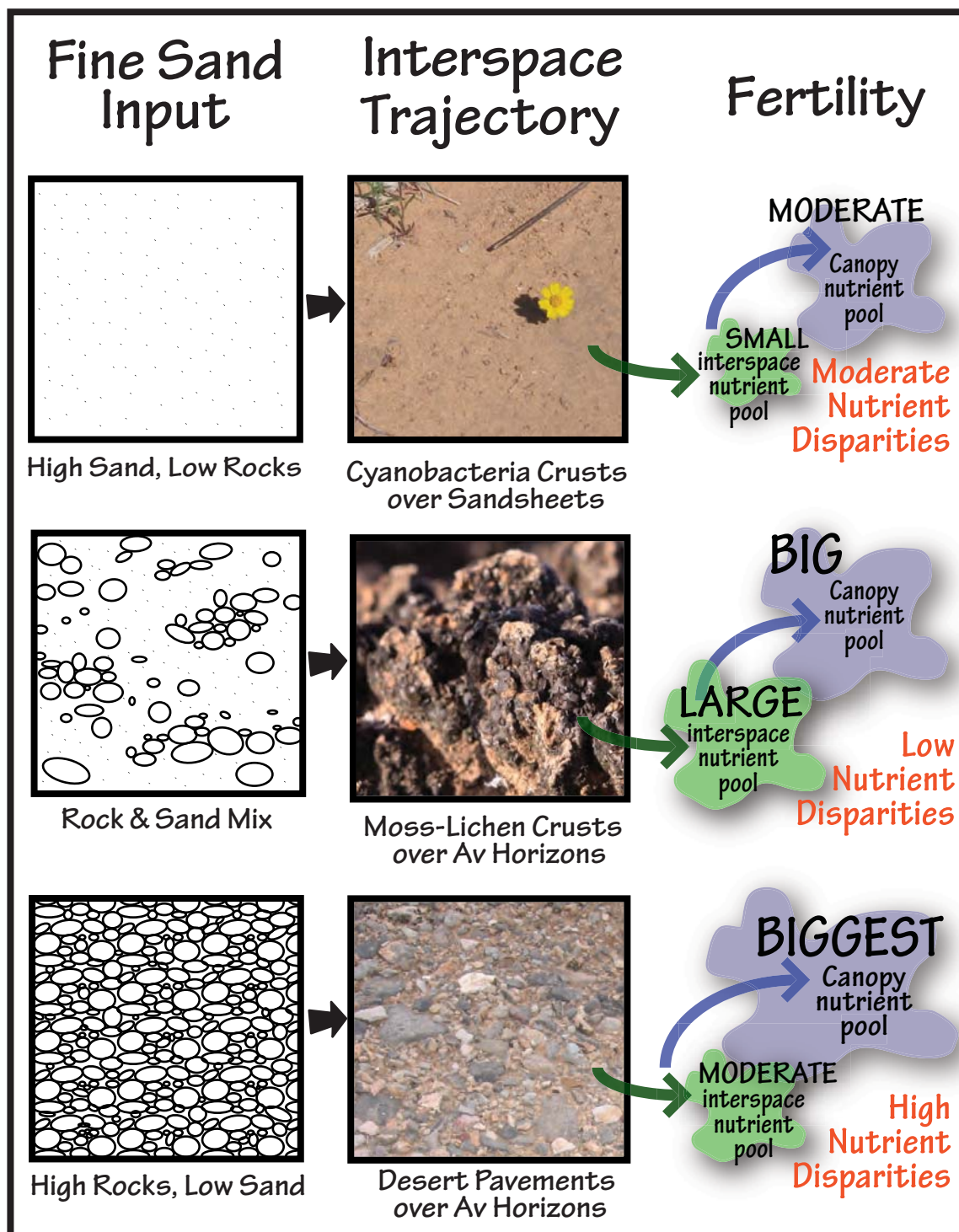


Figure 4.43: Surface particle size controls surface cover and the magnitude of the fertile island effect. Sandy soils support cyanobacteria crusts and lead to low overall fertility and moderate canopy-interspace nutrient disparities. Surfaces composed of sand and rock fragments lead to dense moss-lichen crusts, high interspace fertility, and low canopy-interspace nutrient disparities. Rock-covered surfaces lead to “desert pavements” with scattered moss-lichen crusts and high canopy-interspace nutrient disparities.

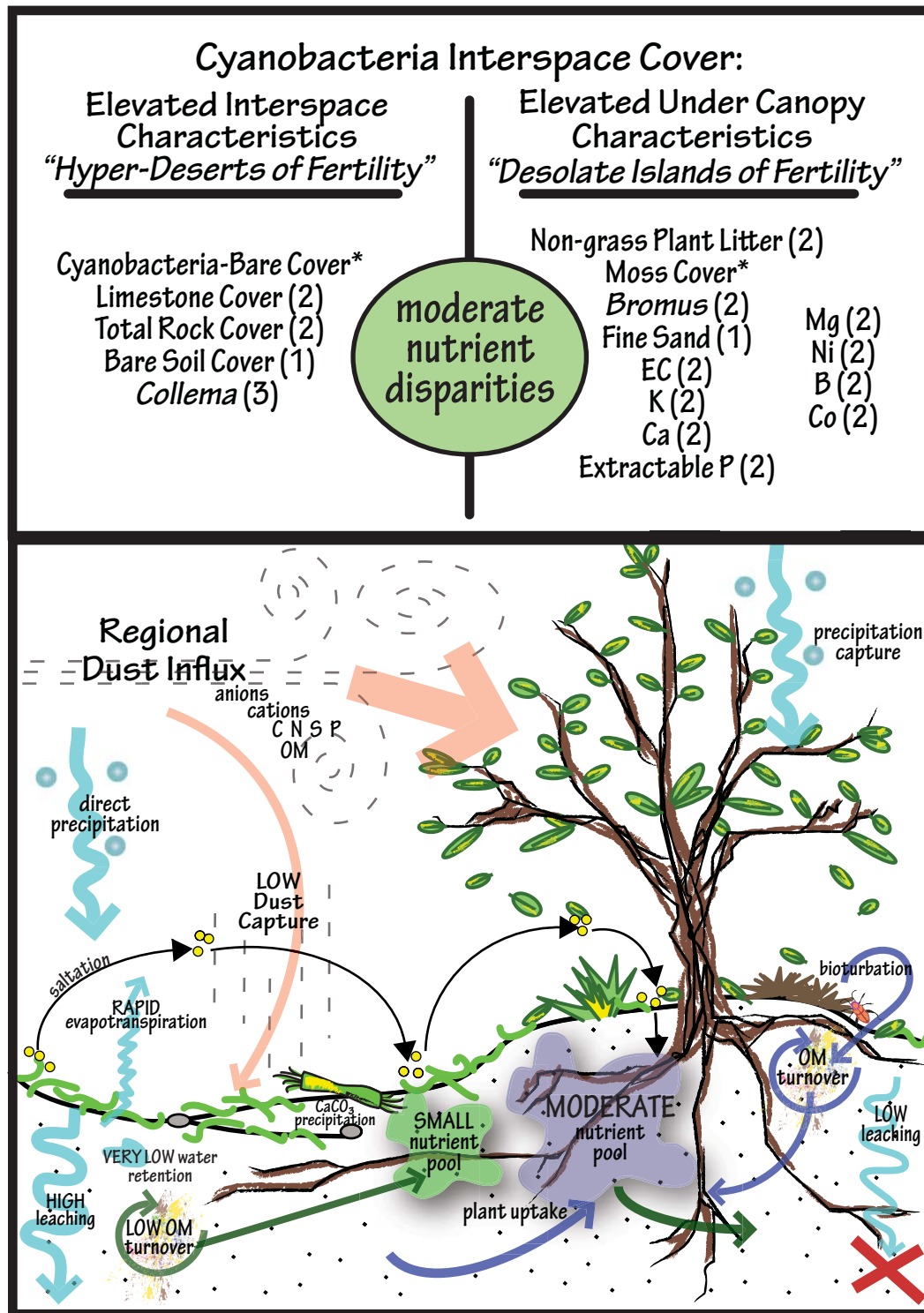


Figure 4.44: Cyanobacteria interspaces (with some bare soil) have low fertility and moderate nutrient disparities from canopies. Low dust capture and low organic matter (OM) produce low nutrient inputs. Sandy soils facilitate leaching and erosion of nutrient-rich substrates. Table above shows interspace-canopy nutrient disparities. Elevated characteristics unique to this cover type are indicated by *. Numbers 1, 2, and 3, show the magnitude of differences in mean/median values compared to other surfaces.

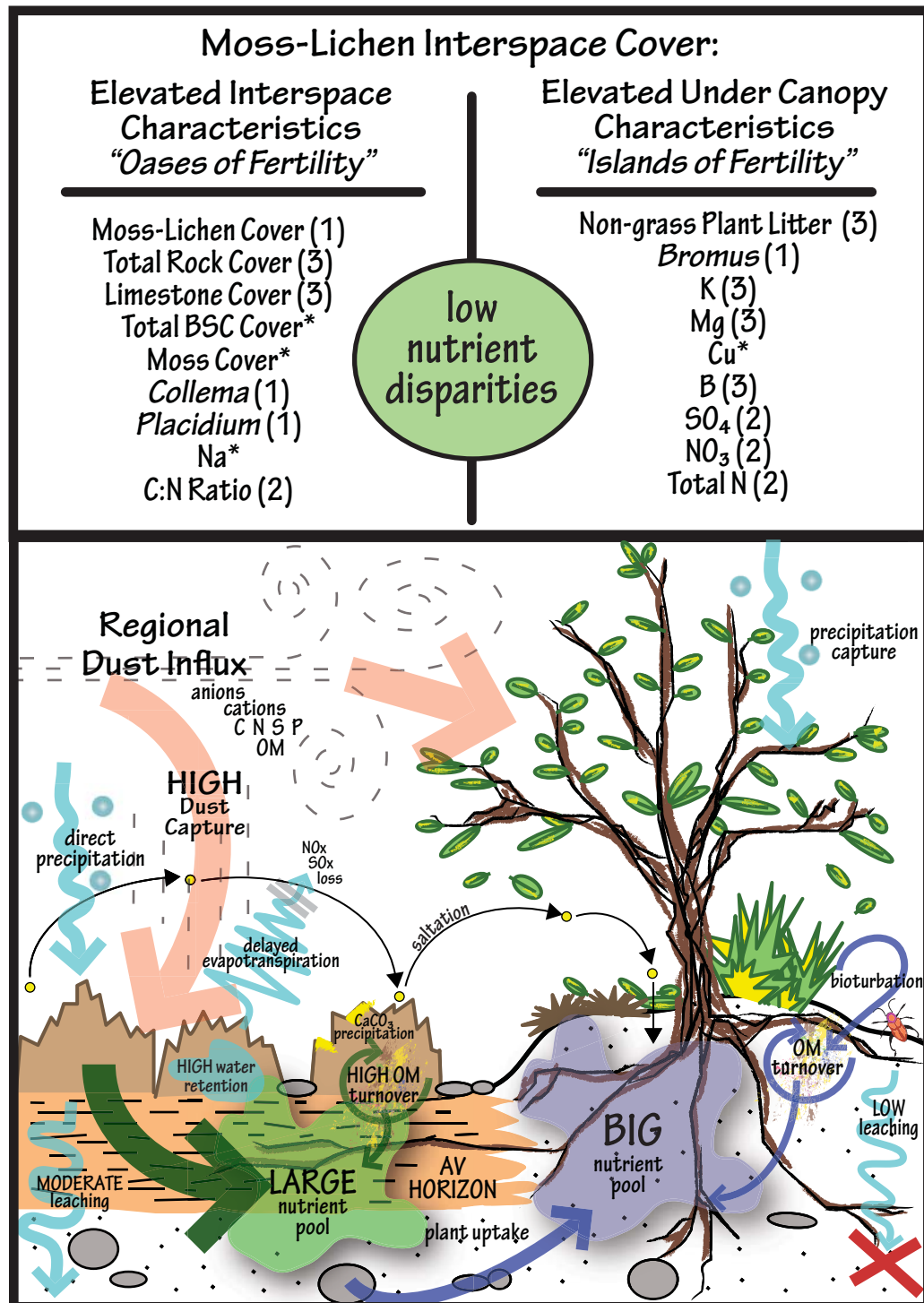


Figure 4.45: Moss-lichen interspaces have high fertility, with low nutrient disparities from shrub canopies. High dust capture leads to high nutrient inputs. Moss-lichen covered loamy-soil prevent erosion and helps maintain soil moisture for organic matter (OM) overturn. Table above shows magnitude of interspace-canopy nutrient disparities. Elevated characteristics unique to this cover type are indicated by *. The numbers 1, 2, and 3, show the relative magnitude of difference in mean/median values as compared to other surfaces.

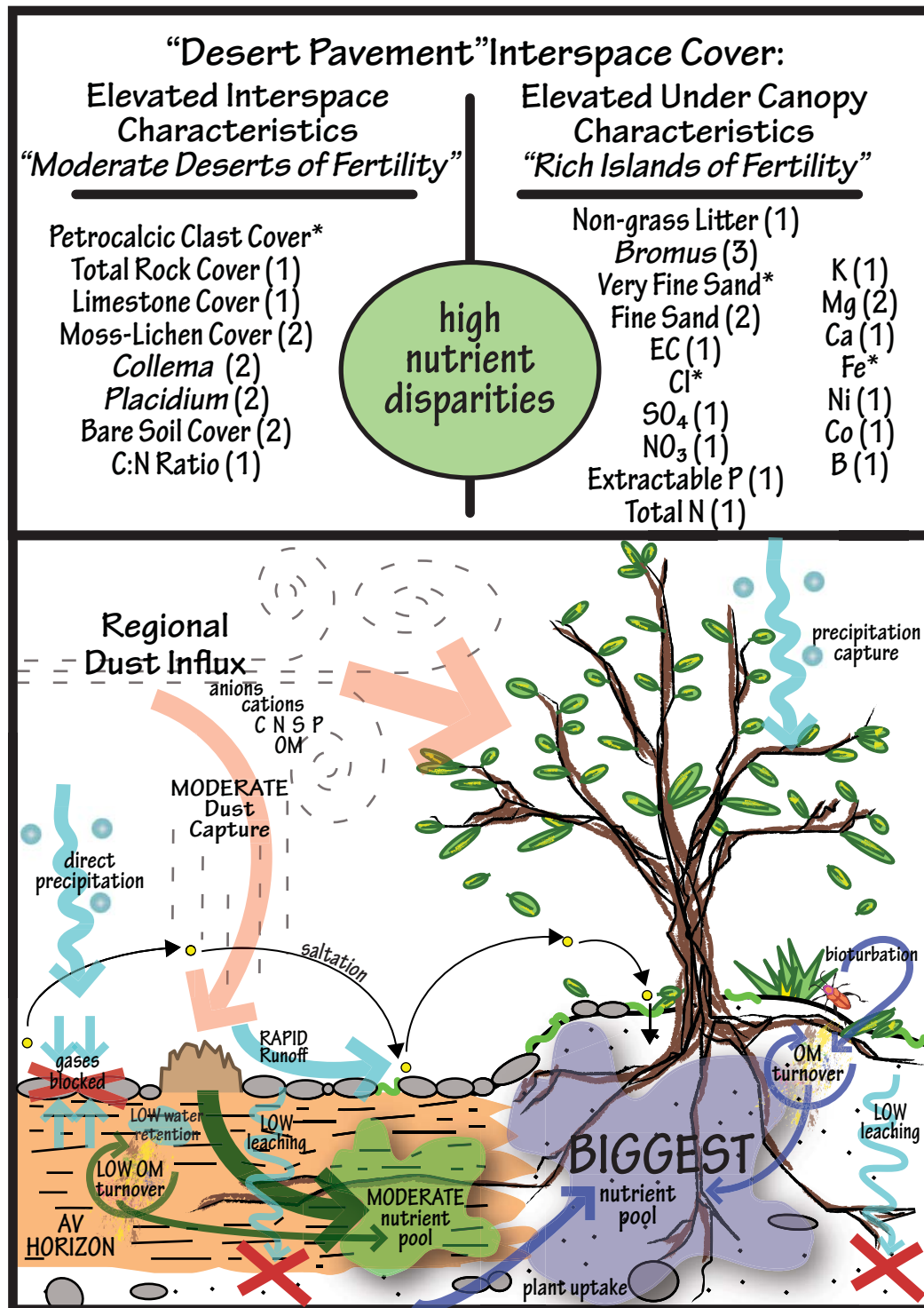


Figure 4.46: “Desert pavement” with scattered moss-lichen crusts have high canopy-nutrient disparities. Low water retention in interspaces leads to low organic matter (OM) turnover and nutrient availability. Low leaching maintains moderate fertility. Table above shows magnitude of interspace-canopy nutrient disparities. Elevated characteristics unique to this cover type are indicated by *. The numbers 1, 2, and 3, show the magnitude of difference in mean/median values as compared to other surfaces.

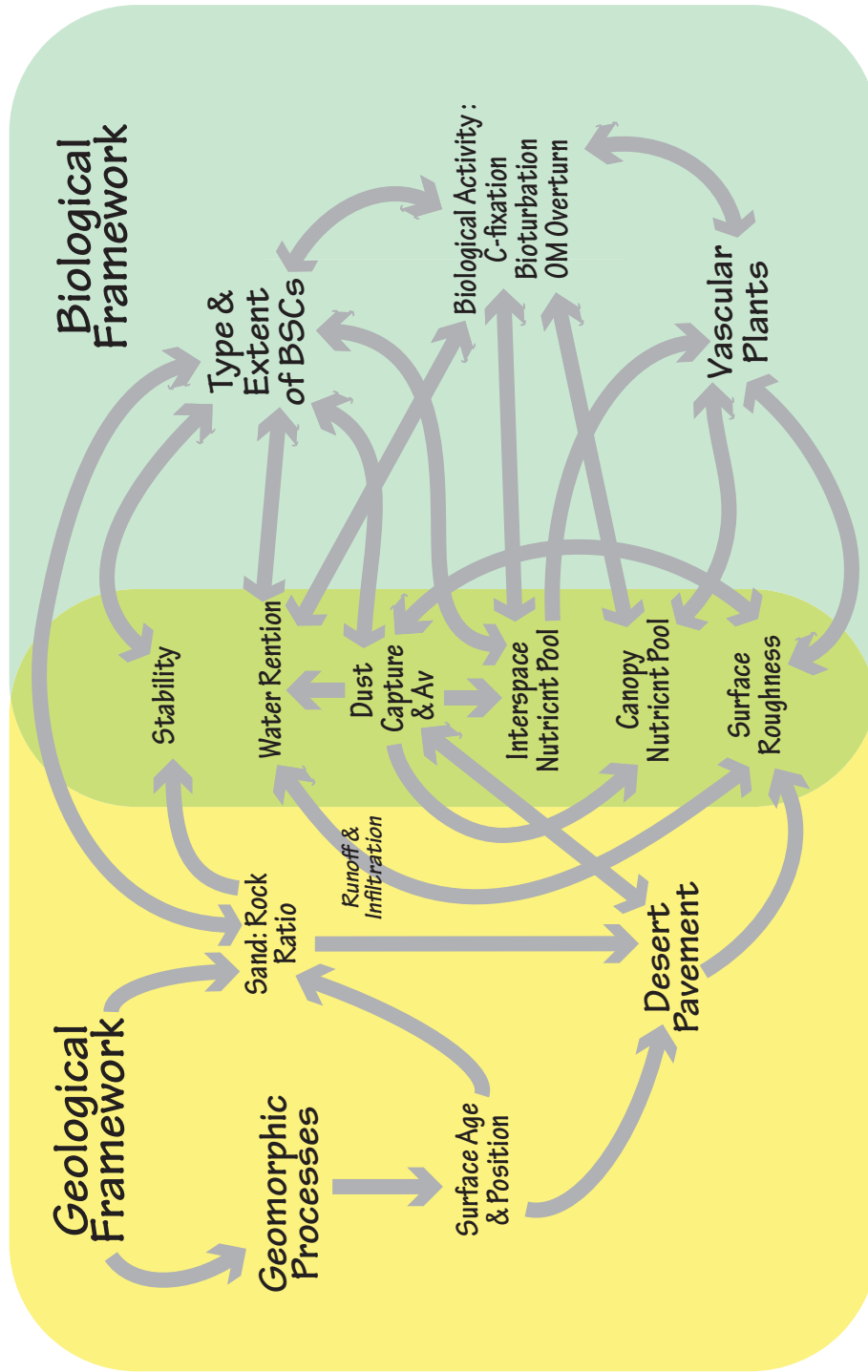


Figure 4.47: Biotic and abiotic factors interact together to determine interspace surface cover and canopy-interspace nutrient dynamics. Sand volume controls soil cover by desert pavement, moss-lichen, and cyanobacteria, which eventually lead to fertile island patterns. Geomorphic and biological self-enhancing feedbacks influence stability, water retention, dust capture, and surface roughness, which support biogeomorphic and biogeochemical stability.

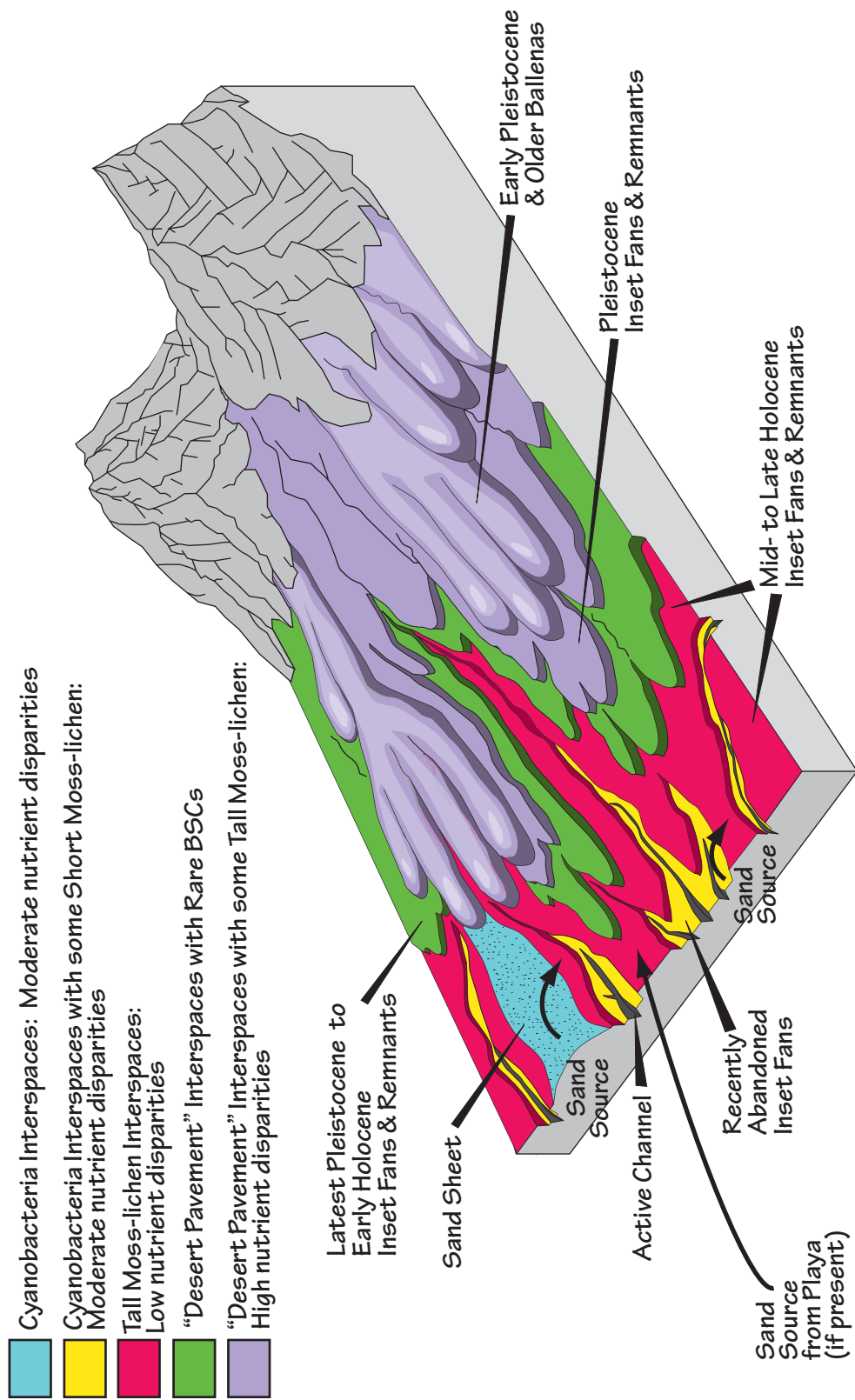


Figure 4.48: Geomorphic surfaces predict interspace cover and fertile island patterns. Sand sources include sand sheets, active channels, and alluvial flats or playas (not shown). Block model adapted after Peterson (1981).

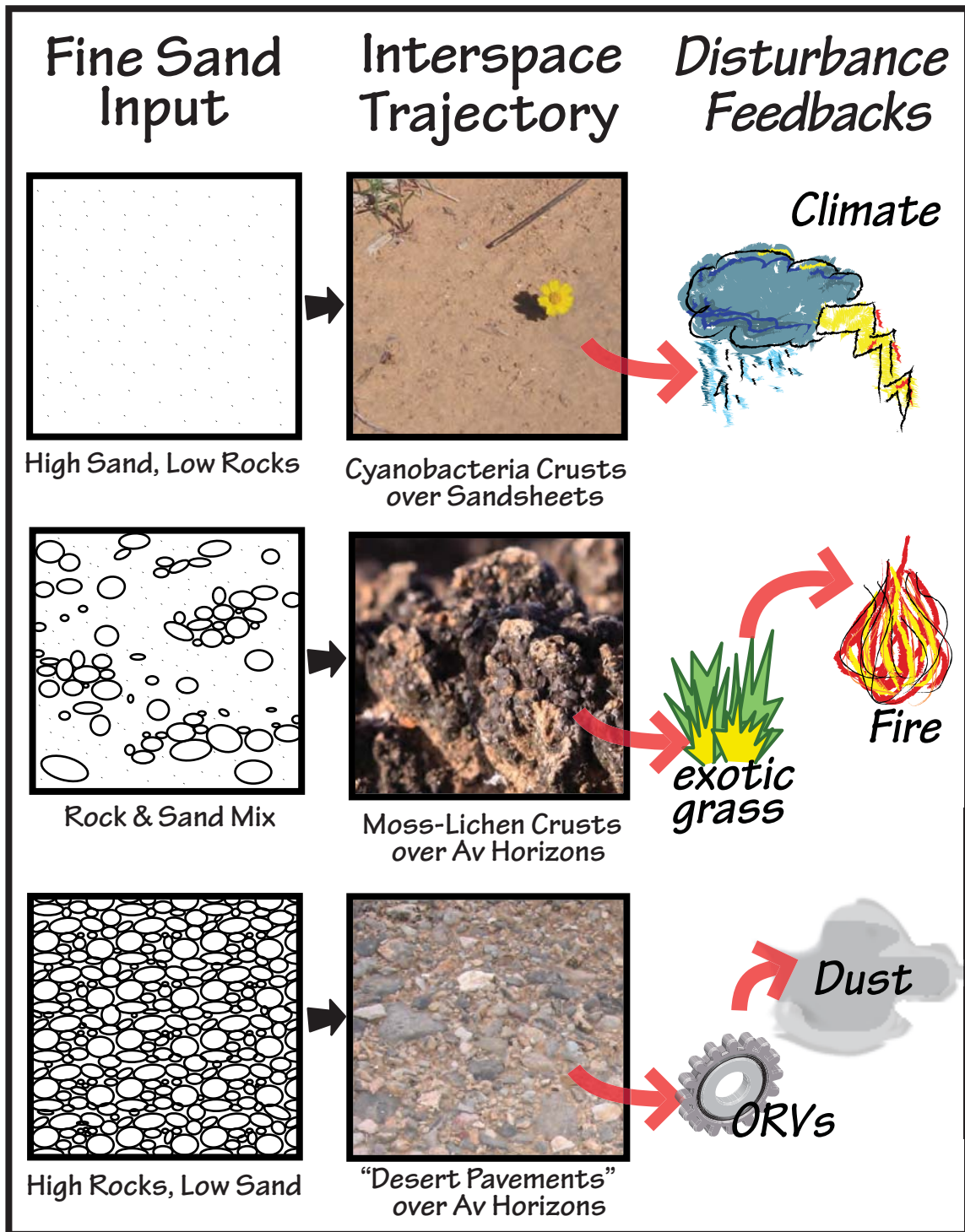


Figure 4.49: Soil profile particle size influences surface cover and disturbance susceptibility. Sandy soils lead to cyanobacteria crusts that are especially susceptible to climate change, as are all BSCs. Mixtures of sand and rock fragments lead to moss-lichen crusts that favor exotic grass invasion and wildfires. Gravel-dominated deposits lead to desert pavements that may emit large volumes of dust with ORV disturbance. These disturbances may disrupt self-enhancing feedbacks and ecological stability.

GIS Overlay Summary

Crust Cover	Dominant Geomorphic Surface (% Overlap)
Cyanobacteria-Bare Crusts BSC Map Unit CB.1	Qea (66%) <i>Deep Holocene Sand Sheets</i>
High Density Tall Moss-Lichen Crusts BSC Map Units ML.1 & ML.2	Qay ₁ & Qay ₂ (57-59%) <i>Alluvium (Mid- to Late Holocene)</i>
Scattered Low to Moderate Density Tall Moss-Lichen Crusts ("Desert Pavement") BSC Map Units S.1, S.2, & S.3	Qai ₃ & Older (63-87%) <i>Alluvium (Pleistocene or older)</i>

Table 4.1: Summary of three dominant crust types and their overlap with geomorphic units. Unit CB.1 has high density cyanobacteria-bare cover and has the greatest overlap with active sand sheets, Qea. Units ML.1 and ML.2 have high density tall moss-lichen pinnacled crusts and have the greatest overlap with mid- to late Holocene inset fans Qay₁ and Qay₂. Units S.1, S.2, and S.3 have low to moderate density tall moss-lichen crusts with and often include "desert pavement" or pavement-like rock cover and have the greatest overlap Pleistocene and older alluvial surfaces.

Geomorphic Map Unit Summary

Geomorphic Unit	Characteristics	Mean Interspace Rock Cover
Qay₄	Youngest alluvium; recent active channels; fresh bar and channel morphology; negligible soil development	not collected
Qay₃	Recently abandoned alluvium; latest Holocene inset fans; fresh bar and swale morphology; negligible soil development	46%
Qay₂	Youngest inactive alluvium; mid- to late Holocene inset fans; muted bar and swale; 15cm Av horizon; Stage I carbonate	18%
Qay₁	Young inactive alluvium; mid-Holocene inset fans; faint bar and swale; 27cm Av horizon; Stage II carbonate	25%
Qai₃	Intermediate alluvium; late Pleistocene inset fans; moderately interlocking pavements; 10cm Av; Stage III Bkkm; Stage I Bk	36%
Qai₂	Intermediate alluvium; mid- to late Pleistocene inset fans; moderately interlocking pavements; 13cm Av; Stage IV Bkkm; Stage I Bk	36%
Qai₁	Intermediate alluvium; early to mid-Pleistocene inset fans; variable pavements morphology; 16cm Av; Stage V Bkkm	49%
Qao₂	Old alluvium; early Pleistocene ballenas; poorly interlocking pavements; 18 cm Av; Stage III-V Bkkm; Stage II Bk with 5% secondary carbonate	63%
Qao₁	Old alluvium; earliest Pleistocene erosional fan remnants; variable pavement morphology; 9 cm Av; Stage V Bkkm	63%
QTa	Oldest alluvium; late Miocene to earliest Pleistocene erosional fan remnants; variable pavements; 8 cm Av; Stage VI Bkkm;	80%
Qc	Latest Pleistocene to Holocene colluvium; variable soils	83%
Qea	Holocene sand sheets with eolian/fluviol gravel lag; sand sheets >1m thick; up to Stage I carbonate morphology	30%

Table 4.2: Summary of geomorphic units and surface characteristics

Surface Cover Composite Classes

Composite Class	Component Categories
Total Canopy Cover	Sum of all plant canopies from line intercept data
Moss-lichen	Sum of moss and all lichen cover from point count data
Total BSCs	Sum of cyanobacteria, moss, and all lichen from point count data
Cyanobacteria-Bare	Sum of cyanobacteria and bare soil cover from point count data
Total Rock	Sum of surface rock cover from limestone, sandstone, and petrocalcic clasts from point count data

Table 4.3: Summary of surface cover composite classes used in data compilation

Paired t-Tests from All Plots

Elevated Interspace Characteristics	Elevated Canopy Characteristics
Total Rock Cover Total BSC Cover Limestone Cover Moss-lichen Cover Bare Soil Cover <i>Collema</i> <i>Placidium</i> Silt Clay Inorganic C Carbonate C:N Ratio Na	Non-grass Plant Litter <i>Bromus</i> Fine Sand Total Sand EC Cl SO ₄ NO ₃ Extractable P Mg Ni K Ca Mn Fe Cu Co B Organic C Total N

Table 4.4: Paired t-tests from all plot data show variable mean/median values for interspace and canopy characteristics. Characteristics are listed where they are found elevated. (See methods in Figure 10.)

Paired t-Tests from Three Interspace Cover Groups

Cyanobacteria-Bare Interspace Cover		Moss-Lichen Interspace Cover		Rock Interspace Cover ("Desert Pavement")	
Elevated Interspace Characteristics	Elevated Canopy Characteristics	Elevated Interspace Characteristics	Elevated Canopy Characteristics	Elevated Interspace Characteristics	Elevated Canopy Characteristics
Limestone Cover (2) Total Rock Cover (2) Cyanobacteria-Bare Cover* Bare Soil Cover (1) Collema (3)	Moss Cover* Non-grass Plant Litter (2) Bromus (2) Fine Sand (1) EC (2) Extractable P (2) K (2) Ca (2) Mg (2) Ni (2) B (2) Co (2)	Total Rock Cover (3) Limestone Cover (3) Total BSC Cover* Moss-Lichen Cover (1) Moss Cover* Collema (1) Placidium (1) Na* C:N Ratio (2)	Non-grass Litter (3) Bromus (1) K (3) Mg (3) Cu* B (3) SO4 (2) NO3 (2) Total N (2)	Total Rock Cover (1) Limestone Cover (1) Petrocalcic Clast Cover* Moss-Lichen Cover (2) Collema (2) Placidium (2) Bare Soil Cover (2) C:N Ratio (1)	Non-grass Litter (1) Bromus (3) Very Fine Sand* Fine Sand (2) EC (1) Cl* SO4 (1) NO3 (1) Extractable P (1) Total N (1) K (1) Mg (2) Ca (1) Fe* Ni (1) Co (1) B (1)

Table 4.5: Paired t-tests from three cover types show variation in mean/median values for interspace and canopy characteristics among three interspace surface cover types. Elevated characteristics unique to one cover type are indicated by *. Characteristics elevated in more than one cover type are indicated by 1, 2, and 3, with 1 being the greatest significant difference in mean/median values between canopy and interspace. (See methods in Figure 11.) Cyanobacteria-bare interspaces have high cyanobacteria crust cover with some bare soil cover. Rock-covered interspaces commonly form some type of "desert pavement".

Parametric Product Moment Correlation Coefficients

	Canopy Cyanobacteria	Canopy Total BSC	Canopy Plant Litter	Canopy Bromus
Canopy Cyanobacteria	1.000	.906**	-.186	-.480**
Canopy Total BSC%_UC	.906**	1.000	-.178	-.558**
Canopy Plant Litter	-.186	-.178	1.000	-.467**
Canopy <i>Bromus</i>	-.480**	-.558**	-.467**	1.000
Canopy Silt	-.316	-.297	.143	.045
Canopy Very Fine Sand	-.298	-.209	.019	.165
Canopy Fine Sand	.260	.251	-.060	-.106
Canopy Sand	.206	.152	-.149	.032
Canopy Total Sand	.264	.264	-.146	-.017
Canopy Na	-.099	-.138	-.033	.058
Canopy Ni	-.325	-.291	.078	-.042
Canopy Extractable P	-.078	-.090	.001	-.037
Canopy Total C	-.429**	-.392*	.290	-.131
Canopy Total N	-.354*	-.218	.041	.009
Canopy C:N Ratio	-.302	-.418*	.517**	-.284
Canopy EC	-.265	-.190	.190	-.134

	Pearson's R < -0.449999, Sig. at 0.05
	Pearson's R > 0.449999, Sig. at 0.05

Table 4.6: Parametric correlation coefficients of canopy cover characteristics are calculated as Pearson's R-values. Cells in blue show significant negative relationships at the 0.05 level, with R-values of -0.45 or less. Cells in orange show significant positive relationships at the 0.05 level, with R-values of 0.45 or greater.

Parametric Product Moment Correlation Coefficients

	Interspace Total BSC	Interspace Limestone
Interspace Total BSC	1.000	-.799**
Interspace Limestone	-.799**	1.000
Interspace Silt	-.229	.439**
Interspace Fine Sand	.265	-.486**
Interspace Sand	-.175	.047
Interspace Total Sand	.226	-.431**
Interspace Mg	.459**	-.258
Interspace Ca	.259	-.087
Interspace Fe	.220	-.075
Interspace Ni	.254	-.065
Interspace Extractable P	-.146	.268
Interspace pH	-.348*	.225
Interspace EC	.285	-.183
Interspace Inorganic C	-.583**	.729**
Interspace Organic C	-.286	.239
Interspace Carbonate	-.583**	.729**

	Pearson's R < -0.449999, Sig. at 0.05
	Pearson's R > 0.449999, Sig. at 0.05

Table 4.7: Parametric correlation coefficients of interspace characteristics are calculated as Pearson's R-values. Cells in blue show significant negative relationships at the 0.05 level, with R-values of -0.45 or less. Cells in orange show significant positive relationships at the 0.05 level, with R-values of 0.45 or greater.

Parametric Correlation Coefficients

	Canopy Cyanobacteria	Canopy Moss	Canopy <i>Collema</i>	Canopy <i>Placidium</i>	Canopy <i>Psora</i>	Canopy <i>Peltula</i>
Canopy Cyanobacteria	1.000	.095	-.056	-.093	-.284	-.187
Canopy Moss	.095	1.000	-.019	.001	-.028	-.106
Canopy <i>Collema</i>	.056	-.019	1.000	.401*	.102	-.057
Canopy <i>Placidium</i>	-.093	.001	.401*	1.000	.173	.227
Canopy <i>Psora</i>	-.284	-.028	.102	.173	1.000	-.041
Canopy <i>Peltula</i>	-.187	-.106	-.057	.227	-.041	1.000
Canopy Moss-Lichen	-.058	.665**	.558**	.404*	.147	-.057
Canopy Total BSC	.903**	.355*	.155	.032	-.260	-.203
Canopy Limestone	-.342*	-.262	.222	.205	.165	-.106
Canopy Sandstone	.205	.025	-.055	-.294	-.086	-.060
Canopy Petrocalcic	-.133	-.217	.039	.352*	.088	.340*
Canopy Total Rock	-.335*	-.415*	.195	.281	.171	.073
Canopy Bare	.211	.215	.086	-.242	-.058	-.157
Canopy Plant Litter	-.187	-.010	-.143	-.109	.158	.138
Canopy <i>Bromus</i>	-.447**	-.049	-.123	-.111	.076	.122
<i>Coleogyne</i>	.087	.121	.022	.283	.139	.218
<i>Pleuraphis</i>	.195	-.151	-.044	-.476**	-.118	-.082
<i>Hymenoclea</i>	-.101	.199	.078	-.055	-.157	-.110
<i>Larrea</i>	.219	.213	-.333*	-.268	-.196	.100
<i>Lycium a.</i>	.350*	-.148	-.060	-.061	-.073	-.051
<i>Dead Shrub</i>	.161	.223	-.339*	-.001	-.156	.090
<i>Psorothamnus</i>	.154	.237	-.034	-.055	-.108	-.075
<i>Menodora</i>	.168	.312	-.153	-.261	-.215	-.150
<i>Krameria</i>	-.175	-.035	.119	.074	-.108	-.075
<i>Encelia</i>	-.106	-.329	.295	.037	.144	-.082
<i>Tiquilia</i>	-.106	-.204	.172	.177	.676**	-.029
<i>Krascheninnikovia</i>	-.285	.155	-.025	.067	.717**	-.029
<i>Eriogonum f.</i>	.016	-.253	.074	-.185	-.041	-.029
<i>Ambrosia</i>	.113	-.278	.047	.011	-.244	.051

	rho<-.0449999, Sig. at 0.05
	rho>0.4499999, Sig. at 0.05

Table 4.8(A): Non-parametric correlation coefficients of canopy characteristics are calculated as rho-values. Cells in blue show significant negative relationships at the 0.05 level, with rho-values of -0.45 or less. Cells in orange show significant positive relationships at the 0.05 level, with rho-values of 0.45 or greater.

Parametric Correlation Coefficients

	Canopy Cyanobacteria	Canopy Moss	Canopy <i>Collema</i>	Canopy <i>Placidium</i>	Canopy <i>Psora</i>	Canopy <i>Peltula</i>
Canopy Clay	.095	-.316	-.063	.191	.124	.171
Canopy Silt	-.293	-.291	.190	.440**	.252	.122
Canopy Very Fine Sand	-.264	-.228	.344*	.292	.056	.268
Canopy Fine Sand	.259	.215	-.232	-.517**	-.217	-.138
Canopy Sand	.164	.329	-.139	-.053	-.032	-.236
Canopy Total Sand	.254	.288	-.162	-.430**	-.229	-.122
Canopy Na	-.095	-.172	-.031	.083	.278	.171
Canopy K	-.382*	-.261	.383*	.414*	.360*	.171
Canopy Mg	-.268	-.003	.416*	.270	.300	.106
Canopy Ca	-.319	-.246	.273	.312	.328	.106
Canopy Mn	-.154	-.148	.166	-.030	-.038	.106
Canopy Fe	-.374*	-.200	.394*	.274	.283	.089
Canopy Ni	-.260	-.273	.248	.352*	.374*	.106
Canopy Cu	-.182	-.018	.004	.358*	.314	-.089
Canopy Zn	-.314	.172	.218	.352*	.328	-.155
Canopy Cobalt	-.301	-.166	.133	.163	.374*	.106
Canopy B	-.391*	-.371*	.342*	.031	.264	.106
Canopy Mo	.005	.048	.367*	.501**	.302	.041
Canopy Cl_UC	.056	-.242	.002	.020	-.281	-.008
Canopy SO ₄	-.101	-.247	.222	.180	-.038	-.155
Canopy NO ₃	-.382*	-.178	.335*	.443**	.066	.220
Canopy Ext. P	-.097	-.003	-.051	.319	.051	-.138
Canopy Total C	-.435**	-.275	.244	.426**	.266	-.008
Canopy Inorganic C	-.358*	-.267	.022	.239	-.087	.122
Canopy Organic C	-.462**	-.158	.347*	.418*	.312	-.122
Canopy Total N	-.378*	.001	.411*	.506**	.210	-.089
Canopy Total S	.134	.403*	.372*	.295	-.136	-.155
Canopy C:N Ratio	-.299	-.546**	-.098	.107	.194	.171
Canopy Carbonate	-.358*	-.267	.022	.239	-.087	.122
Canopy pH	.049	.237	.239	.305	-.081	-.114
Canopy EC	-.290	-.182	.222	.266	.022	.220
Summer Insolation	.218	-.163	.175	.072	-.022	-.220
Equinox Insolation	.146	-.369*	-.006	-.296	-.136	-.252
Winter Insolation	.128	-.395*	-.032	-.318	-.136	-.236
Total Canopy Cover	.258	.228	-.408*	-.210	-.253	-.033



 rho < -0.449999, Sig. at 0.05
 rho > 0.4499999, Sig. at 0.05

Table 4.8(B): Non-parametric correlation coefficients of canopy characteristics are calculated as rho-values. Cells in blue show significant negative relationships at the 0.05 level, with rho-values of -0.45 or less. Cells in orange show significant positive relationships at the 0.05 level, with rho-values of 0.45 or greater.

Parametric Correlation Coefficients

	Canopy Moss-Lichen	Canopy Total BSC	Canopy Limestone	Canopy Sandstone	Canopy Petrocalcic
Canopy Cyanobacteria	-.058	.903**	-.342*	.205	-.133
Canopy Moss	.665**	.355*	-.262	.025	-.217
Canopy Collema	.558**	.155	.222	-.055	.039
Canopy Placidium	.404*	.032	.205	-.294	.352*
Canopy Psora	.147	-.260	.165	-.086	.088
Canopy Peltula	-.057	-.203	-.106	-.060	.340*
Canopy Moss-Lichen	1.000	.301	.039	-.041	-.132
Canopy Total BSC	.301	1.000	-.283	.163	-.157
Canopy Limestone	.039	-.283	1.000	.021	.103
Canopy Sandstone	-.041	.163	.021	1.000	-.033
Canopy Petrocalcic	-.132	-.157	.103	-.033	1.000
Canopy Total Rock	-.091	-.312	.925**	.030	.397*
Canopy Bare	.096	.303	-.073	.163	-.370*
Canopy Plant Litter	-.024	-.182	.411*	-.168	-.081
Canopy <i>Bromus</i>	-.139	-.528**	-.513**	-.091	.021
<i>Coleogyne</i>	.118	.186	.175	.102	.403*
<i>Pleuraphis</i>	-.235	.108	-.399*	.068	-.124
<i>Hymenoclea</i>	.184	.051	.400*	.151	-.057
<i>Larrea</i>	-.177	.119	-.485**	-.128	-.262
<i>Lycium a.</i>	-.184	.312	-.252	-.106	.309
<i>Dead Shrub</i>	-.082	.123	-.407*	-.380*	-.313
<i>Psorothamnus</i>	.268	.219	.196	.290	-.141
<i>Menodora</i>	.171	.208	-.232	.185	-.251
<i>Krameria</i>	.119	-.131	.106	-.157	-.141
<i>Encelia</i>	-.055	-.127	.358*	.028	-.059
<i>Tiquilia</i>	.090	-.106	.220	-.060	-.103
<i>Krascheninnikovia</i>	.114	-.252	.016	-.060	.216
<i>Eriogonum f.</i>	-.187	-.057	.114	.522**	-.103
<i>Ambrosia</i>	-.103	.033	-.094	.062	.158



 rho < -0.449999, Sig. at 0.05
 rho > 0.449999, Sig. at 0.05

Table 4.8(C): Non-parametric correlation coefficients of canopy characteristics are calculated as rho-values. Cells in blue show significant negative relationships at the 0.05 level, with rho-values of -0.45 or less. Cells in orange show significant positive relationships at the 0.05 level, with rho-values of 0.45 or greater.

Parametric Correlation Coefficients

	Canopy Moss-Lichen	Canopy Total BSC	Canopy Limestone	Canopy Sandstone	Canopy Petrocalcic
Canopy Clay	-.199	.002	.262	-.140	.367*
Canopy Silt	.026	-.327	.464**	-.170	.407*
Canopy Very Fine Sand	.052	-.258	.324	-.018	.429**
Canopy Fine Sand	-.107	.276	-.444**	.254	-.383*
Canopy Sand	.141	.145	-.260	-.101	-.353*
Canopy Total Sand	-.014	.289	-.463**	.187	-.397*
Canopy Na	-.125	-.196	.068	-.095	.215
Canopy K	.098	-.362*	.553**	-.050	.356*
Canopy Mg	.327	-.168	.466**	-.248	.088
Canopy Ca	.014	-.309	.503**	-.225	.369*
Canopy Mn	.040	-.084	.136	-.163	-.176
Canopy Fe	.099	-.299	.491**	-.216	.293
Canopy Ni	-.040	-.271	.493**	-.287	.320
Canopy Cu	.089	-.182	.210	-.166	-.005
Canopy Zn	.318	-.265	.277	-.018	.069
Canopy Cobalt	.011	-.268	.311	-.343*	.172
Canopy B	-.016	-.346*	.546**	.019	.198
Canopy Mo	.327	.030	.095	-.053	.060
Canopy Cl_UC	-.230	-.092	.196	.165	.207
Canopy SO ₄	-.042	-.173	.474**	.150	.127
Canopy NO ₃	.162	-.324	.522**	-.226	.217
Canopy Ext. P	-.039	-.191	.333*	-.150	.400*
Canopy Total C	.044	-.452**	.753**	-.072	.350*
Canopy Inorganic C	-.115	-.417*	.671**	-.017	.389*
Canopy Organic C	.154	-.427**	.659**	-.117	.269
Canopy Total N	.269	-.318	.533**	-.142	.306
Canopy Total S	.371*	.282	.084	.026	-.008
Canopy C:N Ratio	-.295	-.410*	.627**	-.012	.204
Canopy Carbonate	-.115	-.417*	.671**	-.017	.389*
Canopy pH	.256	.181	-.119	-.374*	-.114
Canopy EC	.055	-.232	.495**	-.207	.293
Summer Insolation	-.080	.171	.140	.037	-.023
Equinox Insolation	-.388*	.052	.204	.156	-.165
Winter Insolation	-.409*	.035	.235	.174	-.096
Total Canopy Cover	-.023	.225	-.340*	-.020	-.249

rho<-0.449999, Sig. at 0.05
 rho>0.449999, Sig. at 0.05

Table 4.8(D): Non-parametric correlation coefficients of canopy characteristics are calculated as rho-values. Cells in blue show significant negative relationships at the 0.05 level, with rho-values of -0.45 or less. Cells in orange show significant positive relationships at the 0.05 level, with rho-values of 0.45 or greater.

Parametric Correlation Coefficients

	Canopy Total Rock	Canopy Bare	Canopy Plant Litter	Canopy Bromus
Canopy Cyanobacteria	-.335*	.211	-.187	-.447**
Canopy Moss	-.415*	.215	-.010	-.049
Canopy <i>Collema</i>	.195	.086	-.143	-.123
Canopy <i>Placidium</i>	.281	-.242	-.109	-.111
Canopy <i>Psora</i>	.171	-.058	.158	.076
Canopy <i>Peltula</i>	.073	-.157	.138	.122
Canopy Moss-Lichen	-.091	.096	-.024	-.139
Canopy Total BSC	-.312	.303	-.182	-.528**
Canopy Limestone	.925**	-.073	.411*	-.513**
Canopy Sandstone	.030	.163	-.168	-.091
Canopy Petrocalcic	.397*	-.370*	-.081	.021
Canopy Total Rock	1.000	-.194	.338*	-.457**
Canopy Bare	-.194	1.000	.010	-.315
Canopy Plant Litter	.338*	.010	1.000	-.474**
Canopy Bromus	-.457**	-.315	-.474**	1.000
<i>Coleogyne</i>	.259	.172	.294	-.422*
<i>Pleuraphis</i>	-.383*	.096	-.250	.212
<i>Hymenoclea</i>	.308	.482**	.261	-.508**
<i>Larrea</i>	-.514**	-.031	-.222	.295
<i>Lycium a.</i>	-.045	.024	-.252	-.013
<i>Dead Shrub</i>	-.449**	.120	-.090	.186
<i>Psorothamnus</i>	.103	.273	.253	-.402*
<i>Menodora</i>	-.328	.501**	-.111	-.026
<i>Krameria</i>	.036	.193	-.038	.103
<i>Encelia</i>	.313	.020	.260	-.210
<i>Tiquilia</i>	.220	-.157	.244	-.106
<i>Krascheninnikovia</i>	.024	.070	-.016	.203
<i>Eriogonum f.</i>	.138	.165	-.187	.049
<i>Ambrosia</i>	-.020	-.476**	-.120	.154

	rho<-0.449999, Sig. at 0.05
	rho>0.449999, Sig. at 0.05

Table 4.8(E): Non-parametric correlation coefficients of canopy characteristics are calculated as rho-values. Cells in blue show significant negative relationships at the 0.05 level, with rho-values of -0.45 or less. Cells in orange show significant positive relationships at the 0.05 level, with rho-values of 0.45 or greater.

Parametric Correlation Coefficients

	Canopy Total Rock	Canopy Bare	Canopy Plant Litter	Canopy <i>Bromus</i>
Canopy Clay	.397*	-.446**	.185	-.148
Canopy Silt	.572**	-.639**	.188	.009
Canopy Very Fine Sand	.436**	-.523**	.122	.062
Canopy Fine Sand	-.523**	.613**	-.164	.010
Canopy Sand	-.443**	.350*	-.169	.062
Canopy Total Sand	-.569**	.601**	-.206	.032
Canopy Na	.157	-.244	.029	.105
Canopy K	.630**	-.454**	.081	-.031
Canopy Mg	.455**	-.399*	.125	-.069
Canopy Ca	.562**	-.458**	.229	-.080
Canopy Mn	.117	-.062	-.008	.064
Canopy Fe	.525**	-.291	.179	-.077
Canopy Ni	.536**	-.273	.236	-.140
Canopy Cu	.158	.061	.073	-.032
Canopy Zn	.175	.124	-.004	.072
Canopy Cobalt	.339*	-.258	.133	.047
Canopy B	.594**	-.320	.280	-.144
Canopy Mo	.038	-.282	-.223	.095
Canopy Cl_UC	.259	-.056	.145	-.181
Canopy SO ₄	.493**	-.262	.192	-.214
Canopy NO ₃	.558**	-.302	.031	-.036
Canopy Ext. P	.373*	-.531**	-.012	-.022
Canopy Total C	.774**	-.489**	.294	-.146
Canopy Inorganic C	.720**	-.331*	.313	-.200
Canopy Organic C	.646**	-.415*	.230	-.043
Canopy Total N	.494**	-.447**	.079	.026
Canopy Total S	-.017	.081	-.165	-.138
Canopy C:N Ratio	.710**	-.147	.522**	-.317
Canopy Carbonate	.720**	-.331*	.313	-.200
Canopy pH	-.223	.096	-.156	-.008
Canopy EC	.579**	-.463**	.262	-.123
Summer Insolation	.171	-.004	.157	-.226
Equinox Insolation	.238	.119	.231	-.292
Winter Insolation	.284	.109	.257	-.323
Total Canopy Cover	-.385*	.214	-.065	.020

	rho<-0.449999, Sig. at 0.05
	rho>0.4499999, Sig. at 0.05

Table 4.8(F): Non-parametric correlation coefficients of canopy characteristics are calculated as rho-values. Cells in blue show significant negative relationships at the 0.05 level, with rho-values of -0.45 or less. Cells in orange show significant positive relationships at the 0.05 level, with rho-values of 0.45 or greater.

Parametric Correlation Coefficients

	<i>Coleogyne</i>	<i>Pleuraphis</i>	<i>Hymenoclea</i>	<i>Larrea</i>	<i>Lycium andersonii</i>
Canopy Cyanobacteria	.087	.195	-.101	.219	.350*
Canopy Moss	.121	-.151	.199	.213	-.148
Canopy <i>Collema</i>	.022	-.044	.078	-.333*	-.060
Canopy <i>Placidium</i>	.283	-.476**	-.055	-.268	-.061
Canopy <i>Psora</i>	.139	-.118	-.157	-.196	-.073
Canopy <i>Peltula</i>	.218	-.082	-.110	.100	-.051
Canopy Moss-Lichen	.118	-.235	.184	-.177	-.184
Canopy Total BSC	.186	.108	.051	.119	.312
Canopy Limestone	.175	-.399*	.400*	-.485**	-.252
Canopy Sandstone	.102	.068	.151	-.128	-.106
Canopy Petrocalcic	.403*	-.124	-.057	-.262	.309
Canopy Total Rock	.259	-.383*	.308	-.514**	-.045
Canopy Bare	.172	.096	.482**	-.031	.024
Canopy Plant Litter	.294	-.250	.261	-.222	-.252
Canopy <i>Bromus</i>	-.422*	.212	-.508**	.295	-.013
<i>Coleogyne</i>	1.000	-.272	.232	-.488**	-.049
<i>Pleuraphis</i>	-.272	1.000	-.071	.178	.131
<i>Hymenoclea</i>	.232	-.071	1.000	-.407*	-.195
<i>Larrea</i>	-.488**	.178	-.407*	1.000	.231
<i>Lycium andersonii</i>	-.049	.131	-.195	.231	1.000
<i>Dead Shrub</i>	-.031	-.082	-.105	.353*	.011
<i>Psoralea</i>	.126	-.217	.270	-.235	-.134
<i>Menodora</i>	.051	.208	.210	.151	-.049
<i>Krameria</i>	-.235	-.217	.209	-.186	-.134
<i>Encelia</i>	-.029	.053	.230	-.393*	-.147
<i>Tiquilia</i>	-.136	-.082	-.110	-.136	-.051
<i>Krascheninnikovia</i>	.318	-.082	-.110	-.136	-.051
<i>Eriogonum fasciculatum</i>	-.136	.341*	.170	-.136	-.051
<i>Ambrosia</i>	-.109	-.048	-.613**	.109	.171



 rho<-0.449999, Sig. at 0.05
 rho>0.449999, Sig. at 0.05

Table 4.8(G): Non-parametric correlation coefficients of canopy characteristics are calculated as rho-values. Cells in blue show significant negative relationships at the 0.05 level, with rho-values of -0.45 or less. Cells in orange show significant positive relationships at the 0.05 level, with rho-values of 0.45 or greater.

Parametric Correlation Coefficients

	<i>Coleogyne</i>	<i>Pleuraphis</i>	<i>Hymenoclea</i>	<i>Larrea</i>	<i>Lycium andersonii</i>
Canopy Clay	.237	-.255	-.321	-.026	.322
Canopy Silt	.061	-.530**	-.222	-.140	.069
Canopy Very Fine Sand	-.109	-.257	-.113	-.076	-.045
Canopy Fine Sand	-.101	.524**	.214	.179	.018
Canopy Sand	.073	.080	.039	.012	-.246
Canopy Total Sand	-.106	.530**	.201	.167	-.079
Canopy Na	.123	.003	-.175	.037	.144
Canopy K	.031	-.281	.027	-.342*	-.158
Canopy Mg	-.098	-.194	.044	-.142	-.046
Canopy Ca	.170	-.288	-.033	-.198	-.055
Canopy Mn	-.102	-.044	-.080	.107	.046
Canopy Fe	.165	-.237	.117	-.236	-.084
Canopy Ni	.301	-.344*	-.012	-.190	-.083
Canopy Cu	.255	-.353*	.091	-.378*	-.207
Canopy Zn	.096	-.349*	.091	-.319	-.379*
Canopy Cobalt	.088	-.334*	-.085	-.038	.016
Canopy B	.045	-.036	.137	-.389*	-.133
Canopy Mo	.115	-.177	-.344*	-.117	-.225
Canopy Cl_UC	.204	-.099	.109	-.114	.069
Canopy SO ₄	.104	-.313	.204	-.336*	-.137
Canopy NO ₃	.084	-.264	.164	-.208	-.090
Canopy Ext. P	-.025	-.285	-.104	-.139	-.103
Canopy Total C	.087	-.487**	.092	-.418*	-.266
Canopy Inorganic C	.229	-.423*	.145	-.299	-.128
Canopy Organic C	.016	-.434**	.108	-.441**	-.299
Canopy Total N	.016	-.438**	.004	-.349*	-.350*
Canopy Total S	.223	-.206	.107	-.072	-.168
Canopy C:N Ratio	.282	-.304	.264	-.415*	-.018
Canopy Carbonate	.229	-.423*	.145	-.299	-.128
Canopy pH	.050	.178	.012	.123	-.097
Canopy EC	.117	-.255	.163	-.204	-.011
Summer Insolation	.130	-.204	.157	-.402*	.018
Equinox Insolation	-.047	.060	.204	-.081	.041
Winter Insolation	-.061	.088	.234	-.076	.096
Total Canopy Cover	-.018	.007	-.166	.342*	.108



 rho<-0.449999, Sig. at 0.05
 rho>0.449999, Sig. at 0.05

Table 4.8(H): Non-parametric correlation coefficients of canopy characteristics are calculated as rho-values. Cells in blue show significant negative relationships at the 0.05 level, with rho-values of -0.45 or less. Cells in orange show significant positive relationships at the 0.05 level, with rho-values of 0.45 or greater.

Parametric Correlation Coefficients

	<i>Dead Shrub</i>	<i>Psorothamnus</i>	<i>Menodora</i>	<i>Krameria</i>	<i>Encelia</i>
Canopy Cyanobacteria	.161	.154	.168	-.175	-.106
Canopy Moss	.223	.237	.312	-.035	-.329
Canopy <i>Collema</i>	-.339*	-.034	-.153	.119	.295
Canopy <i>Placidium</i>	-.001	-.055	-.261	.074	.037
Canopy <i>Psora</i>	-.156	-.108	-.215	-.108	.144
Canopy <i>Peltula</i>	.090	-.075	-.150	-.075	-.082
Canopy Moss-Lichen	-.082	.268	.171	.119	-.055
Canopy Total BSC	.123	.219	.208	-.131	-.127
Canopy Limestone	-.407*	.196	-.232	.106	.358*
Canopy Sandstone	-.380*	.290	.185	-.157	.028
Canopy Petrocalcic	-.313	-.141	-.251	-.141	-.059
Canopy Total Rock	-.449**	.103	-.328	.036	.313
Canopy Bare	.120	.273	.501**	.193	.020
Canopy Plant Litter	-.090	.253	-.111	-.038	.260
Canopy <i>Bromus</i>	.186	-.402*	-.026	.103	-.210
<i>Coleogyne</i>	-.031	.126	.051	-.235	-.029
<i>Pleuraphis</i>	-.082	-.217	.208	-.217	.053
<i>Hymenoclea</i>	-.105	.270	.210	.209	.230
<i>Larrea</i>	.353*	-.235	.151	-.186	-.393*
<i>Lycium andersonii</i>	.011	-.134	-.049	-.134	-.147
<i>Dead Shrub</i>	1.000	-.127	.150	.128	-.268
<i>Psorothamnus</i>	-.127	1.000	.282	.376*	-.036
<i>Menodora</i>	.150	.282	1.000	.037	-.149
<i>Krameria</i>	.128	.376*	.037	1.000	.164
<i>Encelia</i>	-.268	-.036	-.149	.164	1.000
<i>Tiquilia</i>	-.155	-.075	-.150	-.075	.294
<i>Krascheninnikovia</i>	-.065	-.075	-.150	-.075	-.082
<i>Eriogonum fasciculatum</i>	-.130	-.075	.141	-.075	.271
<i>Ambrosia</i>	-.164	.021	-.173	-.041	-.202

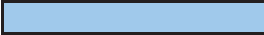

 rho < -0.449999, Sig. at 0.05
 rho > 0.449999, Sig. at 0.05

Table 4.8(I): Non-parametric correlation coefficients of canopy characteristics are calculated as rho-values. Cells in blue show significant negative relationships at the 0.05 level, with rho-values of -0.45 or less. Cells in orange show significant positive relationships at the 0.05 level, with rho-values of 0.45 or greater.

Parametric Correlation Coefficients

	<i>Dead Shrub</i>	<i>Psorothamnus</i>	<i>Menodora</i>	<i>Krameria</i>	<i>Encelia</i>
Canopy Clay	.030	-.045	-.246	-.145	-.016
Canopy Silt	-.209	-.169	-.413*	.007	.193
Canopy Very Fine Sand	-.419*	-.291	-.450**	-.001	.246
Canopy Fine Sand	.175	.045	.306	-.059	-.203
Canopy Sand	.386*	.325	.431**	.142	-.096
Canopy Total Sand	.169	.109	.382*	-.041	-.178
Canopy Na	.048	-.453**	-.093	-.510**	-.113
Canopy K	-.503**	-.284	-.595**	.034	.385*
Canopy Mg	-.247	-.286	-.376*	-.016	.314
Canopy Ca	-.291	-.410*	-.464**	-.155	.268
Canopy Mn	.115	-.354*	-.151	.020	.094
Canopy Fe	-.271	-.413*	-.415*	-.047	.346*
Canopy Ni	-.110	-.464**	-.344*	-.225	.260
Canopy Cu	.076	.032	-.048	.039	-.077
Canopy Zn	-.152	.105	.120	.074	-.049
Canopy Cobalt	-.053	-.433**	-.314	-.099	.181
Canopy B	-.549**	-.245	-.441**	-.087	.465**
Canopy Mo	-.069	-.174	-.138	-.154	-.081
Canopy Cl	-.154	-.159	-.042	-.162	-.023
Canopy SO ₄	-.372*	-.069	-.320	.073	.155
Canopy NO ₃	-.156	-.426**	-.257	-.067	.210
Canopy Ext. P	-.234	.018	-.370*	.111	-.034
Canopy Total C	-.437**	-.039	-.399*	.112	.352*
Canopy Inorganic C	-.249	.162	-.227	.130	.285
Canopy Organic C	-.444**	-.101	-.379*	.149	.244
Canopy Total N	-.339*	-.046	-.359*	.182	.176
Canopy Total S	-.100	.072	.146	.127	-.143
Canopy C:N Ratio	-.214	.078	-.231	.089	.421*
Canopy Carbonate	-.249	.162	-.227	.130	.285
Canopy pH	.113	-.354*	.088	-.182	-.054
Canopy EC	-.156	-.307	-.411*	.014	.310
Summer Insolation	.052	.191	-.113	.367*	.372*
Equinox Insolation	-.140	.004	-.196	.084	.031
Winter Insolation	-.248	-.008	-.191	-.005	.032
Total Canopy Cover	.481**	.373*	.467**	.160	-.449**



 rho < -0.449999, Sig. at 0.05
 rho > 0.449999, Sig. at 0.05

Table 4.8(J): Non-parametric correlation coefficients of canopy characteristics are calculated as rho-values. Cells in blue show significant negative relationships at the 0.05 level, with rho-values of -0.45 or less. Cells in orange show significant positive relationships at the 0.05 level, with rho-values of 0.45 or greater.

Parametric Correlation Coefficients

	<i>Tiquilia</i>	<i>Krascheninnikovia</i>	<i>Eriogonum fasciculatum</i>	<i>Ambrosia</i>
Canopy Cyanobacteria	-.106	-.285	.016	.113
Canopy Moss	-.204	.155	-.253	-.278
Canopy <i>Collema</i>	.172	-.025	.074	.047
Canopy <i>Placidium</i>	.177	.067	-.185	.011
Canopy <i>Psora</i>	.676**	.717**	-.041	-.244
Canopy <i>Peltula</i>	-.029	-.029	-.029	.051
Canopy Moss-Lichen	.090	.114	-.187	-.103
Canopy Total BSC	-.106	-.252	-.057	.033
Canopy Limestone	.220	.016	.114	-.094
Canopy Sandstone	-.060	-.060	.522**	.062
Canopy Petrocalcic	-.103	.216	-.103	.158
Canopy Total Rock	.220	.024	.138	-.020
Canopy Bare	-.157	.070	.165	-.476**
Canopy Plant Litter	.244	-.016	-.187	-.120
Canopy <i>Bromus</i>	-.106	.203	.049	.154
<i>Coleogyne</i>	-.136	.318	-.136	-.109
<i>Pleuraphis</i>	-.082	-.082	.341*	-.048
<i>Hymenoclea</i>	-.110	-.110	.170	-.613**
<i>Larrea</i>	-.136	-.136	-.136	.109
<i>Lycium andersonii</i>	-.051	-.051	-.051	.171
Dead Shrub	-.155	-.065	-.130	-.164
<i>Psorothamnus</i>	-.075	-.075	-.075	.021
<i>Menodora</i>	-.150	-.150	.141	-.173
<i>Krameria</i>	-.075	-.075	-.075	-.041
<i>Encelia</i>	.294	-.082	.271	-.202
<i>Tiquilia</i>	1.000	-.029	-.029	-.170
<i>Krascheninnikovia</i>	-.029	1.000	-.029	-.170
<i>Eriogonum fasciculatum</i>	-.029	-.029	1.000	-.170
<i>Ambrosia</i>	-.170	-.170	-.170	1.000

rho<-0.449999, Sig. at 0.05
rho>0.449999, Sig. at 0.05

Table 4.8(K): Non-parametric correlation coefficients of canopy characteristics are calculated as rho-values. Cells in blue show significant negative relationships at the 0.05 level, with rho-values of -0.45 or less. Cells in orange show significant positive relationships at the 0.05 level, with rho-values of 0.45 or greater.

Parametric Correlation Coefficients

	<i>Tiquilia</i>	<i>Krascheninnikovia</i>	<i>Eriogonum f.</i>	<i>Ambrosia</i>
Canopy Clay	.203	-.024	-.057	.350*
Canopy Silt	.285	.073	-.089	.266
Canopy Very Fine Sand	.106	-.024	.057	.232
Canopy Fine Sand	-.285	-.024	.171	-.217
Canopy Sand	-.106	.057	-.252	-.220
Canopy Total Sand	-.268	-.057	.089	-.258
Canopy Na	.236	.155	.041	-.027
Canopy K	.285	.220	.073	.000
Canopy Mg	.285	.138	.041	-.102
Canopy Ca	.187	.268	.024	.007
Canopy Mn	.041	-.089	.203	-.028
Canopy Fe	.122	.268	.073	-.109
Canopy Ni	.252	.268	-.008	-.120
Canopy Cu	.236	.203	-.236	-.154
Canopy Zn	.187	.268	-.089	-.268
Canopy Cobalt	.252	.268	-.089	-.132
Canopy B	.285	.089	.220	.034
Canopy Mo	.236	.187	-.155	.277
Canopy Cl _{UC}	-.171	-.220	-.057	.228
Canopy SO ₄	.057	-.106	-.041	.156
Canopy NO ₃	.138	-.041	.024	-.124
Canopy Ext. P	-.073	.138	-.252	.196
Canopy Total C	.252	.122	-.024	.053
Canopy Inorganic C	-.220	.089	.024	.140
Canopy Organic C	.285	.155	-.024	-.029
Canopy Total N	.138	.155	-.106	.074
Canopy Total S	-.187	-.008	-.138	.054
Canopy C:N Ratio	.252	.024	.073	-.113
Canopy Carbonate	-.220	.089	.024	.140
Canopy pH	-.074	-.041	-.286	-.049
Canopy EC	.041	-.008	.106	-.047
Summer Insolation	.252	-.268	.057	-.134
Equinox Insolation	.106	-.285	.155	-.101
Winter Insolation	.106	-.285	.155	-.121
Total Canopy Cover	-.269	-.090	-.236	.344*

	rho<-0.449999, Sig. at 0.05
	rho>0.4499999, Sig. at 0.05

Table 4.8(L): Non-parametric correlation coefficients of canopy characteristics are calculated as rho-values. Cells in blue show significant negative relationships at the 0.05 level, with rho-values of -0.45 or less. Cells in orange show significant positive relationships at the 0.05 level, with rho-values of 0.45 or greater.

Non-Parametric Correlation Coefficients

	Interspace Cyanobacteria	Interspace Moss	Interspace <i>Collema</i>	Interspace <i>Placidium</i>
Interspace Cyanobacteria	1.000	-.331 [*]	-.234	-.086
Interspace Moss	-.331 [*]	1.000	.724 ^{**}	.349 [*]
Interspace <i>Collema</i>	-.234	.724 ^{**}	1.000	.586 ^{**}
Interspace <i>Placidium</i>	-.086	.349 [*]	.586 ^{**}	1.000
Interspace <i>Psora</i>	-.370 [*]	.017	.013	.119
Interspace <i>Peltula</i>	-.019	.041	.111	.428 ^{**}
Interspace Moss-Lichen	-.242	.799 ^{**}	.967 ^{**}	.666 ^{**}
Total BSC	.516 ^{**}	.400 [*]	.608 ^{**}	.387 [*]
Interspace Limestone	-.501 ^{**}	-.296	-.336 [*]	-.154
Interspace Sandstone	-.019	.284	.072	-.347 [*]
Interspace Petrocalcic	-.207	.021	-.080	.266
Interspace Total Rock	-.559 ^{**}	-.203	-.328	-.060
Interspace Bare	.169	-.187	-.264	-.465 ^{**}
Interspace Plant Litter	.099	-.075	-.220	-.112
Interspace <i>Bromus</i>	-.206	.081	.356 [*]	.051
Interspace Clay	.268	-.525 ^{**}	-.279	.110
Interspace Silt	-.262	-.152	.017	.463 ^{**}
Interspace Very Fine Sand	-.215	.188	.312	.559 ^{**}
Interspace Fine Sand	.293	.123	-.051	-.550 ^{**}
Interspace Sand	-.081	.101	-.062	-.184
Interspace Total Sand	.145	.237	.053	-.388 [*]

	rho<-.449999, Sig. at 0.05
	rho>0.449999, Sig. at 0.05

Table 4.9(A): Non-parametric correlation coefficients of interspace characteristics are calculated as rho-values. Cells in blue show significant negative relationships at the 0.05 level, with rho-values of -0.45 or less. Cells in orange show significant positive relationships at the 0.05 level, with rho-values of 0.45 or greater.

Non-Parametric Correlation Coefficients

	Interspace Cyanobacteria	Interspace Moss	Interspace <i>Collema</i>	Interspace <i>Placidium</i>
Interspace Na	.039	-.085	.010	-.058
Interspace K	-.209	.378*	.469**	.428**
Interspace Mg	.004	.181	.512**	.450**
Interspace Ca	-.432**	.458**	.554**	.524**
Interspace Mn	.014	.416*	.163	.141
Interspace Fe_	-.312	.343*	.327	.395*
Interspace Ni	-.238	.274	.422*	.477**
Interspace Cu	.262	-.563**	-.626**	-.402*
Interspace Zn	.099	.151	-.189	-.016
Interspace Co	-.033	.137	.181	.157
Interspace B	-.415*	.458**	.528**	.428**
Interspace Mo	.053	-.017	-.068	.194
Interspace Cl	.197	.240	.035	.400*
Interspace SO ₄	-.137	.050	.121	.205
Interspace NO ₃	.014	-.133	-.044	.113
Interspace Extractable P	-.417*	.037	.150	.305
Interspace pH	.017	-.113	-.491**	-.519**
Interspace EC	-.336*	.473**	.566**	.596**
Interspace Total C	-.521**	.021	.059	.331*
Interspace Inorg. C	-.553**	-.107	-.089	.148
Interspace Organic C	-.426**	.156	.178	.413*
Interspace Total N	-.410*	.273	.390*	.501**
Interspace Total S	-.024	-.036	.181	-.106
Interspace C:N Ratio	-.404*	-.094	-.221	-.033
Interspace Carbonate	-.553**	-.107	-.089	.148
Summer Insolation	.065	-.137	.081	.109
Equinox Insolation	.029	.085	.019	-.206
Winter Insolation	.028	.084	-.050	-.239
Maximum Pinnacle Height	-.168	.525**	.710**	.657**

	rho<-0.449999, Sig. at 0.05
	rho>0.449999, Sig. at 0.05

Table 4.9(B): Non-parametric correlation coefficients of interspace characteristics are calculated as rho-values. Cells in blue show significant negative relationships at the 0.05 level, with rho-values of -0.45 or less. Cells in orange show significant positive relationships at the 0.05 level, with rho-values of 0.45 or greater.

Non-Parametric Correlation Coefficients

	Interspace <i>Psora</i>	Interspace <i>Peltula</i>	Interspace Moss-Lichen	Interspace Total BSC
Interspace Cyanobacteria	-.370*	-.019	-.242	.516**
Interspace Moss	.017	.041	.799**	.400*
Interspace <i>Collema</i>	.013	.111	.967**	.608**
Interspace <i>Placidium</i>	.119	.428**	.666**	.387*
Interspace <i>Psora</i>	1.000	-.081	.006	-.248
Interspace <i>Peltula</i>	-.081	1.000	.166	.104
Interspace Moss-Lichen	.006	.166	1.000	.613**
Total BSC	-.248	.104	.613**	1.000
Interspace Limestone	.293	-.109	-.362*	-.801**
Interspace Sandstone	-.050	-.349*	.099	.198
Interspace Petrocalcic	.244	.023	-.006	-.219
Interspace Total Rock	.273	-.017	-.306	-.837**
Interspace Bare	-.087	-.142	-.276	.029
Interspace Plant Litter	.002	-.062	-.227	-.061
Interspace <i>Bromus</i>	.149	.045	.224	.074
Interspace Clay	.187	-.047	-.311	-.156
Interspace Silt	.278	.080	.016	-.322
Interspace Very Fine Sand	.109	.169	.326	.130
Interspace Fine Sand	-.268	-.098	-.060	.320
Interspace Sand	-.205	-.069	-.056	-.167
Interspace Total Sand	-.252	-.055	.061	.301

rho<-0.449999, Sig. at 0.05
rho>0.449999, Sig. at 0.05

Table 4.9(C): Non-parametric correlation coefficients of interspace characteristics are calculated as rho-values. Cells in blue show significant negative relationships at the 0.05 level, with rho-values of -0.45 or less. Cells in orange show significant positive relationships at the 0.05 level, with rho-values of 0.45 or greater.

Non-Parametric Correlation Coefficients

	Interspace <i>Psora</i>	Interspace <i>Peltula</i>	Interspace Moss-Lichen	Interspace Total BSC
Interspace Na	-.082	.164	-.021	.017
Interspace K	-.030	.303	.471**	.328
Interspace Mg	.004	.378*	.485**	.447**
Interspace Ca	.186	.309	.581**	.166
Interspace Mn	.082	.154	.241	.250
Interspace Fe_	.149	.257	.381*	.126
Interspace Ni	.140	.459**	.420*	.170
Interspace Cu	.118	-.155	-.644**	-.329
Interspace Zn	.042	.233	-.115	-.010
Interspace Co	.154	.256	.162	.133
Interspace B	-.022	.073	.547**	.146
Interspace Mo	.113	.165	-.006	.116
Interspace Cl	-.217	.486**	.194	.311
Interspace SO ₄	.042	.052	.132	-.020
Interspace NO ₃	.130	.124	-.031	-.022
Interspace Extractable P	.008	-.026	.168	-.129
Interspace pH	-.070	-.150	-.457**	-.384*
Interspace EC	.102	.457**	.615**	.259
Interspace Total C	.124	.107	.093	-.471**
Interspace Inorg. C	.243	.013	-.081	-.590**
Interspace Organic C	.006	.123	.230	-.261
Interspace Total N	.037	.258	.399*	-.046
Interspace Total S	-.144	.186	.097	.154
Interspace C:N Ratio	.181	-.128	-.189	-.649**
Interspace Carbonate	.243	.013	-.081	-.590**
Summer Insolation	-.119	.129	.075	.035
Equinox Insolation	-.496**	-.198	.045	.060
Winter Insolation	-.543**	-.214	-.010	.026
Maximum Pinnacle Height	.108	.328	.705**	.498**

	rho<-0.449999, Sig. at 0.05
	rho>0.449999, Sig. at 0.05

Table 4.9(D): Non-parametric correlation coefficients of interspace characteristics are calculated as rho-values. Cells in blue show significant negative relationships at the 0.05 level, with rho-values of -0.45 or less. Cells in orange show significant positive relationships at the 0.05 level, with rho-values of 0.45 or greater.

Non-Parametric Correlation Coefficients

	Interspace Total Rock	Interspace Bare	Interspace Plant Litter	Interspace <i>Bromus</i>
Interspace Cyanobacteria	-.559**	.169	.099	-.206
Interspace Moss	-.203	-.187	-.075	.081
Interspace <i>Collema</i>	-.328	-.264	-.220	.356*
Interspace <i>Placidium</i>	-.060	-.465**	-.112	.051
Interspace <i>Psora</i>	.273	-.087	.002	.149
Interspace <i>Peltula</i>	-.017	-.142	-.062	.045
Interspace Moss-Lichen	-.306	-.276	-.227	.224
Total BSC	-.837**	.029	-.061	.074
Interspace Limestone	.867**	-.245	.087	-.021
Interspace Sandstone	-.303	.423*	-.073	-.179
Interspace Petrocalcic	.468**	-.450**	-.217	-.284
Interspace Total Rock	1.000	-.360*	-.042	-.207
Interspace Bare	-.360*	1.000	.046	-.219
Interspace Plant Litter	-.042	.046	1.000	-.030
Interspace <i>Bromus</i>	-.207	-.219	-.030	1.000
Interspace Clay	.352*	-.243	-.097	-.178
Interspace Silt	.582**	-.615**	-.140	.051
Interspace Very Fine Sand	.033	-.464**	.141	.192
Interspace Fine Sand	-.575**	.597**	.154	-.074
Interspace Sand	-.036	.251	-.089	.043
Interspace Total Sand	-.561**	.569**	.149	.002

	rho<-0.449999, Sig. at 0.05
	rho>0.449999, Sig. at 0.05

Table 4.9(E): Non-parametric correlation coefficients of interspace characteristics are calculated as rho-values. Cells in blue show significant negative relationships at the 0.05 level, with rho-values of -0.45 or less. Cells in orange show significant positive relationships at the 0.05 level, with rho-values of 0.45 or greater.

Non-Parametric Correlation Coefficients

	Interspace Total Rock	Interspace Bare	Interspace Plant Litter	Interspace <i>Bromus</i>
Interspace Na	-.015	.037	.031	-.056
Interspace K	-.322	-.171	.045	.411 [*]
Interspace Mg	-.402 [*]	-.096	-.178	.482 ^{**}
Interspace Ca	-.028	-.439 ^{**}	-.232	.375 [*]
Interspace Mn	-.237	-.107	-.042	.072
Interspace Fe	-.076	-.317	-.282	.230
Interspace Ni	-.076	-.423 [*]	-.332 [*]	.440 ^{**}
Interspace Cu	.277	.035	-.017	-.286
Interspace Zn	-.062	-.121	-.083	-.115
Interspace Co	-.145	-.207	-.364 [*]	.354 [*]
Interspace B	.009	-.397 [*]	-.056	.216
Interspace Mo	-.039	-.259	-.171	.086
Interspace Cl	-.184	-.240	.141	-.291
Interspace SO ₄	.041	-.117	-.086	.041
Interspace NO ₃	-.144	-.018	-.067	.340 [*]
Interspace Extractable P	.319	-.256	.096	-.079
Interspace pH	.227	.054	.130	-.229
Interspace EC	-.170	-.300	-.122	.340 [*]
Interspace Total C	.623 ^{**}	-.464 ^{**}	.009	.115
Interspace Inorg. C	.710 ^{**}	-.350 [*]	-.009	.110
Interspace Organic C	.388 [*]	-.415 [*]	.042	.083
Interspace Total N	.147	-.417 [*]	.160	.341 [*]
Interspace Total S	-.203	.062	.323	.334 [*]
Interspace C:N Ratio	.736 ^{**}	-.308	-.190	-.102
Interspace Carbonate	.710 ^{**}	-.350 [*]	-.009	.110
Summer Insolation	.038	.149	-.338 [*]	-.058
Equinox Insolation	-.022	.174	.078	-.269
Winter Insolation	.009	.183	.107	-.355 [*]
Maximum Pinnacle Height	-.327	-.306	-.066	.278

rho<-0.449999, Sig. at 0.05
 rho>0.449999, Sig. at 0.05

Table 4.9(F): Non-parametric correlation coefficients of interspace characteristics are calculated as rho-values. Cells in blue show significant negative relationships at the 0.05 level, with rho-values of -0.45 or less. Cells in orange show significant positive relationships at the 0.05 level, with rho-values of 0.45 or greater.

Parametric Product Moment Correlation Coefficients

	Interspace Moss-Lichen	Interspace Total BSC	Interspace Total Rock
Interspace Moss-Lichen	1.000**	.831**	-.527
Interspace Total BSC	.831**	1.000**	-.796**
Interspace Total Rock	-.527	-.796**	1.000**
Interspace Organic C	.051	.170	-.576*
Interspace Cu	-.332	-.350	.629*

	Pearson's R < -0.449999, Sig. at 0.05
	Pearson's R > 0.449999, Sig. at 0.05

Table 4.10: Parametric correlation coefficients of soil characteristics are calculated as Pearson's R-values in areas where interspaces have >52.9% total rock cover. Cells in blue show significant negative relationships at the 0.05 level, with R-values of -0.45 or less. Cells in orange show significant positive relationships at the 0.05 level, with R-values of 0.45 or greater. No significant canopy correlations were found in these analyses.

Non-Parametric Correlation Coefficients

	Percent Slope	Interspace Moss-Lichen	Interspace Total BSC	Interspace Total Rock
Interspace Moss-Lichen	-.360	1.000	.813**	-.490
Interspace Total BSC	-.590*	.813**	1.000	-.729**
Interspace Total Rock	.343	-.490	-.729**	1.000
Interspace pH	.645*	-.264	-.558*	.394
Interspace Organic C	-.493	.016	.280	-.600*
Interspace Mn	.615*	.176	-.115	.135
Interspace Cu	.180	-.434	-.291	.619*
Interspace Zn	.604*	.027	-.269	.388

	rho<-0.449999, Sig. at 0.05
	rho>0.449999, Sig. at 0.05

Table 4.11: Non-parametric correlation coefficients of soil characteristics are calculated as rho-values in areas where interspaces have >52.9% total rock cover. Cells in blue show significant negative relationships at the 0.05 level, with rho-values of -0.45 or less. Cells in orange show significant positive relationships at the 0.05 level, with rho-values of 0.45 or greater. No significant canopy correlations were found in these analyses.

APPENDIX 1

METHODS

1.1 Thin Section Preparation and Analysis

In June 2009, 70 BSC samples were collected from shrub interspaces in seven locations within the Hidden Valley portion of the Muddy Mountains Wilderness Area, Nevada (Figure 2.3). Three morphological types of BSCs were collected. (1) Cyanobacterial crusts were mostly smooth with some convex surface protrusions (Figure 2.1). (2) Short moss-lichen crusts were composed of mosses and lichens with surface relief of up to 2 cm (Figure 2.2B). (3) Tall, pinnacled moss-lichen crusts were composed of lichens and some mosses with surface relief from 2-5 cm (Figure 2.2 C, E, F)). Moss-lichen samples included moss-dominated crusts with >60% moss cover, lichen-dominated crusts with >50% lichen cover, which commonly include mixtures of mosses and lichens. Cyanobacteria crusts were not sampled exclusively, but sampled in association with short moss-lichen crusts. However, their unique surface morphology and component taxa warrant separation from other crust types.

The seven sampling locations covered a variety of soil and geomorphic settings. Ten moss-lichen samples were collected from each site. Cyanobacteria crusts were collected where they occurred adjacent to short moss-lichen crusts. Sample locations included one site on a recently abandoned inset fan with <20 cm thick sand sheets, two sites within mid- to late Holocene inset fans surfaces, two sites from Pleistocene inset fan surfaces, and one site from a shallow sand sheet over bedrock. Corresponding soil profiles were described using standard methods (Schoeneberger et al. 2002). Extensive

surface characterization was completed, and surface soil samples were collected and analyzed in companion studies (see Chapters 3 and 4, Appendix 1.2)

Prior to sampling, crust surfaces and cross-sections were examined for macro-features, which included pores, cracks, voids, cm-scale surface relief, pedogenic structure, and soil aggregation. Because sampling occurred in June, several weeks after the last precipitation event, specimens were dry and crust organisms were dehydrated. Crusts were carefully excavated from shrub interspaces using a flat hand scoop. Samples ranged from 2-6 cm in diameter with masses from 3-36 g. When possible, sample orientations were recorded. Samples were covered in plastic wrap, placed in padded plastic containers, and carefully transported back to the UNLV Environmental Soil Analysis Laboratory (ESAL). Once in the lab, samples were allowed to equilibrate to the ambient laboratory humidity for a minimum of 24 hours. Ocular estimates of percent cover of genera in dry conditions were made using both unaided and hand lens observations. Samples were examined for physical disturbance and, if damaged, were discarded from the study. Twenty-eight intact specimens were immersed in Spurr low viscosity embedding media. The samples were then placed in a vacuum desiccator for 4-6 hours to remove air bubbles. During this interval, vacuum pressures were incrementally increased from 150 PSI to 600 PSI. Once the epoxy was firm, the samples were placed in an oven at 70° C for 16 hours to harden the epoxy.

The samples were cut into 39 billets using a rock saw equipped with a diamond ISOMET® wafering blade. Oil-based ISOCUT® blade lubricant was used to prevent possible salt mineral dissolution. Billets were prepared by making vertical cuts through the center of each sample parallel to the long axis. One half of the sample was stored,

and the other half was used for thin section preparation. Larger samples were also cut perpendicular to the long axis and provided 1-2 additional billets per sample. National Petrographic Service, Inc., Houston, TX, ground the billets into thin sections using an oil-based lubricant. When possible, orientations of thin sections were recorded.

Thin section characterization began by imaging under a digital flatbed scanner. These scans provided overview maps for subsequent micromorphological analyses. The thin sections were first examined for micromorphological features at 4X, 10X, and 20X magnification under a Nikon Eclipse LV100POL polarized light microscope, and images were recorded using a digital still camera. When authigenic minerals were observed, they were described and their locations were clearly identified. Select thin sections were also examined under a light microscope at lower magnifications of .08X to 3.2X, and photos were taken with a digital still camera. Finally, the thin sections were sputter coated in gold for 30 seconds with a Cressington 108 Auto sputter coater. Samples were then examined and imaged in the UNLV EMIL laboratory using a JEOL-5600 Scanning Electron Microscope (SEM). The thin sections were observed under the SEM's Backscatter Electron detector (BES) at 35-5000X magnifications with working distances of 15-20mm, at 15-20 kV, and at spot sizes of 30-40. Elemental compositions were verified using the attached Oxford INCA Energy Dispersive X-ray Spectroscopy system at 270X to 5000X magnifications with working distances of 15-20 mm, at 15-20 kV, and at spot sizes of 30-40. EDS data were used primarily to determine mineralogy of authigenic precipitates observed during petrographic analyses.

1.2 Mapping and Site Characterization

Two maps were created to delineate (1) BSCs and (2) geomorphology. The BSC map delineates interspace crust species composition and morphology throughout the Hidden Valley basin (Figure 3.4). The geomorphic map outlines distinct geomorphic surfaces within a 2.8 km² subregion of the valley (Figure 3.4, outline). The geomorphic surfaces within the subregion were also correlated to USDA official soil series (Figure 3.4, outline)(Soil Survey Staff 2010a). The maps were created using extensive field reconnaissance and high-resolution remote sensing data and digitized in ESRI ArcGIS 9.3 Desktop and Manifold GIS at a scale of 1:6500. Base map data for digitization included Quickbird® panchromatic and multispectral satellite imagery and NAIP aerial photos. BLM provided access to Quickbird® imagery with resolutions of were 0.61-0.72 m and 2.44-2.88 m for panchromatic and multispectral data, respectively. USDA-NRCS provided natural color NAIP imagery with an average resolution of 1 m. These high-resolution base maps enhanced digitizing precision and efficiency of field reconnaissance.

1.2.1 BSC Mapping

The BSC map delineates differences in interspace BSC species composition and morphology. This digital BSC map was designed to fulfill the following three purposes: (1) to serve as a resource guide for the Bureau of Land Management; (2) to be used for spatial analyses in GIS to determine correlates of BSC distribution; and (3) to characterize and stratify the study area for subsequent data collection and analyses.

BSC map units vary with respect to three interspace surface cover types: (1) cyanobacteria-bare crusts, (2) short moss-lichen crusts, and (3) tall moss-lichen pinnacled

crusts. (Note the cyanobacteria-bare designation is used because crusts formed by filamentous cyanobacteria commonly occur in conjunction with bare soil.) These categories are the dominant crust morphotypes in the area and are easily assessed using the naked eye. Map units were roughly categorized as having high, moderate, and low density tall moss-lichen pinnacled crusts, short moss-lichen crusts, and cyanobacteria-bare crusts. Subsequent surface data collection quantified differences in surface cover among map units. Characteristics of BSCs that occur below plant canopies were not considered in map unit design, but were characterized during surface data collection. Additional classes were created for those areas that do not contain BSCs, such as limestone or sandstone bedrock and areas of off-road vehicle disturbance.

Once the BSC map units were developed, the entire valley was mapped according to these classes. Mapping was primarily field-based. However, remote sensing played an important role in digitization and reconnaissance efficiency. Quickbird® panchromatic satellite base imagery was useful for differentiating various crust unit parameters. For example, areas of high moss-lichen cover generally appeared as darker tones, while areas of high cyanobacteria cover without moss-lichen crusts appeared as smooth, lighter tones. Areas of moderate density moss-lichen cover produce intermediate or gray tones in the panchromatic imagery. Once these remote sensing relationships were solidified, mapping proceeded as follows. Quickbird® panchromatic imagery was examined for subtle differences in surface tones, which were delineated as initial polygon lines. Initial lines were field checked to determine line accuracy and classification of individual polygons. Digitization of units was completed in GIS over Quickbird® panchromatic base images.

During a final series of fieldtrips, accuracy of the digitized map was checked, and corrections to the final map were made as needed.

1.2.2 Ecological Characterization and Sampling

1.2.2.1 Plot Characterization and Sampling

Surface characterization and sampling were completed within 36 plots from the 2.8 km² subregion of Hidden Valley (Figure 3.4), which corresponds to the area covered by the geomorphic map (Appendix 1.2.3). Plot locations were selected using a stratified random sampling design based on the BSC map (see Chapter 3, Appendix 3). A random number generator produced random easting and northing UTM coordinates for the polygons covered by each BSC map unit. A minimum of three random locations were chosen for each of the units. One to three additional plots were selected for the most common map units or units with the greatest aerial extent, yielding 36 plots total.

Surface characterization data were collected within 36 12-m-diameter circular plots during June 2007 and January-February 2008. Plots characterize abiotic and biotic features, including canopy cover by vascular vegetation, soil cover by BSCs and rock fragments, soil cover by plant litter, surface microtopography associated with BSC organisms, and soil physicochemical properties. Three types of data were collected at each plot: (1) line intercept data, (2) point count data, and (3) additional site observations.

Line intercept data were used to characterize the amount and type of vascular plant canopy cover. Line intercepts were established along two perpendicular transects that bisected the plots. The bearing of the perpendicular transects were randomly selected for each plot. Along each transect, a flexible tape measure was used to record

any intercept with vascular plants. The presence/absence and species of vascular plant canopies were recorded along the tape to the nearest cm. The slope and aspect of soil surfaces were recorded along transect lines to the nearest cm.

Point data were used to characterize soil surface cover below shrub canopies and within interspaces. Point counts were collected using a 25 x 25 cm square grid with 25 evenly spaced points (Belnap et al. 2001). At each site, the grid was randomly tossed within the boundaries of the plot and surface cover from 25 grid points was recorded. Within each plot, a minimum of 150 points were recorded from shrub canopies, and a minimum of 150 points were recorded from interspaces. For point counts and for subsequent soil sampling, canopy surface cover was defined as those surfaces lying directly below a shrub canopy. Interspaces were defined as those areas lying between shrubs, or not directly below shrub canopies. Each point was recorded as one of the following cover categories: cyanobacteria crust, moss, *Collema*, *Placidium*, *Peltula*, bare soil, limestone clast, sandstone clast, petrocalcic clast, exotic grass litter, or non-grass plant litter. Although exotic grasses are extensive within the study area, they were too small to be characterized with line intercept data collection. Instead exotic grass species were listed for each plot, and point cover was recorded as “exotic grass litter”.

Additional site observations were recorded for each plot, including hillslope position, slope complexity, interlocking vs. non-interlocking surface clasts, and ocular estimates of percent cover by rock fragment size classes. A vascular plant and BSC species list was compiled, which included those species not recorded in line intercept and point count data. In addition, the maximum height of moss-lichen crust pinnacles was measured using a digital caliper and recorded to the nearest mm. At least 6 caliper

measurements were taken from interspaces at each plot to determine the maximum microtopographic relief associated with BSC surface roughness.

Within each plot, two composite surface soil samples were collected, one from below shrub canopies and one from within interspaces. The composite soil samples were taken from the upper 0-3 cm of soil using a flat, stainless steel scoop. Each interspace/canopy composite sample was collected from a minimum of six points randomly located from the plot. Sub-samples were taken until the composite sample reached 1 L. This yielded a total of 72 composite samples, with 36 canopy and 36 interspace samples. The composite samples were transported in plastic bags to the UNLV Environmental Soil Analysis Laboratory (ESAL).

1.2.2.2 Cyanobacteria Study

Characterization of BSC cover was primarily completed using point counts of organisms visible to the naked eye. Microscopic cyanobacteria present challenges to visually unaided assessment. However other studies have shown that naked-eye estimates can be used to determine the presence and relative concentrations of cyanobacteria in soil crusts (Belnap et al. 2008). A microscopic investigation assessed the accuracy of visual estimates of cyanobacteria presence or absence. A total of 60 crust samples were collected from three locations. All three sample locations lie adjacent to BSC plots. These plots lie along sand sheets and display some degree of physical crusting, which were hypothesized to also contain cyanobacteria. At each site, 10 samples that were hypothesized to have low cyanobacteria cover, or $\leq 10\%$ surface crusting, were collected. Another 10 samples that were hypothesized to have high cyanobacteria cover, or $\geq 35\%$ crusting (Figure 4.1), were also collected. Samples were

chosen in a random manner, but efforts were made to find sufficient numbers of samples with low and high crusting. Surface samples were roughly 100 mm in diameter and up to 10 mm thick. Samples were collected using a flat, stainless steel scoop. Each sample was carefully excavated in order to minimize disturbance and to keep existing surfaces exposed. The samples were carefully placed in 100 mm diameter petri dishes and photographed in the field using a 35 mm digital SLR camera equipped with a macro lens. Visual, or unaided-eye, estimates of percent surface crusting were made for each sample. The petri dishes were covered with lids and wrapped in parafilm. The same day of collection, samples were transported to the UNLV ESAL, where plate covers were removed and samples allowed to equilibrate to ambient humidity at a temperature of 20-25°C for 3 days. Lids were then returned to the samples, and dry masses were measured. Later, the samples were saturated with reverse osmosis (RO) water. Water was carefully added along petri dish sides, to avoid disrupting any surface features. To achieve saturation, water was added incrementally until sample surfaces glistened, similar to the glistening criteria used for saturated paste extracts (Burt 2004), only without sample agitation. Samples were then weighed to determine gravimetric water content and left uncovered for 1 hour at 20-25°C. Next, the samples were observed under a light microscope at 1-4X to determine the relative concentration of cyanobacteria. A grid comprised of 1.4 x 1.4 mm cells was placed over the sample. Sixty random cells were observed for the presence or absence of filamentous cyanobacteria. The number of cells, out of 60, containing filamentous cyanobacteria was recorded for each sample. This value was converted to the percentage of cells showing cyanobacteria filaments. Only one species of filamentous cyanobacteria was identified in this survey. A representative

cyanobacteria filament bundle was removed and grown in sterile soil inside a growth chamber for 3 days, which verified the genus to be *Microcoleus*.

A parametric independent samples t-test was conducted in SPSS PASW Statistics 17 to determine whether samples hypothesized to have high cyanobacteria cover had greater *Microcoleus* concentrations than samples hypothesized to have low concentrations. The two groups tested came from the original sample classifications, which were those samples showing low or $\leq 10\%$ surface crusting and those samples showing high or $\geq 35\%$ surface crusting. Descriptive statistics were calculated for each group, including n , minimum, maximum, range, mean, standard deviation, variance, standard error, and median. Normality was assessed using the Kolmogorov-Smirnov statistic, and homogeneity of variance was calculated by Levene's test, both at the 0.05 level of significance. Samples met the statistical assumptions of normality and homogeneity of variance. The parametric independent t-test assessed the difference in the mean percentage of cells that contained *Microcoleus* filaments, at the 0.05 significance level. The results from this t-test were used to determine whether the presence of physical crusting could be used as a proxy for the presence of filamentous cyanobacteria.

1.2.2.3 Sample Preparation and Laboratory Analyses

To characterize surface soil characteristics, the 72 composite samples from the 36 plots were analyzed for a variety of soil physicochemical properties. The composite samples were transported from the field in plastic bags to the UNLV ESAL, where they were kept refrigerated at 2-3°C for 2 to 30 days. The samples were then air-dried at 20-25°C. After drying, the samples were thoroughly mixed and sieved to 2 mm to remove

rocks and large plant debris. No effort was made to remove BSC material from the mineral soil. Micromorphological investigations have shown that clay and silt-sized particles adhere to microbial structures (see Chapter 2). If BSC bio-structures were removed, any attached silt and clay would also be discarded. Because these silts and clays could be important to the chemistry of the soil, BSC biotic structures were included as part of the bulk sample. Mosses, lichens and cyanobacteria all passed through the 2 mm sieve.

Samples were analyzed for texture using the Malvern Mastersizer 2000 grain size analyzer (Malvern Instruments Ltd., Malvern, UK) in the UNLV ESAL laboratory. This technique uses a laser beam to estimate particle size by volume (International Organization for Standardization 2009). To verify the accuracy of the Mastersizer results, five samples were analyzed using the hydrometer and pipette methods (Dane and Topp 2002, Burt 2004). Results were recorded as percent volume by USDA particle size classes (Schoeneberger et al. 2002). Particle size data were then used to calculate the textural class of each composite sample according to the USDA textural triangle (Schoeneberger et al. 2002).

Soil chemical characteristics were also determined at UNLV ESAL. The samples were saturated with RO water and soil solutions were extracted using the standard USDA saturated paste extractions (Burt 2004). These extractions are commonly used to characterize the chemistry of soil water and can be used as a proxy for the availability of nutrients for plant or microbial uptake (Burt 2004). Extracts were refrigerated at 2-3°C until all analyses were completed. Soil extracts were analyzed for pH and electrical conductivity (EC_e) (Burt 2004). Nitrate (NO_3), sulfate (SO_4), and chloride (Cl^-) from

saturated pasted extracts were analyzed at ESAL using an ICS (Burt 2004). Extractable phosphorus (P) concentrations from bulk sieved soil were analyzed using the Olsen sodium-bicarbonate extraction method (Burt 2004). Total C, total N, and total sulfur (S) were determined for bulk sieved soil using the dry combustion method (Burt 2004). The C:N ratio was calculated from total C and N values (Burt 2004). Carbonate, or inorganic C, was determined by treating a known volume of soil with 3N HCl and measuring CO₂ evolution with a manometer (Burt 2004). To determine organic C, the inorganic fraction was subtracted from the total C (Burt 2004). Remaining soil saturated paste extracts were shipped on ice to California State University, Bakersfield, where ICP-MS was used to determine concentrations of potassium (K), calcium (Ca), iron (Fe), sodium (Na), magnesium (Mg), boron (B), manganese (Mn), sodium (Na), copper (Cu), zinc (Zn), molybdenum (Mo), and nickel (Ni)(Burt 2004). Extracts were diluted by a factor of 20 for ICP-MS analyses. Results are reported as non-diluted concentrations.

1.2.3 Geomorphic Mapping and Characterization

The geomorphic map delineated distinct geomorphic surfaces that vary according to depositional environment and relative age. Relative age was determined using differences in elevation, topography, surface morphology, surface clast characteristics, and degree of pedogenesis (Christenson and Purcell 1985). This map was created to be unique and separate from the BSC map, such that the influence of geomorphic processes on BSC distribution could be tested. This map was the first detailed geomorphic characterization of the field area and was not based upon any previous surficial geologic mapping.

Geomorphic mapping began with extensive field reconnaissance to investigate the geomorphic surfaces represented within the field area and to develop map unit concepts. First, depositional settings were identified and defined as alluvial, colluvial, or eolian. The geomorphic surfaces were assessed with respect to topography and relative age, as determined by cross-cutting relationships (Christenson and Purcell 1985, Bull 1991). Next the surfaces were broadly described according to their landform type (Peterson 1981), secondary pedogenic carbonate stage as viewed along wash exposures (Gile et al. 1966, Bachman and Machette 1977, Machette 1985), surface morphology, and desert pavement development (McFadden et al. 1987, Wells et al. 1987).

Geomorphic units were given labels using conventional alphanumeric nomenclature, similar to that of House et al. (2010). In this nomenclature, the first character reflects the geologic period of that geomorphic surface, where “Q” stands for Quaternary and “T” stands for Tertiary. The next character(s) represent the type of the deposit, where “a” indicates alluvium, “c” indicates colluvium, and “e” indicates eolian. The next character refers to age. I assigned “y” to youngest and generally the lowest topographic surfaces; “i” indicates intermediate-aged surfaces; and “o” refers to the oldest, and generally highest topographic surfaces. The last character, if included, is a numerical identifier that refers to the relative age among the young, intermediate, and old surfaces. These numbers are assigned according to depositional sequence, wherein the oldest surface in the series is labeled 1, and the youngest surface is given the highest numerical number. Additional special units were also delineated, including sandstone or limestone bedrock outcrop and surfaces disturbed by off-road vehicles.

Once geomorphic surfaces were roughly defined, their extent within the subregion was mapped. Similar to BSC mapping, geomorphic mapping incorporated a combination of field reconnaissance and remote sensing. NAIP images were used for base maps in field reconnaissance, digitizing, and final field checks. Once the semi-final geomorphic map was complete, component map units were characterized. Because the geomorphic map corresponded to the same area characterized for the BSC mapping, those surface characteristic data could also be used to characterize the geomorphic map units.

Finally, soil profile descriptions were completed for each geomorphic map unit. Because the study area lies within a BLM wilderness area, soil pit excavation is strictly prohibited. Soil profile descriptions were limited to arroyo exposures and erosional outcrops. Despite these restrictions, 14 soil profiles were described according to standard USDA methods (Schoeneberger et al. 2002), which included soil morphological characteristics and horizon texture according to feel. Additional data were collected including the following observations: ocular estimates of percent surface rock fragment cover by lithology, ocular estimates of percent cover by cyanobacteria, ocular estimates of percent cover by moss-lichen crusts, a BSC species list, a vascular plant species list, secondary carbonate morphology (Schoeneberger et al. 2002), and stage of pedogenic carbonate accumulation (Gile et al. 1966, Bachman and Machette 1977, Machette 1985). Profile data were entered into Pedon PC for more accessible output. Because of budget constraints, the soil profiles were not sampled or analyzed for physicochemical analyses. However, when possible, profiles were chosen adjacent or near to BSC characterization plots. This allowed further verification of ocular surface cover approximations and soil textural estimates.

Once the geomorphic surfaces were characterized, geomorphic surface ages and mapping were finalized. No formal age dating of the geomorphic surfaces was completed. However, ages were estimated using soil surface morphology, desert pavement development, and stage of pedogenic carbonate accumulation and correlated to other soil-geomorphic investigations (Sowers et al. 1989, Bull 1991, Harden et al. 1991, Reheis et al. 1992, Peterson et al. 1995, Bell et al. 1998, 1999, Brock and Buck 2005, Page et al. 2005, Brock and Buck 2009, House et al. 2010).

1.2.4 Soil Correlations

Geomorphic units were correlated with USDA Official Soil Series (Soil Survey Staff 2007, 2010a) to identify soil series that display similar characteristics to geomorphic units. Such correlations would help determine USDA soil components that may effectively predict BSC distribution. The aforementioned soil profile data were used to quantify morphological horizon characteristics from each geomorphic surface. Because soils data were limited to surface exposures from 14 locations, soil characteristics are not comprehensively described nor mapped, but roughly estimated. Soil types were assumed to correlate across a single geomorphic surface and characteristics were extrapolated from arroyo profile descriptions, generally one profile per surface. Within each of the 14 profiles, the thicknesses, depths, and morphological characteristics of individual horizons were used to determine diagnostic horizons, percent secondary carbonate accumulation, particle size control sections, and mineral classes (Soil Survey Staff 2010b). These properties were subsequently used to distinguish each profile's taxonomic classification (Soil Survey Staff 2010b). Next, soil taxonomy was used as the primary criterion through which the USDA Official Soil Series

Descriptions database was searched for potential soil correlates (Soil Survey Staff 2010a). Matching series were further examined for similarities in soil horizons, moisture/temperature regimes, ecological communities, geographic extent, and geomorphology. Those geomorphic surfaces with which no suitable soil series could be correlated were named according to their soil taxonomy (Soil Survey Staff 2010b). Soil map unit correlations were compiled from the BSC surface characterization plots and profile data. The soil type was added to the metadata for each plot.

1.2.5 Insolation Analyses

Potential solar radiation was calculated for each plot to determine the possible impact of insolation on BSCs and vascular plant communities. Solar insolation for each plot location was calculated using a 10 m digital elevation model (DEM). Analyses were conducted using the point solar radiation spatial analyst tool in ESRI ArcGIS 9.3 Desktop. Total daily solar insolation, or hours of insolation per day, were collected for three important dates on the solar calendar, the summer solstice, winter solstice and equinox. The results were incorporated as metadata for each plot.

1.2.6 Data Compilation

Surface characterization data, particle size data, profile data, and plot metadata were compiled to quantify characteristics for individual plots as well as BSC map units, geomorphic map units, and correlated soil types. First, line intercept data, point count data, and metadata from each plot were entered into a Microsoft Excel spreadsheet (Microsoft Office 2007). Intercept data were converted from length data into percent surface area cover, which included percent cover by individual plant canopy species, total canopy cover, and total interspace cover. Point count data were compiled to determine

percent interspace cover and percent canopy cover by each cover category. Categories included cyanobacteria crust, moss, *Collema*, *Placidium*, *Peltula*, bare soil, limestone clast, sandstone clast, petrocalcic clast, exotic grass litter, and non-grass plant litter. In addition, some of these categories were combined into composite classes (Table 3.2), including moss-lichen cover class, cyanobacteria-bare, and total rock cover. Particle size classes were divided into USDA texture classes including clay, silt, very fine sand, fine sand, sand, and total sand (Schoeneberger et al. 2002). The sand category combined medium and coarse sands, while total sand grouped all sand fractions together. Metadata regarding soil geomorphic surface, soil type, hillslope position, slope complexity, maximum pinnacle height, interlocking nature of clasts, ocular estimates of percent cover by rock fragment classes were recorded. Line intercept data, point count, and metadata from each plot were imported as one integrated spreadsheet into SPSS PASW Statistics 17 to quantify the surface characteristics of each map unit. Descriptive statistics for each BSC, geomorphic, and soil map unit included *n*, minimum, maximum, range, mean, standard deviation, variance, standard error, and median.

1.3 GIS Overlays

The geomorphic map was overlain with the BSC map to determine percent overlap between map units. Overlay analyses were conducted using standard methods (House 2005). First, maps were overlain using the “Clip with Intersect” tool in ESRI ArcGIS 9.3 Desktop. Overlay polygons were exported into a spreadsheet. This output was compiled in a Microsoft Excel spreadsheet (Microsoft Office 2007) and expressed as percent compositions of total map unit areas.

1.4 Statistics

A hierarchical approach was taken to explore statistical relationships among biotic and abiotic features. First, mixed response permutation procedures (MRPP) and non-metric multidimensional scaling (NMS) were used as exploratory methods to understand the multivariate relationships among variables. Next, a series of ANOVAs, t-tests, and correlation coefficients explored surface cover and chemistry relationships at multiple scales, starting at the landscape scale and moving down to the meter-scale. At the landscape scale, a series of ANOVAs explored relationships among geomorphic surfaces. Next, a series of ANOVAs and t-tests explored biotic and abiotic characteristics associated with different types of interspace surface cover. T-tests were also used to explore relationships between shrub canopies and interspaces. Finally, to understand the relationship of interspace cover on the fertile island dynamics, t-tests compared shrub canopies to interspaces for all plots as well as plots containing different interspace surface cover. For all data, as well as data for individual groups compared in ANOVAs and t-tests, descriptive statistics were calculated, including n , minimum, maximum, range, mean, standard deviation, variance, standard error, and median. MRPP and ANOVA were conducted in PC-ORD (MjM Software Design), while ANOVAs, t-tests, correlation coefficients and descriptive statistics were completed in SPSS PASW Statistics 17

Several types of data were analyzed. (1) Site metadata include maximum pinnacle height and summer, winter, and equinox solar insolation. (2) Vascular plant canopy cover was calculated from line-intercept data. (3) Biological soil cover from canopies and interspaces includes cyanobacteria crust, moss, *Collema*, *Placidium*,

Peltula, exotic grass litter, and non-grass plant litter. (4) Non-biological soil cover from canopies and interspaces includes, bare soil, limestone clasts, sandstone clasts, and petrocalcic clasts. (5) Composite soil cover classes (Table 4.3) from canopies and interspaces include moss-lichen crusts, total BSCs, cyanobacteria-bare, and total rocks. Because cyanobacteria-dominated crusts most commonly occur with some form of bare soil, cyanobacteria-bare is used as a composite category that includes total cover by bare soil and cyanobacteria crusts. (6) Soil surface chemistry and texture characteristics from canopies and interspaces include clay, silt, very fine sand, fine sand, sand, and total sand, soil pH, EC_e, NO₃, SO₄, Cl, K, Na, Ca, Fe, Mg, B, Mn, Cu, Zn, Mo, Ni, extractable P, total C, total N, total S, C:N ratios, organic C, and inorganic C.

Parametric ANOVAs, t-tests, and correlation coefficients were only conducted on those groups of data that met required assumptions. Data from all parametric tests met assumptions of normality, as calculated using the Kolmogorov-Smirnov statistic at the 0.05 level of significance. Parametric ANOVAs and t-tests met assumptions of homogeneity of variance, as calculated by Levene's test at the 0.05 level of significance. Non-parametric tests were conducted on all variables.

1.4.1 MRPP

MRPP tested differences in soil surface cover among soil map units, among BSC map units, and among geomorphic map units. Biological and non-biological interspace soil cover classes were included in these analyses. Similar to MANOVA, MRPP tests for compositional differences among groups, but it requires no distributional assumptions (McCune and Grace 2002). MRPP tested differences among plots grouped according to their respective BSC, geomorphic, and soil map unit classifications. Groups having less

than 2 plots were removed from the analyses. Analyses were completed using Sørensen (Bray-Curtis) distance measures. Results were reported as chance-corrected within-group agreement (A) with corresponding significance values (p -value).

1.4.2 NMS

NMS analyses were used as an exploratory method to determine relationships among interspace and canopy BSCs, vascular plants, soil surface cover, and soil physicochemical characteristics. NMS analyses were conducted using Sørensen (Bray-Curtis) distance measures for biological soil surface cover from canopies and interspaces and on vascular species composition. For these analyses, surface cover data were weighted by multiplying the percent total interspace cover or percent canopy from each plot by the percent cover by individual cover types in that plot. Experimentation with these analyses indicated this weighting process yielded the most statistically significant ordinations. Environmental variables were overlain on these ordinations and joint plots, which included site metadata, non-biological soil cover, and soil texture and chemistry.

1.4.3 ANOVAs

ANOVAs quantified differences in characteristics among geomorphic surfaces and among soil surface cover types. These tests analyzed differences in site meta data, vascular plant canopy cover, biological and non-biological soil cover, soil cover by composite classes, and soil surface chemistry and texture. Parametric one-way between-groups ANOVAs and post-hoc comparisons using the Tukey HSD test were used to determine differences between groups at the 0.05 significance level. The Kruskal-Wallis H Tests at the 0.05 significance level were used as non-parametric alternative to the ANOVAs. Post-hoc, non-parametric Mann-Whitney U Tests were calculated with

Bonferonni adjustments. Geomorphic ANOVAs had 4 groups and were adjusted to the 0.0125 significance level, while soil surface cover ANOVAs were adjusted to the 0.0167 significance level for 3 groups. Plots that did not fall into one of the ANOVA categories were removed from their respective analyses.

1.4.3.1 ANOVAs of Geomorphic Units

ANOVAs quantified variation in canopy and interspace characteristics between geomorphic units (Figure 4.7). To achieve sufficient n-values for the ANOVAs, geomorphic units were grouped according to similar characteristics (Figure 4.7), including secondary carbonate stage, surface characteristics, depositional setting, and relative surface age. Four groups were used in these analyses to conserve degrees of freedom. Mid- to late Holocene Qay₁ and Qay₂ inset fans were grouped together; eolian units, or Qea sand sheets, comprise another group; all Pleistocene Qai inset fans were grouped together; and the oldest QTa and Qao₁ erosional fan remnants comprise another group (Figure 4.7).

1.4.3.2 ANOVAs of Soil Cover Types

ANOVAs also quantified variation in interspace characteristics, as well as adjacent vascular vegetation for three interspace surface cover types (Figure 4.8). For these analyses, ANOVA groups included plots classified as having >30.9% cyanobacteria-bare interspace cover, > 31.9% moss-lichen interspace cover, and >52.9% rock interspace cover. (Note many moss-lichen crusts also included some cyanobacteria cover.)

1.4.4 t-Tests

1.4.4.1 Independent Samples t-Tests of *Bromus* Cover Groups

Parametric and non-parametric independent samples t-tests quantified variation in characteristics between two surface cover types (Figure 4.9). For these analyses, t-test groups included plots classified as having >14% *Bromus* interspace cover (“high *Bromus*”) or <5% *Bromus* interspace cover (“low *Bromus*”). These tests analyzed differences in site meta data, adjacent vascular plant canopy cover, biological and non-biological interspace soil cover, interspace soil cover by composite classes, and interspace soil surface chemistry and texture. Parametric independent samples t-tests were calculated at the 0.05 level of significance, while Mann-Whitney U Tests were used as a non-parametric alternative at the 0.05 significance level.

1.4.4.2 Paired Samples t-Tests of Interspace and Canopy Characteristics

Parametric and non-parametric paired samples t-tests quantified variation in surface characteristics between interspaces and canopies from all plots (Figure 4.10), as well as plots of different surface cover type (Figure 4.11). These tests analyzed differences in biological and non-biological soil cover, soil cover by composite classes, and soil surface chemistry and texture. Parametric paired samples t-tests were calculated at the 0.05 level of significance, while Wilcoxon signed rank tests were used as a non-parametric alternative at the 0.05 significance level. Because samples were paired for these analyses, characteristics from interspaces and shrub canopies of the same plot were compared directly. The first set of t-tests were completed for all of the plots combined (Figure 4.10). Next, plots from three surface cover classes were tested separately (Figure 4.11). Groups were classified as having >30.9% cyanobacteria-bare interspace cover, >

31.9% moss-lichen interspace cover, or >52.9% rock interspace cover, respectively.

(Note many moss-lichen crusts also included some cyanobacteria cover.) Plots that did not fall into one of these three categories were removed from the analyses.

1.4.5 Correlation Coefficients

Correlation coefficients quantified relationships between soil cover types and soil physiochemical properties. Canopy characteristics were correlated against all other canopy characteristics, while interspace characteristics were correlated to all other interspace characteristics. Variables tested include site meta data, vascular plant canopy cover, biological and non-biological soil cover, soil cover by composite classes, and soil surface chemistry and texture. Parametric Pearson product-moment correlation coefficients were calculated as r values at the 0.05 significance level. Non-parametric Spearman's Rank Order Correlations, or ρ values, were calculated at the 0.05 level of significance. These tests were initially completed on data from all plots. A final series of correlation coefficients were completed on plots with $\geq 53\%$ interspace rock cover for percent slope as well as the aforementioned characteristics.

Literature Cited

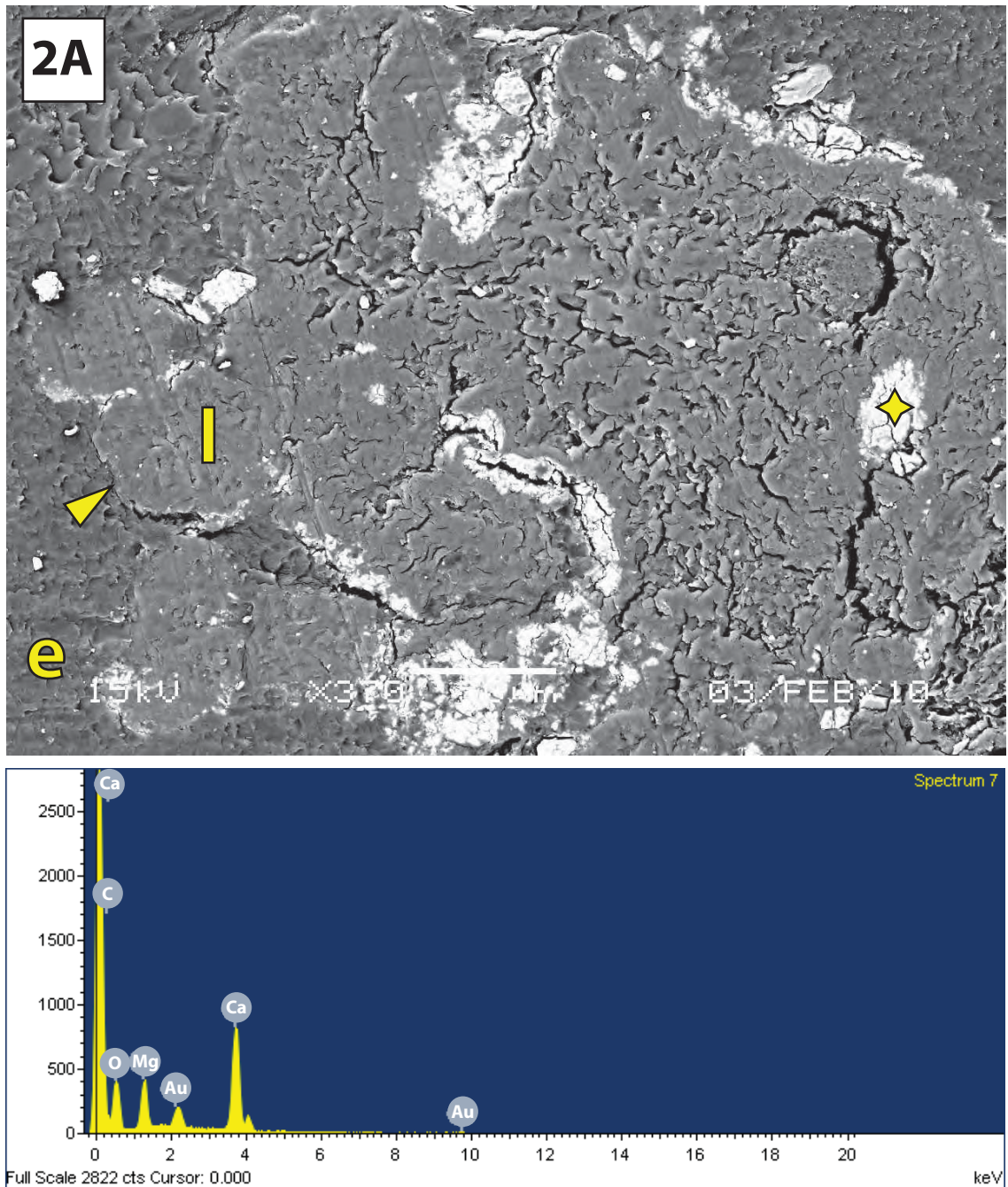
- Bachman GO, M.N. Machette. 1977. Calcic soils and calcretes in the Southwestern United States. USGS Open-File Report 77-794. 163 pp.
- Bell J. W., A. R. Ramelli, and S. J. Caskey. 1998. Geologic map of the Tule Springs Park quadrangle, Nevada. **1:24,000**.
- Bell J. W., A. R. Ramelli, C. M. dePolo, F. Maldonado, and D. L. Schmidt. 1999. Geologic map of the Corn Creek Springs quadrangle, Nevada. **1:24,000**.
- Belnap J., S. L. Phillips, D. L. Witwicky, and M.E. Miller. 2008. Visually assessing the level of development and soil surface stability of cyanobacterially dominated biological soil crusts. *Journal of Arid Environments* **72**:1257-1264.
- Belnap J., Kaltenecker J., Rosentreter R., Williams J., Leonard S., Eldridge D.J. 2001. *Biological Soil Crusts: Ecology and Management*. Denver, CO: U.S. DOI Technical Reference 1730-2. 118 pp.
- Brock A. L., B. J. Buck. 2009. Polygenetic development of the Mormon Mesa, NV petrocalcic horizons: Geomorphic and paleoenvironmental interpretations. *Catena* **77**:65-75.
- Brock A. L., B. J. Buck. 2005. A new formation process for calcic pendants from the Pahrnagat Valley, Nevada, USA, and implication for dating Quaternary landforms. *Quaternary Research* **63**:359-367.
- Bull W. B. 1991. *Geomorphic Responses to Climatic Change*. Oxford University Press, New York.
- Burt R. 2004. *Soil Survey Laboratory Methods Manual*, SSIR No. 42, Version 4.0. 735 pp.
- Christenson G. E., C. Purcell. 1985. Correlation and Age of Quaternary alluvial-fan sequences, Basin and Range province, southwestern United States. Pages 115-122 *In* D. E. Weide, editor. *Soils and Quaternary Geology of the Southwestern United States: Geological Society of America Special Paper 203*, .
- Dane J. H., C. Topp. 2002. *SSSA Method of Soil Analysis, Part 4-Physical Methods*. 866 pp.
- Gile L. H., F. F. Peterson, and R. B. Grossman. 1966. Morphological and genetic sequences of carbonate accumulation. *Soil Science* **101**:347-360.


- Harden J. W., E. M. Taylor, C. Hill, R. K. Mark, L. D. McFadden, M. C. Reheis, J. M. Sowers, and S. G. Wells. 1991. Rates of Soil Development from Four Soil Chronosequences in the Southern Great Basin. *Quaternary Research* **35**:383-399.
- House P. K. 2005. Using geology to improve flood hazard management on alluvial fans - An example from Laughlin, Nevada. *Journal of the American Water Resources Association* **41**:1431-1447.
- House PK, Buck BJ, and A.R., Ramelli. Geologic Assessment of Piedmont and Playa Flood Hazards in the Ivanpah Valley Area, Clark County, Nevada (online only). 2010. NV Bureau of Mines and Geology Report 53, Reno, NV.
- International Organization for Standardization. 2009. Particle size analysis - Laser diffraction methods, ISO13320:2009. International Organization for Standardization, Geneva.
- Machette M. N. 1985. Calcic soils of the southwestern United States. Pages 1-21 *In* D. L. Weide, editor. *Soils and Quaternary geomorphology of the southwestern United States*, Geological Society of America, Boulder, CO.
- McCune B., J. B. Grace. 2002. *Analysis of Ecological Communities*. MjM Software Design, Gleneden Beach, OR.
- McFadden L. D., S. G. Wells, and M. J. Jercinovich. 1987. Influences of eolian and pedogenic processes on the origin and evolution of desert pavements. *Geology* **15**:504-508.
- Page W. R., S. C. Lundstrom, A. G. Harris, V. E. Langenheim, J. B. Workman, S. A. Mahan, J. B. Paces, G. L. Dixon, P. D. Rowley, B. C. Burchfiel, J. W. Bell, and E. I. Smith. 2005. *Geologic and Geophysical Maps of the Las Vegas 30' x 60' Quadrangle, Clark and Nye Counties, Nevada, and Inyo County, California: 1:100,000*.
- Peterson FF. 1981. Landforms of the Basin and Range, Defined for Soil Survey. UNR Max C. Fleishmann College of Agriculture, Nevada Agricultural Experiment Station Technical Bulletin 28. Reno, NV. 52 pp.
- Peterson F. F., J. W. Bell, R. I. Dorn, A. R. Ramelli, and T. L. Ku. 1995. Late Quaternary geomorphology and soils in Crater Flat, Yucca Mountain area, southern Nevada. *GSA Bulletin* **107**:379-395.
- Reheis M. C., J. M. Sowers, E. M. Taylor, L. D. McFadden, and J. W. Harden. 1992. Morphology and genesis of carbonate soils on the Kyle Canyon fan, Nevada, U.S.A. *Geoderma* **52**:303-342.

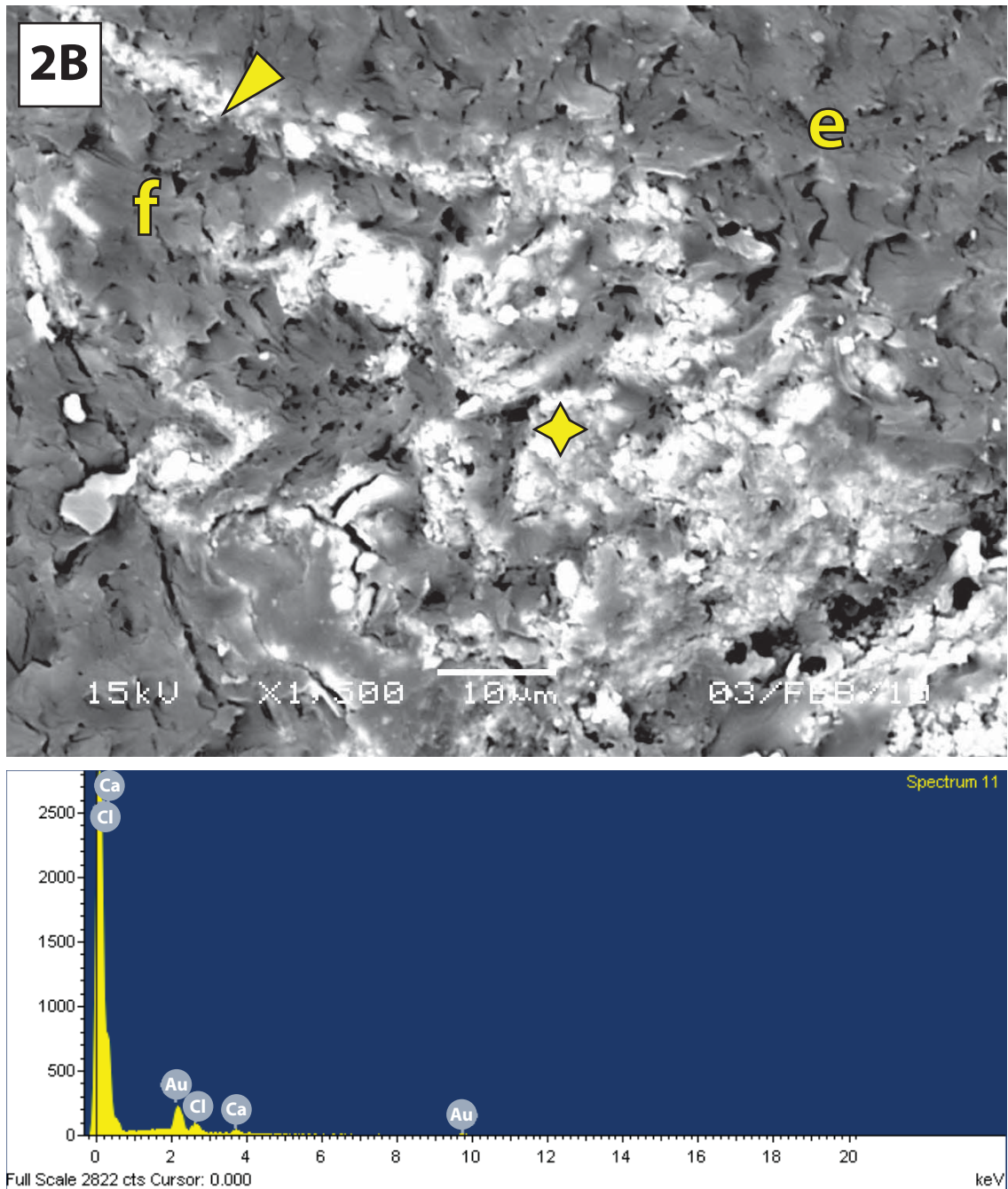
- Schoeneberger P. J., D. A. Wysocki, E. C. Benham, and W. D. Broderson. 2002. Field book for describing and sampling soils, Version 2.0. Natural Resources Conservation Service, National Soil Survey Center, Lincoln, NE.
- Soil Survey Staff. 2010a. Official Soil Series Descriptions. USDA-NRCS, Washington, D.C.
- Soil Survey Staff. 2010b. Keys to Soil Taxonomy. USDA-NRCS, Washington, D.C.
- Soil Survey Staff. 2007. Soil survey of the Clark County area, NV. National Resources Conservation Service. Washington, D.C.:
- Sowers J. M., R. G. Amundson, O. A. Chadwick, J. W. Hardin, A. J. T. Jull, T. L. Ku, L. D. McFadden, M. C. Reheis, E. M. Taylor, and B. J. Szabo. 1989. Geomorphology and pedology on the Kyle Canyon Alluvial Fan, southern Nevada. Pages 93-112 *In* T. J. Rice, editor. Soils, geomorphology, and pedology in the Mojave Desert, California, Nevada: Field Tour Guidebook for the 1989 Soil Science Society of America Annual Meeting Pre-Meeting Tour, October 12-14.
- Wells S. G., L. D. McFadden, and J. C. Dohrenwend. 1987. Influence of late Quaternary climatic changes on geomorphic and pedogenic processes on a desert piedmont, eastern Mojave Desert, California. *Quaternary Research* **27**:130-146.


APPENDIX 2

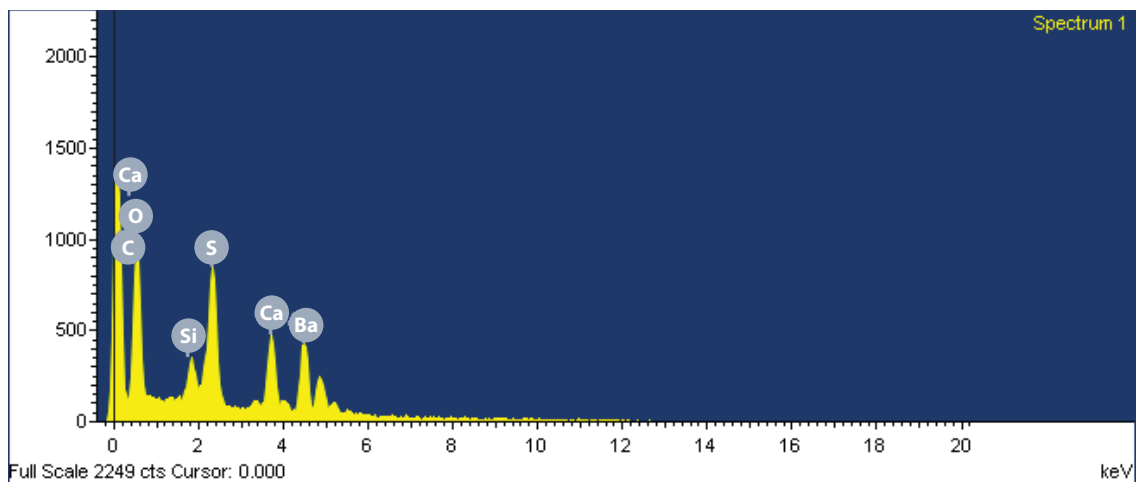
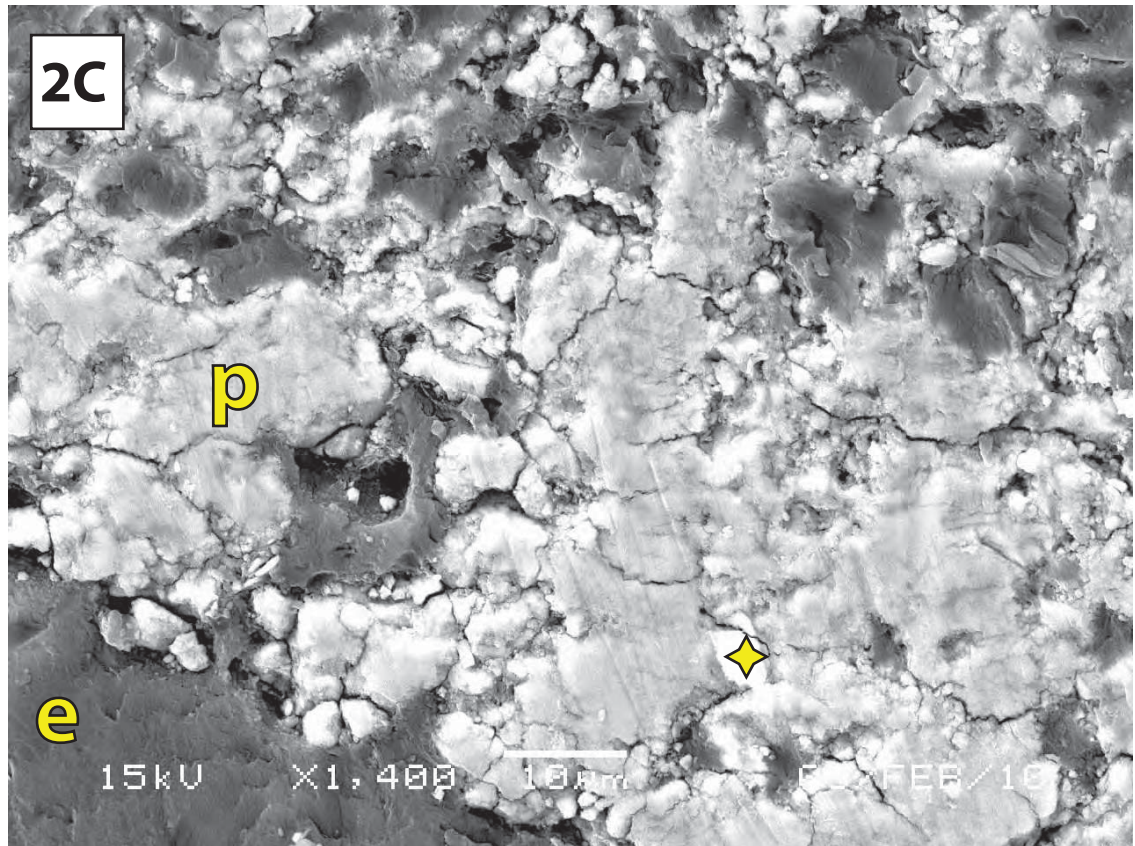
ADDITIONAL MICROMORPHOLOGY OBSERVATIONS



Appendix 2(A): Upper BES image shows authigenic mineral precipitates (white) accumulating inside a gelatinous lichen thallus (Scale 0.05 mm). (An arrow marks outer edge of the lichen thallus (l). Epoxy (e) shows up a darker tones.) Note the precipitates accumulate along fissures or cracks in the lichen thalli. EDS data were collected at the . The lower EDS plot indicates this precipitate to be Ca-carbonate with some inclusions of Mg.



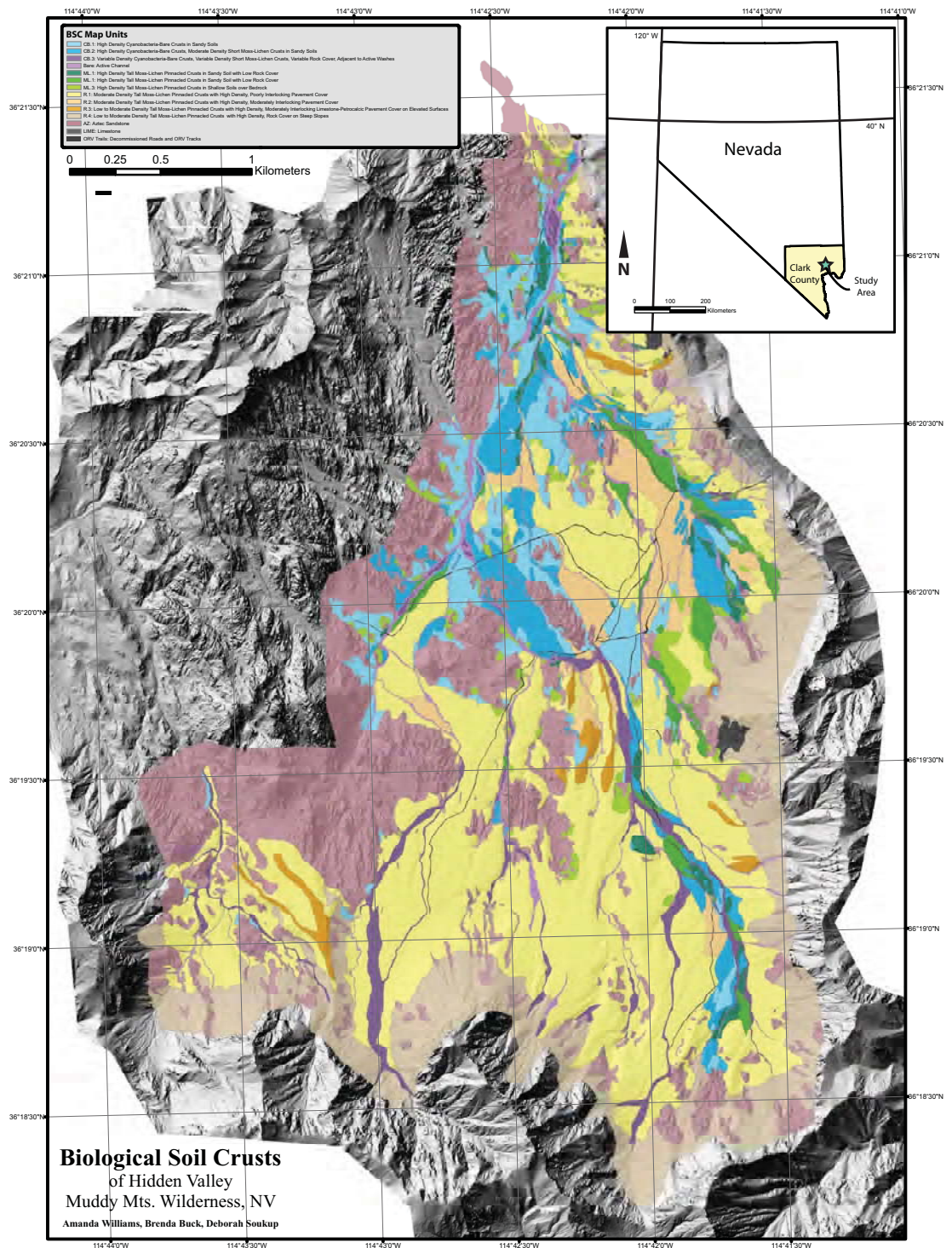
Appendix 2(B): Upper BES image shows authigenic mineral precipitates (white) accumulating along outer edges of filaments (Scale 0.01 mm). (An arrow marks outer edge of one filament (f). Epoxy (e) surrounds filaments.) EDS data were collected at the . The lower EDS plot indicates this precipitate contains high amounts of Ca and may contain Cl. This precipitate could be calcium chloride, but its mineralogy has not been verified.



Appendix 2(C): Upper BES image shows authigenic mineral precipitates (p, white tones) that have accumulated along the outer edge of a squamulose lichen (Scale 0.01 mm). The precipitates are primarily calcium carbonate. However, the EDS data collected at the ♦ indicate a small inclusion of another mineral. The lower EDS plot suggests this grain may be barite. The origin of this crystal and its mineralogy have not been verified. (Epoxy (e) shows up as darker tones.)

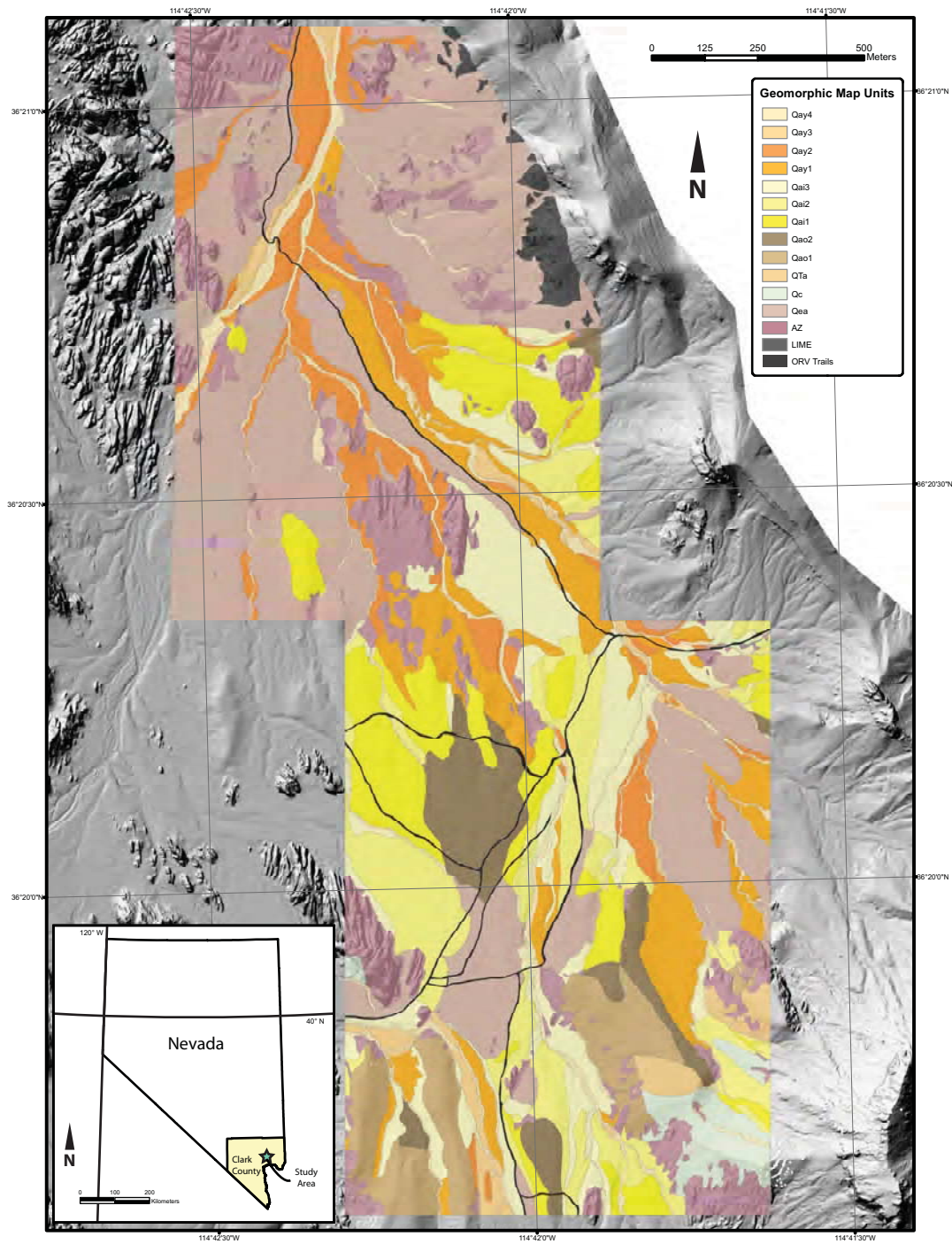
APPENDIX 3

BIOLOGICAL SOIL CRUST MAP



Appendix 3: The BSC map of Hidden Valley delineates unique distributions of cyanobacteria crusts, moss-lichen crusts, and surface characteristics. See full-sized map (attached) and complete map unit descriptions (Chapter 3) for more detail.

APPENDIX 4
GEOMORPHIC MAP



Appendix 4: The geomorphic map delineates geomorphic surfaces within a subregion of Hidden Valley. See full-sized map (attached) and complete map unit descriptions (Chapter 3) for more detail.

VITA

Graduate College
University of Nevada, Las Vegas

Amanda J. Williams

Degrees:

Bachelor of Science, Soil Science, Magna Cum Laude, 2005
University of Missouri – Columbia

Special Honors and Awards:

Recipient ExxonMobil Student Research Grant (2009)
Recipient Geological Society of America (GSA) Student Research Grant (2009)
Recipient GSA Farouk El Baz Student Research Grant (2008); first recipient of the annual award
Recipient UNLV Urban Sustainability Initiative Fellowship (2008-2011)
Recipient NASA-Nevada Space Grant Fellowship (2008; declined due to funding conflicts)
Recipient of the NSF Nevada EPSCOR SEPHAS Graduate Fellowship
Recipient of the UNLV Scholarships: Summer Scholarship (2009); Adams/GPSA Scholarship (2008-2009)
Recipient of the Bernada E. French Scholarship (UNLV Geoscience, 2007, 2008)
Co-wrote funded grant from BLM, Digital Mapping Inventory of Biological Soil Crusts in the Muddy Mts. Wilderness Area, NV, \$99,909
1st place Graduate Student Oral Presentation, 2010 Western CSSA-SSSA Meeting
2nd place Graduate Student Oral Presentation, 2010 Annual Soil Science Society of America Meeting
1st place Graduate Student Oral Presentation, 2009 UNLV Graduate Research Forum
1st place Graduate Student Oral Presentation, 2008 UNLV Geosymposium
Graduated Magna Cum Laude (Undergraduate)
ASA-CSSA-SSSA National Student Recognition Award (2005)

Publications:

Williams, A., Buck, B., Soukup, D., 2010, Biological Soil Crust Ecology and Landscape Relationships in the Muddy Mts. Wilderness, NV, Final Project Report for the Bureau of Land Management.
Williams, A., Buck, B., Soukup, D., Merkler, D., 2010, Geomorphic controls of biological soil crust distribution, Mojave Desert (USA), 19th World Congress of Soil Science Proceedings, Brisbane, Australia. (Short paper)
Williams, A., Buck, B., Beyene, M., Soukup, D., Merkler, D., 2010, Biological Soil Crusts in Mojave Desert, *In:* Fieldtrip Guidebook for the Western CSSA-SSSA Conference, Las Vegas, NV.

- Williams, A.**, Robins, C, Buck, B., Monger, H.C., 2009, Common ground: Discovering a shared purpose in Inner Mongolia, *Soil Survey Horizons*, 49: 96-97.
- Robins, C.R., Buck, B.J., **Williams, A.J**, Morton, J.L., Howell, M.S., Yonovitz, M.L, House, P.K., 2009, Comparison of Flood Hazard Assessments on Desert Piedmonts and Playas: A Case Study in Ivanpah Valley, Nevada, *Geomorphology*, 103: 520-532.

Dissertation Title: Co-Development of Biological Soil Crusts, Soil-Geomorphology, and Landscape Biogeochemistry in the Mojave Desert, Nevada, U.S.A. – Implications for Ecological Management

Dissertation Examination Committee:

- Chairperson, Brenda Buck, Ph.D.
- Committee Member, Margaret (Peg) Rees, Ph.D.
- Committee Member, Stephen Rowland, Ph.D.
- Committee Member, Deborah Soukup, Ph.D.
- Graduate Faculty Representative, Lloyd Stark, Ph.D.